Development of a gene therapy for congenital neutropenia caused by *ELANE* mutations

Dissertation

der Mathematisch-Naturwissenschaftlichen Fakultät

der Eberhard Karls Universität Tübingen

zur Erlangung des Grades eines

Doktors der Naturwissenschaften

(Dr. rer. nat.)

vorgelegt von

Malte Ulrich Ritter

aus Windhuk, Namibia

Tübingen

2024

Gedruckt mit Genehmigung der Mathematisch-Naturwissenschaftlichen Fakultät der Eberhard Karls Universität Tübingen.

Tag der mündlichen Qualifikaiton:	22.11.2024
Dekan:	Prof. Dr. Thilo Stehle
1. Berichterstatter/in:	Prof. Dr. Dr. Julia Skokowa
2. Berichterstatter/in:	Prof. Dr. Peter Ruth

We set sail on this new sea because there is new knowledge to be gained, and new rights to be won, and they must be won and used for the progress of all people. – John F. Kennedy

Table of Contents

Foreword

The figures used in the Results & Discussion section are from previous publications. The original articles are cited in the figure description. I have used the Grammarly software to check spelling and grammar and enhance my text's understandability. Grammarly uses generative artificial intelligence for this purpose.

I am deeply thankful to those who have proofread my work and provided suggestions! The remaining errors are my own and are not intentional.

Eidesstattliche Erklärung

Ich, Malte Ulrich Ritter versichere, dass ich die vorliegende Arbeit selbständig verfasst und keine anderen als die angegebenen Quellen und Hilfsmittel benutzt habe; aus fremden Quellen entnommene Passagen und Gedanken sind als solche kenntlich gemacht.

Datum 19.06.2024 Unterschrift: Malte Ritter

Abbreviations

A-EJ	alternative end joining
AAVS1	adeno-associate viral insertion site 1
AIM2	absent in melanoma 2
AML	acute myeloid leukemia
ATF6	activating transcription factor 6
BiP	binding immunoglobulin protein
BLM	BLM RecQ like helicase
Cas9	CRISPR associated system 9
CAST-seq	chromosomal aberrations analysis by single targeted linker mediated PCR sequencing
CBF	core binding factor
CBFA	core binding factor alpha
CD	cluster of differentiation
CDKN1A	cyclin dependent kinase inhibitor 1A
CEBP	CCAAT enhancer binding protein
CEBPA	CCAAT enhancer binding protein alpha
CFU	colony forming unit assay
CHIP	clonal hematopoiesis of intermediate potential
CN	congenital neutropenia
CN-AML	congenital neutropenia resulting in acute myeloid leukemia
CRISPR	clustered regular interspaced short palindromic repeats
CSF3R	colony stimulating factor 3 receptor
CtIP	C-terminal binding protein 1
CTSG	cathepsin G
CXCR4	C-X-C motif chemokine receptor 4
CyN	cyclic neutropenia
DAMP	danger-associated molecular patterns
DDPI	dipeptidyl peptidase I
DDR	DNA damage response
DNA	deoxyribonucleic acid
DNA2	DNA replication helicase/nuclease 2
DNAPKcs	DNA-dependent protein kinase, catalytic subunit
dPCR	digital polymerase chain reaction

DSBs	double-stranded breaks
eBFP	enhanced blue fluorescent protein
ELANE	elastase neutrophil expressed
ER	endoplasmic reticulum
EXO1	exonuclease 1
fMLP	formylmethionine-leucyl-phenylalanine
G-CSF	granulocyte colony-stimulating factor
G-CSFR	G-CSF-receptor
GADD45A	growth arrest and DNA damage-inducible alpha
GATA2	GATA binding protein 2
gRNA	guide RNA
GRP78	G protein-coupled receptor 78
GUIDE-seq	Genome-wide unbiased identification of double-stranded breaks enabled by sequencing
GvHD	graft versus host disease
h	human
HDR	homology-directed repair
HL-60	human leukemia cell line 60
HNH	histidine – asparagine – histidine domain
HSCs	hematopoietic stem cells
HSPCs	hematopoietic stem and progenitor cells
ID	inhibitory domain
IL-1	interleukin 1
IL-10	interleukin 10
IL-15	interleukin 15
IL-18	interleukin 18
IL-6	interleukin 6
INDELs	insertion or deletion of DNA nucleotides
iPSCs	induced pluripotent stem cells
ISMARA	integrated system for motif activity response analysis
Klf4	krüppel like factor 4
KN	Kongenitale Neutropenie
LEF1	lymphoid enhancer-binding factor 1
LgBiT	lysed and by the addition of the main body of the luciferase protein

LNP	lipid nanoparticles
LOH	loss of heterozygosity
LT-HSCs	long-term hematopoietic stem cells
MDS	myeloid dysplastic syndrome
MILESTONE	modifying ELANE Goldberg–Hogness box to inhibit expression
MMEJ	microhomology-mediated end-joining
MMP	multi-potent progenitors
MRE11	meiotic recombination 11
MRN	MRE11–RAD50–NBS1
mRNA	messenger ribonucleic acid
NBS1	Nijmegen breakage syndrome 1
NE	neutrophil elastase
NETs	neutrophil extracellular traps
NF-kappaB	nuclear factor 'kappa-light-chain-enhancer' of activated B-cells
NGS	next-generation sequencing
NHEJ	non-homologous end joining
NLR	NOD-like receptors
NLS	nuclear localization signal
NmCas9	*Neisseria meningitides* CRISPR associated system 9
NMD	nonsense-mediated decay
NOD	nucleotide-binding oligomerization domain
NSG	nod scid gamma
NSP4	neutrophil serine protease 4
PAM	protospacer adjacent motif
PAMP	PRR binding conserved molecular patterns
PARP	poly(ADP-Ribose)-polymerase
PCR	polymerase chain reaction
PHGDH	phosphoglycerate dehydrogenase
PNK	polynucleotide kinase 3'-phosphatase
PolX	polymerase X
PROTAC	proteases targeting chimeras
PRR	pattern recognition receptors
PRTN3	proteinase 3
PU.1	Spi-1 proto-oncogene

qPCR	quantitative polymerase chain reaction
rAAV6	recombinant adeno-associated virus 6
RAD50	RAD50 double-strand break repair protein
RAD51	RAD51 double-strand break repair protein
RAD52	RAD52 double-strand break repair protein
RHD	runt homology domain
rhG-CSF	recombinant human granulocyte colony-stimulating factor
RIG-I	retinoic acid-inducible gene I
RNA	ribonucleic acid
RNA-seq	ribonucleic acid sequencing
RNP	ribonucleoprotein
ROS	reactive oxygen species
RUNX1	runt-related transcription factor 1
RuvC	crossover junction endodeoxyribonuclease RuvC
SaCas9	*Staphylococcus aureus* CRISPR associated system 9
SAM	synergistic activation mediator
SCN	severe congenital neutropenia
SNP	single nucleotide polymorphism
Sp3	Sp3 transcription factor
SpCas9	*Streptococcus pyogenes* Cas9
SSB	single-strand DNA breaks
ST-HSCs	short-term hematopoietic stem cells
T7E1	T7 endonuclease 1
TAD	transactivation domain
THP-1	Tohoku Hospital pediatrics-1
TLR	toll-like receptor signaling
UPR	unfolded protein response
WNT	wingless-type MMTV integration site family
WRN	Werner syndrome, RecQ helicase-like
WT	wildtype
XRCC3	X-ray repair cross-complementing group 3
XRCC4	X-ray repair cross-complementing group 4

Summary

The monogenetic disease congenital neutropenia (CN) is a pre-leukemia bone marrow failure syndrome. In approximately 50 % of CN patients, the disease is caused by mutations in the *ELANE* gene. This gene encodes the protein neutrophil elastase (NE). Patients suffer from an insufficient number of neutrophils, resulting in frequent severe and life-threatening bacterial infections and sepsis. The current standard of care is regular injections with the recombinant human granulocyte-colony stimulating factor (rhG-CSF), a cytokine produced naturally in the body. This treatment is not curative and does not prevent leukemia development, for which the patients have a 15 – 20 % lifetime risk. If the patient does not respond to rhG-CSF or develops leukemia, the only chance of survival is a bone marrow transplantation, which is associated with a risk of graft-vs-host disease, graft failure, infections, and a mortality risk of about 20 %.

These circumstances create a clear unmet medical need for therapy improvements. The recent development of CRISPR/Cas9 nucleases for gene editing has created a versatile tool ideally suited for genetic manipulation for gene therapy. Here, I present preclinical investigations into the application of CRISPR/Cas9 gene editing tools for the purpose of gene therapy development for patients with CN caused by *ELANE* mutations. Specifically, the development of a knockout strategy for the *ELANE* gene that restores neutrophil development and preserves neutrophil functions. And a novel knockdown strategy that reduces *ELANE* expression by genetically modifying the *ELANE* promotor region using two CRISPR/Cas9 nickases. The therapeutic potential of this approach has been demonstrated *in vitro* and *in vivo*. This approach has been shown to have a favorable genotoxic profile with no detectable off-target gene editing and no chromosomal translocations.

Finally, work on establishing an *in vitro* model with mouse hematopoietic stem and progenitor cells (HSPCs) with the mutations most frequently involved in MDS and AML development in CN patients has provided new insights into the dysregulated pathways and mechanisms underlying the progression from pre-leukemic to leukemic stages. These are mainly driven by increased innate immune activation in HSPCs. These observations are also crucial for disease-specific safety considerations in gene therapy development.

My work has contributed to understanding CN's pathophysiological mechanisms and offers novel gene therapeutic approaches for ELANE mutations that cause CN.

Zusammenfassung

Die hereditäre Erkrankung Kongenitale Neutropenie (KN) ist ein präleukämisches Syndrom, das durch eine Blockade der myeloischen Reifung im Promyelozytenstadium im Knochenmark gekennzeichnet ist. Bei etwa 50 % der KN-Patienten wird die Krankheit durch Mutationen im *ELANE*-Gen verursacht. Dieses Gen kodiert das Protein Neutrophilen-Elastase (NE). Die Patienten leiden an einem Mangel an neutrophilen Granulozyten, welcher häufig zu schweren und lebensbedrohlichen bakteriellen Infektionen und Sepsis führt. Die derzeitige Standardtherapie besteht aus regelmäßigen Injektionen des rekombinanten humanen Granulozyten-Kolonie-stimulierenden Faktors (rh-GCSF), eines körpereigenen Zytokins. Diese Behandlung ist nicht heilend und auch unter rh-GCSF Therapie haben Patienten ein Lebenszeitrisiko von 15 -20 %, an Leukämie zu erkranken. Bei Nichtansprechen auf rhG-CSF oder bei Leukämieentwicklung besteht die einzige Überlebenschance in einer Knochenmarktransplantation welche mit Risiken wie Graft-vs-Host-Disease, Transplantatversagen und einem Mortalitätsrisiko von 20 % verbunden ist.

Diese Umstände verdeutlichen, dass ein klarer medizinischer Bedarf an verbesserten Therapien besteht. Die jüngsten Entwicklungen im Bereich der Geneditierung haben gezeigt, dass sich CRISPR/Cas9-Nukleasen hervorragend für genetische Modifikationen innerhalb der Gentherapie eignen. In dieser Arbeit präsentiere ich präklinische Untersuchungen zur Anwendung von CRISPR/Cas9-Geneditierungs-Werkzeugen zum Zweck der Entwicklung einer Gentherapie für Patienten mit KN, welche durch *ELANE*-Mutationen verursacht werden. Insbesondere wurde in dieser Arbeit der Schwerpunkt auf die Entwicklung einer Knockout-Strategie für das *ELANE*-Gen gelegt, die die Neutrophilenentwicklung wiederherstellt und die Funktionen der Neutrophilen erhält. Zudem zeige ich hier eine neue Knockdown-Strategie, die die *ELANE*-Expression durch eine genetische Modifikation der Promotorregion des Gens mit zwei CRISPR/Cas9-Nickasen reduziert. Das therapeutische Potenzial dieses Ansatzes wurde *in vitro* und *in vivo* nachgewiesen und zeigt ein günstiges genotoxisches Profil ohne nachweisbare Off-Target-Gen-Editierung und ohne chromosomale Translokationen.

Zuletzt ermöglicht diese Arbeit neue Einblicke in fehlregulierte Signalwege und die zugrundeliegenden Mechanismen beim Übergang von der präleukämischen zur leukämischen Phase durch die Etablierung eines *in vitro* Modells mit Mausblutstammzellen mit den häufigsten Mutationen, die an der Entstehung von MDS

und AML bei CN-Patienten beteiligt sind. Diese werden hauptsächlich durch eine erhöhte Immunaktivierung in hämatopoetischen Stamm- und Vorläuferzellen (HSPCs) angetrieben. Diese Beobachtungen sind auch entscheidend für krankheitsspezifische Sicherheitsüberlegungen bei der Entwicklung von Gentherapien.

Zusammenfassend trägt meine Arbeit zum Verständnis der pathophysiologischen Mechanismen der KN bei und beschreibt neue gentherapeutische Ansätze für KN verursachende *ELANE*-Mutationen.

List of publications

Listed are all publications relevant to my PhD thesis.

A. Ritter, M. U., * Nasri M., * Benjamin Dannenmann, Perihan Mir, Benjamin Secker, Diana Amend, Maksim Klimiankou, Karl Welte, Julia Skokowa, J. Side-to-side Comparison of Gene-editing Approaches for Severe Congenital Neutropenia-Causing Mutations in the ELANE Gene – understanding gene editing towards clinical translation. The CRISPR Journal (2024) (* equal contribution)

B. Nasri, M.,* **Ritter, M. U.**,* Mir, P., Dannenmann, B., Kaufmann, M. M., Arreba-Tutusaus, P., Xu, Y., Borboran-Bravo, N., Klimiankou, M., Lengerke, C., Zeidler, C., Cathomen, T., Welte, K. & Skokowa, J. (2024). General CRISPR/Cas9n-mediated gene editing for gene therapy of *ELANE*-related severe congenital neutropenia. Molecular Therapy (2024). (* equal contribution) (DG-GT Paper of the Quarter award Q1 2024)

C. Zeidler, A., Borbaran-Bravo, N., Dannenmann, B., **Ritter, M.**, Nasri, M., Klimiankou, M., Kandabarau, S., Zahabi, A., König, J., Zeidler, C., Skokowa, J., and Welte, K. Differential transcriptional control of hematopoiesis in congenital and cyclic neutropenia patients harboring ELANE mutations. Haematologica. 10.3324/haematol.2023.284033, (2023).

D. Skokowa, J., Hernandez Alvarez, B., Coles, M., **Ritter, M.**, Nasri, M., Haaf, J., Aghaallaei, N., Xu, Y., Mir, P., Krahl, A.-C., Rogers, K. W., Maksymenko, K., Bajoghli, B., Welte, K., Lupas, A. N., Müller, P. & ElGamacy, M. A topological refactoring design strategy yields highly stable granulopoietic proteins. Nature Communications 13, 2948 (2022).

E. Dannenmann, B., Klimiankou, M., Oswald, B., Solovyeva, A., Mardan, J., Nasri, M., **Ritter, M.**, Zahabi, A., Arreba-Tutusaus, P., Mir, P., Stein, F., Kandabarau, S., Lachmann, N., Moritz, T., Morishima, T., Konantz, M., Lengerke, C., Ripperger, T., Steinemann, D., Erlacher, M., Niemeyer, C. M., Zeidler, C., Welte, K. & Skokowa, J. iPSC modeling of stage-specific leukemogenesis reveals BAALC as a key oncogene in severe congenital neutropenia. *Cell Stem Cell* **28**, 906-922.e906 (2021).

F. Mir, P., **Ritter, M.**, Welte, K., Skokowa, J. & Klimiankou, M. in *Methods in Molecular Biology: RNA Interference and CRISPR Technologies: Technical*

Advances and New Therapeutic Opportunities (ed Mouldy Sioud) 455-469 (Springer US, 2020).

G. Nasri, M., **Ritter, M.**,* Mir, P.,* Dannenmann, B.,* Aghaallaei, N., Amend, D., Makaryan, V., Xu, Y., Fletcher, B., Bernhard, R., Steiert, I., Hahnel, K., Berger, J., Koch, I., Sailer, B., Hipp, K., Zeidler, C., Klimiankou, M., Bajoghli, B., Dale, D. C., Welte, K. & Skokowa, J. CRISPR/Cas9-mediated ELANE knockout enables neutrophilic maturation of primary hematopoietic stem and progenitor cells and induced pluripotent stem cells of severe congenital neutropenia patients. *Haematologica* **105**, 598-609 (2020). (* equal contribution)

H. **Ritter, M.**, Klimiankou, M., Klimenkova, O., Schambach, A., Hoffmann, D., Schmidt, A., Kanz, L., Link, D. C., Welte, K. & Skokowa, J. Cooperating, congenital neutropenia–associated Csf3r and Runx1 mutations activate pro-inflammatory signaling and inhibit myeloid differentiation of mouse HSPCs. *Annals of Hematology* **99**, 2329-2338 (2020).

I. Morishima, T., Krahl, A. C., Nasri, M., Xu, Y., Aghaallaei, N., Findik, B., Klimiankou, M., **Ritter, M.**, Hartmann, M. D., Gloeckner, C. J., Stefanczyk, S., Lindner, C., Oswald, B., Bernhard, R., Hähnel, K., Hermanutz-Klein, U., Ebinger, M., Handgretinger, R., Casadei, N., Welte, K., Andre, M., Müller, P., Bajoghli, B. & Skokowa, J. LMO2 activation by deacetylation is indispensable for hematopoiesis and T-ALL leukemogenesis. Blood 134, 1159-1175 (2019).

Personal contribution

This section details the personal contributions to the above-listed publications:

A. Co-first author together with Masoud Nasri. Conceptualization, experimental design, performance, data analysis and *in vitro* liquid culture differentiation, CFU of gene-edited HSPCs, GUIDE-Seq, and manuscript preparation and writing.

B. Co-first author together with Masoud Nasri. Conceptualization, experimental design, performance, data analysis and *in vitro* liquid culture differentiation, xenotransplantation of gene-edited HSPCs, GUIDE-Seq, and manuscript preparation and writing.

C. Fourth author, experimental design, performance, data analysis, and result interpretation of primary patient bone marrow flow cytometric analysis.

D. Third author, experiment design, performance, data analysis, and figure preparation of *de novo* designed G-CSF analog testing in mice.
E. Sixth author, experiment design, execution, and data analysis of lentiviral transduction human HSPCs.
F. The second author was involved in manuscript conceptualization, figure generation, and writing.
G. Co-second author, together with Perihan Mir and Benjamin Dannenmann. Involved in the conceptualization of the study with Masoud Nasri and Julia Skokowa. Planned experiments, conducted them, analyzed data, and participated in manuscript preparation. Was responsible for gene editing of HSPCs, liquid culture differentiation of gene-edited HSPCs, and functional assessment of *in vitro* generated neutrophils.
H. The first author conceptualized the study with Julia Skokowa, planned experiments, conducted them, analyzed data, and wrote the manuscript together with Julia Skokowa.
I. Eigth, author, assisted Ann-Kathrin Krahl in the *in vivo* mouse study.

Participation in academic conferences

A. Ritter, M. U., Nasri, M., Dannenmann, B., Zeidler, K. A., Lengerke, C., Zeidler, C., Klimiankou, M., Welte, K. H. & Skokowa, J. *'A Pipeline for Comparison and Selection of Clinically Applicable Gene Therapy Approaches for ELANE-Associated Severe Congenital Neutropenia'*, Oral presentation, Abstract achievement award *64th Annual meeting of the American Society of Hematology (ASH),* San Diego, USA 2023.
B. **Ritter, M. U**., Nasri, M., Dannenmann, B., Mir, P., Secker, B., Zeidler, C., Klimiankou, M., Welte, K. H. & Skokowa, J. *'A comparison of different strategies for CRISPR/Cas9-based gene therapies of congenital neutropenia associated with ELANE mutations'*, Poster presentation, ESGCT 30th Annual Congress, Brussel, Belgium (2023).
C. **Ritter, M. U.**, Nasri, M., Dannenmann, B., Kaufmann, M. M., Zeidler, K. A., Lengerke, C., Zeidler, C., Klimiankou, M., Cathomen, T., Welte, K. H. & Skokowa, J. *'An Ex Vivo CRISPR/Cas9 and AAV6 Based Gene Therapy Approach for p.W44X HAX1 Mutations in Patients with Severe Congenital*

Neutropenia', Poster presentation, XXIII. Wilsede Meeting 2023, Wilsede Germany 2023.

D. **Ritter, M. U.,** Nasri, M., Dannenmann, B., Mir, P., Secker, B., Zeidler, C., Klimiankou, M., Welte, K. & Skokowa, J. *‚Ein in-vitro Vergleich der bekannten Gentherapieansätzen für Kongenitale Neutropenie auslösende ELANE Mutationen',* Oral presentation, **Young Investigators' Award**, Jahrestagung der Deutschen, Österreichischen und Schweizerischen Gesellschaften für Hämatologie und Medizinische Onkologie (DGHO) Vienna, Austria 2022.

E. **Ritter, M. U.**, Nasri, M., Dannenmann, B., Kaufmann, M. M., Zeidler, K. A., Zeidler, C., Klimiankou, M., Cathomen, T., Welte, K. & Skokowa, J. *'A selection free ex vivo gene therapy approach to congenital neutropenia causing HAX1 mutations'*, Oral presentation, Kind-Philipp-Foundation for Research in Pediatric Oncology XXXV. Annual Meeting Wilsede, Germany 2022.

F. **Ritter, M. U.,** Nasri, M., Zeidler, K. A., Secker, B., Dannenmann, B., Amend, D., Haaf, J., Bernhard, R., Steiert, I., Klimiankou, M., Zeidler, C., Welte, K. H. & Skokowa, J. *'A selection free Ex vivo gene therapy approach for curing the congenital neutropenia causing HAX1 p.W44X mutation',* Oral presentation, Jahrestagung der Deutschen, Österreichischen und Schweizerischen Gesellschaften für Hämatologie und Medizinische Onkologie (DGHO), Berlin, Germany 2021.

G. **Ritter, M. U.**, Secker, B., Nasri, M., Klimiankou, M., Dannenmann, B., Amend, D., Haaf, J., Mir, P., Bernhard, R., Steiert, I., Zeidler, C., Welte, K. & Skokowa, J. *'Efficient Correction of HAX1 Mutations in Primary HSPCs of Severe Congenital Neutropenia Patients Using CRISPR/CAS9 GENE-Editing'*, Oral presentation, Annual meeting of the American Society of Hematology (ASH) Atlanta, USA 2020.

H. Ritter, M. U., Secker, B., Nasri, M., Klimiankou, M., Dannenmann, B., Amend, D., Haaf, J., Mir, P., Bernhard, R., Steiert, I., Zeidler, C., Welte, K. H. & Skokowa, J. *'Efficient Correction of HAX1 Mutations in Primary HSPCS of Severe Congenital Neutropenia Patients Using CRISPR/Cas9 Gene-Editing',* Poster presentation, 25th European Hematology Association (EHA) annual congress, Virtual (2020).

I. **Ritter, M. U.**, Nasri, M., Dannenmann, B., Kaufmann, M. M., Zeidler, K. A., Secker, B., Amend, D., Haaf, J., Zeidler, C., Klimiankou, M., Cathomen, T.,

Welte, K. H. & Skokowa, J. *‘ Safety and Efficacy Evaluation for an Ex Vivo Selection Free CRISPR/Cas9 Based Gene Therapy for HAX1 Associated Congenital Neutropenia’,* Poster presentation, Annual meeting of the American society of gene and cell therapy (ASGCT), Virtual 2020.

J. **Ritter, M. U.**, Secker, B., Klimiankou, M., Nasri, M., Aghaallaei, N., Dannenmann, B., Bernhard, R., Steiert, I., Haehnel, K., Bajoghli, B., Zeidler, C., Welte, K. & Skokowa, J. *‘Efficient Correction of ELANE mutations in Primary HSPCs of Severe Congenital Neutropenia Patients Using CRISPR/Cas9 and rAVV6 HDR Repair Templates’,* Poster presentation, Annual meeting of the American Society of Hematology (ASH), Orlando, USA (2019).

K. **Ritter, M. U.**, Klimenkova, O., Klimiankou, M., Schmidt, A., Stocking, C., Kanz, L., Zeidler, C., Link, D. C., Welte, K. & Skokowa, J. *‘Downstream effect of CSF3R and RUNX1 mutations that underlie leukemic transformations in congenital neutropenia (CN)’*, Oral presentation, Kind-Philipp-Foundation for Research in Pediatric Oncology XXXII. Annual Meeting, Wilsede, Germany 2019.

L. **Ritter, M. U.**, Klimenkova, O., Klimiankou, M., Schmidt, A. E., Stocking, C., Kanz, L., Zeidler, C., Link, D. C., Welte, K. & Skokowa, J. *‘Understanding the Role of CSF3R and Runx1 Runt Homology Domain Missense Mutations in Leukemic Transformation of Hematopoietic Stem Cells.’* Poster presentation, Annual meeting of the American Society of Hematology (ASH), San Diego, USA 2018.

M. **Ritter, M. U.**, Klimiankou, M., Krahl, A.-C., Klimenkova, O., Schmidt, A., Kanz, L., Link, D. C., Andre, M. C., Welte, K. & Skokowa, J. *‚Co-acquisition of RUNX1 and CSF3R mutations transforms hematopoietic progenitor cells of CN patients into more primitive highly proliferative blast’*, Oral presentation, Jahrestagung der Deutschen, Österreichischen und Schweizerischen Gesellschaften für Hämatologie und Medizinische Onkologie (DGHO), Stuttgart, Germany 2017.

I. Introduction

Hematopoiesis

Blood is a liquid organ consisting of plasma, red blood cells (erythrocytes), white blood cells (leukocytes), and platelets (thrombocytes). Circulated through the body's vasculature by the heart, blood supplies, removes, and redistributes metabolites, nutrients, hormones, gases, and heat in the whole body and distributes immune cells for pathogen defense. Broadly speaking, blood contains the following cell types: erythrocytes transport oxygen and carbon dioxide, thrombocytes close wounds by coagulation, and leukocytes defend the body against pathogens.

Blood cells are produced in the bone marrow from hematopoietic stem and progenitor cells (HSPCs). They mature to different stages depending on their cell type before being released into the bloodstream.[1]

The white blood cells are categorized into myeloid and lymphoid cells. Myeloid cells constitute the innate arm of the immune system and are subcategorized into neutrophils, monocytes, basophils, eosinophils, and dendritic cells. The lymphoid cells form the adaptive part of the immune system and consist of T, B, natural killer, and dendritic cells. They further mature and specialize in the other lymphatic organs, namely the thymus, lymph nodes, spleen, and mucosa-associated lymphoid tissue.[2]

The regulation of the number of blood cells is fundamental to the development, homeostasis, and adaptation of the organism to aging, stimuli, and disturbances such as pathogens, environmental influences, toxins, germline, and somatic mutations.[3-5]

To enable adequate reaction of the organism to dynamically changing conditions in homeostasis, blood cells have one of the highest cell turnovers in the human body, requiring the production of roughly 10^{11}-10^{12} cells per day.[6-8] During emergencies such as infections or blood loss, this number can be increased up to 100-fold.[7]

Hematopoietic stem and progenitor cells

The huge nonstop demand for blood cells is covered by the tightly regulated functions of HSPCs residing in niches of the bone marrow.[3,9-11] HSPCs are classified into long-term hematopoietic stem cells (LT-HSCs), short-term hematopoietic stem cells (ST-HSCs), multipotent- and unipotent restricted progenitors, which finally give rise to the different mature blood cells which enter circulation.[6,12] The distinction between these progenitor populations is continuous rather than binary, a finely balanced control of

quiescence, proliferation, and differentiation unique to each population, enabling the continuous production of blood cells over the entire human lifespan and under varying conditions.[13,14] Blood cell production follows a differentiation hierarchy with the most immature LT-HSCs at the top.[6] Current estimates, based on *in vivo* lineage tracing in humans, put the numbers of LT-HSCs between 50,000 – 200,000 in adults.[15,16] These cells are mostly quiescent.[9] When they divide, the division asymmetrically produces one LT-HSC and one ST-HSC, thus maintaining a stable pool of LT-HSC.[17] The ST-HSCs are highly proliferative, produce many ST-HSCs, and differentiate into multi-potent progenitors (MMP), which multiply significantly and differentiate into lineage-committed progenitors.[6] Through this cascade, each LT-HSC is amplified extensively to ensure the production of sufficient mature blood cells, including the most abundant and short-lived white blood cells, granulocytes (Fig. 1).[18]

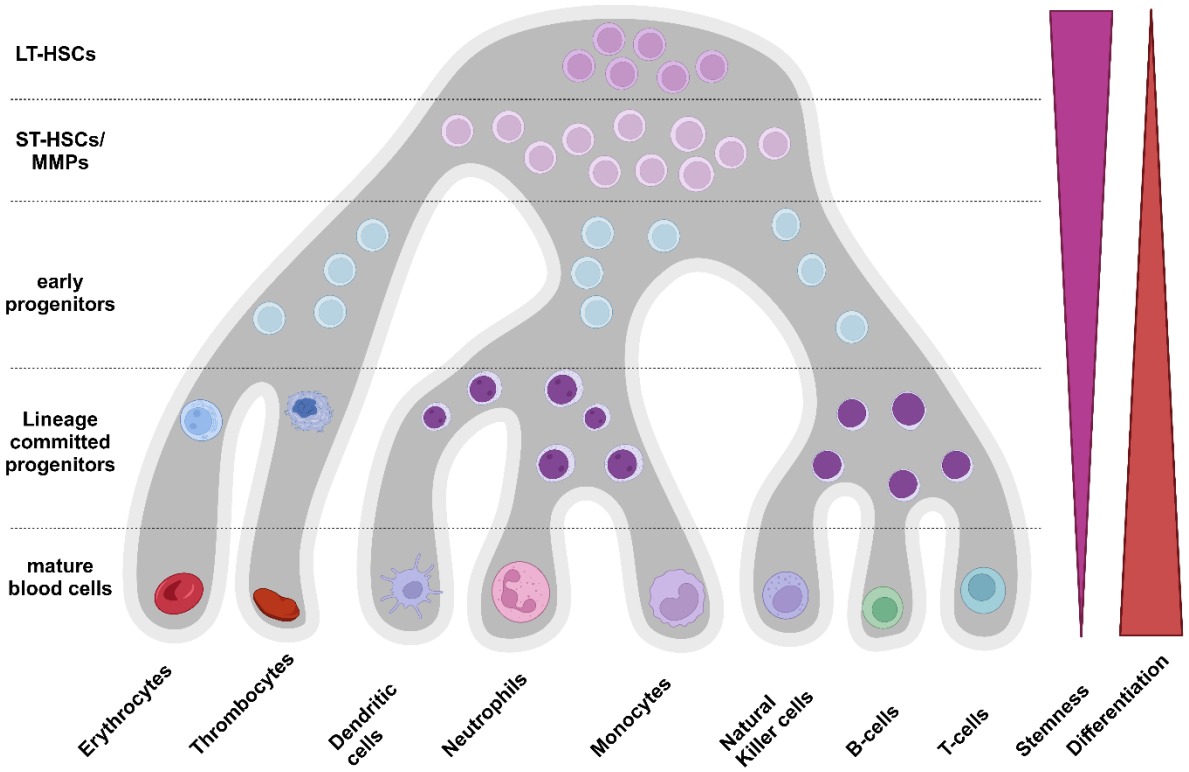

Figure 1. The hematopoietic system. Schematic representation of the hematopoietic hierarchies and lineage differentiation from hematopoietic stem cells to fully mature blood cells. With a qualitative description of stemness and differentiation across the different stages. Adapted from Notta et al.,[12] and Laurenti and Göttgens.[13] This figure was created with BioRender.[19]

Granulocytes

Granulocytes are polymorphonuclear leukocytes of the myeloid lineage, subclassified into neutrophils, basophils, and eosinophils. Neutrophils are the most abundant white blood cells, with a concentration of 1.800-7.500 per µl of blood. They have

characteristically two to five-lobed nuclei and azurophil or basophilic granules of lysosomal origin.[1] Based on the appearance during cell maturation, these granules are also referred to as primary (azurophilic), secondary (basophilic), tertiary (gelatinase), and secretory granules.[20] Neutrophil granules are essential for the primary innate immune response to pathogens, especially against bacteria and fungi.[20-22]

To fulfill their role, neutrophils are equipped with pattern recognition receptors (PRR) such as Toll-like receptors, C-type lectin receptors, nucleic-acid sensing receptors such as AIM2 or RIG-I, and lastly, nucleotide-binding oligomerization domain (NOD) like receptors (NLR). These PRR bind conserved molecular patterns (PAMP) commonly found on bacteria and fungi.[23] Based on the concentration gradient of these PAMP, they find the site of inflammation, enter the infected tissue, where they phagocytose, and kill the pathogens with the cytotoxic content of their lysosomes.[24] They can also form neutrophil extracellular traps (NETs) by dissolving their nucleus and then releasing a mixture of DNA, chromatin, and granular proteins into the extracellular space.[22] This process is an apoptotic pathway that forms web-like structures to immobilize and kill pathogens.[25] Further, activated neutrophils can set free numerous cytokines and other factors that attract and activate other immune cells and assist in wound healing and tissue repair.[22,23,26]

As for all blood cells, the early neutrophil precursors reside in the bone marrow. The first distinct progenitor is the myeloblast, the common progenitor for neutrophils and monocytes. Myeloblasts give rise to promyelocytes, which mature into myelocytes, then develop into metamyelocytes, followed by band neutrophils, finally maturing into neutrophils.[27] Due to the continuous nature of the differentiation process, an alternative simplified classification based on proliferative state and molecular properties has been proposed.[21]

Only band and segmented neutrophils are released into the blood, but under normal circumstances, this makes up only half of the total count of neutrophils in the body. The remaining half of the neutrophils reside in the bone marrow as a reserve that can be rapidly mobilized into the peripheral blood in the case of an emergency.[28]

In the peripheral blood, neutrophils can be in circulation or marginated to blood vessel walls. Marginated neutrophils are not detectable in blood samples. These two pools of neutrophils are distributed equally.[28]

Neutrophils spend around 6-11 hours in circulation in peripheral blood before entering tissues. Some studies have claimed circulation times of up to 5 days.[29] There, they

remain on average for 4-5 days before destruction while serving their phagocytic role or entering senescence.[29,30]

The regulation of the neutrophil production process is classified according to the governing states. One is the homeostatic production of neutrophils, and the other is the emergency granulopoiesis.

Although neutrophils are the most abundant white blood cell type, their heterogeneity and the corresponding impact on physiology and pathophysiology are only partially understood.[27,31,32]

Congenital neutropenia

A neutrophil count below 1000 neutrophils per µl of peripheral blood is called neutropenia.[33] The reason for bone marrow failures, among them neutropenia, can be toxins, chemotherapeutic agents, drugs, infections, autoimmune reactions, or genetic mutations.[33] Genetic mutations can cause benign forms of neutropenia by shifting the distribution of neutrophils, as in the case of benign ethnic neutropenia.[34] When they affect genes essential in the development or maintenance of neutrophils, the results become life-threatening. These cases are referred to as congenital neutropenia (CN). Neutrophil counts below 500 per µl are categorized as severe CN (SCN). The lack of neutrophils is caused by an early-stage maturation block in myeloid differentiation towards neutrophils in the bone marrow, resulting in neutropenia in the peripheral blood.[33,35] This lack of neutrophils leads to severe life-threatening bacterial infections in early life, most frequently otitis, skin infections, deep abscesses, gingivitis, pneumonia, and severe septicemia. It is estimated that 3 – 8.5 per one million individuals suffer from CN.[33,36,37] To date, mutations in more than 100 genes have been shown to impair neutrophil development and cause CN.[38] In approximately 30 % of cases, the genetic cause cannot be resolved.[33,39]

Independent of the mutation, the current standard of care for CN patients is treatment with recombinant human granulocyte colony-stimulating factor (rhG-CSF). Patients administer it subcutaneously daily or every other day at doses ranging up to 50 µg / kg.[33,38] More recently, it has been shown that high doses of nicotinamide (vitamin B3) also increase neutrophil counts and that it can be used as an alternative in mild cases or to reduce the dose of rhG-CSF.[40,41] If both therapies fail to lift the neutrophil count to physiological levels and prevent severe life-threatening infections, the only alternative treatment option is a bone marrow transplantation with the associated risks

and limitations such as but not limited to life-long immune suppression, graft failure, graft versus host disease (GvHD) and secondary malignancies.[33,42]

Mutations in the gene *ELANE* (elastase neutrophil expressed) are the most frequent genetic cause of CN. Positioned on chromosome 19 (19p13.3), the *ELANE* gene consists of 5 exons and 6 introns and encodes the serine protease neutrophil elastase (NE). Depending on the cohort studied, it is the cause in roughly 50 % of all CN cases.[33,43,44]

ELANE transcription is initiated during the promyelocyte cell stage and is then gradually downregulated during maturation to neutrophils[45]. It is expressed as a pre-pro-peptidase[46] and stored in primary granules (azurophilic vesicles) formed at the promyelocyte cell stage.[45]

Different hypotheses have been proposed regarding how *ELANE* mutations cause CN, often depending on the specific mutation studied.[33,47]

In general, three different hypotheses exist with different postulated mechanisms. First is the mistracking or mislocalization hypothesis, according to which incompletely processed mutant NE protease, which is still catalytically active, is routed to the wrong cell compartment and degrades the wrong proteins, leading to maturation arrest. This erroneous routing can be due to incomplete processing of the preforms of NE or due to an overwhelmed transporter system.[48,49] Second is the unfolded protein response (UPR) hypothesis, according to which the mutant NE protein cannot be appropriately folded in the endoplasmic reticulum (ER). When a lot of mutated protein is produced at the promyelocyte stage, this unfolded protein accumulates, triggering (UPR). This explains why the maturation block is specific to the promyelocyte stage, where NE expression massively increases and reaches its peak.[45,48,50] This UPR can be canonical through BiP/GRP78 or ATF6 or alternatively through the activation of excessive reactive oxygen species (ROS) formation caused by UPR. This triggers the synthesis of promyelocytic nuclear bodies, which prevents the response to rhG-CSF at physiological levels.[48,50-52]

Third is the WNT signaling hypothesis postulated by Skokowa et al., which found that the lymphoid enhancer-binding factor 1 (*LEF1*) is severely diminished in promyelocytes, resulting in a lack of CEBPA which causes the observed maturation arrest and corresponding lack of neutrophils.[53]

It is unclear whether the different hypotheses explain the pathophysiology of different mutations, if the described mechanisms act synergistically, or if some described effects are bystanders. This puzzle remains to be fully solved.[47]

Another peculiar observation is the fact that the same mutation can also cause cyclic neutropenia (CyN).[43,44,54] CyN is a condition where patients suffer neutropenia periodically with a 21-day cycling pattern resulting in severe neutropenia for 3-5 days.[33] Death due to sepsis is not the only threat to life for CN patients. Long-term follow-up studies by the patients' registries have revealed that patients carry a 10 - 22 % risk of developing leukemia.[55,56] In the majority of described cases, the developed malignancies were myeloid dysplastic syndrome (MDS) or acute myeloid leukemia (AML).[33] Detailed molecular diagnostics of these AML cases have shown that AML blasts have a dominant pattern of co-acquisition of CSF3R mutations, the gene encoding the G-CSF-receptor (G-CSFR) and the runt-related transcription factor 1 (*RUNX1*). These are not the only genes affected by mutations, but 80 % of patients carry *CSF3R* mutation, and 65 % of these patients co-acquire *RUNX1* mutations.[57]

CSF3R physiology, mutations, and pathophysiological consequences

G-CSFR, encoded by the *CSF3R* gene, is widely expressed in multiple tissues, especially and highly in hematopoietic cells.[58] The receptor belongs to the cytokine receptor class I family and activates proliferative, maturation, and anti-apoptotic pathways. It is essential for the physiological development and survival of myeloid cells, especially neutrophil development.[59] In 1995, the first truncating mutation in the distal intracellular domain of G-CSFR was described.[60] Following studies revealed that these truncating mutations remove the receptor's autoinhibitory domain, resulting in hyperactivating signaling that increases proliferation.[61,62] It was observed in mice that these mutations are not leukemogenic but instead produce a hyperproliferative pre-leukemic phenotype (Fig. 2).[61-63] In our current understanding, these mutations can be classified as mutations conferring a clonal hematopoiesis of intermediate potential (CHIP) phenotype onto HSPCs as they can persist and expand without leukemia development.[64] However, they increase the risk of leukemic transformation.[65]

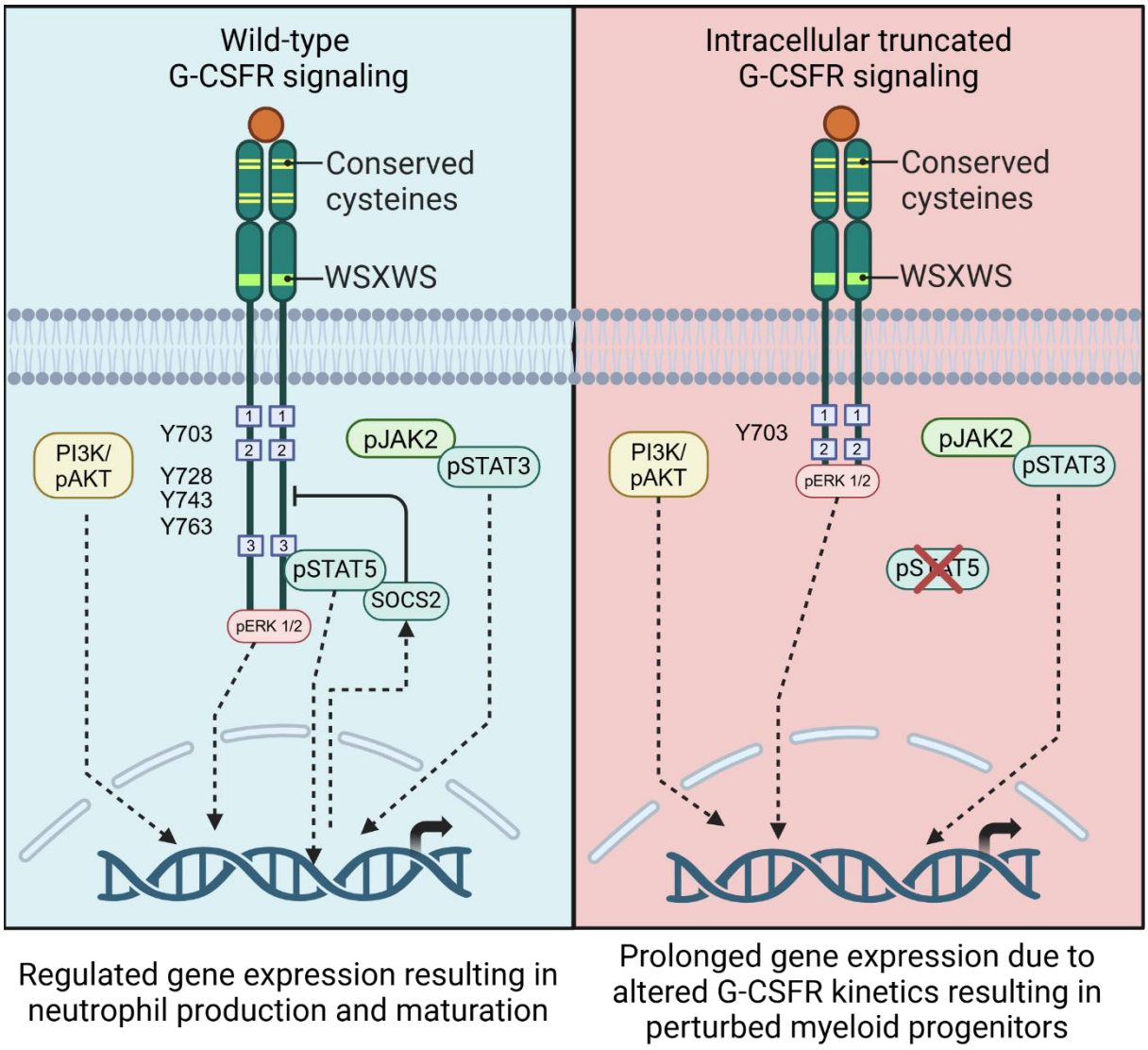

Figure 2. *CSF3R* mutations' impact on the G-CSF signaling pathways. Intracellular signaling pathways of the G-CSF receptor in the wildtype (left) and C-terminally truncated (right) forms. Indicated are the defining extracellular features that group the G-CSFR into the cytokine receptor class I family (conserved cysteines and the WSXWS motif). Blue boxes 1 and 2 are the domains responsible for proliferative signaling, and the domain for differentiation of myeloid progenitors is in blue box 3. Lastly, the signaling molecules and pathways are activated through the four tyrosines. Figure adapted from Dwivedi and Greis.[66] This figure was created with BioRender.[67]

RUNX1 physiology, mutations, and pathophysiology

The transcription factor RUNX1 is an essential transcriptional regulator in the emergence of hematopoietic tissue and plays a critical role in regulating adult hematopoiesis.[68] It is expressed in different isoforms regulated by different promoters and alternative splicing. The three main isoforms in hematopoietic cells are RUNX1A, RUNX1B, and RUNX1C. RUNX1C and RUNX1B contain the same functional elements, namely the Runt homology domain responsible for DNA binding, a nuclear localization signal (NLS), a transactivation domain (TAD), an inhibitory domain (ID), and a preserved C-terminal pentapeptide (Fig. 3A).[68] In definitive hematopoiesis,

RUNX1A and RUNX1B are mainly expressed, with RUNX1A lacking the TAD and thus acting in a dominant negative fashion in regulating the RUNX1 downstream signaling.[69] RUNX1 binds DNA directly, but its effect is strongly enhanced by core binding factor alpha (CBFα), stabilizing the protein-DNA complex.[70] Additionally, RUNX1 can directly interact with many crucial hematopoietic transcription factors, e.g., CEBPα, GATA2, PU.1. Through these interaction partners, RUNX1 is involved in epigenetic regulation besides its role as a direct regulator of transcription.[71] While mutations in RUNX1 during embryonic development are lethal, its mutations, when occurring during adult (definitive) or steady-state hematopoiesis, disrupt the finely tuned production of mature blood cells and the maintenance of HSCs (Fig. 3B).[72] In hematopoietic malignancies, point mutations leading to missense mutation in the RUNT domain, truncating mutations in the RUNT or TAD domains, and longer frameshifts that disrupt the TAD and C-terminal motifs are common (Fig. 3A).[73,74] Additionally, a plethora of translocations creating novel transcription factors involving RUNX1 have been described and extensively studied.[75]

In CN, *RUNX1* mutations were found to affect mainly the RUNT domain.[57,76] They inhibit DNA or CBFA binding, resulting in a dominant negative inhibition of RUNX1 signaling (Fig. 3A).[77] The frequently observed co-acquisition of *RUNX1* and *CSF3R* mutations indicates that they affect cellular signaling in a detrimental synergistic way,[57] but the specific mechanism of this functional interaction remains to be solved. Additionally, the timing of the acquisition of the mutations and the role of additional somatic gene mutations or chromosomal aberrations in the transition to overt leukemia remains unsolved.

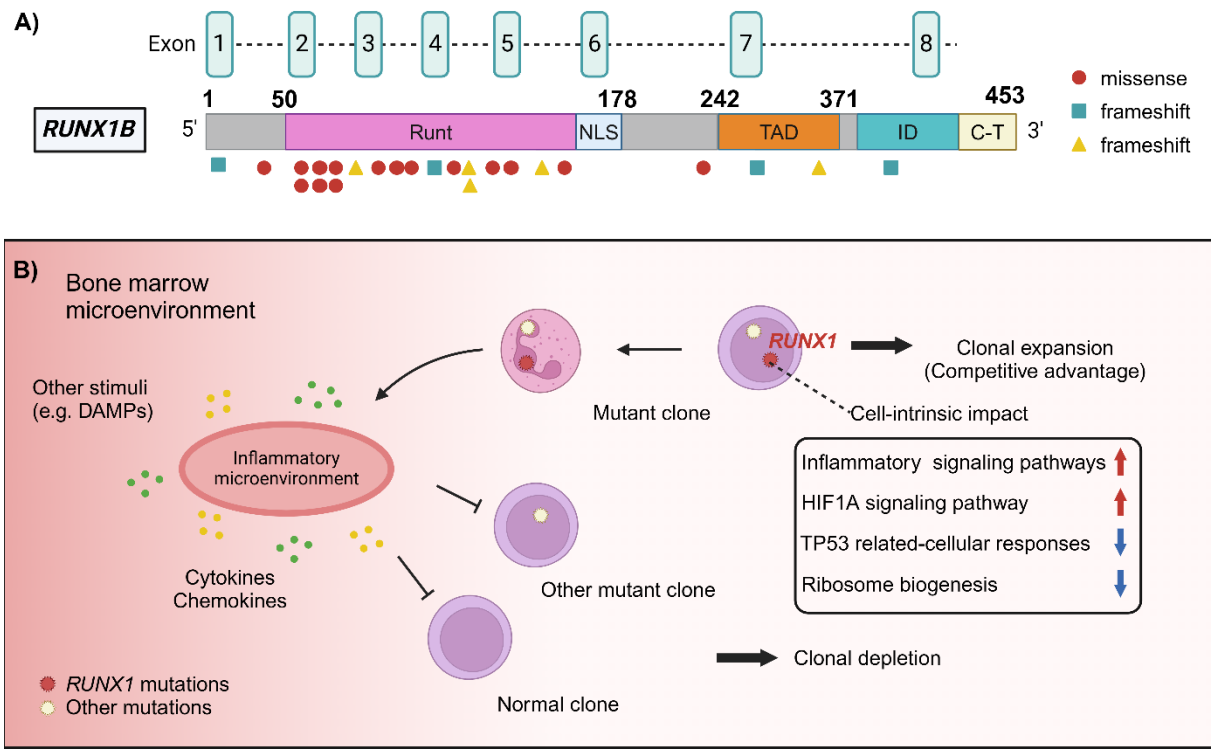

Figure 3. Type of RUNX1 mutations and the impact on the hematopoietic system. A) Representation of the *RUNX1* gene and the corresponding transcription factor domains. Mutations observed in CN patients who developed leukemia are represented by their location in the gene and the type of mutation. Each symbol represents an individual case. **B)** An illustration of the impact of *RUNX1* mutations on the hematopoietic system that contributes to leukemia development. The changes induced by *RUNX1* impact the cellular response to stimuli, the differentiation of stem cells, the secretome, and other behaviors of mature cells that carry the mutation and confer a clonal advantage on HSPCs carrying the mutation, ultimately resulting in leukemia if additional genomic alterations are acquired. This figure was created with BioRender.[78]

CRISPR/Cas9 system for gene therapy of hematopoietic diseases

Editing DNA, the fundamental biological data storage, has been a longstanding aim of science, and many different tools have been developed.[79] Promising but technically challenging to implement have been nucleases that introduce double-stranded breaks (DSB), triggering the cellular repair mechanisms and enabling the alteration of DNA in a precise manner.[80] This technical challenge was solved with the discovery of the clustered regular interspaced short palindromic repeats (CRISPR) and the complementary CRISPR-associated systems (Cas), which are originally a prokaryotic immune defense against viruses.[81,82] These RNA-guided nucleases of prokaryotes were adapted to target DNA and RNA in any cell in a programmable and precise manner by Jinek and Chylinski et al.[83] and subsequently shown by many groups to have the capability also to edit the eukaryotic genome.[84-86] It was the foundation for multiple new tools and applications and has resulted in the Nobel Prize in Chemistry in 2020 for Doudna and Charpentier.[87]

Different CRISPR/Cas systems have been identified and repurposed for gene editing. The most widely used system and backbone for other CRISPR tools, such as base and prime editors, remain *Streptococcus pyogenes* Cas9 (SpCas9) based systems.[88-90] It consists of two components, the SpCas9 nuclease, and guide RNA (gRNA). The SpCas9 nuclease has catalytical domains RuvC and HNH, which are responsible for DNA cleavage. RuvC catalyzes the break in the non-complementary DNA strand, while the HNH domain targets the complementary DNA strand. Together, these cuts result in double-stranded breaks (DSB) in the DNA helix.[91]

For specific DNA cleavage, the *Sp*Cas9 relies on a guide RNA (gRNA) that binds to the genomic DNA through Watson-Crick base pairing. The gRNA is mainly used as a single gRNA (sgRNA), which consists of the spacer sequence required for DNA interaction, a scaffold sequence that enables *Sp*Cas9 to bind the sgRNA, and a linker sequence connecting both. The spacer sequence for *Sp*Cas9 consists of 17–20 nucleotides at the 5'-end of the sgRNA. To activate the nuclease, the complementary DNA must be adjacent to a protospacer adjacent motif (PAM), triggering the nuclease activity of Cas9 and inducing a DSB.[91]

Because DSBs threaten cellular integrity, they immediately trigger a plethora of different proteins and mechanisms to repair the damage in the genetic code, commonly referred to as the DNA damage response (DDR).[92]

For DSB, the repair mechanisms can be divided into the low error frequency homology-directed repair (HDR) and the more error-prone end-joining pathways.[93] The end joining pathways are further distinguished as the canonical nonhomologous end joining (c-NHEJ) and alternative end joining (A-EJ).[94] Mechanistically, c-NHEJ is initiated by a Ku70-Ku80 dimer that binds the free ends originating from a DSB. The bound dimer then recruits other DNA processing proteins, such as DNAPKcs, Artemis, PolX, and PNK, before the ends are connected again by Ligase IV and its cofactors XRCC4 and Xlf/Cenunos.[95] This process can lead to short insertions and deletions (indels) in roughly 30 % of the repairs. The binding of the Ku dimer is the decisive factor determining if c-NHEJ or A-EJ and HDR happen. When no Ku-complex captures the DNA ends, PARP initiates a single-stranded 5'- to 3'-end DNA resection by MRE11-RAD50-NBS1 (MRN) complex and its cofactor CtIP that exposes matching microhomologies around the break site in the undigested strands. Therefore, this process is also known as microhomology-mediated end joining (MMEJ). The paired microhomologies are then stitched together by ligase III with XRCC3 as a cofactor.

This leads to deletions between 2 - 25 long base pairs (bp).[96] The DDR protein 53BP1 inhibits long resections. In case of 53BP1 absence, EXO1 and DNA2, in cooperation with WRN and BLM, produce long ssDNA overhangs. These overhangs can then anneal to homologous sequences, either sister chromatids or exogenous supplied DNA repair templates. The repair is finally processed through the RAD51 or RAD52 recombinases.[96]

Any system allowing targeted and intentional changes of the DNA has high promises for the research and treatment of genetic blood diseases. Since the initial development of SpCas9, this system has been most widely adopted.[97] Today, multiple Cas proteins are available for gene therapeutic applications, e.g., NmCas9, SaCas9, Cas12a. SpCas9 remains the most commonly used nuclease to date, owing to many tools, such as algorithms for predicting editing efficiency and probability of off-target events, commercial availability, and extensive experience.[98] Early on, many groups worked feverishly to improve the efficiency and specificity of the system by introducing point mutations in the nuclease or optimizing the structure and chemistry of the gRNA. This has greatly enhanced research into its use for various genetic hematologic diseases.[97]

Sufficient efficacy and safety are essential for developing a gene therapy for HSPCs that can be translated into clinical practice. Validation of these fundamental aspects of drug development depends on the chosen mode of delivery, the disease, and the gene editing strategy.[99]

Delivery of nucleases into hematopoietic stem cells

Different delivery platforms and methods exist to deliver gene therapy reagents into HSPCs. Broadly, these can be categorized into physical (e.g., electroporation), chemical (e.g., nanoparticles), or biological (e.g., viral vectors or virus-like particles).[100]

The first decision that needs to be made is whether to edit the HSPCs inside the human body (*in vivo*) or to extract and edit the HSPCs outside the body in the laboratory (*ex vivo*). *In vivo,* the delivery of gene editing tools to HSPCs in the bone marrow or in circulation has only recently been achieved in animal models. This route is only beginning to materialize for HSPCs gene therapy.[101,102]

Since HSPCs can be harvested from the bone marrow by puncture or by mobilization into the peripheral blood, where they can be collected by apheresis, *ex vivo* gene editing of HSPCs has been the standard gene therapy approach for hematologic disorders.[103] The modified HSPCs are then infused into the peripheral blood, from

where they return to the bone marrow niches for reconstitution and production of mature blood cells. This is a routine procedure also commonly used in autologous or allogenic bone marrow transplantations.[103]

The components for gene editing should be delivered in transient forms to reduce the possibility of off-target editing or other perturbances, such as activation of the innate immune system.[104] To this end, they can be delivered as non-integrating DNA, mRNA, or proteins. As the progeny to all blood cells, HSPCs are equipped with several receptors to sense viral or bacterial danger-associated molecular patterns (DAMP). Therefore, any entry of nucleic acids into HSPCs will trigger an innate immune response.[105] Additionally, HSPCs are fitted with antiviral enzymes like proteases and nucleases, which makes it challenging for gene editing reagents to perform editing before being neutralized. This has led to the development of degradation-resistant and less immunogenic, chemically modified mRNA.[106,107] By using CRISPR/Cas as a ribonucleoprotein (RNP) complex, the nucleic acid load per cell can be reduced, which, in turn, reduces the activation of the intrinsic cellular innate immune pathways.[108] In addition, it provides a favorable kinetic as the peak of available RNP is lowered, reducing potential oversaturation at the on-target site, and thus, less RNP is available to bind off-target sites.[109,110] Due to the bacterial origin of Cas, there may be pre-existing immunity. Presentation of Cas peptide fragments from gene-edited cells to immune cells can lead to immunological clearance of these cells.[2,111]

The editing reagents can be delivered by lipid transfection reagents,[112] electroporation,[106,113,114] nanoparticles,[101,115] viral vectors,[116,117] virus-like particles,[118,119] and other more recently developed physical delivery systems, such as nanoneedles.[120] To date, delivery by electroporation is the most used system.[121] However, lipid nanoparticles (LNP) are a promising development due to their lower cost and gentler effect on target cells.[101,122]

Efficacy of gene therapy

The first efficacy marker in gene therapy is the extent of intended on-target gene editing at the DNA level. To this end, different methods have been described to analyze DNA editing outcomes. The most available and easy-to-use method is the T7 endonuclease 1 (T7E1) assay, which relies on the structure-selective property of the T7E1 to digest heteroduplexes in DNA. Mutations caused by gene editing result in heteroduplexes, which can be exploited by digesting PCR products from gene-edited

loci with T7E1. The editing efficiency can be determined from the amount of DNA cut by running these digested PCR products on agarose gels.[123] This method is widely available and inexpensive. On the other hand, the margin of error is high and depends on the quality of the gel. It is well suited as an initial screening method for gene editing efficiencies.[124]

A more reliable and widely available assay is the mathematical deconvolution of Sanger sequencing traces of sequenced DNA from gene-edited sites, first described by Brinkmann et al.[125] and the most common choice for many laboratories as it provides the highest accuracy compared to the cost.[124]

The digital PCR-based method is more accurate and delivers rapid, deep sequencing-like depth, but it is not always accessible and requires more extensive assay validation.[126] This assay is especially valuable in projects requiring high sample throughput and simultaneous high accuracy with validated gene editing outcomes.[124]

Finally, next-generation sequencing (NGS) is the most accurate method and is regarded as the gold standard regarding accuracy.[124] However, it is the slowest due to library preparation, service provider turnaround time,[125] and the most expensive method.[124] Lastly, confirming that the intended changes in the DNA result in the desired changes on the protein level is imperative.[127] For this confirmation, any suitable protein detection method can be applied. CRISPR induces reoccurring DNA locus-specific INDELs patterns.[128] Once the pattern has been determined and the consequences on the protein level are established, genetic sequencing becomes a sufficient readout to determine editing efficacy. The disease-specific assays must be applied to determine whether the achievable gene editing induces the intended biological effects.[129,130]

Safety of gene therapy

All therapies must balance efficacy and safety.[131] With genome editing being a permanent and currently irreversible therapy, safety concerns are weighing heavily.[129] Especially, given the tragic and unnecessary death of Jesse Gelsinger in 1999 and multiple other patients in subsequent trials.[132,133] For nuclease-based genome editing approaches, several known unwanted consequences must be minimized, namely genotoxic,[134-136] DNA damage,[137] immunological,[2] cell type, and disease-specific side effects.[138] These are mutations happening outside the gene editing target, so-called off-target effects. At the on-target site, large deletions can be induced at a frequency

of 1-20 %.[134,139] Also, translocations can occur between on- and off-target sites.[135,136] Furthermore, gene editing can potentially induce loss of heterozygosity (LOH) or, worse, chromothripsis.[140,141] These effects depend on the sequence targeted, the sequence similarities in the genome, and the specificity of the nuclease used. The induction of large on-target deletions, translocations, LOH, and chromothripsis depends on several aspects besides the used nuclease and targeted sequence.[142,143] In particular, the culture and delivery process, the activation of repair mechanisms, and immune responses strongly influence the extent and type of genomic aberrations that can occur in gene-edited cells.[104,121,144,145]

These drawbacks prompted the development of multiple improvements, new nucleases, and gene editing tools to quantify, minimize, and prevent these side effects. These include nickases designed to make only single-strand DNA breaks (SSB) instead of DSB. Cellular repair of SSB is more efficient than DSB repair. This results in 100-fold fewer INDELs at the target site than at DSB.[146] When two nickases are combined in proximity, each targeting either the sense or antisense DNA strands, a DSB can still be induced. However, at off-target sites, the probability that both nickases will bind and cut in close proximity is very low. Off-targets are reduced by a factor of 50-100.[147]

New approaches improve the controllability of editing outcomes and, with increased safety profiles, utilize secondary enzymes coupled to nucleases.[148] Based on the secondary enzyme used, single bases are changed by deamination, so-called base-editors.[149] The use of reverse transcriptases and polymerases allows the introduction of any genetic modification at the target site. These constructs are called prime editors[89] and click editors,[150] respectively. Such tools have already been shown to produce fewer INDELs and less activation of DDR, but they do have the potential for novel forms of undesired editing outcomes and should be used critically.[142]

The clinical approval of exagamglogene autotemcel gene editing therapy for beta-thalassemia and sickle cell anemia demonstrates that safe genome editing is possible with the existing tools, provided great care is taken in developing therapies.[151]

II. Aim

The unprecedented fast development from fundamental discovery to clinically approved treatment has demonstrated the immense potential of nucleases, such as CRISPR/Cas9, for gene therapy applications. For safe clinical translation, it is essential to assess the disease specifically to develop and offer this potential for all monogenetic diseases. One such disease is CN. Patients with CN have a high unmet medical need due to the high burden on quality of life and risk of death despite available treatment options. My thesis aims to investigate the preclinical efficacy and safety of an *ex vivo* CRISPR/Cas9 gene therapy approach for CN. Specifically, the aims were:

1) Establishment of reproducible CRISPR/Cas9 genome editing in HSPCs of SCN patients and healthy individuals to facilitate pathophysiological research and development of gene therapy for CN.

2) Application of the established gene editing protocol for investigating the efficacy and safety of gene therapy for CN patients with *ELANE* mutations *ex vivo* and *in vivo.*

3) Modelling the combined intracellular signaling of leukemia causing *CSF3R*-Δ715 and *RUNX1* p.R139G and p.R174L mutations typically acquired by CN patients leading to acute myeloid leukemia *in vitro* using primary mouse lineage negative bone marrow cells.

III. Results and Discussion

(15 -25 pages)

Development of an *ex vivo* gene therapy approach for CN patients with *ELANE* mutations

(This part covers manuscripts A, B, F, and G, including a book chapter)

Autosomal dominant *ELANE* mutations cause half of all CN cases. These mutations are scattered throughout all 5 exons and 2 introns, with the pathophysiology incompletely understood.[33] The current standard of care for CN patients is daily subcutaneous injections of rhG-CSF. Bone marrow transplantation is the ultima ratio when patients are treatment refractive to rhG-CSF or develop leukemia.[38] Thus, a high unmet medical need exists for safer, more accessible, and curative therapy. The large number of different *ELANE* mutations and their autosomal dominant nature make it challenging to develop a gene therapy approach to correct these mutations specifically. Based on the evolution of *ELANE* as a young gene in the met-ase locus, found only in mammals beginning in mice[152,153] and having multiple functionally redundant proteases such as cathepsin G (*CTSG*), proteinase 3 (*PRTN3*), and neutrophil serine protease 4 (*NSP4*),[154,155] we reasoned that it might be dispensable for neutrophil formation and functionality in humans. The fact that *Elane*$^{-/-}$ mice have no detrimental phenotype and normal functional neutrophils[156-158] further strengthened our hypothesis. Lastly, the fact, that Papilloma-Levere Syndrome patients have normal neutrophil counts despite a lack of neutrophil elastase expression due to the absence of dipeptidyl peptidase I (DDPI), the enzyme responsible for processing neutrophil elastase into its active form,[159] indicates its non-essential role in humans. This encouraged us to pursue a knockout approach of *ELANE* as a gene therapy for CN patients with *ELANE* mutations.

For this purpose, a CRISPR/Cas9 gRNA has been designed to target the exon 2 of the *ELANE* gene. Induction of frameshift INDELs in an early exon of a gene typically results in nonsense-mediated decay (NMD), preventing translation and thus resulting in the knockout of the targeted gene. The knockout of *ELANE* with this guide was confirmed in the THP-1 cell line, expressing high levels of neutrophil elastase. In two independent models (HL-60 cells and patient-derived induced pluripotent stem cells

iPSCs), we confirmed the efficient inactivation of mutant *ELANE* and restoration of neutrophil formation.

To enable testing of this approach in primary healthy and CN patient HSPCs, we established an efficient electroporation procedure to deliver CRISPR/Cas9 as an RNP complex *ex vivo* (Fig. 4A). We were able to reach > 80 % of indel induction in the exon 2 of *ELANE* (Fig. 4B). This editing efficiency severely down-regulated neutrophil elastase expression in neutrophils derived from gene-edited HSPCs (Fig. 4C). By *in vitro* differentiation of the edited HSPCs, we found that already ~ 30 % of *ELANE* knockout was sufficient to rescue granulopoiesis significantly. At the same time, high gene knockout efficiencies had no negative impact on granulocyte formation in either edited healthy donors or patient HSPCs. We confirmed this by flow cytometric analysis of commonly used differentiation markers for neutrophils (Fig. 5A), morphological assessment of May-Grünwald-Wright-Giemsa-stained neutrophils in light field microscopy (Fig. 5B), scanning electron microscopy (Fig. 5C) and transmission electron microscopy (Fig. 5D).

In one patient with a p.I120F *ELANE* mutation, we did not observe a neutropenia phenotype by flow cytometry markers (Fig. 5A). This finding may be explained by the fact that this mutation is known to cause clinically mild neutropenia that can be treated with low doses of rhG-CSF. In our experiments up to this point, rhG-CSF concentrations of 10 ng/µl were used. In unpublished follow-up experiments, we found that rhG-CSF concentrations of 1 ng/ml were sufficient for optimal granulocytic differentiation of healthy donor HSPCs but did not differentiate CN patient HSPCs to neutrophils. We used this rhG-CSF concentration for future experiments.

ELANE knockout resulted in a downregulation of the UPR gene *BiP* and an upregulation of the anti-apoptotic factor *Bcl-xl* in hematopoietic cells derived from CN patients' iPSCs. This demonstrates that *ELANE* knockout restores the dysregulated pathways.

In addition to the importance of adequate neutrophil development, the functionality of the cells resulting from maturation has previously been shown to be impaired in CN patients, even with rhG-CSF therapy.[160] Therefore, we performed a functional assessment of *in vitro* generated *ELANE* knockout neutrophils. Specifically, we performed production of ROS upon stimulation with fMLP (Fig. 6A), flow cytometric and live cell imaging of *in vitro* phagocytosis of *E. coli* bioparticles (Fig. 6B & C) and an *in vitro* migration assay to assess chemotaxis in response to N-*formylmethionine-*

leucyl-phenylalanine (fMLP) (Fig. 6D). Lastly, a novel *in vivo* chemotaxis and phagocytosis assay was employed to determine if *ELANE* knockout neutrophils were capable of sensing bacterial infiltration, migrating into the wound and phagocytosing the bacterial particles.

A)

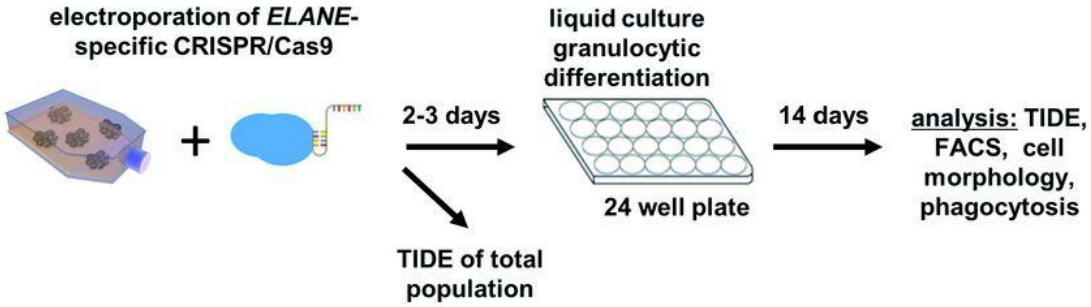

B)

Sample, *ELANE* mutation position	Exon	Indel Efficiency, %	
		day 7	day 14
healthy ctrl 1	-	71	69
healthy ctrl 2	-	57	46
healthy ctrl 3	-	86	94
CN p.A57V	Exon 2	52	63
CN p.I120F	Exon 3	81	90
CN p.S126L	Exon 4	45	57
CN p.C223AfsX17	Exon 5	27	37

C)

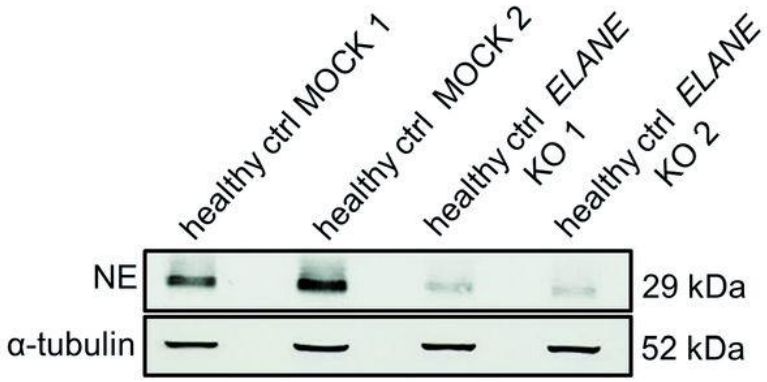

D)

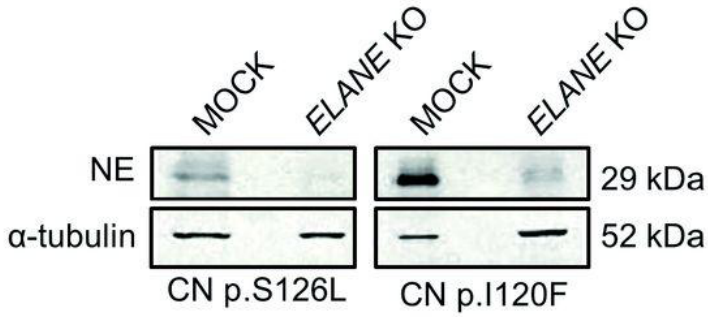

Figure 4. Editing efficiency in primary HSPCs and impact on neutrophil elastase protein expression. A) Workflow for expansions, gene editing, *in vitro* liquid culture differentiation towards neutrophils, and analysis of differentiated cells. **B)** Mutations in used patient HSPCs, the INDEL percentage at day 7 and day 14 of liquid culture differentiation. **C)** Western blot of neutrophil elastase in mock control and ELANE knockout healthy HSPCs. **D)** Effect of gene editing on neutrophil elastase expression in primary congenital neutropenia HSPCs. This data and figure were originally published in Nasri et al.[161]

In summary, we have confirmed that *ELANE* knockout neutrophils retain full functionality in addition to restoring neutrophil development. The observation that knockout of mutant *ELANE* rescues granulopoiesis was independently confirmed by Rao et al.[162]

It could also be argued that correcting the mutant *ELANE* gene would circumvent the question of whether *ELANE* is essential. We and others have shown that this correction is possible *ex vivo* using an *ELANE* repair template for HDR delivered through a recombinant adeno-associated virus 6 (rAAV6) vector.[163,164] This approach faces two fundamental challenges to its application as a potential gene therapy. On the one hand, this approach fundamentally impacts HSPCs biology. First, the only clinical trial to date, the CEDAR study, in which it was attempted to transplant HSPCs that had undergone HDR, was voluntarily stopped. The first patient who was dosed in this study had severe prolonged multilineage cytopenia, which made him dependent on transfusions and growth factor support, indicating poor engraftment or transplant failure.[165] Fundamental studies of comparably edited HSPCs have shown greater activation of the DDR and innate immune response than HSPCs edited with CRISPR/Cas9 alone.[137] On the other hand, it has been shown that LT-HSCs are, for the most part, quiescent. However, HDR is only active in the G2 and S phases of the cell cycle.[166] As the main target cell population for gene therapy is LT-HSC, to achieve multi-lineage engraftment of gene-edited cells, and as these cells are physiologically quiescent, it is essential to stimulate them to enter the cell cycle in culture.[167] Clonal tracking studies have confirmed that the combination of forced cycling, activation of DDR, and immune pathways significantly reduces LT-HSC.[168] Different reagents and methods are being tested to mitigate these engraftment defects induced by HDR-based gene editing, but the clinical translation is currently uncertain.[99,104,169] In addition to these biological limitations, it is on the other hand also challenging from a regulatory standpoint to develop this approach for gene therapy as each individual sgRNA and repair template is treated as individual novel therapies, thus requiring individual clinical trials of efficacy and safety for each mutation targeted. Furthermore, the efficiency of HDR decreases as the size of the locus to be repaired increases. Despite this, Tran et al. showed the successful restoration of exon 4 of *ELANE* with HDR relying on a repair template delivered by an adenovirus-associated virus vector-based approach. One could establish several editing approaches for all ELANE exons or the most frequently mutated exons.[164] This raises the dilemma of how to balance the optimal therapy with

economic viability. This is a fundamental challenge in such rare diseases. Large consortia are currently forming to develop platform approaches for the development of gene editing therapies for rare to individual genetic diseases. Still, under current regulations, each gRNA targeting a different exon, even in the same gene, is treated as an independent therapy.[170]

An approach by Sabo and colleagues to prevent the disadvantage of HDR offers the possibility of allele-specific knockout of the mutated *ELANE* allele. This approach relies on two sgRNAs. One sgRNA cuts inside an intron of *ELANE* on both alleles. INDELs in this intron have no consequences on mRNA or protein expression. By targeting common heterogeneous single nucleotide polymorphism (SNP) upstream or downstream of *ELANE* in the non-coding sequence of the mutated allele, an allele-specific deletion of the mutated *ELANE* is achieved. This approach also preserves *ELANE* expression. However, this approach only applies to 50 - 75 % of CN patients with *ELANE* mutations. The impact of such large deletions and multiple cuts on LT-HSC is yet to be determined.[171]

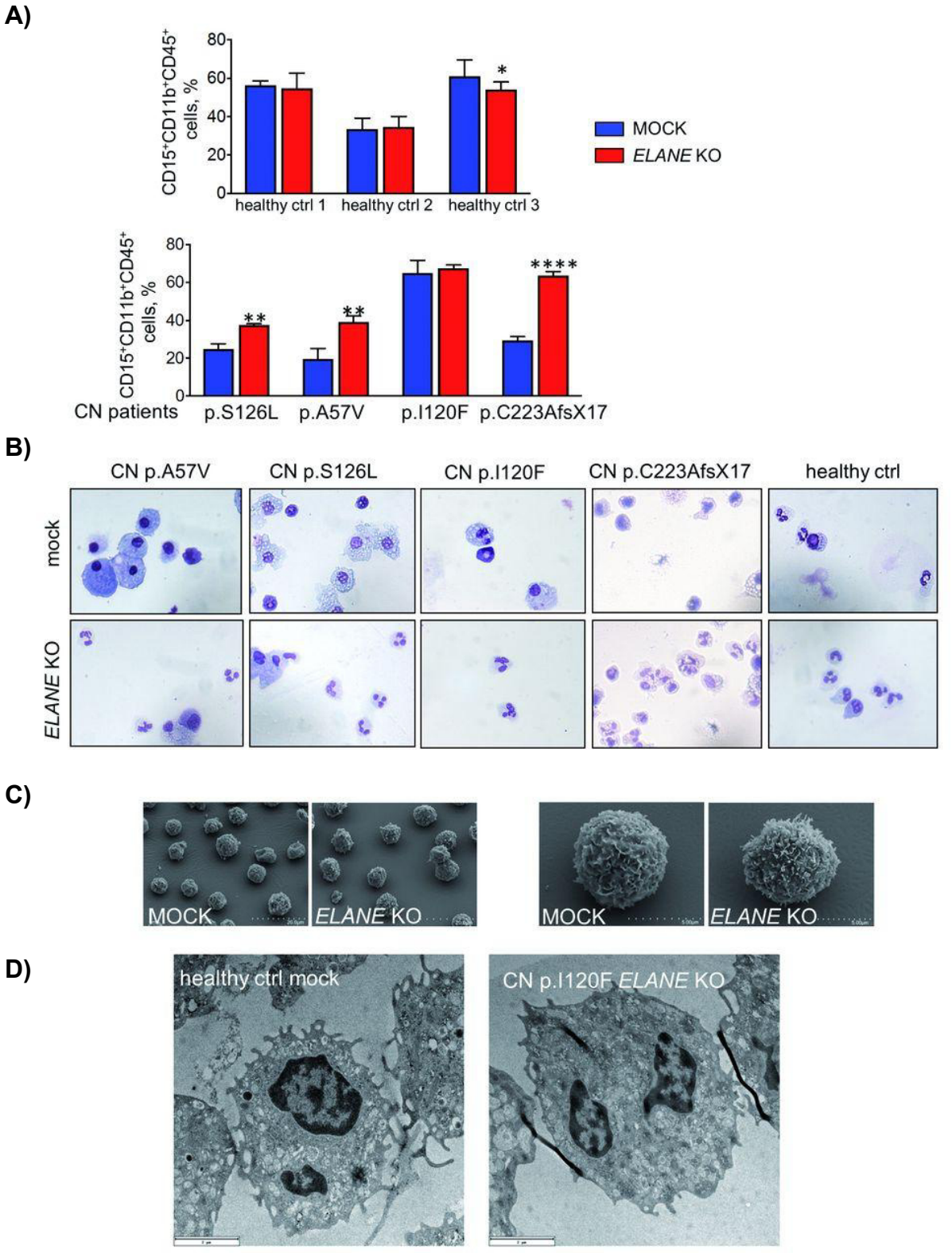

Figure 5 Impact of *ELANE* knockout on *in vitro* neutrophil differentiation. A) Flow cytometric measurement of *in vitro* differentiation towards neutrophils of Mock control or *ELANE* knockout HSPCs from healthy donors or congenital neutropenia patients. Marker combination $CD15^{+}CD11b^{+}CD45^{+}$ constitutes mature neutrophils. * $p < 0,05$, ** $p < 0,01$, **** $p < 0,0001$, **B)** Representative cytospins of HSPCs differentiated *in vitro* to neutrophils. Cells were stained with May-Grünwald and Wright-Giemsa. **C)** Morphological analysis by scanning electron microscopy showing comparable surface development of neutrophils from the Mock control group and *ELANE* knockout group. **D)** Transmission electron microscopy displaying normal morphology of cell organelles in both Mock control and *ELANE* knockout groups. This data and figure were originally published in Nasri et al.[161]

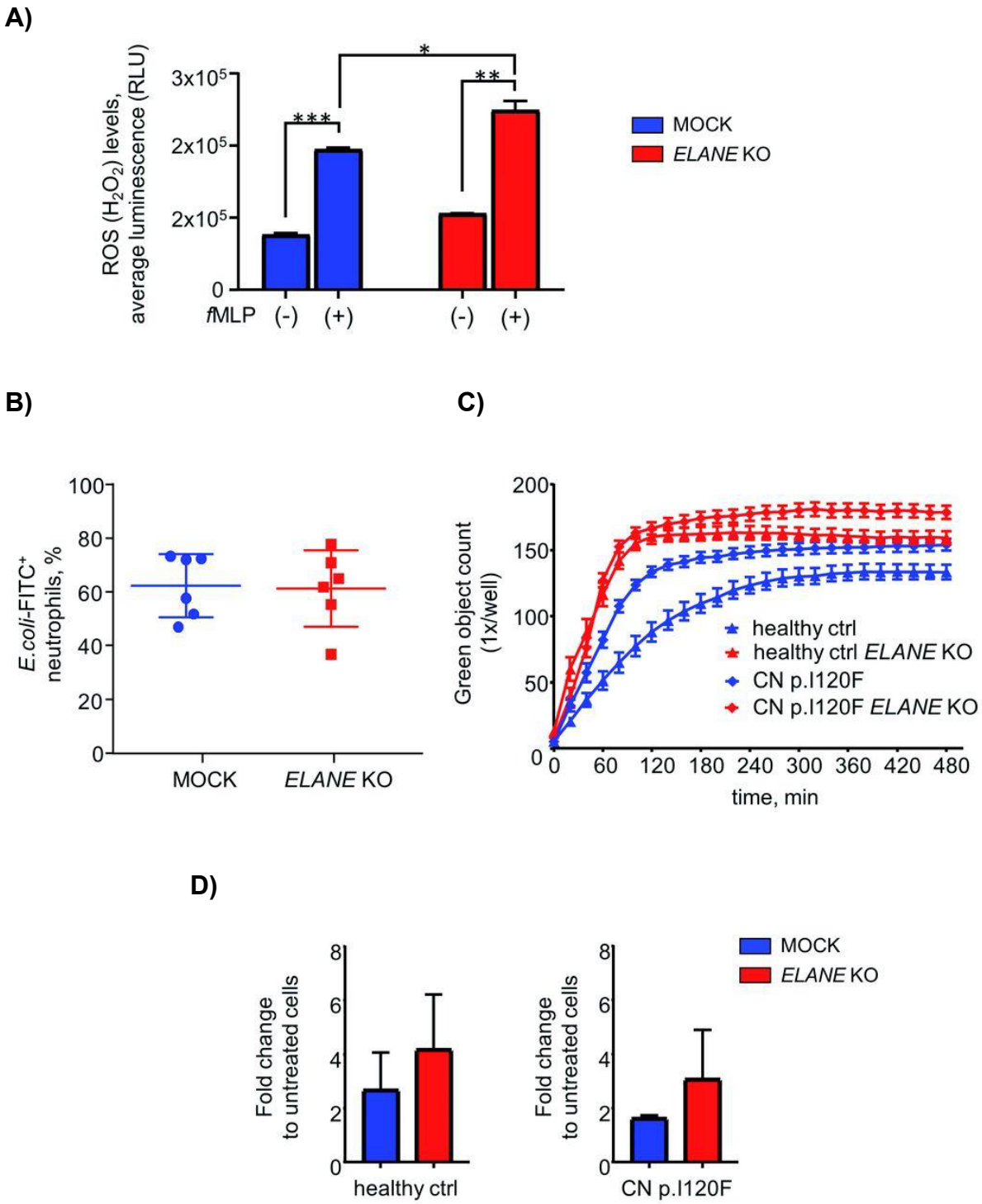

Figure 6 *ELANE* knockout does not affect neutrophil function. A) Formation of ROS upon stimulation with fMLP compared to unstimulated neutrophils, measured by luminescence. Neutrophils were generated by *in vitro* differentiation of gene-edited HSPCs. * $p < 0,05$, ** $p < 0,01$, *** $p < 0,001$ **B)** Percentage of *in vitro* generated neutrophils capable of phagocytosing *E. coli* bioparticles during 1 hour of incubation. **C)** Live cell imaging for phagocytosis of fluorescent *E. coli* bioparticles. Results show the number of cells that performed phagocytosis. **D)** Chemotaxis induced by an fMLP gradient compared to spontaneous migration. The difference is a fold change from spontaneous migration to fMLP-induced migration. All neutrophils used in these experiments were generated *in vitro* by liquid culture differentiation of gene-edited HSPCs to neutrophils. This data and figure were originally published in Nasri et al.[161]

These results have contributed to CN's physiological and pathophysiological studies and are promising as a potential gene therapy approach. To solve some known

challenges, we continued to iterate on the knockout of *ELANE* as a mutation-agnostic approach. One of the concerns raised was the targeting of the coding sequence. Based on a publication by Tuladar et al., CRISPR-generated INDELs have a ~ 50 % probability of inducing novel splicing isoforms, which are translated into *de novo* proteins and have unknown consequences.[127] In addition, new CN-causing ELANE mutations are reported every year, so there is still a chance that INDELs that do not result in knockout will continue to cause CN. While the majority of CRISPR-induced INDEL patterns are reproducible, low-frequency clones with high variability genome editing outcomes are still occurring and have the potential for detrimental outcomes. In theory, these can all be determined by deep-targeted sequencing and subsequent functional studies. However, this is very demanding in terms of resources and time, and one can never be sure if all potential INDELs were detected and if those missed INDELs have potentially harmful effects, warranting an alternative approach.

This led us to the development of gRNAs targeting the promoter of *ELANE.* A reporter cell line for ELANE expression was generated to facilitate an efficient screening process based on THP-1 cells. A split nano luciferase was used as a reporter system. *ELANE* was N-terminally tagged with HiBiT, an eleven amino acid long luciferase fragment. The tag was integrated into the genome of the THP-1 cells by HDR with the help of CRISPR. Cells carrying the tag can be lysed, and by the addition of the main body of the luciferase protein (LgBiT) and its substrate furimazine, the level of NE expression can be determined by measuring the luciferase signal.

Based on the synergistic activation mediator (SAM) tool prediction of regulatory promotor elements, we selected six sgRNAs for screening. All six sgRNAs exhibited the potential to significantly knock down *ELANE* expression by targeting its promoter. The most robust knockdown of NE expression was observed for sgRNAs closest to the transcription start site or inside the predicted TATA box.

Because this iteration aimed to develop an approach suitable for clinical translation, we implemented a dual CRISPR nickase method targeting the sense and antisense strands in the promotor region of *ELANE* to induce a deletion that inactivates the promotor. The induced deletion led to INDELs in the predicted TATA-box of the *ELANE* promotor. The advantage of this dual nickase approach is the off-target reduction by at least 50 to up to 1.000 fold[147]. This approach was termed “MILESTONE for **M**od**i**fying E**L**ANE Goldb**e**rg–Hogne**s**s box **to** i**n**hibit **e**xpression”. The MILESTONE approach was tested in primary healthy donor and CN patients’ HSPCs, which were

edited and subsequently differentiated to neutrophils *in vitro*, confirming no toxicities in healthy HSPCs, neutrophil formation, and a correction of the phenotype in CN HSPCs. By assessing the phagocytotic capacity and ability to produce ROS upon fMLP stimulation, we also confirmed that neutrophils derived from MILESTONE-edited HSPCs were functional.

We further probed if using two nickases impacted the DDR associated with CRISPR genome editing. We used qPCR to measure the expression of *CDKN1A* (the gene encoding p21 protein) and *GADD45A*. The expression of both genes is tightly controlled by p53 activation and is commonly used in gene editing studies to measure DDR activation.[137] Both approaches displayed a non-significant elevation in DDR response genes *CDKN1A* and *GADD45A*. These results indicate that the utilized guides are specific and do not cause significant DNA damage beyond their target sites. This prompted us to transplant MILESTONE-edited healthy and CN HSPCs in immune-compromised nod scid gamma (NSG) mice to evaluate the retention of engraftment potential and to assess the lineage distribution of genome-edited cells (Fig. 7 & 8). We observed no changes in healthy MILESTONE-edited HSPCs compared to AAVS1 control-edited cells (Fig. 8A & B). Distribution of blood cells in the bone marrow, including B, T, and myeloid cells, especially neutrophils, monocytes, and HSPCs, remained constant (Fig. 8C & D). Importantly, for CN HSPCs, the formation of neutrophils was reinstated (Fig. 7D & E). Interestingly, we observed a significant increase in MILESTONE-edited cells in CN HSPCs over the 16 weeks they were engrafted in NSG mice, indicating that low levels of *ELANE* expression already affect HSPCs (Fig. 7B & C). This effect would naturally benefit the patient in a transplant setting as the initial required level of gene editing could be relatively low at approximately 20-30 %. However, it is important to rule out that the expansion of gene-edited HSPCs is driven by off-target INDELs in other genes or other unwanted effects (Fig. 9). To determine the off-target profiles of MILESTONE and the exon 2 targeting approach, we performed GUIDE-seq (Fig. 9B) and CAST-seq (Fig. 9C) in primary healthy HSPCs. With these two methods, we were able to discover potential off-target sites, translocations, and large on-target modifications in MILESTONE-edited cells. The off-target sites found by GUIDE-seq and the highest probable off-targets based on in silico prediction by CRISPRme and CRISPRitz (Fig. 9A) were investigated by targeted NGS (Fig. 9D).

The profiles obtained by GUIDE-Seq, CAST-seq, and targeted sequencing confirmed that developing a dual nickase approach targeting the promotor improved the genome toxicity profile.

Lastly, we utilized RNA-seq to investigate the impact of neutrophil elastase knockdown on the neutrophil transcriptome. While we did observe compensatory up-regulation of other proteases, there was only a slight downregulation of the *PHGDH* gene in addition to the downregulation of *ELANE* when the lowest significance threshold was applied. This is an indication that *ELANE* knockout neutrophils retain their functionality.

Taken together, we developed an effective, safe, and practicable CRISPR/Cas9-based approach for *ex vivo* gene therapy for CN patients carrying *ELANE* mutations. Additionally, this approach has a high potential for fundamental studies on the physiology of neutrophils as it allows the flexible engineering of a wide variety of previously unavailable genotypes.

Also of interest, and with potential for broader application, is the observation that *ELANE* knockout enhances the engraftment ability of CN HSPCs when transplanted into immune-compromised mice. More detailed experiments in healthy HSPCs are necessary to determine if this effect is also transferrable to them. In such a case, temporary silencing of *ELANE*, either by transient CRISPR inhibition, proteolysis targeting chimeras (PROTACs), or short interfering RNA, could be envisaged to enhance the engraftment capacity of stem cells in the autologous setting to increase the number of successful transplantations or to reduce the time window of reconstitution. Mechanistically, we can only speculate about the cause of this engraftment advantage. One promising hypothesis is that the lack of NE increases the CXCR4 level on the surface of HSPCs. It is known that NE is the central protease responsible for the N-terminal degradation of CXCR4.[172] This mechanism is utilized in the mobilization of HSPCs for bone marrow transplantation. It has also been shown in mice that lentiviral overexpression provides an engraftment benefit[173] and that a lack of NE increases CXCR4 levels, which increases chemotaxis of human HSPCs, enhancing their homing to the bone marrow and the retention in the bone marrow niche.[45] Conversely, NE is expressed at low levels in HSPCs.[174] It is, therefore, also possible that mutant NE already has a detrimental effect on HSPCs function, which may be the reason for the high risk of developing leukemia. An alternative possibility is that the low-level expression of NE causes UPR in HSPCs. Thus, the removal of

mutant NE and the subsequent prevention of UPR restore the HSPCs' proliferation.[145,175]

The extent and frequency of large on-target deletions and potential loss of heterozygosity remain open questions for clinical translation. These should be studied by dPCR or optical genome mapping, as recently described by others.[176]

It also remains to be determined if the knockout of *ELANE* is curative for cyclic neutropenia patients with *ELANE* mutations. This might be expected given the common underlying *ELANE* mutations in both syndromes. However, the lack of a model that resembles the disease has prevented this from being tested. The recent discovery of protocols for bone marrow organoids might offer a solution to this challenge.[177]

It is also unclear whether *ELANE* knockout in humans might have unforeseeable consequences. On the one hand, there is the question of whether a knockout of *ELANE* and the subsequent lack of NE influences the formation of neutrophil extracellular traps. Several groups have shown that NE expression is reduced in CN patients.[45,178] Additionally, rhG-CSF increases the neutrophil count to normal levels and prevents infections. Still, it has been shown that neutrophils from CN patients treated with rhG-CSF display abnormal neutrophil behavior.[160] Thus, it is not unreasonable to assume that by restoring normal neutrophil maturation, despite the lack of NE, these neutrophils will display a better function than neutrophils with mutated *ELANE* under rhG-CSF treatment.

On the other hand, NE is active in the hematopoietic niche and is known to play a role in HSPCs mobilization.[45] However, these processes also occur in vertebrates lacking NE expression, and humans have multiple closely related and redundant proteases. Moreover, humans lacking NE survive and prosper, as with Papilloma-Lefevre syndrome.[179]

It is also important to consider how gene editing will impact HSPCs carrying acquired somatic mutations. Will it potentiate the acquisition of such mutations in HSPCs, will the mutant cells retain their leukemic potential, or will the knockdown of ELANE protect them from leukemia development? Therefore, it will be essential to investigate at which age patients should be treated with gene editing, as earlier treatment will result in a lower probability of acquiring somatic mutations. However, the treatment of children is an ethical dilemma between preventing unnecessary harm and hindering treatment improvements by excluding children from clinical studies, which must be carefully

evaluated on a case-by-case basis.[180] Because restoration of neutrophil development should make treatment with rhG-CSF unnecessary, it can be assumed that the selective advantage of HSPCs carrying, e.g., *CSF3R* mutations and other pre-leukemic mutations dependent on rhG-CSF, will be reduced. Further mouse studies are necessary to determine the impact of NE knockdown and gene editing per se on the behaviors and functions of cells carrying pre-leukemic somatic mutations.

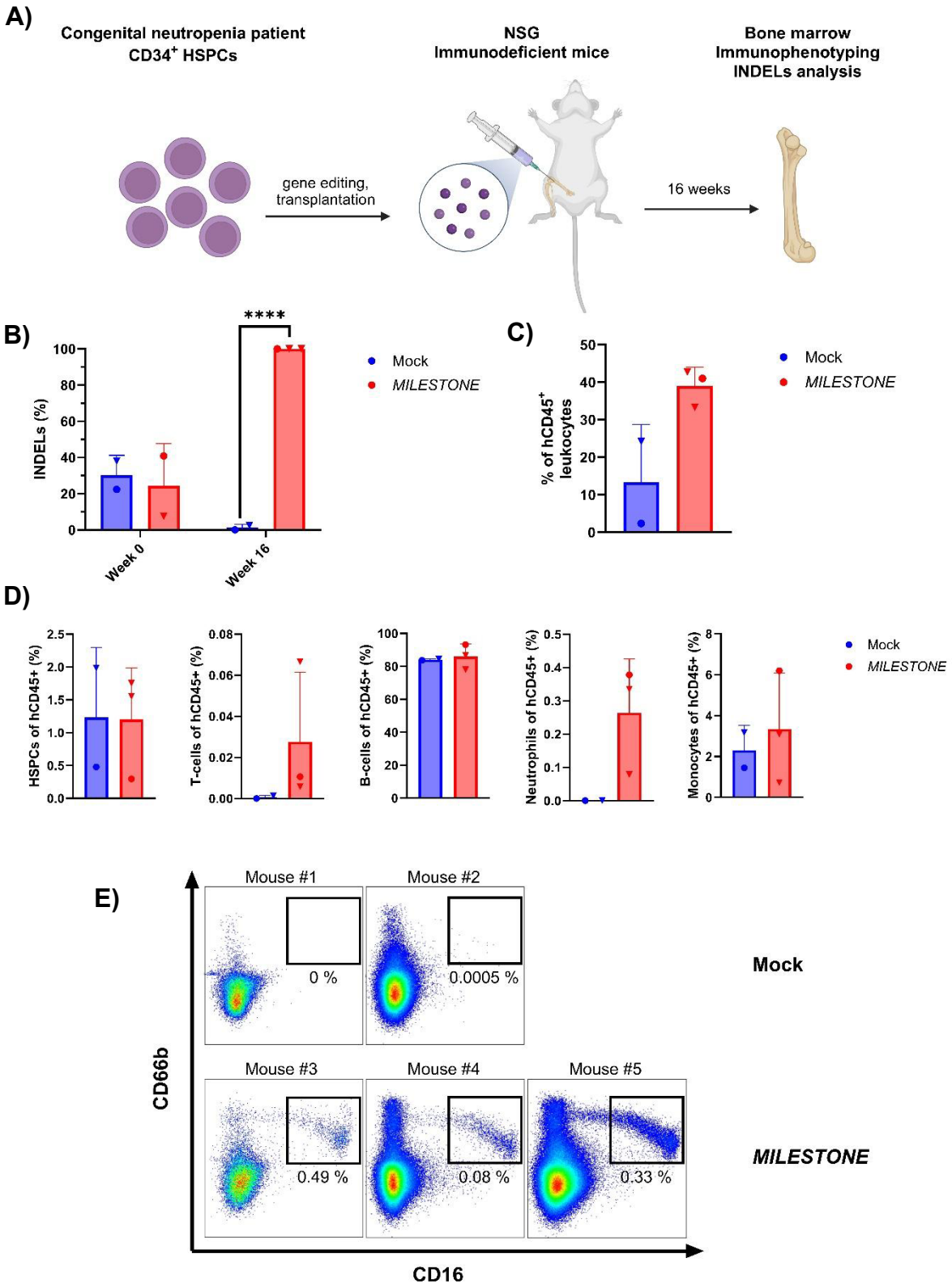

Figure 7 *In vivo* investigation of engraftment of MILESTONE edited CN HSPCs and the effect on leukocyte mature cell formation. A) Conceptual outline of the *in vivo* investigation of MILESTONE edited HSPCs from *ELANE*-CN patients in nod scid gamma (NSG) mice. After *ex vivo* gene editing, Mock control edited HSPCs or MILESTONE-edited HSPCs were intra-femorally injected into individual mice. **B)** Gene editing efficiencies in week 0, meaning before transplantation, and in week 16, when mice were analyzed, showing a significant increase of MILESTONE gene-edited cells compared to Mock edited cells. **** p <0.0001 **C)** Engraftment of human leukocytes in the bone marrow of NSG mice. Showing a non-significant trend of higher engraftment of MILESTONE edited cells. **D)** Leukocyte populations of human CD45$^+$ bone marrow cells. HSPCs (human(h)CD45$^+$CD19$^-$CD3$^-$CD33$^-$ CD66b$^-$CD16$^-$CD34$^+$), T-cells (hCD45$^+$CD19$^-$CD3$^+$), B-cells (hCD45$^+$CD19$^+$CD3$^-$), Neutrophils (hCD45$^+$CD19$^-$CD3$^-$

CD33$^{-/+}$CD66b^{+}CD16^{+}), Monocytes (hCD45^{+}CD19^{-}CD3^{-}CD33^{+}CD14^{+}). **E)** Flow cytometric gates of neutrophil maturation marked by human CD66b^{+}CD16^{+} bone marrow leukocytes. Each symbol represents an individual mouse. Different symbol forms describe mice transplanted with cells from independent HSPCs gene editing batches. Columns indicate the arithmetic mean, and the error bars indicate the standard deviation. This figure was originally published in Nasri and Ritter et al.[181]

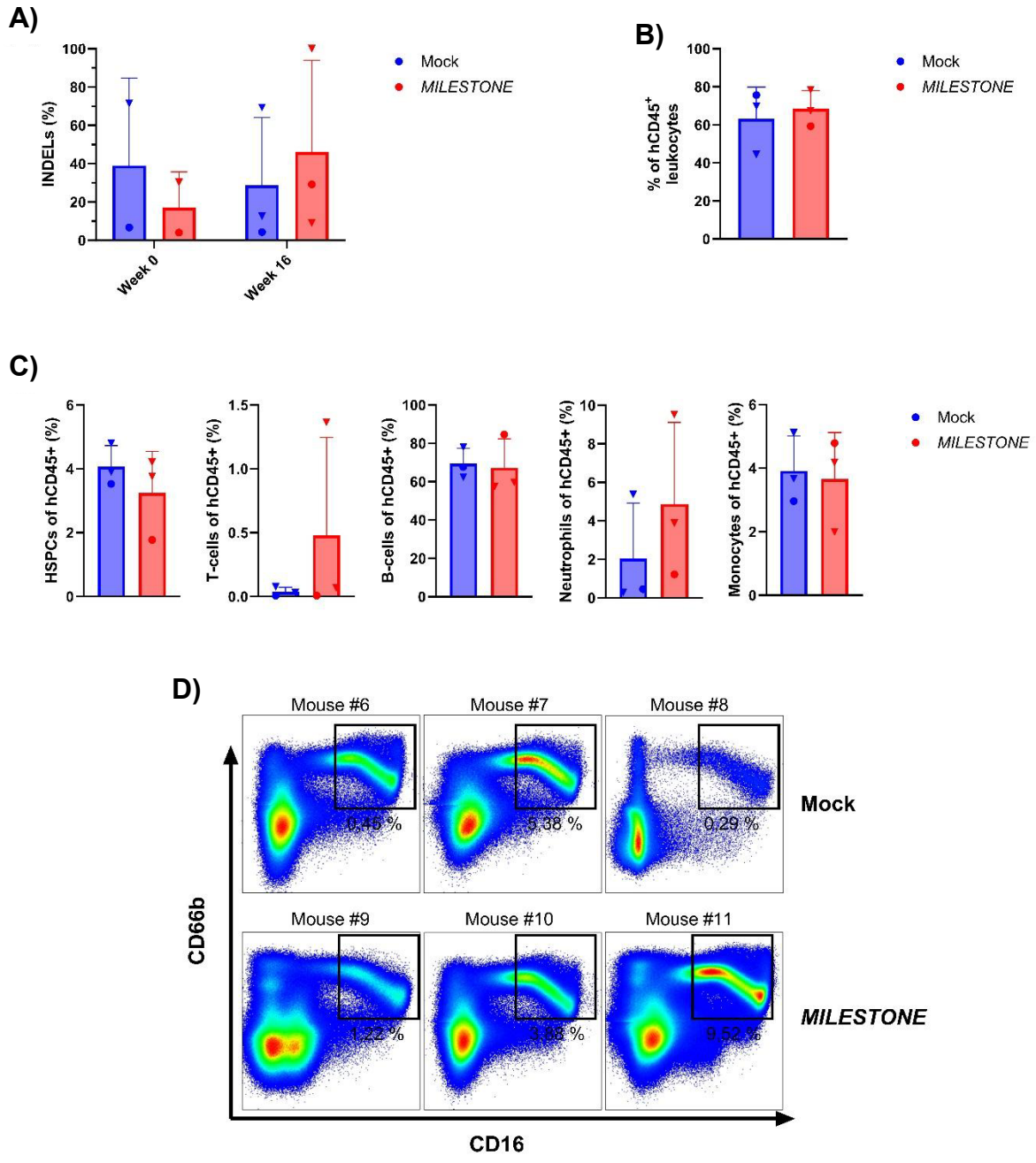

Figure 8 Investigation of the engraftability and differentiation of healthy HSPCs gene-edited with MILESTONE in NSG. A) Editing efficiencies measured as INDELs percentage before transplant (week 0) and at analysis (week 16). **B)** Engraftment efficiency in bone marrow expressed as hCD45^{+} of all bone marrow leukocytes. **C)** Leukocyte populations of human CD45^{+} cells found in bone marrow. HSPCs (human(h)CD45^{+}CD19^{-}CD3^{-}CD33^{-}CD66b^{-}CD16^{-}CD34^{+}), T-cells (hCD45^{+}CD19^{-}CD3^{+}), B-cells (hCD45^{+}CD19^{+}CD3^{-}), Neutrophils (hCD45^{+}CD19^{-}CD3^{-}CD33$^{-/+}$CD66b^{+}CD16^{+}), Monocytes (hCD45^{+}CD19^{-}CD3^{-}CD33^{+}CD14^{+}). **D)** Dot-plots of Neutrophil maturation of CD66b gated against CD16. Double-positive cells are mature neutrophils. This figure was originally published in Nasri and Ritter et al.[181]

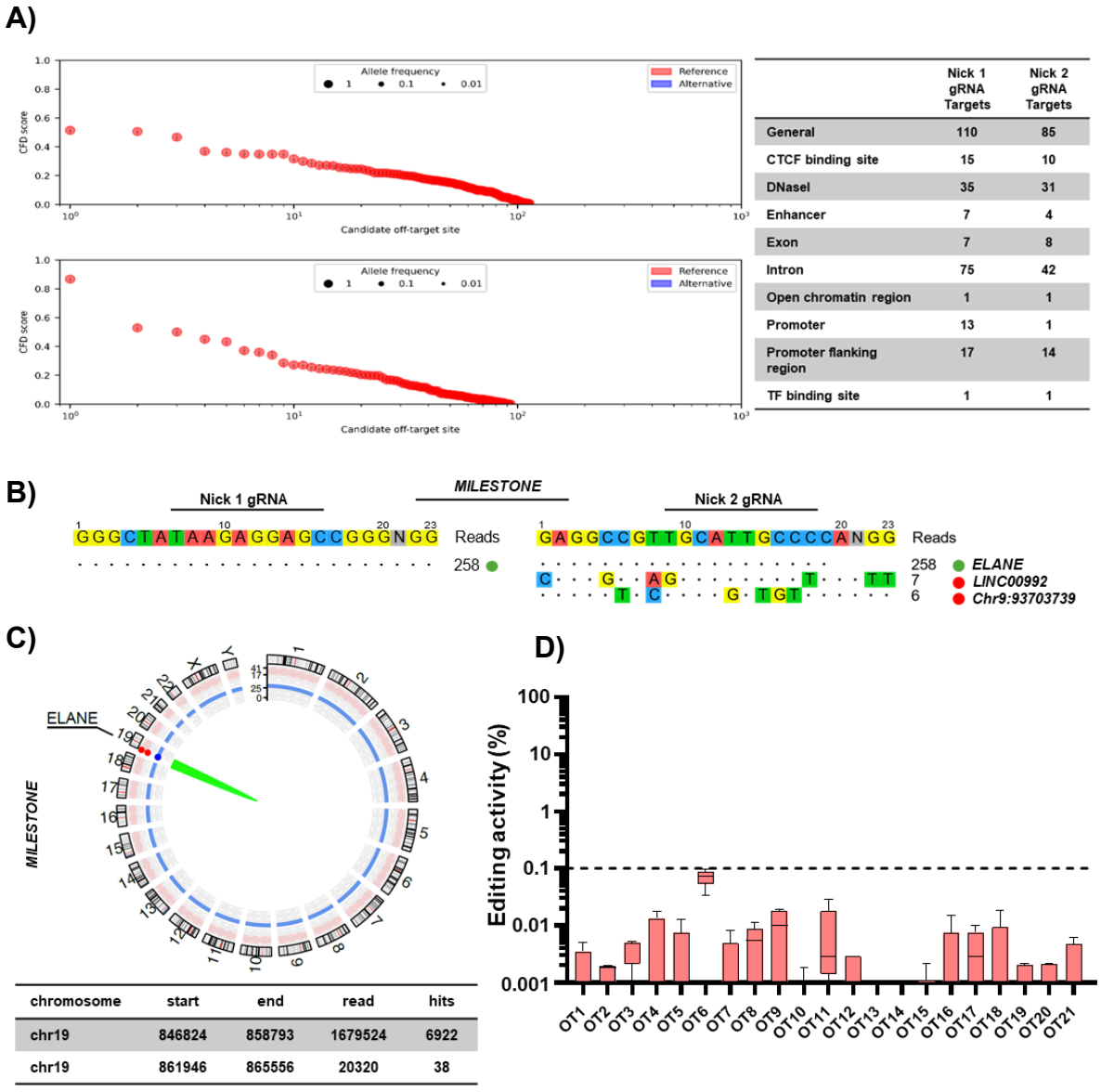

	Nick 1 gRNA Targets	Nick 2 gRNA Targets
General	110	85
CTCF binding site	15	10
DNaseI	35	31
Enhancer	7	4
Exon	7	8
Intron	75	42
Open chromatin region	1	1
Promoter	13	1
Promoter flanking region	17	14
TF binding site	1	1

chromosome	start	end	read	hits
chr19	846824	858793	1679524	6922
chr19	861946	865556	20320	38

Figure 9 Genomic and transcriptionally safety of MILESTONE gene-edited HSPCs and neutrophils. A) *In silico* prediction of off-target sites for both guide RNAs utilized in the MILESTONE approach. Analysis was conducted with CRISPRme and CRISPRitz. **B)** Results from GUIDE-seq screening of the MILESTONE gRNAs. Indicated are 2 potential off-target sites for Nick 2 gRNA. **C)** CAST-seq analysis of MILESTONE gene-edited healthy HSPCs for translocations shows that MILESTONE does not induce translocations. **D)** rhAmp-Seq targeted sequencing of potential off-target sites identified *in silico* by GUIDE-Seq and CAST-Seq showed no detectable INDEL induction at off-target sites. The dotted line marks the detection limit for off-target INDELs. This data and figure were initially published in Nasri and Ritter et al.[181]

Modeling of leukemia development of CN patients in an *in vitro* mouse model

(In this section, manuscripts E and H are summarized and discussed)

The increase in life expectancy of CN patients due to the use of rhG-CSF therapy has revealed CN as a pre-leukemic syndrome. Patients have a 10 % risk of developing

myeloid dysplastic syndrome (MDS) or acute myeloid leukemia (AML).[33] Our group was able to resolve a frequently recurring pattern of mutations consisting of *CSF3R* and *RUNX1* mutations.[57] Since CN is a rare disease and patient leukemia cells are rare, representative models are needed. While iPSCs are an increasingly accurate and essential *in vitro* model, the limited translatability of iPSCs-derived HSPCs, depending on the genetic mutations,[182] prevents their use in currently still required rodent models for *in vivo* pathophysiology studies and therapy testing. Furthermore, questions concerning the immune system's role in leukemia development can only be investigated in syngeneic animal models. Therefore, we developed an *in vitro* approach to model this combination of mutations in HSPCs from mice. We utilized the Δ715-*Csf3r* mouse line, a strain that has a homozygous intracellular *Csf3r* mutation inducing a stop codon in amino acid 715.[61] This truncation mimics the *CSF3R* truncating mutation observed in human CN patients that deletes the three C-terminal intracellular tyrosine residues necessary for autophosphorylation.

We isolated lineage negative (lin^-) cells from Δ715-*Csf3r* mice and transduced them with lentiviral particles carrying either eBFP only, *RUNX1* wildtype (WT), *RUNX1* p.R139G or p.R174L mutations recurrently observed in CN patients' leukemic blasts (Fig. 10B).[57] These mutations are positioned in the Runt homology domain (RHD) of the *RUNX1* transcription factor (Fig. 10A). Since *RUNX1* missense mutations act autosomal dominantly, the overexpression of mutant *RUNX1* is a viable way to mimic the acquisition of these mutations. We investigated the impact on HSPCs differentiation of *Csf3r* and *RUNX1* mutation by colony forming unit assay (CFU) of transduced cells (Fig. 10C). To this end, the differentiation in CFU was analyzed (Fig. 10D), and serial re-plating was evaluated (Fig. 10E). We found that both mutations significantly reduced the number of mature granulocyte colonies (CFU-G) and granulocyte and macrophage colonies (CFU-GM). Simultaneously, the mutant-expressing cells had a more than threefold increased re-plating capacity in the first and second re-plating, displaying two functional hallmarks of leukemia: a differentiation block and an increase in proliferation.

This differentiation block was confirmed in a secondary assay with the transduced cells, subjected to *in vitro* liquid culture differentiation into neutrophils (Fig. 11A).

The functional studies confirmed a close resemblance of this *in vitro* mouse model to the observations in CN patients. Namely the inhibition of myeloid differentiation of HSPCs to mature granulocytes (Fig. 11B) and significantly increased proliferation for

cells transduced with *RUNX1* R139G (Fig. 11C). Therefore, we next performed transcriptional profiling of mRNA of the transduced cells using the microarray method (Fig. 12A & B).

The transcriptional analysis revealed 1814 and 1113 differentially expressed genes for *RUNX1*-R139G and *RUNX1*-R174L mutants, respectively, compared to *RUNX1* wild-type overexpressing cells. Of these differentially expressed genes, 679 were present in both groups (Fig. 12C).

The invariant set of normalized data was analyzed using Ingenuity Pathway Analysis software. Besides a high overlap in the 15 most upregulated and downregulated genes (Fig. 12D), this approach identified most differentially activated pathways as innate immune pathways. Among them were NF-kappaB signaling, toll-like receptor signaling (TLR), acute-phase response signaling, nitric oxide and ROS production, pattern-recognizing receptors, Trem1 signaling, and IL-1 signaling. Furthermore, inflammatory signaling pathways IL-6, interferon signaling, Tec kinase signaling, and leukocyte extravasation were activated (Fig. 12E).

An upstream pathway analysis revealed a misregulation in inflammatory cytokines as probable drivers of these signaling pathways. The upregulation of inflammatory cytokines IL-15 and IL-18, with the addition of pro-survival factor Bcl2a1 and the upregulation of stem cell markers Ly6a, was especially notable. The downregulation of anti-inflammatory cytokine IL-10 and downregulation of *Dpp4*, a cytokine-digesting peptidase, complemented these increased upstream regulators.

Overall, the effect of *RUNX1*-R139G on the intracellular signaling was more substantial than that of *RUNX1*-R174L. In general, however, the type of response was of the same nature and appears to be governed by the same mechanism of activation of innate immune pathways.

To investigate the impact of mutations on the transcription factor activity, we performed an Integrated System for Motif Activity Response Analysis (ISMARA), which revealed the *Irf2_Irf1_Irf8_Irf9_Irf7* motifs to be the most active. Furthermore, the AML-associated motifs of Stat2, Klf4_Sp3, and *Mecp-2* were also significantly enriched.

These observations are important in several ways. First, they provided a novel mechanism contributing to leukemia development in CN: a significant upregulation of proinflammatory pathways that may induce a hyper-proliferative phenotype in HSPCs. This mechanistic observation has been confirmed in human HSPCs with missense *RUNX1* mutations.[183] Many anti-inflammatory drugs are already approved, and many

more specific anti-inflammatory drugs are in development for cancer therapy. This makes it an attractive potential target. It can potentially be used to eliminate pre-leukemic clones before leukemia develops.

Secondly, our findings encourage the possibility of modeling CN-AML in mice. A similar approach has been tried by Olofsen et al.[184] They found that additional mutations were required besides *Csf3r* and *RUNX1* for overt AML *in vivo*. One mouse acquired a Cxxc4 mutation that was responsible for the complete AML phenotype in their specific case. In conclusion, the mainly inflammatory, proliferation-enhancing signaling and downregulation of differentiation signaling induced by combining *Csf3r* and *RUNX1* mutations cause a high-risk pre-leukemic stage requiring only one additional mutation or chromosomal aberration to induce overt MDS or AML (Fig. 13A).

This stepwise combination of mutations and unlimited numbers of cells is precisely the advantage of a murine model system. This allows us to model these mutations independently of the genetic background of individual patients in pure populations. At the precise time point of mutation acquisition, if the phenotype matches the clinical observations seen in patients, an *in vivo* model can be established.

Lastly, these findings highlight a critical safety aspect of gene therapies in pre-leukemic syndromes. As described by different groups and measured for MILESTONE, gene editing induces a DNA damage response and an inflammatory immune response.[104,137] An already elevated inflammatory environment, as observed in our *in vitro* study, may reduce gene editing efficiency or the viability of gene-edited cells because the target cells are already hypersensitized. Additionally, this is a crucial point to consider when selecting patients for gene therapy trials to ensure that pre-leukemic cells are not transformed into leukemic cells, as it has happened previously with lentivirus-based gene therapies.[133] This highlights the importance of disease-specific assessment of the response of target cells to gene editing and processing, which is crucial to ensure an effective and safe treatment development. In the specific case of CN, the treatment of cells or individuals with anti-inflammatory therapies should be explored in the development of gene therapy. This consideration is essential since small cell populations carrying inflammatory mutations can impact the whole organism by producing inflammatory mediators.

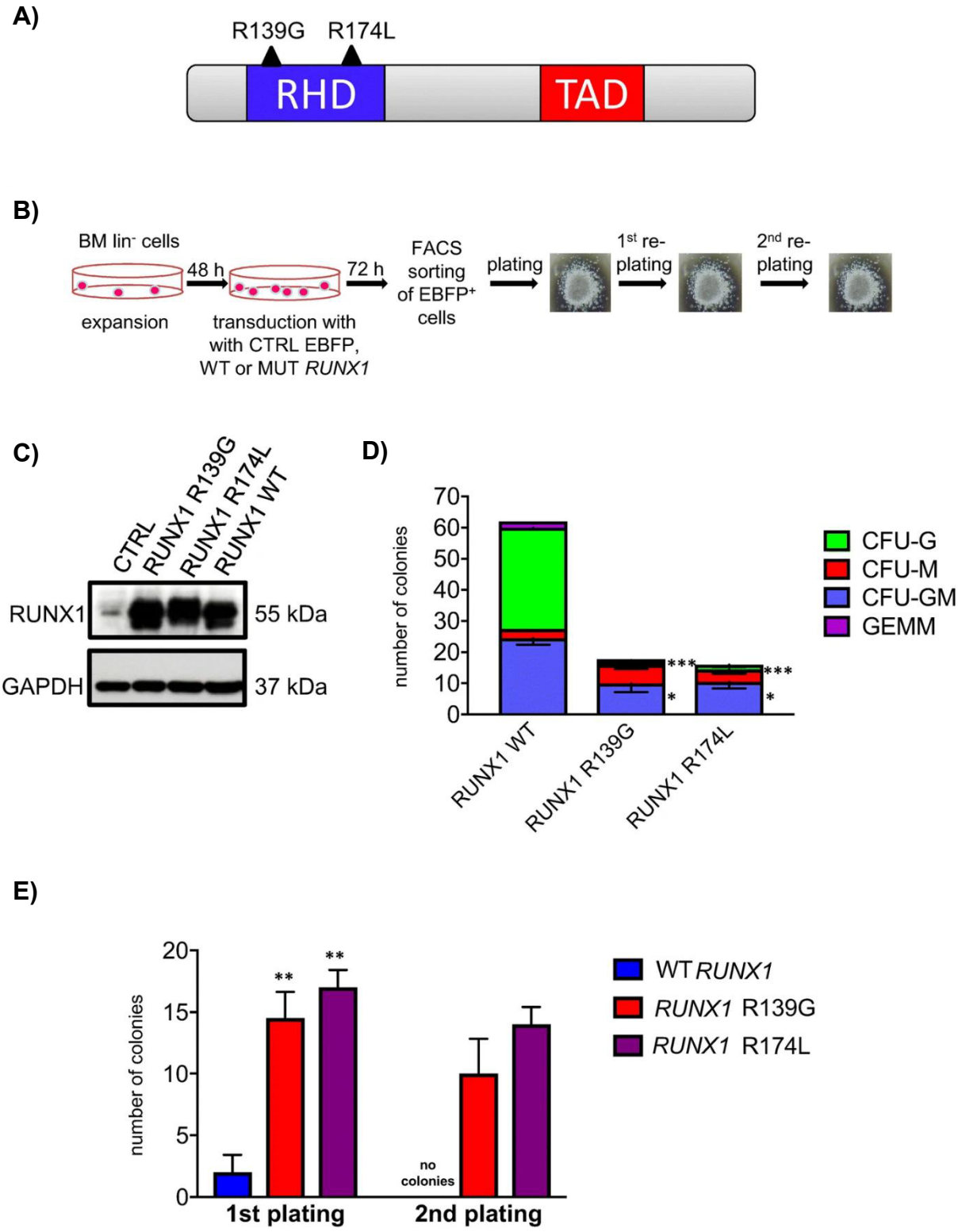

Figure 10 Impact of RUNX1 mutations on colony forming unit potential of transduced mouse lineage negative bone marrow cells. A) Schematic representation of the used *RUNX1* mutations in the RHD. **B)** Workflow of transducing, sorting, and performing CFU assays with mouse lineage negative cells with *csf3r*-truncated cells. **C)** Confirmation of *RUNX1* overexpression by lentiviral transduction with vectors for wildtype *RUNX1*, *RUNX1* R139G mutation, and *RUNX1* R174L mutation. **D)** Number of colonies and phenotype of colonies at day 14 of differentiation. Colonies were scored into CFU-G (granulocytes), M (monocytes), GM (granulocyte and monocytes), and GEMM (granulocytes, erythrocytes, monocytes, and megakaryocytes). **E)** Number of total colonies in 1st and 2nd re-plating. * $p < 0,05$, ** $< 0,01$ and *** $p < 0,001$.These data and figures were originally published in Ritter et al.[185]

A)

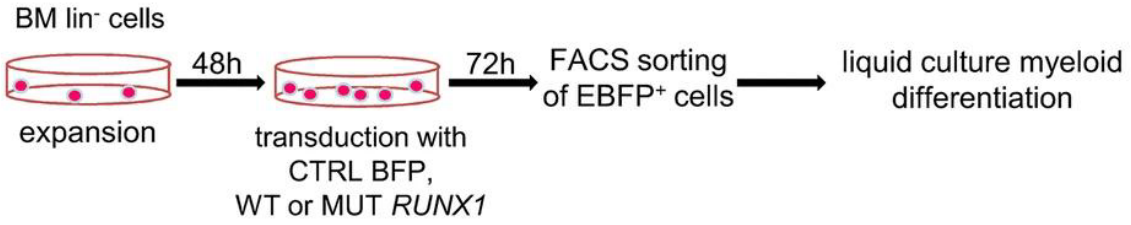

B)

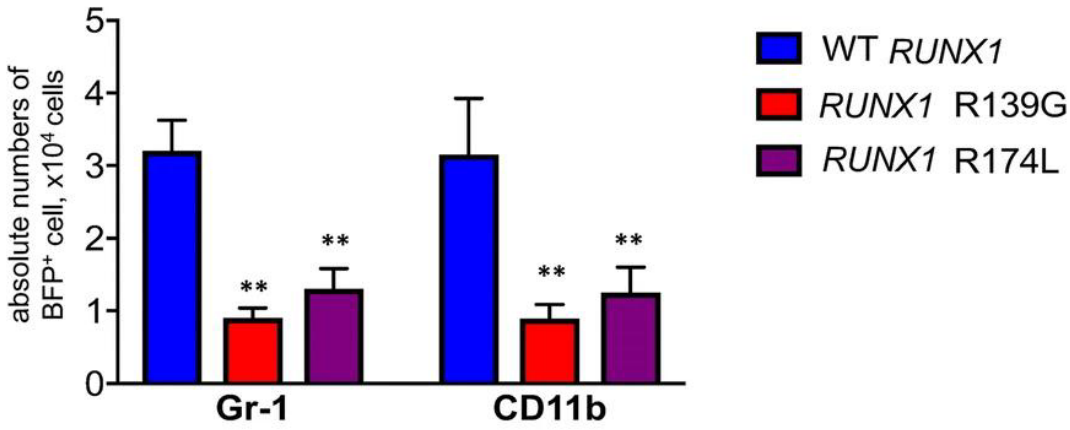

C)

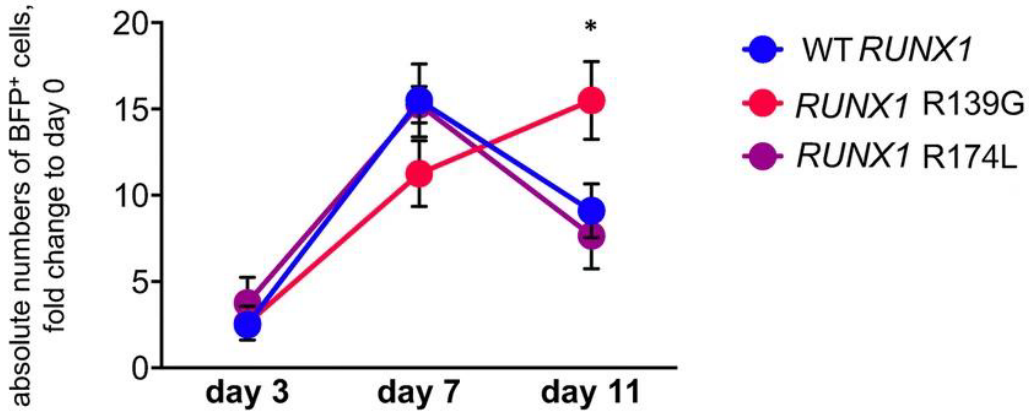

Figure 11 *RUNX1* mutants inhibit *in vitro* liquid culture granulocytic differentiation of transduced truncated *csf3r* mouse lineage negative bone marrow cells. A) Schematic workflow of transduction, sorting, and granulocytic differentiation. **B)** Absolut number of cells expressing granulocytic cell surface markers Gr-1 and CD11b. Significantly downregulated in cells transduced with *RUNX1* mutants R139G or R174L. **C)** Impact of investigated *RUNX1* mutants on proliferation during differentiation. * $p < 0,05$, ** $p < 0,01$. These data and figures were originally published in Ritter et al.[185]

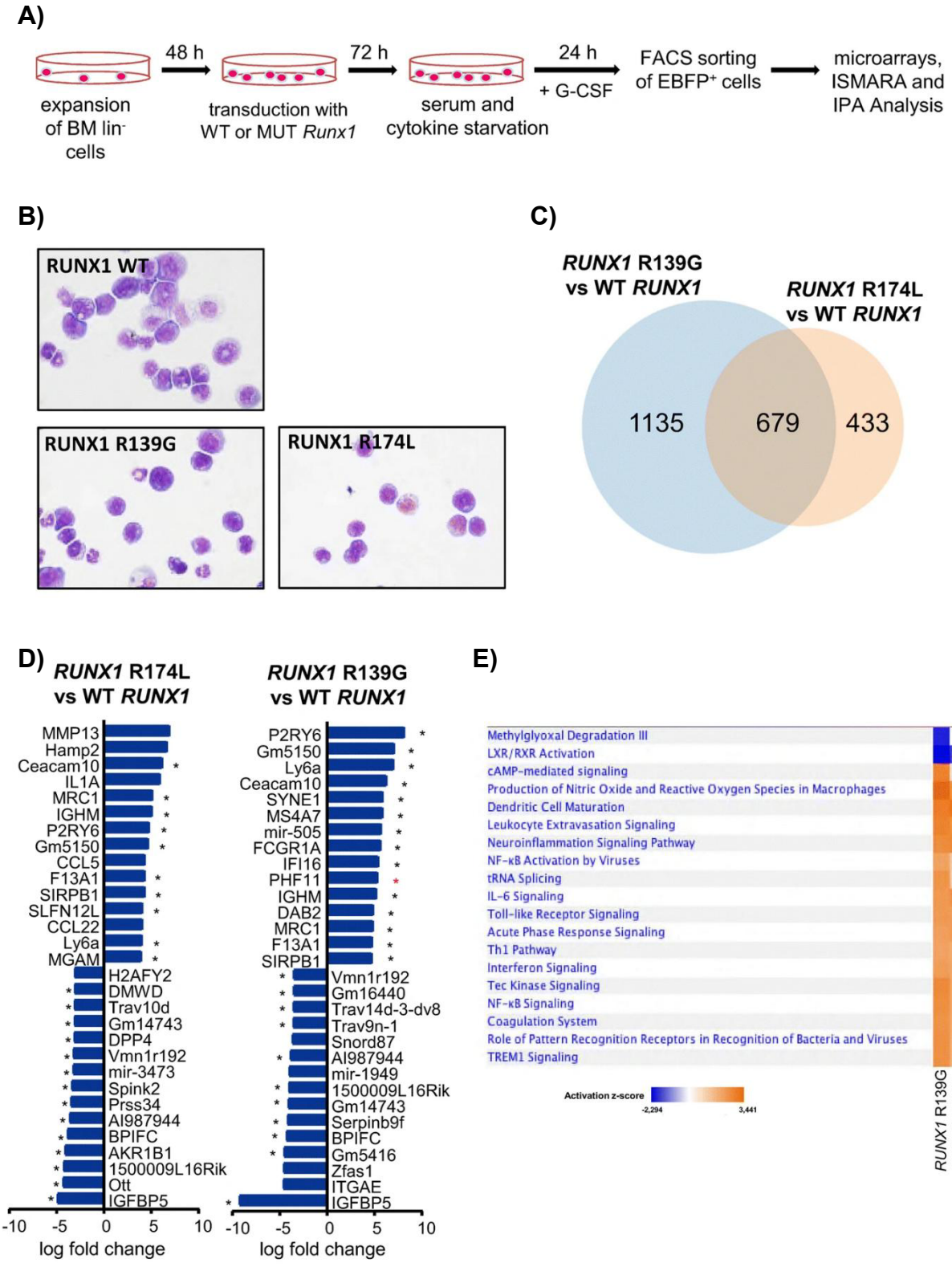

Figure 12. Combining *RUNX1* mutants and truncated *csf3r* induces an inflammatory phenotype, inhibiting myeloid differentiation factors in HSPCs. A) Cell transduction, starvation, G-CSF treatment, and transcriptomics workflow. **B)** Representative cytospins of lineage-negative bone marrow cells used for RNA isolation and analysis. **C)** Overlap of significantly differentially regulated genes between *RUNX1* mutants and RUNX1 wildtype transduced cells. **D)** Top 15 up and down-regulated genes of *RUNX1* R139G and R174L transduced cells. **E)** Ingenuity pathway analysis of significantly up (orange) and down (blue) regulated pathways and functions. This figure was originally published in Ritter et al.[185]

A)

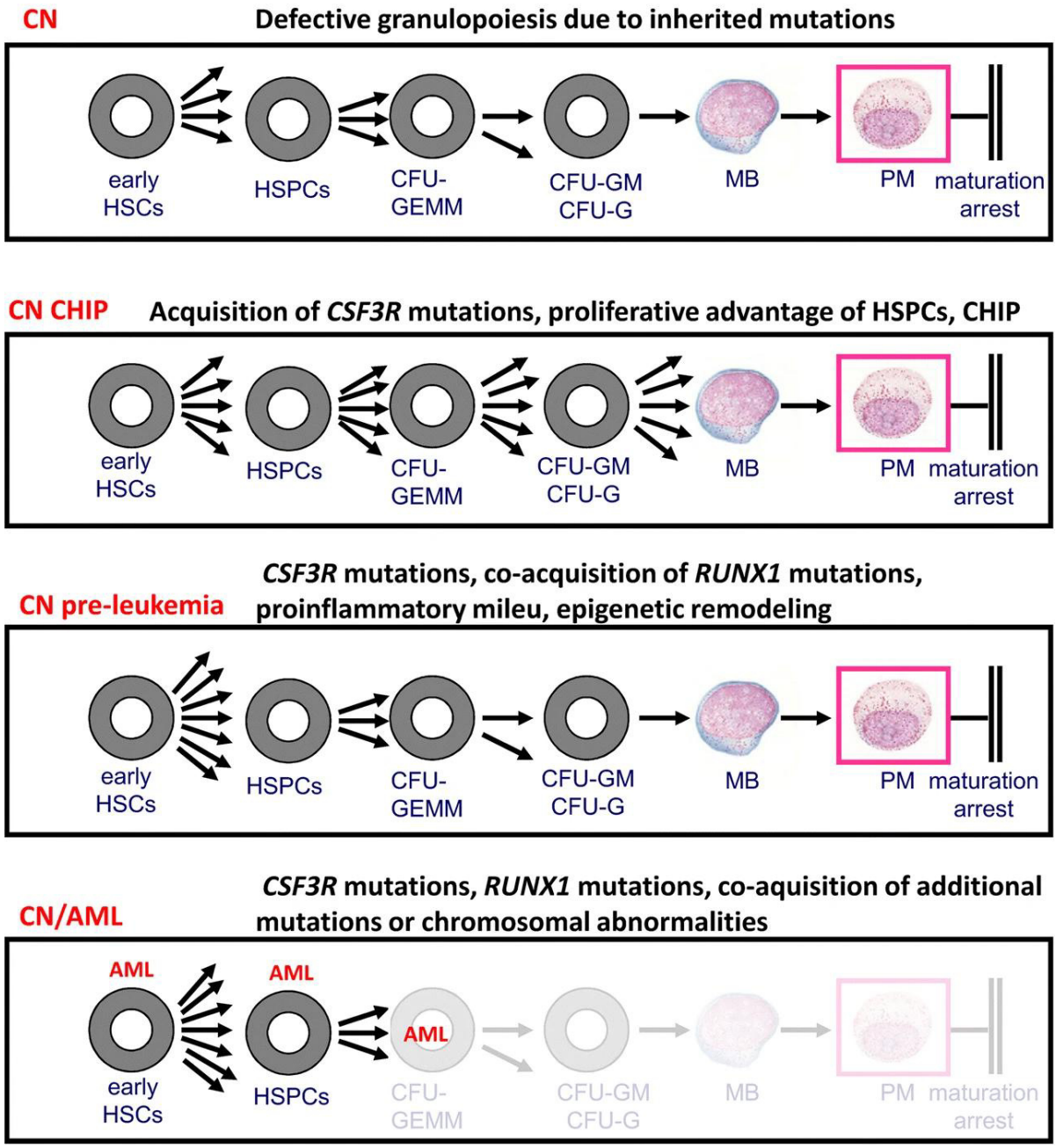

Figure 13. Working hypothesis on leukemia development in CN. A) *CSF3R* mutations most likely constitute a CHIP state in CN. The acquisition of additional mutations associated with leukemia leads to a high-risk pre-leukemia state requiring a last mutation for overt leukemia development. This figure was originally published in Ritter et al.[185]

Outlook

The recent approval of the first CRISPR/Cas-edited stem cell therapy product for sickle cell anemia and beta-thalassemia, exagamglogene autotemcel, just 11 years after the seminal publication by Charpentier and Doudna, has created great optimism that most congenital diseases will soon be treatable. The work in part I presented here and conducted in collaboration with my colleagues offers a therapeutic opportunity for another severe inherited blood disease, CN. Further research will focus on whether *ELANE* is essential and what functions it fulfills in HSPCs to ensure the safety and applicability of this therapeutic approach.

To translate our findings into a clinical trial and hopefully one day into an approved product, another important consideration for the following research questions and experimental design will be the regulatory requirements for advanced medicinal therapeutic products, including *ex vivo* gene-edited cell therapies.[186]

Recent results demonstrating the feasibility of targeting the hematopoietic stem cells *in vivo* with lipid nanoparticles carrying mRNA are encouraging[101]. They will potentially enable us to replace the *ex vivo* gene editing approaches for many hematopoietic diseases, such as CN, with *in vivo* therapy. In addition to reducing cellular stress and, therefore, damage to stem cells, *in vivo* gene editing approaches will democratize gene therapy by lowering the specialization and cost requirements from the required transplant unit and cell production capabilities to a regular hospital ward or doctor`s office capable of performing intravenous infusions of gene therapy products.[187]

A deep understanding of the disease and, based on this, the timing and window of opportunity for gene therapy will be crucial for maximizing efficacy and safety. As the example of CN shows, the acquisition of leukemia-causing mutations raises the concern that pre-leukemic mutated cells may be transformed during the gene editing process due to procedural stressors or unintended consequences of gene editing. Researchers developing these novel gene editing strategies would be well advised to consider the historical failures of gene therapy development in the 1990s and 2000s in the CRISPR/Cas gene therapy development to avoid patient deaths due to premature clinical trials with only partially understood tools and biology.

It will be challenging to overcome the scientific, regulatory, and economic challenges of providing gene editing to all patients and diseases and fulfilling its potential. But this extensive potential excites me for the future, and I have a deep belief in humans' capabilities and that we will be able to solve these challenges.

Acknowledgments

I would like to sincerely thank all past and current members of the Skokowa lab with whom I had the pleasure of working together and sharing the lab. I believe science is a team sport, and the number of collaborative publications would not have been possible without you. I am thankful for all the memories created around work and in external activities; they have and will continue to shape me.

I want to thank Professor Julia Skokowa, my scientific mentor and thesis supervisor, for the opportunity to do science in her lab and for her continuous support. My PhD time with her has been filled with endless learning and personal development.

I thank Karl Welte for being an inspiration, Ann-Christin and Patricia for teaching me how to perform mouse experiments, Masoud for being a sharp discussion partner who sparked many ideas, Benjamin Dannenmann for teaching me many practical tricks in the lab, and Jeremy Haaf for always helping. I also thank our laboratory technicians Ursel, Regine, Karin, and Inge for helping me find my way through the lab and supporting me during experiments.

I want to express my sincere gratitude to Professor Ruth, my PhD supervisor in the pharmacy department, for giving me all the freedom to pursue my scientific path.

Also, I would like to thank my collaboration partners, who taught me new techniques for performing experiments, all the people in the FACS core facility Berg, the Animal facilities FORS and HNO, and the veterinaries for providing an excellent infrastructure at the UKT. I also thank all the other people who accompanied me on this path and whom I was lucky to meet and enjoy their support. Without being mentioned, your support is well-known and sincerely appreciated.

My scientific work would not have been possible without a solid foundation in my private life. I sincerely thank my parents, Heike and Uli, for supporting and encouraging me. I also want to thank my brother Sebastian for taking the tension out of life with his jokes. Lastly, I want to thank my fiancé Simone for being my biggest supporter, cheerleader, and discussion partner, when necessary, as well as a critic, always present, and always loving me unconditionally.

References

1 Hoffbrand, A. V. & Steensma, D. P. *Hoffbrand's Essential Haematology*. Vol. 8 (Wiley Blackwell, 2020).

2 Charlesworth, C. T. *et al.* Identification of preexisting adaptive immunity to Cas9 proteins in humans. *Nature Medicine* **25**, 249-254 (2019). https://doi.org/10.1038/s41591-018-0326-x

3 Olson, O. C., Kang, Y. A. & Passegué, E. Normal Hematopoiesis Is a Balancing Act of Self-Renewal and Regeneration. *Cold Spring Harb Perspect Med* **10** (2020). https://doi.org/10.1101/cshperspect.a035519

4 Boettcher, S. & Manz, M. G. Regulation of Inflammation- and Infection-Driven Hematopoiesis. *Trends in Immunology* **38**, 345-357 (2017). https://doi.org/https://doi.org/10.1016/j.it.2017.01.004

5 Kasbekar, M., Mitchell, C. A., Proven, M. A. & Passegué, E. Hematopoietic stem cells through the ages: A lifetime of adaptation to organismal demands. *Cell Stem Cell* **30**, 1403-1420 (2023). https://doi.org/10.1016/j.stem.2023.09.013

6 Doulatov, S., Notta, F., Laurenti, E. & Dick, John E. Hematopoiesis: A Human Perspective. *Cell Stem Cell* **10**, 120-136 (2012). https://doi.org/10.1016/j.stem.2012.01.006

7 Fliedner, T. M., Graessle, D., Paulsen, C. & Reimers, K. Structure and Function of Bone Marrow Hemopoiesis: Mechanisms of Response to Ionizing Radiation Exposure. *Cancer Biotherapy and Radiopharmaceuticals* **17**, 405-426 (2002). https://doi.org/10.1089/108497802760363204

8 Trumpp, A. & Haas, S. Cancer stem cells: The adventurous journey from hematopoietic to leukemic stem cells. *Cell* **185**, 1266-1270 (2022). https://doi.org/10.1016/j.cell.2022.03.025

9 Wilson, A. *et al.* Hematopoietic Stem Cells Reversibly Switch from Dormancy to Self-Renewal during Homeostasis and Repair. *Cell* **135**, 1118-1129 (2008). https://doi.org/https://doi.org/10.1016/j.cell.2008.10.048

10 Baryawno, N., Severe, N. & Scadden, D. T. Hematopoiesis: Reconciling Historic Controversies about the Niche. *Cell Stem Cell* **20**, 590-592 (2017). https://doi.org/https://doi.org/10.1016/j.stem.2017.03.025

11 Pinho, S. & Frenette, P. S. Haematopoietic stem cell activity and interactions with the niche. *Nat Rev Mol Cell Biol* **20**, 303-320 (2019). https://doi.org/10.1038/s41580-019-0103-9

12 Notta, F. *et al.* Distinct routes of lineage development reshape the human blood hierarchy across ontogeny. *Science* **351**, aab2116 (2016). https://doi.org/10.1126/science.aab2116

13 Laurenti, E. & Göttgens, B. From haematopoietic stem cells to complex differentiation landscapes. *Nature* **553**, 418-426 (2018). https://doi.org/10.1038/nature25022

14 Velten, L. *et al.* Human haematopoietic stem cell lineage commitment is a continuous process. *Nature Cell Biology* **19**, 271-281 (2017). https://doi.org/10.1038/ncb3493

15 Lee-Six, H. *et al.* Population dynamics of normal human blood inferred from somatic mutations. *Nature* **561**, 473-478 (2018). https://doi.org/10.1038/s41586-018-0497-0

16 Mitchell, E. *et al.* Clonal dynamics of haematopoiesis across the human lifespan. *Nature* **606**, 343-350 (2022). https://doi.org/10.1038/s41586-022-04786-y

17 Loeffler, D. & Schroeder, T. Symmetric and asymmetric activation of hematopoietic stem cells. *Curr Opin Hematol* **28** (2021).
18 Cosgrove, J., Hustin, L. S. P., de Boer, R. J. & Perié, L. Hematopoiesis in numbers. *Trends in Immunology* **42**, 1100-1112 (2021). https://doi.org/10.1016/j.it.2021.10.006
19 Ritter, M. in *Biorender Arreba, P. (2025) https://BioRender.com/y85f401* (2024).
20 Othman, A., Sekheri, M. & Filep, J. G. Roles of neutrophil granule proteins in orchestrating inflammation and immunity. *The FEBS Journal* **289**, 3932-3953 (2022). https://doi.org/https://doi.org/10.1111/febs.15803
21 Evrard, M. *et al.* Developmental Analysis of Bone Marrow Neutrophils Reveals Populations Specialized in Expansion, Trafficking, and Effector Functions. *Immunity* **48**, 364-379.e368 (2018). https://doi.org/10.1016/j.immuni.2018.02.002
22 Kruger, P. *et al.* Neutrophils: Between Host Defence, Immune Modulation, and Tissue Injury. *PLOS Pathogens* **11**, e1004651 (2015). https://doi.org/10.1371/journal.ppat.1004651
23 Thomas, C. J. & Schroder, K. Pattern recognition receptor function in neutrophils. *Trends Immunol* **34**, 317-328 (2013). https://doi.org/10.1016/j.it.2013.02.008
24 Burn, G. L., Foti, A., Marsman, G., Patel, D. F. & Zychlinsky, A. The Neutrophil. *Immunity* **54**, 1377-1391 (2021). https://doi.org/10.1016/j.immuni.2021.06.006
25 Rosazza, T., Warner, J. & Sollberger, G. NET formation – mechanisms and how they relate to other cell death pathways. *The FEBS Journal* **288**, 3334-3350 (2021). https://doi.org/https://doi.org/10.1111/febs.15589
26 de Oliveira, S., Rosowski, E. E. & Huttenlocher, A. Neutrophil migration in infection and wound repair: going forward in reverse. *Nature Reviews Immunology* **16**, 378-391 (2016). https://doi.org/10.1038/nri.2016.49
27 Yvan-Charvet, L. & Ng, L. G. Granulopoiesis and Neutrophil Homeostasis: A Metabolic, Daily Balancing Act. *Trends in Immunology* **40**, 598-612 (2019). https://doi.org/10.1016/j.it.2019.05.004
28 Rankin, S. M. The bone marrow: a site of neutrophil clearance. *Journal of Leukocyte Biology* **88**, 241-251 (2010). https://doi.org/https://doi.org/10.1189/jlb.0210112
29 Hidalgo, A., Chilvers, E. R., Summers, C. & Koenderman, L. The Neutrophil Life Cycle. *Trends in Immunology* **40**, 584-597 (2019). https://doi.org/10.1016/j.it.2019.04.013
30 Koenderman, L., Tesselaar, K. & Vrisekoop, N. Human neutrophil kinetics: a call to revisit old evidence. *Trends in Immunology* **43**, 868-876 (2022). https://doi.org/https://doi.org/10.1016/j.it.2022.09.008
31 Aroca-Crevillén, A., Vicanolo, T., Ovadia, S. & Hidalgo, A. Neutrophils in Physiology and Pathology. *Annual Review of Pathology: Mechanisms of Disease* **19**, 227-259 (2024). https://doi.org/10.1146/annurev-pathmechdis-051222-015009
32 McKenna, E. *et al.* Neutrophils: Need for Standardized Nomenclature. *Frontiers in Immunology* **12** (2021).
33 Skokowa, J., Dale, D. C., Touw, I. P., Zeidler, C. & Welte, K. Severe congenital neutropenias. *Nat Rev Dis Primers* **3**, 17032 (2017). https://doi.org/10.1038/nrdp.2017.32

34 Atallah-Yunes, S. A., Ready, A. & Newburger, P. E. Benign ethnic neutropenia. *Blood Rev* **37**, 100586 (2019). https://doi.org/10.1016/j.blre.2019.06.003
35 KOSTMANN, R. INFANTILE GENETIC AGRANULOCYTOSIS. *Acta Paediatrica* **64**, 362-368 (1975). https://doi.org/https://doi.org/10.1111/j.1651-2227.1975.tb03847.x
36 Carlsson, G. *et al.* Incidence of severe congenital neutropenia in Sweden and risk of evolution to myelodysplastic syndrome/leukaemia. *Br J Haematol* **158**, 363-369 (2012). https://doi.org/10.1111/j.1365-2141.2012.09171.x
37 Donadieu, J., Beaupain, B., Mahlaoui, N. & Bellanné-Chantelot, C. Epidemiology of congenital neutropenia. *Hematol Oncol Clin North Am* **27**, 1-17, vii (2013). https://doi.org/10.1016/j.hoc.2012.11.003
38 Fioredda, F. *et al.* The European Guidelines on Diagnosis and Management of Neutropenia in Adults and Children: A Consensus Between the European Hematology Association and the EuNet-INNOCHRON COST Action. *Hemasphere* **7**, e872 (2023). https://doi.org/10.1097/hs9.0000000000000872
39 Gauthier-Vasserot, A. *et al.* Application of whole-exome sequencing to unravel the molecular basis of undiagnosed syndromic congenital neutropenia with intellectual disability. *American Journal of Medical Genetics Part A* **173**, 62-71 (2017). https://doi.org/https://doi.org/10.1002/ajmg.a.37969
40 Skokowa, J. *et al.* NAMPT is essential for the G-CSF–induced myeloid differentiation via a NAD+–sirtuin-1–dependent pathway. *Nature Medicine* **15**, 151-158 (2009). https://doi.org/10.1038/nm.1913
41 Deordieva, E. *et al.* Nicotinamide (vitamin B3) treatment improves response to G-CSF in severe congenital neutropenia patients. *British Journal of Haematology* **192**, 788-792 (2021). https://doi.org/https://doi.org/10.1111/bjh.17313
42 Fioredda, F. *et al.* Stem cell transplantation in severe congenital neutropenia: an analysis from the European Society for Blood and Marrow Transplantation. *Blood* **126**, 1885-1892 (2015). https://doi.org/10.1182/blood-2015-02-628859
43 Makaryan, V. *et al.* The diversity of mutations and clinical outcomes for ELANE-associated neutropenia. *Curr Opin Hematol* **22**, 3-11 (2015). https://doi.org/10.1097/MOH.0000000000000105
44 Germeshausen, M. *et al.* The Spectrum of ELANE Mutations and their Implications in Severe Congenital and Cyclic Neutropenia. *Human Mutation* **34**, 905-914 (2013). https://doi.org/https://doi.org/10.1002/humu.22308
45 Skokowa, J., Fobiwe, J. P., Dan, L., Thakur, B. K. & Welte, K. Neutrophil elastase is severely down-regulated in severe congenital neutropenia independent of ELA2 or HAX1 mutations but dependent on LEF-1. *Blood* **114**, 3044-3051 (2009). https://doi.org/10.1182/blood-2008-11-188755
46 Hajjar, E., Broemstrup, T., Kantari, C., Witko-Sarsat, V. & Reuter, N. Structures of human proteinase 3 and neutrophil elastase – so similar yet so different. *The FEBS Journal* **277**, 2238-2254 (2010). https://doi.org/https://doi.org/10.1111/j.1742-4658.2010.07659.x
47 Rydzynska, Z., Pawlik, B., Krzyzanowski, D., Mlynarski, W. & Madzio, J. Neutrophil Elastase Defects in Congenital Neutropenia. *Frontiers in Immunology* **12** (2021). https://doi.org/10.3389/fimmu.2021.653932
48 Köllner, I. *et al.* Mutations in neutrophil elastase causing congenital neutropenia lead to cytoplasmic protein accumulation and induction of the unfolded protein response. *Blood* **108**, 493-500 (2006). https://doi.org/https://doi.org/10.1182/blood-2005-11-4689

49 Salipante, S. J. *et al.* Contributions to Neutropenia from PFAAP5 (N4BP2L2), a Novel Protein Mediating Transcriptional Repressor Cooperation between Gfi1 and Neutrophil Elastase. *Molecular and Cellular Biology* **29**, 4394-4405 (2009). https://doi.org/10.1128/MCB.00596-09

50 Nustede, R. *et al.* ELANE mutant–specific activation of different UPR pathways in congenital neutropenia. *British Journal of Haematology* **172**, 219-227 (2016). https://doi.org/https://doi.org/10.1111/bjh.13823

51 Grenda, D. S. *et al.* Mutations of the ELA2 gene found in patients with severe congenital neutropenia induce the unfolded protein response and cellular apoptosis. *Blood, The Journal of the American Society of Hematology* **110**, 4179-4187 (2007).

52 Olofsen, P. A. *et al.* PML-controlled responses in severe congenital neutropenia with ELANE-misfolding mutations. *Blood Advances* **5**, 775-786 (2021). https://doi.org/https://doi.org/10.1182/bloodadvances.2020003214

53 Skokowa, J. *et al.* LEF-1 is crucial for neutrophil granulocytopoiesis and its expression is severely reduced in congenital neutropenia. *Nature Medicine* **12**, 1191-1197 (2006). https://doi.org/10.1038/nm1474

54 Newburger, P. E. *et al.* Cyclic neutropenia and severe congenital neutropenia in patients with a shared ELANE mutation and paternal haplotype: evidence for phenotype determination by modifying genes. *Pediatric blood & cancer* **55**, 314-317 (2010).

55 Donadieu, J. *et al.* Analysis of risk factors for myelodysplasias, leukemias and death from infection among patients with congenital neutropenia. Experience of the French Severe Chronic Neutropenia Study Group. *Haematologica* **90**, 45-53 (2005). https://doi.org/10.3324/%x

56 Rosenberg, P. S. *et al.* Stable long-term risk of leukaemia in patients with severe congenital neutropenia maintained on G-CSF therapy. *British Journal of Haematology* **150**, 196-199 (2010). https://doi.org/https://doi.org/10.1111/j.1365-2141.2010.08216.x

57 Skokowa, J. *et al.* Cooperativity of RUNX1 and CSF3R mutations in severe congenital neutropenia: a unique pathway in myeloid leukemogenesis. *Blood* **123**, 2229-2237 (2014). https://doi.org/10.1182/blood-2013-11-538025

58 Uhlén, M. *et al.* Tissue-based map of the human proteome. *Science* **347**, 1260419 (2015). https://doi.org/10.1126/science.1260419

59 Nguyen-Jackson, H. T., Zhang, H. & Watowich, S. S. in *Twenty Years of G-CSF: Clinical and Nonclinical Discoveries* (eds Graham Molineux, MaryAnn Foote, & Tara Arvedson) 83-105 (Springer Basel, 2012).

60 Dong, F. *et al.* Mutations in the Gene for the Granulocyte Colony-Stimulating–Factor Receptor in Patients with Acute Myeloid Leukemia Preceded by Severe Congenital Neutropenia. *New England Journal of Medicine* **333**, 487-493 (1995). https://doi.org/10.1056/NEJM199508243330804

61 McLemore, M. L., Poursine-Laurent, J. & Link, D. C. Increased granulocyte colony-stimulating factor responsiveness but normal resting granulopoiesis in mice carrying a targeted granulocyte colony-stimulating factor receptor mutation derived from a patient with severe congenital neutropenia. *The Journal of Clinical Investigation* **102**, 483-492 (1998). https://doi.org/10.1172/JCI3216

62 Hermans, M. H. A. *et al.* Perturbed Granulopoiesis in Mice With a Targeted Mutation in the Granulocyte Colony-Stimulating Factor Receptor Gene Associated With Severe Chronic Neutropenia. *Blood* **92**, 32-39 (1998). https://doi.org/10.1182/blood.V92.1.32.413k42_32_39

63 Liu, F. *et al.* Csf3r mutations in mice confer a strong clonal HSC advantage via activation of Stat5. *The Journal of Clinical Investigation* **118**, 946-955 (2008). https://doi.org/10.1172/JCI32704
64 Touw, I. P. Game of clones: the genomic evolution of severe congenital neutropenia. *Hematology* **2015**, 1-7 (2015). https://doi.org/10.1182/asheducation-2015.1.1
65 Xia, J. *et al.* Somatic mutations and clonal hematopoiesis in congenital neutropenia. *Blood* **131**, 408-416 (2018). https://doi.org/10.1182/blood-2017-08-801985
66 Dwivedi, P. & Greis, K. D. Granulocyte colony-stimulating factor receptor signaling in severe congenital neutropenia, chronic neutrophilic leukemia, and related malignancies. *Experimental Hematology* **46**, 9-20 (2017). https://doi.org/https://doi.org/10.1016/j.exphem.2016.10.008
67 Ritter, M. in *BioRender. Arreba, P. (2025)* *https://BioRender.com/i58j620* (2024).
68 Hayashi, Y., Harada, Y. & Harada, H. Myeloid neoplasms and clonal hematopoiesis from the RUNX1 perspective. *Leukemia* **36**, 1203-1214 (2022). https://doi.org/10.1038/s41375-022-01548-7
69 Tanaka, T. *et al.* An acute myeloid leukemia gene, AML1, regulates hemopoietic myeloid cell differentiation and transcriptional activation antagonistically by two alternative spliced forms. *Embo j* **14**, 341-350 (1995). https://doi.org/10.1002/j.1460-2075.1995.tb07008.x
70 Goetz, T. L., Gu, T. L., Speck, N. A. & Graves, B. J. Auto-inhibition of Ets-1 is counteracted by DNA binding cooperativity with core-binding factor alpha2. *Molecular and cellular biology* **20**, 81-90 (2000). https://doi.org/10.1128/mcb.20.1.81-90.2000
71 Bonifer, C., Levantini, E., Kouskoff, V. & Lacaud, G. in *RUNX Proteins in Development and Cancer* (eds Yoram Groner *et al.*) 65-81 (Springer Singapore, 2017).
72 Lam, K. & Zhang, D.-E. RUNX1 and RUNX1-ETO: roles in hematopoiesis and leukemogenesis. *FBL* **17**, 1120-1139 (2012). https://doi.org/10.2741/3977
73 Osato, M. *et al.* Biallelic and Heterozygous Point Mutations in the Runt Domain of theAML1/PEBP2αB Gene Associated With Myeloblastic Leukemias. *Blood* **93**, 1817-1824 (1999). https://doi.org/https://doi.org/10.1182/blood.V93.6.1817.406k36_1817_1824
74 Harada, H. *et al.* High incidence of somatic mutations in the AML1/RUNX1 gene in myelodysplastic syndrome and low blast percentage myeloid leukemia with myelodysplasia. *Blood* **103**, 2316-2324 (2004). https://doi.org/10.1182/blood-2003-09-3074
75 Huret, J. L. *et al.* Atlas of genetics and cytogenetics in oncology and haematology in 2013. *Nucleic Acids Res* **41**, D920-924 (2013). https://doi.org/10.1093/nar/gks1082
76 Beekman, R. *et al.* Sequential gain of mutations in severe congenital neutropenia progressing to acute myeloid leukemia. *Blood* **119**, 5071-5077 (2012). https://doi.org/10.1182/blood-2012-01-406116
77 Tsai, S.-C. *et al.* Biological Activities of RUNX1 Mutants Predict Secondary Acute Leukemia Transformation from Chronic Myelomonocytic Leukemia and Myelodysplastic Syndromes. *Clinical Cancer Research* **21**, 3541 - 3551 (2015).
78 Ritter, M. in *BioRender. Arreba, P. (2025)* *https://BioRender.com/n56o822* (2024).

79 Williams, D. A., Lemischka, I. R., Nathan, D. G. & Mulligan, R. C. Introduction of new genetic material into pluripotent haematopoietic stem cells of the mouse. *Nature* **310**, 476-480 (1984). https://doi.org/10.1038/310476a0
80 Urnov, F. D. *et al.* Highly efficient endogenous human gene correction using designed zinc-finger nucleases. *Nature* **435**, 646-651 (2005). https://doi.org/10.1038/nature03556
81 Mojica, F. J., Díez-Villaseñor, C., García-Martínez, J. & Soria, E. Intervening sequences of regularly spaced prokaryotic repeats derive from foreign genetic elements. *J Mol Evol* **60**, 174-182 (2005). https://doi.org/10.1007/s00239-004-0046-3
82 Barrangou, R. *et al.* CRISPR Provides Acquired Resistance Against Viruses in Prokaryotes. *Science* **315**, 1709-1712 (2007). https://doi.org/10.1126/science.1138140
83 Jinek, M. *et al.* A programmable dual-RNA–guided DNA endonuclease in adaptive bacterial immunity. *science* **337**, 816-821 (2012).
84 Cong, L. *et al.* Multiplex Genome Engineering Using CRISPR/Cas Systems. *Science* **339**, 819-823 (2013). https://doi.org/10.1126/science.1231143
85 Mali, P. *et al.* RNA-Guided Human Genome Engineering via Cas9. *Science* **339**, 823-826 (2013). https://doi.org/10.1126/science.1232033
86 Hwang, W. Y. *et al.* Efficient genome editing in zebrafish using a CRISPR-Cas system. *Nat Biotechnol* **31**, 227-229 (2013). https://doi.org/10.1038/nbt.2501
87 NobelPrize.org. *Nobel Prize Outreach AB 2023.*, <https://www.nobelprize.org/prizes/chemistry/2020/press-release/> (2020).
88 Komor, A. C., Kim, Y. B., Packer, M. S., Zuris, J. A. & Liu, D. R. Programmable editing of a target base in genomic DNA without double-stranded DNA cleavage. *Nature* **533**, 420-424 (2016). https://doi.org/10.1038/nature17946
89 Anzalone, A. V. *et al.* Search-and-replace genome editing without double-strand breaks or donor DNA. *Nature* **576**, 149-157 (2019). https://doi.org/10.1038/s41586-019-1711-4
90 Zhang, F. Development of CRISPR-Cas systems for genome editing and beyond. *Quarterly Reviews of Biophysics* **52**, e6 (2019). https://doi.org/10.1017/S0033583519000052
91 Nishimasu, H. *et al.* Crystal Structure of Cas9 in Complex with Guide RNA and Target DNA. *Cell* **156**, 935-949 (2014). https://doi.org/https://doi.org/10.1016/j.cell.2014.02.001
92 Jasin, M. & Haber, J. E. The democratization of gene editing: Insights from site-specific cleavage and double-strand break repair. *DNA Repair* **44**, 6-16 (2016). https://doi.org/https://doi.org/10.1016/j.dnarep.2016.05.001
93 Porteus, M. H. A New Class of Medicines through DNA Editing. *New England Journal of Medicine* **380**, 947-959 (2019). https://doi.org/10.1056/NEJMra1800729
94 Xue, C. & Greene, E. C. DNA Repair Pathway Choices in CRISPR-Cas9-Mediated Genome Editing. *Trends in Genetics* **37**, 639-656 (2021). https://doi.org/https://doi.org/10.1016/j.tig.2021.02.008
95 Bétermier, M., Bertrand, P. & Lopez, B. S. Is Non-Homologous End-Joining Really an Inherently Error-Prone Process? *PLOS Genetics* **10**, e1004086 (2014). https://doi.org/10.1371/journal.pgen.1004086
96 Nambiar, T. S., Baudrier, L., Billon, P. & Ciccia, A. CRISPR-based genome editing through the lens of DNA repair. *Molecular Cell* **82**, 348-388 (2022). https://doi.org/https://doi.org/10.1016/j.molcel.2021.12.026

97 Li, T. *et al.* CRISPR/Cas9 therapeutics: progress and prospects. *Signal Transduction and Targeted Therapy* **8**, 36 (2023). https://doi.org/10.1038/s41392-023-01309-7
98 Elliott, E. K., Haupt, L. M. & Griffiths, L. R. Mini review: genome and transcriptome editing using CRISPR-cas systems for haematological malignancy gene therapy. *Transgenic Research* **30**, 129-141 (2021). https://doi.org/10.1007/s11248-020-00232-9
99 Ferrari, S. *et al.* Genetic engineering meets hematopoietic stem cell biology for next-generation gene therapy. *Cell Stem Cell* **30**, 549-570 (2023). https://doi.org/10.1016/j.stem.2023.04.014
100 Mohammadian Gol, T. *et al.* CRISPR medicine for blood disorders: Progress and challenges in delivery. *Frontiers in Genome Editing* **4** (2023). https://doi.org/10.3389/fgeed.2022.1037290
101 Breda, L. *et al.* In vivo hematopoietic stem cell modification by mRNA delivery. *Science* **381**, 436-443 (2023). https://doi.org/doi:10.1126/science.ade6967
102 Li, C. *et al.* In vivo HSC prime editing rescues sickle cell disease in a mouse model. *Blood* **141**, 2085-2099 (2023). https://doi.org/10.1182/blood.2022018252
103 Kohn, D. B., Chen, Y. Y. & Spencer, M. J. Successes and challenges in clinical gene therapy. *Gene Therapy* **30**, 738-746 (2023). https://doi.org/10.1038/s41434-023-00390-5
104 Ferrari, S. *et al.* Gene Editing of Hematopoietic Stem Cells: Hopes and Hurdles Toward Clinical Translation. *Frontiers in Genome Editing* **3** (2021). https://doi.org/10.3389/fgeed.2021.618378
105 Schmid, M. A., Takizawa, H., Baumjohann, D. R., Saito, Y. & Manz, M. G. Bone marrow dendritic cell progenitors sense pathogens via Toll-like receptors and subsequently migrate to inflamed lymph nodes. *Blood* **118**, 4829-4840 (2011). https://doi.org/10.1182/blood-2011-03-344960
106 Hendel, A. *et al.* Chemically modified guide RNAs enhance CRISPR-Cas genome editing in human primary cells. *Nature Biotechnology* **33**, 985-989 (2015). https://doi.org/10.1038/nbt.3290
107 Vaidyanathan, S. *et al.* Uridine Depletion and Chemical Modification Increase Cas9 mRNA Activity and Reduce Immunogenicity without HPLC Purification. *Mol Ther Nucleic Acids* **12**, 530-542 (2018). https://doi.org/10.1016/j.omtn.2018.06.010
108 Cromer, M. K. *et al.* Global Transcriptional Response to CRISPR/Cas9-AAV6-Based Genome Editing in CD34(+) Hematopoietic Stem and Progenitor Cells. *Mol Ther* **26**, 2431-2442 (2018). https://doi.org/10.1016/j.ymthe.2018.06.002
109 Liang, X. *et al.* Rapid and highly efficient mammalian cell engineering via Cas9 protein transfection. *Journal of Biotechnology* **208**, 44-53 (2015). https://doi.org/https://doi.org/10.1016/j.jbiotec.2015.04.024
110 Kim, S., Kim, D., Cho, S. W., Kim, J. & Kim, J. S. Highly efficient RNA-guided genome editing in human cells via delivery of purified Cas9 ribonucleoproteins. *Genome Res* **24**, 1012-1019 (2014). https://doi.org/10.1101/gr.171322.113
111 Wagner, D. L. *et al.* High prevalence of Streptococcus pyogenes Cas9-reactive T cells within the adult human population. *Nature Medicine* **25**, 242-248 (2019). https://doi.org/10.1038/s41591-018-0204-6
112 Pensado, A., Seijo, B. & Sanchez, A. Current strategies for DNA therapy based on lipid nanocarriers. *Expert Opinion on Drug Delivery* **11**, 1721-1731 (2014). https://doi.org/10.1517/17425247.2014.935337

113 Genovese, P. *et al.* Targeted genome editing in human repopulating haematopoietic stem cells. *Nature* **510**, 235-240 (2014). https://doi.org/10.1038/nature13420
114 Dever, D. P. *et al.* CRISPR/Cas9 β-globin gene targeting in human haematopoietic stem cells. *Nature* **539**, 384-389 (2016). https://doi.org/10.1038/nature20134
115 El-Kharrag, R. *et al.* Efficient polymer nanoparticle-mediated delivery of gene editing reagents into human hematopoietic stem and progenitor cells. *Molecular Therapy* **30**, 2186-2198 (2022). https://doi.org/https://doi.org/10.1016/j.ymthe.2022.02.026
116 Wilbie, D., Walther, J. & Mastrobattista, E. Delivery Aspects of CRISPR/Cas for in Vivo Genome Editing. *Accounts of Chemical Research* **52**, 1555-1564 (2019). https://doi.org/10.1021/acs.accounts.9b00106
117 Gillmore, J. D. *et al.* CRISPR-Cas9 In Vivo Gene Editing for Transthyretin Amyloidosis. *New England Journal of Medicine* **385**, 493-502 (2021). https://doi.org/doi:10.1056/NEJMoa2107454
118 Segel, M. *et al.* Mammalian retrovirus-like protein PEG10 packages its own mRNA and can be pseudotyped for mRNA delivery. *Science* **373**, 882-889 (2021). https://doi.org/doi:10.1126/science.abg6155
119 Mangeot, P. E. *et al.* Genome editing in primary cells and in vivo using viral-derived Nanoblades loaded with Cas9-sgRNA ribonucleoproteins. *Nature Communications* **10**, 45 (2019). https://doi.org/10.1038/s41467-018-07845-z
120 Chiappini, C. *et al.* Tutorial: using nanoneedles for intracellular delivery. *Nature Protocols* **16**, 4539-4563 (2021). https://doi.org/10.1038/s41596-021-00600-7
121 Ferrari, G., Thrasher, A. J. & Aiuti, A. Gene therapy using haematopoietic stem and progenitor cells. *Nature Reviews Genetics* (2020). https://doi.org/10.1038/s41576-020-00298-5
122 Vavassori, V. *et al.* Lipid nanoparticles allow efficient and harmless ex vivo gene editing of human hematopoietic cells. *Blood* **142**, 812-826 (2023). https://doi.org/10.1182/blood.2022019333
123 Mashal, R. D., Koontz, J. & Sklar, J. Detection of mutations by cleavage of DNA heteroduplexes with bacteriophage resolvases. *Nature Genetics* **9**, 177-183 (1995). https://doi.org/10.1038/ng0295-177
124 Bennett, E. P. *et al.* INDEL detection, the 'Achilles heel' of precise genome editing: a survey of methods for accurate profiling of gene editing induced indels. *Nucleic Acids Research* **48**, 11958-11981 (2020). https://doi.org/10.1093/nar/gkaa975
125 Brinkman, E. K., Chen, T., Amendola, M. & van Steensel, B. Easy quantitative assessment of genome editing by sequence trace decomposition. *Nucleic Acids Research* **42**, e168-e168 (2014). https://doi.org/10.1093/nar/gku936
126 Mock, U. *et al.* mRNA transfection of a novel TAL effector nuclease (TALEN) facilitates efficient knockout of HIV co-receptor CCR5. *Nucleic Acids Research* **43**, 5560-5571 (2015). https://doi.org/10.1093/nar/gkv469
127 Tuladhar, R. *et al.* CRISPR-Cas9-based mutagenesis frequently provokes on-target mRNA misregulation. *Nature Communications* **10**, 4056 (2019). https://doi.org/10.1038/s41467-019-12028-5
128 Chakrabarti, A. M. *et al.* Target-Specific Precision of CRISPR-Mediated Genome Editing. *Mol Cell* **73**, 699-713.e696 (2019). https://doi.org/10.1016/j.molcel.2018.11.031

129 Cox, D. B. T., Platt, R. J. & Zhang, F. Therapeutic genome editing: prospects and challenges. *Nature Medicine* **21**, 121-131 (2015). https://doi.org/10.1038/nm.3793
130 Shim, G. *et al.* Therapeutic gene editing: delivery and regulatory perspectives. *Acta Pharmacologica Sinica* **38**, 738-753 (2017). https://doi.org/10.1038/aps.2017.2
131 Geisslinger, G., Menzel, S., Gudermann, T., Hinz, B. & Ruth, P. *Mutschler Arzneimittelwirkungen: Pharmakologie – Klinische Pharmakologie – Toxikologie*. (Wissenschaftliche Verlagsgesellschaft Stuttgart, 2020).
132 Baker, D. E. (ed FDA regulatory affairs) (2002).
133 Morgan, M. A., Galla, M., Grez, M., Fehse, B. & Schambach, A. Retroviral gene therapy in Germany with a view on previous experience and future perspectives. *Gene Therapy* **28**, 494-512 (2021). https://doi.org/10.1038/s41434-021-00237-x
134 Kosicki, M., Tomberg, K. & Bradley, A. Repair of double-strand breaks induced by CRISPR–Cas9 leads to large deletions and complex rearrangements. *Nature Biotechnology* **36**, 765-771 (2018). https://doi.org/10.1038/nbt.4192
135 Turchiano, G. *et al.* Quantitative evaluation of chromosomal rearrangements in gene-edited human stem cells by CAST-Seq. *Cell Stem Cell* **28**, 1136-1147.e1135 (2021). https://doi.org/https://doi.org/10.1016/j.stem.2021.02.002
136 Tsai, S. Q. *et al.* GUIDE-seq enables genome-wide profiling of off-target cleavage by CRISPR-Cas nucleases. *Nature Biotechnology* **33**, 187-197 (2015). https://doi.org/10.1038/nbt.3117
137 Schiroli, G. *et al.* Precise Gene Editing Preserves Hematopoietic Stem Cell Function following Transient p53-Mediated DNA Damage Response. *Cell Stem Cell* **24**, 551-565.e558 (2019). https://doi.org/10.1016/j.stem.2019.02.019
138 Wienert, B. & Cromer, M. K. CRISPR nuclease off-target activity and mitigation strategies. *Frontiers in Genome Editing* **4** (2022). https://doi.org/10.3389/fgeed.2022.1050507
139 Adikusuma, F. *et al.* Large deletions induced by Cas9 cleavage. *Nature* **560**, E8-E9 (2018). https://doi.org/10.1038/s41586-018-0380-z
140 Alanis-Lobato, G. *et al.* Frequent loss of heterozygosity in CRISPR-Cas9-edited early human embryos. *Proc Natl Acad Sci U S A* **118** (2021). https://doi.org/10.1073/pnas.2004832117
141 Leibowitz, M. L. *et al.* Chromothripsis as an on-target consequence of CRISPR–Cas9 genome editing. *Nature Genetics* **53**, 895-905 (2021). https://doi.org/10.1038/s41588-021-00838-7
142 Tao, J., Bauer, D. E. & Chiarle, R. Assessing and advancing the safety of CRISPR-Cas tools: from DNA to RNA editing. *Nat Commun* **14**, 212 (2023). https://doi.org/10.1038/s41467-023-35886-6
143 Kosicki, M. *et al.* Cas9-induced large deletions and small indels are controlled in a convergent fashion. *Nature Communications* **13**, 3422 (2022). https://doi.org/10.1038/s41467-022-30480-8
144 Ferrari, S. *et al.* Choice of template delivery mitigates the genotoxic risk and adverse impact of editing in human hematopoietic stem cells. *Cell Stem Cell* **29**, 1428-1444.e1429 (2022). https://doi.org/10.1016/j.stem.2022.09.001
145 Canarutto, D. *et al.* Unbiased assessment of genome integrity and purging of adverse outcomes at the target locus upon editing of CD4+ cells for the

treatment of Hyper IgM1. *The EMBO Journal* **42**, e114188 (2023). https://doi.org/https://doi.org/10.15252/embj.2023114188
146 Metzger, M. J., McConnell-Smith, A., Stoddard, B. L. & Miller, A. D. Single-strand nicks induce homologous recombination with less toxicity than double-strand breaks using an AAV vector template. *Nucleic Acids Research* **39**, 926-935 (2011). https://doi.org/10.1093/nar/gkq826
147 Ran, F. A. *et al.* Double nicking by RNA-guided CRISPR Cas9 for enhanced genome editing specificity. *Cell* **154**, 1380-1389 (2013). https://doi.org/10.1016/j.cell.2013.08.021
148 Adli, M. The CRISPR tool kit for genome editing and beyond. *Nature Communications* **9**, 1911 (2018). https://doi.org/10.1038/s41467-018-04252-2
149 Porto, E. M., Komor, A. C., Slaymaker, I. M. & Yeo, G. W. Base editing: advances and therapeutic opportunities. *Nature Reviews Drug Discovery* **19**, 839-859 (2020). https://doi.org/10.1038/s41573-020-0084-6
150 Joana Ferreira da, S. *et al.* Click editing enables programmable genome writing using DNA polymerases and HUH endonucleases. *bioRxiv*, 2023.2009.2012.557440 (2023). https://doi.org/10.1101/2023.09.12.557440
151 Wong, C. UK first to approve CRISPR treatment for diseases: what you need to know. *Nature* (2023). https://doi.org/10.1038/d41586-023-03590-6[^1^][1]
152 Akula, S., Fu, Z., Wernersson, S. & Hellman, L. The Evolutionary History of the Chymase Locus -a Locus Encoding Several of the Major Hematopoietic Serine Proteases. *Int J Mol Sci* **22** (2021). https://doi.org/10.3390/ijms222010975
153 Akula, S., Thorpe, M., Boinapally, V. & Hellman, L. Granule Associated Serine Proteases of Hematopoietic Cells - An Analysis of Their Appearance and Diversification during Vertebrate Evolution. *PLoS One* **10**, e0143091 (2015). https://doi.org/10.1371/journal.pone.0143091
154 Fu, Z., Thorpe, M., Akula, S., Chahal, G. & Hellman, L. T. Extended Cleavage Specificity of Human Neutrophil Elastase, Human Proteinase 3, and Their Distant Ortholog Clawed Frog PR3—Three Elastases With Similar Primary but Different Extended Specificities and Stability. *Frontiers in Immunology* **9** (2018). https://doi.org/10.3389/fimmu.2018.02387
155 Isles, H. M. *et al.* Pioneer neutrophils release chromatin within in vivo swarms. *eLife* **10**, e68755 (2021). https://doi.org/10.7554/eLife.68755
156 Allport, J. R. *et al.* Neutrophils from MMP-9- or neutrophil elastase-deficient mice show no defect in transendothelial migration under flow in vitro. *Journal of Leukocyte Biology* **71**, 821-828 (2002). https://doi.org/https://doi.org/10.1189/jlb.71.5.821
157 Young, R. E. *et al.* Neutrophil elastase (NE)-deficient mice demonstrate a nonredundant role for NE in neutrophil migration, generation of proinflammatory mediators, and phagocytosis in response to zymosan particles in vivo. *J Immunol* **172**, 4493-4502 (2004). https://doi.org/10.4049/jimmunol.172.7.4493
158 Hirche, T. O., Atkinson, J. J., Bahr, S. & Belaaouaj, A. Deficiency in neutrophil elastase does not impair neutrophil recruitment to inflamed sites. *Am J Respir Cell Mol Biol* **30**, 576-584 (2004). https://doi.org/10.1165/rcmb.2003-0253OC
159 Pham, C. T., Ivanovich, J. L., Raptis, S. Z., Zehnbauer, B. & Ley, T. J. Papillon-Lefèvre syndrome: correlating the molecular, cellular, and clinical consequences of cathepsin C/dipeptidyl peptidase I deficiency in humans. *J Immunol* **173**, 7277-7281 (2004). https://doi.org/10.4049/jimmunol.173.12.7277

160 Spiekermann, K., Roesler, J., Emmendoerffer, A., Elsner, J. & Welte, K. Functional features of neutrophils induced by G-CSF and GM-CSF treatment: differential effects and clinical implications. *Leukemia* **11**, 466-478 (1997). https://doi.org/10.1038/sj.leu.2400607
161 Nasri, M. *et al.* CRISPR/Cas9-mediated ELANE knockout enables neutrophilic maturation of primary hematopoietic stem and progenitor cells and induced pluripotent stem cells of severe congenital neutropenia patients. *Haematologica* **105**, 598-609 (2020). https://doi.org/10.3324/haematol.2019.221804
162 Rao, S. *et al.* Dissecting ELANE neutropenia pathogenicity by human HSC gene editing. *Cell Stem Cell* **28**, 833-845. e835 (2021).
163 Ritter, M. U. *et al.* Efficient Correction of ELANE mutations in Primary HSPCs of Severe Congenital Neutropenia Patients Using CRISPR/Cas9 and rAVV6 HDR Repair Templates. *Blood* **134**, 1036-1036 (2019). https://doi.org/10.1182/blood-2019-131708
164 Tran, N. T. *et al.* CRISPR-Cas9-Mediated ELANE Mutation Correction in Hematopoietic Stem and Progenitor Cells to Treat Severe Congenital Neutropenia. *Mol Ther* **28**, 2621-2634 (2020). https://doi.org/10.1016/j.ymthe.2020.08.004
165 Bio, G. Graphite Bio Announces Voluntary Pause of Phase 1/2 CEDAR Study of Nulabeglogene Autogedtemcel (Nula-Cel) for Sickle Cell Disease.[Press Release]. *Businesswire (5 January 2023)* (2023).
166 Mao, Z., Bozzella, M., Seluanov, A. & Gorbunova, V. DNA repair by nonhomologous end joining and homologous recombination during cell cycle in human cells. *Cell Cycle* **7**, 2902-2906 (2008). https://doi.org/10.4161/cc.7.18.6679
167 Shin, J. J. *et al.* Controlled Cycling and Quiescence Enables Efficient HDR in Engraftment-Enriched Adult Hematopoietic Stem and Progenitor Cells. *Cell Reports* **32**, 108093 (2020). https://doi.org/https://doi.org/10.1016/j.celrep.2020.108093
168 Ferrari, S. *et al.* Efficient gene editing of human long-term hematopoietic stem cells validated by clonal tracking. *Nature Biotechnology* **38**, 1298-1308 (2020). https://doi.org/10.1038/s41587-020-0551-y
169 Haltalli, M. L. R., Wilkinson, A. C., Rodriguez-Fraticelli, A. & Porteus, M. Hematopoietic stem cell gene editing and expansion: State-of-the-art technologies and recent applications. *Experimental Hematology* **107**, 9-13 (2022). https://doi.org/https://doi.org/10.1016/j.exphem.2021.12.399
170 Murdock, A., Doudna, J., Urnov, F. & Ringeisen, B. *The Beacon for CRISPR Cures aims to create a roadmap for rapidly developing genome-editing therapies[^1^][1]*, <https://innovativegenomics.org/news/igi-danaher-crispr-cures/> (2024).
171 Sabo, P. *et al.* Mutant allele knockout with novel CRISPR nuclease promotes myelopoiesis in ELANE neutropenia. *Molecular Therapy - Methods & Clinical Development* **26**, 119-131 (2022). https://doi.org/https://doi.org/10.1016/j.omtm.2022.06.002
172 Valenzuela-Fernaéndez, A. *et al.* Leukocyte Elastase Negatively Regulates Stromal Cell-derived Factor-1 (SDF-1)/CXCR4 Binding and Functions by Amino-terminal Processing of SDF-1 and CXCR4*. *Journal of Biological Chemistry* **277**, 15677-15689 (2002). https://doi.org/https://doi.org/10.1074/jbc.M111388200

173 Lai, C. Y. *et al.* Stage-specific roles for CXCR4 signaling in murine hematopoietic stem/progenitor cells in the process of bone marrow repopulation. *Stem Cells* **32**, 1929-1942 (2014). https://doi.org/10.1002/stem.1670
174 Gíslason, M. H. *et al.* BloodSpot 3.0: a database of gene and protein expression data in normal and malignant haematopoiesis. *Nucleic Acids Research* **52**, D1138-D1142 (2023). https://doi.org/10.1093/nar/gkad993
175 van Galen, P. *et al.* The unfolded protein response governs integrity of the haematopoietic stem-cell pool during stress. *Nature* **510**, 268-272 (2014). https://doi.org/10.1038/nature13228
176 Nahmad, A. D. *et al.* Frequent aneuploidy in primary human T cells after CRISPR–Cas9 cleavage. *Nature Biotechnology* **40**, 1807-1813 (2022). https://doi.org/10.1038/s41587-022-01377-0
177 Khan, A. O. *et al.* Human Bone Marrow Organoids for Disease Modeling, Discovery, and Validation of Therapeutic Targets in Hematologic Malignancies. *Cancer Discov* **13**, 364-385 (2023). https://doi.org/10.1158/2159-8290.Cd-22-0199
178 Sprenkeler, E. G. G. *et al.* Lack of eosinophil extracellular trap formation due to failure of plasma membrane breakdown in the absence of elastase. *Blood Advances* (2023). https://doi.org/10.1182/bloodadvances.2022009432
179 Dalgıc, B., Bukulmez, A. & Sarı, S. Eponym. *European Journal of Pediatrics* **170**, 689-691 (2011). https://doi.org/10.1007/s00431-010-1367-4
180 *Ethik in der Medizin. Ein Studienbuch*. (Reclam, 2004).
181 Nasri, M. *et al.* CRISPR/Cas9n-mediated ELANE promoter editing for gene therapy of severe congenital neutropenia. *Molecular Therapy* (2024). https://doi.org/10.1016/j.ymthe.2024.03.037
182 Wesely, J. *et al.* Acute Myeloid Leukemia iPSCs Reveal a Role for RUNX1 in the Maintenance of Human Leukemia Stem Cells. *Cell Reports* **31** (2020). https://doi.org/10.1016/j.celrep.2020.107688
183 Marion, W. *et al.* RUNX1 mutations mitigate quiescence to promote transformation of hematopoietic progenitors in Fanconi anemia. *Leukemia* **37**, 1698-1708 (2023). https://doi.org/10.1038/s41375-023-01945-6
184 Olofsen, P. A. *et al.* Malignant Transformation Involving CXXC4 Mutations Identified in a Leukemic Progression Model of Severe Congenital Neutropenia. *Cell Reports Medicine* **1**, 100074 (2020). https://doi.org/https://doi.org/10.1016/j.xcrm.2020.100074
185 Ritter, M. *et al.* Cooperating, congenital neutropenia–associated Csf3r and Runx1 mutations activate pro-inflammatory signaling and inhibit myeloid differentiation of mouse HSPCs. *Annals of Hematology* **99**, 2329-2338 (2020). https://doi.org/10.1007/s00277-020-04194-0
186 Tavridou, A., Rogers, D., Farinelli, G., Gravanis, I. & Jekerle, V. Genome-editing medicinal products: the EMA perspective. *Nature Reviews Drug Discovery* **23**, 242-243 (2024). https://doi.org/10.1038/d41573-024-00050-2
187 Bulaklak, K. & Gersbach, C. A. The once and future gene therapy. *Nature Communications* **11**, 5820 (2020). https://doi.org/10.1038/s41467-020-19505-2

Appendix I: List of accepted publications

A) Ritter, M. U. & Nasri, M. et *a*l., 2024, *The CRISPR Journal*

B) Nasri M. & Ritter M. U. et al., 2024, *Molecular Therapy*

C) Zeidler, A. et al., 2023, *Haematologica*

D) Skokowa, J. and Hernandez Alvarez, B. et al., 2022, *Nature Communications*

E) Dannenmann, B. and Klimiankou, M. et al., 2021, *Cell Stem Cell*

F) Mir, P. et al., 2020, *Methods in Molecular Biology*

G) Nasri, M. et al., 2020, *Haematologica*

H) Ritter, M. et al., 2020, *Annals of Hematology*

I) Morishima, T. et al., 2019, *Blood*

A) Ritter, M. U. & Nasri, M. et *a*l., 2024, *The CRISPR Journal*

The CRISPR Journal
Volume 7, Number 5, 2024

DOI: 10.1089/crispr.2024.0006

The CRISPR Journal

RESEARCH ARTICLE CRISPR Trials

Comparison of Gene-Editing Approaches for Severe Congenital Neutropenia-Causing Mutations in the *ELANE* Gene

Malte Ulrich Ritter,[1,†] Masoud Nasri,[1,†] Benjamin Dannenmann,[1] Perihan Mir,[1] Benjamin Secker,[1,‡] Diana Amend,[1,§] Maksim Klimiankou,[1] Karl Welte,[2] and Julia Skokowa[1,3,*]

Abstract

Safety considerations for gene therapies of inherited preleukemia syndromes, including severe congenital neutropenia (CN), are paramount. We compared several strategies for CRISPR/Cas9 gene editing of autosomal-dominant *ELANE* mutations in $CD34^+$ cells from two CN patients head-to-head. We tested universal and allele-specific *ELANE* knockout, *ELANE* mutation correction by homology-directed repair (HDR) with AAV6, and allele-specific HDR with ssODN. All strategies were not toxic, had at least 30% editing, and rescued granulopoiesis *in vitro*. In contrast to published data, allele-specific indels in the last exon of *ELANE* also restored granulopoiesis. Moreover, by implementing patient-derived induced pluripotent stem cells for GUIDE-Seq off-target analysis, we established a clinically relevant "personalized" assessment of off-target activity of gene editing on the background of the patient's genome. We found that allele-specific approaches had the most favorable off-target profiles. Taken together, a well-defined head-to-head comparison pipeline for selecting the appropriate gene therapy is essential for diseases with several gene editing strategies available.

Introduction

The design and selection of the optimal gene therapy for a particular disease-causing mutation must consider the nature and pathological function of the mutant gene and its resulting protein, the pattern of its inheritance, the affected cell types, and the available genome-editing tools. Base editing and prime editing promise high precision and low toxicities but also contain the potential for unanticipated risks.[1] We have focused on classical approaches utilizing the CRISPR/Cas9 nuclease. Patients with inherited bone marrow failure syndromes (iBMFS) are candidates for *ex vivo* gene therapies. iBMFS manifest as single cytopenia (e.g., erythroid, myeloid, or megakaryocytic) or as pancytopenia and often culminate in leukemia.[2,3] Most iBMFS patients require allogeneic bone marrow transplantation, which can cure the condition but simultaneously carries severe risks.[4] This therapy can be potentially replaced by autologous transplantation of gene-edited hematopoietic stem and progenitor cells (HSPCs). To this end, evaluating the efficacy and safety of gene-editing-based therapies is critical to preserve the integrity and functionality of gene-edited HSPCs. In the case of preleukemia iBMFS, the increased risk for leukemic transformation and the possible presence of preleukemic clones with somatic mutations in a pool of gene-edited cells require a thorough evaluation of gene editing strategies. If several potential gene editing strategies are possible, these should be compared head-to-head to determine the most suitable approach for clinical development. What constitutes an acceptable, effective, and safe gene therapy approach depends on the disease-specific mutation, affected cell type, disease prognosis, risks, and existing therapy options.

Severe congenital neutropenia (CN) is a preleukemia iBMFS that usually manifests as severe neutropenia shortly

[1]*Department of Hematology, Oncology, Immunology and Rheumatology, University Hospital Tübingen, Tübingen, Germany;* [2]*Department of Pediatric Hematology, Oncology and Bone Marrow Transplantation, University Hospital Tübingen, Tübingen, Germany; and* [3]*Gene and RNA Therapy Center, Tübingen University, Tübingen, Germany.*
[†]*These authors contributed equally to the work.*
[‡]*Present address: Cegat GmbH, Tübingen Germany.*
[§]*Present address: Paris Lodron University, Salzburg, Austria.*

*Address correspondence to: *Julia Skokowa, Division of Translational Oncology, Department of Hematology, Oncology, Clinical Immunology and Rheumatology, University Hospital Tübingen, Otfried-Müller Strasse 10, 72076 Tübingen, Germany,* E-mail: Julia.skokowa@med.uni-tuebingen.de

after birth owing to the inability of bone marrow myeloid progenitor cells to differentiate into mature neutrophils.[3] Most CN patients can be treated with lifelong subcutaneous recombinant human granulocyte colony-stimulating factor (rhG-CSF) injections. rhG-CSF markedly improves the quality of life, but some CN patients do not respond to this cytokine, and ~15% of patients develop leukemia.[3] CN is a heterogeneous disease, and the largest patient cohort harbors autosomal-dominant heterozygous mutations in the *ELANE* gene (*ELANE*-CN patients).[5] *ELANE* mutations are distributed throughout all exons and two introns (3 and 4).[5] Mutated *ELANE* has a gain-of-function effect, inducing pathological intracellular processes in myeloid progenitor cells that result in maturation arrest of granulopoiesis.[3] *ELANE* is a relatively recently evolved gene in the met-ase locus on the short arm of chromosome 19 that is not present in lower organisms, including zebrafish. It encodes neutrophil elastase (NE) protein, a serine protease specifically expressed and secreted by neutrophilic granulocytes.[6]

Autosomal-dominant gain-of-function mutations can be corrected, mutated genes with redundant nonessential functions can be knocked out, or allele-specific KO can be performed. Several approaches for CRISPR/Cas-based gene editing of *ELANE* mutations in CN patients' HSPCs have been recently described.[7–10] Our group developed a practical approach based on universal *ELANE* knockout (uEKO)[7] and, more recently, an approach to knockdown *ELANE* expression.[11] An independent group subsequently reproduced our findings.[9] Tran et al. demonstrated that correction of the specific *ELANE* mutation with AAV6-based delivery of repair template in HSPCs of one *ELANE*-CN patient effectively restored granulocytic differentiation *in vitro* and *in vivo*.[8] Allele-specific knockout (ASKO) of the mutated *ELANE* allele would preserve NE expression. A recent approach, estimated to apply to 75% of patients, utilizes common single-nucleotide polymorphisms (SNPs) outside of the coding region to achieve the ASKO of the mutant *ELANE* allele.[10] Although this strategy seems promising, introducing two simultaneous double-strand breaks increases the probability of genotoxic events. More than 150 pathogenic *ELANE* variants have been reported to date,[5,12] and it is almost impossible to establish clinical-grade gene-editing therapy for each reported *ELANE* mutation under the current regulatory and fiscal framework. Additionally, AAV vectors can induce TLR2/9 signaling and TP53-triggered DNA damage responses (DDR), which results in reduced engraftment rate of gene-edited hematopoietic stem cells.[13] In the present study, we designed and compared head-to-head several CRISPR/Cas9-based gene-editing strategies reflecting different therapeutic principles to establish the optimal *ELANE*-CN gene therapy translational strategy.

Results

Experimental design to compare gene-editing strategies for mutated *ELANE*

The proposed gene-editing strategies for *ELANE*-CN have advantages and disadvantages (Fig. 1A). The *ELANE* uEKO approach restores granulopoiesis and can be applied to nearly all *ELANE*-CN patients. However, the biological functions of NE are not fully defined, and inhibition of its wild-type (WT) form might have unanticipated side effects. Additionally, introducing *ELANE* variants due to CRISPR/Cas9 in-frame indels can produce *de novo* protein variants with unforeseeable effects.[14] In this regard, homology-directed repair-based correction using AAV6 (HDR-AAV) preserves NE expression but may also introduce *de novo*

FIG. 1. Scheme of designed gene editing strategies along with potential outcomes. **(A)** Graphical overview of compared CRISPR/Cas9-based strategies targeting CN-causing *ELANE* mutations. These are the universal *ELANE* knockout (uEKO), correction of *ELANE* mutation by homology-directed repair (HDR) relying on a template introduced by recombinant AAV6 referred to as HDR-AAV, the allele-specific knockout (ASKO) of the mutant allele through an allele-specific sgRNA, and the mutation correction through HDR in an allele-specific manner (AS-HDR). The impact on granulopoiesis, neutrophil elastase expression, and the potential to produce novel mutations is summarized for each strategy. Plus annotates a positive improvement; two pluses indicate that this approach is superior to approaches with one plus. The minus indicates that a feature is completely blocked. For each approach, we also summarized the outcomes graphically. If an outcome continues to lead to neutropenia, it is shown in the box marked in red. Outcomes that cure neutropenia are marked in a blue box. **(B)** Detailed genomic DNA sequences of exon 2 surrounding *ELANE* mutation p.A57V and of exon 5 surrounding the p.G214V *ELANE* mutation. The sgRNAs used to target indicated mutations with SpCas9 have been annotated in light red if they act as allele-specific and in light purple if they target both alleles, independent of the mutation. The wild-type and HDR template sequences are marked in blue. Red marks the mutant allele sequences causing CN. Yellow-marked nucleotides are silent mutations used to enhance HDR rates. The figures were created with Biorender.com. CN, congenital neutropenia.

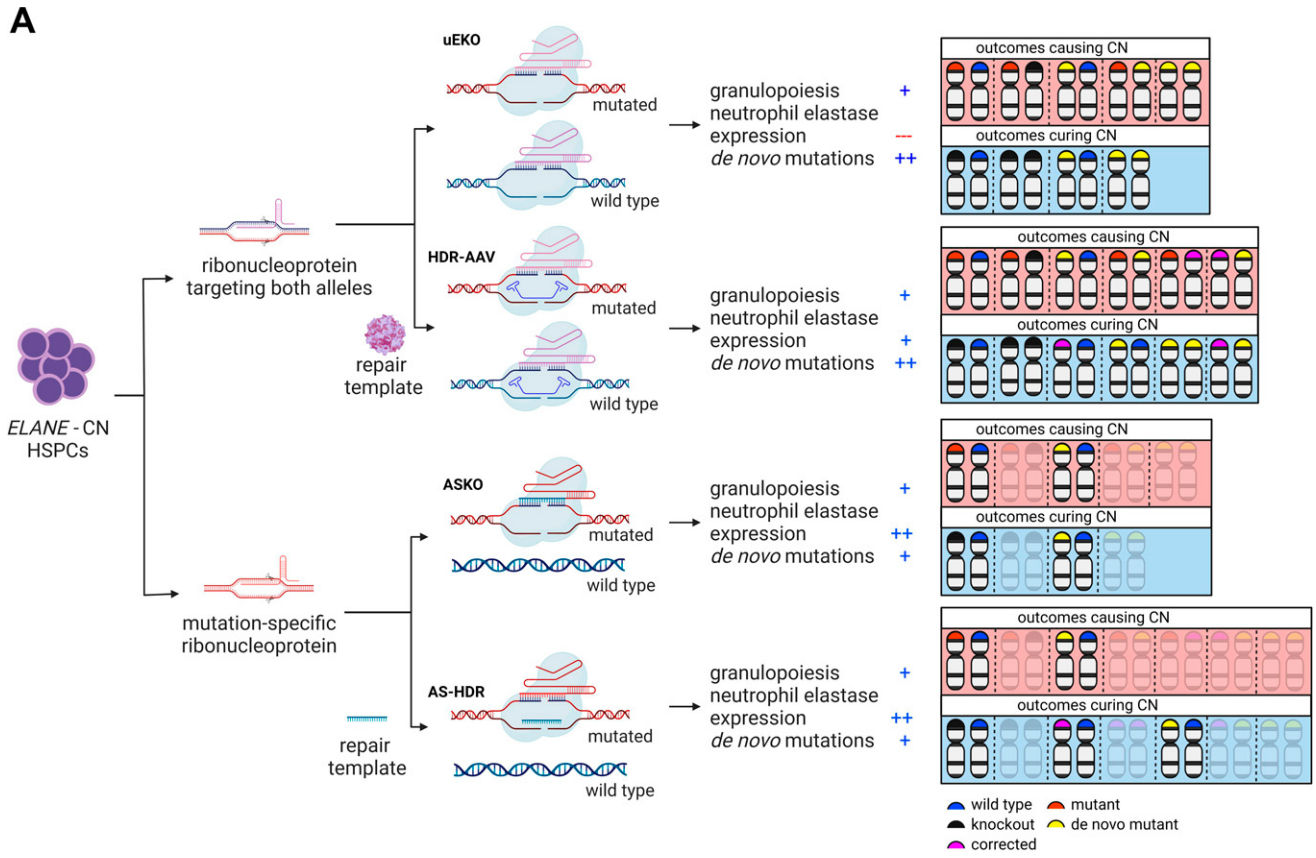

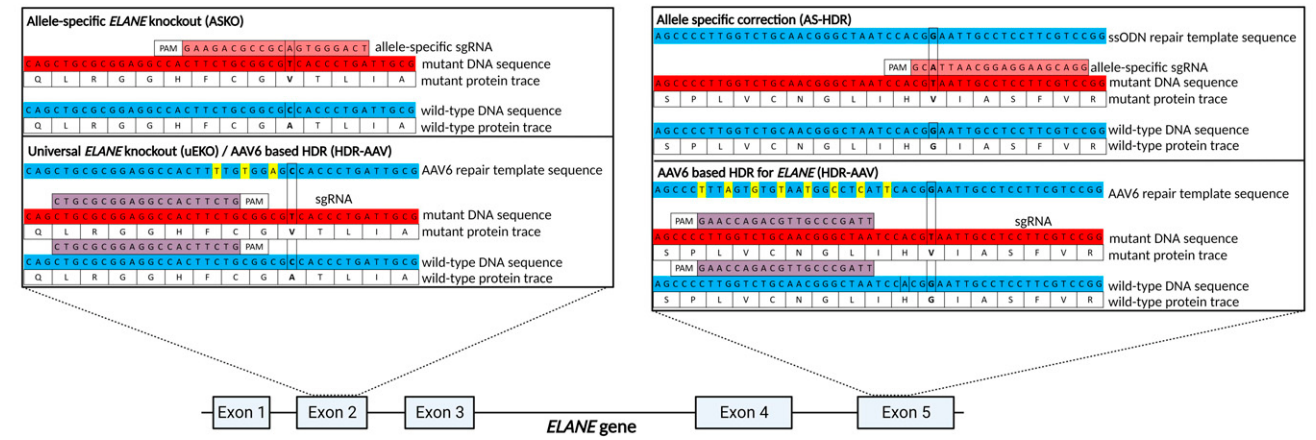

ELANE variants. Neither uEKO nor HDR-AAV discriminates between mutated and WT *ELANE*. The ASKO approach precisely cuts the mutated *ELANE* allele and limits the generation of *de novo* mutations. However, not all *ELANE* mutation positions are suitable for the design of allele-specific gRNAs. This raises a limitation of the ASKO approach, as some *ELANE*-CN patients (such as CN p.A57V and CN p.G214R) have a promising therapeutic option, while others might not have access to ASKO. In theory, as Rao et al.[9] suggested, allele-specific gene editing can only knock out mutated *ELANE* in the first four exons, where indels trigger nonsense-mediated decay. Therefore,

we tested the possibility of performing allele-specific editing of the mutant allele of *ELANE* in exon 5.

To compare the proposed strategies, we selected two *ELANE*-CN patients with hotspot mutations—NM_001972.4:c.170C>T, p.A57V (CN patient 1) and NM_001972.4:c.639C>T, p.G214V (CN patient 2)—who showed no or low response to G-CSF and a high risk of developing leukemia.[5] For uEKO and HDR-AAV approaches, we utilized the sgRNA targeting exon 2 as previously described by us.[7] To repair *ELANE* mutations, we designed AAV6-HDR with silent mutations to prevent the re-cutting of the repaired allele, as has been described for the *HBB* gene previously.[15] We then designed an allele-specific sgRNA that targets the mutant (p.A57V) allele (sg-ASKO-2). For the correction of the *ELANE* mutation (p.G214V), we utilized a specific sgRNA (sg-HDR-AAV-5) with an accompanying AAV6 repair template. Last, to correct the p.G214V mutation in an allele-specific manner *via* HDR (AS-HDR), we designed a patient-specific sgRNA targeting p.G214V that is combined with a wild-type *ELANE* repair template, delivered as a single-strand oligonucleotide (ssODN) (Fig. 1B).

All tested gene-editing strategies show equal efficacy in restoring granulopoiesis for the p.A57V *ELANE* mutation

We compared the therapeutic effects of proposed gene editing using primary bone marrow $CD34^+$ HSPCs from two *ELANE*-CN patients, performing colony-forming unit (CFU) and *in vitro* granulocytic liquid culture differentiation (LCD) assays (Supplementary Fig. S1). For CN patient 1, we compared uEKO, AAV-HDR, and ASKO editing. In all experiments, we used cells edited in the AAVS1 gene, a "safe harbor" site, applying a previously described sgRNA[16] as a control. After 14 days of *in vitro* LCD, we observed 62% insertion–deletion mutations (indels) in control cells, 70% knockout with the uEKO approach, 10.5% ± 3.3% HDR, with an additional 49.5% ± 32.1% knockout, with the HDR-AAV approach, and 54.6% knockout of the mutant allele with the ASKO approach (Fig. 2A). Gene editing did not markedly affect the number of viable HSPCs, as assessed 2 days post-editing (Fig. 2B).

All gene-editing approaches corrected the neutropenia phenotype in CFU assays (Fig. 2C). For uEKO, the percentage of CFU-G (granulocyte) and CFU-GM (granulocyte/macrophage) colonies was elevated compared with AAVS1-edited control cells. In contrast, the proportion of CFU-M (macrophage) and erythroid burst-forming (BFU-E) colonies significantly declined. The same changes were observed in the HDR-AAV group, with CFU-G and CFU-GM colony numbers rising significantly and CFU-M and BFU-E colonies significantly reduced compared with control cells. Similar trends were observed for the ASKO condition, but only CFU-G colonies significantly increased, and only CFU-M colonies significantly decreased

FIG. 2. All proposed gene-editing approaches demonstrated equal efficacy in restoring neutrophil maturation for p.A57V *ELANE* mutation. **(A)** Gene-editing efficiencies determined on day 14 of *in vitro* liquid culture differentiation of HSPCs to neutrophils, two independent experiments. **(B)** Number of viable HSPCs on day 2 postelectroporation per 10^5 electroporated cells, two independent experiments. **(C, D)** Distribution **(C)** and absolute counts **(D)** of CFU colonies generated from gene-edited HSPCs. The percentage and the total colony counts were tested for significance by two-way ANOVA and Dunnett's multiple comparisons to control cells, two independent experiments. **(E)** Distribution of gene-editing outcomes in CFU-G colonies of ASKO-edited cells. **(F)** Impact of gene-editing of HSPCs on their *in vitro* differentiation to neutrophils. Neutrophil numbers are shown normalized to 1×10^5 HSPCs used for differentiation. One-way ANOVA with multiple comparisons analysis of all treatment conditions to control was used to determine statistical significance, two independent experiments. **(G)** Neutrophil differentiation efficiency, as assessed by flow cytometry analysis of cells at day 14 of liquid culture differentiation. Neutrophils are defined as $CD11b^+CD15^+$ of $CD45^+$ cells. One-way ANOVA with multiple comparisons analysis of all treatment conditions to control was used to determine statistical significance, two independent experiments. **(H)** Histological assessment of neutrophil maturation on May-Grünwald-Giemsa–stained cytospins and **(I)** representative cytospin images from gene-edited and differentiated HSPCs assessed at day 14 of differentiation. Data in **(H)** were tested for significance by two-way ANOVA and multiple comparisons to control cells, two independent experiments. **(J)** ROS forming potential of *in vitro* derived neutrophils upon fMLP stimulation. Unpaired Student's *t*-test was used to determine the statistical significance. Results are depicted as the mean of biological replicates. Error bars represent the standard deviations in all figures, two independent experiments. Statistical significance is marked by $*p \le 0.05$, $**p \le 0.01$, $***p \le 0.001$, and $****p \le 0.001$. ANOVA, analysis of variance; CFU, colony-forming unit; HSPCs, hematopoietic stem and progenitor cells; ROS, reactive oxygen species.

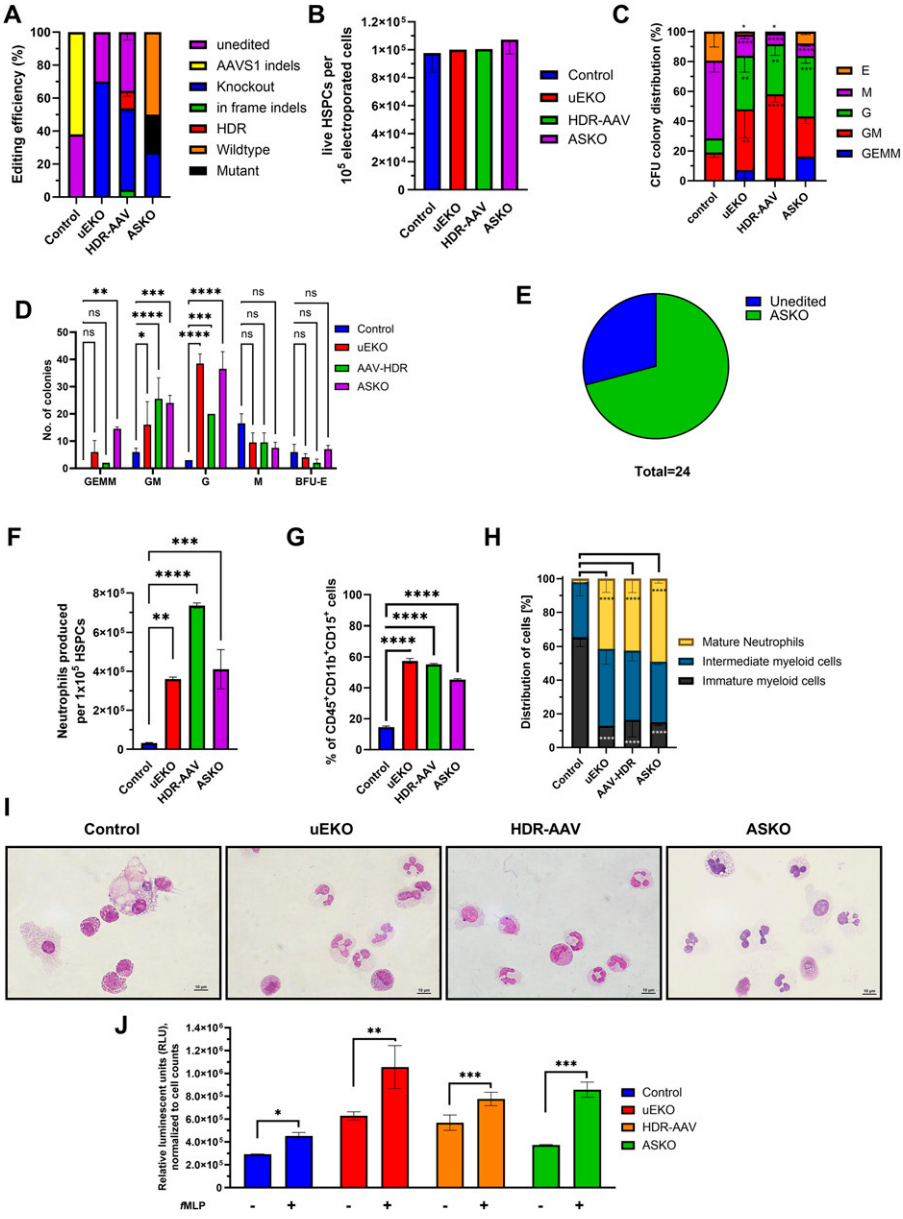

compared with the control group. The same patterns were observed for absolute colony counts (Fig. 2D). In addition to the significant increase in the numbers of CFU-G and CFU-GM colonies under all conditions, CFU-GEMM (granulocyte, erythroid, macrophage, and megakaryocyte) counts showed a trend to increase in all conditions but only significantly increased in the ASKO group. The reduction in CFU-M and BFU-E colonies was insignificant when expressed as absolute counts. Sanger sequencing of selected CFU-G colonies from ASKO editing revealed the presence of an ASKO in 70.8% of analyzed colonies (Fig. 2E and Fig. S2A).

In line with CFU results, in *in vitro* liquid culture granulocytic differentiation, all gene-edited HSPCs produced significantly more neutrophils compared to control cells. Specifically, compared to control cells, neutrophil output increased 11.1-fold for uEKO, 22.7-fold for HDR-AAV, and 12.7-fold for ASKO (Fig. 2F). Flow cytometry analyses also revealed a significant increase in the percentage of $CD11b^{+}CD15^{+}$ neutrophils on day 14 of *in vitro* differentiation (Fig. 2G). Morphological assessments of May-Grünwald-Giemsa–stained cytospin preparations of cells generated on day 14 of liquid culture granulocytic differentiation also showed a significant reduction in immature

neutrophil precursors and a significantly increased number of mature neutrophils for all gene-editing approaches compared with control cells (Fig. 2H, I). These findings unequivocally demonstrate that all explored treatment options for CN patient 1 were effective in reestablishing granulopoiesis.

Previous studies have demonstrated that neutrophils produced by CN patients through rhG-CSF treatment have functional defects.[17–19] Among the functional impairments is a reduced capacity to produce reactive oxygen species (ROS) upon formyl-methionine-leucin-proline (fMLP) stimulation. Therefore, we compared ROS production upon fMLP stimulation in neutrophils derived from gene-edited HSPCs. All treatment conditions showed at least a 2-fold higher ROS level than the control groups. A slight difference was observed between the unstimulated cells of the treatment conditions, where the ASKO-generated neutrophils had a lower ROS level compared to the uEKO and HDR-AAV groups (Fig. 2J).

Knockout, HDR, and ASKO restore granulopoiesis for the p.G214V *ELANE* mutation

The gene-editing efficiency for control group from CN patient 2 harboring p.G214V *ELANE* mutation was 77%. In uEKO conditions, the knockout efficiency was 35.3% ± 6.8%. For the AAV-HDR approach, the correction efficiency was 83.1% ± 2.8%, with 13.6% ± 3.5% frameshift indels. Last, the AS-HDR group showed no HDR but exhibited 46% frameshift indels, corresponding to the knockout of 92% of all mutant alleles (Fig. 3A). None of the gene editing approaches significantly affected the number of viable HSPCs (Fig. 3B).

CFU assays with gene-edited HSPCs showed a significant increase in CFU-G and CFU-GM colonies and a significant decrease in CFU-M colonies with uEKO, HDR-AAV, and AS-HDR approaches ($p < 0.0001$ for all conditions and colony types) compared with control cells. BFU-E percentages were significantly reduced in HDR-AAV ($p < 0.0001$) and AS-HDR ($p = 0.0073$) groups (Fig. 3C). These observations remained significant in analyses of absolute colony counts (Fig. 3D). More specifically, compared to control-edited cells, CFU-G and CFU-GM colony numbers significantly increased for uEKO, HDR-AAV, and AS-HDR conditions. Absolute CFU-M colony counts decreased significantly for all conditions, whereas BFU-E colonies were significantly reduced only in the HDR-AAV group.

We further performed Sanger sequencing of CFU-G colonies to determine if frameshift indels in exon 5 led to the correction of the CN phenotype. Surprisingly, contrary to a previous report,[9] we observed that 88.9% of all sequenced CFU-G colonies contained a knockout mutant allele, 3.7% were unedited, and 7.4% had indels in the wild-type allele (Fig. 3E and Fig. S3A).

In line with CFU results, LCD showed a significant increase in the absolute number of neutrophils and percentage of neutrophils produced during 14 days for all gene-editing approaches (Fig. 3F, G) compared to control samples. A morphological assessment showed comparable neutrophil increases and simultaneous decreases in immature myeloid cells in HDR-AAV and AS-HDR groups (Fig. 3H). May-Grünwald-Giemsa–stained cytospin preparations also showed a clear formation of segmented mature neutrophils in these groups compared with mainly immature and apoptotic cells in the control samples (Fig. 3I).

FIG. 3. Tested gene-editing designs demonstrated comparable efficacy in the restoration of granulopoiesis for p.G214V *ELANE* mutation. **(A)** Gene-editing efficiencies on day 14 of liquid culture granulocytic differentiation of edited HSPCs, two independent experiments. **(B)** Number of viable cells on day 2 after electroporation are shown per 105 HSPCs, two independent experiments. **(C, D)** CFU assay of gene-edited patient HSPCs, assessed on day 14 after seeding. The distribution of colonies in percentage **(C)** and absolute colony numbers **(D)** are shown and tested for significance by two-way ANOVA and multiple comparisons to control cells, two independent experiments. **(E)** Sanger sequencing results of 27 CFU-G colonies. **(F)** Impact of gene-editing on the total number of neutrophils generated on day 14 of *in vitro* liquid culture differentiation. One-way ANOVA with multiple comparisons analysis of all treatment conditions to control was used to determine statistical significance, two independent experiments. **(G)** Flow cytometry analysis of granulocytic differentiation of gene-edited HSPCs on day 14 of liquid culture differentiation. One-way ANOVA with multiple comparisons analysis of all treatment conditions to control was used to determine statistical significance, two independent experiments. **(H, I)** Histological assessment of neutrophil maturation on May-Grünwald-Giemsa–stained cytospins **(H)** and **(I)** representative cytospin images derived from gene-edited and differentiated HSPCs at day 14 of differentiation. Results are depicted as the mean of replicates. Error bars represent the standard deviation. Statistical significance is marked by $*p \leq 0.05$, $**p \leq 0.01$, $***p \leq 0.001$, and $****p \leq 0.001$. CFU-G, colony-forming unit-granulocyte.

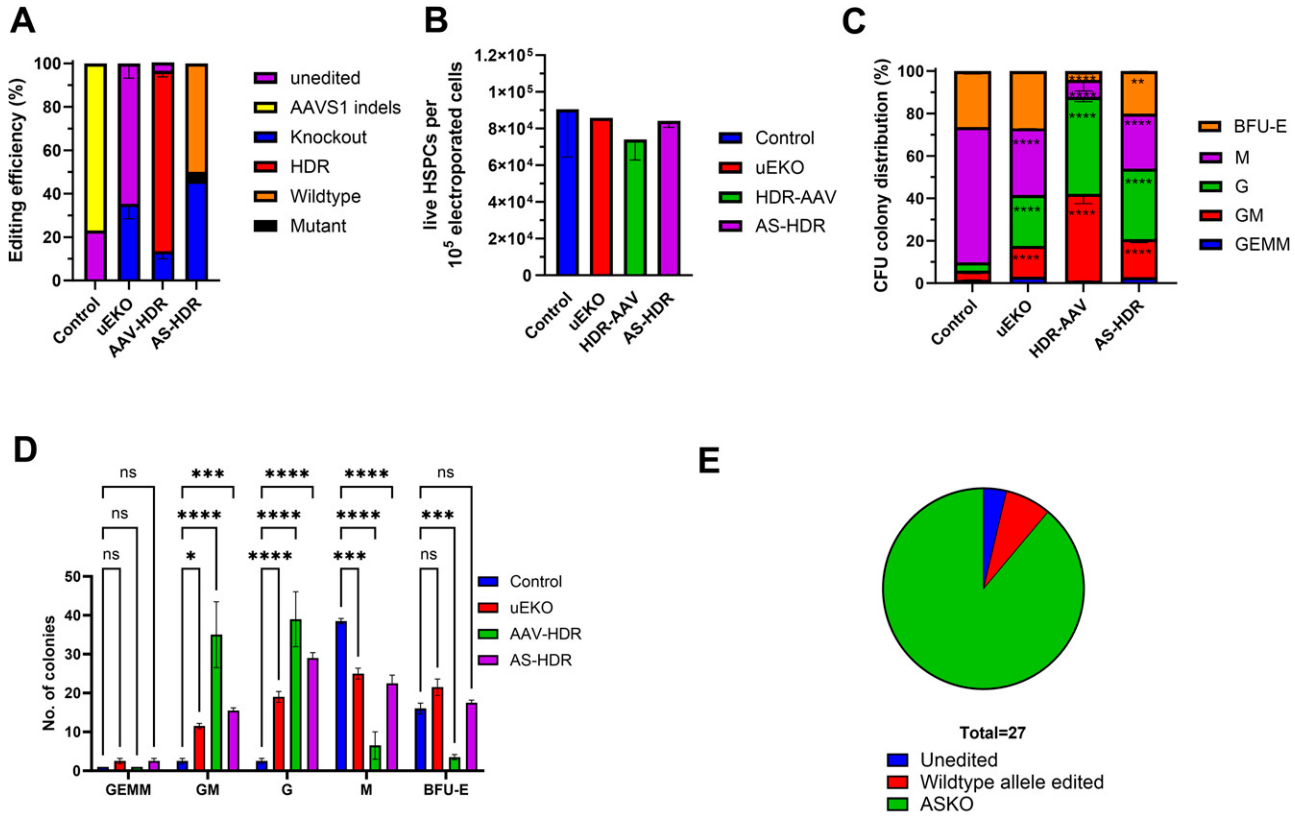
A
Editing efficiency (%)
unedited
AAVS1 indels
Knockout
HDR
Wildtype
Mutant
Control
uEKO
AAV-HDR
AS-HDR
B
live HSPCs per 10^5 electroporated cells
Control
uEKO
HDR-AAV
AS-HDR
C
CFU colony distribution (%)
BFU-E
M
G
GM
GEMM
D
No. of colonies
GEMM
GM
G
M
BFU-E
E
Total=27
Unedited
Wildtype allele edited
ASKO
F
Neutrophils produced per 1x10^5 HSPCs
Control
uEKO
HDR-AAV
ASKO
G
% of CD45+CD11b+CD15+ cells
H
Distribution of cells [%]
Mature Neutrophils
Intermediate myeloid cells
Immature myeloid cells
I
Control
HDR-AAV
AS-HDR

Allele-specific targeting of mutations in exon 2 and exon 5 of *ELANE* restores granulopoiesis

We utilized two *ELANE*-CN patient-derived induced pluripotent stem cells (iPSC) lines to further investigate the ASKO of mutant *ELANE*. As a control, we used the corresponding unedited iPSC lines, iPSC-CN Ex2 harboring *ELANE* p.A57V mutation and iPSC-CN Ex5 with *ELANE* p.G214R mutation. Both iPSC cell lines and methods for gene editing of iPSCs have been described by us previously.[20–23] Allele-specific *ELANE* editing resulted in 14.7% ASKO of *ELANE* in iPSC-CN-Ex2 and 12% in iPSC-CN-Ex5. We further observed 18.1% and 12.8% HDR in iPSC-CN-Ex2 and iPSC-CN-Ex5, respectively, with corresponding in-frame indels values of 6.3% and 1.6%, and remaining mutant allele values of 10.9% and 23.6% for respective iPSC lines (Fig. 4A). The wild-type allele was not edited. To confirm the specificity of the mutant-specific sgRNAs, we electroporated control iPSCs with the allele-specific guides for p.A57V or p.G214R. We observed no editing, confirming the *ELANE* mutant-allele specificity of the utilized guides (Fig. 4B).

To evaluate the functional outcome of allele-specific editing of *ELANE* mutations, we assessed granulopoietic differentiation of edited iPSCs, according to our previous publication.[22] CFU assays employing $CD34^+$ cells derived from gene-edited iPSCs ($iCD34^+$ cells) showed a significant increase in CFU-G colonies and a significant decrease in CFU-M colonies compared with unedited $iCD34^+$ cells. CFU-GM colonies were also significantly increased for iPSC-CN-Ex2–derived HSPCs with ASKO performed on exon 2 (Fig. 4C). Total colony counts showed the same trend as the CFU distribution (Fig. 4D). We also observed restored granulopoiesis in the *in vitro* EB-based granulocytic differentiation of ASKO-edited iPSC-CN-Ex2 and iPSC-CN-Ex5, as assessed by the percentage of cells expressing pan-granulocyte markers $CD45^+CD11b^+CD15^+$ and the neutrophil-specific markers $CD45^+CD15^+CD16^+$ on day 28 of differentiation and compared to mock electroporated cells (Fig. 4E–H). These findings confirmed the observation in primary HSPCs that ASKO resolved the CN phenotype not only in exon 2 but also in the last exon 5 of *ELANE*.

Patient-specific off-target profiling using GUIDE-Seq of patient-derived iPSCs

Recent publications have demonstrated that population-specific SNPs lead to substantial off-targets in individuals carrying this SNP. Using healthy donor-derived primary cells or cell lines may lead to underestimate the potential off-targets effects of gene editing tools due to the patients-specific genetic background.[24–26] Thus, to avoid possible off-target profile inconsistency, we established an approach for patient-specific genetic background off-target profiling in patient-derived iPSCs. An initial *in silico* screen with CRISPRitz did find between 33 and 138 potential off-target sites but no clear trend favoring any of the strategies (Fig. 5A). We further performed a patient-specific GUIDE-Seq screen in *ELANE*-CN patient-derived iPSCs (Fig. 5B). To this end, we utilized three iPSC cell lines: iPSC-CN-Ex2, iPSC-CN-Ex4 (p.C151Y), and iPSC-CN-Ex5.[20,23] In the iPSC-CN-Ex2 line, we compared the profiles of sg-uEKO and sg-ASKO-2 used in previous experiments. In the iPSC-CN-Ex4 line, we compared sgRNA-E4 (E4), which targets both *ELANE* alleles for HDR, and sgRNA-E4PS (E4PS), which targets the p.C151Y allele specifically for knockout or repair. Finally, in the iPSC-CN-Ex5 line, we compared sg-HDR-AAV and sg-AS-HDR, also tested above. In iPSC-CN-Ex2 cells, we found 10 off-target sites for sg-uEKO and 3 off-target sites for sg-ASKO-2. All three

FIG. 4. Targeting of *ELANE* mutations with an allele-specific sgRNA restores granulopoiesis in patient-derived iPSCs. **(A)** Gene-editing efficiency of allele-specific knockout of mutation p. A57V in Exon 2 and p. G214R in Exon 5 of *ELANE*, as assessed in total gene-edited iPSCs population. **(B)** Representative Sanger sequencing of a control, unedited and gene-edited iPSCs. **(C, D)** CFU assay of gene-edited cells shown as distribution **(C)** and as an absolute number **(D)** of colonies, two independent experiments. **(E)** FACS analysis of granulocytic number **(D)** of colonies, two independent experiments. **(E)** FACS analysis of granulocytic differentiation of gene-edited iPSCs at day 28 of EB-based granulocytic differentiation. Statistical test used: unpaired two-sided Student's *t*-test. **(F)** Absolute number of neutrophils produced by EB-based granulocytic differentiation of gene-edited iPSCs on day 28 of culture. An unpaired two-sided Student's *t*-test was used to calculate statistical significance. **(G)** Histological assessment of neutrophil maturation on May-Grünwald-Giemsa–stained cytospins. Tested for significance by two way ANOVA and secondary multiple comparison to control cells for two independent experiments. **(H)** Representative images of cytospins of cells from day 28 of EB-based iPSC differentiation to neutrophils. Where shown, results are depicted as the mean of biological and technical replicates. Error bars represent the standard deviation. Statistical significance is marked by $*p \leq 0.05$, $**p \leq 0.01$, and $****p \leq 0.001$.

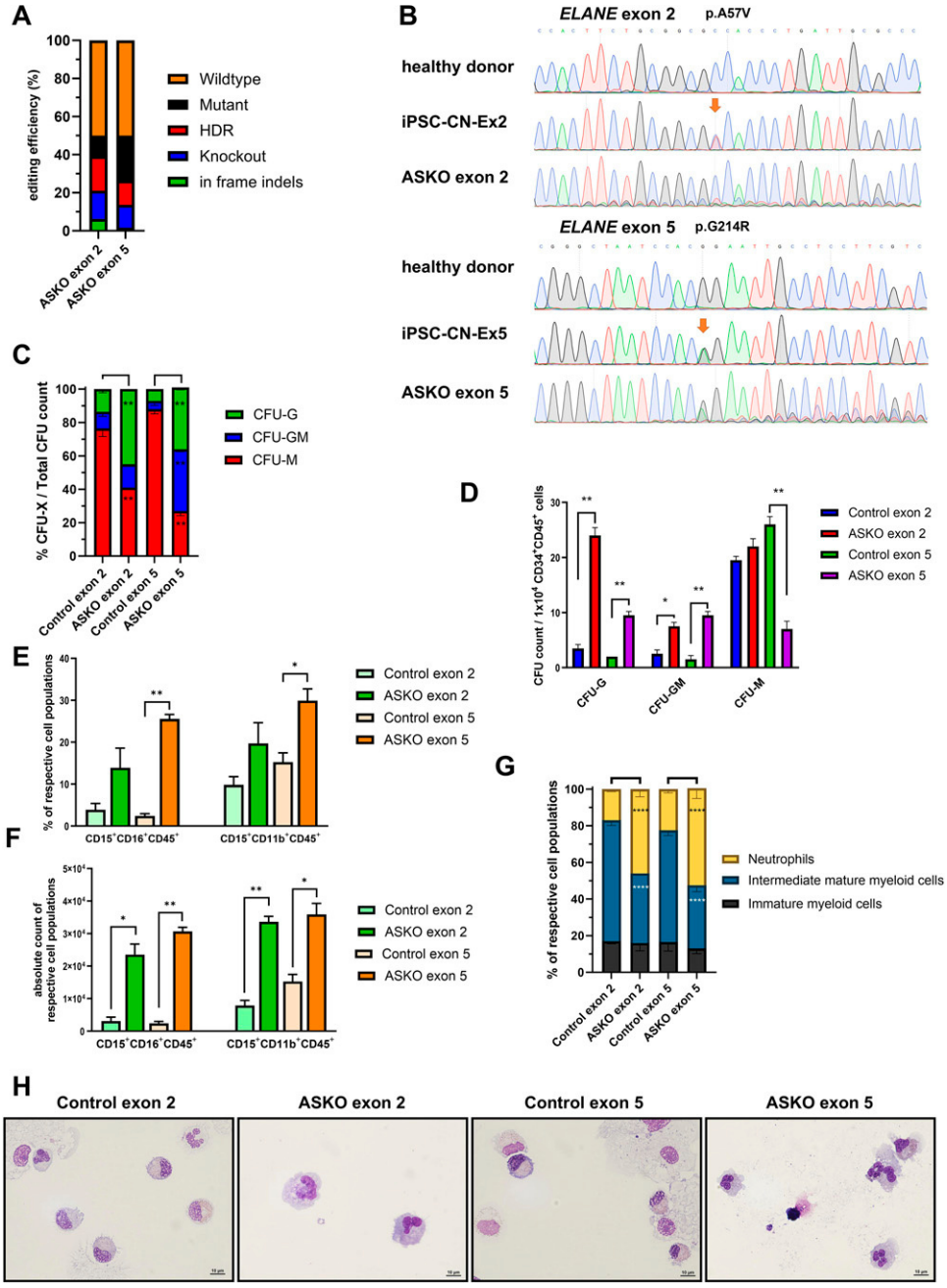

sg-ASKO-2 off-targets were positioned in introns (Fig. 5C and Fig. S4A). Among the off-targets of sg-uEKO, seven were intergenic, two were intronic, and one was in a mitochondrial gene. Analysis of the iPSC-CN-Ex4 line revealed two potential off-targets for E4 sgRNA in unplaced genomic sequences[33] and three off-targets for E4PS sgRNA: two intronic and one intergenic (Fig. 5C and Fig. S4A). Finally, comparing sg-HDR-AAV and sg-AS-HDR in the iPSC-CN-Ex5 line revealed three off-targets for both guides. Whereas sg-HDR-AAV had two intronic and one intergenic off-target, only one intronic and two intergenic off-targets were detected for sg-AS-HDR (Fig. 5C and Fig. S4A). Taken together, we have successfuly established patient-specific off-target screening using iPSC model.

Discussion

In this study, we have performed an *in vitro* comparison of several gene-editing approaches for *ELANE* mutations in patients' HSPCs and patient-derived iPSCs. We

believe that such analysis should be done for preclinical gene therapy trials and preceding animal experiments. We have focused on the disease-specific needs of *ELANE*-CN patients for effective and safe gene therapy,[27,28] which includes the efficacy, stemness conservation, functional assessment of mature neutrophils produced from gene-edited HSPCs, and genotoxicity.[27,28]

Concerning efficacy, the uEKO, AAV-HDR, and ASKO approaches were equally good in rescuing granulopoiesis in two independent assays, and no relevant differences in cell viability were observable. The observed gene editing efficiencies range from 30% to 80%, resulting in comparable phenotype correction, pointing to a broad therapeutic window. We recently reported that 8% of *ELANE* knockdown in *ELANE*-CN HSPCs was sufficient to rescue the CN phenotype after engraftment of gene-edited cells in immune-compromised NSG mice.[11] Also, estimates from mosaic *ELANE* patients with a normal neutrophil count reach a similar level of 11%.

Double-stranded breaks by Cas9 nuclease, intracellular ssODNs, and AAV6 transduction can cause activation of TP53-triggered DNA damage and inflammatory responses, reducing the engraftment potential of gene-edited HSCs.[15,29–34] The assessment of stemness and transplantability by CFU assay, an *in vitro* surrogate for engraftment efficiency[35,36] confirmed the known impact of AAV6 transduction to reduce the transplantability of gene-edited stem cells, most probably, through the immunogenic reactions caused by the viral transduction.[37] In line with published data, we observed a noticeably lower number of CFU-GEMM colonies, that are derived from more immature HSCs and a stronger increase in CFU-GM and CFU-G colonies that are produced by more mature and less engraftable myeloid progenitor cells. The next step in this evaluation should be an *in vivo* engraftment of gene-edited cells from groups pre-selected from the *in vitro* studies in immunocompromised mice.[29] To assess the impact of individual gene editing components and processes, ideally, individual controls for electroporation, ribonucleoprotein, AAV6 vectors, and ssODNs are necessary. Due to limited primary patient cells available, we could only perform one control, for which we chose gene editing at the safe harbor site AAVS1. We believe this to be the optimal control in this material limited scenario, as it accounts for the most factors across the different conditions.

In terms of the functionality of the generated neutrophils, HDR-AAV and ASKO maintain the production of wild-type NE, whereas uEKO eliminates the *ELANE* gene. The importance of wild-type NE for neutrophil functions requires a more detailed investigation in the future. Our data prove the comparable efficacy for uEKO, HDR-AAV, and ASKO regarding ROS capacity restoration. Recent data show that knocking out *ELANE* in HSPCs does not interrupt granulopoiesis or other blood lineage development.[7,9,11] Moreover, *ELANE*-KO neutrophils can produce ROS and can perform phagocytosis and chemotaxis *in vitro* (as tested for some Gram-positive and Gram-negative bacteria) and *in vivo* (for Gram-positive bacteria).[7] Neutrophil counts in *Elane*$^{-/-}$ mice are normal, but they have reduced capacity for clearing Gram-negative bacteria and sensing zymosan particles.[38,39] The redundancy of *ELANE* is likely a result of its origin as a duplicated paralog of the proteinase 3 (*PRTN3*) gene of the neutrophil serine protease family, which also includes cathepsin G (*CTSG*), leukocidin (*AZU1*), and serine protease 57 (*PRSS57*).[6]

For the genome integrity analysis, we performed GUIDE-seq and found that allele-specific gRNAs have a favorable off-target profile compared with all other tested gRNAs. However, safety could vary between different allele-specific gRNAs targeting other *ELANE* mutations. Additional evaluations, including rhAMP-seq, CAST-seq,[40] and the presence of large on-target insertions and deletions[41] should also be performed. It is also essential to evaluate the safety of each gRNA in a patient-specific manner to account for possible additional off-targets or reduced on-target efficiency owing to patient-specific genomic variations.[25,26] *In silico* modeling is the standard way to predict patient-specific off-targets.[42] By applying

FIG. 5. Safety profiling of designed gene-editing approaches in CN patient-derived iPSCs. **(A)** CRISPRitz profile of six sgRNAs used in this study for three *ELANE* hotspot mutations p.A57V, p.C151Y, and p.G214R. For each mutation, one guide RNA targeting both the wild-type and the mutant allele was compared to an allele-specific guide RNA, which targets only the CN-causing *ELANE* mutation. The comparison was performed for up to four mismatches. **(B)** Proposed workflow for patient genomic background specific GUIDE-Seq off-target screening in CN patients-derived iPSC, including reprogramming of peripheral blood mononuclear cells, GUIDE-Seq screening in patient-derived iPSC, DNA isolation, library preparation, and *in silico* analysis. Workflow visualization was created using Biorender.com. **(C)** Off-target sites found by GUIDE-seq for gRNAs tested in patient derived iPSCs. Detailed information on which guide RNA was tested in each cell line-can be found in the results section.

A

gRNA	sg-uEKO	sg-ASKO-2	sgRNA-E4	sgRNA-E4PS	sg-HDR-AAV-5	sg-AS-HDR
Targets	88	93	138	64	33	130
CTCF binding site	6	6	13	4	2	9
DNase I	45	23	46	25	15	42
Enhancer	5	3	1	2	2	3
Exon	16	15	18	17	1	15
Intron	59	54	91	38	24	80
Open chromatin region	1	0	1	1	1	1
Promoter	16	14	32	8	3	6
Promoter flanking region	10	10	13	12	6	18
TF binding site	0	1	2	1	0	2

B

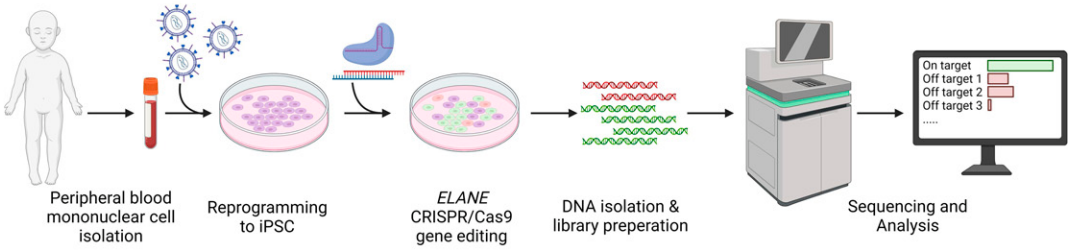

C

sg-uEKO

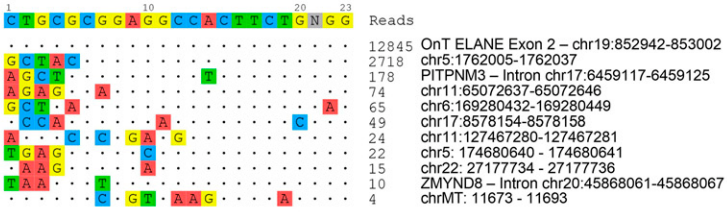

sg-ASKO-2

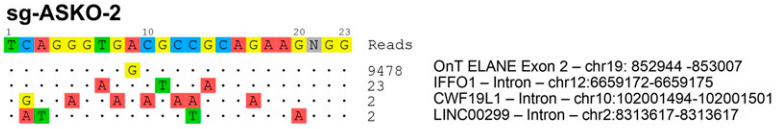

sgRNA-E4

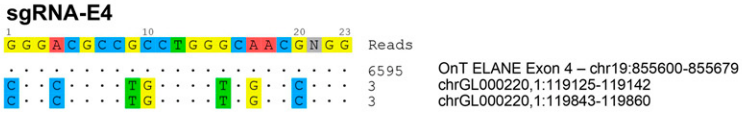

sgRNA-E4PS

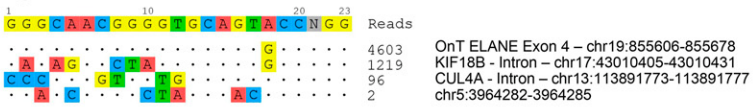

sg-HDR-AAV-5

sg-AS-HDR

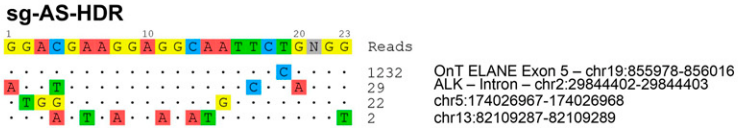

GUIDE-Seq to patient-derived iPSC, we found an efficient way to generate patient-specific personalized off-target profiles. This method can be broadly used for personalized safety assessments of gene-editing therapies in the future.

The next important factor in establishing gene therapy is its feasibility for patients with rare diseases, including *ELANE*-CN. Universal knockout of *ELANE* is by far the most technically feasible approach. The universal nature of uEKO results in lower overall costs for patients and insurance providers, potentially bringing gene therapy equity and fairness to all *ELANE*-CN patients.[43] However, in addition to the abovementioned question about the physiological role of NE, gene knockout targeting the coding sequence has the risk of introducing *de novo* mutations and potentially inducing on-target mRNA misregulation.[14] To mitigate this risk, we recently established a knockdown approach by targeting the *ELANE* promoter.[11] The *ELANE* ASKO approach requires only one double-strand break to inactivate the mutant allele, as compared to the study by Sabo et al., which introduces three DNA double-strand breaks and introduces a large deletion,[10] altogether elevating the DDR.[31,44] However, each *ELANE* mutation requires its own sgRNA with individual efficacy and safety assessment, making it time—and money-intensive. Interestingly, our ASKO-HDR approach for the p.G214V *ELANE* mutation, relying on an ssODN repair template, resulted in no measurable HDR, despite evidence of successful HDR in this exon in HSPCs in the literature.[45] The use of higher ssODN concentrations might produce favorable results, but we faced dose-limiting toxicities of ssODN (data not shown).[30,46] However, indels induced by allele-specific gene editing in exon 5 of *ELANE* in HSPCs and iPSCs resulted in the restoration of granulopoiesis. This outcome is unexpected, as frameshift mutations in this region should not cause nonsense-mediated decay, as suggested elsewhere.[9,47] The exact mechanism underlying this observation remains to be elucidated. One potential mechanism—reduced translation efficiency and, therefore, effective knockdown due to a shortened 3′-UTR, as proposed by Rao et al.[9]—does not fully explain our observation, given that this type of editing creates a high number of +1 indels.[9]

Recent proof-of-concept studies of *in vivo* gene editing of HSPCs can overcome the challenges of *ex vivo* gene editing and offer a simpler, faster, cheaper, and more accessible treatment for patients.[48–50] Theoretically, this approach will be superior to *ex vivo* gene therapy. However, the field is in the initial stages, and many questions remain to be solved before it can move into the clinic safely.[51]

In summary, we suggested a head-to-head pipeline for the *in vitro* comparison of several gene editing approaches prior to *in vivo* validation of the best performing *in vitro* strategies. We also establish a personalized GUIDE-Seq off-target screening in patient-derived iPSC. The iPSC platform has high potential for personalized genotoxicity investigations. Thus, our work demonstrates the feasibility of a comparison of patient-specific gene therapy appr-oaches and challenges for rare disease patients.

Materials and Methods

Isolation and culture of CD34$^+$ HSPCs

To isolate CD34$^+$ cells, mononuclear cells were obtained from bone marrow. Briefly, mononuclear cells were obtained by centrifugation through a Ficoll gradient (GE Healthcare #17-1440-03) and subsequently used for CD34$^+$ purification with magnetic beads (Miltenyi #130-046-703). CD34$^+$ cells were cultured in StemSpan SFEM II hematopoietic cell culture medium supplemented with 20 ng/mL interleukin-3, 50 ng/mL stem cell factor, 20 ng/mL interleukin-6, 20 ng/mL thrombopoietin, 50 ng/mL fms-related receptor tyrosine kinase 3 ligand, 2 mM L-glutamine, 100 U/mL penicillin, and 0.1 mg/mL streptomycin at a density of $2.5–5 \times 10^5$ cells/mL.

Analysis of gene-editing efficiency

Gene-editing efficiency was measured on day 14 of differentiation. Briefly, cells were lysed in a quick-extract solution (Lucigen # QE09050) to obtain genomic DNA. The edited genomic region was amplified using Go-Taq DNA polymerase (Promega # M3005) or Primestar max DNA polymerase (Takara # R045A) and respective PCR primers (Supplementary Table S3), according to the manufacturer's protocol. In the case of using HDR-AAV6 as a repair template, the *ELANE* locus was amplified using primers targeting a region outside of the HDR-template sequence. The editing efficiency was calculated from Sanger sequencing traces of the amplified genomic regions using ICE synthego.[52]

Ethics

All experiments were carried out under the approval of the ethics committee of the University of Tuebingen. The study was conducted according to Helsinki's declaration. Informed written consent was obtained from the study participants.

Statistical analysis

Statistical analyses were carried out using GraphPad Prism version 9 software. Shapiro–Wilk test was used to test

for normal distribution. We used a two-sided, unpaired Student's *t*-test, one-way analysis of variance (ANOVA) with multiple comparisons, or two-way ANOVA with multiple comparisons to determine statistical significance. Details are indicated in the figure legends.

Data access

Data access is available through the corresponding author upon request.

Acknowledgments

The authors thank Matthew Porteus and Volker Wiebkind for their advice on experiment design and AAV virus production. The authors thank the Flow Cytometry Core Facility—Berg of the University Hospital Tübingen for technical support regarding flow cytometric experiments. The authors thank Cornelia Zeidler for providing patient samples and Claudia Lengerke for support as Department Head. The authors thank Dr. Lina Maria Serna Higuita for advice on statistical analysis. Special thanks to the patients and their families for their cooperation.

Authors' Contributions

Conceptualization: M.U.R., M.N., P.M., and J.S. Performance of the experiments: M.U.R., M.N., P.M., B.D., B.S., and D.A. Data analysis: M.U.R., M.N., P.M., and B.D. Funding acquisition: J.S. Resources: J.S. Supervision: J.S. Writing—original draft: M.U.R., M.N., and J.S. Writing—reviewing and editing: all authors.

Author Disclosure Statement

M.N., P.M., and J.S. have filed a patent relating to the presented work.

AI-assisted technologies (Grammarly) were used to improve readability and language. The authors reviewed and edited the content after using these tools as needed and take full responsibility for the content of the publication.

Funding Information

This work was supported by the DFG, BMBF "MyPred," NIH, M. Schickedanz Kinderkrebsstiftung, and the COST EU action "InnoChron."

Supplementary Material

Supplementary Data S1
Supplementary Figure S1
Supplementary Figure S2
Supplementary Figure S3
Supplementary Figure S4
Supplementary Table S1
Supplementary Table S2
Supplementary Table S3

References

1. Fiumara M, Ferrari S, Omer-Javed A, et al. Genotoxic effects of base and prime editing in human hematopoietic stem cells. Nat Biotechnol 2023; 42(6):877–891; doi: 10.1038/s41587-023-01915-4
2. Skokowa J, Steinemann D, Katsman-Kuipers JE, et al. Cooperativity of RUNX1 and CSF3R mutations in severe congenital neutropenia: A unique pathway in myeloid leukemogenesis. Blood 2014;123(14): 2229–2237; doi: 10.1182/blood-2013-11-538025
3. Skokowa J, Dale DC, Touw IP, et al. Severe congenital neutropenias. Nat Rev Dis Primers 2017;3(1):17032; doi: 10.1038/nrdp.2017.32
4. Fioredda F, Iacobelli S, Van Biezen A, et al. Severe Aplastic Anemia the Inborn Error, and the Pediatric Disease Working Parties of the European Society for Blood and Bone Marrow Transplantation (EBMT) and Stem Cell Transplant for Immunodeficiencies in Europe (SCETIDE). Stem cell transplantation in severe congenital neutropenia: An analysis from the European Society for Blood and Marrow Transplantation. Blood J Am Soc Hematol 2015;126(16):1885–1892; quiz 1970.
5. Makaryan V, Zeidler C, Bolyard AA, et al. The diversity of mutations and clinical outcomes for ELANE-associated neutropenia. Curr Opin Hematol 2015;22(1):3–11; doi: 10.1097/MOH.0000000000000105
6. Pham CT. Neutrophil serine proteases: Specific regulators of inflammation. Nat Rev Immunol 2006;6(7):541–550; doi: 10.1038/nri1841
7. Nasri M, Ritter M, Mir P, et al. CRISPR/Cas9-mediated ELANE knockout enables neutrophilic maturation of primary hematopoietic stem and progenitor cells and induced pluripotent stem cells of severe congenital neutropenia patients. Haematologica 2020;105(3):598–609; doi: 10 .3324/haematol.2019.221804
8. Tran NT, Graf R, Wulf-Goldenberg A, et al. CRISPR-Cas9-Mediated ELANE Mutation Correction in Hematopoietic Stem and Progenitor Cells to Treat Severe Congenital Neutropenia. Mol Ther 2020;28(12):2621–2634; doi: 10.1016/j.ymthe.2020.08.004
9. Rao S, Yao Y, de Brito JS, et al. Dissecting ELANE neutropenia pathogenicity by human HSC gene editing. Cell Stem Cell 2021;28(5):833–845. e5.
10. Sabo P, Makaryan V, Dicken Y, et al. Mutant allele knockout with novel CRISPR nuclease promotes myelopoiesis in ELANE neutropenia. Mol Ther Methods Clin Dev 2022;26:119–131; doi: 10.1016/j.omtm.2022.06 .002
11. Nasri M, Ritter MU, Mir P, et al. CRISPR-Cas9n-mediated ELANE promoter editing for gene therapy of severe congenital neutropenia. Mol Ther 2024;32(6):1628–1642; doi: 10.1016/j.ymthe.2024.03.037
12. Germeshausen M, Deerberg S, Peter Y, et al. The Spectrum of ELANE Mutations and their Implications in Severe Congenital and Cyclic Neutropenia. Hum Mutat 2013;34(6):905–914; doi: 10.1002/humu.22308
13. Charlesworth CT, Hsu I, Wilkinson AC, et al. Immunological barriers to haematopoietic stem cell gene therapy. Nat Rev Immunol 2022;22(12): 719–733; doi: 10.1038/s41577-022-00698-0
14. Tuladhar R, Yeu Y, Tyler Piazza J, et al. CRISPR-Cas9-based mutagenesis frequently provokes on-target mRNA misregulation. Nat Commun 2019; 10(1):4056; doi: 10.1038/s41467-019-12028-5
15. Dever DP, Bak RO, Reinisch A, et al. CRISPR/Cas9 β-globin gene targeting in human haematopoietic stem cells. Nature 2016;539(7629):384–389; doi: 10.1038/nature20134
16. Cho SW, Kim S, Kim Y, et al. Analysis of off-target effects of CRISPR/Cas-derived RNA-guided endonucleases and nickases. Genome Res 2013; 24(1):132–141; doi: 10.1101/gr.162339.113
17. Spiekermann K, Roesler J, Emmendoerffer A, et al. Functional features of neutrophils induced by G-CSF and GM-CSF treatment: Differential effects and clinical implications. Leukemia 1997;11(4):466–478; doi: 10 .1038/sj.leu.2400607
18. Donini M, Fontana S, Savoldi G, et al. G-CSF treatment of severe congenital neutropenia reverses neutropenia but does not correct the underlying functional deficiency of the neutrophil in defending against microorganisms. Blood 2007;109(11):4716–4723; doi: 10.1182/blood-2006-09-045427
19. Liu Q, Zhang L, Shu Z, et al. Two paternal mosaicism of mutation in ELANE causing severe congenital neutropenia exhibit normal neutrophil morphology and ROS production. Clin Immunol 2019;203:53–58. (
20. Dannenmann B, Zahabi A, Mir P, et al. Human iPSC-based model of severe congenital neutropenia reveals elevated UPR and DNA damage in CD34+ cells preceding leukemic transformation. Exp Hematol 2019; 71:51–60; doi: 10.1016/j.exphem.2018.12.006

21. Nasri M, Mir P, Dannenmann B, et al. Fluorescent labeling of CRISPR/-Cas9 RNP for gene knockout in HSPCs and iPSCs reveals an essential role for GADD45b in stress response. Blood Adv 2019;3(1):63–71; doi: 10.1182/bloodadvances.2017015511
22. Dannenmann B, Nasri M, Welte K, et al. CRISPR/Cas9 genome editing of human-induced pluripotent stem cells followed by granulocytic differentiation. In: RNA Interference and CRISPR Technologies: Technical Advances and New Therapeutic Opportunities. (Sioud M ed.) Springer US: New York, NY; 2020; pp. 471–483.
23. Dannenmann B, Klimiankou M, Oswald B, et al. iPSC modeling of stage-specific leukemogenesis reveals BAALC as a key oncogene in severe congenital neutropenia. Cell Stem Cell 2021;28(5):906–922.e6; doi: 10.1016/j.stem.2021.03.023
24. Scott DA, Zhang F. Implications of Human Genetic Variation in CRISPR-Based Therapeutic Genome Editing. Nature Medicine 2017;23:1095–1101; doi: 10.1038/nm.4377
25. Cancellieri S, Zeng J, Lin LY, et al. Human genetic diversity alters off-target outcomes of therapeutic gene editing. Nat Genet 2023;55(1):34–43; doi: 10.1038/s41588-022-01257-y
26. Cromer MK, Majeti KR, Rettig GR, et al. Comparative analysis of CRISPR off-target discovery tools following ex vivo editing of CD34+ hematopoietic stem and progenitor cells. Mol Ther 2023;31(4):1074–1087; doi: 10.1016/j.ymthe.2023.02.011
27. Wienert B, Cromer MK. CRISPR nuclease off-target activity and mitigation strategies. Front Genome Ed 2022;4:1112956; doi: 10.3389/fgeed.2022.1050507
28. Porteus MH. A new class of medicines through DNA editing. N Engl J Med 2019;380(10):947–959; doi: 10.1056/NEJMra1800729
29. Bak RO, Dever DP, Porteus MH. CRISPR/Cas9 genome editing in human hematopoietic stem cells. Nat Protoc 2018;13(2):358–376; doi: 10.1038/nprot.2017.143
30. Romero Z, Lomova A, Said S, et al. Editing the sickle cell disease mutation in human hematopoietic stem cells: Comparison of endonucleases and homologous donor templates. Mol Ther 2019;27(8):1389–1406; doi: 10.1016/j.ymthe.2019.05.014
31. Schiroli G, Conti A, Ferrari S, et al. Precise gene editing preserves hematopoietic stem cell function following transient p53-mediated DNA damage response. Cell Stem Cell 2019;24(4):551–565.e8; doi: 10.1016/j.stem.2019.02.019
32. Ferrari S, Jacob A, Beretta S, et al. Efficient gene editing of human long-term hematopoietic stem cells validated by clonal tracking. Nat Biotechnol 2020;38(11):1298–1308; doi: 10.1038/s41587-020-0551-y
33. Dudek AM, Porteus MH. Answered and unanswered questions in early-stage viral vector transduction biology and innate primary cell toxicity for ex-vivo gene editing. Front Immunol 2021;12:660302; doi: 10.3389/fimmu.2021.660302
34. Lee B-C, Grice M, Wu C, et al. Clonal dynamics of HDR-Edited HSPCs targeting the CD33 locus in rhesus macaques. Blood 2022;140(Supplement 1):309–310; doi: 10.1182/blood-2022-166504
35. Demirci S, Khan MBN, Hinojosa G, et al. Ex vivo culture resting time impacts transplantation outcomes of genome-edited human hematopoietic stem and progenitor cells in xenograft mouse models. Cytotherapy 2024;26(6):641–648; doi: 10.1016/j.jcyt.2024.02.011
36. Xu L, Lahiri P, Skowronski J, et al. Molecular dynamics of genome editing with CRISPR-Cas9 and rAAV6 virus in human HSPCs to treat sickle cell disease. Mol Ther Methods Clin Dev 2023;30:317–331; doi: 10.1016/j.omtm.2023.07.009
37. Bio G. Graphite Bio Announces Voluntary Pause of Phase 1/2 CEDAR Study of Nulabeglogene Autogedtemcel (Nula-Cel) for Sickle Cell Disease [Press Release]. Businesswire; 2023.
38. Belaaouaj A, McCarthy R, Baumann M, et al. Mice lacking neutrophil elastase reveal impaired host defense against gram negative bacterial sepsis. Nat Med 1998;4(5):615–618; doi: 10.1038/nm0598-615
39. Young RE, Thompson RD, Larbi KY, et al. Neutrophil elastase (NE)-deficient mice demonstrate a nonredundant role for NE in neutrophil migration, generation of proinflammatory mediators, and phagocytosis in response to zymosan particles in vivo. J Immunol 2004;172(7):4493–4502; doi: 10.4049/jimmunol.172.7.4493
40. Turchiano G, Andrieux G, Klermund J, et al. Quantitative evaluation of chromosomal rearrangements in gene-edited human stem cells by CAST-Seq. Cell Stem Cell 2021;28(6):1136–1147.e5; doi: 10.1016/j.stem.2021.02.002
41. Höijer I, Emmanouilidou A, Östlund R, et al. CRISPR-Cas9 induces large structural variants at on-target and off-target sites in vivo that segregate across generations. Nat Commun 2022;13(1):627; doi: 10.1038/s41467-022-28244-5
42. Bao XR, Pan Y, Lee CM, et al. Tools for experimental and computational analyses of off-target editing by programmable nucleases. Nat Protoc 2021;16(1):10–26; doi: 10.1038/s41596-020-00431-y
43. Hildebrandt CCM, J M. Justice in CRISPR/Cas9 research and clinical applications. AMA J Ethics 2018;20(9):E826–E833; doi: 10.1001/amajethics.2018.826
44. Dorset SR, Bak RO. The p53 challenge of hematopoietic stem cell gene editing. Mol Ther Methods Clin Dev 2023;30:83–89; doi: 10.1016/j.omtm.2023.06.003
45. DeWitt MA, Magis W, Bray NL, et al. Selection-free genome editing of the sickle mutation in human adult hematopoietic stem/progenitor cells. Sci Transl Med 2016;8(360):360ra134; doi: 10.1126/scitranslmed.aaf9336
46. Pattabhi S, Lotti SN, Berger MP, et al. In vivo outcome of homology-directed repair at the HBB gene in HSC using alternative donor template delivery methods. Mol Ther Nucleic Acids 2019;17:277–288; doi: 10.1016/j.omtn.2019.05.025
47. Lindeboom RGH, Vermeulen M, Lehner B, et al. The impact of nonsense-mediated mRNA decay on genetic disease, gene editing and cancer immunotherapy. Nat Genet 2019;51(11):1645–1651; doi: 10.1038/s41588-019-0517-5
48. Li C, Georgakopoulou A, Newby GA, et al. In vivo HSC prime editing rescues sickle cell disease in a mouse model. Blood 2023;141(17):2085–2099; doi: 10.1182/blood.2022018252
49. Shi D, Toyonaga S, Anderson DG. In vivo RNA delivery to hematopoietic stem and progenitor cells via targeted lipid nanoparticles. Nano Lett 2023;23(7):2938–2944; doi: 10.1021/acs.nanolett.3c00304
50. Breda L, Papp TE, Triebwasser MP, et al. In vivo hematopoietic stem cell modification by mRNA delivery. Science 2023;381(6656):436–443; doi: 10.1126/science.ade6967
51. Ferrari S, Naldini L. A step toward stem cell engineering in vivo. Science 2023;381(6656):378–379; doi: 10.1126/science.adj0997
52. Hsiau T, Conant D, Rossi N, et al. Inference of CRISPR edits from Sanger trace data. bioRxiv 2019;251082; doi: 10.1101/251082

Received: January 17, 2024
Accepted: September 03, 2024
Online Publication Date: October 18, 2024

B) Nasri M. & Ritter M. U. et al., 2024, *Molecular Therapy*

Molecular Therapy
Original Article

CRISPR-Cas9n-mediated *ELANE* promoter editing for gene therapy of severe congenital neutropenia

Masoud Nasri,[1,8] Malte U. Ritter,[1,8] Perihan Mir,[1] Benjamin Dannenmann,[1] Masako M. Kaufmann,[2,3,4] Patricia Arreba-Tutusaus,[1] Yun Xu,[1] Natalia Borbaran-Bravo,[1] Maksim Klimiankou,[1] Claudia Lengerke,[1] Cornelia Zeidler,[1,5] Toni Cathomen,[2,3] Karl Welte,[1,6] and Julia Skokowa[1,7]

[1]Department of Oncology, Hematology, Clinical Immunology, and Rheumatology, University Hospital Tübingen, 72076 Tübingen, Germany; [2]Institute for Transfusion Medicine and Gene Therapy, Medical Center – University of Freiburg, 79106 Freiburg, Germany; [3]Center for Chronic Immunodeficiency, Faculty of Medicine, University of Freiburg, 79106 Freiburg, Germany; [4]Spemann Graduate School of Biology and Medicine, University of Freiburg, 79106 Freiburg, Germany; [5]Pediatric Hematology and Oncology, Hannover Medical School, 30625 Hannover, Germany; [6]Department of Pediatric Hematology, Oncology and Bone Marrow Transplantation, Children`s Hospital, University Hospital Tübingen, 72076 Tübingen, Germany; [7]Gene and RNA Therapy Center (GRTC), University Hospital Tübingen, 72076 Tübingen, Germany

Severe congenital neutropenia (CN) is an inherited pre-leukemia bone marrow failure syndrome commonly caused by autosomal-dominant *ELANE* mutations (*ELANE*-CN). *ELANE*-CN patients are treated with daily injections of recombinant human granulocyte colony-stimulating factor (rhG-CSF). However, some patients do not respond to rhG-CSF, and approximately 15% of *ELANE*-CN patients develop myelodysplasia or acute myeloid leukemia. Here, we report the development of a curative therapy for *ELANE*-CN through inhibition of *ELANE* mRNA expression by introducing two single-strand DNA breaks at the opposing DNA strands of the *ELANE* promoter TATA box using CRISPR-Cas9D10A nickases—termed *MILESTONE*. This editing effectively restored defective neutrophil differentiation of *ELANE*-CN CD34$^+$ hematopoietic stem and progenitor cells (HSPCs) *in vitro* and *in vivo*, without affecting the functions of the edited neutrophils. CRISPResso analysis of the edited *ELANE*-CN CD34$^+$ HSPCs revealed on-target efficiencies of over 90%. Simultaneously, GUIDE-seq, CAST-Seq, and rhAmpSeq indicated a safe off-target profile with no off-target sites or chromosomal translocations. Taken together, *ex vivo* gene editing of *ELANE*-CN HSPCs using *MILESTONE* in the setting of autologous stem cell transplantation could be a universal, safe, and efficient gene therapy approach for *ELANE*-CN patients.

INTRODUCTION

Patients with severe congenital neutropenia (CN), an inherited pre-leukemia bone marrow failure syndrome, suffer from severe bacterial infections that generally occur shortly after birth.[1] The reason for these infections is a myeloid differentiation defect of hematopoietic stem and progenitor cells (HSPCs) with an almost complete inability to form mature neutrophils. In addition to defective granulopoiesis, CN patients are at risk of developing hematological malignancies, including myelodysplastic syndrome, acute myeloid leukemia (AML), and, in some rare cases, chronic myelomonocytic leukemia, acute lymphoblastic leukemia, or bi-phenotypic leukemia. Autosomal-dominant mutations in the *ELANE* gene encoding neutrophil elastase (NE) protein frequently cause CN.[1–3]

Since its clinical use in 1987, rhG-CSF[4] became the standard treatment option for CN patients. Although most *ELANE*-CN patients respond to daily treatment with subcutaneous injections of rhG-CSF, some do not, even at doses up to 50 μg/kg/d.[5] Some patients continue suffering from frequent infections despite rhG-CSF therapy; in others, especially in puberty or adulthood, rhG-CSF causes severe bone pain, leading to discontinuation of treatment and a subsequent high risk of developing severe infections.[1,5] The only potentially curative treatment available for CN is allogeneic hematopoietic stem cell (HSCs) transplantation, which, despite its benefits, still has a 3-year mortality rate of 17% and causes severe side effects in 21% of patients.[6] Thus, there is an unmet need for an alternative curative treatment for CN patients.

Understanding the pathophysiology of defective granulopoiesis in CN patients downstream of *ELANE* mutations is essential for developing alternative therapies. NE is a proteolytic enzyme of the neutrophil serine protease family whose members also include the proteases cathepsin G

Received 29 June 2023; accepted 28 March 2024;
https://doi.org/10.1016/j.ymthe.2024.03.037.

[8]These authors contributed equally

Correspondence: Masoud Nasri, Division of Translational Oncology, Department of Hematology, Oncology, Clinical Immunology and Rheumatology, University Hospital Tübingen, Otfried-Müller Strasse 10, 72076 Tübingen, Germany.
E-mail: masoud.nasri@med.uni-tuebingen.de
Correspondence: Malte U. Ritter, Division of Translational Oncology, Department of Hematology, Oncology, Clinical Immunology and Rheumatology, University Hospital Tübingen, Otfried-Müller Strasse 10, 72076 Tübingen, Germany.
E-mail: malte.ritter@med.uni-tuebingen.de

(CG), proteinase 3 (PRTN3), azurocidin 1 (AZU1), and serine protease 57 (PRSS57, previously referred to as NSP4).[7,8] These proteases, stored in cytoplasmic granules and secreted into extracellular and pericellular spaces upon cellular activation, are considered crucial components of bacterial defense.[8] *ELANE* mutations in CN patients are distributed throughout all five exons and introns (but mainly intron 4) of the *ELANE* gene, affecting different functional domains of the NE protein.[3,9] The ultimate mechanisms underlying the defective granulocytic differentiation of HSPCs with *ELANE* mutations are not yet fully understood. We and others have reported that the inhibition of HSPC proliferation and differentiation observed in CN patients harboring *ELANE* mutations is caused by an enhanced unfolded protein response (UPR) in the endoplasmic reticulum instigated by misfolded mutant NE protein.[10–13] Therefore, we recently hypothesized that *ELANE*-CN could be treated and its associated "maturation arrest" corrected by CRISPR-Cas9–sgRNA–mediated *ELANE* knockout.[14] Indeed, we reported that knocking out the *ELANE* gene in CN HSPCs successfully rescued defective granulopoiesis, an approach that was later validated by others.[15] However, editing *ELANE*'s coding sequence (CDS) region with CRISPR-Cas9 could introduce new *ELANE* variants in the CDS—an unwanted outcome of on-target editing.

Therefore, to mitigate potential safety concerns, it is beneficial to establish a universal strategy for modulating *ELANE* mRNA expression without targeting the CDS region of *ELANE*. There are multiple possible approaches for safely inhibiting the expression of a gene of interest, including RNA interference (RNAi), CRISPR interference (CRISPRi), and CRISPR-Cas9-based editing of gene enhancer regulatory elements. Such approach, previously described for targeting the enhancer region of the *BCL11A* gene to inhibit suppression of γ-globin, has been approved as a treatment for sickle cell disease and transfusion-dependent β-thalassemia (TDT).[16,17] Some studies have reported that introducing a double-strand break (DSB) using paired Cas9 nickases (Cas9n) greatly increases genome-editing precision, adding a safety factor.[18–23] Using nickase-based gene editing for gene therapy has also been shown to enhance the safety profile 50 to 1,000-fold.[21] Thus, replacing Cas9 with Cas9D10A/H840A nickases adds an extra level of safety in clinical gene therapy strategies. Although a dual-nickase strategy is generally thought to be less efficient, in the specific case of SpCas9D10A nickase (CRISPR-Cas9n), it has been shown that this approach can be as efficient or even more efficient in inducing double-stranded breaks than native Cas9, depending on the single guide RNA (sgRNA) design and the targeted genomic locus.[20]

In addition to genomic safety, assessing the functional safety of gene-edited cells is essential for *ex vivo* HSPCs-modified therapies. Given that *ELANE* mutations are autosomal dominant, the inability of the *ELANE*-KO approach to discriminate between wild-type and mutated alleles leads to reduced levels of both mutated and wild-type NE. Nevertheless, we recently found that eliminating mutated *ELANE* completely restored granulopoiesis despite simultaneous suppression of wild-type *ELANE* *in vitro* and *in vivo*, causing no harmful effects on neutrophil differentiation or functions, including reactive oxygen species (ROS) production, chemotaxis, and phagocytosis of Alexa 594–conjugated *Staphylococcus aureus* BioParticles.[14] *Elane*$^{-/-}$ mice also have average neutrophil counts and no defects in neutrophil maturation.[24–26] Moreover, neutrophils from patients with Papillon-Lefevre Syndrome (PLS), a rare autosomal-recessive syndrome caused by loss-of-function mutations in the *CTSC* (cathepsin C) gene locus (encoding dipeptidylpeptidase I [DPPI]) that leads to severe defects in neutrophil serine proteases, including NE, can effectively kill bacteria, such as *S. aureus* (gram positive) and *Escherichia coli* (gram negative).[27] These data suggest that, because of existing redundancies in the bactericidal mechanisms of neutrophils in humans, serine proteases are not essential for killing common bacteria, allowing us to conclude that therapeutic NE inhibition is safe and preserves neutrophil functions.

Here, we report the successful development of a universal and efficient approach for inhibiting *ELANE* mRNA expression by disrupting the regulatory region in the promoter upstream of the *ELANE* gene transcription start site (TSS). To establish this, we applied CRISPR-Cas9n and sgRNAs with excellent safety profiles, as assessed by GUIDE-seq, rhAmpSeq validation of off-targets, and CAST-seq of edited primary HSPCs. Editing *ELANE* in primary HSPCs of CN patients using this strategy led to successful granulocytic differentiation of edited cells *in vitro* and *in vivo*.

RESULTS

CRISPR-Cas9-based targeting of the *ELANE* TATA box inhibits *ELANE* transcription

CRISPR-Cas9-mediated gene editing of the *ELANE* CDS in CN patients' HSPCs, either for knockout or mutation-correction purposes, can lead to the generation of *de novo* mutations in subpopulations of cells and could potentially raise long-term safety concerns regarding its clinical application in the setting of autologous transplantation of gene-edited HSPCs. In particular, we previously demonstrated the presence of small undesired in-frame deletions and insertions in gene-edited cells after targeting exon 2 of *ELANE*.[14] Therefore, while the rationale underlying potential safety concerns of gene-editing approaches targeting the *ELANE* CDS will require further investigation in long-term *in vivo* studies, we here sought to circumvent this concern by designing an alternative CRISPR-Cas9-based genome-editing strategy that does not target the CDS of *ELANE* and so sidesteps these concerns.

We established a CRISPR-Cas9n-based gene-editing approach for inhibiting NE expression that targets the non-coding region of *ELANE* and thus does not generate new, unwanted *ELANE* variants. To screen the efficiency of different guides and their combinations, we engineered a NE-reporter cell line using THP-1 AML cells[28] expressing high levels of NE. We used a split nano luciferase reporter system (see materials and methods). It consists of a large (18 kDa) protein (LgBiT) and a small (11 amino acid) protein termed HiBiT,[29] the latter of which can be used to tag endogenous proteins. Adding LgBiT protein and the luciferase substrate furimazine to lysed HiBiT reporter cells for a tagged protein makes it possible to quantitatively determine the expression of the tagged protein by measuring its luminescence signal.[29] The HiBiT tag was fused to the N terminus of the NE protein by CRISPR-Cas9-mediated

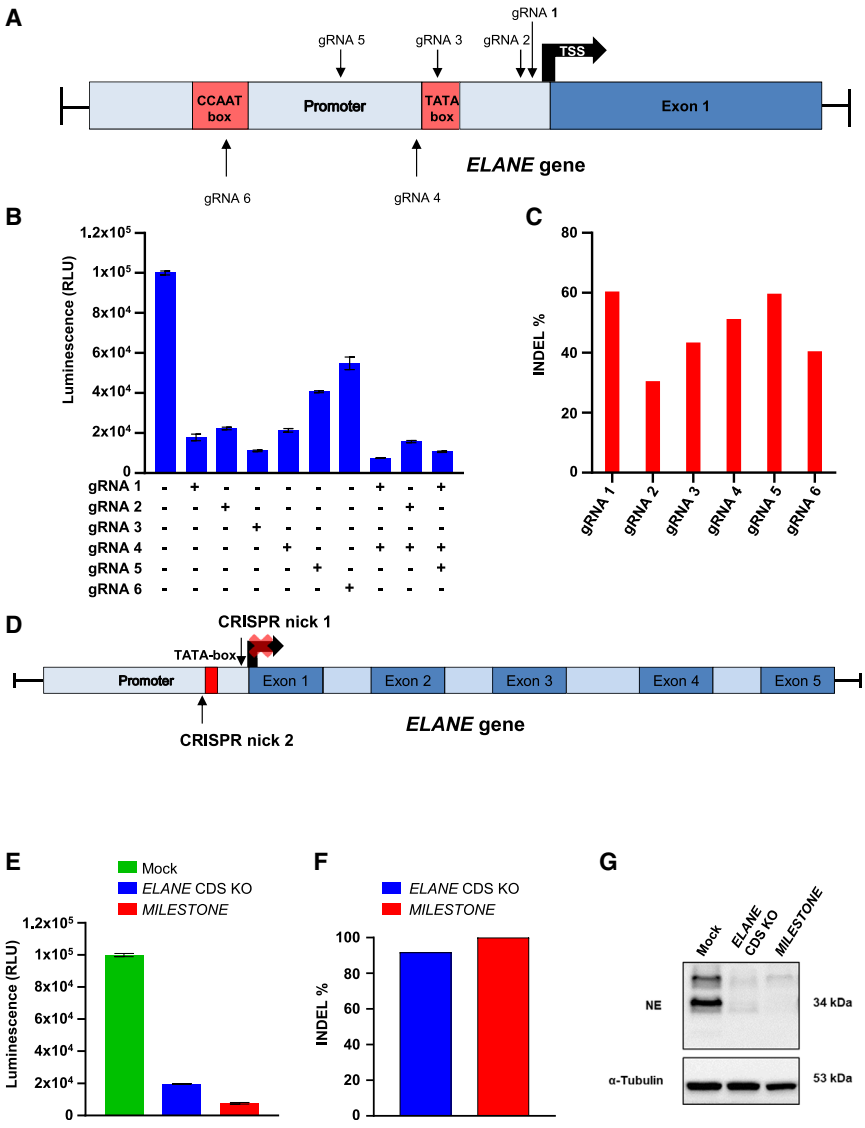

Figure 1. Development of a CRISPR-Cas9n-based gene-editing strategy to inhibit the *ELANE* transcription process by targeting its promoter's TATA box

(A) Schematic representation of the sgRNA selection. HiFi-Cas9 protein guided by sgRNAs targeting multiple areas of the *ELANE* gene promoter was used to find the region critical for repression of the *ELANE* mRNA transcription. CCAAT-box (−146 nucleotide from TSS) and TATA box −29 nucleotides from TSS were predicted using the eukaryotic promoter database (EPD) with p value <0.001. (B) Neutrophil elastase (NE)-HiBiT-tagged THP-1 single cell-derived cells were electroporated with the indicated sgRNAs. Seventy-two hours after electroporation, the bioluminescence signal of the HiBiT-tagged NE protein was assessed using a GloMax bioluminescent plate reader. Data represent means ± standard deviation (SD) from triplicates of a representative experiment. (C) On-target editing efficiency of each sgRNA 72 h post-electroporation of NE-HiBiT-tagged THP-1 cells of a representative experiment. (D) Schematic representation of the *MILESTONE* genome-editing strategy. Cas9D10A nickase guided by a pair of gRNAs targeting opposite strands of *ELANE* TATA box was used to introduce a double-strand break followed by small deletion to reduce the *ELANE* mRNA transcription. (E) NE-HiBiT-tagged THP1 cells were electroporated using *ELANE* CDS KO, *MILESTONE,* or Mock control. Seventy-two hours post-electroporation, the bioluminescence signal of the HiBiT-tagged NE protein was assessed using a GloMax bioluminescent plate reader. Data represent means ± SD from triplicates. (F) On-target editing efficiency of the *ELANE* CDS KO and *MILESTONE* 72 h post-electroporation of NE-HiBiT-tagged THP-1 cells. (G) Representative western blotting (WB) images of NE and α-tubulin protein expression are depicted. NE-HiBiT-tagged THP1 cells were electroporated using *ELANE* CDS KO or *MILESTONE*. Seventy-two hours post-electroporation, western blotting analysis of the NE protein was performed.

homology-directed repair (HDR), as described in materials and methods. A pure single-cell-derived clone of the NE-reporter THP-1 cell line was successfully generated by limiting dilutions on the bulk-edited cell population. This was followed by screening luminescence levels of single-cell-derived populations after 3 weeks of culture by assessing luminescence signals, with verification by Sanger sequencing (Figures S1A–S1C). The TSS and promoter motifs of the *ELANE* gene were previously identified using the synergistic activation mediator (SAM) web tool (http://sam.genome-engineering.org)[30] and the eukaryotic promoter database (EPD).[31] Combining these publicly available data, we designed six sgRNAs targeting nucleotides −2 to −146 bp relative to the *ELANE* TSS. We screened editing results obtained using sgRNAs 1–6 and the sgRNA combinations 1 + 4, 2 + 4, and 1 + 4 + 5 using HiFi Cas9-based gene editing (Figure 1A; Figure S1D). Although all selected sgRNAs reduced NE expression, the combination of sgRNAs 1 and 4, targeting the predicted TATA box (Goldberg-Hogness box) at position −29 bp relative to the TSS, led to the most pronounced reduction in NE levels according to the measured luminescent signal (Figure 1B). sgRNAs on-target efficiencies assessed by applying the DECODR (Deconvolution of Complex DNA Repair) algorithm[32] to Sanger sequencing traces of gene-edited THP-1 cells obtained 72 h post-electroporation were over 50% (Figure 1C). To implement an extra layer of safety in the *ELANE*-knockdown procedure, we used a double-nickase Cas9D10A strategy for sgRNA 1 (nick 1) and sgRNA 4 (nick 2), to target opposite strands of the *ELANE* promoter TATA box, thereby introducing a DSB that led to deletions that reduced the efficiency of *ELANE* mRNA transcription (Figure 1D). We termed the proposed strategy *MILESTONE*: Modifying *ELANE* Goldberg-Hogness box to inhibit expression.

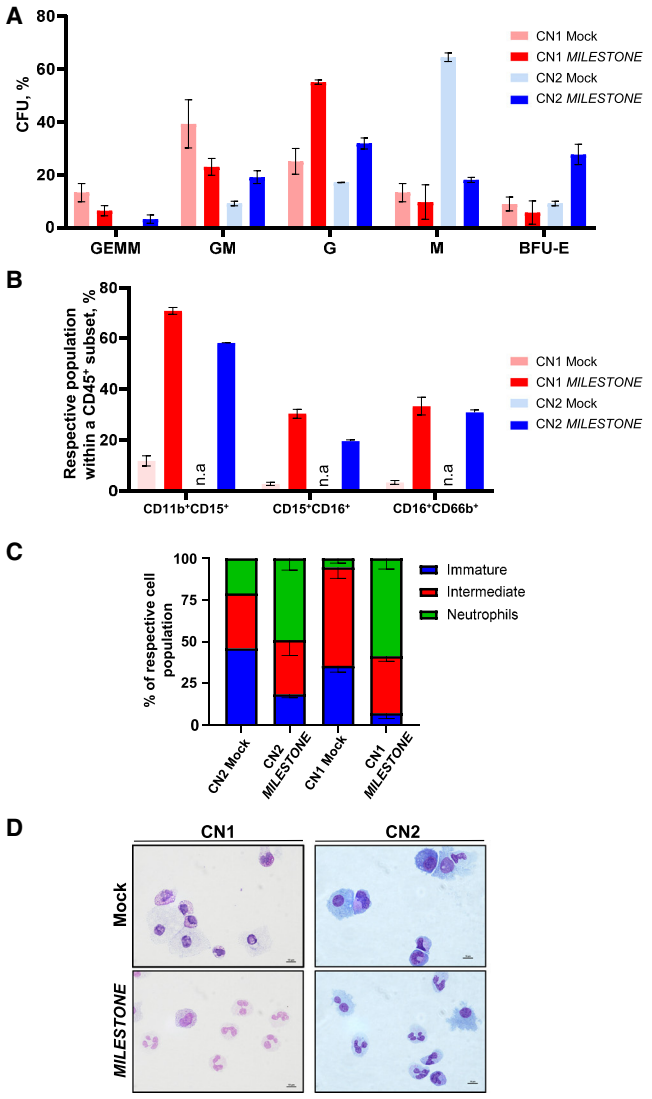

Figure 2. Restored granulocytic differentiation of *MILESTONE*-edited primary *ELANE*-CN HSPCs

(A) Colony-forming unit (CFU) assay of gene-edited *ELANE*-CN CD34$^+$ HSPCs (n = 2) on day 14 of differentiation (CFU-GEMM: granulocytes, erythrocytes, monocytes, megakaryocytes; CFU-GM: granulocytes, monocytes; CFU-G: granulocytes; CFU-M: monocytes. BFU E: burst-forming unit–erythroid. Data represent means ± SD from duplicates. (B) Granulocytic differentiation of *MILESTONE*-edited *ELANE*-CN CD34$^+$ HSPCs (n = 2) was assessed by liquid culture differentiation after 14 days of culture analyzing neutrophilic surface marker expression by flow cytometry. Data represent means ± SD from duplicates. n.a = not applicable. (C) May-Grunwald-Giemsa staining of *in vitro* differentiated cells from *ELANE*-CN CD34$^+$ HSPCs was conducted on day 14, allowing morphologic discrimination of the cells. Data represent means ± standard deviation (SD) from duplicates except for the CN2 mock which, due to the severity of the phenotype, only yielded enough cells for one cytopsin. (D) Representative cytopsin images of May-Grunwald-Giemsa staining of *ELANE*-CN HSPCs derived from the *in vitro* neutrophil differentiation culture on day 14 are depicted.

We compared *MILESTONE* with a previously reported *ELANE* CDS knockout (CDS KO) strategy[14] by measuring the luminescence signal of NE protein in NE-reporter THP-1 cells, used as a readout of NE protein levels 72 h post-electroporation. We found that *MILESTONE* efficiently decreased NE protein levels compared with Mock-electroporated cells (Figure 1E). The editing efficiencies of *ELANE* CDS KO and *MILESTONE* approaches were 91.8% and 100%, respectively, as assessed by applying the DECODR algorithm to Sanger sequencing traces of edited THP-1 cells obtained 72 h post-electroporation (Figure 1F). In a separate experiment, western blot analyses using an NE-specific antibody confirmed the reduction in NE levels after *ELANE* editing (Figure 1G).

Collectively, these findings demonstrate the successful development of a novel gene-editing strategy for knocking down *ELANE* mRNA expression. This strategy prevents the emergence of *de novo ELANE* mutations from INDELs or novel splice variants induced by INDELs in the *ELANE* CDS, as described by Tuladhar et al.[33]

MILESTONE restores granulocytic differentiation of primary *ELANE*-CN CD34$^+$ HSPCs

To further evaluate the clinical applicability of *MILESTONE* as a treatment option for *ELANE*-CN, we performed *MILESTONE* editing on primary bone marrow-derived CD34$^+$ HSPCs from two *ELANE*-CN patients—one, CN1, harboring p.Ala57Val (GenBank: NM_001972.4) and the other, CN2, bearing p.Ala79_Arg81del (GenBank: NM_001972.4) *ELANE* mutations—and evaluated their granulocytic differentiation using colony-forming unit (CFU) and *in vitro* liquid culture neutrophil differentiation assays. CFU assays showed a remarkable increase in granulocytic colony-forming units (CFU-G) in the *MILESTONE* group compared with the Mock-electroporated control group (Figure 2A). In line with this, *in vitro* granulocytic liquid culture differentiation assays revealed that granulopoiesis was restored on day 14 of differentiation compared with Mock-electroporated cells, assessed based on the percentage of cells expressing the pan-granulocyte marker status, CD45$^+$CD11b$^+$CD15$^+$, and neutrophils with the two neutrophil-specific marker combinations, CD45$^+$CD15$^+$CD16$^+$ and CD45$^+$CD16$^+$CD66b$^+$[34] (Figures 2B and S2A). The phenotype of the CN2 patient was extremely severe and resulted in very low numbers of cells in a control Mock group generated on day 14 of granulocytic differentiation, which were not sufficient for flow cytometry analysis. Remarkably, even these cells differentiated efficiently into neutrophils following *ELANE* editing with *MILESTONE*. A morphological examination of cytospin preparations of cells of both CN patients on day 14 of culture confirmed restoration of granulopoiesis upon *MILESTONE* treatment compared with controls (Figures 2C and 2D). The editing efficiency of *MILESTONE* was greater than 90%, as assessed by applying the DECODR algorithm to Sanger sequencing data for cells obtained on day 14 of differentiation (Figures S3A and S3B). These latter results were further confirmed by next-generation sequencing of rhAMPseq-generated targeted PCR amplicons from gene-edited cells from CN1 patient on day 7 of differentiation, as analyzed using the CRISPResso tool[35] (Figures S4A–S4C). Taken together, the *in vitro* neutrophilic differentiation data of

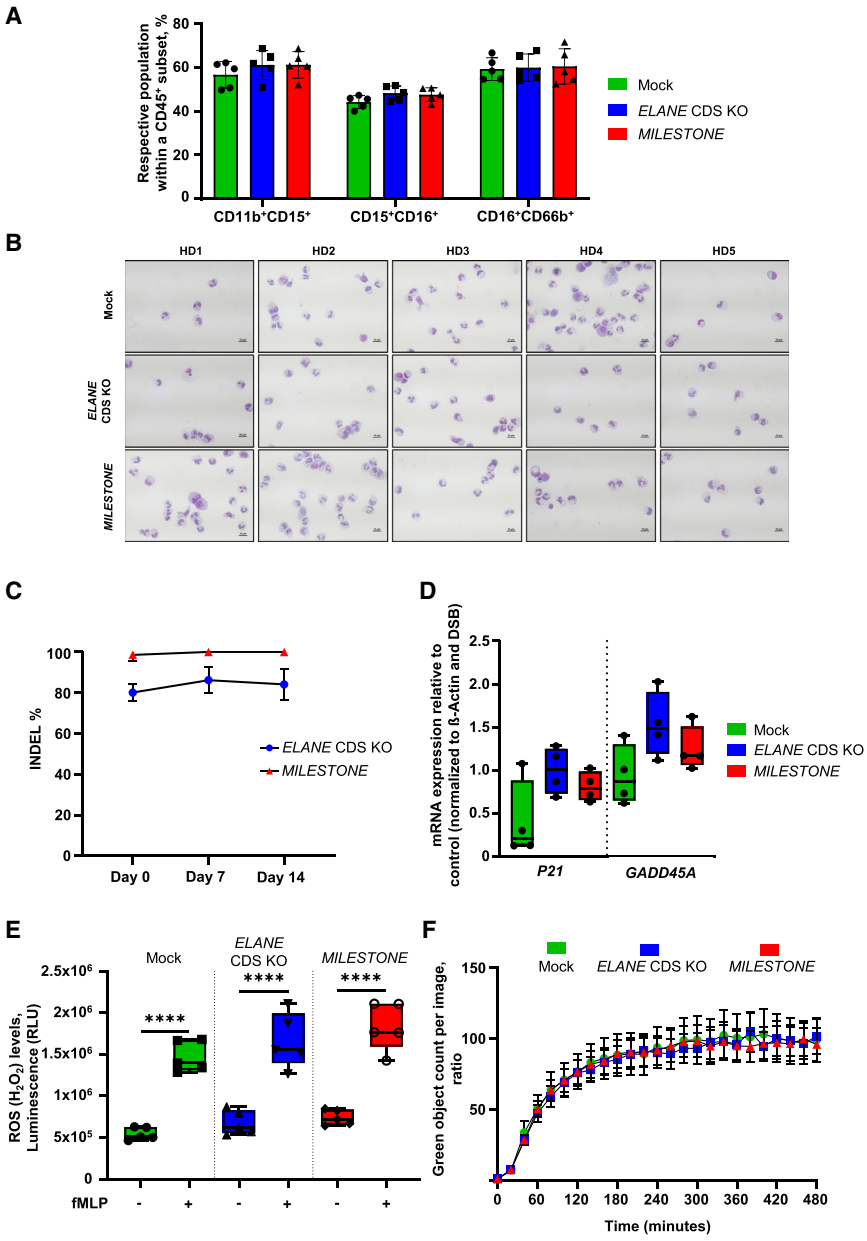

Figure 3. Healthy donors' primary HSPCs granulocytic differentiation remained unaffected upon applying *MILESTONE*

(A) Granulocytic differentiation of gene-edited CD34$^+$ HSPCs of healthy donors was assessed by analyzing neutrophilic surface marker expression using flow cytometry. Data represent means ± SD from five biological replicates. (B) Representative cytopsin images of May-Grunwald-Giemsa staining of *in vitro* differentiated neutrophils from CD34$^+$ HSPCs of healthy donors at day 14 are depicted. (C) On-target editing efficiency of the *ELANE* CDS KO, or *MILESTONE*-edited CD34$^+$ HSPCs of healthy donors 4 days post-electroporation (day 0 of *in vitro* differentiation), 7 and 14 (*in vitro* differentiation end time point). Data represent means ± SD from five biological replicates. (D) qRT-PCR analysis of mRNA expression of *P21* and *GADD45A* in HSPCs collected 48 h post-electroporation of the Mock, *ELANE* CDS KO, or *MILESTONE*-edited healthy donors CD34$^+$ HSPCs. Data were normalized to non-electroporated cells, β-actin, and double-strand breaks. Data represent means ± SD from four biological replicates. (E) Level of hydrogen peroxide (H_2O_2) reactive oxygen species (ROS), measured after stimulation of *in vitro* differentiated Mock, *ELANE* CDS KO, and *MILESTONE*-derived neutrophils (see A–C) with formylmethionine-leucyl-phenylalanine (fMLP) for 30 min. Data represent means ± SD from five biological replicates. ****$p < 0.0001$, unpaired t test. (F) Phagocytosis kinetic of pHrodo green *S. aureus* bioparticles of *in vitro* differentiated Mock, *ELANE* CDS KO, and *MILESTONE* neutrophils derived from CD34$^+$ HSPCs of healthy donors at day 14 of differentiation, using IncuCyte ZOOM System. Data represent means ± SD from five biological replicates.

MILESTONE-edited cells from two *ELANE*-CN patients confirmed previous observation by our group[14] and others[15] that inhibition of *ELANE* expression in HSPCs from *ELANE*-CN patients effectively restores granulocytic differentiation.

MILESTONE DOES NOT AFFECT GRANULOCYTIC DIFFERENTIATION OF PRIMARY HSPCs FROM HEALTHY DONORS

To investigate whether *MILESTONE* has any adverse effects on granulopoiesis or neutrophil functions *in vitro*, we electroporated CD34$^+$ HSPCs from five healthy donors with the CRISPR-Cas9 RNP complex of *ELANE* CDS KO or *MILESTONE* and processed cells for *in vitro* neutrophilic differentiation 4 days later. We found that knockout or inhibition of *ELANE* expression did not impair neutrophil differentiation compared with Mock-electroporated cells (Figure 3A). May-Grunwald-Giemsa staining of neutrophils differentiated *in vitro* from CD34$^+$ HSPCs of healthy donors at day 14, either with *ELANE* CDS knockout or *MILESTONE* editing, also confirmed this observation (Figure 3B). The editing efficiency of *ELANE* CDS KO averaged 80%, 86%, and 84% on days 0, 7, and 14 of differentiation, respectively. *MILESTONE*'s editing efficiency was greater than 99% at the start of *in vitro* differentiation and remained stable through day 14 (Figures 3C and S5A). Similar results were also obtained with targeted next-generation sequencing (NGS), which showed an editing efficiency for *MILESTONE* of 97% on day 0, as analyzed with the Cas-analyzer tool[36] (Figure S5B).

To evaluate TP53-triggered DNA damage responses upon genome editing, we measured the mRNA expression levels of the TP53 targets, *P21* and *GADD45A*, 48 h after electroporation. No significant

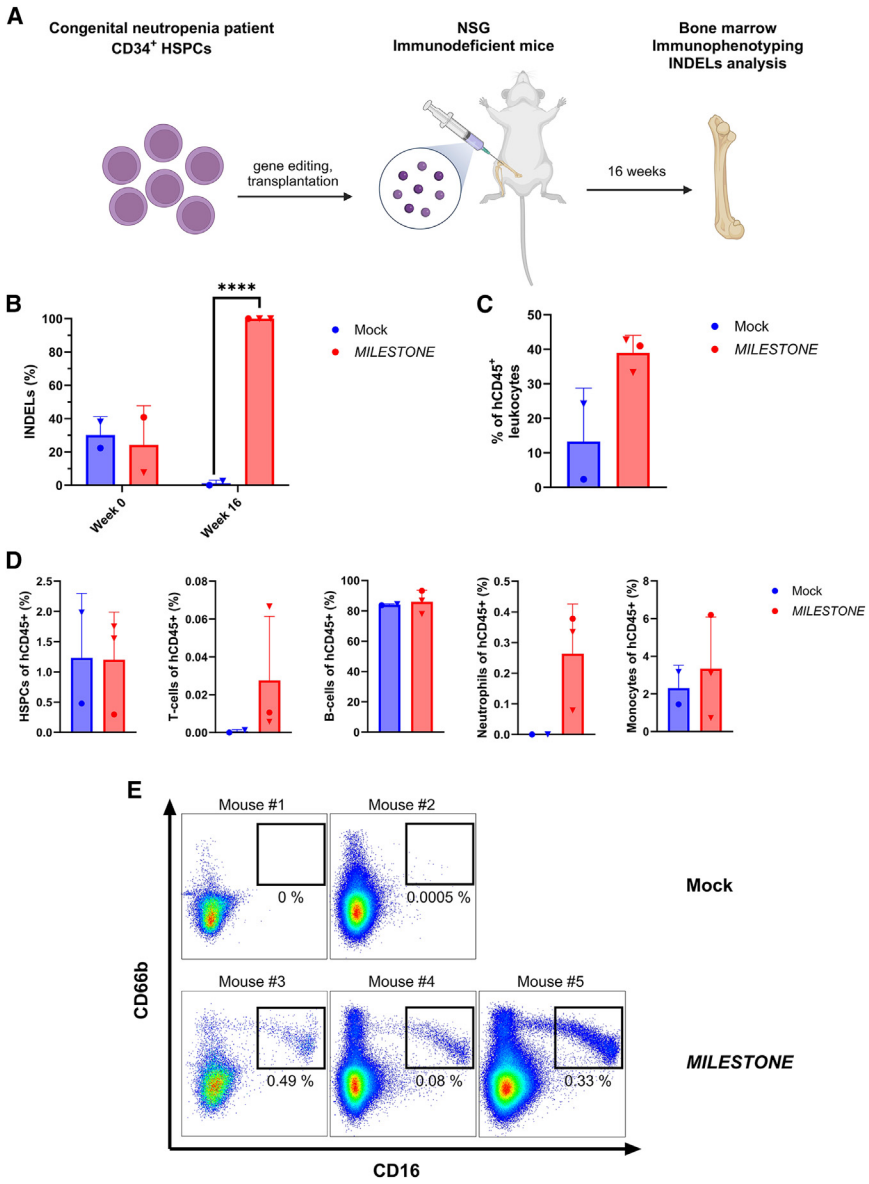

Figure 4. Xenotransplantation of *MILESTONE*-edited *ELANE*-CN HSPCs

(A) Schematic workflow of *in vivo* experiments. Depicted are genome editing, intra-femoral injection of edited cells, flow cytometry-based immunophenotyping, and INDELs analysis of bone marrow 16 weeks after transplantation. Created with BioRender.com. (B) INDELs frequencies observed 72 h post *ex vivo* editing (week 0) and at the experimental endpoint 16 weeks post-transplantation in engrafted human bone marrow cells (CN3). Data represent means ± SD from two independent experiments. $^{****}p < 0.0001$, unpaired t test. (C) Engraftment efficiency of human CD45$^+$ cells 16 weeks post-transplantation. Data are shown as means ± SD, and dots represent individual animals. (D) Frequency of HSPCs (mCD45$^-$hCD45$^+$hCD19$^-$hCD3$^-$hCD33$^-$hCD66b$^-$hCD34$^+$), T cells (mCD45$^-$hCD45$^+$hCD19$^-$hCD3$^+$), B cells (mCD45$^-$hCD45$^+$hCD19$^+$hCD3$^-$), neutrophils (mCD45$^-$hCD45$^+$hCD19$^-$hCD3$^-$hCD33$^{+/-}$hCD66b$^+$hCD16$^+$), and monocytes (mCD45$^-$hCD45$^+$hCD19$^-$hCD3$^-$hCD33$^+$hCD14$^+$) shown as the percentage of total human CD45$^+$ cells in the bone marrow. Data are shown as means ± SD, and dots represent individual animals. (E) Representative FACS images showing CD16$^+$CD66b$^+$ mature neutrophils (black gate) in Mock or *MILESTONE* recipient mice. The percentage of neutrophils in human CD45$^+$ cells is shown below the gate. Symbols mark individual mice. Symbols with the same shape mark animals from the same experiment.

difference was observed for *ELANE* CDS KO or *MILESTONE* compared with control Mock-electroporated cells (Figure 3D).

We further analyzed the *in vitro* generated neutrophils for their functional capabilities. We first assessed ROS in formyl methionyl-leucyl-phenylalanine (fMLP)-activated neutrophils by measuring H_2O_2 levels and found that both *ELANE* CDS KO and *MILESTONE* neutrophils were able to generate ROS at levels comparable to Mock-electroporated cells (Figure 3E). We next assessed phagocytosis using live-cell imaging of neutrophils incubated with pHrodo Green *S. aureus* bioparticles using the IncuCyte ZOOM system. We observed similar phagocytosis activity in Mock, *ELANE* CDS KO, or *MILESTONE* neutrophils (Figure 3F).

Next, we evaluated whether *MILESTONE* gene-editing affected mRNA expression levels of *PRTN3* and *AZU1*, genes adjacent to the *ELANE* gene that encode two other serine proteases. To this end, we measured *ELANE, PRTN3,* and *AZU1* mRNA expression in neutrophils derived from liquid culture-differentiated *MILESTONE*-edited HSPCs from two healthy donors compared with that in the Mock group. Meanwhile, *ELANE* mRNA expression was markedly reduced in *MILESTONE*-edited neutrophils compared with control cells, and *PRTN3* and *AZU1* levels remained unaffected (Figures S6A–S6C).

MILESTONE editing enables granulocytic differentiation of primary *ELANE*-CN HSPCs in immune-deficient NSG mice

To assess the effect of *MILESTONE* editing on engraftment, proliferation, and granulocytic differentiation of edited HSPCs *in vivo*, we performed xenotransplantation studies in immune-deficient NSG (NOD SCIDγ) mice.[37,38] We analyzed their bone marrow 16 weeks post-transplantation (Figure 4A; Figure S7A). As a control, cells were edited with a sgRNA assembled with HiFi Cas9 targeting the safe harbor locus, AAVS1, within the *PPP1R12C* gene (Mock control). Two independent experiments were performed with primary

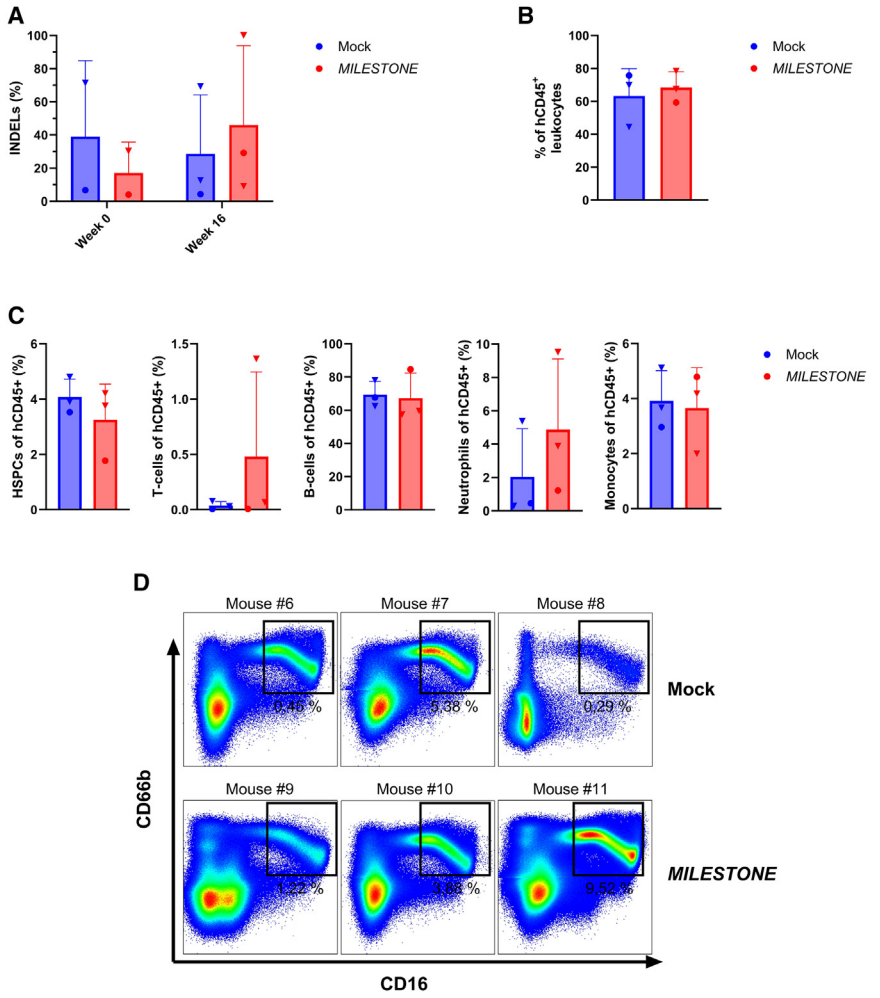

Figure 5. Xenotransplantation of *MILESTONE*-edited healthy donor primary HSPCs

(A) INDELs frequencies observed 72 h post *ex vivo* editing (week 0) and at experimental endpoint 16 weeks post-transplantation in engrafted human bone marrow cells (HD8 and HD9). Data represent means ± SD from two independent experiments. (B) Engraftment efficiency of human $CD45^+$ cells 16 weeks post-transplantation. Data are shown as means ± SD, and dots represent individual animals. (C) Frequency of human HSPCs ($CD45^+CD19^-CD3^-CD33^-CD66b^-CD34^+$), T cells ($CD45^+CD19^-CD3^+$), B cells ($CD45^+CD19^+CD3^-$), neutrophils ($CD45^+CD19^-CD3^-CD33^{+/-}CD66b^+CD16^+$), and monocytes ($CD45^+CD19^-CD3^-CD33^+CD14^+$) shown as the percentage of total human $CD45^+$ cells in bone marrow. Data are shown as means ± SD, and dots represent individual animals. (D) Flow cytometry analysis showing $CD16^+CD66b^+$ mature neutrophils (black gate) in Mock or *MILESTONE* recipient mice. The percentage of neutrophils in human $CD45^+$ cells is shown below the gate. Symbols mark individual mice. Symbols with the same shape mark animals from the same experiment.

$CD34^+$ HSPCs from one *ELANE*-CN patient (*ELANE* mutation GenBank: NM_001972.4, p.Val101Glu) and two healthy donors. *Ex vivo* gene-editing efficiency of the CN patient's HSPCs before transplantation was comparable between Mock (30.2%) and *MILESTONE* (24.3%) groups. However, editing in engrafted human leukocytes differed strongly and significantly ($p < 0.001$) between Mock- and *MILESTONE*-edited cells. Whereas Mock-edited cells engrafted poorly, with fewer than 5% of cells in the AAVS1 locus carrying INDELs, *MILESTONE*-edited cells showed a strong engraftment advantage, with 100% INDELs in all recipient mice (Figure 4B). We further found that engraftment of human $CD45^+$ leukocytes was increased in *MILESTONE*-edited recipient mice compared with that in the control group (Figure 4C). In line with this superior engraftment, we found that the percentage of neutrophils was also markedly increased in *MILESTONE*-edited cells compared with that in the control group (Figures 4D and 4E). No significant differences were observed in other cellular compartments, including HSPCs, T cells, B cells, and monocytes (Figure 4D). *Ex vivo*, *MILESTONE* editing resulted in editing efficiencies in healthy donor HSPCs comparable to those in CN HSPCs. *In vivo*, Mock- and *MILESTONE*-edited healthy donor HSPCs showed engraftment potentials that were similar to each other and slightly higher than *MILESTONE*-edited CN HSPCs (Figures 5A and 5B). Furthermore, *MILESTONE* editing did not severely alter the distribution of the engrafted immature and mature populations compared with that in the Mock control group (Figure 5C). A direct comparison of Mock- and *MILESTONE*-edited cells showed no differences in neutrophil maturation that exceeded inter-mouse differences (Figure 5D). A comparison of neutrophil maturation between Mock-edited healthy cells and *MILESTONE*-edited CN HSPCs further highlighted the fact that the *MILESTONE* strategy fully restored granulocytic differentiation in CN HSPCs to the levels of healthy HSPCs *in vivo* (Figures 4E and 5D). These data further support our *in vitro* observations and are consistent with previously published observations by Rao et al.[15] who reported successful restoration of *in vivo* neutrophilic differentiation upon *ELANE* KO in an *ELANE*-CN xenograft mouse model, that was established based on gene edited healthy donor HSPCs.

The safety profile of the *MILESTONE* approach

Currently, no algorithms are available for *in silico* off-target prediction of CRISPR-Cas9n double nickases. Therefore, we performed two independent *in silico* off-target predictions for *MILESTONE* guide RNAs, calculating up to four mismatches and annotating the predicted potential of off-target sites using CRISPRitz and CRISPRme tools[39,40]; we identified 110 targets for nick 1 sgRNA and 85 targets for nick 2 sgRNA (Figure 6A). Since the simultaneous activity of both nickases on opposing strands of the genome is

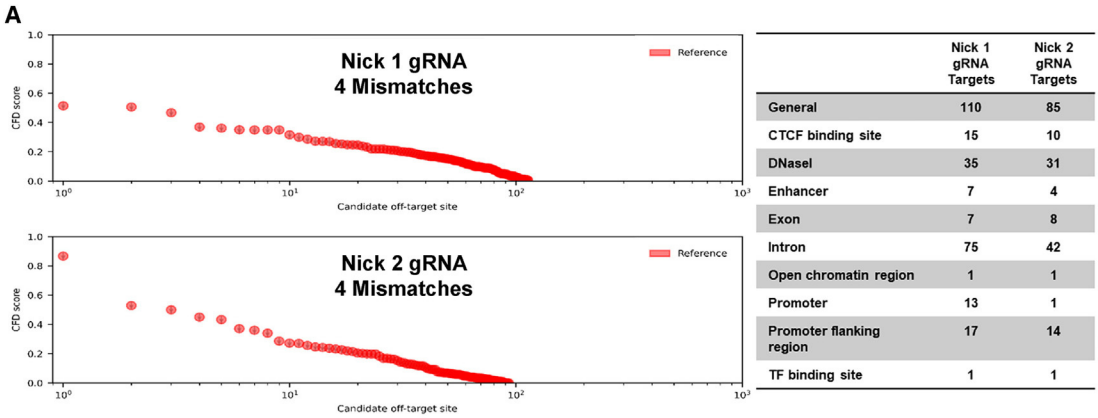

	Nick 1 gRNA Targets	Nick 2 gRNA Targets
General	110	85
CTCF binding site	15	10
DNaseI	35	31
Enhancer	7	4
Exon	7	8
Intron	75	42
Open chromatin region	1	1
Promoter	13	1
Promoter flanking region	17	14
TF binding site	1	1

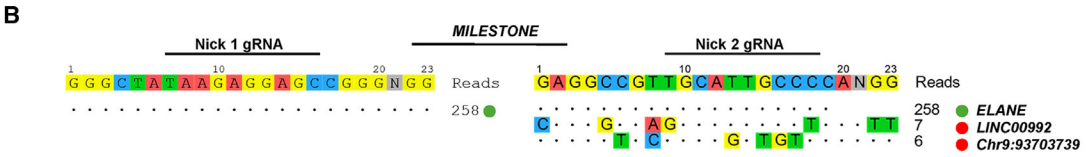

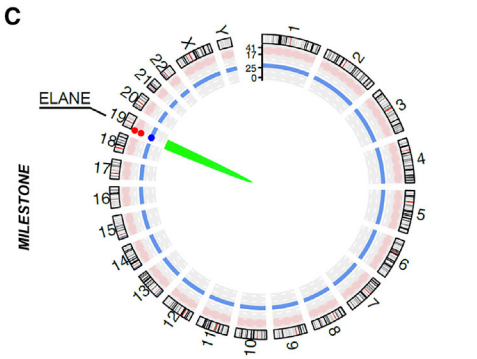

chromosome	start	end	read	hits
chr19	846824	858793	1679524	6922
chr19	861946	865556	20320	38

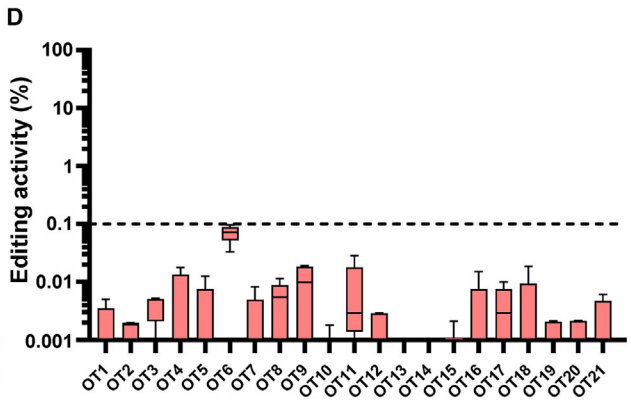

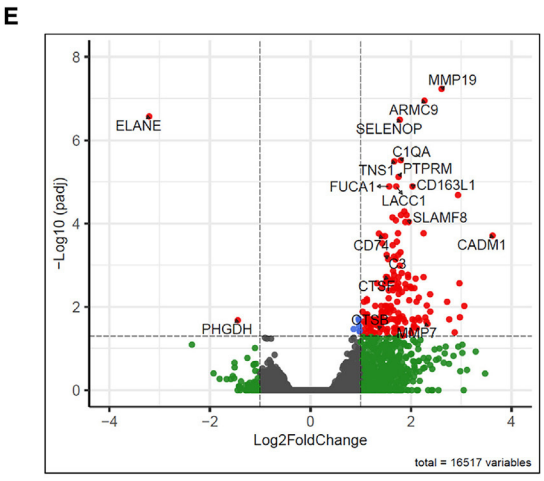

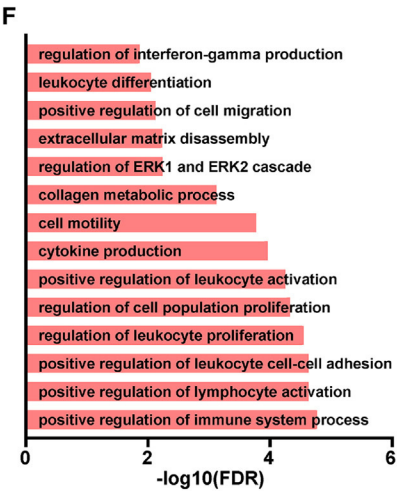

(legend on next page)

necessary to introduce a DNA DSB, we used two genome-wide off-target profiling methods, GUIDE-Seq and CAST-Seq, in our study. With GUIDE-Seq, we profiled the *MILESTONE* approach in primary $CD34^+$ HSPCs from one healthy donor. We observed two potential off-target sites for Nick2 sgRNA—LINC00992 (Long Intergenic Non-Protein Coding RNA 992) and Chr9:93703739, a non-coding intergenic region—which contained six or seven mismatches relative to the on-target site (Figure 6B). To determine whether genome editing triggered structural variations, we additionally performed a quantitative evaluation of chromosomal rearrangements in *MILESTONE*-edited primary $CD34^+$ HSPCs using CAST-Seq,[41,42] which detected on-target aberrations but no translocations (Figure 6C). We also performed *in silico* off-target prediction, GUIDE-seq, and CAST-seq for our previously reported *ELANE* CDS KO approach[14] and identified seven potential off-target sites starting with four mismatches compared with the target site. In contrast, CAST-seq revealed large deletions/inversions at the on-target site but no translocations (Figures S8A–S8C).

For off-target site validation, we designed an rhAmpSeq panel that included all potential off-target sites identified by GUIDE-seq and CRISPRitz based on the CFD (cutting frequency determination) score for both *ELANE* CDS KO and *MILESTONE* (Table S1). Genomic DNA from five healthy donors 4 days post-nucleofection with *ELANE* CDS KO or *MILESTONE* gene-editing (Figures 3C and S5A) was used for rhAmpSeq library preparation and NGS. The analysis of sequencing data with CRISPECTOR[43] revealed INDELs above the noise threshold in GUIDE-seq–identified off-target site 5 (OT5) (Chr5:1762021-1762044) at an average of 0.8% in all five biological samples (Figure S8D). We found no INDELs in the *MILESTONE* off-target site that exceeded threshold levels, indicating a high specificity that was even higher than the already specific *ELANE* CDS KO approach (Figure 6D).

To further investigate the specificity of the *MILESTONE* approach in reducing *ELANE* mRNA expression levels, we performed RNA sequencing of neutrophils generated by *in vitro* liquid culture differentiation of *MILESTONE*- or Mock-edited primary bone marrow $CD34^+$ HSPCs from two healthy donors (HD12 and HD13) (Figures S9A–S9C). Differentially expressed genes (DEGs) between *MILESTONE*- and Mock-electroporated neutrophils were extracted by analyzing RNA sequencing results using the nf-core pipeline (Figures 6E; Table S2). This analysis revealed a more than 9-fold (log2-fold = 3.21) downregulation of *ELANE* mRNA expression, with an adjusted p value of 2.68×10^{-7}. Only one additional gene, *PHGDH* (phosphoglycerate dehydrogenase), was significantly downregulated (log2-fold 1.44, adjusted p value 2.10×10^{-2}). *PHGDH,* which is involved in L-serine synthesis, should be further investigated to determine whether its downregulation is an outcome of *MILESTONE* or indicates a feedback mechanism related to the downregulation of NE. We also evaluated whether the *MILESTONE* approach affected mRNA levels of the *ELANE*-neighboring genes, *AZU1*, *PRTN3*, *CFD,* and *MED16*, which lie within an approximately 68-kb genetic; we found that none of them was among identified DEGs (Table S2). Functional enrichment analysis of upregulated genes among the list of DEGs using the ShinyGO web server[44] (database version 0.80) identified "positive regulation of immune system process," "positive regulation of leukocyte proliferation," "cytokine production," and "positive regulation of cell migration" as enriched biological processes activated upon inhibition of *ELANE* expression (Figures 6F; Table S3). The fact that only one gene, besides *ELANE*, is downregulated by less than 2 log2fold supports our hypothesis that *ELANE* is not an essential gene for activating transcriptional programs, including those critical for neutrophil development and activation.

DISCUSSION

This study presents a pioneering approach for suppressing *ELANE* expression without introducing novel variants in the CDS of the edited gene utilizing a straightforward and highly effective method termed *MILESTONE*. This method, based on a recent proof-of-principle—restoration of granulopoiesis in CN HSPCs through *ELANE* knockout targeting its CDS—that we and others recently described,[14,15] successfully restored granulocytic differentiation of *ELANE*-CN HSPCs both *in vitro* and *in vivo*. The main advantage of *MILESTONE* editing is that it does not modify the *ELANE* CDS and thus avoids creating new mutant variants of *ELANE* and NE protein, which can be deleterious for HSPC functions. Additionally,

Figure 6. *MILESTONE* safety profile

(A) *In silico* off-target profiling of each gRNA, performed using CRISPRme tool to determine potential off-target sites for up to four mismatches with calculated cutting frequency determination (CFD) score of each possible off-target site according to the human reference genome assembly GRCh38. The genomic region functional annotation of off-target sites was annotated using the CRISPRitz tool. (B) Genome-wide profiling of off-target cleavage in *MILESTONE*-edited healthy donor $CD34^+$ HSPCs (HD10) using GUIDE-seq. The *ELANE* promoter target sequence is shown in the top line, with cleaved sites underneath. Mismatches to the on-target site are highlighted in color. GUIDE-seq read counts are displayed to the right of each site. The on-target site is marked with a green circle, and off-target sites are marked with a red circle. All the genomic coordinates are based on human reference genome assembly GRCh37. (C) CAST-Seq for the quantitative evaluation of chromosomal rearrangements in *MILESTONE*-edited healthy donor $CD34^+$ HSPCs (HD11). The Circos plot shows on-target site aberrations (ON, green). From the outer to the inner layer, black rectangles show the DNA location of the translocation sites. All the genomic coordinates are based on human reference genome assembly GRCh38. (D) Validation of potential off-target sites determined by rhAmpSeq in healthy donor $CD34^+$ HSPCs (HD1-5). NGS data were analyzed using the CRISPECTOR pipeline. Data represent means ± SD from five independent experiments. (E) Volcano plot showing differentially expressed genes (DEGs) in *MILESTONE*-edited terminally differentiated neutrophils derived from healthy donor $CD34^+$ HSPCs ($n = 2$). The x axis shows the log2 fold change (magnitude of change), and the y axis shows the −log10 adjusted p value (statistical significance). Colors represent the significance of the genes in terms of p value and log2 fold change. Selected differentially expressed genes are annotated. (F) Functional enrichment analysis using a list of significantly upregulated genes in *MILESTONE*-edited terminally differentiated neutrophils from healthy donor $CD34^+$ HSPCs ($n = 2$). A complete list of pathways is provided in Table S3. Data are displayed as −log10 adjusted p value (FDR).

using the nickase variant of Cas9 nuclease reduces the probability of unintended double-strand breaks, which can lead to INDELs at off-target sites. Our novel approach for modifying the expression of a gene with a gain-of-function mutation through targeting the promoter region of the target gene using Cas9 nickases is not only uniquely applicable to *ELANE*; it can be applied to many other genetic syndromes caused by gain-of-function mutations in genes with redundant functions. Because *ELANE* mutations are autosomal dominant, neither CDS- nor promoter-based approaches discriminate between wild-type and mutated alleles of *ELANE*, simultaneously knocking out both forms of the NE protein. Despite strongly reducing NE levels, *MILESTONE* did not affect the functions of neutrophils differentiated from gene-edited cells, a finding in line with our previous observations on CN patients' *ELANE*-KO gene-edited HSPCs[14] and reports on PLS patients[27] and *Elane*$^{-/-}$ mice.[24,26,45] Moreover, incomplete gene-editing efficiency and the consequent residual expression of *ELANE* mRNA in *MILESTONE*-edited cells *in vivo* will result in some neutrophils that express normal (unedited cells) in addition to those that express reduced (edited cells) levels of NE, thus sustaining bactericidal activity. Simultaneously, our data argue for the dose-dependent effects of mutated NE on granulocytic differentiation—even with remaining levels of mutated NE, HSPCs could efficiently differentiate into mature neutrophils. The high level of the *ELANE* gene editing achieved by *MILESTONE* suffices to reach the current estimate for a therapeutic threshold of *ELANE* knockout of 11%, as evaluated in healthy individuals with mosaic congenital neutropenia-causing *ELANE* mutations.[15] Whether the remaining mutant *ELANE* may still contribute to leukemogenic transformation in CN patients remains to be investigated. Because *MILESTONE* successfully restored granulopoiesis, we assume that the probability of developing leukemia in *MILESTONE*-treated patients will be at least reduced because these patients will not require chronic therapy with rhG-CSF anymore, and the endogenous G-CSF levels are expected to normalize.

To achieve clinical translation, gene-editing technology must demonstrate both safety and efficacy.[23,46,47] Our comprehensive analysis of on-target and off-target activity employing rhAmpSeq, GUIDE-seq, and CAST-seq revealed a high on-target editing efficiency and superior off-target profile of MILESTONE editing. In contrast, this analysis identified INDELs in OT5 for the *ELANE* CDS KO guide. Together, these results underscore the enhanced safety profile of the *MILESTONE* approach. Multiple groups recently described unintended on-target aberrations after targeting different cell types with Cas nucleases.[48–51] Given these new data, further validation of *MILESTONE* editing, for example, using drop-off ddPCR or single-cell RNA sequencing of edited HSPCs, as performed by Nahmad et al.,[49] will be required to preclude potential on-target aberrations, including large deletions and aneuploidy. Another safety concern highlighted by recent studies is that DNA double-strand breaks can induce DNA damage response through TP53 activation, leading to reduced proliferation, engraftment, and clonogenic capacity of edited HSPCs.[52,53] Approaches for HSPC gene editing in an autologous transplantation setting must preserve the stemness features of gene-edited HSPCs. We demonstrated no significant difference in expression levels of the p53 downstream targets, *P21* and *GADD45A*, between HSPCs edited with *MILESTONE*, *ELANE* CDS KO and Mock samples 48 h after electroporation, indicating that both approaches limit DNA damage to their intended on-target site, largely without affecting TP53-initiated responses.

Additionally, we found that efficient engraftment and multilineage potential of *MILESTONE*-edited HD and *ELANE*-CN HSPCs were preserved in immunodeficient NSG mice and were accompanied by granulocytic differentiation *in vivo*. The fact that primary *ELANE*-CN *MILESTONE*-edited HSPCs exhibited a significant engraftment advantage—with 100% engraftment of edited cells, even in cell populations that do not constitutively express NE (e.g., lymphocytes)—indicates that mutant NE has pathological effects on early self-renewing HSPCs, in addition to its impact on myeloid progenitors. This exciting observation warrants further investigation and provide new insights on the pathogenesis of *ELANE*-CN.

An essential feature of *MILESTONE* is its universality—a considerable advantage given that pathogenic *ELANE* mutations occur at any exon and even in some introns of the *ELANE* gene, and more than 120 *ELANE* mutations have been reported to date.[3,9] In a recent study, Tran et al. demonstrated the successful correction of a single *ELANE* mutation at exon 4 (p. L172P) using AAV-based delivery of the repair template.[54] However, such *ELANE* mutation position-specific gene-editing strategies are extraordinarily costly and time-intensive. Moreover, recent reports suggest poor engraftment and reduced repopulating activity of HSPCs after gene editing using AAV-based constructs *in vivo*.[55–61] In the *MILESTONE* approach, only two sgRNAs and Cas9D10A protein are sufficient to correct neutropenia in all *ELANE*-CN patients, independent of the position of the *ELANE* mutation. Moreover, no AAV-based delivery of an HDR template is required. In another study, researchers demonstrated the successful restoration of defective granulocytic differentiation through allele-specific editing of *ELANE* mutations in *ELANE*-CN HSPCs *in vitro*.[62] This group developed a CRISPR-based strategy utilizing single-nucleotide polymorphisms (SNPs) identified in the human population (healthy or CN) with two sgRNAs. These sgRNAs independently introduce DSBs, facilitating the introduction of a monoallelic knockout. Although this method is promising, introducing two double-strand breaks may increase genotoxicity, chromosomal aberrations, and risk of off-target effects, especially if the extensively cut genomic region is greater than 3 kb in size. This approach may also affect the expression of the neighboring genes, e.g., *CFD,* located ~240 base pairs (bp) from one of the proposed cut sites. Notably, such allele-specific gene editing only applies to *ELANE*-CN patients carrying the obligatory SNPs; all other patients are precluded from exploiting this type of therapy.

Taken together, our findings establish *MILESTONE* as a universal, safe, and effective gene therapy approach that reduces *ELANE* mRNA expression level by using a CRISPR-Cas9n double-nickase based editing of the *ELANE* promoter without targeting the *ELANE* CDS. The *MILESTONE* approach rescues granulopoiesis in

ELANE-CN patients. It offers a potentially curative therapy in the setting of autologous transplantation of gene-edited HSPCs for these patients, replacing daily rhG-CSF therapy and potentially decreasing the risk of leukemia development. This approach is also useful in gene engineering for the knockdown of genes, especially for targeting genomic sequences highly similar to other loci or genes with multiple isoforms not targetable with one guide RNA. We also envision the potentially broad applicability of this approach in gene therapy applications for example inhibition of the expression of genes with gain-of-function mutations or cell engineering.

MATERIAL AND METHODS

Cell isolation and culture

Human $CD34^+$ HSPCs were isolated from the bone marrow mononuclear cell fraction from three *ELANE*-CN patients and 13 healthy donors by Ficoll gradient centrifugation and magnetic bead separation using the Human CD34 Progenitor Cell Isolation Kit (Miltenyi Biotech, #130-046-703). $CD34^+$ cells were cultured in a density of 2×10^5 cells/mL in StemSpan SFEM II stem cell expansion medium (Stemcell Technologies, # 09605) supplemented with 1% penicillin/streptomycin, 1% L-Glutamine and a cytokine cocktail consisting of 20 ng/mL interleukin (IL)-3, 20 ng/mL IL-6, 20 ng/mL TPO, 50 ng/mL SCF, and 50 ng/mL FLT-3L (all cytokines were purchased from R&D Systems). Samples were collected during the routine annual follow-up recommendation by the Severe Chronic Neutropenia International Registry or prior bone marrow transplantation. Informed written consent was obtained from the study participants. The study was conducted according to Helsinki's declaration. Study approval was obtained from the Ethical Review Board of the Medical Faculty, University of Tübingen.

THP-1 cells were maintained in RPMI-1640 supplemented with 10% fetal bovine serum (FBS) (Gemini Bio Products, West Sacramento, CA, USA), 2 mM L-glutamine, and 1% penicillin/streptomycin (Thermo Fisher Scientific) at 37°C and 5% CO_2.

Design of the sgRNAs and repair template for HiBiT tagging of *ELANE*

Specific single-guide RNA (sgRNA) for endogenous bioluminescence tagging of the *ELANE* gene (cut site: chr19 [5′ TCGGCGGCCGA GGGTCATGG 3′, +852,330: −852,330], NM_001972.3 Exon 1, NP_001963.1 p. M1) and repair template to knock in HiBiT tag (5′-GGCAATGCAACGGCCTCCCAGCACAGGGCTATAAGAGG AGCCGGGCGGGCACGGAGGGGCAGAGACCCCGGAGCCCCA GCCCCACCATGGTGAGCGGCTGGCGGCTGTTCAAGAAGATT AGCACCCTCGGCCGCCGACTCGCGTGTCTTTTCCTCGCCTGT GTCCTGCCGGCCTTGCTGCTGGGGGGTGAGTTTTTGAGT -3′) were designed using Benchling [Biology Software] retrieved from ensemble.org and ordered via Integrated DNA Technologies (IDT). Specific sgRNAs for targeting the non-coding regulatory regions of the *ELANE* gene (cut site: chr19 [5′ GGGCTATAAGAGGA GCCGGG 3′, +852,258] and [5′ GAGGCCGTTGCATTGCCCCA 3′, −852,243] were designed using SAM webtool (http://sam.genome-engineering.org [30]) and ordered via IDT.

CRISPR-Cas gRNA RNP mediated gene editing

According to the manufacturer's instructions, electroporation was carried out using the Amaxa nucleofection system (P3 primary kit, #V4XP-3024). Briefly, 1×10^6 THP-1 cells or human $CD34^+$ HSPCs were electroporated with assembled gRNA (8 μg) and HiFiCas9 or Cas9D10A (15 μg) protein (IDT); 1 μM of ssODN was added to the electroporation mix in the case of the HiBiT knockin experiment. Single-cell HiBiT-tagged *ELANE* clones were selected by single-cell subculturing of edited THP-1 cells as described by Ran et al.[63] Briefly, gene-edited cells were diluted to 0.5 cells per 100 μL. The diluted cell suspension was distributed on two 96-well plates. Plates were incubated for 2 weeks with bi-weekly media changes. After 2 weeks, half the cells were lysed, and luminescence was measured, as described below. Cells with a strong luminescence signal were selected and expanded for subsequent experiments.

NE protein measurement through HiBiT-based luminescence

To measure HiBiT-based NE protein levels, we followed the manufacturer's instructions. Briefly, 1×10^5 cells were suspended in 100 μL of RPMI supplemented with 10% FBS per well of a white 96-well tissue culture plate. Next, cells were lysed by adding an equal volume of Nano-Glo HiBiT Lytic Reagent (Promega N3030) and incubated at room temperature for 30 min while shaking. Nano-Glo HiBiT Lytic reagent consists of Nano-Glo HiBiT Lytic Buffer, Nano-Glo HiBiT Lytic Substrate, and LgBiT Protein. Luminescence was then measured with a GloMax Multidetection System plate reader.

Western blotting

A total of 1×10^6 cells were lysed in 200 μL 3X Laemmli buffer, and protein was denatured for 10 min at 95°C. Five microliters of cell lysate in Laemmli buffer were loaded per lane. Proteins were separated on a 12% polyacrylamide gel and transferred on a nitrocellulose membrane (GE Healthcare) (1 h, 100V, 4°C). The membrane was blocked for 1 h in 5% BSA/TBST and incubated with primary anti-NE (Santa Cruz, #sc-9520) or α-Tubulin (Cell Signaling, #4970) antibody overnight at 4°C. After that, membranes were washed and incubated with a secondary HRP-conjugated antibody (Santa Cruz, #sc-2004) for 1 h at room temperature. Pierce ECL solution (Thermo Fisher) and Amersham Hyperfilms were used to detect the chemiluminescence signal of proteins.

CFU assay

$CD34^+$ cells were resuspended in IMDM supplemented with 2% FBS (Stemcell Technologies, #07700) and enriched Methocult (Stemcell Technologies, #H4435). The cell suspension was plated on 3.5-cm dishes (3×10^3 cells/dish) for 14 days at 37°C and 5% CO_2.

Liquid culture differentiation of $CD34^+$ cells

$CD34^+$ cells were seeded at 2×10^5 cells/mL density. Cells were incubated for 7 days in RPMI 1640 GlutaMAX supplemented with 10% FBS, 1% penicillin/streptomycin, 5 ng/mL SCF, 5 ng/mL IL-3, 5 ng/mL GM-CSF, and 1 ng/mL G-CSF. The medium was exchanged every second day. On day 7, cells were plated in RPMI 1640 GlutaMAX supplemented with 10% FBS, 1% penicillin/streptomycin, and 1 ng/mL G-CSF. On day 14, cells were analyzed by flow cytometry using the

following mouse anti-human antibodies: CD34 (BD, #348811), CD33 (BioLegend, #303416), CD45 (BioLegend, #304036), CD11b (BD, #557754), CD15 (BD, #555402), CD66b (BioLegend, #305114), and CD16 (BD, #561248). The morphology of the cells was investigated on cytospin slides by May-Grunwald-Giemsa staining.

Assessing genome-editing efficiency

Genomic DNA was isolated using the QuickExtract DNA extraction kit (Lucigen, #QE09050). PCR was carried out using the primeSTAR max Polymerase Kit (Takara, #R045B) and gene-specific primers (Table S4). The PCR products were purified by ExoSAP, which is a master mix of one part of Exonuclease I 20 U/μl (Thermo Fisher Scientific, #EN0581) and two parts of FastAP thermosensitive alkaline phosphatase 1 U/μL (Thermo Fisher Scientific, #EF0651). Microsynth performed Sanger sequencing of purified PCR products. CRISPR-Cas9-based genome editing was analyzed using the Deconvolution of Complex DNA Repair (DECODR) web tools.

In vitro ROS assay

Granulocytes from day 14 of liquid culture differentiation were cultured in RPMI 1640 medium supplemented with 0.5% BSA at the density of 5×10^4 per well of 96-well white-walled plate with or without fMLP (Sigma, #F3506) at a final concentration of 10 nM and incubated for 30 min at 37°C, 5% CO_2. According to the manufacturer's protocol, the hydrogen peroxide (H_2O_2) level, an ROS, was measured by ROS-Glo H2O2 Assay kit (Promega, #G8820) on a GloMax Multidetection System plate reader.

Assessment of phagocytosis kinetics using the IncuCyte ZOOM system

Granulocytes from day 14 of liquid culture differentiation were cultured in RPMI 1640 medium supplemented with 0.5% BSA and pHrodo Green *S. aureus* bioparticles (#4620 Essen Bio) according to the manufacturer's protocol in IncuCyte ZOOM system (Essen Bio) at 37°C, 5% CO_2. Briefly, 10^4 cells were seeded in 90 μL of medium, and 10 μg of Bioparticles were added to a final volume of 100 μL. The cells were monitored for 6 h. The analysis was conducted in IncuCyte S3 Software.

Xenotransplantation of HSPCs in NSG mice

HSPCs were thawed and cultured for 14–16 h before electroporation. Following electroporation, cells were cultured for an additional 6 h before transplantation. Bulk electroporated cells were distributed among different mice. Mock cells were electroporated with sgRNA targeting the AAVS1 safe harbor site (5 CTCCCTCCCAGGATCC TCTC 3).[64] Eight- to 16-week-old NOD.Cg-Prkdcscid Il2rgtm1Wjl/SzJ (NSG) mice (Charles River Laboratory # 001976) were sublethally (170 cGy) irradiated 4 h prior to transplantation. HSPCs were transplanted intra-femorally. To this end, 1×10^5 HSPCs were injected per mouse in the right femur. Mice were euthanized 16 weeks post-transplantation. Bone marrow cells were isolated and immunophenotyped by flow cytometry on a FACS ARIA. The following antibodies were used for staining: 7AAD (BD # 559925), anti-mouse CD45 PerCP (BioLegend # 103130), anti-human CD45 BV510 (BioLegend # 304036), anti-human CD19 BV421 (BioLegend # 302234), anti-human CD3 BV711 (BioLegend # 300464), anti-human CD14 BV650 (BioLegend # 301836), anti-human CD16 APC (BioLegend # 302012), anti-human CD33 APC-Cy7 (BioLegend # 303442), anti-human CD66b FITC (BioLegend #305104), and anti-human CD34 Pe-Cy7 (BD #348811). Genome-editing efficiencies were determined as described in the "assessing genome-editing efficiency" section above. Mouse experiments were approved by the Institutional Animal Care and Use Committee of the University of Tübingen according to German state and federal regulations, protocol M 23/21G.

Quantitative real-time PCR

RNA was isolated using RNeasy Micro Kit (Qiagen, #74004), and cDNA was prepared from 1 μg of total RNA with Omniscript RT Kit (Qiagen, # 205111). qPCR was performed using SYBR Green 3 qPCR master mix (Roche, # 04887352001) and Light Cycler 480 (Roche). Target genes were normalized to *ACTB* or *GAPDH* genes. Primer sequences are presented in Table S5.

GUIDE-seq

MILESTONE was applied on primary healthy donor $CD34^+$ HSPCs along with annealed dsODN (/5Phos/GTTTAATTGAGTTGTCA TATGTTAATAACGGT*A*T and/5Phos/ATACCGTTATTAACA TATGACAACTCAATTAA*A*C, Phos represents a 5′ phosphorylation and * indicates a phosphorothioate linkage). Four days post-electroporation, genomic DNA was isolated with the QIAamp DNA Mini Kit (Qiagen, # 51304) according to the manufacturer's protocol. NGS library preparation was performed as described by Malinin et al.[65] and sequenced by NovoGene. NGS files were analyzed using the pipeline provided by Tsai lab in Git Hub (https://github.com/tsailabSJ/guideseq).

CAST-seq

MILESTONE was applied on the primary healthy donor $CD34^+$ HSPCs. According to the manufacturer's protocol, genomic DNA was isolated 4 days after electroporation using QIAamp DNA Micro Kit (Qiagen, #56304). CAST-seq library preparation for NGS and data analysis was performed, as Turchiano et al. explained,[41] with an improved bioinformatics pipeline.[42]

rhAmpSeq

Targeted amplicon sequencing was performed using IDT rhAmpSeq CRISPR analysis system. Briefly, the rhAMP primers to amplify multiple *ELANE* regions (promoter region, exon 2, exon 3, exon 4, and exon 5) or potential off-target sites (Table S1) were designed using the IDT rhAMP primer design software and ordered via IDT. Library preparation was performed according to the manufacturer's protocol, and Novogene performed NGS. CRISPRESSO package[35] and CAS-analyzer[36] were used to analyze the on-target data. CRISPECTOR[43] tool was used to analyze the off-target data.

RNA-seq

MILESTONE was applied on primary healthy donor $CD34^+$ HSPCs, followed by granulocytic liquid culture differentiation for 14 days.

According to the manufacturer's protocol, the RNA was extracted using an RNeasy Micro Kit (Qiagen, #74004). Strand-specific paired-end RNA-seq was performed by Novogene. The nf-core RNAseq pipeline[66] - a framework for community-curated bioinformatics pipelines - was used to extract the gene-level count matrix for each sample. Differential analysis of count data was performed using the DESeq2 package and the iDEP web tool to obtain the differentially expressed genes (DEGs) (Table S2). The volcano plot of DEGs was generated using the Enhance volcano plot R-package.

Statistical analysis

Differences in mean values between groups were analyzed using two-sided, unpaired Student's t tests in GraphPad Prism software.

DATA AND CODE AVAILABILITY

For original data, please get in touch with Julia.skokowa@med.uni-tuebingen.de.

SUPPLEMENTAL INFORMATION

Supplemental information can be found online at https://doi.org/10.1016/j.ymthe.2024.03.037.

ACKNOWLEDGMENTS

We thank Dr. Olg aKlimenkova for excellent support during submission of the manuscript. We thank Geoffroy Andrieux for bioinformatics support and the Flow Cytometry Core Facility – Berg of the University Hospital Tübingen for technical support. This work was supported by the BMBF consortium MyPred, the German Research Foundation, M. Schickedanz Leukämia-Stiftung, J. Carreras Leukemia Foundation, the InnoChron COST EU action, and the Horizon Europe Pathfinder Challenge X-PAND consortium (ID 101070950 to T.C.).

AUTHOR CONTRIBUTIONS

M.N., P.M., and J.S. made initial observations and designed and supervised the experiments; M.N., M.R., and J.S. interpreted the results and wrote the manuscript. M.N. performed CRISPRITZ and CRISPRme *in silico* analysis, rhAmpSeq off-target validation, RNA-seq and analyzed the data; M.N., M.R., and P.M. performed experiments with primary HSPCs with the help from B.D. and N.B.B.; M.R. and M.N. conducted GUIDE-seq and analyzed data; M.M.K., T.C., and M.N. performed CAST-seq; M.N. performed endogenous tagging of *ELANE* in THP1 with Y.X. assistance; M.R. designed and performed *in vivo* experiments and analyzed data. P.A.-T. assisted in *in vivo* experiments and wrote the manuscript. K.W. and C.Z. provided patients' material; K.W., M.K., C.Z., C.L., and T.C. gave insightful comments.

DECLARATION OF INTERESTS

M.N., P.M., and J.S. have filed a patent on the invention described in this study. T.C. is an advisor to Cimeio Therapeutics and Excision BioTherapeutics and holds a patent on CAST-Seq.

REFERENCES

1. Skokowa, J., Dale, D.C., Touw, I.P., Zeidler, C., and Welte, K. (2017). Severe congenital neutropenias. Nat. Rev. Dis. Primers *3*, 17032. https://doi.org/10.1038/nrdp.2017.32.

2. Dale, D.C., Person, R.E., Bolyard, A.A., Aprikyan, A.G., Bos, C., Bonilla, M.A., Boxer, L.A., Kannourakis, G., Zeidler, C., Welte, K., et al. (2000). Mutations in the gene encoding neutrophil elastase in congenital and cyclic neutropenia. Blood *96*, 2317–2322. https://doi.org/10.1182/blood.V96.7.2317.

3. Makaryan, V., Zeidler, C., Bolyard, A.A., Skokowa, J., Rodger, E., Kelley, M.L., Boxer, L.A., Bonilla, M.A., Newburger, P.E., Shimamura, A., et al. (2015). The diversity of mutations and clinical outcomes for ELANE-associated neutropenia. Curr. Opin. Hematol. *22*, 3–11. https://doi.org/10.1097/MOH.0000000000000105.

4. Souza, L.M., Boone, T.C., Gabrilove, J., Lai, P.H., Zsebo, K.M., Murdock, D.C., Chazin, V.R., Bruszewski, J., Lu, H., Chen, K.K., et al. (1986). Recombinant human granulocyte colony-stimulating factor: effects on normal and leukemic myeloid cells. Science *232*, 61–65. https://doi.org/10.1126/science.2420009.

5. Zeidler, C., Gerschmann, N., Mellor-Heineke, S., Frömling, F., Skokowa, J., and Welte, K. (2019). Response to High Dose G-CSF Treatment (20µg/kg/d or Higher) of Patients with Congenital Neutropenia: An Analysis By the Scnir in Europe. Blood *134*, 1225. https://doi.org/10.1182/blood-2019-129844.

6. Fioredda, F., Iacobelli, S., van Biezen, A., Gaspar, B., Ancliff, P., Donadieu, J., Aljurf, M., Peters, C., Calvillo, M., Matthes-Martin, S., et al. (2015). Stem cell transplantation in severe congenital neutropenia: an analysis from the European Society for Blood and Marrow Transplantation. Blood *126*, 1885–1970. https://doi.org/10.1182/blood-2015-02-628859.

7. Perera, N.C., Schilling, O., Kittel, H., Back, W., Kremmer, E., and Jenne, D.E. (2012). NSP4, an elastase-related protease in human neutrophils with arginine specificity. Proc. Natl. Acad. Sci. USA *109*, 6229–6234.

8. Pham, C.T.N. (2006). Neutrophil serine proteases: specific regulators of inflammation. Nat. Rev. Immunol. *6*, 541–550. https://doi.org/10.1038/nri1841.

9. Germeshausen, M., Deerberg, S., Peter, Y., Reimer, C., Kratz, C.P., and Ballmaier, M. (2013). The Spectrum of ELANE Mutations and their Implications in Severe Congenital and Cyclic Neutropenia. Hum. Mutat. *34*, 905–914. https://doi.org/10.1002/humu.22308.

10. Köllner, I., Sodeik, B., Schreek, S., Heyn, H., von Neuhoff, N., Germeshausen, M., Zeidler, C., Krüger, M., Schlegelberger, B., Welte, K., and Beger, C. (2006). Mutations in neutrophil elastase causing congenital neutropenia lead to cytoplasmic protein accumulation and induction of the unfolded protein response. Blood *108*, 493–500. https://doi.org/10.1182/blood-2005-11-4689.

11. Grenda, D.S., Murakami, M., Ghatak, J., Xia, J., Boxer, L.A., Dale, D., Dinauer, M.C., and Link, D.C. (2007). Mutations of the ELA2 gene found in patients with severe congenital neutropenia induce the unfolded protein response and cellular apoptosis. Blood J. Am. Soc. Hematol. *110*, 4179–4187.

12. Nanua, S., Murakami, M., Xia, J., Grenda, D.S., Woloszynek, J., Strand, M., and Link, D.C. (2011). Activation of the unfolded protein response is associated with impaired granulopoiesis in transgenic mice expressing mutant Elane. Blood J. Am. Soc. Hematol. *117*, 3539–3547.

13. Nustede, R., Klimiankou, M., Klimenkova, O., Kuznetsova, I., Zeidler, C., Welte, K., and Skokowa, J. (2016). ELANE mutant–specific activation of different UPR pathways in congenital neutropenia. Br. J. Haematol. *172*, 219–227. https://doi.org/10.1111/bjh.13823.

14. Nasri, M., Ritter, M., Mir, P., Dannenmann, B., Aghaallaei, N., Amend, D., Makaryan, V., Xu, Y., Fletcher, B., Bernhard, R., et al. (2020). CRISPR/Cas9-mediated ELANE knockout enables neutrophilic maturation of primary hematopoietic stem and progenitor cells and induced pluripotent stem cells of severe congenital neutropenia patients. Haematologica *105*, 598–609. https://doi.org/10.3324/haematol.2019.221804.

15. Rao, S., Yao, Y., Soares de Brito, J., Yao, Q., Shen, A.H., Watkinson, R.E., Kennedy, A.L., Coyne, S., Ren, C., Zeng, J., et al. (2021). Dissecting ELANE neutropenia pathogenicity by human HSC gene editing. Cell Stem Cell *28*, 833–845.e5. https://doi.org/10.1016/j.stem.2020.12.015.

16. Frangoul, H., Altshuler, D., Cappellini, M.D., Chen, Y.-S., Domm, J., Eustace, B.K., Foell, J., de la Fuente, J., Grupp, S., Handgretinger, R., et al. (2021). CRISPR-Cas9

Gene Editing for Sickle Cell Disease and β-Thalassemia. N. Engl. J. Med. *384*, 252–260. https://doi.org/10.1056/NEJMoa2031054.

17. FDA. (2023). FDA Approves First Gene Therapies to Treat Patients with Sickle Cell Disease. https://www.fda.gov/news-events/press-announcements/fda-approves-first-gene-therapies-treat-patients-sickle-cell-disease.
18. Cho, S.W., Kim, S., Kim, Y., Kweon, J., Kim, H.S., Bae, S., and Kim, J.S. (2014). Analysis of off-target effects of CRISPR/Cas-derived RNA-guided endonucleases and nickases. Genome Res. *24*, 132–141. https://doi.org/10.1101/gr.162339.113.
19. Frock, R.L., Hu, J., Meyers, R.M., Ho, Y.J., Kii, E., and Alt, F.W. (2015). Genome-wide detection of DNA double-stranded breaks induced by engineered nucleases. Nat. Biotechnol. *33*, 179–186. https://doi.org/10.1038/nbt.3101.
20. Gopalappa, R., Suresh, B., Ramakrishna, S., and Kim, H.H. (2018). Paired D10A Cas9 nickases are sometimes more efficient than individual nucleases for gene disruption. Nucleic Acids Res. *46*, e71. https://doi.org/10.1093/nar/gky222.
21. Ran, F.A., Hsu, P.D., Lin, C.Y., Gootenberg, J.S., Konermann, S., Trevino, A.E., Scott, D.A., Inoue, A., Matoba, S., Zhang, Y., and Zhang, F. (2013). Double nicking by RNA-guided CRISPR Cas9 for enhanced genome editing specificity. Cell *154*, 1380–1389. https://doi.org/10.1016/j.cell.2013.08.021.
22. Shen, B., Zhang, W., Zhang, J., Zhou, J., Wang, J., Chen, L., Wang, L., Hodgkins, A., Iyer, V., Huang, X., and Skarnes, W.C. (2014). Efficient genome modification by CRISPR-Cas9 nickase with minimal off-target effects. Nat. Methods *11*, 399–402. https://doi.org/10.1038/nmeth.2857.
23. Tao, J., Bauer, D.E., and Chiarle, R. (2023). Assessing and advancing the safety of CRISPR-Cas tools: from DNA to RNA editing. Nat. Commun. *14*, 212. https://doi.org/10.1038/s41467-023-35886-6.
24. Allport, J.R., Lim, Y.-C., Shipley, J.M., Senior, R.M., Shapiro, S.D., Matsuyoshi, N., Vestweber, D., and Luscinskas, F.W. (2002). Neutrophils from MMP-9- or neutrophil elastase-deficient mice show no defect in transendothelial migration under flow in vitro. J. Leukoc. Biol. *71*, 821–828. https://doi.org/10.1189/jlb.71.5.821.
25. Young, R.E., Thompson, R.D., Larbi, K.Y., La, M., Roberts, C.E., Shapiro, S.D., Perretti, M., and Nourshargh, S. (2004). Neutrophil elastase (NE)-deficient mice demonstrate a nonredundant role for NE in neutrophil migration, generation of proinflammatory mediators, and phagocytosis in response to zymosan particles in vivo. J. Immunol. *172*, 4493–4502. https://doi.org/10.4049/jimmunol.172.7.4493.
26. Hirche, T.O., Atkinson, J.J., Bahr, S., and Belaaouaj, A. (2004). Deficiency in neutrophil elastase does not impair neutrophil recruitment to inflamed sites. Am. J. Respir. Cel Mol. Biol. *30*, 576–584. https://doi.org/10.1165/rcmb.2003-0253OC.
27. Pham, C.T.N., Ivanovich, J.L., Raptis, S.Z., Zehnbauer, B., and Ley, T.J. (2004). Papillon-Lefèvre syndrome: correlating the molecular, cellular, and clinical consequences of cathepsin C/dipeptidyl peptidase I deficiency in humans. J. Immunol. *173*, 7277–7281. https://doi.org/10.4049/jimmunol.173.12.7277.
28. Tsuchiya, S., Yamabe, M., Yamaguchi, Y., Kobayashi, Y., Konno, T., and Tada, K. (1980). Establishment and characterization of a human acute monocytic leukemia cell line (THP-1). Int. J. Cancer *26*, 171–176. https://doi.org/10.1002/ijc.2910260208.
29. Schwinn, M.K., Machleidt, T., Zimmerman, K., Eggers, C.T., Dixon, A.S., Hurst, R., Hall, M.P., Encell, L.P., Binkowski, B.F., and Wood, K.V. (2018). CRISPR-mediated tagging of endogenous proteins with a luminescent peptide. ACS Chem. Biol. *13*, 467–474.
30. Joung, J., Konermann, S., Gootenberg, J.S., Abudayyeh, O.O., Platt, R.J., Brigham, M.D., Sanjana, N.E., and Zhang, F. (2017). Genome-scale CRISPR-Cas9 knockout and transcriptional activation screening. Nat. Protoc. *12*, 828–863. https://doi.org/10.1038/nprot.2017.016.
31. Dreos, R., Ambrosini, G., Groux, R., Cavin Périer, R., and Bucher, P. (2017). The eukaryotic promoter database in its 30th year: focus on non-vertebrate organisms. Nucleic Acids Res. *45*, D51–D55. https://doi.org/10.1093/nar/gkw1069.
32. Bloh, K., Kanchana, R., Bialk, P., Banas, K., Zhang, Z., Yoo, B.C., and Kmiec, E.B. (2021). Deconvolution of Complex DNA Repair (DECODR): Establishing a Novel Deconvolution Algorithm for Comprehensive Analysis of CRISPR-Edited Sanger Sequencing Data. Crispr J. *4*, 120–131. https://doi.org/10.1089/crispr.2020.0022.
33. Tuladhar, R., Yeu, Y., Tyler Piazza, J., Tan, Z., Rene Clemenceau, J., Wu, X., Barrett, Q., Herbert, J., Mathews, D.H., Kim, J., et al. (2019). CRISPR-Cas9-based mutagenesis frequently provokes on-target mRNA misregulation. Nat. Commun. *10*, 4056. https://doi.org/10.1038/s41467-019-12028-5.
34. Mir, P., Ritter, M., Welte, K., Skokowa, J., and Klimiankou, M. (2020). Gene Knockout in Hematopoietic Stem and Progenitor Cells Followed by Granulocytic Differentiation. Methods Mol. Biol. *2115*, 455–469. https://doi.org/10.1007/978-1-0716-0290-4_26.
35. Pinello, L., Canver, M.C., Hoban, M.D., Orkin, S.H., Kohn, D.B., Bauer, D.E., and Yuan, G.-C. (2016). Analyzing CRISPR genome-editing experiments with CRISPResso. Nat. Biotechnol. *34*, 695–697. https://doi.org/10.1038/nbt.3583.
36. Park, J., Lim, K., Kim, J.-S., and Bae, S. (2017). Cas-analyzer: an online tool for assessing genome editing results using NGS data. Bioinformatics *33*, 286–288. https://doi.org/10.1093/bioinformatics/btw561.
37. Shultz, L.D., Lyons, B.L., Burzenski, L.M., Gott, B., Chen, X., Chaleff, S., Kotb, M., Gillies, S.D., King, M., Mangada, J., et al. (2005). Human lymphoid and myeloid cell development in NOD/LtSz-scid IL2R gamma null mice engrafted with mobilized human hemopoietic stem cells. J. Immunol. *174*, 6477–6489. https://doi.org/10.4049/jimmunol.174.10.6477.
38. Coughlan, A.M., Harmon, C., Whelan, S., O'Brien, E.C., O'Reilly, V.P., Crotty, P., Kelly, P., Ryan, M., Hickey, F.B., O'Farrelly, C., and Little, M.A. (2016). Myeloid Engraftment in Humanized Mice: Impact of Granulocyte-Colony Stimulating Factor Treatment and Transgenic Mouse Strain. Stem Cells Dev. *25*, 530–541. https://doi.org/10.1089/scd.2015.0289.
39. Cancellieri, S., Canver, M.C., Bombieri, N., Giugno, R., and Pinello, L. (2020). CRISPRitz: rapid, high-throughput and variant-aware in silico off-target site identification for CRISPR genome editing. Bioinformatics *36*, 2001–2008. https://doi.org/10.1093/bioinformatics/btz867.
40. Cancellieri, S., Zeng, J., Lin, L.Y., Tognon, M., Nguyen, M.A., Lin, J., Bombieri, N., Maitland, S.A., Ciuculescu, M.-F., Katta, V., et al. (2023). Human genetic diversity alters off-target outcomes of therapeutic gene editing. Nat. Genet. *55*, 34–43. https://doi.org/10.1038/s41588-022-01257-y.
41. Turchiano, G., Andrieux, G., Klermund, J., Blattner, G., Pennucci, V., el Gaz, M., Monaco, G., Poddar, S., Mussolino, C., Cornu, T.I., et al. (2021). Quantitative evaluation of chromosomal rearrangements in gene-edited human stem cells by CAST-Seq. Cell Stem Cell *28*, 1136–1147.e5. https://doi.org/10.1016/j.stem.2021.02.002.
42. Rhiel, M., Geiger, K., Andrieux, G., Rositzka, J., Boerries, M., Cathomen, T., and Cornu, T.I. (2023). T-CAST: An optimized CAST-Seq pipeline for TALEN confirms superior safety and efficacy of obligate-heterodimeric scaffolds. Front. Genome Ed. *5*, 1130736.
43. Amit, I., Iancu, O., Levy-Jurgenson, A., Kurgan, G., McNeill, M.S., Rettig, G.R., Allen, D., Breier, D., Ben Haim, N., Wang, Y., et al. (2021). CRISPECTOR provides accurate estimation of genome editing translocation and off-target activity from comparative NGS data. Nat. Commun. *12*, 3042. https://doi.org/10.1038/s41467-021-22417-4.
44. Ge, S.X., Jung, D., and Yao, R. (2020). ShinyGO: a graphical gene-set enrichment tool for animals and plants. Bioinformatics *36*, 2628–2629.
45. Belaaouaj, A., McCarthy, R., Baumann, M., Gao, Z., Ley, T.J., Abraham, S.N., and Shapiro, S.D. (1998). Mice lacking neutrophil elastase reveal impaired host defense against gram negative bacterial sepsis. Nat. Med. *4*, 615–618. https://doi.org/10.1038/nm0598-615.
46. Naldini, L. (2019). Genetic engineering of hematopoiesis: current stage of clinical translation and future perspectives. EMBO Mol. Med. *11*, e9958. https://doi.org/10.15252/emmm.201809958.
47. Haltalli, M.L.R., Wilkinson, A.C., Rodriguez-Fraticelli, A., and Porteus, M. (2022). Hematopoietic stem cell gene editing and expansion: State-of-the-art technologies and recent applications. Exp. Hematol. *107*, 9–13. https://doi.org/10.1016/j.exphem.2021.12.399.
48. Kosicki, M., Tomberg, K., and Bradley, A. (2018). Repair of double-strand breaks induced by CRISPR–Cas9 leads to large deletions and complex rearrangements. Nat. Biotechnol. *36*, 765–771. https://doi.org/10.1038/nbt.4192.
49. Nahmad, A.D., Reuveni, E., Goldschmidt, E., Tenne, T., Liberman, M., Horovitz-Fried, M., Khosravi, R., Kobo, H., Reinstein, E., Madi, A., et al. (2022). Frequent aneuploidy in primary human T cells after CRISPR–Cas9 cleavage. Nat. Biotechnol. *40*, 1807–1813. https://doi.org/10.1038/s41587-022-01377-0.
50. Ferrari, S., Valeri, E., Conti, A., Scala, S., Aprile, A., Di Micco, R., Kajaste-Rudnitski, A., Montini, E., Ferrari, G., Aiuti, A., and Naldini, L. (2023). Genetic engineering

meets hematopoietic stem cell biology for next-generation gene therapy. Cell Stem Cell *30*, 549–570. https://doi.org/10.1016/j.stem.2023.04.014.

51. Ferrari, S., Vavassori, V., Canarutto, D., Jacob, A., Castiello, M.C., Javed, A.O., and Genovese, P. (2021). Gene Editing of Hematopoietic Stem Cells: Hopes and Hurdles Toward Clinical Translation. Front. Genome Ed. *3*, 618378. https://doi.org/10.3389/fgeed.2021.618378.
52. Schiroli, G., Conti, A., Ferrari, S., Della Volpe, L., Jacob, A., Albano, L., Beretta, S., Calabria, A., Vavassori, V., Gasparini, P., et al. (2019). Precise Gene Editing Preserves Hematopoietic Stem Cell Function following Transient p53-Mediated DNA Damage Response. Cell Stem Cell *24*, 551–565.e8. https://doi.org/10.1016/j.stem.2019.02.019.
53. Dorset, S.R., and Bak, R.O. (2023). The p53 challenge of hematopoietic stem cell gene editing. Mol. Ther. Methods Clin. Dev. *30*, 83–89. https://doi.org/10.1016/j.omtm.2023.06.003.
54. Tran, N.T., Graf, R., Wulf-Goldenberg, A., Stecklum, M., Strauß, G., Kühn, R., Kocks, C., Rajewsky, K., and Chu, V.T. (2020). CRISPR-Cas9-Mediated ELANE Mutation Correction in Hematopoietic Stem and Progenitor Cells to Treat Severe Congenital Neutropenia. Mol. Ther. *28*, 2621–2634. https://doi.org/10.1016/j.ymthe.2020.08.004.
55. Bio, G. (2023). Graphite Bio Announces Voluntary Pause of Phase 1/2 CEDAR Study of Nulabeglogene Autogedtemcel (Nula-Cel) for Sickle Cell Disease.[Press Release] (Businesswire).
56. Pattabhi, S., Lotti, S.N., Berger, M.P., Singh, S., Lux, C.T., Jacoby, K., Lee, C., Negre, O., Scharenberg, A.M., and Rawlings, D.J. (2019). In Vivo Outcome of Homology-Directed Repair at the HBB Gene in HSC Using Alternative Donor Template Delivery Methods. Mol. Ther. Nucleic Acids *17*, 277–288. https://doi.org/10.1016/j.omtn.2019.05.025.
57. Dever, D.P., Bak, R.O., Reinisch, A., Camarena, J., Washington, G., Nicolas, C.E., Pavel-Dinu, M., Saxena, N., Wilkens, A.B., Mantri, S., et al. (2016). CRISPR/Cas9 β-globin gene targeting in human haematopoietic stem cells. Nature *539*, 384–389. https://doi.org/10.1038/nature20134.
58. De Ravin, S.S., Reik, A., Liu, P.-Q., Li, L., Wu, X., Su, L., Raley, C., Theobald, N., Choi, U., Song, A.H., et al. (2016). Targeted gene addition in human CD34+ hematopoietic cells for correction of X-linked chronic granulomatous disease. Nat. Biotechnol. *34*, 424–429. https://doi.org/10.1038/nbt.3513.
59. Ferrari, S., Jacob, A., Beretta, S., Unali, G., Albano, L., Vavassori, V., Cittaro, D., Lazarevic, D., Brombin, C., Cugnata, F., et al. (2020). Efficient gene editing of human long-term hematopoietic stem cells validated by clonal tracking. Nat. Biotechnol. *38*, 1298–1308. https://doi.org/10.1038/s41587-020-0551-y.
60. Lee, B.-C., Lozano, R.J., and Dunbar, C.E. (2021). Understanding and overcoming adverse consequences of genome editing on hematopoietic stem and progenitor cells. Mol. Ther. *29*, 3205–3218. https://doi.org/10.1016/j.ymthe.2021.09.001.
61. Dudek, A.M., and Porteus, M.H. (2021). Answered and Unanswered Questions in Early-Stage Viral Vector Transduction Biology and Innate Primary Cell Toxicity for Ex-Vivo Gene Editing. Front. Immunol. *12*, 660302. https://doi.org/10.3389/fimmu.2021.660302.
62. Sabo, P., Makaryan, V., Dicken, Y., Povodovski, L., Rockah, L., Bar, T., Gabay, M., Elinger, D., Segal, E., Haimov, O., et al. (2022). Mutant allele knockout with novel CRISPR nuclease promotes myelopoiesis in ELANE neutropenia. Mol. Ther. Methods Clin. Dev. *26*, 119–131. https://doi.org/10.1016/j.omtm.2022.06.002.
63. Ran, F.A., Hsu, P.D., Wright, J., Agarwala, V., Scott, D.A., and Zhang, F. (2013). Genome engineering using the CRISPR-Cas9 system. Nat. Protoc. *8*, 2281–2308. https://doi.org/10.1038/nprot.2013.143.
64. Kim, S., Kim, D., Cho, S.W., Kim, J., and Kim, J.S. (2014). Highly efficient RNA-guided genome editing in human cells via delivery of purified Cas9 ribonucleoproteins. Genome Res. *24*, 1012–1019. https://doi.org/10.1101/gr.171322.113.
65. Malinin, N.L., Lee, G., Lazzarotto, C.R., Li, Y., Zheng, Z., Nguyen, N.T., Liebers, M., Topkar, V.V., Iafrate, A.J., Le, L.P., et al. (2021). Defining genome-wide CRISPR–Cas genome-editing nuclease activity with GUIDE-seq. Nat. Protoc. *16*, 5592–5615. https://doi.org/10.1038/s41596-021-00626-x.
66. Ewels, P.A., Peltzer, A., Fillinger, S., Patel, H., Alneberg, J., Wilm, A., Garcia, M.U., Di Tommaso, P., and Nahnsen, S. (2020). The nf-core framework for community-curated bioinformatics pipelines. Nat. Biotechnol. *38*, 276–278. https://doi.org/10.1038/s41587-020-0439-x.

YMTHE, Volume *32*

Supplemental Information

CRISPR-Cas9n-mediated *ELANE* promoter editing for gene therapy of severe congenital neutropenia

Masoud Nasri, Malte U. Ritter, Perihan Mir, Benjamin Dannenmann, Masako M. Kaufmann, Patricia Arreba-Tutusaus, Yun Xu, Natalia Borbaran-Bravo, Maksim Klimiankou, Claudia Lengerke, Cornelia Zeidler, Toni Cathomen, Karl Welte, and Julia Skokowa

Supplemental material

Table S1. rhAMPseq panel list

name	Chr	start	stop	study	gRNA	Method
OT1	chr11	14667818	14667997	ELANE_CDS_KO	ELANE_CDS_KO	GUIDEseq
OT2	chr11	65072596	65072776	ELANE_CDS_KO	ELANE_CDS_KO	GUIDEseq
OT3	chr16	82627660	82627830	ELANE_CDS_KO	ELANE_CDS_KO	GUIDEseq
ON	chr19	852827	852999	ELANE_CDS_KO	ELANE_CDS_KO	-
OT4	chr5	116337885	116338074	ELANE_CDS_KO	ELANE_CDS_KO	GUIDEseq
OT5	chr5	1761858	1762095	ELANE_CDS_KO	ELANE_CDS_KO	GUIDEseq
OT6	chr7	366213	366387	ELANE_CDS_KO	ELANE_CDS_KO	CRISPRitz
OT7	chr18	46385064	46385274	ELANE_CDS_KO	ELANE_CDS_KO	CRISPRitz
OT8	chr6	36760988	36761177	ELANE_CDS_KO	ELANE_CDS_KO	CRISPRitz
OT9	chr8	126460448	126460620	ELANE_CDS_KO	ELANE_CDS_KO	CRISPRitz
OT10	chr1	162678252	162678445	ELANE_CDS_KO	ELANE_CDS_KO	CRISPRitz
OT11	chr8	146146277	146146515	ELANE_CDS_KO	ELANE_CDS_KO	CRISPRitz
OT12	chr12	24459444	24459621	ELANE_CDS_KO	ELANE_CDS_KO	CRISPRitz
OT13	chr20	45867973	45868146	ELANE_CDS_KO	ELANE_CDS_KO	CRISPRitz
OT14	chr20	61399089	61399287	ELANE_CDS_KO	ELANE_CDS_KO	CRISPRitz
ON	chr19	852182	852373	MILESTONE	gRNA1, gRNA4	-
OT1	chr5	116869021	116869225	MILESTONE	gRNA4	GUIDEseq
OT2	chr9	93703651	93703824	MILESTONE	gRNA4	GUIDEseq
OT3	chr12	53094901	53095078	MILESTONE	gRNA1	CRISPRitz
OT4	chr20	4900020	4900192	MILESTONE	gRNA1	CRISPRitz
OT5	chr6	135626960	135627144	MILESTONE	gRNA1	CRISPRitz
OT6	chr1	103572978	103573162	MILESTONE	gRNA1	CRISPRitz
OT7	chr8	131180916	131181085	MILESTONE	gRNA1	CRISPRitz
OT8	chrX	147885026	147885200	MILESTONE	gRNA1	CRISPRitz
OT9	chr12	93770665	93770871	MILESTONE	gRNA1	CRISPRitz
OT10	chr4	25010289	25010462	MILESTONE	gRNA1	CRISPRitz
OT11	chr2	242925583	242925750	MILESTONE	gRNA1	CRISPRitz
OT12	chr6	126281343	126281526	MILESTONE	gRNA4	CRISPRitz
OT13	chr15	80014395	80014560	MILESTONE	gRNA4	CRISPRitz
OT14	chr1	24948541	24948735	MILESTONE	gRNA4	CRISPRitz
OT15	chr7	139782707	139782869	MILESTONE	gRNA4	CRISPRitz
OT16	chr4	10239890	10240070	MILESTONE	gRNA4	CRISPRitz
OT17	chr17	17762732	17762904	MILESTONE	gRNA4	CRISPRitz
OT18	chr2	17663517	17663707	MILESTONE	gRNA4	CRISPRitz
OT19	chr20	6834023	6834238	MILESTONE	gRNA4	CRISPRitz
OT20	chr13	31664325	31664543	MILESTONE	gRNA4	CRISPRitz
OT21	chr11	67201125	67201290	MILESTONE	gRNA4	CRISPRitz

Name and chromosomal coordinates of on- and off-target sites for *MILESTONE* and *ELANE* CDS KO gene editing are shown. It is also mentioned how each off-target was determined. All the genomic coordinates are based on human reference genome assembly GRCh37.

Table S2. Differentially expressed genes (DEGs)

Submitted as supplemental Excel table. DEGs were derived as described in the Material and Methods section.

Table S3. Functional pathway enrichment list

Submitted as supplemental Excel table. Differentially regulated pathways were assessed as described in the Material and Methods and Results section.

Table S4. PCR primers used for Sanger sequencing

Primer name	**Sequence (5' to 3')**	**Amplified region**
*ELANE*_Exon1_F	GCAATGCAACGGCCTCCCA	Exon 1
*ELANE*_Exon1_R	CAGAACCTCAGTCTCTTCTG	Exon 1
*ELANE*_Prom_F	GGTAAACTGAGGCAGGCGAGGC	Promoter
*ELANE*_Prom_R	AGAGGTGGGAACAGAACCCGGG	Promoter
AAVS1 F1	CACCTTATATTCCCAGGGCCG	PPP1R12C
AAVS1 R1	CCTAGGACGCACCATTCTCAC	PPP1R12C

Table S5. qRT-PCR primers

Target gene	**Forward primer (5` -> 3')**	**Reverse primer (5` -> 3')**
ELANE	GTGTCTTTTCCTCGCCTGTGTC	CCCACAATCTCCGAGGCCAG
PRTN3	CACCCAGCAGCACTTCTCGGTG	GACGGAGGCACTGAGGTTGGCT
AZU1	AGTTCCCGTTCCTGGCCTCCAT	GGAAAACGTCTGGCGGGACTGC
GAPDH	CTGGGCTACACTGAGCACC	AAGTGGTCGTTGAGGGCAATG
P21	TGTCCGTCAGAACCCATGC	AAAGTCGAAGTTCCATCGCTC
GADD45A	GAGAGCAGAAGACCGAAAGGA	CAGTGATCGTGCGCTGACT
ACTB	TTCCTGGGCATGGAGTC	CAGGTCTTTGCGGATGATGTC

Supplemental figures

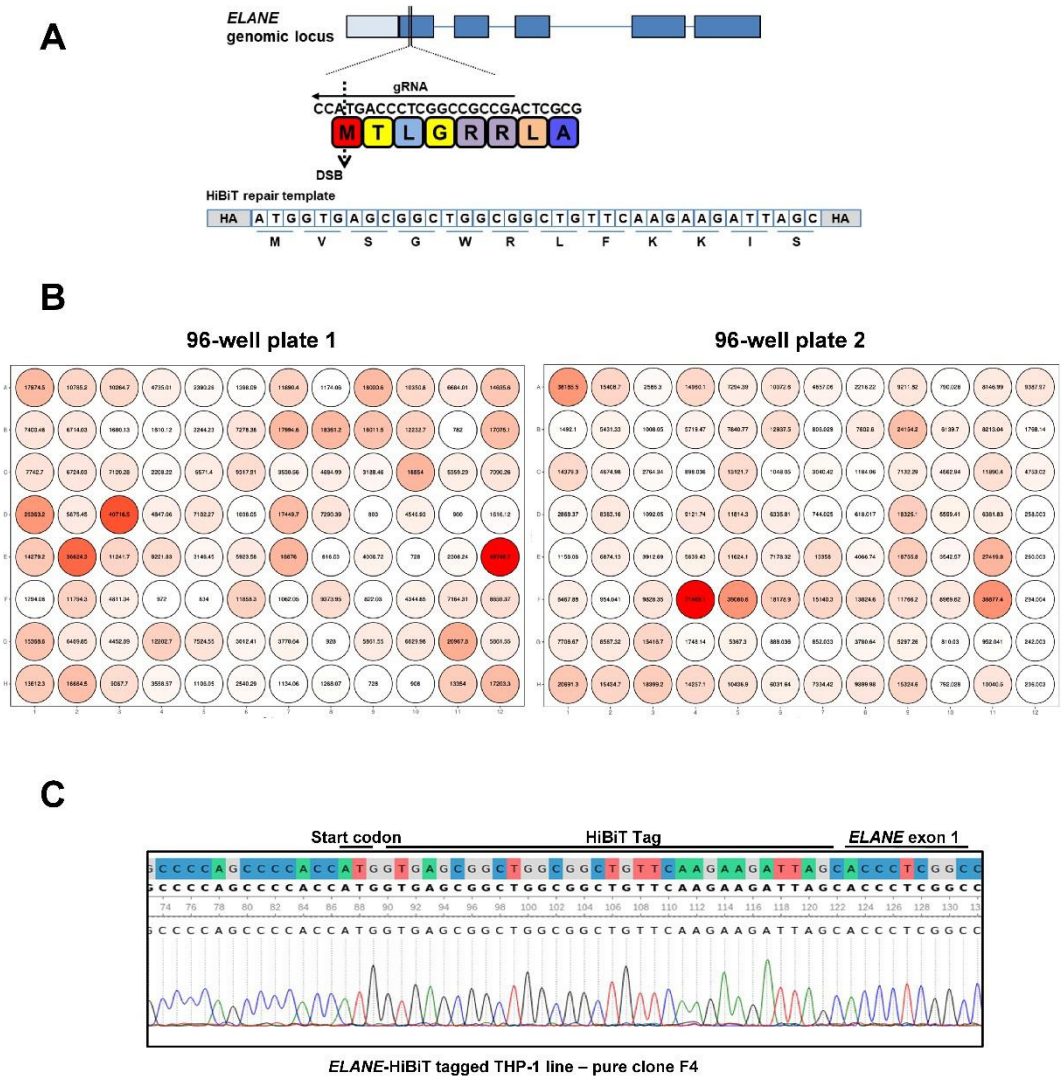

Guide-RNA	Sequence (5‘ to 3‘)	Distance to TSS
gRNA 1	GGGCTATAAGAGGAGCCGGG	-2
gRNA 2	ACAGGGCTATAAGAGGAGCC	-5
gRNA 3	TCCCAGCACAGGGCTATAAG	-29
gRNA 4	GAGGCCGTTGCATTGCCCCA	-30
gRNA 5	TCATCAACGCCCTGTGCCAG	-81
gRNA 6	AGGGGGACAAGACGCTGGAT	-146

Figure S1. HiBiT-tagging of *ELANE* in THP-1 cells and selected sgRNAs information

A, Luminescence-based tagging strategy of the *ELANE* gene to quantify NE protein levels upon gene editing. HDR template with DNA sequence encoding eleven amino acids long HiBiT peptide tag was introduced into the *ELANE* gene using CRISPR/Cas9 gene-editing to provide sensitive bioluminescent

detection of the endogenous NE protein. **B,** Luminescence-based screening of single-cell derived THP-1 cells after neutrophil elastase tagging (NE-HiBiT). The values in each well show the relative luminescent units (RLU) for each single-cell derived population of cells. **C,** Confirmatory Sanger sequencing traces of single-cell derived NE-HiBiT tagged THP-1 cell clone. **D,** A list of sgRNAs used to establish the *MILESTONE* gene editing. sgRNA sequences and distance to the transcription start site (TSS) are presented.

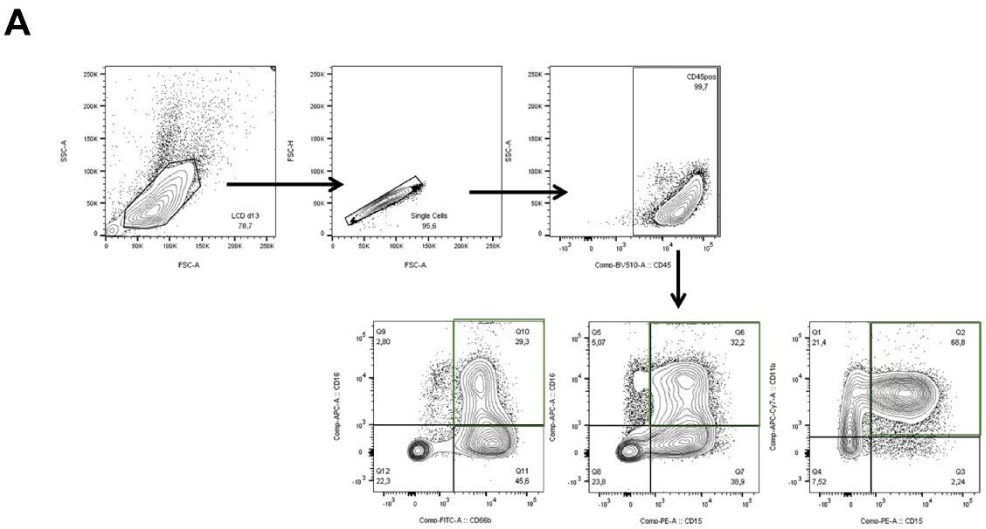

Figure S2. Gating strategies used for assessing granulocytic differentiation of primary human HSPCs *in vitro* by FACS

A, Neutrophils were identified from $CD45^+$ cells as $CD16^+CD66b^+$ or $CD16^+$ $CD15^+$ cells. The combination of $CD11b^+CD15^+$ marks all granulocytic precursor and mature cells.

A

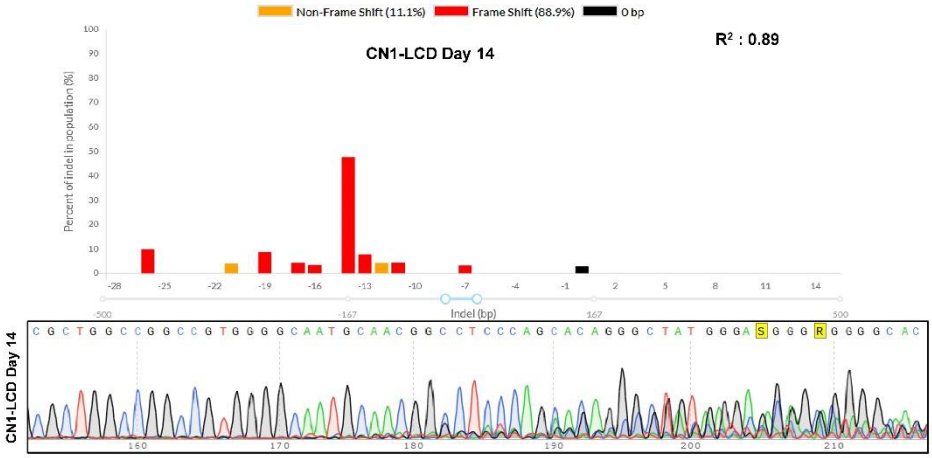

Contribution %	Net Indel
31.1	-14
16.4	-14
9.9	-26
8.7	-19
7.7	-13
4.3	-11
4.2	-17
3.9	-21
3.4	-16
3.3	-17

B

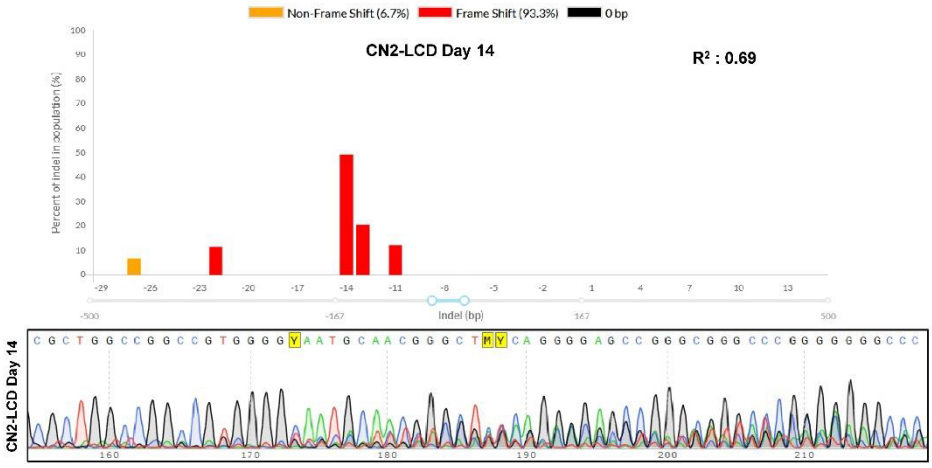

Contribution %	Net Indel
49.1	-14
20.5	-13
12.1	-11
11.5	-22
6.7	-27

Figure S3. Assessment of the gene editing efficiency in *MILESTONE*-edited *ELANE*-CN patients` primary HSPCs by Sanger sequencing

A-B, *MILESTONE* gene editing efficiency in *ELANE*-CN patients` primary HSPCs CN1 (**A**) and CN2 (**B**) *ELANE*-CN was analyzed from Sanger sequencing traces using deconvolution of complex DNA repair (DECODR) algorithm on day 14 of granulocytic liquid culture differentiation.

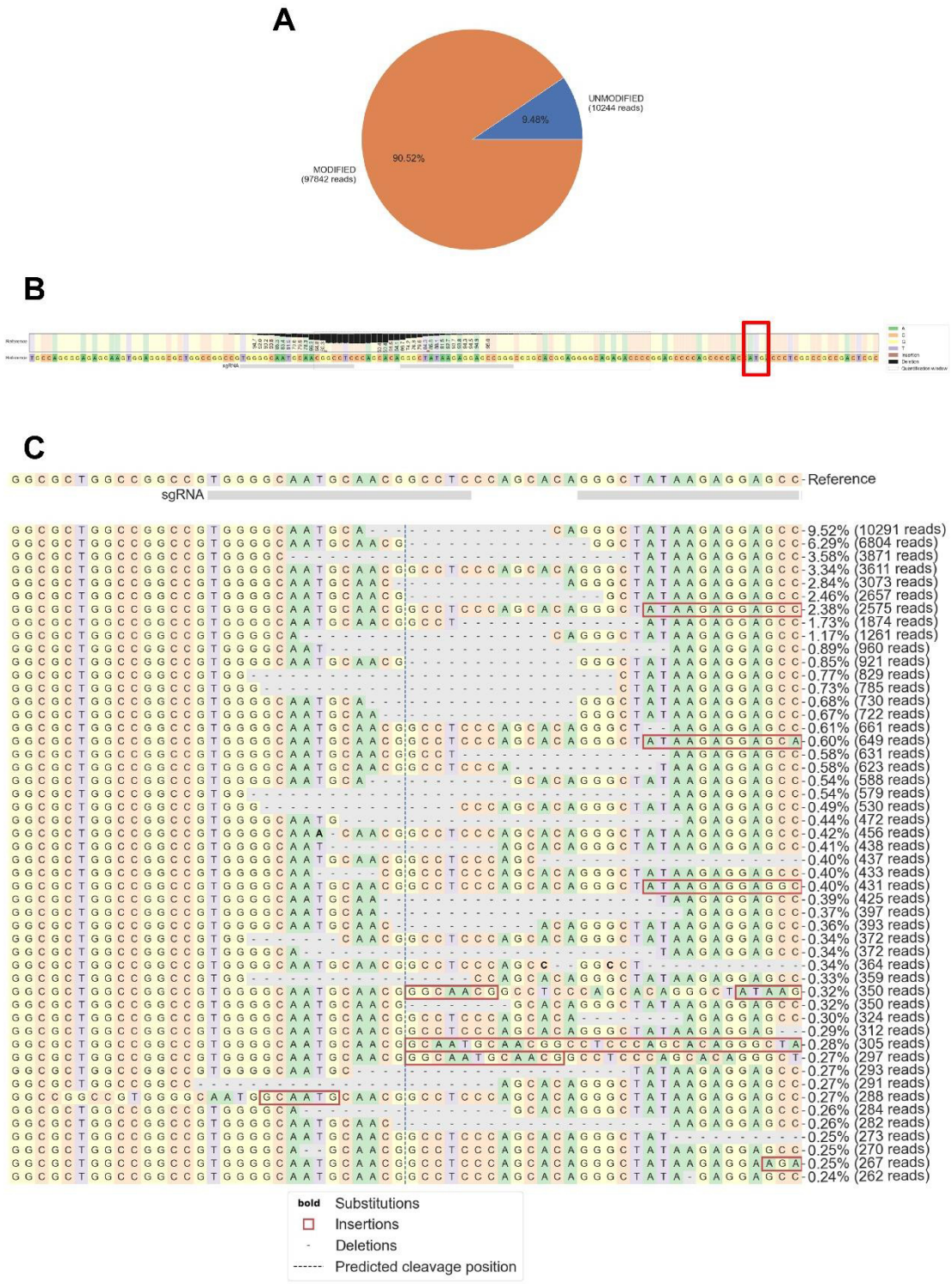

Figure S4. Assessment of *MILESTONE* gene editing efficiency in *ELANE*-CN patients` primary HSPCs by rhAMPseq

A-C, *MILESTONE* gene editing efficiency in *ELANE*-CN patients` primary HSPCs (CN1) was assessed by analyzing rhAMPseq deep sequencing data using the CRISPResso package on day 7 of granulocytic liquid culture differentiation. **A,** Alignment and editing frequency of reads, determined by the percentage

and number of the sequence reads. **B,** Nucleotide distribution across amplicon. At each base in the reference amplicon, the percentage of each base in sequencing reads is shown (A = green; C = orange; G = yellow; T = purple). Black bars show the percentage of deleted reads for the corresponding base. Brown bars between bases show the percentage of reads inserted at the corresponding position. The starting methionine is highlighted in the red box. **C,** Visualization of the distribution of identified alleles around the cleavage site. Nucleotides are indicated by unique colors (A = green; C = red; G = yellow; T = purple). Nucleotide substitutions are shown in bold font. Red rectangles highlight inserted sequences. Horizontal dashed lines indicate deleted sequences.

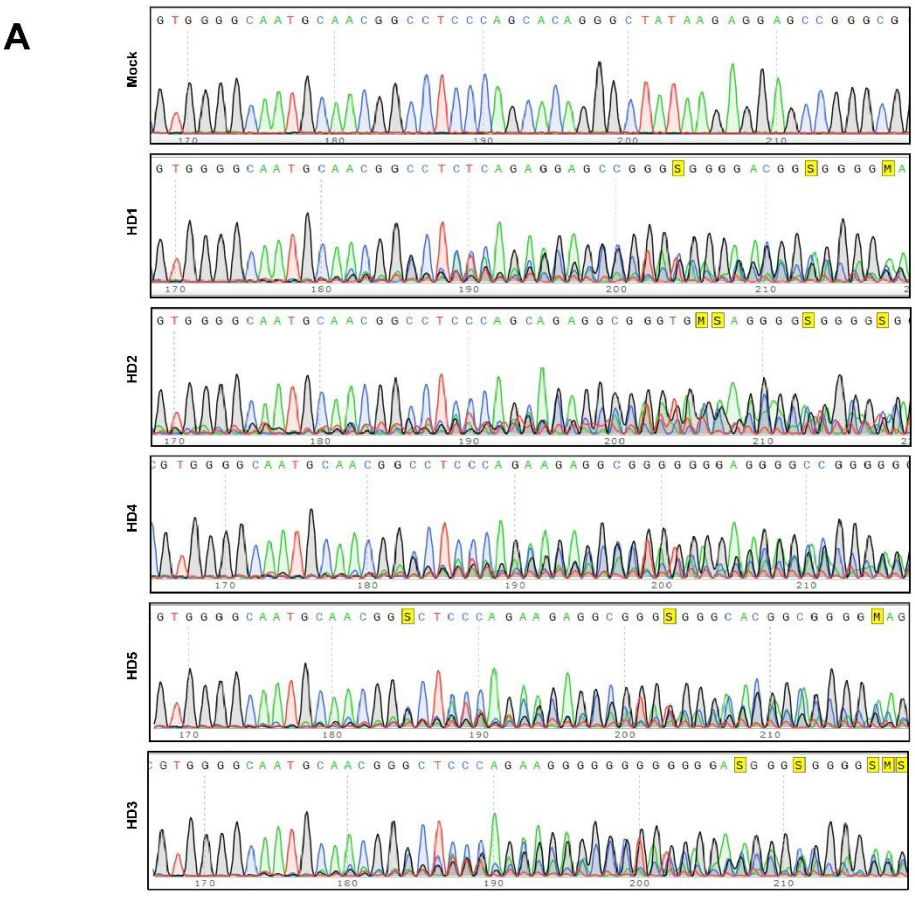

Figure S5. On target genome-editing efficiency in CD34$^+$ healthy donor HSPCs

A, Representative Sanger sequencing traces of DNA isolated from CD34$^+$ HSPCs of healthy donors 1-5 (n = 5) 4 days post-electroporation when starting the liquid culture differentiation (LCD day 0). The same DNA samples were used in the off-target validation assay by rhAMPseq analysis. **B,** *MILESTONE* on-target editing efficiency was assessed using NGS data generated from the rhAMPseq library using the CAS analyzer tool for paired nickases. Data represent means ± SD from five independent experiments.

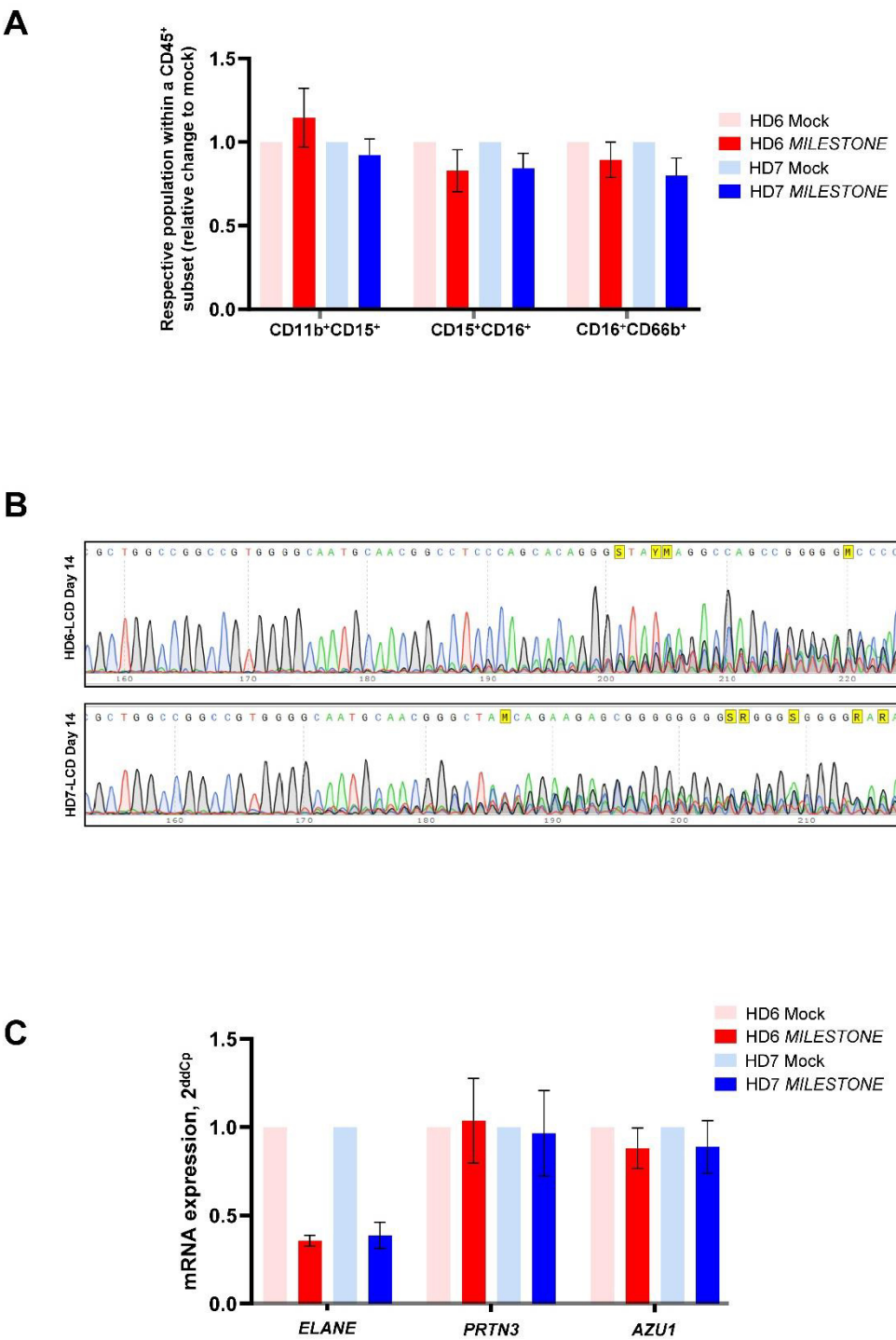

Figure S6. Specific reduction of *ELANE*, but not *PRTN3* and *AZU1* mRNA expression levels in *MILESTONE* edited HSPCs

A, Granulocytic differentiation of gene-edited $CD34^+$ HSPCs of healthy donors (n = 2) was assessed by liquid culture differentiation after 14 days of culture analyzing neutrophilic surface marker expression by FACS. Data were normalized to the respective Mock control group and represented as means ± SD from duplicates. **B,** Representative Sanger sequencing traces of *in vitro* generated gene-edited neutrophils on day 14 of *in vitro* liquid culture differentiation. **C,** qRT-PCR analysis of *ELANE*, *PRTN3*, and *AZU1* mRNA expression in HSPCs-derived neutrophils collected at day 14 of liquid culture differentiation. Data were normalized to the respective Mock control group. Data represent means ± SD from duplicates.

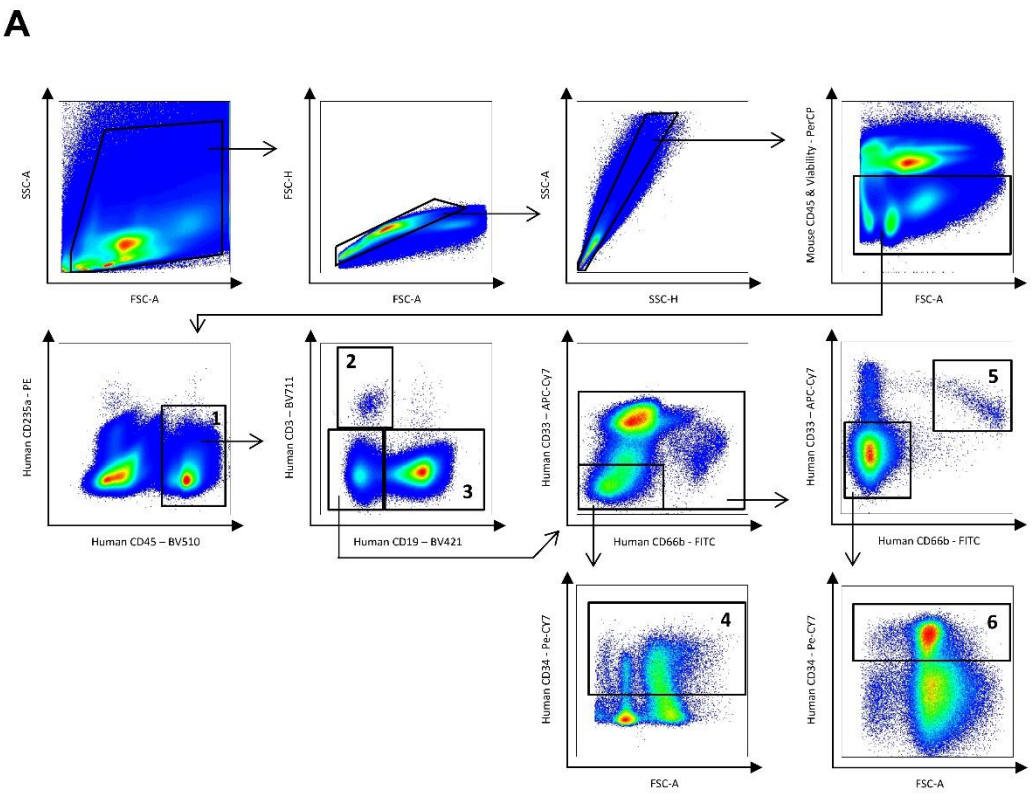

Figure S7. Gating strategy used for immunophenotyping of granulocytic differentiation *in vivo*

A, Gating strategy used to immunophenotype bone marrow of NSG mice 16 weeks post-transplantation. Population (1) marks human leukocytes selected based on the expression of CD45. B cells are characterized by CD19 expression (2) and T cells by CD3 antigen (3). Cells negative for both markers were then separated based on CD33 and CD66b expression. We considered cells to be HSPCs (4) if they were negative for CD33 and CD66b but expressed the CD34 antigen. Leukocytes that were CD33 and/or CD66b positive and also expressed high CD16 are neutrophils (5). Monocytes (6) lack CD66b expression and stained positive for CD14.

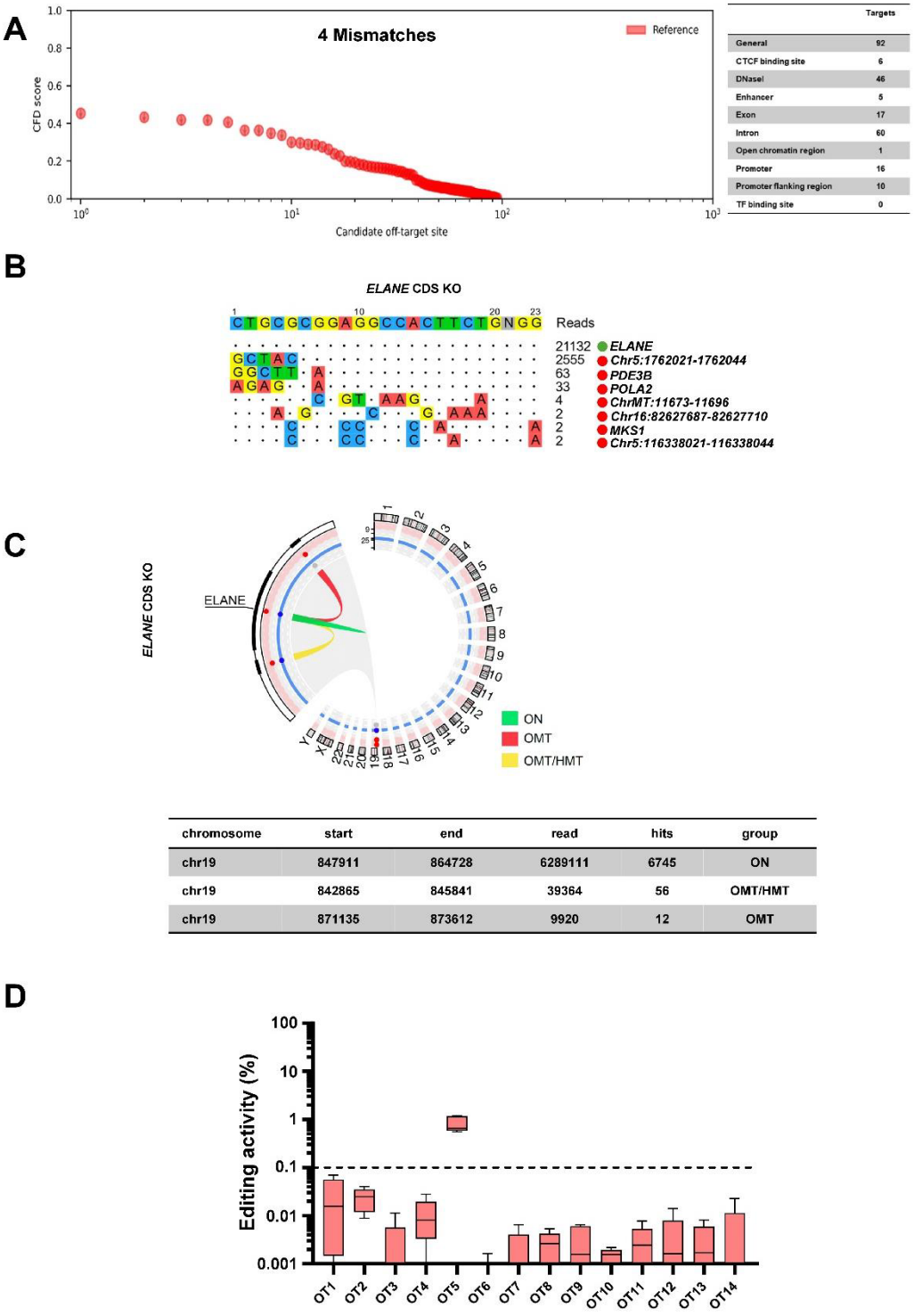

Figure S8. The safety profile of the *ELANE* CDS KO gene editing

A, *In silico* off-target profiling of the *ELANE* CDS KO sgRNA was performed using CRISPRme tool to determine potential off-target sites for up to 4 mismatches with calculated cutting frequency determination (CFD) score of each possible off-target site according to the human reference genome assembly GRCh38. The genomic region functional annotation of off-target sites was done using the

CRISPRitz tool. **B,** Genome-wide profiling of off-target cleavage in *ELANE* CDS KO gene-edited healthy donor $CD34^+$ HSPCs (HD10) using GUIDE-seq. The *ELANE* CDS target sequence is shown in the top line, with cleaved sites shown underneath. Mismatches to the on-target site are displayed and highlighted in color. GUIDE-seq read counts are shown to the right of each site. The on-target site is marked with a green circle, and the off-target sites are marked with a red circle. All genomic coordinates are based on the human reference genome assembly GRCh37. **C,** CAST-Seq for detecting chromosomal rearrangements in *ELANE* CDS KO gene-edited healthy donor $CD34^+$ HSPCs (HD11). The Circos plot indicates on-target aberrations in green and large deletions/inversion in red. All the genomic coordinates are based on human reference genome assembly GRCh38. **D,** Validation of potential off-target (OT) sites determined by rhAmpSeq in healthy donor $CD34^+$ HSPCs (HD 1-5). NGS data were analyzed using the CRISPECTOR pipeline. Data represent means ± SD from five independent experiments.

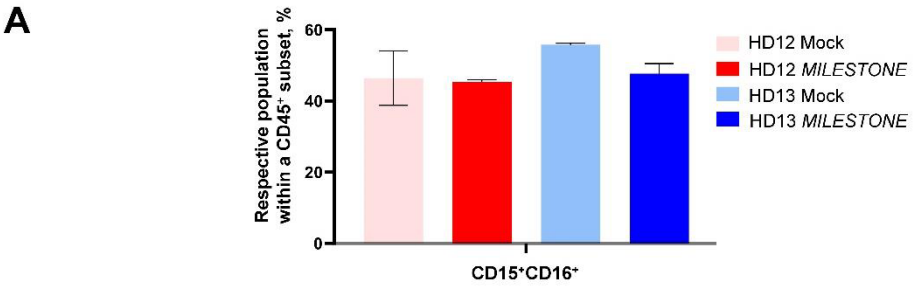

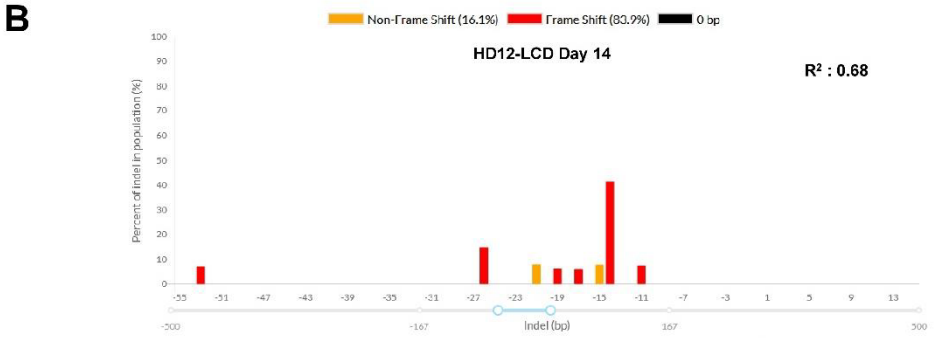

Contribution %	Net Indel
30.7	-14
15	-26
10.8	-14
8.1	-21
8	-15
7.6	-11
7.1	-53
6.4	-19
6.2	-17

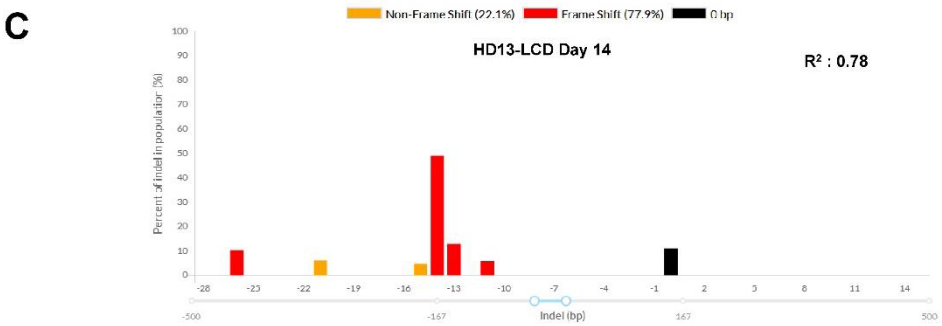

Contribution %	Net Indel
35.2	-14
13	-13
11.1	0
10.2	-26
8.4	-14
6.2	-21
5.8	-11
5.4	-14
4.8	-15

Figure S9. Differentiation status and gene-editing efficiency of *MILESTONE*-generated neutrophils used for transcriptomic profiling

A, *In vitro* generated neutrophils from *MILESTONE*-edited healthy donor CD34$^+$ HSPCs (n = 2) or Mock electroporated control group. Granulocytic differentiation of gene-edited CD34$^+$ HSPCs of healthy donors was assessed after 14 days of liquid culture differentiation, analyzing neutrophilic surface

marker expression by FACS. Data represent means ± SD from duplicates. **B, C,** *MILESTONE* gene editing efficiency in healthy donors` primary HSPCs was assessed by analyzing Sanger sequencing traces using deconvolution of complex DNA repair (DECODR) algorithm on day 14 of granulocytic liquid culture differentiation in HD12 (**B**) and HD13 (**C**) samples. Tables show exact values displayed in the corresponding bar diagram for the frequency and size of INDEL based on the DECODR algorithm.

C) Zeidler, A. et al., 2023, *Haematologica*

Differential transcriptional control of hematopoiesis in congenital and cyclic neutropenia patients harboring *ELANE* mutations

Alexander Zeidler,[1*] Natalia Borbaran-Bravo,[1*] Benjamin Dannenmann,[1] Malte Ritter,[1] Masoud Nasri,[1] Maksim Klimiankou,[1] Sergey Kandabarau,[1] Azadeh Zahabi,[1] Josef König,[2] Cornelia Zeidler,[3] Julia Skokowa[1] and Karl Welte[1,4]

[1]Department of Oncology, Hematology, Clinical Immunology, and Rheumatology, University Hospital Tübingen, Tübingen, Germany; [2]Hematology and Oncology, Ordensklinikum Elisabethinen, Linz, Austria; [3]Department of Oncology, Hematology, Immunology and Bone Marrow Transplantation, Hannover Medical School, Hannover, Germany and [4]Department of Pediatric Hematology and Oncology, University Children's Hospital Tübingen, Tübingen, Germany

AZ and NB-B contributed equally as first authors.

Correspondence: K. Welte
karl.welte@med.uni-tuebingen.de

Received: August 7, 2023.
Accepted: October 10, 2023.
Early view: October 19, 2023.

https://doi.org/10.3324/haematol.2023.284033

Abstract

Mutations in the *ELANE* gene, encoding the neutrophil elastase (NE) protein, are responsible for most cyclic neutropenia (CyN) cases and approximately 25% of congenital neutropenia (CN) cases. In CN and in CyN, a median of 2.8% of CD34$^+$ cells were early CD49f$^+$ hematopoietic stem cells (eHSC) that did not express *ELANE* and thus escape from the unfolded protein response (UPR) caused by mutated NE. In CyN, the CD49f$^+$ cells respond to granulocyte colony-stimulating factor (G-CSF) with a significant upregulation of the hematopoietic stem cell-specific transcription factors, C/EBPα, *MLL1, HOXA9, MEIS1*, and HLF during the ascending arm of the cycle, resulting in the differentiation of myeloid cells to mature neutrophils at the cycle peak. However, NE protein released by neutrophils at the cycle's peak caused a negative feedback loop on granulopoiesis through the proteolytic digestion of G-CSF. In contrast, in CN patients, CD49f$^+$ cells failed to express mRNA levels of HSC-specific transcription factors mentioned above. Rescue of C/EBPα expression in CN restored granulopoiesis.

Introduction

Cyclic neutropenia (CyN) and severe congenital neutropenia (CN) are autosomal-dominant inherited disorders of hematopoiesis that markedly differ in disease severity.[1] Mutations in the *ELANE* gene are considered largely responsible for most cases of CyN and CN. Because several identical *ELANE* mutations have been identified in both groups of patients,[2] genotyping alone is insufficient to establish a clinical diagnosis. CyN is characterized by regular oscillations of peripheral blood neutrophils from nearly normal to severely low counts, generally within 21-day cycles. Absolute neutrophil count (ANC) at nadir is often less than 200/mm^3 and is associated with fever, mouth ulcers, pharyngitis, sinusitis, and in some cases more severe infections with gram-negative bacteria.[3] By contrast, CN is characterized by recurrent, severe infections that develop in the first months of life, with ANC persistently less than 200/mm^3.[1,4] The availability of recombinant human granulocyte colony-stimulating factor (G-CSF) for clinical use in CN since 1987 and its successful application to CyN patients has changed the outcome for these patients, providing a markedly improved quality of life.[4-7] However, during the course of the disease, 53% of CN patients who harbor *ELANE* mutations and 17% of CyN patients acquire mutations in the gene for the G-CSF receptor, *CSF3R*.[1,8] Together with subsequently acquired mutations in, e.g., *RUNX1, CSF3R* mutations precede the development of myelodysplastic syndrome (MDS) or acute myeloid leukemia (AML).[8-11] The risk of developing leukemia in CN is considered to be 20%.[10] In CyN patients, G-CSF treatment does not abrogate the cycling of neutrophil counts but increases the amplitude of neutrophil counts during the cycle, leading to a shorter period of severe neutropenia and a reduction in the cycle length from 21 days to approximately 14 days.[5] This suggests an influence of G-CSF on the neutrophil cycling pathomechanism. There are reported cases of AML also in CyN patients.[11]

Recently, we and others reported that inhibition of the

proliferation and differentiation of hematopoietic stem and progenitor cells (HSPC) from CN patients harboring *ELANE* mutations is caused by an enhanced unfolded protein response (UPR) in the endoplasmic reticulum (ER) instigated by misfolded mutant NE protein.[1,12] This enhanced UPR is also recapitulated in induced pluripotent stem cells (iPSC) derived from CN patients with *ELANE* mutations.[13,14] However, the UPR does not equally affect all cells, for instance, the least primed early HSC (eHSC) expressing CD49f (integrin-α6)[15] escape from the damage since they do not express *ELANE*.[16] Most CD34$^+$ cells are lineage-restricted progenitors, and true self-renewing CD49f$^+$ eHSC are rare.[17,18] CD49f plays an important, conserved role in stem cell biology that has been reaffirmed by its importance in maintaining the self-renewal of stem cells in more than 30 tissues.[19]

The transcriptional control of differentiation from eHSC to primed myeloid cells is mainly regulated by C/EBPα.[20,21] Knockout of the *cebpa* gene or its 137 kb upstream enhancer in mice showed two major findings: (i) neutropenia in bone marrow (BM) and peripheral blood (PB); (ii) decrease in long-term HSC (LT-HSC) numbers.[22] In co-immunoprecipitation experiments, Collins *et al*. showed that C/EBPα is an essential collaborator of HOXA9 and MEIS1.[23] In addition, C/EBPα regulates the expression of the histone H3 lysine 4 (H3K4) methyltransferase MLL1, which, in turn, coordinates self-renewal, proliferation, and lineage-specific gene expression in HSC.[24] MLL1 dynamically and selectively regulates *Hox* gene expression.[25] Thus, C/EBPα induces the expression of HOXA9/MEIS1 and subsequent proliferation and differentiation of HSC directly or indirectly via MLL1. Combining gene expression analysis with genome-wide assessment of C/EBPα binding and epigenetic configurations, Hasemann *et al*. showed that C/EBPα modulates the epigenetic states of genes important for HSC function.[26] Another study also demonstrated that C/EBPα positively regulates HSC self-renewal, protects adult HSC from apoptosis, and maintains their quiescent state.[27]

In one of our earlier studies on the pathomechanism of CN, we demonstrated that the expression of C/EBPα is greatly reduced in the arrested promyelocytes of CN patients but normal in CyN patients.[28] We found that C/EBPα is directly regulated by the transcription factor lymphoid enhancer-binding factor 1 (LEF-1).[28] The significant reduction of C/EBPα in CN has been confirmed in iPSC derived from CN patients.[13,29]

The targets of C/EBPα, HOXA9 and MEIS1, are homeodomain transcription factors that are co-expressed in the most primitive eHSC subpopulation (i.e., CD49f$^+$). Their expression induce robust self-renewal of eHSC and expansion of the HSC pool.[30-32] Diminished HOXA9 function results in a reduction in multilineage long-term repopulating ability and diminished numbers of peripheral blood leukocytes in mice,[33] whereas overexpression of HOXA9 in bone marrow cells induces stem cell expansion.[34] HOXA9 might be the primary physiological determinant of HSC self-renewal.[35] Using single-cell transcriptomes of HSPC from cord blood, adult bone marrow, and fetal liver to search for human HSC markers with self-renewal capacity, Lehnertz *et al*. identified the master transcription factor HLF as one of the most selectively expressed genes in human HSC and proposed *HLF* as the defining gene of the human HSC state.[36] Giladi *et al*. also identified HLF as the most highly enriched transcription factor in HSC.[37]

Here, we demonstrate that the defective expression of C/EBPα, its targets MLL1, HOXA9, MEIS1, and HLF in CN but not in CyN discriminate between both disorders. During the ascending arm of the CyN cycle, G-CSF induced the proliferation of CD49f$^+$ eHSC and their differentiation into more mature CD34$^+$CD49f$^-$ cells, which respond to the transcription factor C/EBPα to differentiate into neutrophils. Moreover, during the downward arm of the cycle, NE released from neutrophils at the peak of the cycle causes negative feedback through proteolytic digestion of G-CSF, again causing neutropenia.

Methods

Patient samples

Five healthy donors, 13 CyN harboring *ELANE* mutations, and 13 *ELANE*-CN patients were used (*Online Supplementary Table S1*). All patients were treated with subcutaneous injections of Neupogen. BM samples of CN and CyN patients were collected in accordance with an annual follow-up recommendation of the SCNIR and the EHA.[38] The study was conducted under the approval of the Ethical Board of the Medical Faculty, University of Tübingen. Written informed consent was obtained from all participants.

Isolation of human CD34$^+$ cells

Human CD34$^+$ cells were isolated from BM mononuclear cells using Ficoll gradient centrifugation followed by magnetic bead separation using EasySep™ human CD34$^+$ selection kit II (STEMCELL Technologies, #17856).

Multicolor fluorescence-activated cell sorting analysis

Cells were washed with ice-cold phosphate-buffered saline (PBS) and stained with corresponding antibodies in PBS containing 2% fetal bovine serum and 0.02% sodium azide. We used: mouse anti-human CD38 (BD, #563964), mouse anti-human CD34 (BD, #348811), rat anti-human CD49f (BD, #563271), mouse anti-human CD90 (BD, #562685), and mouse anti-human CD45RA (BD, #560673). For intracellular NE protein analysis, cells were subsequently fixed and permeabilized using the Fix&Perm kit (Nordic Mubio, #GAS-002FOC), followed by incubation with a rabbit anti-human NE (abcam, #ab131260) antibody for 15 minutes (min) at room temperature, and subsequent incubation with a goat polyclonal secondary antibody to rabbit IgG-H&L (Alexa Fluor 488) (abcam, #ab150077) for 15 min at room

temperature. Cells were fixed with 0.5% paraformaldehyde and measured using a BD LSRFortessa.
Additional methods are available in the *Online Supplementary Appendix*.

Results

Dynamic cycle-dependent expression of C/EBPα and its target genes in hematopoietic stem cells from cyclic neutropenia patients

We first measured the percentage of CD34⁺CD49f⁺ early HSC in the BM of CN (N=3), CyN (N=8) and healthy donors' (HD) cord blood (CB) cells (N=6) by flow cytometry. Since the percentages of CD49f⁺ cells from CB CD34⁺ cells are comparable to the percentages of CD34⁺CD49f⁺ cells from the BM of children and young adults[39] we used them for comparison. We observed a median of 2.8% (range, 1.2-4.6%) and 2.8% (range, 1.7-7.3%) CD34⁺CD49f⁺ eHSC in CN and CyN patients` BM, respectively. HD CB cells contained 7.3% (range, 3.4-9.3%) CD34⁺CD49f⁺ eHSC. In CyN patients the percentage of CD49f⁺ cells was independent of the granulocyte cycle stage (Figure 1A).
We further evaluated possible cycle-dependent changes

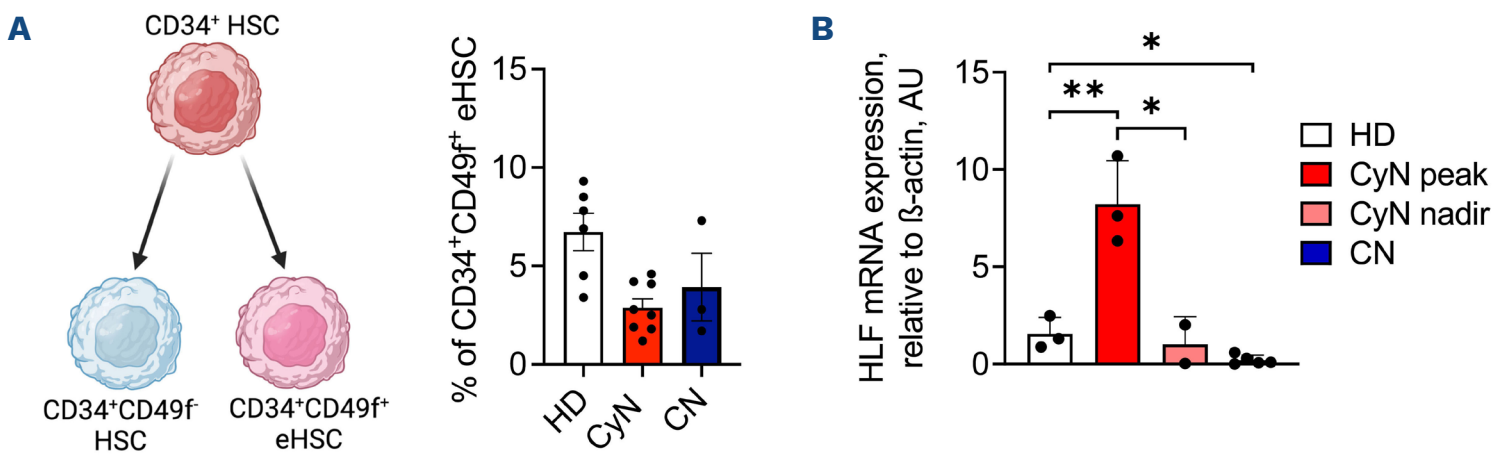

Figure 1. Cycle-dependent dynamics of transcription factors expression in hematopoietic stem and progenitor cells of cyclic neutropenia patients. (A) Left: schema of early CD49f⁺ hematopoietic stem cell (eHSC) specification, where eHSC with self-renewal capacity, but not more committed HSC, express the CD49f marker. Right: percentage of CD34⁺CD49f⁺ cells as assessed by fluorescence-activated cell sorting. Mean ± standard error of the mean are shown. (B, C) mRNA expression of the indicated genes in CD34⁺ bone marrow cells from healthy individuals (HD), cyclic neutropenia (CyN) patients at peak and nadir of neutrophil counts, and congenital neutropenia (CN) patients, measured by quantitative real-time polymerase chain reaction. Data were normalized to β-actin and are represented as mean ± standard deviation in duplicates. Unpaired *t* test, **P*<0.05, ***P*<0.01; ****P*<0.001.

in mRNA expression levels of the stemness marker HLF as well as the transcription factor C/EBPα and its target genes MEIS1, HOXA9, and MLL1, in CD34⁺ HSPC of CyN and CN patients, and healthy individuals. We found that HLF mRNA levels were upregulated at the CyN peak of neutrophil counts, as compared to CyN nadir where HLF levels were comparable to healthy individuals. In CN, HLF expression was significantly downregulated as compared to healthy individuals (Figure 1B; *Online Supplementary Table S2*). C/EBPα mRNA expression was also upregulated at the peak of the cycle and reduced to the levels of healthy individuals at the nadir of the cycle. As already published, we observed almost no C/EBPα expression in CN patients (Figure 1C). Next, we aimed to assess C/EBPα activity during the CyN cycle by measuring the expression of its target genes. Using the UCSC Genome Browser and data from the ReMap Atlas of regulatory regions,[40] we confirmed previous reports that showed C/EBPα binding to the promoters and upstream regulatory regions of HLF, MEIS1, and MLL1 (*Online Supplementary Figure S1A*). In the context of HOXA9 regulation by C/EBPα, it is known that C/EBPα acts as part of a multiprotein complex that contains HOXA9 to promote HOXA9 mRNA expression in an autocrine manner.[41] We found that mRNA levels of all selected factors were strongly upregulated at the peak of the cycle in CyN compared to healthy individuals and were only moderately expressed at the nadir (Figure 1C). In CN, expression of all these factors was diminished when compared to healthy controls (Figure 1C).

Early CD49f⁺ hematopoietic stem cells lack *ELANE* mRNA and neutrophil elastase protein expression

Knowing that CyN and CN patients harbor *ELANE* mutations, and that mutated elastase protein may damage hematopoiesis, we evaluated at which stage of hematopoietic differentiation *ELANE* mRNA and protein are expressed in physiological conditions in healthy individuals. We found the absence of NE protein expression in bone marrow CD49f⁺ eHSC of three HD (Figure 2A). Single-cell RNA-sequencing analysis of CD34⁺ HSC from two HD revealed that only 10% of CD49f⁺ (ITGA6⁺) eHSC co-expressed *ELANE* mRNA (58/560 cells), 90% of the cells express either *ELANE* or *ITGA6*, but not both (Figure 2B). The discrepancy in the *ELANE* mRNA and NE protein expression levels can be explained by different kinetics and efficiencies of *ELANE* mRNA transcription and NE protein translation. The most important finding is that NE protein is absent in CD49f⁺CD34⁺ cells.

Granulocytic differentiation of cyclic neutropenic induced pluripotent stem cells is comparable to healthy donor cells

We further generated induced pluripotent stem cells (iPSC) from peripheral blood mononuclear cells (PBMNC) of three *ELANE*-CyN patients. iPSC showed reliable expression levels of mRNA (*SOX2, NANOG*, and *DNMT3A*) and cell surface proteins (*TRA-1-60* and *SSEA4*) that are markers of pluripotency (*Online Supplementary Figure S2A, B; data not shown*). They also had the potential to spontaneously differentiate into ectoderm and endoderm (*Online Supplementary Figure S2C*). We applied *ELANE*-CN iPSC, already available in the laboratory,[14,29] to compare their hematopoietic and granulocytic differentiation potential between CN and CyN using the embryoid body (EB) based hematopoietic differentiation.[42] Flow cytometry analysis of iPSC-derived hematopoietic cells obtained at day 14 of differentiation revealed that the majority of HSC were early HSC (CD34⁺CD43⁺) in CN iPSC (Figure 3A), which corresponded to up to 50% CD49f⁺ eHSC in CyN and HD iPSC (Figure 3B). On day 28 of differentiation, the percentage of mature neutrophils was severely reduced in iPSC derived from CN patients while, interestingly, the proportion of neutrophils produced by CyN iPSC was comparable to HDr iPSC (Figure 3C). The mRNA expression levels of C/EBPα and MEIS1 in iPSC-derived HSC collected on day 14 of differentiation recapitulated the results obtained from primary HSC. C/EBPα levels were severely downregulated in HSC derived from CN iPSC as compared to CyN HSC (Figure 3D). MEIS1 levels were markedly higher in CyN HSC as compared to CN and HD HSC (Figure 3E, left). Intriguingly, HOXA9 expression in iPSC-derived HSC was very low in all samples (Figure 3E)

A

	HSPC CD34⁺CD38⁻	HSC CD34⁺CD38⁻ CD45RA⁻ CD90⁺	CD49f⁺ HSC CD34⁺CD38⁻ CD45RA⁻ CD90⁺CD49f⁺	MPP CD34⁺CD38⁻ CD45RA⁻ CD90⁻	CMP/MEP CD34⁺CD38⁺ CD45RA⁻
HD 1	7,29	1,34	0,0	62,1	99,6
HD 2	13	0,8	0,0	66,8	97,8
HD 3	15,8	1,0	0,0	43,3	97,6

B

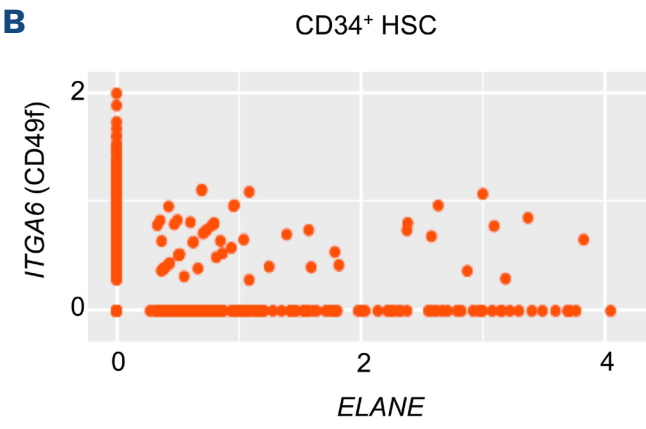

Figure 2. *ELANE* mRNA and protein expression in hematopoietic stem cell subsets. (A) Percentage of neutrophil elastase (NE) expressed in different human stem and progenitor cell subsets in the bone marrow of 3 healthy donors (HD) measured by flow cytometry. (B) Co-expression plot of ITGA6 (y-axis) and ELANE (x-axis) expression in single CD34⁺ hematopoietic stem cells (HSC) from 2 HD. Values plotted were normalized to read counts. MPP: multipotent progenitors; CMP: common myeloid progenitors; MEP: megakaryocytic-erythroid progenitors.

and more than ten times lower than in primary cells from e.g., CyN patients (Figure 1E). This is in agreement with reports from other laboratories, that HOXA9 expression in iPSC or in ESC is very low.[43] Therefore, it is hard to make any solid conclusions based on these data. However, there is a clear difference in the expression levels of C/EBPα, and MEIS1 and thus myeloid differentiation between CyN and CN iPSC.

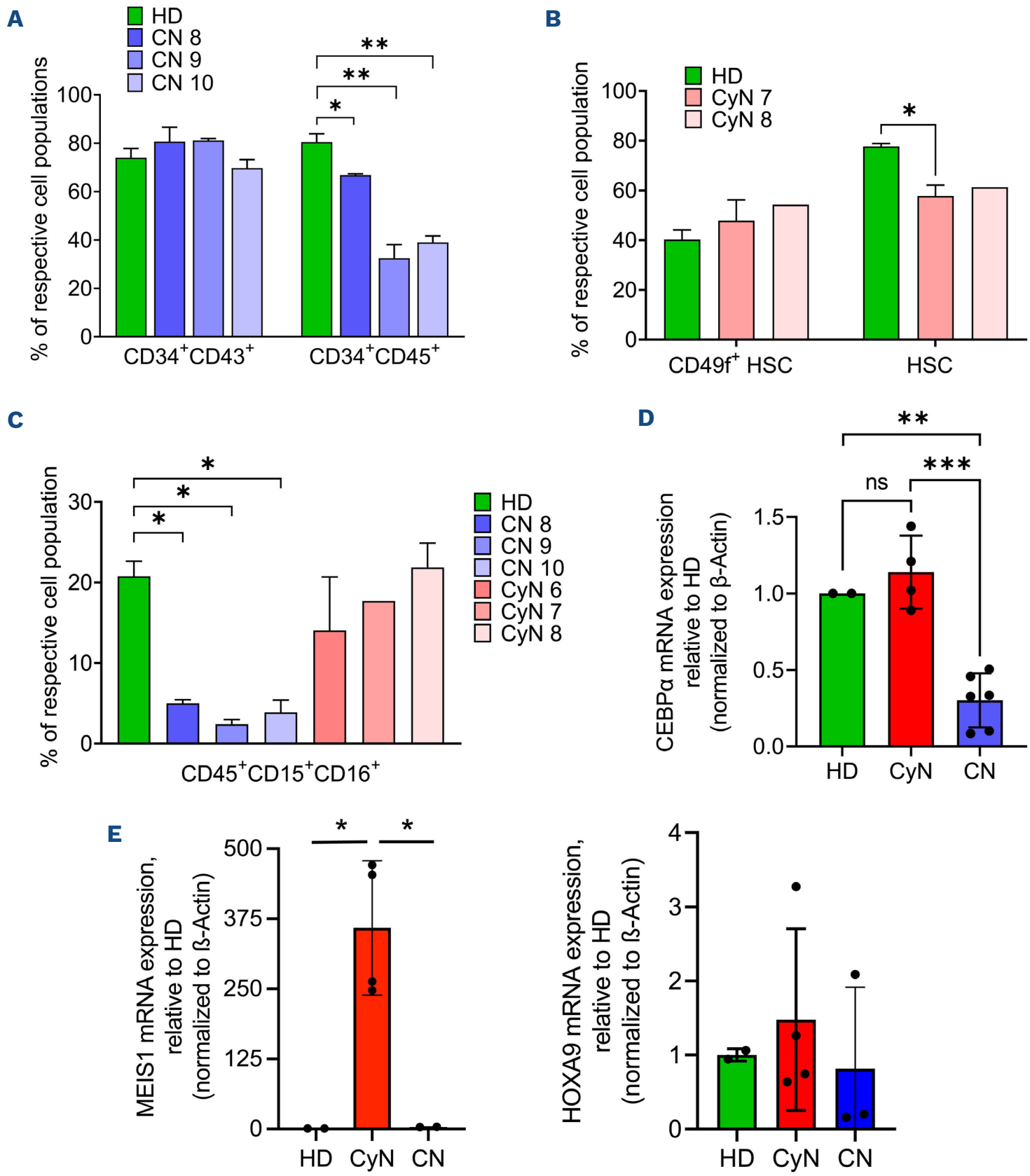

Figure 3. Evaluation of granulocytic differentiation of induced pluripotent stem cells derived from congenital neutropenia and cyclic neutropenia patients harboring *ELANE* mutations. (A) Evaluation of early hematopoietic differentiation of induced pluripotent stem cells derived (iPSC) derived from 1 healthy donor (HD) and 3 congenital neutropenia (CN) patients using flow cytometry. Data are represented as mean ± standard deviation (SD) from 2 independent experiments, in duplicates; unpaired *t* test, **P*<0.05; ***P*<0.01. (B) Evaluation of early hematopoietic differentiation of iPSC derived from 1 healthy donor (HD) and 2 cyclic neutropenia (CyN) patients using flow cytometry. Data are represented as mean ± SD from 2 independent experiments, in duplicates, Unpaired *t* test, **P*<0.05. (C) Granulocytic differentiation of iPSC generated from 1 HD, 3 CN and 3 CyN patients. The percentage of $CD45^+CD15^+CD16^+$ neutrophils was assessed by flow cytometry of suspension cells on day 28 of embryoid body-based differentiation. Data are represented as mean ± SD from 2 independent experiments, each in duplicates. Unpaired *t* test, **P*<0.05. (D, E) Relative mRNA expression of C/EBPα (D), MEIS1 and HOXA9 (E) in $CD34^+$ cells derived from iPSC of CyN patients and CN patients to HD cells measured by quantitative real-time polymerase chain reaction. Data were normalized to β-actin and are represented as mean ± SD in duplicates. Unpaired *t* test, **P*<0.05.

Rescue with C/EBPα restored defective granulopoiesis in primary hematopoietic stem cells of two *ELANE* congenital neutropenia patients

We next tested whether restoration of the diminished C/EBPα expression in primary CD34$^+$ HSPC of CN patients harboring *ELANE* mutations would affect their granulocytic differentiation *in vitro*. We used an RFP$^+$-lentiviral vector to overexpress C/EBPα in CD34$^+$ HSPC obtained from three *ELANE*-CN patients and then differentiated transduced cells to neutrophils in liquid culture (Figure 4A). After 14 days of differentiation, we found a reduction in granulocyte-monocyte progenitor cells (GMP/MB: RFP$^+$CD45$^+$CD33^{high}), while promyelocytes/myelocytes (PM/MY: RFP$^+$CD45$^+$CD33^{DIM}CD16$^-$) and band cells/polymorphonuclear neutrophils (BC/PMN: RFP$^+$CD45$^+$CD33^{DIM}CD16$^+$) were markedly higher in C/EBPα transduced cells as compared to RFP control (Figure 4B; *Online Supplementary Figure S3A*). Cytospin morphology of one *ELANE*-CN patient confirmed the improved granulocytic differentiation in C/EBPα transduced cells, as compared to RFP control (Figure 4C).

Strong correlation of cyclic neutrophil elastase plasma levels with absolute neutrophil count in a cyclic neutropenia patient

Finally, we investigated whether the cyclic behavior of NE protein expression is also observed in CyN plasma. We collected blood samples from one CyN patient over three cycles and assessed NE values using a NE-specific enzyme-linked immunosorbent assay (ELISA). This assay revealed a dramatic difference in NE levels according to the phase of the cycle, with high expression during the cycle peak and very low levels at the cycle nadir (Figure 5A). NE protein levels strongly correlated with ANC during the cycles (Figure 5A, B). The NE levels in the plasma of three healthy individuals not treated with G-CSF were 66.98+1.94 ng/mL and of three individuals treated with 5 mg/kg/day of G-CSF for 3 days were 374.3+123.0 ng/mL (Figure 5A). In order to prove the cycle-dependent correlation between NE levels and ANC, more patients should be analyzed in the future.

Discussion

By searching for the different pathomechanisms of CN and CyN, we found that C/EBPα expression discriminates between CN and CyN. C/EBPα, one of the key factors in granulopoiesis,[20] was greatly reduced in CN, but not in CyN. In addition to C/EBPα, mRNA expression levels of its target genes *MLL1, MEIS1, HOXA9*, and *HLF* were substantially decreased, or even absent, in CD34$^+$ cells from CN patients

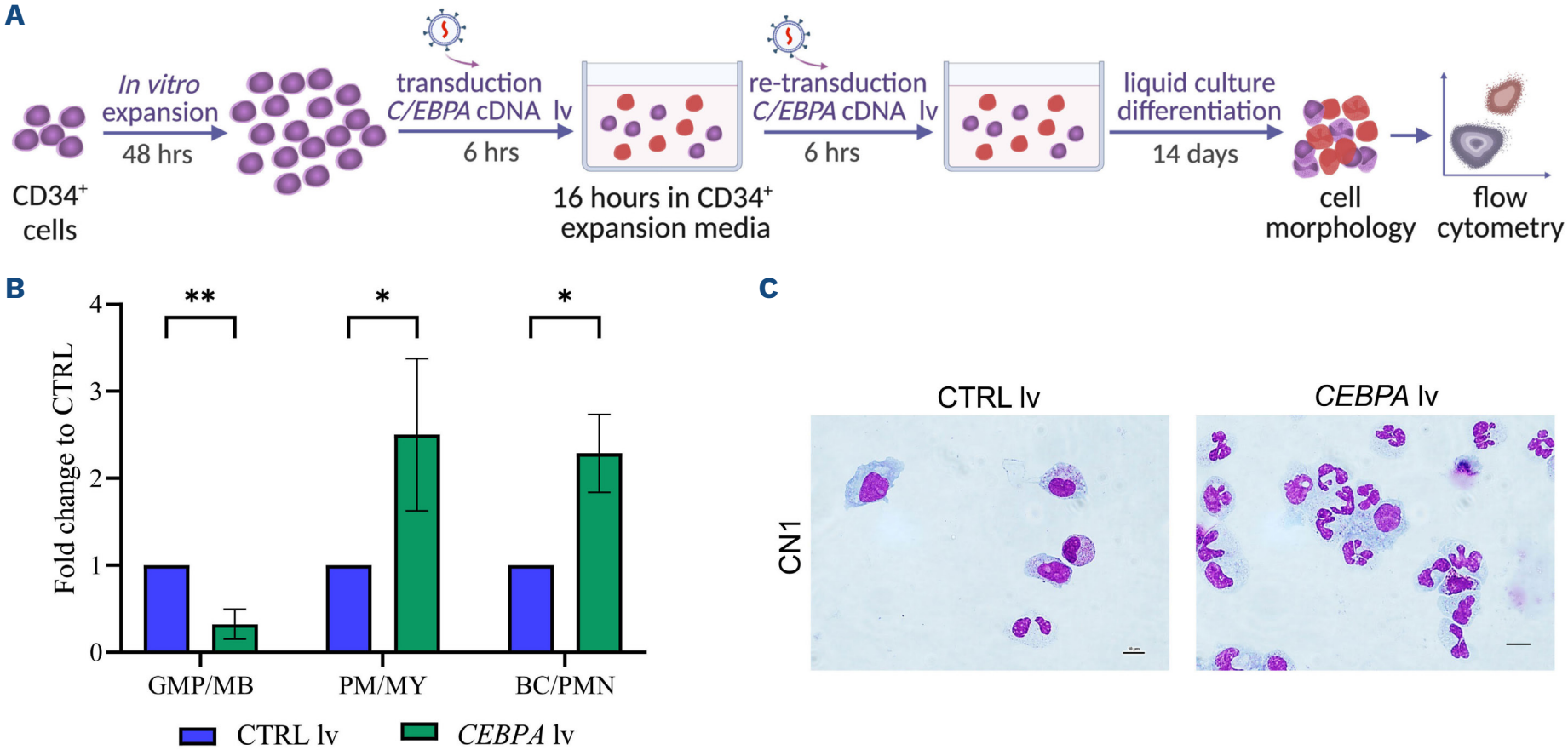

Figure 4. Ectopic expression of C/EBPα rescues neutrophilic differentiation of CD34$^+$ hematopoietic stem and progenitor cells of congenital neutropenia patients. (A) Schematic of the experimental procedure: CD34$^+$ hematopoietic stem and progenitor cells (HSPC) of 3 *ELANE* congenital neutropenia (CN) patients were expanded *in vitro*, transduced with lentivirus particles containing C/EBPα cDNA or a control (CTRL) virus with the red fluorescent marker RFP, and differentiated in liquid culture for 14 days. (B) Flow cytometry analysis of granulocyte-monocyte progenitors/myeloblasts (GMP/MB; RFP$^+$CD45$^+$CD33^{high}), promyelocytes/myelocytes (PM/MY; RFP$^+$CD45$^+$CD33^{DIM}CD16$^-$) and band cells/polymorphonuclear cells (BC/PMN; RFP$^+$CD45$^+$CD33^{DIM}CD16$^+$) at day 14 of differentiation. Data are represented as fold-change increase to control RFP transduced cells and as mean ± standard deviation, in duplicates. Unpaired *t* test, *P<0.05, **P<0.01. (C) Representative images of May-Grunwald-Giemsa-stained preparations of differentiated cells on day 14 of culture (60X magnification, scale bars =10 μm).

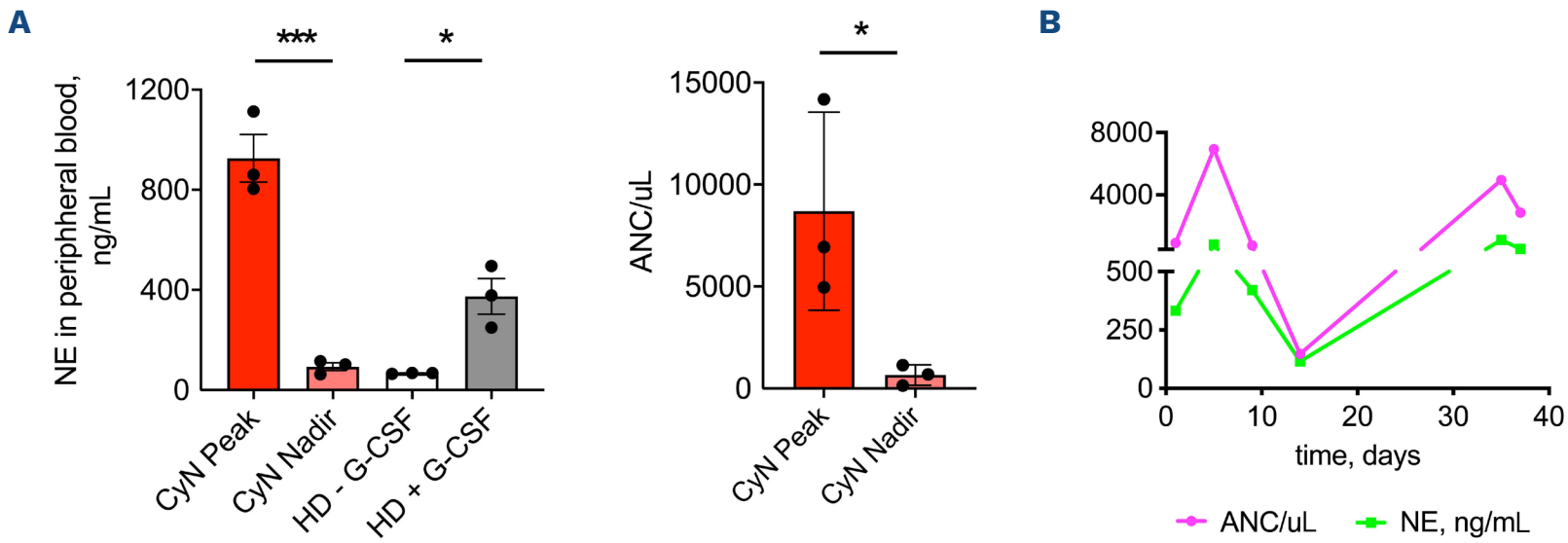

Figure 5. Correlation of neutrophil elastase plasma levels and absolute neutrophil count in cyclic neutropenia cycle. (A) Neutrophil elastase (NE) plasma levels (left panel) assessed by enzyme-linked immunosorbant assay and absolute neutrophil counts (ANC) (right panel) in peripheral blood at peaks and nadirs of neutrophil cycles of 1 cyclic neutropenia (CyN) patient over 3 cycles. NE plasma levels were also evaluated in healthy donors (HD) treated or not with recombinant human granulocyte colony-stimulating factor (rhG-CSF). Data are represented as mean ± standard deviation. Unpaired *t* test, **P*<0.05, ****P*<0.001. (B) Time course of NE levels and ANC in 1 CyN patient.

compared with CD34$^+$ cells from healthy controls (Figure 1C). Indeed, self-renewal, proliferation, and differentiation of HSC are dependent on the epigenetic activation, e.g,. by histone-acetylation of transcription factors such as C/EBPα, the C/EBPα-target genes MLL1, MEIS1, and HOXA9[23-25,30,31,33,35] and HLF, all of them abrogated in CN. We need to emphasize, that we were able to acquire a relatively small number of patient samples for this investigation and further studies should be performed on large patient cohorts.

The severely diminished expression of HSC-specific transcription factors CEBPA and MEIS1 in CN, as compared to CyN, could be recapitulated and confirmed in iPSC established from these group of patients. Intriguingly, HOXA9 was expressed at least ten times lower in iPSC-derived HSC than in primary CD34$^+$ cells. The low expression of HOXA9 in iPSC or in ESC was already reported by others[43] supporting our data in Figure 3E. Ramos-Meja *et al*. identified HOXA9 as the most downregulated gene in hESC-derived HSPC as compared with CB-derived CD34$^+$ cells, HOXA9 expression was 60-fold lower in differentiating day 15 EB than in CB-CD34$^+$ cells. The principal problem of low HOXA9 expression in iPSC cells was not the subject of our study. The low expression of C/EBPα in iPSC derived from CN patients was already reported.[13]

In contrast to CN patients, at the peak of the cycle, CD34$^+$ cells from CyN patients, which included CD49f$^+$ eHSC, expressed C/EBPα, MLL1, MEIS1, HOXA9, and HLF at levels significantly higher than those in healthy controls (Figure 1B, C). Increased expression of these stem-cell-specific transcription factors during the ascending arm of the neutrophil cycle in CyN induces self-renewal, proliferation, and differentiation of CD49f$^+$ eHSC, which give rise to more mature HSC, myeloid progenitor cells, and mature neutrophils. The high expression of HLF at the peak of the cycle (Figure 1B) ensures the high self-renewal capacity of the CD49f$^+$ eHSC in CyN and can be used as a biomarker for the presence of self-renewing, naïve HSC. Indeed, HLF is one of the most selectively expressed genes in human HSC with self-renewal capacity and the defining factor of the human HSC state.[36,37] Intriguingly, the same *ELANE* mutation can cause CN and CyN. We demonstrated that the UPR-induced inhibition of proliferation and differentiation of HSC reported in CN is incomplete in CyN[16] reflecting the fact that some eHSC escape from UPR-related damage. In this study, we showed that these escaper cells are CD34$^+$CD49f$^+$ eHSC. The asymmetrical self-renewal of CD34$^+$CD49f$^+$ eHSC gives rise to equal numbers of CD49f$^+$ eHSC and committed CD34$^+$CD49f$^-$ HSC that differentiate to progenitor cells and ultimately to mature neutrophils.[17] CD49f$^+$ cells are eHSC with the capacity for self-renewal that only exist at low frequencies within the CD34$^+$ cell population.[15,16] The CD49f$^+$ escaper cells in CN and in CyN are not affected by UPR, since they do not express *ELANE* but respond to G-CSF.[15,46] Indeed, single-cell RNA-sequencing analyses of individual CD34$^+$ cells revealed that *ELANE* is not co-expressed with integrin α6 (CD49f antigen), indicating that CD49f$^+$ eHSC do not express *ELANE* (Figure 2B). Additionally, we found no NE protein in CD49f$^+$ eHSC by FACS analysis (Figure 2A). Avellino *et al*. also reported that *ELANE* is not expressed in LT-HSC,[22] further supporting our hypothesis that escaper eHSC are not affected by the UPR. In CN, CD49f$^+$ eHSC are not capable of asymmetric division, proliferation, and differentiation due to the lack of hematopoiesis-specific transcription factors, C/EBPα, MLL1, MEIS1, HOXA9, and HLF. However, rescue of C/EBPα expression by ectopic expression of C/EBPα, cDNA in CD34$^+$ cells of three *ELANE* CN patients led to strongly improved differentiation to neutrophils *in vitro*, confirming the crucial role of C/EBPα in the pathomechanism of CN and in discriminating between CN and CyN.

During the downward arm of the cycle, there is a decrease

in HSC-specific transcription factor expression caused by negative feedback mediated by an inhibitor/s released by mature neutrophils at the peak of the cycle. Early reports suggested that, in CyN, disruption of such an autoregulatory feedback loop would explain cycling.[45,46] Horwitz *et al*. favored a feedback model in which mature neutrophils elaborate an inhibitor of myelopoiesis whose concentration depends upon the number of neutrophils present.[47] Indeed, we were able to demonstrate that the concentration of NE in CyN correlates with the number of neutrophils in one CyN patient (Figure 5A, B), suggesting that the NE released from neutrophils at the peak of the cycle is a strong candidate mediator of the negative feedback loop. This correlation needs to be confirmed by the evaluation of more patients in the future. NE is already known to provide feedback regulation of granulopoiesis through direct proteolytic action on G-CSF and the G-CSF receptor.[48,49] We further demonstrated that treatment with NE digests human recombinant G-CSF.[50] Li and Horwitz hypothesized that the CN phenotype is unlikely to result from haploinsufficiency in the proteolytic activity of mutated NE toward native substrates.[51] Their study also proposed the "chalone" hypothesis, in which neutrophils homeostatically regulate their production by inhibiting granulopoiesis. Efforts to track down the chalone led to the purification of NE protein.[52] The relatively high numbers of neutrophils at the peak of the cycle release NE causing proteolytic digestion of G CSF. Intriguingly, in CN, levels of NE in mature neutrophils and in plasma were decreased, whereas in CyN they were comparable to healthy individuals,[53] which is dependent on the cycle stage (Figure 5A, B). Therefore, there is a sufficient amount of proteolytically active NE in the plasma of CyN patients, especially at the peak of the cycle, to promote the digestion of G-CSF. Indeed, Watari *et al*. showed G-CSF levels below the detection limit at the peak of the cycle and 165 pg/mL at the nadir of the cycle in a patient with CyN.[54] The lack of biologically active G-CSF at the peak leads to a decrease in the expression of transcription factors in CD49f$^+$ eHSC (escaper cells), which is normally triggered by G-CSF. The amount of NE released by neutrophils at the peak is sufficient to abrogate the proliferation and differentiation of CD49f$^+$ eHSC. Moreover, the majority of NE-expressing, more mature CD34$^+$CD49f$^-$ cells are affected by the UPR.

In healthy individuals, the NE protein released by neutrophils and the degree of proteolytic digestion of G-CSF is not sufficient to completely block the proliferation of the relatively high number of CD34$^+$ cells but instead functions only as an autoregulatory feedback loop for granulopoiesis. At the nadir of the cycle, high UPR activity in CD34$^+$ cells containing CD49f$^+$ eHSC, as measured by elevated ATF6, BiP, and PERK expression,[16] again leads to the damage of the newly generated NE-expressing CD34$^+$ HSPC. Because of its low release at the nadir attributable to the low neutrophil counts, NE no longer affects G-CSF levels, and thus G-CSF is available for the induction of proliferation and differentiation of the remaining CD49f$^+$ eHSC during the ascending arm of the cycle. The reduction in the cycle length from 21 to 14 days upon G-CSF therapy might be attributable to G-CSF-induced increases in the proliferation of CD49f$^+$ eHSC during the ascending arm of the cycle. Indeed, CD49f$^+$ eHSC can respond to treatment with G-CSF.[46] Therefore, the cycling of neutrophils is caused by cycling G-CSF-triggered transcriptional activities of CD49f$^+$ eHSC, which are not affected by the UPR. Therefore, high levels of the stem cell factors, HLF, C/EBPα, MLL1, HOXA9, and MEIS1, at the peak of the cycle induce proliferation and self-renewal of HSC which differentiate to progenitor cells and neutrophils.

In CN, G-CSF is unable to induce the proliferation of CD34$^+$ cells because they are impacted by the UPR and the CD49f$^+$ cells fail to express stem cell-specific transcription factors. This disables the generation of sufficient numbers of HSC and neutrophils. CN patients require treatment with high dosages of G-CSF to overcome this UPR-mediated block of granulocytic differentiation. How much G-CSF is required to produce more than 1,000 neutrophils/μL is, therefore, most likely dependent on the degree to which G-CSF is degraded by NE.

In summary, by searching for different molecular pathomechanisms of CyN and CN, we identified that C/EBPα expression and its targets HLF, MLL1, MEIS1, and HOXA9, in CD34$^+$ HSC discriminate between CN and CyN. Whereas in CN patients, expression of these factors was defective or absent, in CyN we observed a cycle-dependent increase in the expression of these five factors, leading to the self-renewal, proliferation, and differentiation of CD49f$^+$ eHSC. Ectopic expression of C/EBPα in CN rescued the differentiation to neutrophils. In CyN, CD49f$^+$ eHSC within the CD34$^+$ cell population escape UPR damage because they do not express *ELANE*. This reveals the high transcriptional activity of CD49f$^+$ eHSC (escaper cells) in response to G-CSF at the peak of the cycle, which ensures their differentiation to sufficient neutrophil numbers. However, the neutrophils at the peak of the cycle release NE causing proteolytic digestion of G CSF leading to a lack of biologically active G-CSF and a subsequent decrease in the expression of transcription factors in CD49f$^+$ eHSC (escaper cells). On the basis of these findings, we propose that the therapeutic options for patients suffering from CN or CyN would be either to inhibit the mutated NE activity with, for example, an elastase inhibitor,[55] or to delete or correct the *ELANE* gene using gene therapy.[56] Another approach could be to treat CN patients with a newly designed G-CSF that is resistant to proteolytic digestion by NE.[50]

Disclosure

No conflicts of interest to disclose.

Contributions

KW designed the study. KW and JS supervised the experimentation and wrote the manuscript. AZ and NB-B performed main experiments and analyzed the data. MR performed FACS analysis. BD, AZa and MN assisted with iPSC experiments. MK and SK performed scRNA-seq data analysis. MK performed

prediction of C/EBPα binding to target genes. KH assisted with qRT-PCR and FACS. CZ and JK provided patients material.

Acknowledgments

We thank K. Hähnel and R. Bernhard for their excellent technical support.

Funding

This work was supported by the Intramural Fortüne program of the Medical Faculty of the UKT (to MK, AZ), Madeleine Schickedanz Kinderkrebsstiftung (to JS, KW, MK, MN), DFG (to JS, AZ), BMBF (to JS, KW, CZ, SK), and the COST Action European Network for Innovative Diagnosis and Treatment of Chronic Neutropenias (EuNet-INNOCHRON) (to KW, CZ, MK, JS). We acknowledge the support by the Open Access Publishing Fund of the University of Tübingen.

Data-sharing statement

All data are available on request from the corresponding author.

References

1. Skokowa J, Dale DC, Touw IP, Zeidler C, Welte K. Severe congenital neutropenias. Nat Rev Dis Primers. 2017;3:17032.
2. Makaryan V, Zeidler C, Bolyard AA, et al. The diversity of mutations and clinical outcomes for ELANE-associated neutropenia. Curr Opin Hematol. 2015;22(1):3-11.
3. Dale DC, Welte K. Cyclic and chronic neutropenia. Cancer Treat Res. 2011;157:97-108.
4. Bonilla MA, Dale D, Zeidler C, et al. Long-term safety of treatment with recombinant human granulocyte colony-stimulating factor (r-metHuG-CSF) in patients with severe congenital neutropenias. Br J Haematol. 1994;88(4):723-730.
5. Hammond WP, Price TH, Souza LM, Dale DC. Treatment of cyclic neutropenia with granulocyte colony-stimulating factor. N Engl J Med. 1989;320(20):1306-1311.
6. Bonilla MA, Gillio AP, Ruggeiro M, et al. Effects of recombinant human granulocyte colony-stimulating factor on neutropenia in patients with congenital agranulocytosis. N Engl J Med. 1989;320(24):1574-1580.
7. Dale DC, Bolyard A, Marrero T, et al. Long-term effects of G-CSF therapy in cyclic neutropenia. N Engl J Med. 2017;377(23):2290-2292.
8. Klimiankou M, Uenalan M, Kandabarau S, et al. Ultra-sensitive CSF3R deep sequencing in patients with severe congenital neutropenia. Front Immunol. 2019;10:116.
9. Skokowa J, Steinemann D, Katsman-Kuipers JE, et al. Cooperativity of RUNX1 and CSF3R mutations in severe congenital neutropenia: a unique pathway in myeloid leukemogenesis. Blood. 2014;123(14):2229-2237.
10. Rosenberg PS, Zeidler C, Bolyard AA, et al. Stable long-term risk of leukaemia in patients with severe congenital neutropenia maintained on G-CSF therapy. Br J Haematol. 2010;150(2):196-199.
11. Klimiankou M, Mellor-Heineke S, Klimenkova O, et al. Two cases of cyclic neutropenia with acquired CSF3R mutations, with 1 developing AML. Blood. 2016;127(21):2638-2641.
12. Nustede R, Klimiankou M, Klimenkova O, et al. ELANE mutant-specific activation of different UPR pathways in congenital neutropenia. Br J Haematol. 2016;172(2):219-227.
13. Nayak RC, Trump LR, Aronow BJ, et al. Pathogenesis of ELANE-mutant severe neutropenia revealed by induced pluripotent stem cells. J Clin Invest. 2015;125(8):3103-3116.
14. Dannenmann B, Zahabi A, Mir P, et al. Human iPSC-based model of severe congenital neutropenia reveals elevated UPR and DNA damage in CD34+ cells preceding leukemic transformation. Exp Hematol. 2019;71:51-60.
15. Velten L, Haas SF, Raffel S, et al. Human haematopoietic stem cell lineage commitment is a continuous process. Nat Cell Biol. 2017;19(4):271-281.
16. Mir P, Klimiankou M, Findik B, et al. New insights into the pathomechanism of cyclic neutropenia. Ann N Y Acad Sci. 2020;1466(1):83-92.
17. Notta F, Doulatov S, Laurenti E, Poeppl A, Jurisica I, Dick JE. Isolation of single human hematopoietic stem cells capable of long-term multilineage engraftment. Science. 2011;333(6039):218-221.
18. Belluschi S, Calderbank EF, Ciaurro V, et al. Myelo-lymphoid lineage restriction occurs in the human haematopoietic stem cell compartment before lymphoid-primed multipotent progenitors. Nat Commun. 2018;9(1):4100.
19. Krebsbach PH, Villa-Diaz LG. The role of integrin α6 (CD49f) in stem cells: more than a conserved biomarker. Stem Cell Dev. 2017;26(15):1090-1099.
20. Radomska HS, Huettner CS, Zhang P, Cheng T, Scadden DT, Tenen DG. CCAAT/enhancer binding protein alpha is a regulatory switch sufficient for induction of granulocytic development from bipotential myeloid progenitors. Mol Cell Biol. 1998;18(7):4301-4314.
21. Iida S, Watanabe-Fukunaga R, Nagata S, Fukunaga R. Essential role of C/EBPalpha in G-CSF-induced transcriptional activation and chromatin modification of myeloid-specific genes. Genes Cells. 2008;13(4):313-327.
22. Avellino R, Mulet-Lazaro R, Havermans M, et al. Induced cell-autonomous neutropenia systemically perturbs hematopoiesis in Cebpa enhancer-null mice. Blood Adv. 2022;6(5):1406-1419.
23. Collins C, Wang J, Miao H, et al. C/EBPalpha is an essential collaborator in Hoxa9/Meis1-mediated leukemogenesis. Proc Natl Acad Sci U S A. 2014;111(27):9899-9904.
24. Artinger EL, Mishra BP, Zaffuto KM, et al. An MLL-dependent network sustains hematopoiesis. Proc Natl Acad Sci U S A. 2013;110(29):12000-12005.
25. Milne TA, Briggs SD, Brock HW, et al. MLL targets SET domain methyltransferase activity to Hox gene promoters. Mol Cell. 2002;10(5):1107-117.
26. Hasemann MS, Lauridsen FK, Waage J, et al. C/EBPalpha is required for long-term self-renewal and lineage priming of hematopoietic stem cells and for the maintenance of epigenetic configurations in multipotent progenitors. PLoS Genet. 2014;10(1):e1004079.
27. Ye M, Zhang H, Amabile G, et al. C/EBPa controls acquisition and maintenance of adult haematopoietic stem cell quiescence. Nat Cell Biol. 2013;15(4):385-394.
28. Skokowa J, Cario G, Uenalan M, et al. LEF-1 is crucial for neutrophil granulocytopoiesis and its expression is severely

reduced in congenital neutropenia. Nat Med. 2006;12(10):1191-1197.
29. Dannenmann B, Klimiankou M, Oswald B, et al. iPSC modeling of stage-specific leukemogenesis reveals BAALC as a key oncogene in severe congenital neutropenia. Cell Stem Cell. 2021;28(5):906-922.
30. Calvo KR, Knoepfler PS, Sykes DB, Pasillas MP, Kamps MP. Meis1a suppresses differentiation by G-CSF and promotes proliferation by SCF: potential mechanisms of cooperativity with Hoxa9 in myeloid leukemia. Proc Natl Acad Sci U S A. 2001;98(23):13120-13125.
31. Pineault N, Helgason CD, Lawrence HJ, Humphries RK. Differential expression of Hox, Meis1, and Pbx1 genes in primitive cells throughout murine hematopoietic ontogeny. Exp Hematol. 2002;30(1):49-57.
32. Argiropoulos B, Yung E, Humphries RK. Unraveling the crucial roles of Meis1 in leukemogenesis and normal hematopoiesis. Genes Dev. 2007;21(22):2845-2849.
33. Lawrence HJ, Christensen J, Fong S, et al. Loss of expression of the Hoxa-9 homeobox gene impairs the proliferation and repopulating ability of hematopoietic stem cells. Blood. 2005;106(12):3988-3994.
34. Thorsteinsdottir U, Mamo A, Kroon E, et al. Overexpression of the myeloid leukemia-associated Hoxa9 gene in bone marrow cells induces stem cell expansion. Blood. 2002;99(1):121-129.
35. Argiropoulos B, Humphries RK. Hox genes in hematopoiesis and leukemogenesis. Oncogene. 2007;26(47):6766-6776.
36. Lehnertz B, Chagraoui J, MacRae T, et al. HLF expression defines the human hematopoietic stem cell state. Blood. 2021;138(25):2642-2654.
37. Giladi A, Paul F, Herzog Y, et al. Single-cell characterization of haematopoietic progenitors and their trajectories in homeostasis and perturbed haematopoiesis. Nat Cell Biol. 2018;20(7):836-846.
38. Fioredda F, Skokowa J, Tamary H, et al. The European Guidelines on Diagnosis and Management of Neutropenia in Adults and Children: a consensus between the European Hematology Association and the EuNet-INNOCHRON COST action. Hemasphere. 2023;7(4):e872.
39. Hammond CA and Eaves C. Postnatal conservation of human blood- and marrow-specific CD34+ hematopoietic phenotypes. Exp Hematol. 2022;109:18-26.
40. Cheneby J, Menetrier Z, Mestdagh M, et al. ReMap 2020: a database of regulatory regions from an integrative analysis of human and arabidopsis DNA-binding sequencing experiments. Nucleic Acids Res. 2020;48(D1):D180-D188.
41. Huang Y, Sitwala K, Bronstein J, et al. Identification and characterization of Hoxa9 binding sites in hematopoietic cells. Blood. 2012;119(2):388-398.
42. Dannenmann B, Nasri M, Welte K, Skokowa J. CRISPR/Cas9 genome editing of human-induced pluripotent stem cells followed by granulocytic differentiation. Methods Mol Biol. 2020;2115:471-483.
43. Ramos-Mejía V, Navarro-Montero O, Ayllon V, et al. HOXA9 promotes hematopoietic commitment of human embryonic stem cells. Blood. 2014;124(20):3065-3075.
44. Knapp DJ, Hammond CA, Aghaeepour N, et al. Distinct signaling programs control human hematopoietic stem cell survival and proliferation. Blood. 2017;129(3):307-318.
45. Morley A. Cyclic hemopoiesis and feedback control. Blood Cells. 1979;5(2):283-296.
46. von Schulthess GK, Mazer NA. Cyclic neutropenia (CN): a clue to the control of granulopoiesis. Blood. 1982;59(1):27-37.
47. Horwitz MS, Duan Z, Korkmaz B, Lee HH, Mealiffe ME, Salipante SJ. Neutrophil elastase in cyclic and severe congenital neutropenia. Blood. 2007;109(5):1817-1824.
48. Hunter MG, Druhan LJ, Massullo PR, Avalos BR. Proteolytic cleavage of granulocyte colony-stimulating factor and its receptor by neutrophil elastase induces growth inhibition and decreased cell surface expression of the granulocyte colony-stimulating factor receptor. Am J Hematol. 2003;74(3):149-155.
49. El Ouriaghli F, Fujiwara H, Melenhorst JJ, Sconocchia G, Hensel N, Barrett AJ. Neutrophil elastase enzymatically antagonizes the in vitro action of G-CSF: implications for the regulation of granulopoiesis. Blood. 2003;101(5):1752-1758.
50. Skokowa J, Hernandez Alvarez B, Coles M, et al. A topological refactoring design strategy yields highly stable granulopoietic proteins. Nat Commun. 2022;13(1):2948.
51. Li FQ, Horwitz M. Characterization of mutant neutrophil elastase in severe congenital neutropenia. J Biol Chem. 2001;276(17):14230-14241.
52. Horwitz M, Benson KF, Duan Z, et al. Role of neutrophil elastase in bone marrow failure syndromes: molecular genetic revival of the chalone hypothesis. Curr Opin Hematol. 2003;10(1):49-54.
53. Skokowa J, Fobiwe JP, Dan L, Thakur BK, Welte K. Neutrophil elastase is severely down-regulated in severe congenital neutropenia independent of ELA2 or HAX1 mutations but dependent on LEF-1. Blood. 2009;114(14):3044-3051.
54. Watari K, Asano S, Shirafuji N, et al. Serum granulocyte colony-stimulating factor levels in healthy volunteers and patients with various disorders as estimated by enzyme immunoassay. Blood. 1989;73(1):117-122.
55. Makaryan V, Kelley ML, Fletcher B, Bolyard AA, Aprikyan AA, Dale DC. Elastase inhibitors as potential therapies for ELANE-associated neutropenia. J Leukoc Biol. 2017;102(4):1143-1151.
56. Skokowa J. Circumventing mutation to nix neutropenia. N Engl J Med. 2021;384(20):1956-1958.

D) Skokowa, J. and Hernandez Alvarez, B. et al., 2022, *Nature Communications*

nature COMMUNICATIONS

ARTICLE

https://doi.org/10.1038/s41467-022-30157-2 OPEN

A topological refactoring design strategy yields highly stable granulopoietic proteins

Julia Skokowa[1,8✉], Birte Hernandez Alvarez[2,8], Murray Coles[2], Malte Ritter[1], Masoud Nasri[1], Jérémy Haaf[1], Narges Aghaallaei[1], Yun Xu[1], Perihan Mir[1], Ann-Christin Krahl[1], Katherine W. Rogers[3,5], Kateryna Maksymenko[2,3], Baubak Bajoghli[1], Karl Welte[1], Andrei N. Lupas[2], Patrick Müller[3,6] & Mohammad ElGamacy[1,3,4,7✉]

Protein therapeutics frequently face major challenges, including complicated production, instability, poor solubility, and aggregation. De novo protein design can readily address these challenges. Here, we demonstrate the utility of a topological refactoring strategy to design novel granulopoietic proteins starting from the granulocyte-colony stimulating factor (G-CSF) structure. We change a protein fold by rearranging the sequence and optimising it towards the new fold. Testing four designs, we obtain two that possess nanomolar activity, the most active of which is highly thermostable and protease-resistant, and matches its designed structure to atomic accuracy. While the designs possess starkly different sequence and structure from the native G-CSF, they show specific activity in differentiating primary human haematopoietic stem cells into mature neutrophils. The designs also show significant and specific activity in vivo. Our topological refactoring approach is largely independent of sequence or structural context, and is therefore applicable to a wide range of protein targets.

[1] Division of Translational Oncology, Department of Hematology, Oncology, Clinical Immunology and Rheumatology, University Hospital Tübingen, 72076 Tübingen, Germany. [2] Max Planck Institute for Biology, 72076 Tübingen, Germany. [3] Friedrich Miescher Laboratory of the Max Planck Society, 72076 Tübingen, Germany. [4] Heliopolis Biotechnology Ltd, Cambridge CB24 9RX, UK. [5] Present address: Division of Developmental Biology, Eunice Kennedy Shriver National Institute of Child Health and Human Development, National Institutes of Health, Bethesda, MD 20892, USA. [6] Present address: Department of Biology, University of Konstanz, 78464 Konstanz, Germany. [7] Present address: Max Planck Institute for Biology, 72076 Tübingen, Germany. [8] These authors contributed equally: Julia Skokowa, Birte Hernandez Alvarez. ✉email: julia.skokowa@med.uni-tuebingen.de; mohammad.elgamacy@tuebingen.mpg.de

De novo protein design can serve as a powerful tool for protein therapeutics discovery and development, having enabled unprecedented strides in navigating the protein sequence and structure spaces[1,2], and tailoring novel functions[3]. A central objective in the design of functional proteins is to tailor a scaffold structure that best supports the function encoded on a fraction of the template protein's surface. In addition to high activity levels, other criteria are pivotal for the successful deployment of a protein drug, such as activity half-life, folding rates, structural stability, solubility, and molecular weight[4,5]. These properties depend on a set of controllable protein parameters such as a protein's sequence, topology, and size.

Computational design can offer control over these parameters to radically alter the final properties of a protein. The design process can be carried out under the structural constraints encoded by the prior knowledge of the active epitope. First, the sequence can be optimised to maximise the enthalpies of the core residues ("core repacking") or to minimise the solvent-exposed hydrophobic residues, with the aim to improve the thermostability and the solubility, respectively. Second, topology can be changed to objectively optimise folding rate and folding free energy. The topological contact order, a metric that describes the average sequence distance of contacting residues, has been shown to inversely correlate with the logarithm of folding rates[6]. Topological simplification also tends to affect the folding thermodynamics, for instance, removing long, flexible loops tends to decrease the absolute difference in entropy between the unfolded and folded states (i.e. $|\Delta S|$)[7,8]. Third, a protein's size has significant influence on its folding rate[6], as well as on its folding free energy, where the latter is impacted by the magnitude of configurational entropy change upon folding, that, in turn, increases quadratically with the length of the polypeptide chain[9].

In this work, we demonstrate a generalisable refactoring strategy, which aims at preserving a protein's functional epitope, while reconstructing the protein's fold and composition around it. The basis of the proposed strategy relies on constructing more than one structured loop de novo into the same protein at once, which enables the reordering of secondary structural elements along the primary structure. This simplifies the topology from around the active epitope, disposes of entire secondary structures along the sequence, and reduces the protein size down to the necessary scaffolding required to maintain the structural integrity of the functional epitope. Furthermore, spatially distant residues from the functional epitope are optimised to best encode information necessary to improve folding or solvation free energies.

Here, we sought to demonstrate this in silico design strategy as a means for conceiving novel receptor modulators by remodelling a natural cytokine: the granulocyte-colony stimulating factor (G-CSF) (Fig. 1A). G-CSF is a cytokine that stimulates the proliferation and myeloid differentiation of haematopoietic stem and progenitor cells (HSPCs) in the bone marrow and mobilises them into the blood stream[10]. Recombinant human G-CSF (rhG-CSF) has demonstrated great immunotherapeutic utility due to its potent activity in the stimulation of granulopoiesis, boosting the immunity of neutropenic patients, who suffer from a severely reduced number of neutrophils due to genetic factors or chemotherapy[11–16]. Like most other protein therapeutics, rhG-CSF is clinically deployed in its native form or with a few modifications. This is reflected in several suboptimal pharmaceutical features, such as its low recombinant production yield, poor solubility and stability, and short shelf- and serum half-lives. Only classical engineering strategies have thus far been pursued to improve rhG-CSF, spanning point-mutagenesis[17–20], PEGylation[21,22] and circularisation[23,24].

Our strategy aimed to minimise the loss of entropy during folding and receptor binding by reducing structural complexity and rigidifying the bound conformation, respectively (Fig. 1). This resulted in designs that possess minimal sequence similarity with the native G-CSF and contain no disulfide bonds, representing a miniaturised G-CSFR binding domain. We evaluated the biophysical properties of the resulting proteins and determined the structure of the most active one, which showed atomic-level agreement with the design. We found that the designed proteins, especially in tandem, are highly effective receptor activators, and are potent and specific in inducing proliferation and differentiation of primary human haematopoietic stem cells into functional neutrophils. Strikingly, the designs also had significant granulopoietic activity in vivo in zebrafish and mice.

Results

Computational design of G-CSFR binders. Human G-CSF induces JAK/STAT signalling and downstream granulopoiesis by binding to the ectodomains of the G-CSF receptor (G-CSFR)[25]. Biochemical and structural studies have shown that binding site II —comprising residues K16, E19, Q20, R22, K23, D27, D109, and D112—is the dominant binding motif on the surface of G-CSF (Fig. 1A). Our refactoring process sought to reduce the topological complexity, improve thermodynamic and kinetic stabilities, reduce the size, increase the solubility, and eliminate the need for post-translational modifications (PTMs) in G-CSF. The PTMs in human G-CSF are comprised of two disulfide bridges across C69 and C75 and C97 and C107, and an O-glycosylation at T133 (Swiss-Prot numbering). The refactoring process was achieved by rewiring the topology (Fig. 1B), repacking the core, and optimising solvent-exposed residues (Fig. 1C). The first step was to eliminate two segments from the primary structure that are 32- and 22-residue long, which structurally encode three long loops and a helix. This reduced size architecture was redesigned to optimise the packing of core residues, with the goal of rigidifying the binding epitope. The initial structural template was extracted from the G-CSF–G-CSFR complex structure (PDB: 2D9Q)[26], which shows that G-CSF has a similar binding conformation when compared to unbound G-CSF structures. Moreover, solvent-exposed residues distal to the binding epitope were also designed to replace hydrophobic side chains that were used to efface the removed motifs and to enhance the helical character of the assembled protomers (see the "Methods" section). While the design protocol used optimised decoys for their *talaris13* energy score, after several rounds of design the final hits were filtered purely based on their packing quality. The top several hundred candidates were subject to equilibrium molecular dynamics (MD) for the inspection of their structural stability, where the most structurally stable decoy was forwarded for the next design stage (loop design). At the end of this first step it was critical to choose a single decoy for the following loop design, as the design protocol entails unrestrained backbone motions that would generate diverse conformations at the disjoint junctions.

The second step aimed at arriving at single-chain variants to minimise the contact order, which was done through the design of two short loops across the gaps. The two gaps extended approximately across 10 and 13 Å, hence we sought to connect them by 3- and 4-residue de novo loops, respectively. Since the sequence space of 3- or 4-residue loops is sufficiently tractable for nearly exhaustive exploration, we picked the amino acids with the highest loop propensity and generated all the possible sequence combinations. For the 3-residue loop, 9 amino acid types were used to generate 729 (9^3) combinations, and for the 4-residue loop 8 amino acid types were used to generate 4096 (8^4) combinations (see the "Methods" section). These sequences were modelled in and refined across their respective junction. This was followed by conformational homogeneity evaluation across

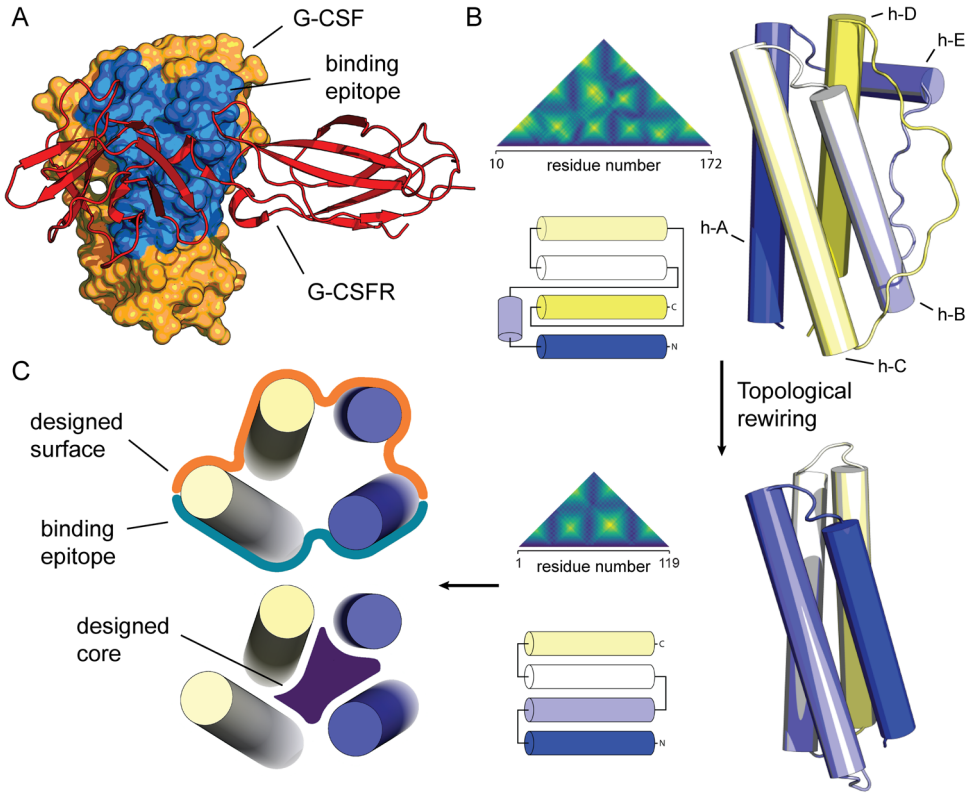

Fig. 1 Computational design stages of the topological refactoring strategy. A X-ray structure of G-CSF (orange) bound to its cognate receptor (red) through its binding epitope (blue). **B** According to the *topological refactoring* strategy, the topology of the native G-CSF was rewired from around the fixed binding epitope. This was done by replacing the two long, bundle-spanning loops, by two short, de novo designed loops; reconstructing an up-up-down-down bundle into an up-down helical bundle. This resulted in much simpler contact maps, a lower contact-order, and a smaller protein (G-CSF residue numbering is based on PDB: 2D9Q). **C** The design models were further optimised in order to idealise the core packing (blue volume) and to hydrophilise residues distal from the binding epitope (orange crust).

repeated MD simulations. Initially, loops across each junction were modelled individually, whereby the other loop was modelled as a constrained tri- or tetra-glycine. The 50 conformationally most stable loops were from each junction, and combined together to generate 2500 spliced models (50^2). The simulations were repeated for the combined loops models and the four most conformationally stable molecules were chosen for experimental evaluation.

The four designs were named Boskar1–4, and were 123-amino acid long—a substantial size reduction from rhG-CSF, which is 174 amino acid-long. Moreover, the reshuffling of the secondary structural elements along the primary structure during the topological reconstruction, combined with the sequence optimisation, resulted in low full-length sequence homology, where the sequence identity with rhG-CSF is below 32% for all of the designs (Supplementary Table 1). In addition to their new topology, lower contact order, and idealised sequences, the designs were also devoid of the native form's PTMs. The designs lacked glycosylation sites and disulfide bonds, which are normally important for hG-CSF folding. In fact, our proteins were designed not to contain any cysteine residues, which have been implicated in misfolding of rhG-CSF[17].

The designs possess granulocytic proliferative potential. To query the potential biological activity of the four experimentally tested designs, we used murine NFS-60 cells, a hematopoietic cell line that is routinely deployed to quantify G-CSF-triggered proliferative potential[27]. Cell densities were assessed by a fluorescence redox-based assay 48 h after treatment with the designs or rhG-CSF, where the average EC_{50} values (i.e. the concentration that gave half-maximal cell density response) ranged from micromolar to nanomolar (Supplementary Table 1). Boskar1, Boskar2, Boskar3, and Boskar4 showed EC_{50} values of 164.5 ± 19.9, 241.8 ± 74.3, 58.5 ± 6.0 and 2.05 ± 0.2 nM, respectively. The most active designs, Boskar3 and Boskar4, exhibited dose–response curves in the nanomolar range upon 48-hour treatment of NFS-60 cells (Fig. 2A). We then set out to investigate the dose- and time-response kinetics of the two most active designs, which showed that our designs possess slower proliferation induction kinetics than rhG-CSF. The proliferative concentrations Boskar4 and Boskar3 were found to reach sub-nanomolar levels for longer-duration treatments in time-lapse microscopy analyses of the cell proliferation kinetics over longer treatment durations (Fig. 2B–D, Supplementary Fig. 1 and Supplementary Movies 1–4).

Activation of G-CSFR signalling by Boskar3 and Boskar4. To evaluate the dependency of the response to the designed proteins on G-CSFR expression, we knocked out G-CSFR in NFS-60 cells using CRISPR/Cas9-mediated mutagenesis. For this, we synthesised guide RNA (gRNA) specifically targeting exon 4 of *CSF3R* (cut site: chr4 [+126,029,810:−126,029,810]) to introduce stop-codon or frameshift mutations in the extracellular part of all G-CSFR isoforms. We generated pure G-CSFR KO NFS-60 cell clones that have one nucleotide deletion on each allele, as assessed by Sanger sequencing and tracking of indels by decomposition (TIDE) analysis (Supplementary Fig. 2)[28]. In contrast to wild type cells, G-CSFR KO NFS-60 cells did not respond to treatment with

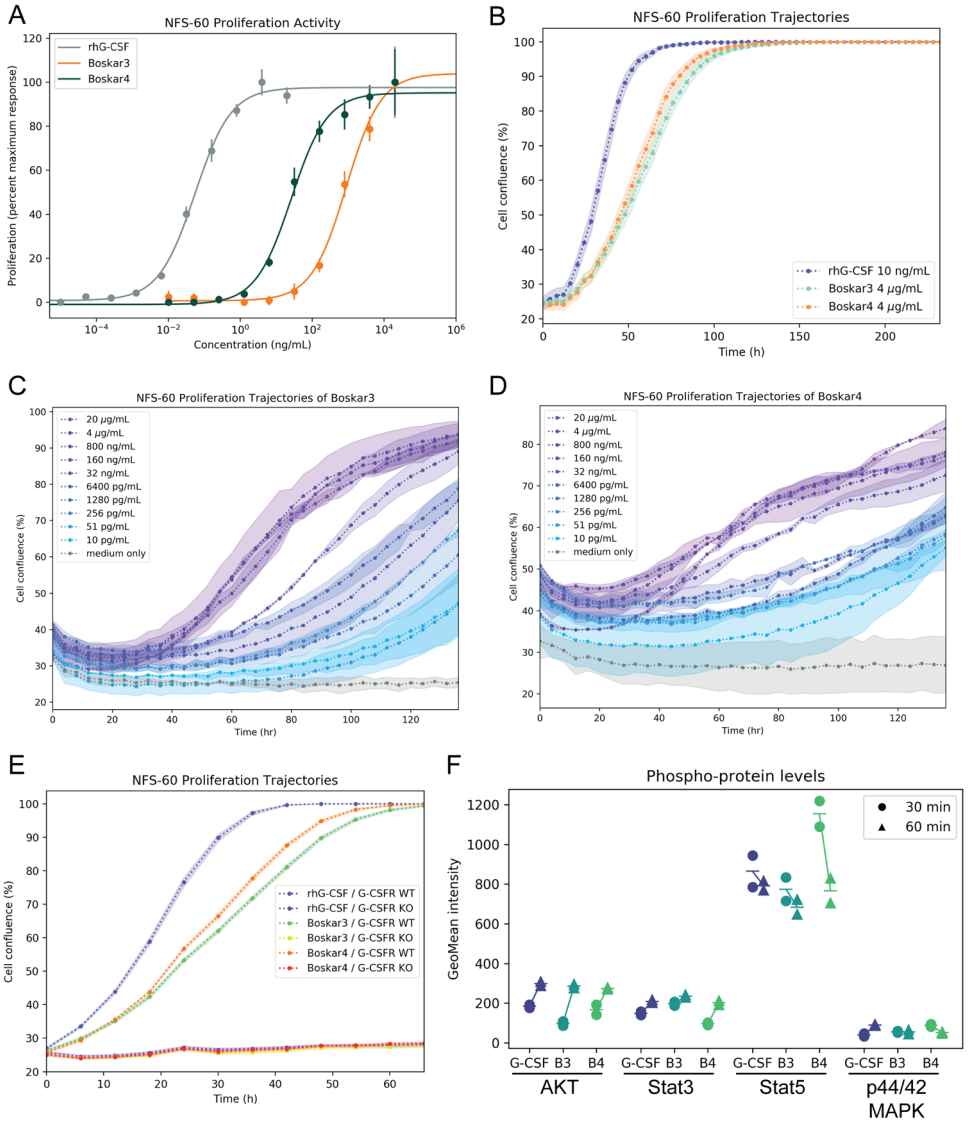

Fig. 2 The designs display potent and specific activity in cell-based assays. A Dose–response curves of NFS-60 proliferation upon 48 h treatment with Filgrastim (rhG-GCSF), Boskar3, or Boskar4. Datapoints and error bars represent mean ± standard deviations of three biologically independent replicates. **B** Time-dependent proliferation trajectory of surface-immobilised NFS-60 cells over a 10-day treatment. Data points and shades represent mean and standard deviation values of three biologically independent replicates. Experiments were performed three times in triplicates. Data of one representative experiment is shown. **C**, **D** Dose- and time-dependent proliferation trajectories over a 5-day treatment of free-floating NFS-60 cells, under the influence of Boskar3 and Boskar4 treatments, respectively. Data points and shades represent mean and standard deviation values of three biologically independent replicates. **E** G-CSFR-deficient primary stem cells (G-CSFR KO), show abolished proliferative responses to either rhG-CSF or the designs. Experiment was performed twice in triplicates. Data points and shades represent mean and standard deviation values of three biologically independent replicates. **F** Intracellular levels of phospho-AKT (Thr308), phospho-ERK1/2 (p44/42 MAPK), phospho-STAT3 (Tyr705), and phospho-STAT5 (Tyr694) in $CD34^+$ HSPCs treated with rhG-CSF or the designs (see the "Methods" section). Geometric mean of the expression intensity of each phospho-protein (GeoMean intensity) is shown on the *y*-axis. The experiment was performed twice.

rhG-CSF, Boskar3 or Boskar4 (Fig. 2E). These data demonstrate that the designed proteins act via G-CSFR.

Binding of G-CSF to G-CSFR rapidly activates a cascade of intracellular events, including phosphorylation of downstream effectors, e.g. Akt, STAT3, STAT5 or MAPK, that ultimately induce granulocytic differentiation[29]. To test whether our designed proteins directly induce G-CSFR signalling, we measured these immediate phosphorylation targets of G-CSFR signalling in $CD34^+$ HSPCs. Indeed, we found that Akt, STAT3, STAT5 and p44/42 MAPK (Erk1/2) were tyrosine phosphorylated in HSPCs treated with Boskar3 or Boskar4 to a similar degree as in rhG-CSF-treated cells (Fig. 2F). Together, this shows that the biological activity of the designs is directly attributable to G-CSFR activation.

The designed protein Boskar4 has enhanced stability characteristics. Expression of the designs in *E. coli* showed that all designs were highly expressed in the soluble cell fraction. We focused our biophysical and structural characterisation on one design; Boskar4, which showed the highest activity in endpoint dose–response assays. In contrast to rhG-CSF which is expressed insolubly to a yield of 3 mg/l culture and has to be refolded[30], Boskar4 was expressed solubly in *E. coli* to a yield of >80 mg/l culture as final yield after tandem affinity and size-exclusion chromatography. The solubility of Boskar4 also outstripped that of rhG-CSF, where Boskar4 could be readily concentrated to >20 mg/ml in PBS buffer, while rhG-CSF precipitated above a concentration of about 4 mg/ml in PBS buffer. Circular dichroism

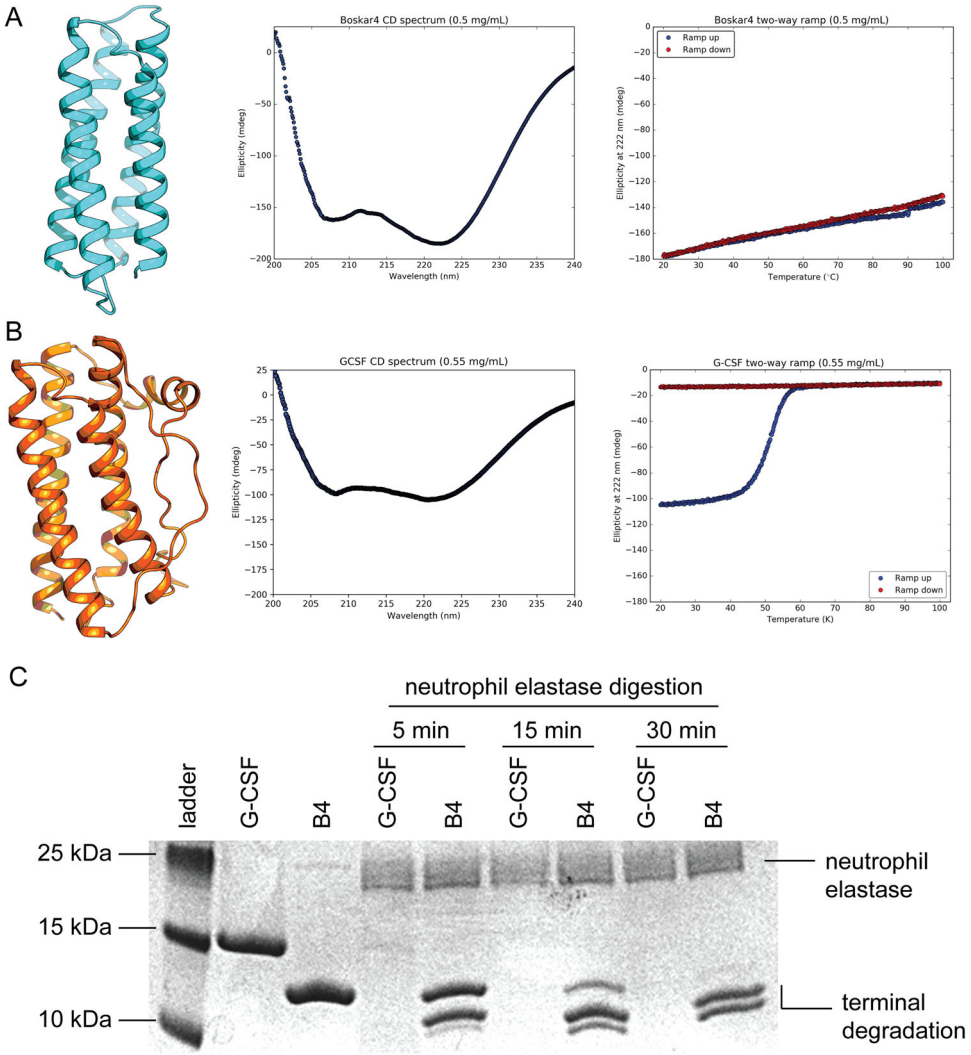

Fig. 3 The designed protein Boskar4 is substantially more stable than rhG-CSF. A Design model of Boskar4 (left pane) has a CD spectrum that shows a strong helical content (middle pane). The melting curve of Boskar4 shows exceptional stability since it does not undergo a melting transition up to 100 °C (blue curve) and shows a full regain of residual ellipticity at 222 nm upon cooling (red curve). **B** In contrast, rhG-CSF appears to display weaker helical signal compared to the design (middle pane), and melts irreversibly at 57 °C. **C** Neutrophil elastase treatment of Boskar4 (B4) and rhG-CSF shows Boskar4 to be substantially more resistant to proteolytic digestion in comparison to rhG-CSF. Expected neutrophil elastase and degradation bands are indicated.

(CD) spectra of Boskar4 show it to possess strong helical character, with almost two-fold the mean residual ellipticity magnitude of rhG-CSF, when measured at the same concentration (middle pane of Fig. 3A, B). CD spectroscopy was also used to assess thermal unfolding of Boskar4 and rhG-CSF. Boskar4 appeared to remain stably folded up until 100 °C, with completely reversible residual ellipticity recovery upon cooling. Conversely, the melting curves of native rhG-CSF showed irreversible thermal unfolding at a temperature of 57 °C, whereby the protein heavily precipitates upon cooling (right pane of Fig. 3A, B). To investigate if the disulfide bond formation has an impact on the irreversible denaturation or thermostability of rhG-CSF, we sought to repeat these melting and cooling experiments with addition of reducing agents to the buffer. Due to high buffer absorbance, we carried out these experiments using nanoDSF, for rhG-CSF in standard PBS buffer, PBS buffer supplemented with a mixture reduced and oxidised glutathione (2.5 mM and 0.5 mM, respectively), or in PBS buffer supplemented with 5 mM dithiothreitol (DTT). These melting curves showed similar melting points in either PBS alone or in a mixture of reduced and oxidised gluthathione, as the latter condition should accelerate the equilibrium for formation or breaking of disulfide bonds, at 50 and 51.6 °C, respectively (Supplementary Figs. 3 and 4). Conversely, the purely reducing effect of DTT resulted in a lower thermostability of rhG-CSF where the melting point was 35.4 °C, and a clear scattering change could be observed, indicative of aggregation (Supplementary Fig. 5). In all three cases, the unfolding of rhG-CSF was irreversible.

To test whether the enhanced thermostability of the designs can be of potential pharmacokinetic advantage, we tested the protease resistance of Boskar4 in comparison to rhG-CSF. Neutrophil elastase (NE) is a serine protease that has broad substrate specificity. Secreted by neutrophils and macrophages during inflammation, NE enzymatically degrades G-CSF, inhibiting its activity, which constitutes a negative feedback loop against excessive cytokine-induced granulopoiesis[31,32]. Analysing the products of NE treatment showed that rhG-CSF was almost entirely digested after a five-minute-treatment (Fig. 3C). Boskar4, however, was largely protease-resistant even after 30 min. Most of the partial digestion of Boskar4 appears to be restricted to terminal fragments, possibly representing the unstructured hexa-Histidine and thrombin cleavage purification tag. Therefore, we

sought to identify the composition of these degradation bands using nanoflow liquid chromatography–tandem mass spectrometry (nano-LC–MS/MS). While the mass spectrometry analysis (Supplementary Fig. 6) for the band corresponding to full-length Boskar4 shows complete sequence coverage, peptides of partial degradation bands 1 and 2 do not cover, or only partially cover, the N-terminus and C-terminus, indicating these bands to be terminal degradation products of Boskar4 by neutrophil elastase.

To expand our analysis, we further tested the protease sensitivity of Boskar4 and rhG-CSF against a set of diverse human proteases representing different classes of proteolytic enzymes. These were the lysosomal aspartyl protease Cathepsin D, the metalloprotease ADAM10, the cysteine protease Cathepsin L, and the serine protease Cathepsin G. While these results showed both Boskar4 and rhG-CSF are not sensitive to Cathepsin L or ADAM10, rhG-CSF was sensitive to Cathepsin D and Cathepsin G degradation, whereas Boskar4 was resistant to them under the same conditions (Supplementary Fig. 7). Collectively, these results indicate that Boskar4 is less likely to partially or fully unfold, and hence less accessible to proteolytic digestion.

The solution structure of the Boskar4 design matches its design model to atomic-accuracy. To evaluate the structural precision of the design process we determined the solution structure of Boskar4, since it showed well-dispersed NMR spectra (Supplementary Fig. 8). The structure was determined using the CoMAND method (Conformational Mapping by Analytical NOESY Decomposition), a protocol that provides unbiased structure determination driven by a residue-wise R-factor tracking the match between experimental and back-calculated NOESY spectra[33]. In the CoMAND protocol, a 3D-CNH-NOESY spectrum[34] is divided into 1D sub-spectra (referred to as strips), each representing contacts to a single backbone amide proton, thus representing the structural environment of the respective residue (see the "Methods" section). Spectral decomposition is then performed to yield local backbone dihedral angles for all residues where strips are available, which are used for initial model building. In subsequent stages, the *R*-factor is used both to extract further geometric data and as a selection criterion for frame-picking from MD trajectories, yielding the final structure ensemble. For Boskar4, the CNH-NOESY spectra provided 107 strips for CoMAND analysis. Of the 118 non-proline residues, 11 were not observed, presumably due to fast exchange with solvent. Accordingly, all of these residues are at the C-termini of helices or the subsequent loops, including 5 residues (K89-R93) in the α3-α4 loop. We performed CoMAND factorisation calculations for 98 of these strips (strips containing significant overlapped intensities were excluded at this stage), yielding backbone dihedrals that were used as input for model building in Rosetta. The angles obtained were both consistent with the values predicted from chemical shift profiles by TALOS-N[35] (Supplementary Fig. 9). To refine this initial model, we applied a protocol employing alternate rounds of unrestrained and restrained molecular dynamics simulations, with the aim of producing a set of unrestrained structures close to the average structure. To achieve this we applied restraints derived from *R*-factor optimisation and from conventional "boot-strapping" based on the initial model. These included 76 inter-helical distance restraints (Supplementary Table 3 and Supplementary Fig. 10), primarily between well-resolved aromatic and methyl groups, derived from two further NOESY experiments (see the "Methods" section). We then selected a final ensemble of 17 structures from this pool by *R*-factor optimisation over all available strips, resulting in an average *R*-factor of 0.31 ± 0.11 (Fig. 4A, C, Supplementary Table 2). The ensemble deviated by an average of 0.80 Å from the average structure, and 2.0 Å from the design model (Fig. 4A). Locally aligning the NMR ensemble to the designed binding epitope residues showed a backbone RMSD of 1.0 Å and an all-atom RMSD of 1.2 Å (Fig. 4B), thus demonstrating atomic precision in re-sculpting the binding epitope.

The overall structure of Boskar4 is very similar to the design model in the lengths of the four helices, the bundle architecture, helical register and packing. On the global level, the largest deviation is across narrow end of the bundle (corresponding to the α1–α2 and α3–α4 loops), where the helices of the solution structure are less tightly packed than for the model. This difference is well captured by *R*-factor optimisation for A97, which shows contacts to methyl groups of L22 and I25 (Supplementary Fig. 11). This region is also the site of the largest deviation on the local level, where the capping motif for the α1 helix of the design is incompatible with the CNH-NOESY data (Supplementary Fig. 12). Here the CoMAND analysis identifies a backbone polymorphism at L22, where 4 of the 17 models adopt an alternate conformation (Supplementary Fig. 12). To take this into account, we rebuilt the α1–α2 loop, constructing a range of trial structures for each of the alternate forms and selected frames to minimise *R*-factors across the segment. Under the NMR measurements conditions, Boskar4 appeared to be monomeric and thermostable, where temperature and concentration ramps did not influence the reference ^{1}H–^{15}N HSQC spectrum (Supplementary Fig. 13).

To further examine the internal dynamics of the Boskar4 structure, we measured ^{15}N $\{^{1}H\}$-heteronuclear NOE values and water exchange rates for backbone amide protons. The former report on internal motions over fast (i.e. sub-nanosecond) timescales, while the latter primarily report on hydrogen bond stability on timescales of milliseconds to seconds. Both measures are consistent with stable secondary structure elements; NOE values indicative of high-amplitude fast motions (NOE < 0.8) and shorter exchange times are only observed in the inter-helical loops (Fig. 4D). Thus, the Boskar4 design provides a stable and accurate scaffold for presenting the binding epitope. Analysis of the solubility character of the Boskar4 NMR structure (PDB: 7NY0; 1st model) and G-CSF crystal structure (PDB: 2D9Q), indicates that sequence- and structure-based solubility prediction methods show fewer exposed hydrophobic outliers on the Boskar4 surface, as compared to G-CSF (Supplementary Fig. 14).

The designs binding to human G-CSFR is enhanced by bivalency. To characterise the kinetics and affinity of interactions between the designs and the G-CSF receptor, we performed surface plasmon resonance-based measurements for Boskar3, Boskar4 in comparison to rhG-CSF (Fig. 5A–C, Table 1, and Supplementary Fig. 15A–C). Analysis of the kinetics across the injection dilution series, assuming 1:1 binding, resulted in dissociation constants (K_d) of 156 and 195 nM for Boskar3 (Fig. 5B), Boskar4 (Fig. 5C), respectively. In comparison, the K_d determined for rhG-CSF was 1 nM (Fig. 5A). Previous studies have reported K_d values for the G-CSF:G-CSFR interaction between 200 pM using SPR[36] and 1.4 nM using ITC[37].

We noticed that titrating higher concentrations of designs (i.e. 10–50 μM) resulted in sensograms that better fit with a 2:2 binding model. Size-exclusion chromatography of the Boskar3 (Supplementary Fig. 16) and Boskar4 (Supplementary Fig. 17) designs indeed showed that the designs partition between monomeric and dimeric forms. This monomer–dimer equilibrium however seems to follow a very slow interchange, even at room temperature (Supplementary Figs. 18 and 19). Nonetheless, in all of the measurements and assays described, both monomer and dimer fractions were pooled together and used as a single

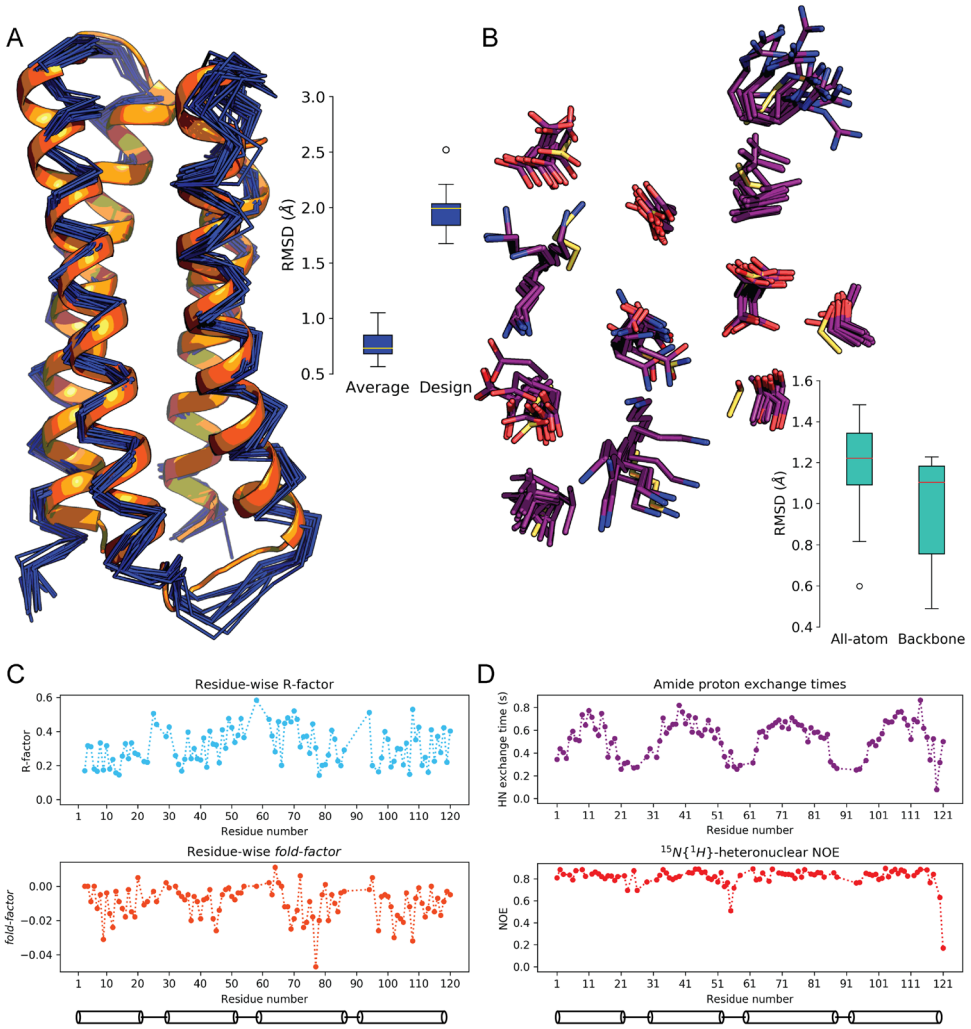

Fig. 4 The design model shows atomic-level agreement with its NMR solution structure. A Boskar4 solution structure shows an ensemble deviation from the average structure of 0.8, and 2.0 Å from the designed coordinates. The design model (orange) is shown against the NMR ensemble (dark blue). The boxplot shows the median and spread across the ensemble frames. **B** The backbone atoms RMSD of the binding epitope averaged at 1.0 Å, while all-atom RMSD of averaged at 1.2 Å, highlighting the design precision. The design model residues (yellow) are shown against the NMR ensemble (purple), and the box plot shows the deviations across the ensemble. The boxplot shows the median and spread across the ensemble frames. The box plots represent median (central line), 1st and 3rd interquartile range (box), and minimum and maximum of 1.5 times the latter interquartile range (whiskers). **C** Residue-wise *R*-factor values for the covered residues are shown (top), indicating the normalised CNH-NOESY RMSD from the expected spectra by the final ensemble. The *fold-factor* shown (bottom), a metric which signifies the *R*-factor reduction by non-local residue-residue contacts, shows the contribution of buried helical residues to Boskar4 folding. **D** Both amide proton exchange (top) and $^{15}N\{^1H\}$NOEs (bottom) show the backbone amides of the helical residues to be solvent-shielded and conformationally rigid, respectively.

sample. We next sought to construct a truely bivalent design form by linking two Boskar4 domains in tandem by means of a 24-residue linker (i.e. $(GGGGSS)_4$), named Boskar4_t2 (Fig. 6A). Boskar4_t2 binding to G-CSFR showed a K_d of 5 nM (Fig. 5D, Table 1, Supplementary Fig. 15D), which constitutes a 39-fold improvement of affinity in comparison to Boskar4. This further suggested that Boskar4_t2 may exhibit avidity, thus can be a more efficient dimeriser and subsequently a more active G-CSFR agonist.

G-CSFR activation is sensitive to its dimerisation spacing. To study the biological relevance of this affinity enhancement of Boskar4_t2, we evaluated its proliferative potential through end-point NFS-60 proliferation assay, where it showed an EC_{50} of 180 nM; 11-fold better than Boskar4 (Fig. 6A, C, and Supplementary Table 1). We reasoned this improved activation may be sensitive to the receptor subunit spacing as was reported with other cytokine receptors[38–40]. Therefore, we created another 2-copy tandem construct with a shorter (6-residue) flexible linker (i.e. GGGGSS), named Boskar4_st2. While Boskar4_st2 showed similar affinity to Boskar4_t2 against G-CSFR (i.e. 6 nM; Table 1), it was indeed even more active in inducing proliferation of NFS-60 cells ($EC_{50} = 7.6$ pM), with a 263-fold improvement in activity over the single domain Boskar4, and 24-fold over the two-domain construct Boskar4_t2 (Fig. 6B, C, and Supplementary Table 1). Repeating the dose- and time-dependent proliferation assays resulted in a similar picture, emphasising the activity gain from efficient dimerisation and linker length reduction (Fig. 6E, F). To further evaluate the generality of this observation, we created the Boskar3_st2 construct, and a mixed Boskar3_Boskar4 construct, where either two Boskar3 domains or one Boskar3 and one Boskar4 domains are connected in tandem using a 6-residue linker (i.e. GGGGSS), respectively. The same pattern was

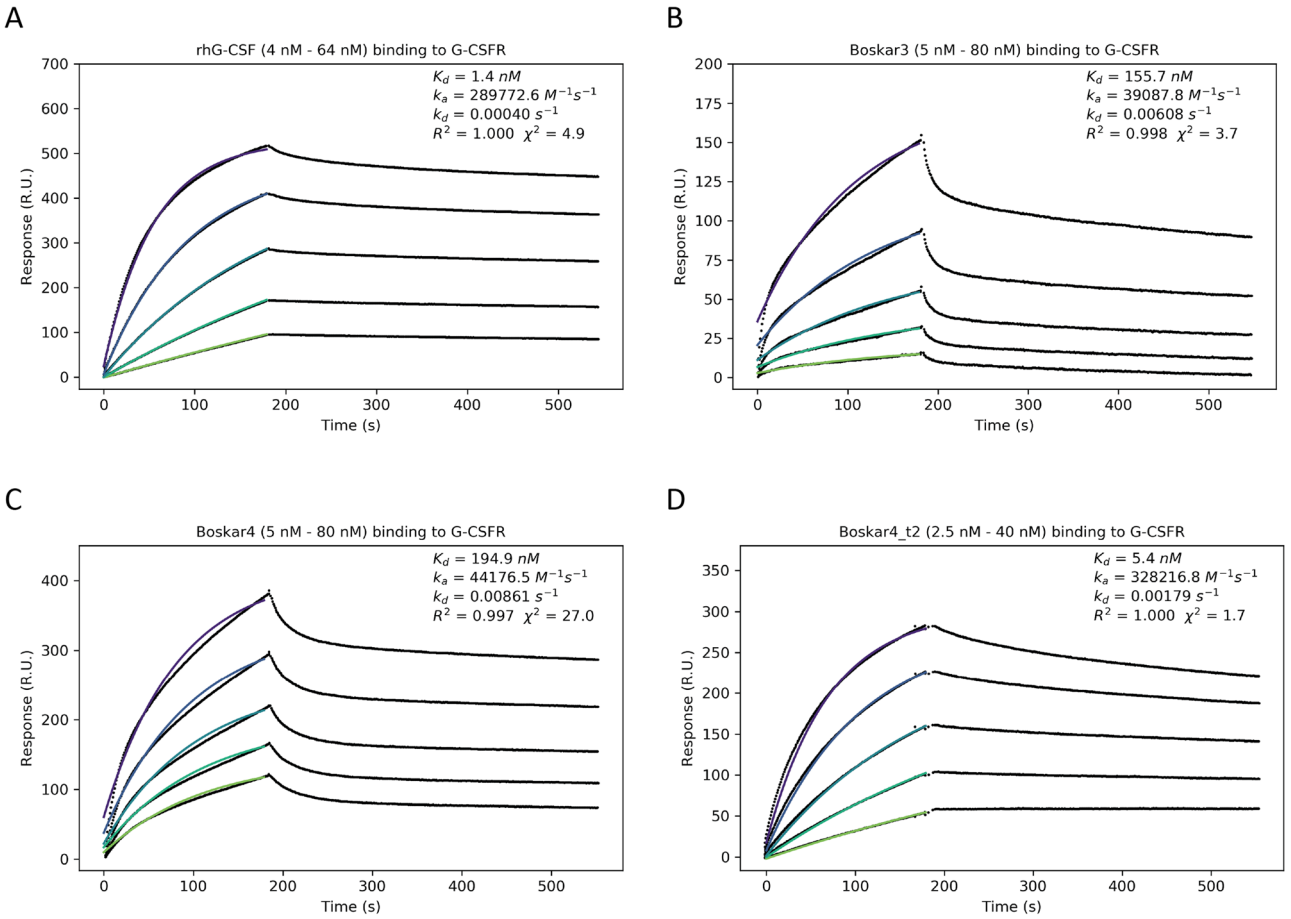

Fig. 5 The designs bind to the human G-CSF receptor. SPR titration sensorgrams of the binding kinetics of **A** rhG-CSF (Filgrastim), **B** Boskar3, **C** Boskar4, and **D** Boskar4_t2. The binding kinetics analysis (association curve fits shown in spectrum colours) indicates higher apparent binding affinity of inherently bivalent ligands, whereby rhG-CSF and Boskar4_t2 represent two distinct modes of bivalent binding to the G-CSFR.

Table 1 SPR binding parameters.

Analyte	k_a ($M^{-1}s^{-1}$)	k_d (s^{-1})	K_d (M)
rhG-CSF	$(3.0 \pm 0.3) \times 10^5$	$(4.9 \pm 2.8) \times 10^{-4}$	$(1.1 \pm 1.6) \times 10^{-9}$
Boskar3	$(3.8 \pm 0.4) \times 10^4$	$(6.1 \pm 0.1) \times 10^{-3}$	$(1.6 \pm 0.2) \times 10^{-7}$
Boskar4	$(4.3 \pm 0.3) \times 10^4$	$(8.6 \pm 0.1) \times 10^{-3}$	$(2.0 \pm 0.2) \times 10^{-7}$
Boskar4_t2	$(3.4 \pm 0.5) \times 10^5$	$(1.7 \pm 0.5) \times 10^{-3}$	$(5.1 \pm 1.9) \times 10^{-9}$
Boskar4_st2	$(5.3 \pm 0.7) \times 10^5$	$(2.9 \pm 1.9) \times 10^{-3}$	$(5.9 \pm 4.4) \times 10^{-9}$
Boskar3_B4	$(4.8 \pm 0.7) \times 10^5$	$(1.1 \pm 0.32) \times 10^{-3}$	$(2.4 \pm 0.9) \times 10^{-9}$
Boskar3_st2	$(4.\ 9 \pm 0.8) \times 10^5$	$(2.3 \pm 0.39) \times 10^{-3}$	$(4.8 \pm 1.4) \times 10^{-9}$
Boskar3 monomeric	$(1.6 \pm 0.1) \times 10^5$	$(6.3 \pm 0.16) \times 10^{-3}$	$(3.9 \pm 2.2) \times 10^{-8}$
Boskar3 dimeric	$(1.5 \pm 0.2) \times 10^5$	$(2.7 \pm 0.19) \times 10^{-3}$	$(1.8 \pm 3.0) \times 10^{-8}$
Boskar4 monomeric	$(1.4 \pm 0.1) \times 10^4$	$(1.8 \pm 0.32) \times 10^{-2}$	$(1.2 \pm 123.3) \times 10^{-6}$
Boskar4 dimeric	$(2.4 \pm 0.2) \times 10^5$	$(3.7 \pm 0.23) \times 10^{-3}$	$(1.5 \pm 1.9) \times 10^{-8}$

observed where the short-linker tandems are more active than the dimeric species, that is in turn more active than the monomeric species of the respective design (Supplementary Figs. 20 and 21).

The designs induce proliferation and neutrophilic differentiation of HSPCs in vitro. To investigate the clinical potential of our designs, we further evaluated their biological activity in human primary $CD34^+$ hematopoietic stem and progenitor cells (HSPCs). We started by assaying the stimulation of $CD34^+$ HSPCs with the original designs (Boskar3 or Boskar4), which induced an increase in cell proliferation that subsequently plateaued, similar to that observed in rhG-CSF-treated cells (Supplementary Figs. 22, 23, and 24). We then assessed granulocytic differentiation of $CD34^+$ HSPCs from two healthy donors in the presence of rhG-CSF or the different designs using a liquid culture system. In all of the HSPCs experiments, rhG-CSF was used at a concentration of 10 ng/mL, Boskar3 and Boskar4 were used at of 1 µg/mL, and Boskar4_t2 or Boskar4_st2 at 100 ng/mL (except for the CFU and phagocytosis assays where both 10 and 100 ng/ml of Boskar4_t2 or Boskar4_st2 were used). As expected, a majority of cells cultured in the presence of rhG-CSF or designed proteins exhibited the typical and highly specific morphology of neutrophilic granulocytes with multilobed nuclei (Fig. 7A, B). A FACS analysis also revealed differentiation of HSPCs into neutrophilic granulocytes ($CD45^+CD11b^+CD15^+$, $CD45^+CD11b^+CD16^+$, and $CD45^+CD15^+CD16^+$ cells) in the presence of the Boskar3 and Boskar4 to levels comparable to that induced by rhG-CSF (Supplementary Figs. 25 and 26). A more detailed FACS analysis of granulocytic differentiation for Boskar4_t2 and Boskar4_st2 revealed a strong neutrophilic differentiation bias of the treated cells (Fig. 7C, and Supplementary Fig. 27). Additionally, we observed the formation of colony-forming units (CFUs) from healthy donor $CD34^+$ cells in the presence of the designed proteins (Fig. 7D, E, and Supplementary Fig 28). Although the number of CFU colonies induced by the designs was relatively lower than that stimulated by rhG-CSF (Fig. 7D), the typical myeloid cell morphology of CFUs was evident in all groups (Fig. 7E).

We further tested whether the neutrophils differentiated in vitro from HSPCs by our designs can execute neutrophil-specific functions such as production of reactive oxygen species

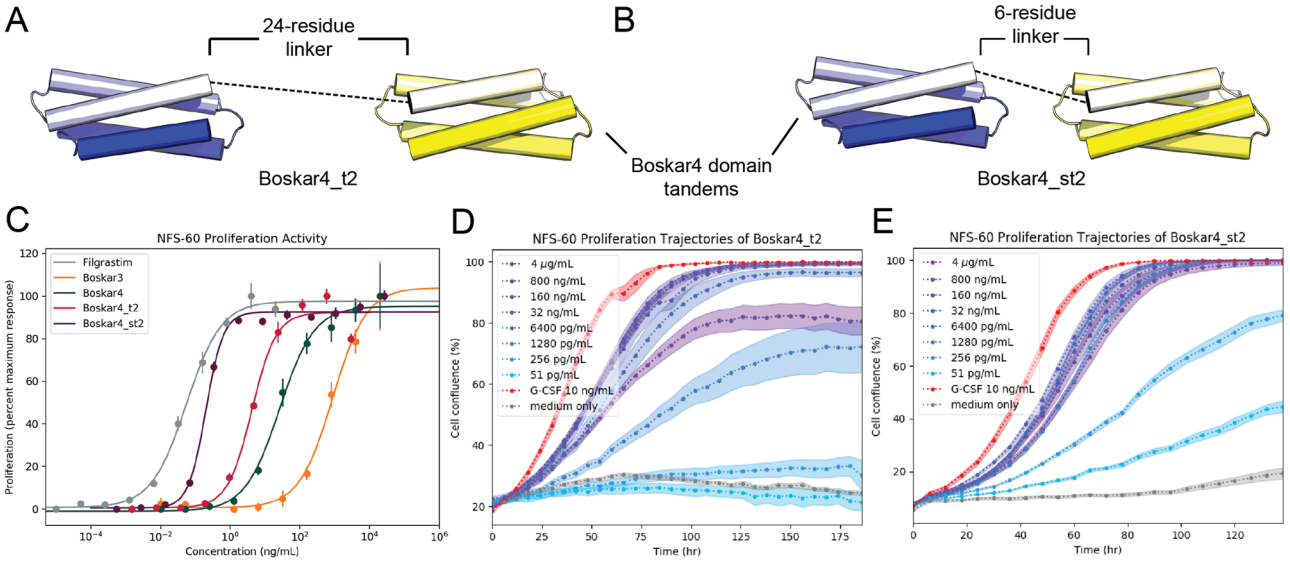

Fig. 6 The potency of designs can be greatly enhanced by the optimal tandem spacing. The creation of two-copy Boskar4 tandems with different flexible spacers, through **A** a 24-residue-linker (Boskar4_t2), and **B** a short 6-residue-linker (Boskar4_st2). **C** Dose-response curves in NFS-60 cells show Boskar4_t2 (EC_{50} = 180 pM), and Boskar4_st2 (EC_{50} = 7.6 pM) to be 11- and 263-fold more active than the single domain Boskar4, respectively. Datapoints and error bars represent mean ± standard deviations of 3 biologically independent replicates. **D**, **E** This greatly enhanced potency is also evident in the dose- and time-dependent NFS-60 proliferation kinetics, highlighting the requirement for an optimal G-CSFR dimerisation spacing to achieve maximal G-CSFR activation. The experiments in **C**, **E** were performed as described in figure legend to Fig. 2.

(ROS), neutrophil extracellular traps (NETs) formation, and phagocytosis. We first assessed H_2O_2 levels in *N*-Formylmethionyl-leucyl-phenylalanine (fMLP)-stimulated neutrophils and detected elevated ROS levels in designs-generated neutrophils, comparable or even higher to rhG-CSF-stimulated samples (Fig. 7F, and Supplementary Fig. 29). Phagocytosis was evaluated using live cell imaging of neutrophils incubated with pHrodo Green *E. coli* bioparticles. We observed similar phagocytosis behaviour of rhG-CSF- and designs-generated neutrophils (Fig. 7G and Supplementary Fig. 30). These neutrophils were also capable of producing NETs upon stimulation with phorbol myristate acetate (PMA) (Fig. 7H). Taken together, designed proteins induce formation of functionally active neutrophils.

The design proteins induce chemotaxis of neutrophils in vitro. To study the effects of design proteins on the chemotactic activity on neutrophils, we assessed chemotaxis of healthy donor peripheral blood neutrophils in vitro by incubating cells with rhG-CSF or the designs and measuring chemotactic activity using IncuCyte® Chemotaxis Cell Migration Assay on an IncuCyte S3 Live cell analysis system. Indeed, we found that our designs induced neutrophils chemotaxis to a similar degree as in with rhG-CSF (Fig. 7I). These results highlight the activity of design proteins not only on the granulocytic differentiation, but also migration of neutrophils.

Boskar4 tandems induce neutrophil production in zebrafish. To investigate the potential in vivo activity of our most active design Boskar4_t2 and Boskar4_st2, we used a fluorescent neutrophil reporter zebrafish line, *Tg(mpx:GFP)*[41]. Equal volumes (4 nL) of PBS solution containing 8 ng of rhG-CSF, 16 ng Boskar4_t2, or 16 ng Boskar4_st2 were injected into the cardinal vein of transgenic embryos at 1.5 days post-fertilisation (dpf). As negative control, 16 ng Moevan_control (a protein lacking binding or activation capacity of G-CSFR[28], but expressed and purified under the same conditions) was injected. All injected embryos survived without displaying morphological abnormalities. The number of GFP^+ neutrophils was assessed in each embryo 24- and 72-h post-injection. Compared to the PBS-injected counterparts, the number of neutrophils was almost unchanged in the Moevan_control-injected embryos, whereas it was significantly higher in embryos injected with rhG-CSF, Boskar_t2 and Boskar_st2 treatments (Fig. 8A, B, and Supplementary Table 4). We also observed an increased neutrophil localisation near the caudal hematopoietic tissue in the rhG-CSF and Boskar_st2 injected embryos (Fig. 8C) indicating strong granulopoietic activity for these designs in zebrafish.

The designed proteins induce granulopoiesis in mice. We next evaluated the effects of the designed proteins on the induction of granulopoiesis in mice. We treated C57BL/6 mice with rhG-CSF or G-CSF designs, Boskar4_t2 and Boskar4_st2 at a concentration of 300 μg/kg by intraperitoneal injection (i.p.) every second day for a total of five injections. Mice in the control group were treated with PBS, or a protein incapable of G-CSFR binding (Moevan_control[28]) using the same treatment scheme. One day after the fifth injection, the number of $Ly6G^+Ly6C^+$ neutrophils in the bone marrow of treated mice was evaluated. We found that treatment of mice with rhG-CSF, Boskar4_t2, or Boskar4_st2 induces production of neutrophils, as compared to the control PBS-treated group (Fig. 8D, and Supplementary Fig. 31). No toxic effects of the designed proteins and no significant effects of Moevan_control on neutrophil numbers were observed. These results demonstrate the granulopoietic activity of our designed proteins in vivo.

Discussion

Proteins can uniquely offer large, diverse, and highly restrained physicochemical environments that undergo minimal or tightly controlled modes of motion, as encoded by their primary structure. Cytokines are a class of proteins that exert their function by modulating their cognate receptors in a lock-and-key manner. The latter appears to mostly take place through cytokines dimerising their receptors' ectodomains[42]. Existing structures of helical cytokines undergo minimal conformational change between the receptor-bound and the isolated cytokine structures,

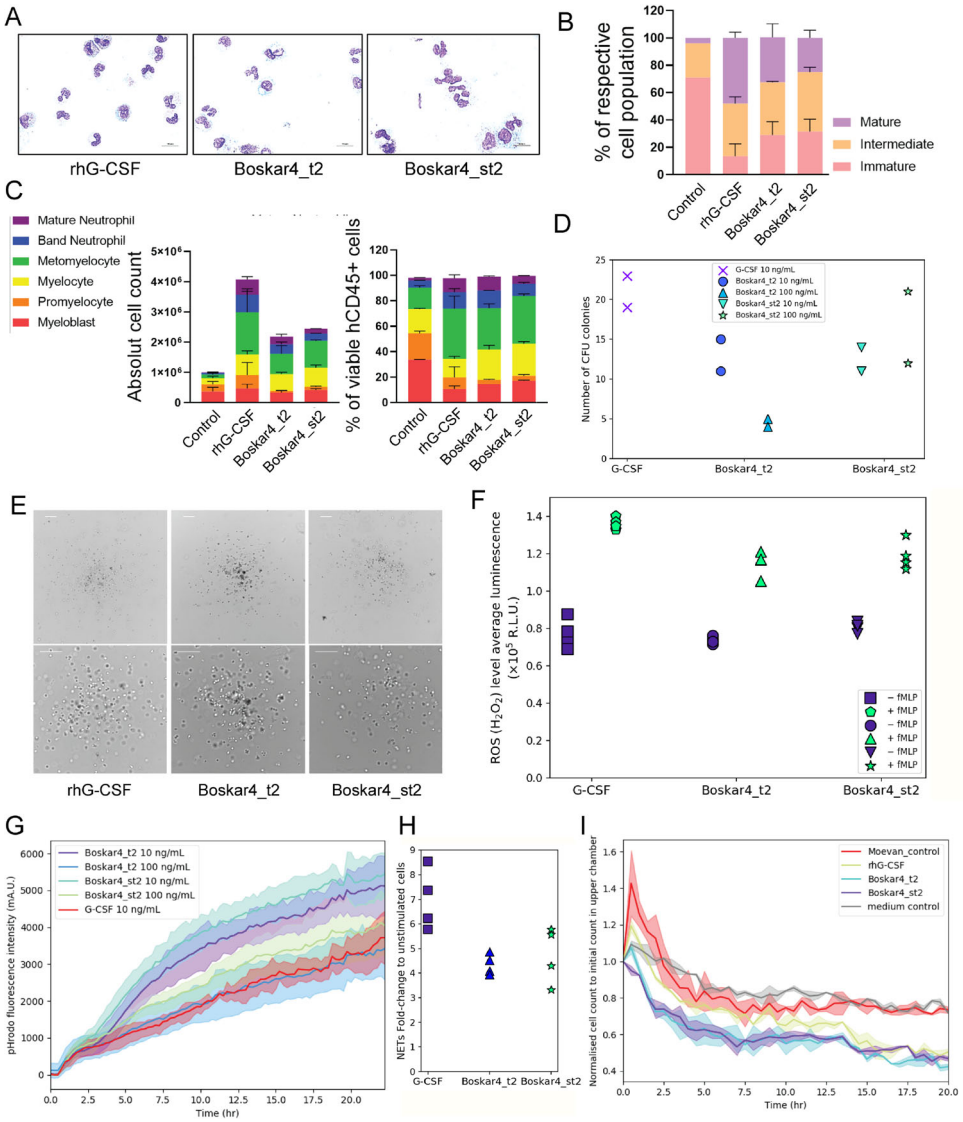

Fig. 7 The designs are functionally active in human primary cells. Cell morphology (**A**, **B**) and FACS (**C**) analysis of neutrophils generated from human healthy donors' $CD34^+$ HSPCs in the presence of either the inactive protein Moevan_control (control, 100 ng/ml), rhG-CSF (10 ng/ml), Boskar4_t2 (B4_t2, 100 ng/ml), or Boskar4_st2 (B4_st2, 100 ng/ml) using in vitro liquid culture. Data represent mean ± standard deviation of triplicate samples from two healthy donors. **D**, **E** Quantification (**D**) and representative images (**E**) of myeloid colonies induced by the rhG-CSF (10 ng/ml), Boskar4_t2 (10 or 100 ng/ml), or Boskar4_st2 (10 or 100 ng/ml) from human healthy donors' $CD34^+$ HSPCs after 14 days of culture. **F**–**H** Evaluation of functions of in vitro generated granulocytes using rhG-CSF, Boskar4_t2 or Boskar4_st2 (see the "Methods" section). **F** Reactive oxygen species (ROS) formation in fMLP-stimulated neutrophils. **G** Phagocytosis kinetic analysis using IncuCyte ZOOM System. Lines represent mean, shades represent ± standard deviation. **H** Formation of neutrophil extracellular traps (NETs) was determined by DNA staining in IncuCyte live-cell imaging. The green area was normalised to the phase area at the experiment start, and the results are depicted as fold change from unstimulated to PMA stimulated cells. Data show four biologically independent replicates after 19 h of treatment. **I** Chemotactic migration of peripheral blood healthy donors' neutrophils (solid lines represent the average of duplicates, and shades represent standard deviation) (see the "Methods" section).

indicating a rigid binding mode. However, owing to their regulatory roles, most cytokines are quickly eliminated, and possess poor stability and fairly short serum half-life[43]. The aim of this work was to reconstruct a cytokine to improve its stability and solubility. This was done under the constraint of minimally perturbing the receptor binding epitope, with the goal of preserving the receptor binding affinity, and consequently the underlying pharmacodynamics.

Here, we followed a three-pronged approach of optimising topology, size, and sequence; demonstrating that a functional protein can be fully refactored from around its active epitope. The most critical step in this strategy is the topological rewiring. For instance, a protein architecture with a defined number N of structural segments (e.g. helices, strands, or motifs), can be rewired into $N(N-1)!$ folds and circular permutations. Thus, the successful design of multiple structured loops is crucial to tap into a huge pool of accessible folds, with distinct biophysical features. We have previously shown a cytokine binding epitope could be rescaffolded onto geometrically accomodating structures with simpler folds[28]. Another recent attempt to redesign a cytokine has utilised a combination of helical extensions and template-based loop design, which successfully yielded highly active Interleukin-2 mimics[44]. The latter strategies, however, are contingent upon finding existing structural templates for either epitope or loop grafting. In contrast, here we deploy a more generalisable approach of de novo loop design that obviates the reliance on

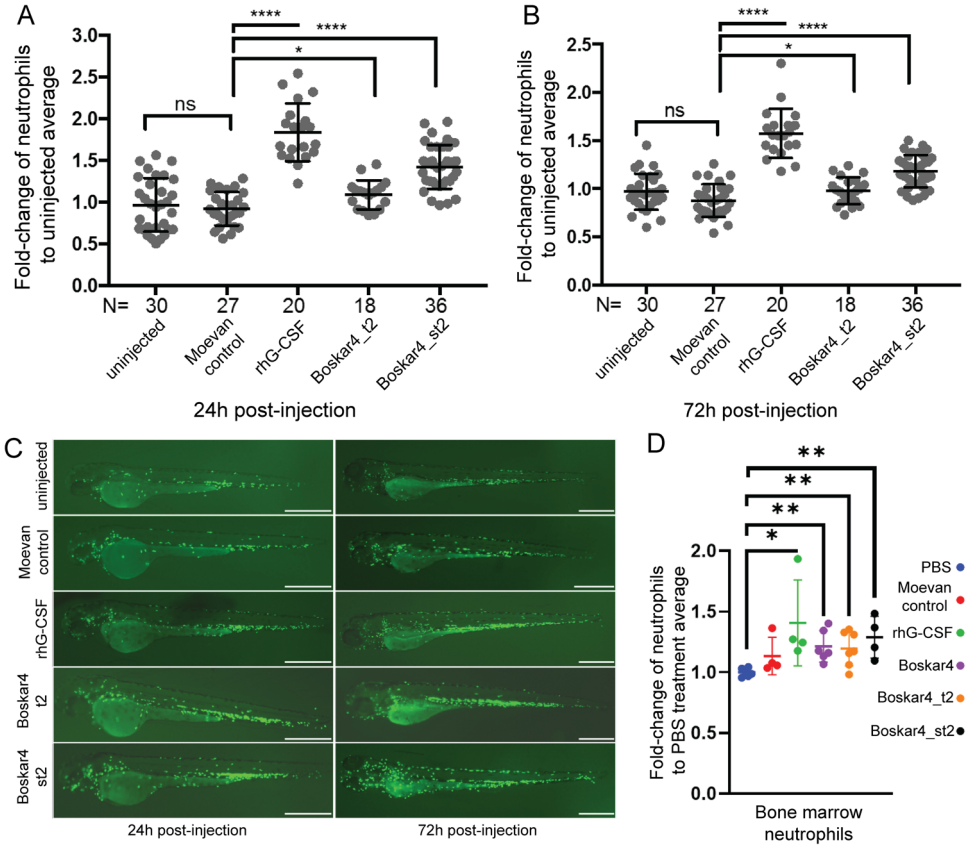

Fig. 8 The designs show in vivo activity in zebrafish and mouse models. A, **B** Interval plots of the fluorescent neutrophils in zebrafish (*Tg:mpxGFP*) that were either not injected, or injected with the inactive protein Moevan_control, rhG-CSF, Boskar4_t2, or Boskar4_st2, after (**A**) 24 h or (**B**) 72 h of treatment. Data show mean ± standard deviation, and the number of treated embryos under each condition is show as *N* (under the *x*-axis), $^{*}p < 0.05$, or $^{****}p < 0.0001$ vs. the Moevan_control group (*p*-values are listed in Supplementary Table 4). **C** Representative images of 1- and 3-day embryos that were not injected, or injected with inactive protein (Moevan_control), Boskar4_t2, or Boskar4_st2. Fluorescently labelled neutrophils can be observed and quantified across the tail region (scale bar: μm). **D** Ly5.1 mice were treated with PBS, the inactive protein Moevan_control, rhG-CSF, Boskar4, Boskar4_t2, or Boskar4_st2 ($n = 7$ per group for each condition). Fold change of mouse neutrophils ($DAPI^{-}CD45^{+}Ly6G^{+}Ly6C^{+}$) in the bone marrow of treated mice compared to PBS group is shown. Statistical significance was calculated by Fisher's two-sided *t*-test ($^{*}p < 0.05$, or $^{**}p < 0.01$ vs. the PBS group). The exact *p*-values are provided in the source data files.

existing loop structures database. Topological rewiring also brings the advantage of eliminating structural segments from across the primary structure, providing an effective means for reducing protein size. The combined effect of topology simplification and size reduction increases the probability of folded contact formation and narrows down the folding landscape, improving the folding rate and free energy, in turn[18,45]. In the last step, core and surface residues must be optimised to maximise conformational stability and solubility. Improving solubility of therapeutic proteins is particularly important to penalise the desolvation energy of off-target interactions, and also to avoid aggregation, which is related to immunogenic effects[46].

We applied our topological refactoring strategy (Fig. 1) to design novel haematopoietic agents that activate the G-CSFR pathway, which induces the proliferation and differentiation of haematopoietic stem and progenitor cells into mature granulocytes. The G-CSF:G-CSFR binding is assumed to occur in a 2:2 complex, through two binding sites on the G-CSF surface; site II and site III[26,47]. Ligand-receptor co-crystal structures, alanine scanning, and NMR studies[26,47–50] point to a minor receptor-binding contribution from site III. Therefore, we sought to design binding domains that maintain the high-affinity binding site II of G-CSF, eliminating site III from the reconstructed designs. Initial cell-based experiments showed nanomolar activity of 2 out of 4 testing designs, bearing only one binding site. Further biophysical characterisation showed these designs to exist in both monomeric and dimeric forms, whereby the dimeric species were more affine and more active in cell-based assays. This tendency to dimerise of a single binding site-bearing domain appeared to be the reason behind the observed activity. Guided by these results, we set out to create two-copy tandems with different linker lengths to evaluate the impact of purely dimerising ligands with varying receptor subunit spacing. This has surprisingly led us to discover extremely active design variants with low picomolar EC_{50} (Fig. 6). Our findings are in line with previous findings that the CRH domains in the G-CSF:G-CSFR complex are less than 55 Å apart, highlighting the distance-sensitivity of G-CSFR activation[37]. These findings also motivate further exploration of the G-CSFR subunits sensitivity to their dimeric orientation and spacing, and its impact on activation magnitude and the relative balance of downstream effects (i.e. AKT, ERK, and STAT messaging).

To the end of our design objectives, our biophysical and functional investigations demonstrate that the refactoring strategy enabled the successful creation of novel granulopoietic proteins with sequence and structure starkly distinct from native human G-CSF. The designs have a recombinant expression yield more than 20-fold higher than rhG-CSF, lack any post-translational modifications, and are expressed in a soluble form, unlike rhG-CSF. Moreover, the most active design is highly thermostable, unlike rhG-CSF. The most active design also appears to be more

resistant to proteolytic digestion when compared to rhG-CSF, where Boskar4 digestion is restricted to terminal fragments. Such protease resistance is a feature that may contribute to a potentially longer serum half-life. Deploying this design strategy, a single computational design iteration has shown to be sufficient to yield leads with nanomolar proliferative activity in NFS-60 cells. Additionally, tandem design variants could reach single-digit picomolar activity in the same assay. Combined with the relative proteolytic resistance, such stabilised active proteins can be of great therapeutic potential, especially given that rhG-CSF possesses a very short serum and shelf half-lives. In spite of the stark sequence and structure differences between the designs and native G-CSF, our results from the SPR binding experiments, testing G-CSFR knock-out cells activation, and the analysis of the downstream protein phosphorylation patterns show the designs specifically bind and activate G-CSFR. Detailed functional characterisation of the designs showed very specific activity when used to treat human healthy donor-derived hematopoietic stem cell ex vivo, where the designs induce their differentiation into mature functionally active granulocytes. These design-generated granulocytes were capable of executing a range of functions, such as NETs formation, ROS generation, and phagocytosis. Strikingly, the designs also appear to be pharmacologically active in vivo—in both zebrafish and mouse models. This further highlights the translational power of the computational protein design in creating novel therapeutic leads, without recourse to excessive experimental screening and selection.

Future development of these novel granulopoietic proteins should also evaluate their utility against clinical shortcomings of rhG-CSF. For instance, unmodified rhG-CSF is not orally bioavailable owing to its proteolytic instability[51]. Thus, orally bioavailable formulations of the Boskar designs can greatly improve the quality of life of congenital neutropenia patients that require daily subcutaneous administration of rhG-CSF. Another is the treatment of congenital neutropenia patients with compromising mutations to the Ig-like domain and its binding site in G-CSFR, where such patients are unresponsive to rhG-CSF, which requires two different binding sites to dimerise the receptor, unlike the designs. Conversely, optimising the Boskar designs into strictly monomeric forms can yield G-CSFR signalling inhibitors, that can be useful for different types of cancers[52]

Methods

Protein design. The protein design calculations were done in two stages. The first design stage was the sequence optimisation of the reduced bundle (Fig. 1B), while the second was the design of loops de novo, to rewire the topology (Fig. 1C). The reduced bundle was determined to be the minimal 4-helix-bundle sufficient to scaffold G-CSFR site II; eliminating helix E and three long loops distal to site II. The remaining fragments comprised of the peptide segments 71–123, 10–39, and 145–171, which are made of helices A, B–C and D, where B and C were left connected by a short native loop. This minimal bundle should fully host the essential site II residues, namely: K16, E19, Q20, R22, K23, D27, D109, and D112 (blue patch in Fig. 1A). This helical architecture was reordered to a permutation that would move the native B-C motive to the N-terminus, and wire it with the remaining helices to achieve the shortest gaps (and thus, loops) across the bundle. This transformed the old arrangement: A—E—B–C—D into the new arrangement: B'- C'- A'- D', where "-" and "—" represent short and long loops, respectively. This gapped template was used directly for sequence optimisation (i.e. the first design stage), which was done through sequence and conformer sampling performed within the RosettaScripts framework[53]. With the addition of a root-mean-square deviation (RMSD) constraint on the binding epitope, a previously described core packing protocol was used[54]. This comprised steps of interleaved Monte Carlo sequence, as well as side-chain and backbone conformer sampling iterations. The sequence sampling was directed to most core residues and to solvent-exposed hydrophobic residues. The scoring functions used were the *talaris2013* energy function[55] and the *packstat* packing score[56] (Supplementary methods). While the energy function was used to bias the sampling towards lower energy decoys, the top decoys were forwarded for further evaluation based on the packing quality, where the latter was further judged by the ruggedness of the radial distribution function $g(r)$ as given by the definite integral $\int_0^4 \left|\frac{dg(r)}{dr}\right| dr$.

The second design stage was to construct loops de novo across the junctions C'- A' and A'- D'. The N-C distance gap across the C'- A' junction was approximately 10 Å, while the N-C distance across the A'- D' was approximately 13 Å. Therefore, we sought to build 3- and 4-residue loops at junctions C'- A' and A'- D', respectively. The 3-residue were constructed by covering all sequence combinations of the residues G, D, P, S, L, N, T, E, and K, while the 4-residue loops were constructed by covering all combinations of the residues G, D, P, S, L, N, T, and K. The G, D, P, S, and T amino acids were chosen for their higher propensity to exist in loops[57], L was included due its abundance in helix-helix-turns[58]. E, D and K were included for their helix-capping roles[58], where E was removed from the 4-residue optimisation to reduce the sequence space. Novel loops were constructed through automatic modelling[59], followed by molecular dynamics-based evaluation, which relied on repeated generalised-ensemble sampling (GS)[60] simulations. These simulations were deployed to temper the decoys serially between 250 and 390 K, over 6 and 8 ps, respectively per cycle (through $N = 25$ serial cycles per decoy). These cycles were interlaced with 100 conjugate gradient minimisation steps to revert to local minima along the serial conformational divergence. These simulations were done in restrained and unrestrained formats, initial simulations constrained all atoms except for loop residues, and 5 flanking residues up- and down-stream, later simulations combining top 50 sequences at each loop where recombined and underwent unrestrained simulations. A conformational homogeneity metric was calculated as the average all-against-all RMSD, which is a proxy of the misfolding or basin hopping tendency of each decoy, as $S_h = \sum_{i \neq j}^{N^2} \frac{S_{\mathrm{RMSD}_{i,j}}}{N^2}$, where $S_{\mathrm{RMSD}_{i,j}}$ is the aligned backbone RMSD between frames i, j. All molecular dynamics simulations relied on conjugate gradient minimisation and a perturbation time step of 2 fs, under Langevin temperature control. A long-range interactions cutoff of 12.0 Å, a switching distance of 10.0 Å, and a Langevin temperature control set to 310 K with a damping coefficient of 1.0 ps^{-1} were used. Generalised Born solvation was used for GS simulations. TIP3P water and Langevin barostat were used for NMR refinement simulations, with a Langevin piston oscillation period of 200 fs and a piston decay period of 50 fs. The systems were neutralised with 0.15 M sodium chloride. All simulations were either conducted using the OpenMM library[61] or the NAMD engine[62]. A schematic of the design workflow is shown in Supplementary Fig. 32.

For computational evaluation of the solubility analysis, we used three different metrics. The first metric was the Damietta solvation energy function, which is based on a CHARMM-compatible solvation model[63]. Using a single round of the Damietta software `ra` (repack all, v0.22) protocol, residues side chains were repacked, and the residue-wise solvation energy extracted from the output PDB file. The Damietta protein design software is available at https://bio.mpg.de/damietta/. The second metric was the Kyte-Doolittle hydropathy scale[64] as implemented on the ProtScale server (https://web.expasy.org/protscale/). The third metric was the Rosetta residue-wise solvation energy sub-score[65] after a single run of Rosetta Relax protocol using *talaris14* scoring function.

Protein expression and purification. Synthetic genes encoding the designs were cloned into the pET28a(+) expression vector carrying a kanamycin resistance gene using *NdeI* and *XhoI* cloning sites in-frame with an N-terminal hexaHis-tag and a thrombin cleavage site (Synbio Technologies, Inc.). The plasmids were used to transform chemically competent *E. coli* BL21(DE3) by heat-shock. Transformed cells were grown in LB medium and induced with IPTG at OD600 of about 0.5–1 with overnight expression at 25 °C. For expression of isotopically labelled protein, a preculture in LB medium was grown, cells collected, washed twice in PBS buffer, and resuspended in M9 minimal medium (240 mM Na_2HPO_4, 110 mM KH_2PO_4, 43 mM NaCl), supplemented with 10 µM $FeSO_4$, 0.4 µM H_3BO_3, 10 nM $CuSO_4$, 10 nM $ZnSO_4$, 80 nM $MnCl_2$, 30 nM $CoCl_2$ and 38 µM kanamycin sulfate, to an OD600 of about 0.5–1. After 40 min of incubation at 25 °C, 2.0 g ^{15}N-labelled ammonium chloride (Sigma-Aldrich 299251) and 6.25 g ^{13}C D-glucose (Cambridge Isotope Laboratories, Inc., CLM-1396) were added in a 2.5 l culture. After another 40 min IPTG was added to a final concentration of 1 mM for overnight expression. Cells were collected by centrifugation at 5000 × *g* for 15 min, lysed by a Branson Sonifier S-250 (Fisher Scientific) in hypotonic 50 mM Tris–HCl buffer supplemented with one tablet of the cOmplete protease inhibitor cocktail (Sigma-Aldrich 4693159001) and 3 mg of lyophilised DNase I (5200 U/mg; Applichem A3778). The insoluble fraction was pelleted by centrifugation at 30,000 × *g* for 50 min, and the soluble fraction was passed through a 0.45 µm filter and directly applied to a Ni-NTA HisTrap column (GE Healthcare). For wild-type G-CSF, refolding extraction was performed from the insoluble fraction of the *E. coli* cell pellet by stirring in 8 M guanidinium chloride solution for 2 h at 4 °C. The mixture was gradually diluted to 1 M guanidinium chloride in 4 steps over 4 h and loaded directly onto an affinity purification column. A 5 ml HisTrapFF immobilised nickel column (GE Healthcare Life Sciences 17-5255-01) was used for this purpose, washed consecutively with 30 ml 150 mM NaCl, 30 mM Tris buffer (pH 8.5) at 0, 30 and 60 mM imidazole. Fractions were collected by gradient elution at >60 mM imidazole. The eluate was concentrated using 3 kDa MWCO centrifugal filters (Merck Millipore UFC901024) and loaded onto an equilibrated Superdex 75 gel filtration column (GE Healthcare Life Sciences 17517401). The gel filtration buffer used was 150 mM sodium phosphate buffer, pH 7.5, for NMR and CD transparency as well as cell culture compatibility. An Äkta Pure system (GE Healthcare Life

Sciences) was used for all chromatography runs. All experiments involving wild-type G-CSF were initially conducted using in-house purified rhG-CSF, and later reproduced using USP filgrastim as a standard reference (Sigma-Aldrich 1270435), except the CD experiments, which were performed only using in-house produced rhG-CSF.

Endotoxin removal and quantification from bacterially produced designs. We used a special two-step purification protocol to produce low-endotoxin protein samples for in the in vivo experiments. Firstly, we optimised a detergent-based purification protocol based on two previous protocols[66,67]. The cell pellets from overnight expression 2 l cultures were reconstituted in PBS buffer to 25 ml with 3 mg of lyophilised DNase I (5200 U/mg; Applichem A3778) and protease inhibitor cocktail (Sigma-Aldrich 4693159001) and lysed by sonication, as described above. This total lysate was added to chilled 25 ml of 1% Triton-X114 (Sigma Aldrich X114-100ML) and sonicated further at 4 °C for another 30 min interval. This total lysate was then incubated for 5 min in a 42 °C water bath in order to phase out most of the Triton-X114. This was spun at 3000 × *g*, and the supernatant was decanted for further ultracentrifugation at 30,000 × *g*. The supernatant was then loaded on a 5 ml HisTrap NiNTA column, which was prewashed with 0.1% Triton-X114 in PBS (6 column volumes) at 4 °C. After loading, an on-column wash was done with 0.1% Triton-X114 in PBS (10 column volumes), followed by the affinity purification protocol as described above. Size exclusion was performed as described above, with the addition of a pre-equilibration wash with 1 column volume of 3 M urea and 1 M NaOH. Both washes in affinity and size-exclusion purification were flushed through the fraction collector tubing. The second step of the depyrogenation protocol was done using a specialised endotoxin binding resin; the 0.5 ml Pierce high capacity endotoxin removal spin column (ThermoFisher, 88274) according to the supplier's protocol. The amount of endotoxin in protein preparations was quantified using the Pierce chromogenic endotoxin quant kit (ThermoFisher, A39552S) according to the supplier's protocol. A calibration curve was plotted between standard endotoxin concentrations of 0 and 1.0 EU/ml, and samples were diluted to obtain 410 nm absorbance values within this range.

The endotoxin content of the purified designs using this protocol ranged from <0.4 to 6.64 EU/mg, which was considered an acceptable level for in vivo experiments.

Thermostability analysis. Circular dichroism (CD) spectra were recorded using a JASCO J-810 spectrometer. Samples (0.5 ml) with concentrations between 0.5 and 0.6 mg/ml of the respective proteins in PBS buffer (pH 7.1) were loaded into 2 mm path length cuvettes. Spectral scans of mean residual ellipticity were measured at a resolution of 0.1 nm across a range of 240–195 nm. The mean residual ellipticity at a wavelength of 222 nm across a temperature range of 20–100 °C (with an increase of 1 °C/min) was tracked in melting curves. Additional thermostability analysis was performed to rhG-CSF to evaluate the influence of disulfide bonds on folding, nanoscale differential scanning fluorimetry (nanoDSF) was performed using Prometheus NT.48 (Nanotemper) and standard Prometheus capillaries (Nanotemper, PR-C002). The same temperature ramp parameters used for CD were set for melting and cooling, using 1 mg/ml protein samples in PBS, in 5 mM Dithiothreitol (DTT) in PBS, and in 2.5 mM reduced glutathione (GSH) and 0.5 mM oxidised glutathione (GSSG) in PBS.

Protease sensitivity analysis. Purified human neutrophil elastase was obtained from Enzo Life Science (#BML-SE284-0100). The elastase was reconstituted in PBS buffer (pH 7.1) to a stock concentration of 20 IU/ml. Digestion reactions were conducted in PBS buffer with final concentrations of 300 µg/ml of the tested protein, and 1 U/ml of neutrophil elastase. The reaction mixture was incubated at 37 °C and digestion samples were withdrawn, immediately mixed with SDS sample buffer (450 mM Tris–HCl, 12% glycerol, and 10% SDS) and flash-frozen in a liquid nitrogen bath to stop the reaction after 5, 15 and 30 min from the reaction start. Frozen samples were then heated at 85 °C for 10 min before loading on Novex™ 16% Tricine Protein Gels (Thermo Fisher Scientific #EC6695BOX). Protein gels were incubated overnight in fixing solution (30% ethanol, 10% acetic acid) and then stained using colloidal Coomassie dye (Serva; 35050).

Nano-HPLC–MS/MS was used to analyse the protein bands resulting from the digest of Boskar 4 with Neutrophile elastase. Boskar4 samples incubated with neutrophil elastase (as described above) were separated on SDS-PAGE, where each lane of the gel (16% Tricine protein gel, ThermoFisher Scientific, #EC6695) contains 6 µg Boskar4 digested with neutrophile elastase for 30 min. Excised protein bands were digested in-gel using Arg-C. LC–MS/MS analysis was done on an Easy-nLC 1200 (Thermo Scientific) coupled to a QExactive HF mass spectrometer (Thermo Scientific) as described elsewhere[68]. Peptide mixtures were injected onto the column in HPLC solvent A (0.1% formic acid) at a flow rate of 500 nL/min and subsequently eluted with a 46 min gradient of 5–33% HPLC solvent B (80% ACN in 0.1% formic acid) at a flow rate of 200 nl/min. The seven most intense precursor ions were sequentially fragmented in each scan cycle using HCD fragmentation.

MS data were processed using the MaxQuant software suite v.1.5.2.8[69]. Database search was performed using the Andromeda search engine[70]. Spectra were searched against a Uniprot *E. coli* database, a database containing 248 commonly observed contaminants and against the sequence of human Neutrophil elastase (UniProtKB-P08246 (ELNE_HUMAN)) as well as a database comprising the sequence of Boskar4 and it's truncated forms. For the latter, all sequences derived from consecutively shortening the amino acid sequence of Boskar4 (including the purification tag), once starting at the N terminus and once at the C terminus, respectively, were unified into one database. In the database search, full specificity was required for Arg-C and up to two missed cleavages were allowed. Carbamidomethylation of cysteine was set as fixed modification, protein N-terminal acetylation, and oxidation of methionine were set as variable modifications. False discovery rate (FDR) was set to 1% on protein as well as peptide level. The posterior error probability (PEP) was calculated for each peptide[71].

The proteolytic stability of Boskar4 and rhG-CSF was tested against a spectrum of different proteases including recombinant human Cathepsin D (bio-techne, #1014-AS), recombinant human ADAM10 Protein (bio-techne, #936-AD), Cathepsin L from Human Liver (Merck, #219402), and Cathepsin G from human leucocytes (Merck, #C4428). In detail, 300 µg/ml of Boskar4 (23 µM) or rhG-CSF (µM) were incubated with Cathepsin D (10 µg/ml) in 0.1 M NaOAc, 0.2 M NaCl, pH 3.5, ADAM10 (5 µg/ml) in 25 mM Tris, 2 µM $ZnCl_2$, 0.005 % (w/v) Brij-35, pH 9.0, Cathepsin L (50 µg/ml) and Cathepsin G (0.5 U/µl) in phosphate buffered saline, pH 7.4, at 37 °C. Samples were taken after 5, 15, and 30 min and the reaction was stopped immediately by addition of SDS sample buffer (450 mM Tris–HCl, 12% glycerol, and 10% SDS) and flash-freezing in liquid nitrogen. For analysis frozen samples were heated at 85 °C for 10 min and loaded on Novex™ 16 % Tricine Protein Gels (Thermo Fisher Scientific, #EC6695). Protein gels were incubated overnight in fixing solution (30% ethanol, 10% acetic acid) and stained using colloidal Coomassie dye (Serva, #35050).

NMR structure determination. All spectra were recorded at 310 K on Bruker AVIII-600 and AVIII-800 spectrometers. All spectra were acquired for samples of Boskar4 in PBS buffer with a concentration between 400 and 800 µM, where the measuring temperature throughout (showing best dispersion) was 313 K. Backbone sequential and aliphatic side chain assignments were completed using standard triple resonance experiments (HNCO, HNCA, HNCAB, CC(CO)NH-TOCSY). A CCH-TOCSY experiment was used to aid aliphatic sidechain assignments. The CNH-NOESY for CoMAND analysis was acquired at 800 MHz with a mixing time of 80 ms, and consisted of 112 complex time points in the ^{13}C dimension, processed to 256 points in the final matrix. The experimental strips extracted for each residue have been submitted with the PDB entry for the *boskar4* structure. Two further NOESY spectra were acquired at 800 MHz: a ^{13}C-HSQC NOESY and a 2D-NOESY spectrum acquired with suppression of signals from ^{15}N-bound protons, which is intended to isolate contacts to aromatic protons. The latter aided aromatic assignment by linking aromatic spin systems to the respective $C^{\beta}H_2$ protons.

Structures were determined using the CoMAND method, which exploits the high accuracy that can be obtained in back-calculating NOESY spectra with indirect ^{13}C dimensions[33]. The CoMAND method involves spectral decomposition of one-dimensional sub-spectra extracted from a 3D-CNH-NOESY spectrum[34]. These sub-spectra (strips) are chosen from a search area centred on assigned ^{15}N-HSQC positions and thus contain cross-peaks to a specific amide proton. For residues with overlapping search areas, strips were extracted at the estimated maximum for each component, and a scaling factor calculated expressing the contribution of each component to the strip. These 1D strips were decomposed against a library of spectra back-calculated by systematic sampling over a local dihedral angle space, yielding estimates of backbone and side chain dihedral angles for each residue. Although it is possible to decompose even heavily overlapped strips with this procedure[33], we did not do so here, due to the relatively low number of such cases. Later stages of the protocol involve conformer selection aimed at minimising a quantitative *R*-factor expressing the match between the experimental strips and back-calculated spectra, or a fold-factor designed to isolate the contribution to the *R*-factor from long-range NOESY contacts[33].

For initial model building, unrestrained Rosetta ab initio[72] folding simulations were performed and generated 10,222 decoys. The corresponding CNH-NOESY spectra of these decoys were back-calculated to evaluate the structure-averaged fold-factors. The decoy with the lowest fold-factor was used to seed five independent unrestrained molecular dynamics simulations. These refinement simulations were carried out using the CHARMM36 force field[73] in explicit solvent using the polarisable TIP3P water model. Trajectories of a total length of approximately 1 µs were run, with frames collected every 100 ps. An initial refined ensemble was compiled through a global greedy minimisation of the R-factor as previously described[33], which converged on a total of 12 frames.

The 12 selected frames represent a thermodynamically relevant ensemble, thermalized to the experiment's temperature (313 K). It may not, however, optimise *R*-factors well, as this depends on the ability of the MD trajectory to reproduce the distributions of conformers present in the sample, particularly for sidechain rotamers. To optimise *R*-factors further, we have developed an extended protocol that proceeds via a restrained intermediate ensemble. Restraints for this ensemble were derived from sub-sets of the trajectory selected by greedy *R*-factor optimisation for single residues. These typically converge on *R*-factors close to the noise level, and the distributions of backbone dihedrals, sidechain rotamers, H-bond parameters and other distances extracted from these subsets are thus

directly associated with low *R*-factors. This procedure was applied for all 107 observed strips, while jointly optimising any strips with overlapped intensities. Restraints derived in this manner were supplemented by 56 NOE contacts identified using the initial ensemble as a bootstrapping model. These were primarily well-resolved contacts between aromatic sidechains and methyl groups observed either in a ^{13}C-HSQC-NOESY or in a 2D NOESY acquired with suppression of signals from ^{15}N-bound protons. The extracted restraints are summarised in Table S2.

The intermediate ensemble was calculated in Xplor-NIH[74] using short, low-temperature simulated annealing runs, cooling from 300 to 100 K via 2000 steps of molecular dynamics in vacuo (timestep 3 fs) with randomised initial velocities. Each of the 12 structures from the initial ensemble was used to calculate five restrained models. Each of these 60 models was then used to seed short, unrestrained simulated annealing runs using a similar protocol, primarily aimed at exploring surface sidechain conformations. Each run yielded a further five models and the intermediate ensemble was formed by pooling the 360 resulting restrained and unrestrained frames. A final set of 17 structures was selected by applying greedy optimisation over all available strips. Accordingly, the selected ensemble had improved *R*-factors relative to the initial ensemble, but can no longer be considered thermodynamically relevant. In this respect it is closer in nature to conventionally calculated structures based on NMR-derived restraints, however it differs in that individual structures are allowed to deviate from restraints. For this reason, restraint violations are not tabulated in Table S2.

For one residue, E23 at the C-terminus of α1, greedy optimisation failed to produce *R*-factors commensurate with the quality of the strip, while factorisation suggested a backbone polymorphism. This had not been resolved during greedy optimisation, as it had not been adequately sampled in Rosetta model building, nor during the MD simulations (Supplementary Fig. 12). The polymorphism was localised to the backbone ψ angle of L22. To accommodate this, the α1–α2 loop was remodelled by restraining L22 to either the canonical helical angles derived from the greedy optimisation ($\varphi/\psi = -56 \pm 10°/-31 \pm 8°$), or the alternate conformer suggested by factorisation $\psi = -135 \pm 30°$. These restraints were applied during further simulated annealing rounds, where the residues of the α1–α2 loop were free (L22–L29) and all other coordinates fixed. Loop models were selected to optimise *R*-factors for residues across the segment. This procedure also identified multiple backbone conformations for S26, despite the low signal-to-noise of this strip.

The $^{15}N\{^1H\}$-heteronuclear NOE experiment[75] was acquired at 800 MHz as a pseudo-3D spectrum with interleaving of data points. The reported values are the ratio of the intensity for each residue in an experiment with NOE mixing (mixing time 3 s) versus a reference without mixing. MEXICO water exchange experiments[76] were acquired as a pseudo-3D spectrum at 800 MHz with 5 mixing times (τ) spaced linearly between 50 and 250 ms. The reported values are time constants for backbone amide water exchange processes, calculated for each residue by first subtracting and then normalising by a reference value representing $\tau = 0$. The resulting exponential was fitted after linearising using the polyfit routine in NumPy.

NFS-60 cell proliferation analysis. NFS-60 cells were cultured in IL-3-containing RPMI 1640 medium, supplemented with L-glutamine, 10% KMG-5 and 10% FBS (CLS, cell line services). Before each assay, cells were pelleted and washed three times with cold non-supplemented RPMI 1640 medium. After the last washing step, cells were diluted at a density of 6×10^5 cells/ml in RPMI 1640 containing glutamine and 10% FBS. In order to analyse cell proliferation, NFS-60 cells were grown in the presence of varying concentrations of G-CSF wild-type and designed variants. For this, five-fold dilution series were prepared from stock solutions of wild-type G-CSF (40 ng/ml) and the designs (40 µg/ml) in RPMI 1640 medium supplemented with glutamine and 10% FBS. 75 µl of each dilution were mixed with the same volume of washed cells in a 96-well plate yielding a final cell density of 3×10^5 cells/ml and G-CSF concentrations varying from 0.00001 to 20 ng/ml for wild-type and 0.01–20,000 ng/µl for the designs. Each 96-well plate contained triplicates of each dilution and the according blanks, including wells containing cells seeded in RPMI 1640 medium supplemented with L-glutamine, 10% KMG-5 and 10% FBS (cls, cell line services) and wells containing medium only. For end-point analysis, following incubation for 48 h at 37 °C and 5% CO_2, 30 µl of the redox dye resazurin (CellTiter-Blue® Cell Viability Assay, Promega) was added to the wells, and incubation was continued for another hour. Cell viability was measured by monitoring the fluorescence of each well at a H4 Synergy Plate Reader (BioTek) using the following settings: excitation = 560 ± 9 nm, Emission = 590 ± 9 nm, read speed = normal, delay = 100 ms, measurements per data point = 10. The data were analysed and curves were plotted applying a four-parameter sigmoid fit using SigmaPlot (Systat Software). For time-kinetics analysis, cells were monitored for 136 h in the IncuCyte S3 Live-Cell Analysis System (Essen Bio) with a ×10 objective. Cell proliferation was analysed using IncuCyte S3 Software.

Surface plasmon resonance (SPR) binding assays. Multi-cycle kinetics experiments were performed on a Biacore X100 system (GE Healthcare Life Sciences). G-CSF Receptor (G-CSFR) (R&D systems 381-GR-050/CF) was diluted to 50 µg/ml in 10 mM acetate buffer pH 5.0 and immobilised on the surface of a CM5 sensor chip (GE Healthcare 29149604) using standard amine coupling chemistry. The designs and rhG-CSF (USP RS Filgrastim, Sigma-Aldrich 1270435) were diluted in running buffer (10 mM HEPES, pH 7.4, 150 mM NaCl, 3.4 mM EDTA, 0.005% v/v Tween-20). Analyses were conducted at 25 °C at a flow rate of 30 µl/min. Five sequential 2-fold increasing concentrations of the sample solution (for Boskar3 and Boskar4 from 5 to 80 nM; for Boskar4_t2 from 2.5 to 40 nM; for Boskar4_st2 from 6.5 to 100 nM; for rhG-CSF from 4 to 64 nM) were injected over the functionalized sensor chip surface for 180 s, followed by a 360 s dissociation with running buffer. At the end of each run, the sensor surface was regenerated with a 60 s injection of 10 mM glycine–HCl pH 2.0. The reference responses and zero-concentration sensograms were subtracted from each dataset (double-referencing). Association rate (k_a), dissociation rate (k_d), and equilibrium dissociation (K_d) constants were obtained using the linearization method described in ref. [77] and were derived as follows. Global fitting of the association curves to a 1:1 interaction model was performed using the following equation:

$$\Gamma(t) = \Gamma_{GG} - \Gamma_{GG} \cdot e^{-k_{obs} \cdot t} \quad (1)$$

where $\Gamma(t)$ describes the surface load capacity over time (t), Γ_{GG} is the equilibrium surface load capacity, and k_{obs} is the observed binding rate constant. The previous equation was rewritten as:

$$\Gamma(t) = c + a \cdot e^{-b \cdot t}$$

where the parameters a, b, and c were fit to the data to minimise the value of χ^2, which is evaluated by the expression:

$$\chi^2 = \frac{\sum(\Gamma_{fit} - \Gamma_{obs})^2}{n - p} \quad (2)$$

where Γ_{fit} is the $\Gamma(t)$ function with minimum sum of squared deviations from the observed sensogram Γ_{obs}, n is the number of data points ($n = 900$), and p is the number of parameters fitted by optimiser ($p = 3$). The optimisation was performed using the Nelder–Mead method at a tolerance of 10^{-12} and a maximum number of 10^6 iterations. The optimisation bounds for parameters a, b, and c were $(-7 \times 10^2, 0)$, $(10^{-4}, 10^{-1})$, $(0, 7 \times 10^2)$, respectively. After fitting, the resulting k_{obs} values were plotted against the corresponding analyte concentrations (C) to perform a linear regression according to the following equation:

$$k_{obs} = k_a \cdot C + k_d \quad (3)$$

where k_a represents the slope, and k_d represents the y-axis intercept of the linear fit. The dissociation constant K_d was calculated as follows:

$$K_d = \frac{k_d}{k_a} \quad (4)$$

To measure the dispersion of a dataset, five additional linear fits of $k_{obs}(C)$ function were performed as described above, but excluding one analyte concentration at a time. Standard deviations of k_a, k_d, and K_d values were calculated as follows:

$$s = \sqrt{\frac{\sum(x_i - \bar{x})^2}{N - 1}} \quad (5)$$

where x_i is the value of k_a, k_d, or K_d derived from the ith linear fit, $\bar{x}$ is the mean value of k_a, k_d, or K_d, and N is the total number of performed linear fits ($N = 5$).

CRISPR/Cas9-sgRNA RNP-mediated *CSF3R* KO in NFS-60 cells. A specific guide RNA (sgRNA) for knock-out of the *CSF3R* gene (cut site: chr4 [+126.029.810: −126.029.810], NM_007782.3 and NM_001252651.1, exon 4, 112 bp after ATG; NP_031808.2 and NP_001239580.1 p.L38) was designed using CCTop at (http://crispr.cos.uni-heidelberg.de)[78]. Electroporation of NFS-60 cells was carried out using the Amaxa nucleofection system (SF cell line 4D-Nucleofector kit, #V4XC-2012) according to the manufacturer's instructions. Briefly, 1×10^6 cells were electroporated with assembled sgRNA (8 µg) and HiFi Cas9 nuclease protein (15 µg) (Integrated DNA Technologies). Clonal isolation of single-cell derived NFS-60 cells was performed by limiting dilution followed by an expansion period of 3 weeks. Genomic DNA of each single-cell derived NFS-60 clones was isolated using QuickExtract DNA extraction solution (Lucigen #QE09050). PCR was carried out with mouse *CSF3R*-specific primers (forward: 5′-GGCATTCACACCATGGGGCACA-3′, reverse: 5′-GCCTGCGTGAAGCT CAGCTTGA-3′) and the GoTaq Hot Start Polymerase Kit (Promega, #M5006) using 2 µl of gDNA template for each PCR reaction. In vitro cleavage assay was done by adding 1 µM Cas9 RNP assembled by the same sgRNA used for the knock-out experiment to 3 µl of each PCR product. The PCR reactions were incubated at 37 °C for 60 min and run on a 1% agarose gel. The PCR products that showed no cleavage were purified by ExoSAP (ratio 3:1), which is a master mix of one-part Exonuclease I 20 U/µl (Thermo Fisher Scientific, #EN0581) and two parts of FastAP thermosensitive alkaline phosphatase 1 U/µl (Thermo Fisher Scientific, #EF0651). Sanger sequencing of purified PCR products was performed by Microsynth and analysed using the TIDE (Tracking of Indels by Decomposition) webtool[79].

Evaluation of time-dependent effects of the designs on the proliferation of CD34$^+$ HSPCs and NFS-60 cells. Cells were incubated in poly-L-lysine-coated

96-well plates (2×10^4 cells/well) in an IncuCyte S3 Live-Cell Analysis System (Essen Bio) with a ×10 objective at 37 °C and 5% CO_2, and cell proliferation over time was analysed. The $CD34^+$ HSPC cell culture medium contained Stemline II Hematopoietic Stem Cell Expansion medium (Sigma Aldrich; #50192) supplemented with 10% FBS, 1% penicillin/streptomycin, 1% L-glutamine and 1 µg/ml Boskar3, 1 µg/ml Boskar4, or 100 ng/ml rhG-CSF. Cell proliferation was analysed using IncuCyte S3 Software.

Colony-forming unit (CFU) assay of human HSPCs. $CD34^+$ HSPCs at a concentration of 1×10^4 cells/ml were plated in 35 mm cell culture dishes in 1 ml Methocult H4230 medium (Stemcell Technologies) supplemented with 2% FBS, 10 µg/ml 100× Antibiotic–Antimycotic Solution (Sigma) and 50 ng/ml rhG-CSF, or 1 µg/ml Boskar3 or Boskar4. Cells were cultured at 37 °C and 5% CO_2. Colonies were counted on day 10–14.

In vitro granulocytic differentiation of HSPCs. Human $CD34^+$ HSPCs were isolated from the bone marrow mononuclear cell fraction of two healthy donors by magnetic bead separation using the Human CD34 Progenitor Cell Isolation Kit (Miltenyi Biotech Germany; #130-046-703). $CD34^+$ cells were cultured at a density of 2×10^5 cells/ml in Stemline II Hematopoietic Stem Cell Expansion medium (Sigma Aldrich; #50192) supplemented with 10% FBS, 1% penicillin/streptomycin, 1% L-glutamine and 20 ng/ml IL-3, 20 ng/ml IL-6, 20 ng/ml TPO, 50 ng/ml SCF, and 50 ng/ml FLT-3L. For liquid culture granulocytic differentiation, expanded $CD34^+$ cells (2×10^5 cells/ml) were incubated for 7 days in RPMI 1640 GlutaMAX supplemented with 10% FBS, 1% penicillin/streptomycin, 5 ng/ml SCF, 5 ng/ml IL-3, 5 ng/ml GM-CSF and 10 ng/ml rhG-CSF, 1 µg/ml of Boskar3 or Boskar4, or 100 ng/ml of Boskar4_t2 or Boskar4_st2 (10 ng/mL of Boskar4_t2 or Boskar4_st2 were also tested in some experiments as indicated in the Fig. 7). Medium was exchanged every second day. On day 7, medium was replaced by RPMI 1640 GlutaMax supplemented with 10% FBS, 1% penicillin/streptomycin and 10 ng/ml rhG-CSF, or 1 µg/ml of Boskar3, or 1 µg/ml of Boskar4, or 10 or 100 ng/ml Boskar4_t2, or 10 or 100 ng/ml Boskar4_st2, or PBS. Medium was exchanged every second day until day 14. On day 14, cells were analysed by flow cytometry on a FACSCanto II instrument using the following antibodies: mouse anti-human CD45 (Biolegend; #304036), mouse anti-human CD11b (BD; #557754), mouse anti-human CD15 (BD; #555402), mouse anti-human CD16 (BD; #561248), and mouse anti-human CD66b (BD; #555724). For all FACS analyses, vital mononuclear cells were selected, and doublets were excluded based on scatter characteristics.

Cell morphology was evaluated on cytospin preparations on day 14 of culture. 10×10^4 cells per cytospin slide were centrifuged at $400 \times g$ for 5 min at room temperature using a Thermo Scientific cytospin 4 cytocentrifuge. Wright-Giemsa-stained cytospin slides were prepared using a Hema-Tek slide stainer (Ames) and evaluated using a Nikon Eclipse TS 100 microscope with a ×10 objective.

Assessment of phagocytosis kinetics. Neutrophils from day 14 of liquid culture differentiation were cultured in RPMI 1640 medium supplemented with 0.5 % BSA and pHrodo Green *E. coli* Bioparticles Conjugate (Essen Bio; #4616) according to the manufacturer's protocol (Essen Bio) at 37 °C and 5% CO_2. Briefly, 1×10^4 cells were seeded in 90 µl medium, and 10 µg of Bioparticles were added to a final volume of 100 µl. The cells were monitored for 8 h in an IncuCyte S3 Live-Cell Analysis System (Essen Bio) with a ×10 objective. The analysis was conducted in IncuCyte S3 Software.

In vitro reactive oxygen species (ROS) production assay. Cells were seeded at a density of 1×10^5 cells/ml with or without 10 nM *f*MLP (Sigma, #F3506) and incubated for 30 min at 37 °C and 5% CO_2. The level of hydrogen peroxide (H_2O_2), a reactive oxygen species (ROS), was measured with the ROS-Glo H_2O_2 Assay kit (Promega, #G8820) according to the manufacturer's protocol.

Quantitative analysis of NETosis formation. Ex vivo generated neutrophils were seeded at a density of 2×10^4 per well in a poly-L-lysin-coated 96-well plate in RPMI without phenol red supplemented with 0.5% BSA and 250 nM IncuCyte® Cytotox Green Dye (Incucyte #4633). NETosis was induced by adding 0,5 µM Phorbol-12-myristate-13-acetate (PMA). Cells were analysed every 30 min at ×20 magnification on the IncuCyte S3 Live cell analysis system. Data analysis was performed using IncuCyte Basic Software, as recommended by the manufacturer.

Chemotaxis. Neutrophils were isolated from peripheral blood of healthy donors using EasySep Direct Human Neutrophil isolation kit (StemCell technologies #19666) and resuspended in assay medium RPMI (Gibco, # 72400-054) supplemented with 0.5% FBS (Sigma Aldrich, # A8412-100) at a density of 8.3×10^5/ml. The pre-cooled IncuCyte ClearView migration plate, including insert and reservoir plate (Essen BioScience, cat. 4582), were coated with recombinant human fibronectin fragment (Takara Clonetech, #T100B) and incubated at room temperature for 60 min. After fibronectin was removed, an insert was placed in a new reservoir plate filled with 200 µl of PBS, and 60 µl of neutrophil cell suspension (5000 cells/well) with or without rhG-CSF, Boskar4_t2 and Boskar4_st2 at a final concentration of 10 ng/ml were loaded into the insert, followed by incubation at room temperature for 45 min in a sterile condition. After that, the inserts were placed in a fibronectin-coated reservoir plate containing 200 µl/well of rhG-CSF, Boskar4_t2 and Boskar4_st2 at a concentration of 100 ng/ml or control medium (RPMI with 0.5% FBS). The plate was placed into an IncuCyte S3 Live cell analysis system. After 30 min of incubation at 37 °C, recurrence scanning at ×10 magnification for every 45 min was scheduled for 24 h, according to the manufacturer's manual. The IncuCyte's automated algorithms quantified the chemotaxis of neutrophils, using whole-well images of the insert membrane from the top of the ClearView migration plate. The chemotaxis results were reported as a decrease of cell numbers on the top side area of the membrane.

Neutrophil reporter zebrafish experiments. The mpx:gfp Zebrafish reporter line was used as a readout for neutrophil number. The embryos were collected at 1.5-day post fertilization (dpf) and anaesthetised with 0.1% MS 222 (tricaine methansulfonate), then injected with 4 nl of Moevan_control (16 ng), rhG-CSF (8 ng), Boskar_t2(16 ng), or Boskar_st2 (16 ng) proteins into the cardinal vein. After the injection by one and three days, embryos were positioned and orientated laterally within cavities formed in 1% agarose on a 96-well plate and imaged by a Nikon-stereomicroscope (SMZ18). Imaris software was used to count the number of neutrophils (GFP-positive cells) in each embryos in the tail region. Fold-change of the cell numbers were calculated by normalising to the average of uninjected mpx:gfp groups.

Induction of granulopoiesis by designed proteins in C57BL/6 mice. B6.SJL-PtprcaPepcb/BoyCrl mice (Ly5.1 mice) were maintained under pathogen-free conditions in the research animal facility of the University of Tübingen, according to German federal and state regulations (Regierungspräsidium Tübingen, M 05-20G). Mice, aged between 6 and 8 weeks, were treated with intraperitoneal injections (i.p.) of rhG-CSF, Boskar4, Boskar4_t2, or Boskar4_st2 at a concentration of 300 µg/kg every second day for a total of five injections. Mice were sacrificed one day after the last injection. Mice in the control group were treated with PBS, or Moevan_control using the same schema. Bone marrow cells were isolated by flushing with a 22 G syringe, and filtered through a 0.45 µm cell strainer prior to counting and staining for flow cytometry analyses. Cells were stained with DAPI (Sigma#D9542), anti-mouse CD45.1 PerCP (Biolegend#110725), anti-mouse Ly6C AF488 (Biolegend#128022), and anti-mouse Ly6G APC (Biolegend#127614). Flow cytometry was carried out on a FACS Canto II (BD), and data were analysed using FlowJo (BD). Vital mononuclear cells were selected, and doublets were excluded based on scatter characteristics. Gates were set according to fluorescence minus one (FMO) controls.

Analysis of signalling effector activation in $CD34^+$ HSPCs. $CD34^+$ cells were cultured in Stemline II Hematopoietic Stemcell Expansion Medium (Sigma-Aldrich; #50192) supplemented with 10% FBS (Sigma-Aldrich; #F7524), 1% L-glutamine (Biochrom; #K0283), 1% penicillin/streptomycin (Biochrom; #A2213) and a premixed cytokine cocktail containing IL-3 (PeproTech; #200-03), IL-6 (Novus Biologicals; #NBP2-34901), TPO (R&D Systems; #288-TP200), rhSCF (R&D Systems; #255-SC-200) and Flt-3L (BioLegend; #550606). Final concentrations were 20 ng/ml for IL-3, IL-6 and TPO, and 50 ng/ml for SCF and Flt-3L. On day 6 of culture, serum- and cytokine-starved (4 h) $CD34^+$ HSPCs were treated with 20 ng/ml of rhG-CSF, 10 µg/ml of Boskar3 or 10 µg/ml of Boskar4 for 30 or 60 min, fixed in 4% PFA (Merck; #P6148) for 15 min at room temperature, and permeabilised by slowly adding ice-cold methanol (C. Roth; #7342.1) to a final concentration of 90% and incubating for 30 min. Cells were left overnight in methanol at −20 °C and stained on the next day by incubation for 20 min on ice in PBS/2% BSA with specific antibodies recognising the phosphorylated signalling effectors, phospho-Stat3 (Tyr705) (D3A7) XP rabbit mAb (Cell Signalling; #9145); phospho-Stat5 (Tyr694) (C11C5) rabbit mAb (Cell Signalling; #9359); phospho AKT (Thr308) (244F9) rabbit mAb (Cell Signalling; #4056S), and phospho-p44/42 MAPK (Erk1/2) (Thr202/Tyr204) (E10) mouse mAb (Cell Signalling; #9106), or the respective Alexa Fluor 488-conjugated isotype control antibody, anti-mouse IgG (H+L) F(ab')2 fragment (Cell Signalling; #4408) or goat anti-rabbit IgG H+L (Abcam; #ab150077). Thereafter, cells were washed twice in ice-cold PBS/2% BSA and analysed by FACS. The background-corrected fluorescence signal was distinguished from the corresponding phosphorylated proteins by subtracting the fluorescence signal of the appropriate isotype control, estimated at each time point of stimulation, from the specific phospho-protein signal.

Reporting summary. Further information on research design is available in the Nature Research Reporting Summary linked to this article.

Data availability

The data that support this study are available from the corresponding authors upon reasonable request. The NMR structural data generated in this study have been deposited in the Protein Data Bank under the accession code 7NY0, and in the Biological Magnetic Resonance Data Bank under the accession code 34613. Source data are provided with this paper.

Received: 29 May 2020; Accepted: 19 April 2022;
Published online: 26 May 2022

References

1. Huang, P.-S., Boyken, S. E. & Baker, D. The coming of age of de novo protein design. *Nature* **537**, 320 (2016).
2. Woolfson, D. N. et al. De novo protein design: how do we expand into the universe of possible protein structures? *Curr. Opin. Struct. Biol.* **33**, 16–26 (2015).
3. Kuhlman, B. & Bradley, P. Advances in protein structure prediction and design. *Nat. Rev. Mol. Cell Biol.* **20**, 681–697 (2019).
4. Kintzing, J. R., Filsinger Interrante, M. V. & Cochran, J. R. Emerging strategies for developing next-generation protein therapeutics for cancer treatment. *Trends Pharmacol. Sci.* **37**, 993–1008 (2016).
5. Cicerone, M., Giri, J., Shaked, Z. E. & Roberts, C. Protein stability—an underappreciated but critical need for drug delivery systems. *Adv. Drug Deliv. Rev.* **93**, 1 (2015).
6. Ivankov, D. N. et al. Contact order revisited: influence of protein size on the folding rate. *Protein Sci.* **12**, 2057–2062 (2003).
7. Dagan, S. et al. Stabilization of a protein conferred by an increase in folded state entropy. *Proc. Natl Acad. Sci. USA* **110**, 10628–10633 (2013).
8. Zhou, H.-X. Loops, linkages, rings, catenanes, cages, and crowders: entropy-based strategies for stabilizing proteins. *Acc. Chem. Res.* **37**, 123–130 (2004).
9. Xu, D. & Nussinov, R. Favorable domain size in proteins. *Fold. Des.* **3**, 11–17 (1998).
10. Bendall, L. J. & Bradstock, K. F. G-CSF: from granulopoietic stimulant to bone marrow stem cell mobilizing agent. *Cytokine Growth Factor Rev.* **25**, 355–367 (2014).
11. Annabel Strife, C. L. et al. Activities of four purified growth factors on highly enriched human hematopoietic progenitor cells. *Blood* **69**, 1508–1523 (1987).
12. Welte, K. et al. Recombinant human granulocyte colony-stimulating factor. Effects on hematopoiesis in normal and cyclophosphamide-treated primates. *J. Exp. Med.* **165**, 941–948 (1987).
13. Körbling, M. & Anderlini, P. Peripheral blood stem cell versus bone marrow allotransplantation: does the source of hematopoietic stem cells matter? *Blood* **98**, 2900–2908 (2001).
14. Welte, K., Gabrilove, J., Bronchud, M. H., Platzer, E. & Morstyn, G. Filgrastim (r-metHuG-CSF): the first 10 years. *Blood* **88**, 1907–1929 (1996).
15. Kuwabara, T., Kobayashi, S. & Sugiyama, Y. Pharmacokinetics and pharmacodynamics of a recombinant human granulocyte colony-stimulating factor. *Drug Metab. Rev.* **28**, 625–658 (1996).
16. Souza, L. M. et al. Recombinant human granulocyte colony-stimulating factor: effects on normal and leukemic myeloid cells. *Science* **232**, 61 (1986).
17. Arakawa, T., Prestrelski, S. J., Narhi, L. O., Boone, T. C. & Kenney, W. C. Cysteine 17 of recombinant human granulocyte-colony stimulating factor is partially solvent-exposed. *J. Protein Chem.* **12**, 525–531 (1993).
18. Luo, P. et al. Development of a cytokine analog with enhanced stability using computational ultrahigh throughput screening. *Protein Sci.* **11**, 1218–1226 (2002).
19. Sarkar, C. A. et al. Rational cytokine design for increased lifetime and enhanced potency using pH-activated "histidine switching". *Nat. Biotechnol.* **20**, 908 (2002).
20. Bishop, B., Koay, D. C., Sartorelli, A. C. & Regan, L. Reengineering granulocyte colony-stimulating factor for enhanced stability. *J. Biol. Chem.* **276**, 33465–33470 (2001).
21. Piedmonte, D. M. & Treuheit, M. J. Formulation of Neulasta® (pegfilgrastim). *Adv. Drug Deliv. Rev.* **60**, 50–58 (2008).
22. Kinstler, O. B. et al. Characterization and stability of N-terminally PEGylated rhG-CSF. *Pharm. Res.* **13**, 996–1002 (1996).
23. Miyafusa, T. et al. Backbone circularization coupled with optimization of connecting segment in effectively improving the stability of granulocyte-colony stimulating factor. *ACS Chem. Biol.* **12**, 2690–2696 (2017).
24. Popp, M. W., Dougan, S. K., Chuang, T.-Y., Spooner, E. & Ploegh, H. L. Sortase-catalyzed transformations that improve the properties of cytokines. *Proc. Natl Acad. Sci. USA* **108**, 3169 (2011).
25. Dwivedi, P. & Greis, K. D. Granulocyte colony-stimulating factor receptor signaling in severe congenital neutropenia, chronic neutrophilic leukemia, and related malignancies. *Exp. Hematol.* **46**, 9–20 (2017).
26. Tamada, T. et al. Homodimeric cross-over structure of the human granulocyte colony-stimulating factor (GCSF) receptor signaling complex. *Proc. Natl Acad. Sci. USA* **103**, 3135 (2006).
27. Hara, K. et al. Bipotential murine hemopoietic cell line (NFS-60) that is responsive to IL-3, GM-CSF, G-CSF, and erythropoietin. *Exp. Hematol.* **16**, 256–261 (1988).
28. Alvarez, B. H. et al. Design of novel granulopoietic proteins by topological rescaffolding. *PLoS Biol.* **18**, e3000919 (2020).
29. Skokowa, J. & Welte, K. Defective G-CSFR signaling pathways in congenital neutropenia. *Hematol./Oncol. Clin. North Am.* **27**, 75–88 (2013).
30. Vanz, A. L. S. et al. Human granulocyte colony stimulating factor (hG-CSF): cloning, overexpression, purification and characterization. *Microb. Cell Factories* **7**, 13 (2008).
31. Carter, C. R. D., Whitmore, K. M. & Thorpe, R. The significance of carbohydrates on G-CSF: differential sensitivity of G-CSFs to human neutrophil elastase degradation. *J. Leukoc. Biol.* **75**, 515–522 (2004).
32. El Ouriaghli, F. et al. Neutrophil elastase enzymatically antagonizes the in vitro action of G-CSF: implications for the regulation of granulopoiesis. *Blood* **101**, 1752 (2003).
33. ElGamacy, M., Riss, M., Zhu, H., Truffault, V. & Coles, M. Mapping local conformational landscapes of proteins in solution. *Structure* **27**, 853–865.e5 (2019).
34. Diercks, T., Coles, M. & Kessler, H. An efficient strategy for assignment of cross-peaks in 3D heteronuclear NOESY experiments. *J. Biomol. NMR* **15**, 177–180 (1999).
35. Shen, Y., Delaglio, F., Cornilescu, G. & Bax, A. TALOS+: a hybrid method for predicting protein backbone torsion angles from NMR chemical shifts. *J. Biomol. NMR* **44**, 213–223 (2009).
36. Heinzelman, P., Schoborg, J. A. & Jewett, M. C. pH responsive granulocyte colony-stimulating factor variants with implications for treating Alzheimer's disease and other central nervous system disorders. *Protein Eng. Des. Sel.* **28**, 481–489 (2015).
37. Mine, S. et al. Thermodynamic analysis of the activation mechanism of the GCSF receptor induced by ligand binding. *Biochemistry* **43**, 2458–2464 (2004).
38. Syed, R. S. et al. Efficiency of signalling through cytokine receptors depends critically on receptor orientation. *Nature* **395**, 511–516 (1998).
39. Staerk, J. et al. Orientation-specific signalling by thrombopoietin receptor dimers. *EMBO J.* **30**, 4398–4413 (2011).
40. Moraga, I. et al. Tuning cytokine receptor signaling by re-orienting dimer geometry with surrogate ligands. *Cell* **160**, 1196–1208 (2015).
41. Renshaw, S. A. et al. A transgenic zebrafish model of neutrophilic inflammation. *Blood* **108**, 3976–3978 (2006).
42. Spangler, J. B., Moraga, I., Mendoza, J. L. & Garcia, K. C. Insights into cytokine-receptor interactions from cytokine engineering. *Annu. Rev. Immunol.* **33**, 139–167 (2015).
43. Aziz, N. et al. Stability of cytokines, chemokines and soluble activation markers in unprocessed blood stored under different conditions. *Cytokine* **84**, 17–24 (2016).
44. Silva, D.-A. et al. De novo design of potent and selective mimics of IL-2 and IL-15. *Nature* **565**, 186–191 (2019).
45. Viguera, A.-R. & Serrano, L. Loop length, intramolecular diffusion and protein folding. *Nat. Struct. Biol.* **4**, 939–946 (1997).
46. Chirino, A. J., Ary, M. L. & Marshall, S. A. Minimizing the immunogenicity of protein therapeutics. *Drug Discov. Today* **9**, 82–90 (2004).
47. Young, D. C., Zhan, H., Cheng, Q. L., Hou, J. & Matthews, D. J. Characterization of the receptor binding determinants of granulocyte colony stimulating factor. *Protein Sci.* **6**, 1228–1236 (1997).
48. Aritomi, M. et al. Atomic structure of the GCSF–receptor complex showing a new cytokine–receptor recognition scheme. *Nature* **401**, 713–717 (1999).
49. Layton, J. E., Hall, N. E., Connell, F., Venhorst, J. & Treutlein, H. R. Identification of ligand-binding site III on the immunoglobulin-like domain of the granulocyte colony-stimulating factor receptor. *J. Biol. Chem.* **276**, 36779–36787 (2001).
50. Zink, T. et al. Structure and dynamics of the human granulocyte colony-stimulating factor determined by NMR spectroscopy. Loop mobility in a four-helix-bundle protein. *Biochemistry* **33**, 8453–8463 (1994).
51. Jensen-Pippo, K. E., Whitcomb, K. L., DePrince, R. B., Ralph, L. & Habberfield, A. D. Enteral bioavailability of human granulocyte colony stimulating factor conjugated with poly(ethylene glycol). *Pharm. Res.* **13**, 102–107 (1996).
52. Liu, L., Liu, Y., Yan, X., Zhou, C. & Xiong, X. The role of granulocyte colony-stimulating factor in breast cancer development: a review. *Mol. Med. Rep.* **21**, 2019–2029 (2020).
53. Fleishman, S. J. et al. RosettaScripts: a scripting language interface to the rosetta macromolecular modeling suite. *PLoS ONE* **6**, e20161 (2011).
54. ElGamacy, M., Coles, M. & Lupas, A. Asymmetric protein design from conserved supersecondary structures. *J. Struct. Biol.* **204**, 380–387 (2018).
55. Leaver-Fay, A. et al. Scientific benchmarks for guiding macromolecular energy function improvement. In *Methods in Enzymology*, Vol. 523 (ed. Keating, A.E.) 109–143 (Academic Press, 2013).
56. Sheffler, W. & Baker, D. RosettaHoles: rapid assessment of protein core packing for structure prediction, refinement, design, and validation. *Protein Sci.* **18**, 229–239 (2009).
57. Costantini, S., Colonna, G. & Facchiano, A. M. Amino acid propensities for secondary structures are influenced by the protein structural class. *Biochem. Biophys. Res. Commun.* **342**, 441–451 (2006).

58. Wintjens, R. T., Rooman, M. J. & Wodak, S. J. Automatic classification and analysis of alpha alpha-turn motifs in proteins. *J. Mol. Biol.* **255**, 235–253 (1996).
59. Webb, B. & Sali, A. Comparative protein structure modeling using MODELLER. *Curr. Protoc. Bioinforma.* **54**, 5.6.1–5.6.37 (2016).
60. Nymeyer, H. Serial tempering without exchange. *J. Chem. Phys.* **133**, 114113 (2010).
61. Eastman, P. et al. OpenMM 7: rapid development of high performance algorithms for molecular dynamics. *PLoS Comput. Biol.* **13**, e1005659 (2017).
62. Phillips, J. C. et al. Scalable molecular dynamics with NAMD. *J. Comput. Chem.* **26**, 1781–1802 (2005).
63. Ferrara, P., Apostolakis, J. & Caflisch, A. Evaluation of a fast implicit solvent model for molecular dynamics simulations. *Proteins: Struct. Funct. Bioinforma.* **46**, 24–33 (2002).
64. Kyte, J. & Doolittle, R. F. A simple method for displaying the hydropathic character of a protein. *J. Mol. Biol.* **157**, 105–132 (1982).
65. Alford, R. F. et al. The Rosetta all-atom energy function for macromolecular modeling and design. *J. Chem. Theory Comput.* **13**, 3031–3048 (2017).
66. Reichelt, P., Schwarz, C. & Donzeau, M. Single step protocol to purify recombinant proteins with low endotoxin contents. *Protein Expr. Purif.* **46**, 483–488 (2006).
67. Aida, Y. & Pabst, M. J. Removal of endotoxin from protein solutions by phase separation using Triton X-114. *J. Immunol. Methods* **132**, 191–195 (1990).
68. Kelstrup, C. D. et al. Rapid and deep proteomes by faster sequencing on a benchtop quadrupole ultra-high-field orbitrap mass spectrometer. *J. Proteome Res.* **13**, 6187–6195 (2014).
69. Cox, J. & Mann, M. MaxQuant enables high peptide identification rates, individualized p.p.b.-range mass accuracies and proteome-wide protein quantification. *Nat. Biotechnol.* **26**, 1367–1372 (2008).
70. Cox, J. et al. Andromeda: a peptide search engine integrated into the maxquant environment. *J. Proteome Res.* **10**, 1794–1805 (2011).
71. Käll, L., Storey, J. D., MacCoss, M. J. & Noble, W. S. Posterior error probabilities and false discovery rates: two sides of the same coin. *J. Proteome Res.* **7**, 40–44 (2008).
72. Bradley, P., Misura, K. M. S. & Baker, D. Toward high-resolution de novo structure prediction for small proteins. *Science* **309**, 1868–1871 (2005).
73. Best, R. B. et al. Optimization of the additive CHARMM all-atom protein force field targeting improved sampling of the backbone ϕ, ψ and side-chain χ1 and χ2 dihedral angles. *J. Chem. Theory Comput.* **8**, 3257–3273 (2012).
74. Schwieters, C. D., Kuszewski, J. J., Tjandra, N. & Clore, G. M. The Xplor-NIH NMR molecular structure determination package. *J. Magn. Reson.* **160**, 65–73 (2003).
75. Farrow, N. A. et al. Backbone dynamics of a free and phosphopeptide-complexed Src homology 2 domain studied by 15N NMR relaxation. *Biochemistry* **33**, 5984–6003 (1994).
76. Gemmecker, G., Jahnke, W. & Kessler, H. Measurement of fast proton exchange rates in isotopically labeled compounds. *J. Am. Chem. Soc.* **115**, 11620–11621 (1993).
77. Krämer, S. D., Wöhrle, J., Rath, C. & Roth, G. Anabel: an online tool for the real-time kinetic analysis of binding events. *Bioinforma. Biol. Insights* **13**, 1177932218821383 (2019).
78. Stemmer, M., Thumberger, T., del Sol Keyer, M., Wittbrodt, J. & Mateo, J. L. CCTop: an intuitive, flexible and reliable CRISPR/Cas9 target prediction tool. *PLoS ONE* **10**, e0124633 (2015).
79. Brinkman, E. K., Chen, T., Amendola, M. & van Steensel, B. Easy quantitative assessment of genome editing by sequence trace decomposition. *Nucleic Acids Res.* **42**, e168–e168 (2014).

Acknowledgements

This research was funded by the Max Planck Society, the DFG, the German Federal Ministry of Education and Research, and the Madeleine Schickedanz Kinderkrebs-stiftung. We thank the European Zebrafish Resource Center for providing *Tg(mpx:GFP)^{i114}* fish. We also acknowledge the Garching Computing Centre of the Max Planck Society for computing time on the COBRA and DRACO supercomputers.

Author contributions

Conceived and designed the experiments: J.S., B.H.A, M.C., K.M., B.B., K.W., A.L., P.M., M.E. Performed the experiments: B.H.A, M.C., M.R., M.N., J.H., N.A., Y.X., P.Mir, A-.C.K., K.M., K.W.R., M.E. Analysed the data: J.S., B.H.A, M.C., M.R., M.N., J.H., N.A., Y.X., P.Mir, A-.C.K., K.M., B.B., M.E. Contributed materials/analysis tools: J.S., M.C., A.L., P.M., M.E. Wrote the paper: J.S., B.H.A, M.C., N.A., K.W.R., K.M., B.B., K.W., A.L., P.M., M.E.

Funding

Open Access funding enabled and organized by Projekt DEAL.

Competing interests

The designed proteins in this study are included as part of the priority patent application number EP19217185. J.S., B.H.A. and M.E. are the inventors, and the application is filed by MAX-PLANCK-Gesellschaft zur Förderung der Wissenschaften e.V., and Eberhard Karls Universität Tübingen. The other authors declare no competing interests.

Additional information

Supplementary information The online version contains supplementary material available at https://doi.org/10.1038/s41467-022-30157-2.

Correspondence and requests for materials should be addressed to Julia Skokowa or Mohammad ElGamacy.

Peer review information *Nature Communications* thanks the anonymous reviewers for their contribution to the peer review of this work. Peer reviewer reports are available.

Reprints and permission information is available at http://www.nature.com/reprints

Publisher's note Springer Nature remains neutral with regard to jurisdictional claims in published maps and institutional affiliations.

E) Dannenmann, B. and Klimiankou, M. et al., 2021, *Cell Stem Cell*

Cell Stem Cell

Article

iPSC modeling of stage-specific leukemogenesis reveals BAALC as a key oncogene in severe congenital neutropenia

Graphical abstract

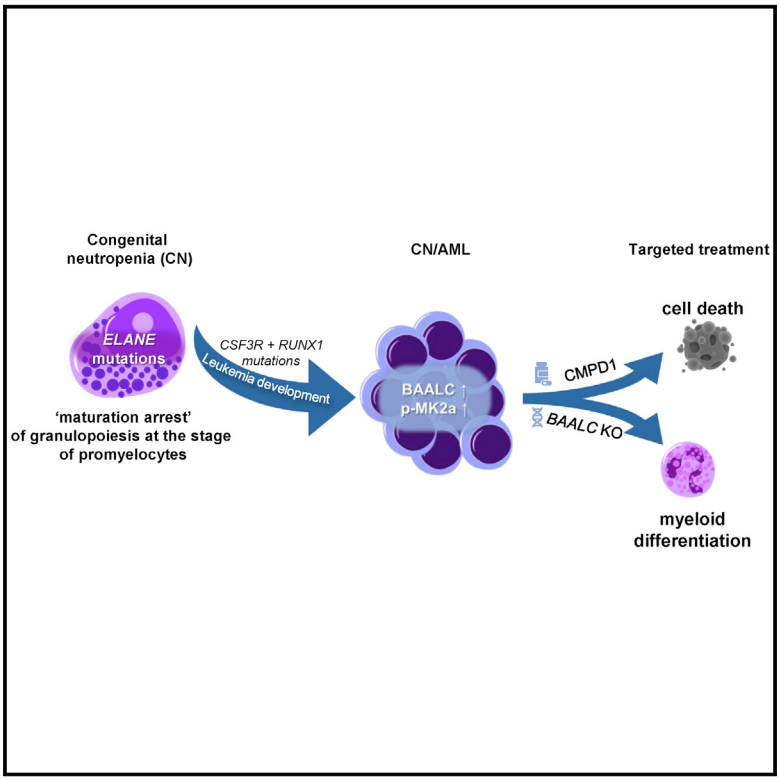

Highlights

- Generation of an iPSC model of leukemic development in severe congenital neutropenia
- High BAALC expression leads to MK2a hyperphosphorylation in CN/AML leukemogenesis
- Loss of BAALC restores myeloid differentiation and inhibits blasts proliferation
- The MK2a inhibitor CMPD1 selectively blocks the growth of CN/AML cells

Authors

Benjamin Dannenmann, Maksim Klimiankou, Benedikt Oswald, ..., Cornelia Zeidler, Karl Welte, Julia Skokowa

Correspondence

julia.skokowa@med.uni-tuebingen.de

In brief

Dannenmann, Klimiankou et al. developed a stepwise leukemogenesis model of severe congenital neutropenia, an inherited pre-leukemic bone marrow failure syndrome, using CRISPR-Cas9 gene editing of patient-derived iPSCs. They identified a leukemogenic role of elevated BAALC, showing that BAALC knockout or MK2a inhibition induces differentiation and inhibits proliferation of BAALC(hi) AML blasts.

Dannenmann et al., 2021, Cell Stem Cell *28*, 906–922
May 6, 2021
https://doi.org/10.1016/j.stem.2021.03.023

CellPress

CellPress

Cell Stem Cell

Article

iPSC modeling of stage-specific leukemogenesis reveals BAALC as a key oncogene in severe congenital neutropenia

Benjamin Dannenmann,[1,11] Maksim Klimiankou,[1,11] Benedikt Oswald,[1] Anna Solovyeva,[1] Jehan Mardan,[1] Masoud Nasri,[1] Malte Ritter,[1] Azadeh Zahabi,[1] Patricia Arreba-Tutusaus,[1] Perihan Mir,[1] Frederic Stein,[1] Siarhei Kandabarau,[2] Nico Lachmann,[3] Thomas Moritz,[3] Tatsuya Morishima,[1] Martina Konantz,[4] Claudia Lengerke,[1,4] Tim Ripperger,[5] Doris Steinemann,[5] Miriam Erlacher,[6,7,8] Charlotte M. Niemeyer,[6,7,8] Cornelia Zeidler,[9] Karl Welte,[10] and Julia Skokowa[1,12,*]

[1]Department of Oncology, Hematology, Immunology, and Rheumatology, University Hospital Tuebingen, 72074 Tuebingen, Germany
[2]Dr. Margarete Fischer-Bosch-Institute of Clinical Pharmacology (IKP), 70376 Stuttgart, Germany
[3]Institute of Experimental Hematology, Hannover Medical School, 30625 Hannover, Germany
[4]Department of Biomedicine, University Hospital Basel, 4031 Basel, Switzerland
[5]Institute of Human Genetics, Hannover Medical School, 30625 Hannover, Germany
[6]Faculty of Medicine, Division of Pediatric Hematology and Oncology Medical Center, Department of Pediatrics and Adolescent Medicine, University of Freiburg, 79106 Freiburg, Germany
[7]German Cancer Consortium (DKTK), 79106 Freiburg, Germany
[8]German Cancer Research Center (DKFZ), 69120 Heidelberg, Germany
[9]Department of Oncology, Hematology, Immunology and Bone Marrow Transplantation, Hannover Medical School, 39625 Hannover, Germany
[10]University Children's Hospital Tuebingen, 72074 Tuebingen, Germany
[11]These authors contributed equally
[12]Lead contact
*Correspondence: julia.skokowa@med.uni-tuebingen.de
https://doi.org/10.1016/j.stem.2021.03.023

SUMMARY

Severe congenital neutropenia (CN) is a pre-leukemic bone marrow failure syndrome that can evolve to acute myeloid leukemia (AML). Mutations in *CSF3R* and *RUNX1* are frequently observed in CN patients, although how they drive the transition from CN to AML (CN/AML) is unclear. Here we establish a model of stepwise leukemogenesis in CN/AML using CRISPR-Cas9 gene editing of CN patient-derived iPSCs. We identified BAALC upregulation and resultant phosphorylation of MK2a as a key leukemogenic event. BAALC deletion or treatment with CMPD1, a selective inhibitor of MK2a phosphorylation, blocked proliferation and induced differentiation of primary CN/AML blasts and CN/AML iPSC-derived hematopoietic stem and progenitor cells (HSPCs) without affecting healthy donor or CN iPSC-derived HSPCs. Beyond detailing a useful method for future investigation of stepwise leukemogenesis, this study suggests that targeting BAALC and/or MK2a phosphorylation may prevent leukemogenic transformation or eliminate AML blasts in CN/AML and *RUNX1* mutant BAALC(hi) *de novo* AML.

INTRODUCTION

Pre-leukemia bone marrow (BM) failure syndromes are characterized by abnormal differentiation and functions of hematopoietic stem and progenitor cells (HSPCs). They frequently culminate in the development of myelodysplastic syndrome (MDS) or acute myeloid leukemia (AML) (Alter, 2017; Collins and Dokal, 2015; Feurstein et al., 2016; Göhring et al., 2007; Savage and Dufour, 2017; Skokowa et al., 2007, 2017; Wegman-Ostrosky and Savage, 2017). The prevailing hypothesis of leukemia development in inborn pre-leukemia syndromes postulates that homeostasis, self-renewal, proliferation, or differentiation of HSPCs is disturbed because of inherited mutations (Alter, 2017; Collins and Dokal, 2015; Feurstein et al., 2016; Göhring et al., 2007; Skokowa et al., 2007, 2017; Wegman-Ostrosky and Savage, 2017). These "unfit" HSPCs are exposed to constant stress through intrinsic HSPCs defects and extrinsic abnormalities within the HSPC niche, which together may lead to the acquisition of mutations and/or chromosomal abnormalities in leukemia-associated genes (Quentin et al., 2011; Skokowa et al., 2017). The background of an inherited disease can create selective pressure that supports the outgrowth and evolution of mutant HSPCs clones (Lensch et al., 1999). Severe congenital neutropenia (CN) is a pre-leukemia syndrome that, in the majority of patients,

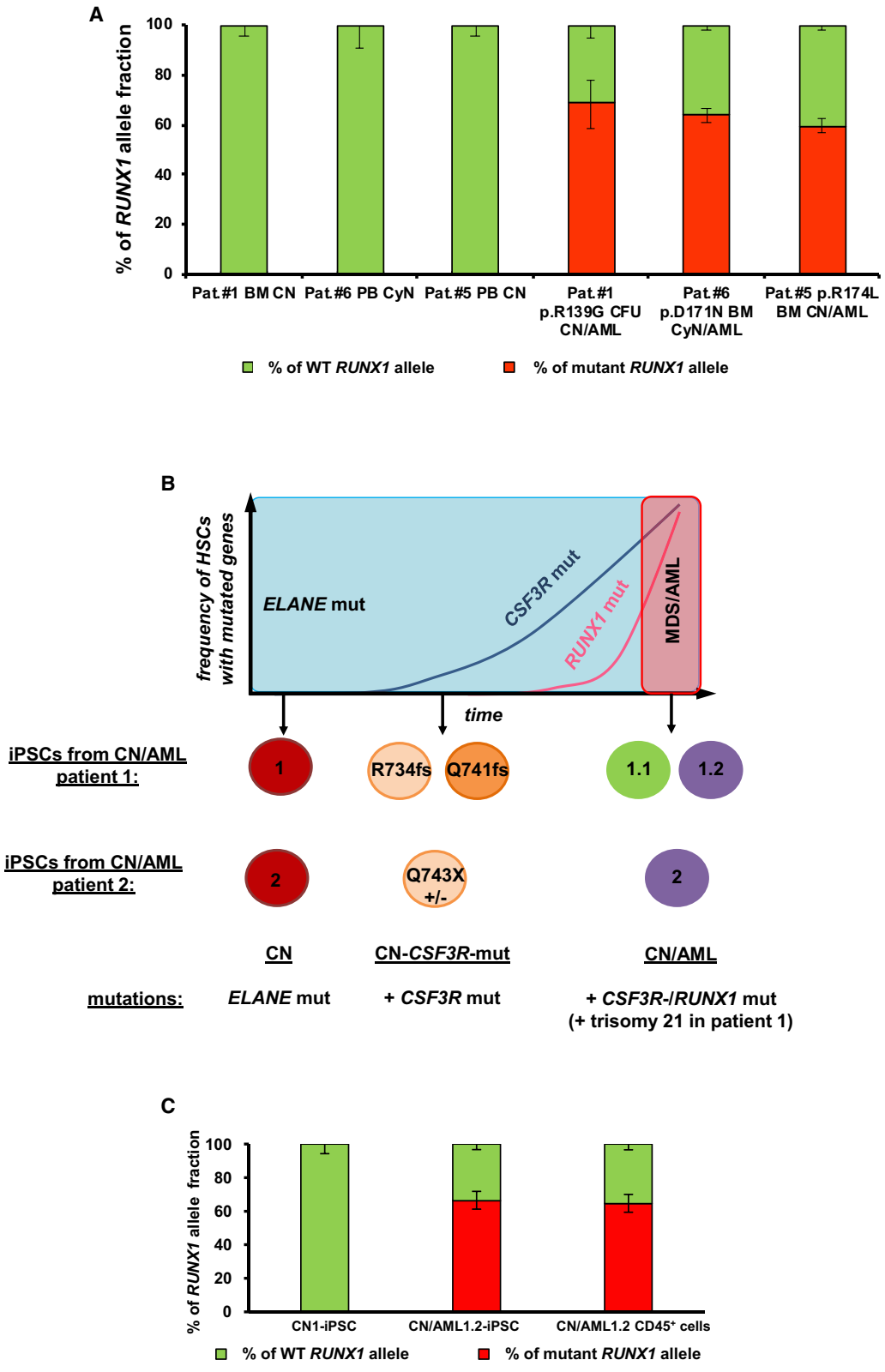

Figure 1. Allele frequencies of missense *RUNX1* mutations in CN/AML and CyN/AML with trisomy 21

(A) Analysis of the allele frequencies (AF) of wild-type (WT) and corresponding mutant *RUNX1* in CN patients before and after onset of AML (CN/AML). Each bar represents percentage of WT (green) and mutant (red) *RUNX1* AF quantified using dPCR. In the CN phase, genotyping of BM or PB samples revealed an absence

(legend continued on next page)

is caused by heterogeneous *ELANE* mutations encoding neutrophil elastase (NE) (Dale et al., 2000). The HSPCs of CN patients fail to differentiate into neutrophilic granulocytes, without any severe maturation defects in other blood lineages (Skokowa et al., 2007, 2017; Welte and Dale, 1996; Welte et al., 2006). The cumulative incidence of MDS or AML in CN patients is approximately 20% after 20 years (Rosenberg et al., 2006, 2010; Skokowa et al., 2017). Exposure of CN HSPCs to high concentrations of granulocyte colony-stimulating factor (G-CSF) partially reverses granulocytic maturation defects (Skokowa et al., 2017; Welte et al., 2006). However, there is a correlation between susceptibility to G-CSF therapy and frequency of leukemia (Rosenberg et al., 2006, 2010). We recently reported a high frequency of acquired cooperative mutations in *CSF3R* (encoding the G-CSF receptor) and *RUNX1* (runt-related transcription factor 1) in 55% of CN/AML patients (31 patients were studied) (Skokowa et al., 2014). Recently, we described a clinical case of two cyclic neutropenia (CyN) patients with acquired *CSF3R* mutations. One of these patients co-acquired *RUNX1* mutation, trisomy 21, and developed AML (Klimiankou et al., 2016a). In the majority of CN and CyN patients who developed AML or MDS, the emergence of HSPCs clones carrying a *CSF3R* mutation preceded the co-acquisition of *RUNX1* mutations in the same cells (Skokowa et al., 2014). The mechanism of leukemogenic transformation of HSPCs downstream of acquired *CSF3R* and *RUNX1* mutations on the pathological background caused by CN-associated inherited mutations is unclear. *CSF3R* mutations are stop-codon mutations localized in the intracellular domain of the G-CSF receptor, which is responsible for the inhibition of STAT5-mediated proliferative signals by SOCS3, and the activation of STAT3-dependent differentiation (Dong et al., 1995, 1997; Germeshausen et al., 2008; Gupta et al., 2014; Klimiankou et al., 2016b; Skokowa et al., 2007). Missense and nonsense *RUNX1* mutations in the DNA-binding Runt homology domain (RHD), or truncating mutations in the transactivation domain (TAD), have been detected in CN/AML patients (Beekman et al., 2012; Skokowa et al., 2014). Numerous studies have reported a diversity of mechanisms underlying the pathogenesis of missense and nonsense *RUNX1* mutations (Harada and Harada, 2011; Imai et al., 2000; Michaud et al., 2002). Most of these studies are performed in a mouse system or by overexpressing mutated *RUNX1*. Interestingly, *RUNX1* maps to chromosome 21, and leukemic blasts from some CN/AML patients harbor trisomy 21 (Skokowa et al., 2014). Thus, the ratio of mutant to wild-type (WT) *RUNX1* alleles may contribute to leukemogenesis.

The establishment of a viable experimental model would be essential for studying multistep leukemogenesis in CN. Transgenic mice with a knockin of the human *ELANE* mutation exhibit no neutropenia phenotype under steady-state conditions (Nanua et al., 2011). Despite some limitations, patient-specific induced pluripotent stem cells (iPSCs) are an excellent alternative to animal models. Generation of CN patient-specific iPSCs that recapitulate the maturation arrest of granulopoiesis has been previously described (Hiramoto et al., 2013; Morishima et al., 2014; Nayak et al., 2015). iPSCs have been used to study leukemogenesis and to identify compounds targeting AML (Chang et al., 2018; Chao et al., 2017; Hsu et al., 2019; Papapetrou, 2019; Ruiz-Gutierrez et al., 2019; Wesely et al., 2020). Using CRISPR-Cas9 gene editing, it is possible to introduce distinct mutations in iPSCs and to study stepwise, stage-specific leukemia progression (Kotini et al., 2017). This approach allows the development of leukemia models to compare different types of mutations (e.g., missense versus nonsense) in endogenously expressed proteins (e.g., RUNX1).

In the present study, we established an *in vitro* model of leukemia evolution in CN using patient-derived iPSCs and CRISPR-Cas9-mediated introduction of gene mutations. Using this model, we described the upregulation of *BAALC* (brain and acute leukemia, cytoplasmic) as a key leukemogenic event. We identified a small-molecule inhibitor of MK2a phosphorylation that targets CN/AML blasts without affecting healthy HSPCs. This strategy could be applied to treat CN/AML or *de novo* AML patients with *RUNX1* mutations and/or elevated BAALC expression.

RESULTS

Missense *RUNX1* mutations are associated with trisomy 21 in CN/AML patients

A comparison of cytogenetic abnormalities and type of acquired *RUNX1* mutations in 23 CN/AML patients revealed that 7 of 14 CN/AML patients with missense *RUNX1* mutations only co-acquired numerical or structural abnormalities of chromosome 21 (trisomy 21, add [21q]). In contrast, tetrasomy 21 was detected in 1 of 5 CN/AML patients with nonsense or frameshift *RUNX1* mutations (Table S1). Digital PCR (dPCR) revealed two copies of mutated missense *RUNX1* in two CN/AML and one CyN/AML patient with trisomy 21, suggesting a crucial role of the dosage of missense *RUNX1* for leukemia initiation (Figure 1A; Figure S1A).

iPSC model of stepwise leukemogenic transformation in CN/AML

We generated iPSCs from two CN/AML patients harboring *ELANE* mutations, p.C151Y and p.G214R (Figure 1B). Using mononuclear cells (MNCs) isolated from peripheral blood (PBMNCs) of CN patient 1 at time of overt AML, we generated an iPSC clone carrying *ELANE* p.C151Y mutation only (CN1) and two iPSC clones carrying *ELANE* mutation and acquired nonsense *CSF3R* p.Q741X mutation in combination with missense *RUNX1* p.R139G mutation and trisomy 21 (CN/AML1.1 and 1.2) (Figures S2A and S2B). dPCR showed one

of mutant *RUNX1* allele, whereas in overt AML, 59%–68% of leukemia cells acquired *RUNX1* mutations, indicating the gain of a second mutant *RUNX1* allele. Data are represented as mean ± SD.

(B) A stepwise *in vitro* model of leukemogenesis in congenital neutropenia through the generation of patient-specific iPSCs and the insertion of additional mutations using CRISPR-Cas9 gene editing. Top panel represents the timescale of leukemic transformation in CN/AML patients; bottom panel represents the generation of single iPSC clones for specific time points during disease progression.

(C) dPCR analysis of the allele frequency of WT and mutant (p.R139G) *RUNX1* in $CD45^+$ cells derived from CN1, CN/AML1.1, and CN/AML1.2 iPSCs.

See also Figures S1 and S2 and Table S1.

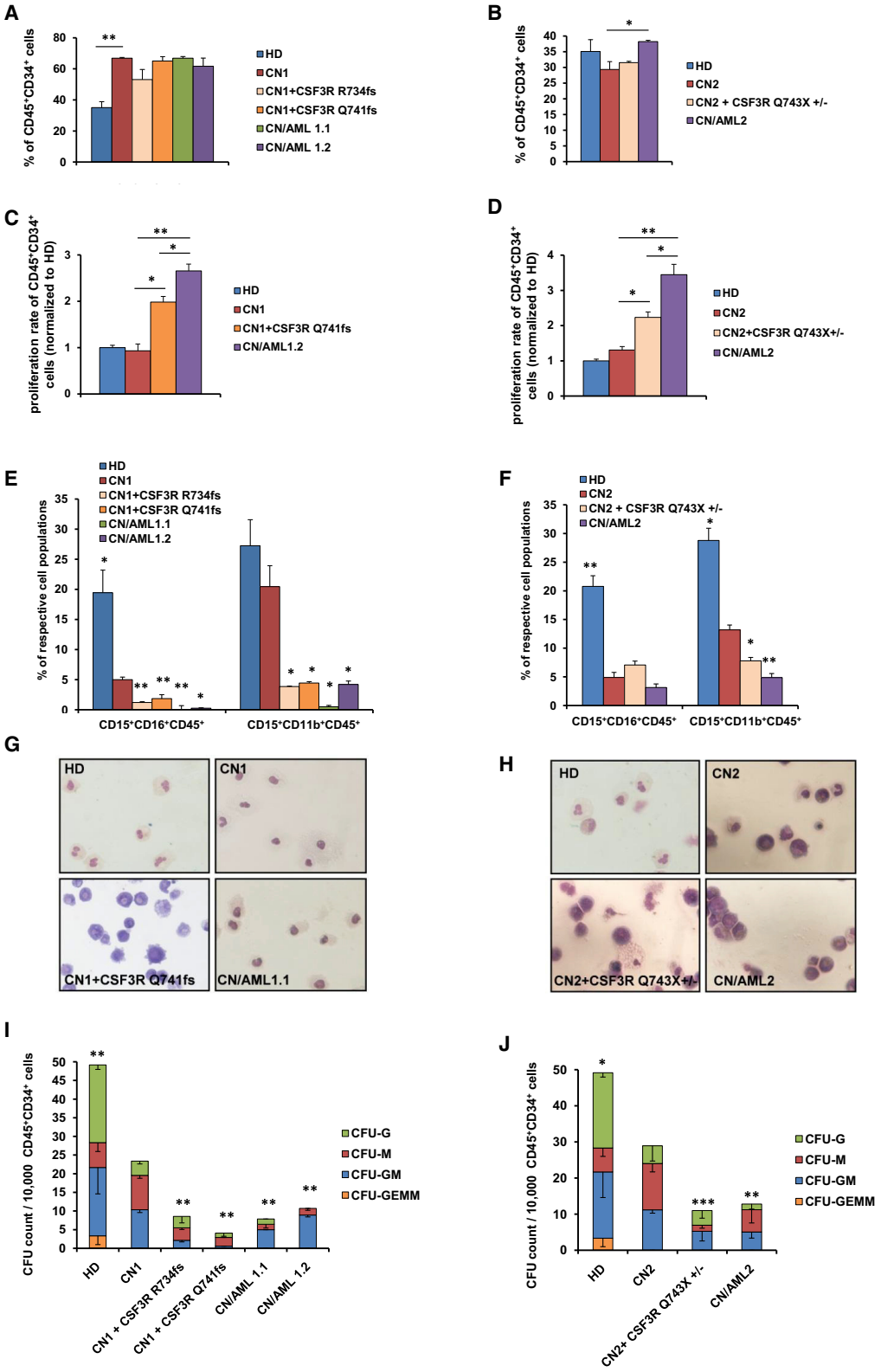

(legend on next page)

copy of WT and two copies of mutated *RUNX1* in iPSCs and CD45$^+$ cells (Figure 1C), in line with observations in primary CN/AML blasts. Using CRISPR-Cas9 gene editing (Table S2), we generated two iPSC lines, one carrying the heterozygous *CSF3R* mutation p.Arg734SerfsX35 (CN1+*CSF3R* R734fs) and another carrying the compound heterozygous *CSF3R* mutations p.Gln741AsnfsX59 and p.Ser742PhefsX29 (CN1+*CSF3R* Q741fs) (Figure 1B; Figures S2C and S2D).

iPSC clones of CN patient 2 carrying *ELANE* p.G214R mutation only (CN2) or *ELANE* mutation and acquired *CSF3R* p.Q743X mutation (CN2+*CSF3R* Q743X$^{+/-}$) were generated from BMMNCs isolated at AML stage (Figure 1B; Figure S2A). Heterozygous frameshift *RUNX1* p.Glu175SerfsX7 mutation was introduced in CN2+*CSF3R* Q743X$^{+/-}$ iPSC clone using CRISPR-Cas9 (CN/AML2) (Figure 1B; Figure S2E).

We observed no off-target effects in the CRISPR-Cas9 gene-edited iPSCs (Table S3). Array-CGH confirmed no chromosomal abnormalities in CN1 iPSC clone, trisomy 21 in CN/AML1.1 and 1.2 iPSC clones, and the additional gain of a part of chromosome 12 in CN/AML1.1 iPSC clone (Figure S2B). The chromosome 12 gain is a frequent finding during iPSC maintenance, reflecting high proliferation of these cells (Liang and Zhang, 2013). No chromosomal abnormalities were detected in iPSC clones derived from CN patient 2 (Figure S2B).

All iPSC lines expressed pluripotent stem cell markers (Figures S3A–S3C), displayed alkaline phosphatase activity (Figures S3D and S3E), differentiated into three germ layers (data not shown), and had inactivated lentiviral plasmid used for reprogramming (Figures S3A and S3B).

Impaired differentiation and elevated proliferation of CN/AML iPSC-derived HSPCs

We performed *in vitro* embryoid body (EB)-based hematopoietic and myeloid differentiation (Dannenmann et al., 2020; Lachmann et al., 2015) in generated iPSC lines (Figure S4A). The proportions of immature cells showed only slight differences between CN1 and CN/AML1 iPSC lines (Figure 2A; Figure S4B). For CN/AML2, the percentages of CD45$^+$CD34$^+$ and CD34$^+$CD43$^+$ cells, but not of CD41a$^+$CD235a$^+$CD45$^-$ cells, were increased compared with CN2 (Figure 2B; Figure S4C).

To assess proliferation, HSPCs were collected at day 14 of EB differentiation and cultured on FLT3-L-secreting feeder cells. We observed a substantial increase in proliferation of CN/AML iPSC-derived HSPCs from both patients compared with CN or healthy donor (HD) HSPCs (Figures 2C and 2D). Proliferation of HSPCs expressing mutated *CSF3R* was significantly higher than in CN cells, but much lower than in CN/AML cells (Figures 2C and 2D). Granulocytic differentiation was markedly reduced in CN and CN-*CSF3R* iPSCs compared with HD iPSCs and practically abolished in CN/AML iPSCs (Figures 2E and 2F). Morphological analysis of cytospin preparations revealed almost no mature granulocytes in CN/AML samples (Figures 2G and 2H). CD34$^+$ cells derived from CN iPSCs produced smaller numbers of CFU-G and CFU-GM colonies compared with HD iPSCs. These numbers were further decreased in *CSF3R*-mutated CN iPSCs and CN/AML iPSCs (Figures 2I and 2J).

AML-associated gene expression signature in CN/AML iPSC-derived HSPCs

We next examined whether top genes that we found to be upregulated in primary CN/AML blasts (*BAALC*, *HPGDS* [hematopoietic prostaglandin D synthase], *CD34*, and *CD109* [own unpublished observations of transcriptome studies]) might be also elevated in CN/AML iPSC-derived HSPCs. We confirmed increased mRNA levels of *BAALC*, *HPGDS*, *CD34*, and *CD109* in primary blasts of five CN/AML patients carrying *RUNX1* and *CSF3R* mutations compared with CD34$^+$CD33$^+$ BM cells isolated from three CN patients prior to leukemia development (Figure 3A). *BAALC*, *CD34*, *HPGDS*, and *CD109* expression was also increased in CD34$^+$ cells derived from CN/AML1.1 and 1.2 iPSC lines compared with CN1 iPSCs, and *BAALC* mRNA was higher in CN/AML2 HSPCs compared with CN2 cells (Figures 3B and 3C). BAALC protein was elevated in CN/AML HSPCs of both patients (Figure 3D).

We further tested whether elevated *BAALC* level is caused by mutated *RUNX1*. Indeed, introduction of mutated *RUNX1* (p.R139G or p.R174L) in healthy individuals' CD34$^+$ cells led to markedly increased *BAALC* mRNA, compared with WT *RUNX1* transduced cells (Figure 3E).

We have reported elevated levels of STAT5a in primary CN/AML blasts (Gupta et al., 2014). Here, upregulated STAT5a mRNA and protein were detected in CN/AML iPSC-derived HSPCs (Figures 3F–3I). Interestingly, *RUNX1* mRNA and protein expression was markedly increased in CN/AML1 cells with missense *RUNX1* and trisomy 21, whereas in CN/AML2, with truncated *RUNX1*, only *RUNX1* mRNA was elevated. G-CSFR

Figure 2. Hematopoietic differentiation of CN/AML patient-derived iPSCs

(A and B) Percentage of CD34$^+$ cells derived from CN/AML1 (A) and CN/AML2 (B) iPSCs on day 14 of culture. Data are represented as mean ± SD from two independent experiments. Group comparisons were done between CN and all other iPSC clones. Significant differences between groups to CN are indicated (*$p < 0.05$ and **$p < 0.01$).

(C and D) Proliferation rate of CD34$^+$ cells derived from CN/AML1 (C) and CN/AML2 (D) iPSCs on day 14 of culture. HSPCs were expanded on SL/SL feeder for 7 days. Data were normalized to healthy donor (HD) control and are represented as mean ± SD from two independent experiments. Significant differences between groups to CN are indicated (*$p < 0.05$ and **$p < 0.01$).

(E and F) Percentage of iPSC-derived granulocytes (CD15$^+$CD16$^+$CD45$^+$ and CD15$^+$CD11b$^+$CD45$^+$) in CN/AML1 (E) and CN/AML2 (F). iPSCs were cultured under EB differentiation conditions for 32 days. Data are represented as mean ± SD from two independent experiments. Group comparisons were done between CN and all other iPSC clones. Significant differences between groups to CN are indicated (*$p < 0.05$ and **$p < 0.01$).

(G and H) Representative images of iPSC-derived hematopoietic cells at day 32 of differentiation stained with Wright Giemsa are shown for CN/AML1 (G) and CN/AML2 (H). Magnification at 40× is shown.

(I and J) CFU assay of iPSC-derived CD34$^+$ cells isolated from EBs culture at day 14. Total CFU counts are shown for CN/AML1 (I) and CN/AML2 (J). Data are represented as mean ± SD from two independent experiments in triplicate. Group comparisons were done between CN and all other iPSC clones. Significant differences between groups to CN are indicated (*$p < 0.05$, **$p < 0.01$, and ***$p < 0.001$).

See also Figures S2–S4 and Tables S2 and S3.

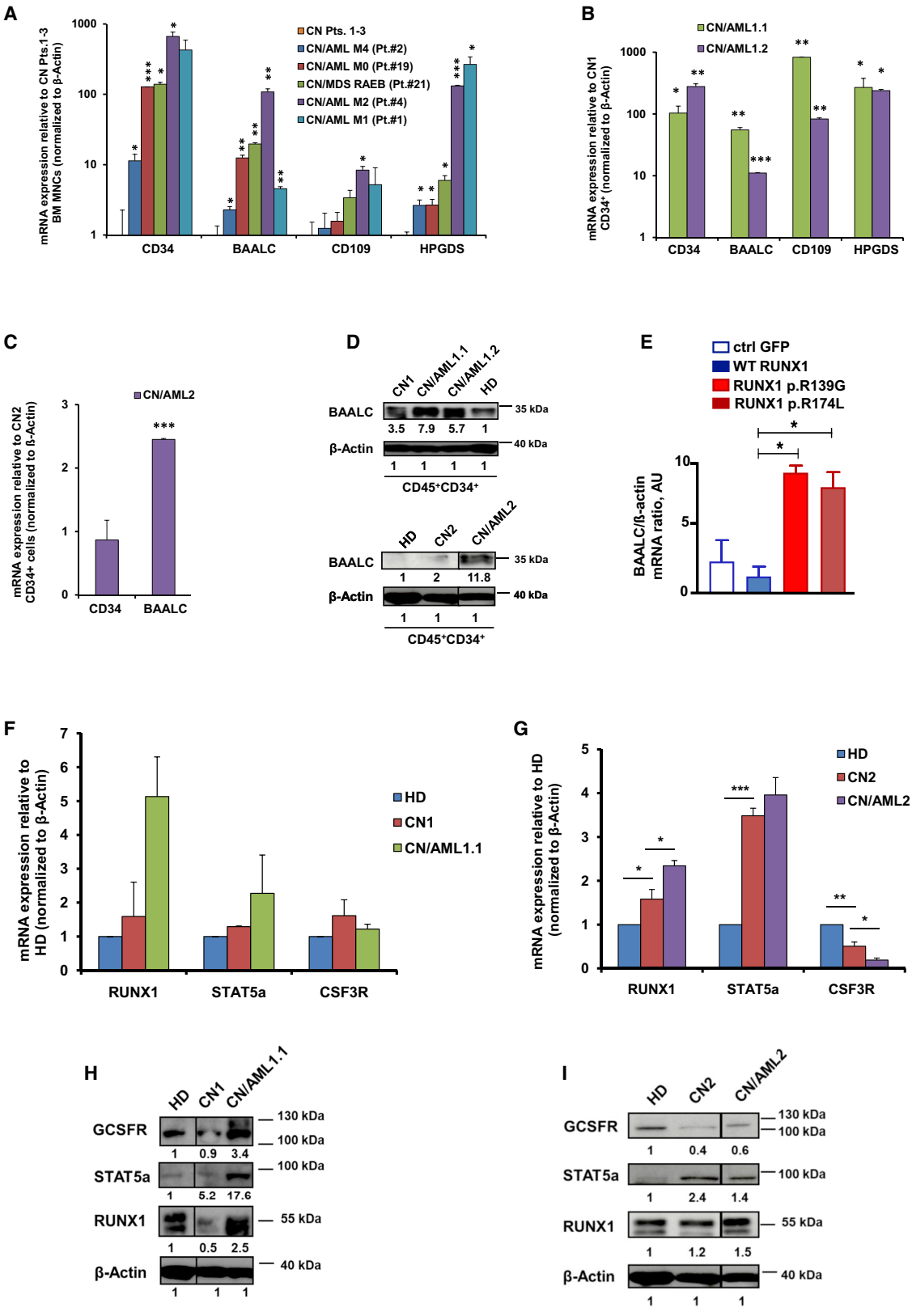

(legend on next page)

protein expression was enhanced in CN/AML1 but not in CN/AML2 (Figures 3F–3I).

Leukemogenic effects of elevated *BAALC* in CN

To determine which of the candidate genes, *BAALC*, *HPGDS*, *CD109*, or *RUNX1*, is responsible for the leukemogenic transformation in CN, we generated knockout (KO) CN/AML1 iPSCs for each of these genes (Figure 4A). We created single guide RNAs (sgRNAs) targeting the first coding exons of each gene, cloned them into a pSpCas9(BB)-2A-GFP (PX458) construct (Ran et al., 2013) (Table S2), and generated single-cell-derived CN/AML1 iPSC clones with homozygous (*RUNX1*, *BAALC*) or compound heterozygous (*CD109*, *HPDGS*) mutations (Figures S5A–S5F). Pluripotency of selected iPSC clones was unaffected (data not shown), and there was no evidence of CRISPR-Cas9 off-target activity (Table S3).

BAALC, but not *CD109*, *RUNX1*, or *HPGDS*, KO resulted in a dramatic induction of granulocytic differentiation and a significant reduction in proliferation of CN/AML1 iPSC-derived HSPCs (Figures 4B–4E; Figure S5G). Similarly, we observed a striking increase in granulocytic differentiation along with a marked reduction in proliferation in CN/AML2 iPSC-derived HSPCs after *BAALC* KO (Figures 4F–4I; Figure S5H). In contrast, *BAALC* KO did not affect granulocytic differentiation in HD iPSCs but induced granulopoiesis in CN iPSCs (Figure 4J; Figures S5I–S5K).

We also assessed the inhibitory effect of *BAALC* KO on proliferation of primary blasts from three CN/AML patients. *BAALC* KO (CRISPR-Cas9 KO efficiency was about 80%) led to a marked reduction of cell proliferation measured on day 14 of culture compared with mock electroporated cells (Figure 4K).

Leukemia-specific gene expression signature in CN/AML iPSC-derived HSPCs

We compared the transcriptome of CN and CN/AML iPSC-derived HSPCs from both patients. Differential gene expression analyses using DESeq2 R package (Love et al., 2014) identified 132 up- and 570 downregulated genes, as well as 570 up- and 1,422 downregulated genes between CN/AML and CN stages for patient 1 and patient 2, respectively ($\log_2$ fold change [$\log_2$FC] > 1 or < −1, adjusted $p < 0.05$; Figures 5A and 5B; Figures S6A and S6B; Tables S4 and S5). Gene set enrichment analysis (GSEA) revealed E2F targets, MYC targets, and the oxidative phosphorylation pathway as top significant altered pathways in CN/AML1, whereas platelet-specific genes were enriched in CN1 (Figure 5C). G2M checkpoint signaling, E2F targets, and TGF-β signaling were significantly deregulated in CN/AML2, whereas the structural integrity of the ribosomes was enriched in CN2 (Figure 5D).

To predict transcription factors that control differentially expressed (DE) genes, we performed eXpression2Kinases analysis (Clarke et al., 2018). We detected RUNX1 binding motifs, GATA1 and GATA2 motifs, and AML-associated SUZ12 and EZH2 motifs (Figure 5E) to be significantly enriched in CN/AML cells of both patients. TRIM28 and TP53 motifs were specifically enriched in CN/AML1 and CEBPB, NANOG, and KLF4 in CN/AML2 (Figure 5E).

Using kinase enrichment analysis (KEA), we predicted kinases that phosphorylate proteins regulated by the subnetwork of prioritized transcription factors (Clarke et al., 2018). A majority of enriched kinases, including HIPK2, MAPK1/3/14, CSNK2A1, ERK1, and AKT1, were shared between both patients at the selected threshold ($p < 10^{-8}$) (Figure 5F). Unique enriched kinases (e.g., CDK1, JNK1, ERK2) were detected in CN/AML2 only (Figure 5F).

To determine the effects of SUZ12 and EZH2 differential binding in CN/AML, we measured total levels of H3K27me3 in CN and CN/AML iPSC-derived $CD34^+$ cells. SUZ12 and EZH2 belong to a core subunit of PRC2 (polycomb repressive complex 2), responsible for H3K27 methylation. We detected reduced H3K27me3 levels in CN/AML cells compared with CN cells (Figure S6C), suggesting a modulatory effect of *RUNX1* mutations on the H3K27me3 status in CN/AML.

BAALC-dependent leukemogenic pathways in CN/AML

To identify BAALC-dependent leukemia-associated gene expression, we compared the transcriptomes of CN/AML iPSCs before and after *BAALC* KO. We identified 165 up- and 254 downregulated genes between CN/AML1 and CN/AML1 *BAALC* KO, as well as 185 up- and 381 downregulated genes between CN/AML2 and CN/AML2 *BAALC* KO ($\log_2$FC > 1 or < −1, adjusted $p < 0.05$) (Figures 6A and 6B; Figures S6D and S6E; Tables S6 and S7). *BAALC* KO led to a dramatic shift in the gene expression signature (Figures 6C and 6D). GSEA revealed enrichment of oxidative phosphorylation, tricarboxylic acid

Figure 3. Upregulation of AML-associated genes in primary CN/AML blasts and CN/AML iPSC-derived $CD34^+$ cells

(A) mRNA expression of indicated genes in BMMNCs from three CN and five CN/AML patients, measured using qRT-PCR. Gene expression levels were normalized to β-actin and are shown relative to CN. Data are represented as mean ± SD from two independent experiments. *$p < 0.05$, **$p < 0.01$, and ***$p < 0.001$ compared with CN.

(B and C) mRNA expression of indicated genes in $CD34^+$ cells derived from CN1 and CN/AML1 (B) as well as CN2 and CN/AML2 (C) iPSCs, measured using qRT-PCR. Gene expression levels were normalized to β-actin and are shown relative to CN. Data are represented as mean ± SD from two independent experiments. *$p < 0.05$, **$p < 0.01$, and ***$p < 0.001$ compared with CN.

(D) Western blotting of BAALC protein expression in $CD34^+$ cells derived from HD, CN, and CN/AML iPSCs. Numbers indicate protein expression levels normalized to β-actin and shown relative to HD. The results are representative of two independent experiments.

(E) mRNA expression of *BAALC* in $CD34^+$ cells from healthy individuals (n = 2) transduced with control GFP, WT *RUNX1*, or mutant *RUNX1* (p.R139G and p.R174L) lentiviral constructs, measured using qRT-PCR. Gene expression levels were normalized to β-actin. Data are represented as mean ± SD from two independent experiments. *$p < 0.05$.

(F and G) mRNA expression of indicated genes in $CD34^+$ cells derived from (F) HD, CN1, and CN/AML1 and (G) HD, CN2, and CN/AML2 iPSCs. Gene expression levels were normalized to β-actin and are shown relative to HD. Data are represented as mean ± SD from two independent experiments. *$p < 0.05$, **$p < 0.01$, and ***$p < 0.001$.

(H and I) Western blotting of indicated proteins in $CD34^+$ cells derived from (H) HD, CN1, and CN/AML1 and (I) HD, CN2, and CN/AML2 iPSCs. Numbers indicate protein expression levels relative to HD and normalized to β-actin. The results are representative of two independent experiments.

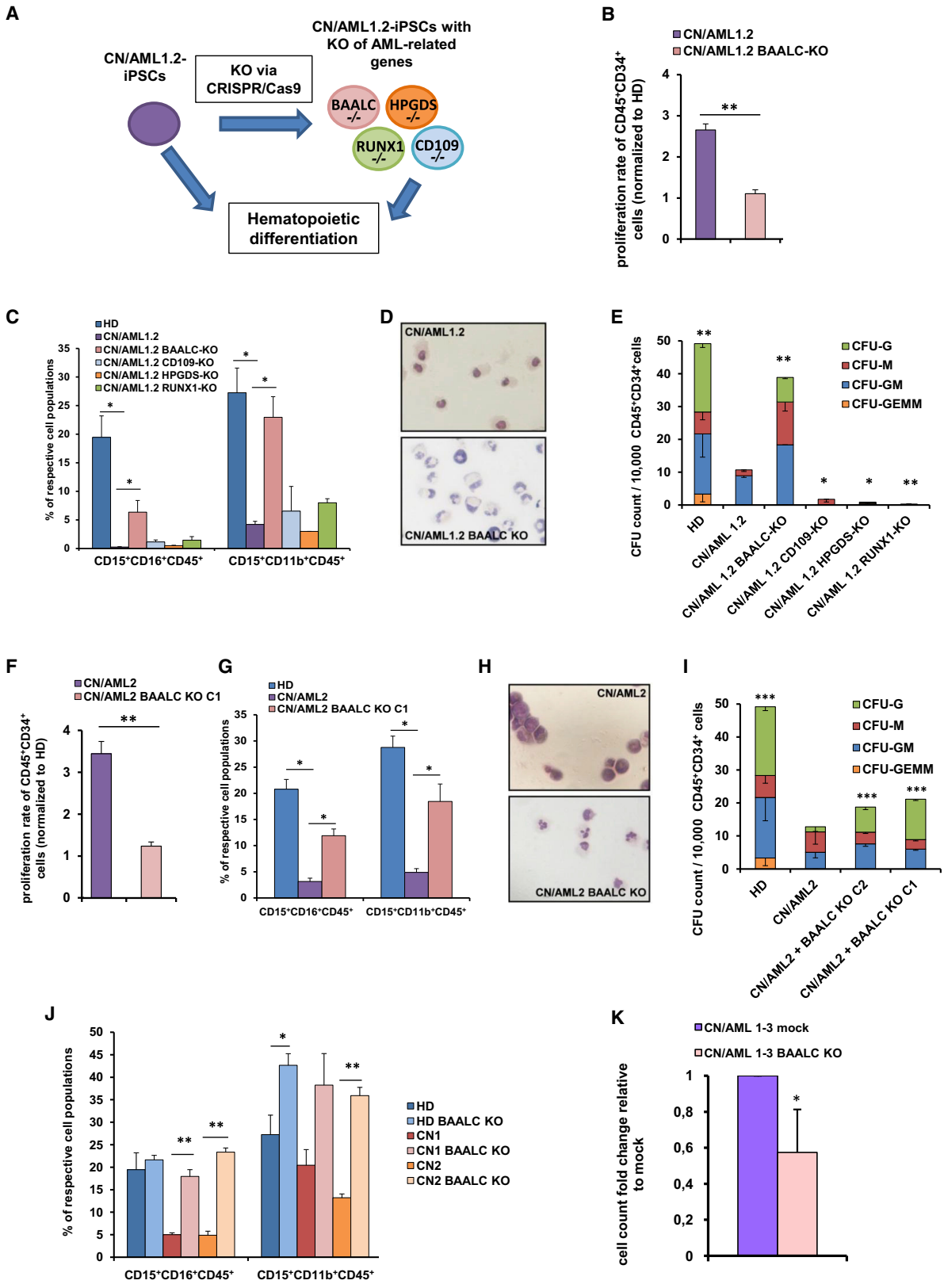

(legend on next page)

(TCA) cycle, p53 signaling, and inhibition of platelet-specific genes in CN/AML1 sample compared with *BAALC* KO (Figure 6E). E2F targets, G2M checkpoint-associated genes, TGF-β signaling, and MYC targets were enriched in CN/AML2 cells (Figure 6F).

Transcription factor enrichment analysis (TFEA) of DE genes revealed RUNX1, GATA1/2, and SUZ12 transcription factor binding motifs to be BAALC dependent in both patients. AR, TCF3, RAD21, and NANOG motifs were deregulated in CN/AML1 only. ERG1, STAT3, and ZC3H11A motifs were CN/AML2 specific (Figure 6G).

CSNK2A1, CDK1, GSK3B, HIPK2, and MAPK14/p38α were among the top BAALC-dependent kinases in both patients (Figure 6H). CN/AML2, but not CN/AML1, showed patient-specific kinase enrichment (Figure 6H).

Key transcription factor motifs such as RUNX1, GATA1/2, SUZ12, and SMAD4 as well as 7 of 12 kinases (e.g., MAPK14, MAPK1, ERK1, AKT1) were enriched in CN/AML compared with either CN or CN/AML *BAALC* KO stages in both patients (Figures 6I and 6J). These data indicate that *BAALC* KO at least partially restores CN phenotype in CN/AML cells irrespective of the *RUNX1* mutation type.

The anti-proliferative effect of a selective inhibition of MAPK14/p38α-mediated MK2a phosphorylation in CN/AML

Using Connectivity Map (CMAP) analysis (Lamb et al., 2006) of DE genes between CN/AML and CN/AML *BAALC* KO HSPCs, we evaluated drug candidates inducing a gene expression profile similar to *BAALC* KO. A selective inhibitor of p38α-mediated MK2a phosphorylation, CMPD1, was the first hit (Figure S7A). This result is in line with the KEA: MAPK14/p38α was among the top BAALC-dependent kinases in CN/AML (Figures 5F and 6H).

We assessed MK2a and p38α phosphorylation levels in CN and CN/AML iPSC-derived HSPCs as well as in CN/AML cells treated with CMPD1 and CN/AML *BAALC*-KO cells. We detected elevated phospho-MK2a but not phospho-p38α levels in CN/AML cells compared with CN (Figure 7A). At the same time, CMPD1 treatment or *BAALC* KO resulted in a reduction of MK2a but not p38α phosphorylation in CN/AML (Figure 7A). Basal levels of non-phosphorylated MK2a and p38α proteins remained unchanged in all groups (Figure S7B). These data confirm BAALC-dependent phosphorylation of MK2a in CN/AML.

We next tested the effects of CMPD1-dependent reduction of MK2a phosphorylation on the growth of CN/AML cells. We treated the BAALC^{high} AML cell line Kasumi-1 with CMPD1 and found markedly reduced cell proliferation compared with DMSO control (Figure S7C). Importantly, CMPD1 treatment of CN/AML iPSC-derived HSPCs from both patients significantly reduced cell growth without affecting the proliferation of HD and CN iPSC-derived HSPCs (Figure 7B), compared with DMSO groups. Moreover, treatment of primary blasts from three BAALC^{high} CN/AML patients with CMPD1 led to a dramatic suppression of proliferation, without affecting HD cells (Figures 7C and 7D). A less prominent effect of CMPD1 was observed in *de novo BAALC*^{high} AML samples (Figures 7E and 7F). *BAALC* KO partially protected CN/AML cells from CMPD1-induced death (Figure 7G). Additionally, *BAALC* mRNA levels were slightly but significantly reduced after CMPD1 treatment (Figure 7H), suggesting feedback regulation of *BAALC* expression by MK2a.

It has been reported that MEK1/2 inhibitor U0126, in combination with KLF4 activation, reduces the growth of *BAALC*-expressing *de novo* AML cells (Morita et al., 2015). We thus compared the effects of two MEK inhibitors, U0126 and AZD-6244, on the proliferation of CN/AML and *BAALC*^{high} *de novo* AML cells. U0126 treatment had no effects on cell proliferation (Figure S7D), whereas AZD-6244 had a moderate effect (Figures S7E–S7G). No effect of AZD-6244 was observed in Kasumi-1 cells (Figure S7C). The KLF-4 activator APTO-253, in combination with 1 μM AZD-6244, was either not effective at a dose of

Figure 4. *BAALC* upregulation is essential for leukemogenic transformation in CN/AML

(A) Schematic overview of the experimental design. CRISPR-Cas9-mediated gene editing of indicated genes was performed in CN/AML iPSCs followed by EB-based differentiation. Hematopoietic differentiation was compared with unedited CN/AML iPSCs and HD iPSCs.

(B) Proliferation rate of CD34$^+$ cells derived from CN/AML1 and CN/AML1 *BAALC*-KO iPSCs. CD34$^+$ cells were expanded on SL/SL feeder for 7 days. Data were normalized to HD and are represented as mean ± SD from two independent experiments. **$p < 0.01$.

(C) Percentage of iPSCs derived granulocytes (CD15$^+$CD16$^+$ CD45$^+$ and CD15$^+$CD11b$^+$CD45$^+$) on day 32 of culture. Data are represented as mean ± SD from two independent experiments. *$p < 0.05$.

(D) Representative images of iPSC-derived hematopoietic cells at day 32 of differentiation stained with Wright Giemsa at 40× magnification are shown.

(E) CFU assay of iPSC-derived CD34$^+$ cells isolated at day 14 of culture. Total CFU counts are shown. Data are represented as mean ± SD from two independent experiments in triplicate. Group comparisons were done between CN/AML1 and all other iPSC clones. Significant differences between groups to CN/AML1 are indicated (*$p < 0.05$ and **$p < 0.01$).

(F) Proliferation rate of CD34$^+$ cells derived from CN/AML2 and CN/AML2 *BAALC*-KO iPSCs. CD34$^+$ cells were expanded on SL/SL feeder for 7 days. Data were normalized to HD and are represented as mean ± SD from two independent experiments. **$p < 0.01$.

(G) Percentage of iPSC-derived granulocytes (CD15$^+$CD16$^+$CD45$^+$ and CD15$^+$CD11b$^+$CD45$^+$) on day 32 of culture. Data are represented as mean ± SD from two independent experiments. *$p < 0.05$.

(H) Representative images of iPSC-derived hematopoietic cells at day 32 of differentiation stained with Wright Giemsa at 40× magnification are shown.

(I) CFU assay of iPSC-derived CD34$^+$ cells isolated at day 14 of culture. Total CFU counts are shown. Data are represented as mean ± SD from two independent experiments in triplicate. Group comparisons were done between CN/AML2 and all other iPSC clones. Significant differences between groups to CN/AML2 are indicated (*$p < 0.05$, **$p < 0.01$, and ***$p < 0.001$).

(J) Percentage of iPSC-derived granulocytes (CD15$^+$CD16$^+$CD45$^+$ and CD15$^+$CD11b$^+$CD45$^+$) on day 32 of culture. Data are represented as mean ± SD from two independent experiments. *$p < 0.05$ and **$p < 0.01$.

(K) Proliferation rate of primary CN/AML mock and CN/AML *BAALC*-KO blasts from three CN/AML patients. Gene-edited primary CN/AML blasts were expanded on SL/SL feeder for 14 days. Data were normalized to mock cells and are represented as mean ± SD. *$p < 0.05$.

See also Figure S5 and Tables S2 and S3.

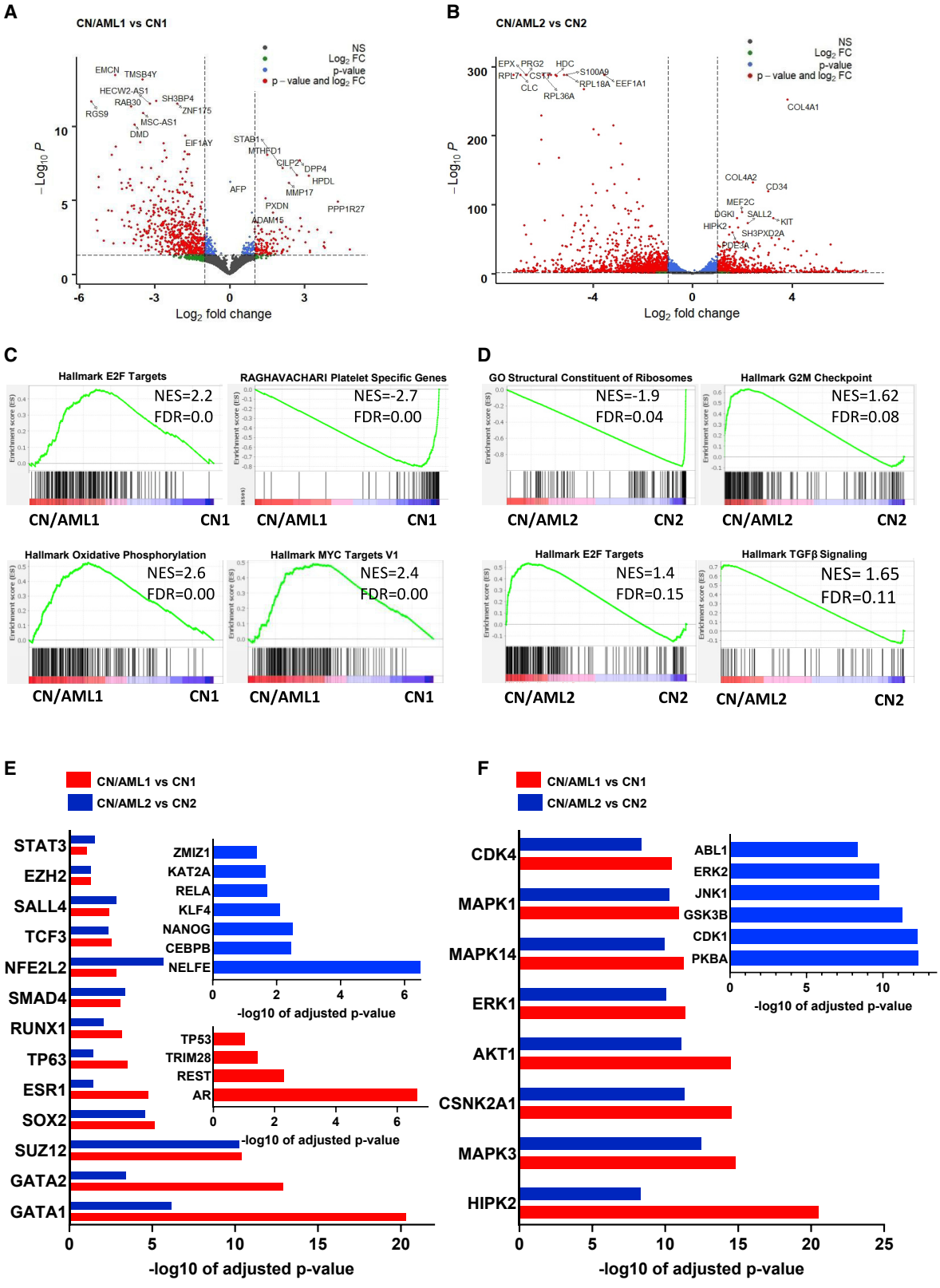

(legend on next page)

10 nM of ATO-253 or toxic at 100 and 1,000 nM concentrations (data not shown).

DISCUSSION

We present here an *in vitro* model of stepwise leukemia development in pre-leukemia BM failure syndromes, exemplified by CN. Using CRISPR-Cas9 gene editing, we introduced gene alterations associated with pre-leukemia and leukemia conditions in iPSC lines of CN patients. By generating iPSCs recapitulating non-leukemic and leukemia conditions, we were able to evaluate hematopoietic differentiation and intracellular signaling differences between these two conditions. We observed almost completely abrogated myeloid differentiation and elevated proliferation of CN/AML iPSCs compared with control or CN iPSCs. The elevated levels of AML-associated genes (e.g., *BAALC*, *STAT5*) in HSPCs derived from CN/AML iPSCs along with their increased proliferation and diminished differentiation argues for their leukemic features. Therefore, our *in vitro* model recapitulates stepwise leukemia development in CN. Given the absence of animal models of *ELANE*-CN, *in vitro* modeling of CN and leukemia using CRISPR-Cas9 gene editing of patient-derived iPSCs is of high importance.

Different *RUNX1* mutation types (missense, nonsense, and frameshift) were detected in CN/AML (Beekman et al., 2012; Skokowa et al., 2014). CRISPR-Cas9 gene editing allows a comparison of the effects of different mutations in endogenously expressed proteins. We provided evidence for dose-dependent outcomes of missense mutations versus *RUNX1* haploinsufficiency: missense *RUNX1* mutations, but not nonsense or frameshift mutation in RHD, require trisomy 21 to amplify the leukemogenic effect of the mutated *RUNX1*. We generated iPSC lines carrying *ELANE*, *CSF3R*, and, additionally, mutations and chromosomal abnormalities mimicking CN/AML phenotype: (1) missense *RUNX1* mutation and trisomy 21 with two copies of mutated *RUNX1* or (2) *RUNX1* haploinsufficiency without trisomy 21. In both conditions, myeloid differentiation was severely abrogated, and proliferation was elevated. We identified signaling pathways deregulated by both missense and frameshift *RUNX1* mutations in CN/AML cells or affected explicitly by each mutation. The vast majority of crucial signaling leukemia-causing pathways, such as the activation of the *E2F* pathway, an enrichment of RUNX1, GATA1/2, SUZ12, and EZH2 targets, and targets of MAPK1/3/14, HIPK2, AKT1, and ERK1 kinases were overlapped in $CD34^+$ CN/AML cells with missense or frameshift *RUNX1* mutations. Interestingly, some transcription factors and signaling pathways were regulated on the *RUNX1* mutation type-specific manner: missense p.R139G *RUNX1* regulated MYC targets and oxidative phosphorylation, while truncated *RUNX1* affected the constituents of ribosomes, G2M checkpoint genes, and TGF-β signaling. These data provide a better understanding of the mechanistic outcomes of different types of *RUNX1* mutations in leukemogenesis. Particularly interesting is the fact of the differential activity of SUZ12 and EZH2 in CN/AML versus CN. SUZ12 and EZH2 are core PRC2 subunits, suggesting possible changes of H3K27me3 distribution in *RUNX1* mutant cells. There is an enrichment of *EZH2* mutations in *RUNX1* mutant AML (Gaidzik et al., 2016; Stengel et al., 2018), and H3K27 mutations cooperate with *RUNX1* mutations in AML (Lehnertz et al., 2017). In line with this, we detected reduced H3K27me3 levels in CN/AML samples compared with CN samples. It would be interesting to further investigate a specific H3K27me3 distribution in CN/AML cells.

We identified elevated *BAALC* levels in CN/AML blasts, and CRISPR-Cas9-mediated *BAALC* KO inhibited proliferation, simultaneously inducing myeloid differentiation of CN/AML cells. *BAALC* is upregulated in *RUNX1*-mutated *de novo* AML (Mendler et al., 2012; Metzeler et al., 2013), and we found that mutated *RUNX1* induced *BAALC* expression in HD HSPCs. High *BAALC* expression is associated with aggressive AML and poor prognosis (Weber et al., 2014). To study the mechanism of leukemogenesis downstream of *BAALC* activation, we performed RNA sequencing (RNA-seq) of $CD34^+$ cells derived from CN/AML and CN/AML *BAALC*-KO cells. *BAALC* KO led to a marked shift in gene expression in CN/AML cells independent of the *RUNX1* mutation type. We detected oxidative phosphorylation, MYC, TGF-β, E2F, and G2M checkpoint-controlling pathways to be *BAALC* dependent in CN/AML. Moreover, RUNX1, SUZ12, SOX2, GATA1/2, SMAD4 and SALL4 transcription factors as well as MAPK14, GSK3B, CSNK2A1, and CDK1/2 kinase pathways were found to be downstream of *BAALC* in both CN/AML patients. These findings clearly demonstrate the fundamental role of *BAALC* in leukemia development downstream of missense and truncated *RUNX1* mutations.

Searching for the translational applications of our findings, we identified the selective MK2a inhibitor, CMPD1, as the best drug candidate mimicking *BAALC*-KO expression signature, when comparing CN/AML with CN/AML *BAALC* KO using CMAP. CMPD1 treatment effectively reduced proliferation of iPSC-derived and primary CN/AML blasts without affecting HD and CN HSPCs. This result was in line with inhibition of MK2a but not p38α phosphorylation by CMPD1 treatment or *BAALC* KO. These data argue for BAALC-dependent activation of MK2a phosphorylation in CN/AML. Thus, CMPD1, or alternative MK2a inhibitors, might be implemented in the treatment of CN/AML and $BAALC^{high}$ *de novo* AML. CN/AML and $BAALC^{high}$

Figure 5. Gene expression signature of $CD34^+$ cells derived from CN and CN/AML iPSCs

(A and B) Volcano plot showing differentially expressed genes (DEGs; $\log_2FC > 1$ or < -1, adjusted $p < 0.05$) in iPSC-derived $CD34^+$ cells from (A) CN/AML1 versus CN1 and (B) CN/AML2 versus CN2 group comparisons. The x axis shows the $\log_2$ fold change, and the y axis shows the $-\log_{10}$ adjusted p value. Colors represent the significance of the genes in terms of p value and $\log_2$ fold change. Gene names are indicated for the top ten upregulated and top ten downregulated genes.
(C and D) GSEA version 4.0.3 analysis of normalized read counts of iPSC-derived HSPCs from CN/AML1 versus CN1 (C) and CN/AML2 versus CN2 (D) groups.
(E) Transcription factors predicted by TFEA of DEGs in CN/AML1 versus CN1 (red) and CN/AML2 versus CN2 (blue) groups. Common transcription factors are plotted on the same graph. Data are displayed as $-\log_{10}$ adjusted p value.
(F) Kinases predicted by KEA of DEGs in CN/AML1 versus CN1 (red) and CN/AML2 versus CN2 (blue). Common kinases with p values $< 10^{-8}$ are plotted on the same graph. Data are displayed as $-\log_{10}$ adjusted p values.
See also Figure S6 and Table S5.

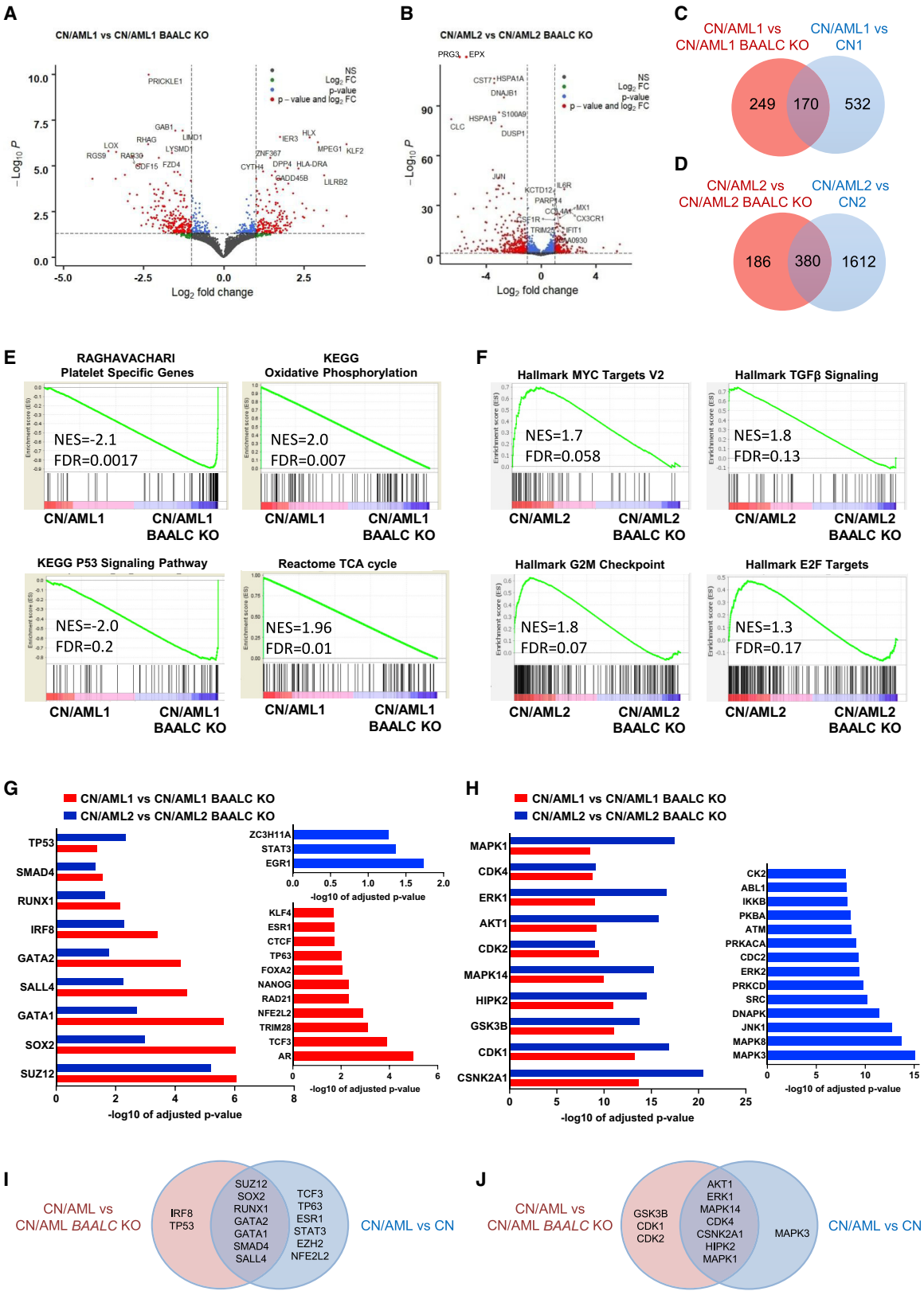

(legend on next page)

de novo AML patients have aggressive leukemia with poor prognosis, and our findings represent a first step toward the establishment of advanced therapies for these leukemias. Of note, CMPD1 treatment was partially effective in CN/AML *BAALC*-KO cells. At the same time, *BAALC* expression was reduced upon CMPD1 treatment, suggesting a feedback regulation of *BAALC* expression by MK2a pathway.

In summary, the present iPSC-based *in vitro* model is reliable for investigating stepwise leukemogenesis in pre-leukemia BM failure syndromes. Implementation of this model led to the characterization of high *BAALC* expression and elevated MK2a phosphorylation as ultimate leukemia-causing events in CN/AML and the identification of CMPD1 as a potential therapeutic drug for CN/AML and *BAALC*^{high} *de novo* AML patients. Inhibition of BAALC or treatment with MK2a inhibitors might prevent leukemia development in CN/AML and eliminate *RUNX1*-mutated BAALC^{high} *de novo* AML blasts (Figure 7I).

Limitations of study

Although we were able to identify a key signaling pathway of CN/AML development and a potential drug targeting CN/AML blasts, the CN patient-specific iPSCs model used in our study has some caveats. The most important one involves the impossibility to go further and study the *in vivo* behavior of iPSC-derived CN/AML blasts and their sensitivity to CMPD1 therapy using xenograft models in NSG mice. Up to now, it has been almost impossible to efficiently engraft iPSC-derived HSPCs or leukemia cells into NSG mice, with a limited number of studies reporting successful engraftment.

Another limitation is the limited number of patients who were evaluated here. Taken into consideration a relative rarity of CN with even less CN/AML cases, *BAALC* expression levels and MK2a phosphorylation status should be evaluated in a bigger cohort of CN/AML patients and iPSC models with different CN-associated mutations in, for example, *HAX1*, *JAGN1*, or *SRP54*.

STAR★METHODS

Detailed methods are provided in the online version of this paper and include the following:

SUPPLEMENTAL INFORMATION

Supplemental information can be found online at https://doi.org/10.1016/j.stem.2021.03.023.

ACKNOWLEDGMENTS

We thank the UKT fluorescence-activated cell sorting (FACS) and cATG core facilities for assistance in cell sorting and RNA-seq, respectively. This work was supported by the Excellence Initiative of the Faculty of Medicine, University of Tuebingen (J.S.); Bundesministerium für Bildung und Forschung (BMBF) MyPred (J.S., K.W., C.Z., T.R., C.M.N., and M.E.); The Else Kroener-Fresenius Foundation (B.D. and M. Klimiankou); the Jose Carreras Leukemia Foundation (J.S. and B.D.); Madeleine Schickedanz Kinderkrebsstiftung (J.S.); Deutsche

Figure 6. BAALC-dependent gene expression profile of CN/AML iPSC-derived CD34$^+$ cells

(A and B) Volcano plot showing DEGs in iPSC-derived CD34$^+$ cells from (A) CN/AML1 versus CN/AML1 *BAALC* KO and (B) CN/AML2 versus CN/AML2 *BAALC* KO group comparisons. The x axis shows the $\log_2$ fold change, and the y axis shows the $-\log_{10}$ adjusted p value. Colors represent the significance of the genes in terms of p value and $\log_2$ fold change. Gene names are indicated for the top ten upregulated and top ten downregulated genes.

(C and D) Venn diagram showing overlap of DEGs between (C) CN/AML1 versus CN/AML1 *BAALC* KO (red) and CN/AML1 versus CN1 (blue) groups, as well as (D) CN/AML2 versus CN/AML2 *BAALC* KO (red) and CN/AML2 versus CN2 (blue) groups.

(E and F) GSEA 4.0.3 analysis of normalized read counts of RNA-seq from iPSC-derived HSPCs from (E) CN/AML1 versus CN/AML1 *BAALC* KO and (F) CN/AML2 versus CN/AML *BAALC* KO groups.

(G) Transcription factors predicted by TFEA of DEGs in CN/AML1 versus CN/AML1 *BAALC* KO (red) and CN/AML2 versus CN/AML2 *BAALC* KO (blue) groups. Common transcription factors ($p < 0.05$) are plotted on the same graph. Data are displayed as $-\log_{10}$ of adjusted p value.

(H) Kinases predicted by KEA of DEGs in CN/AML1 versus CN/AML1 *BAALC* KO (red) and CN/AML2 versus CN/AML2 *BAALC* KO (blue) groups. Common kinases ($p < 10^{-8}$) are plotted on the same graph. Data are displayed as $-\log_{10}$ of adjusted p value.

(I and J) Venn diagram showing overlap of transcription factors (I) and kinases (J) between CN/AML versus CN/AML *BAALC* KO (red) and CN/AML versus CN (blue) groups of both CN/AML patients.

See also Figure S6 and Tables S6 and S7.

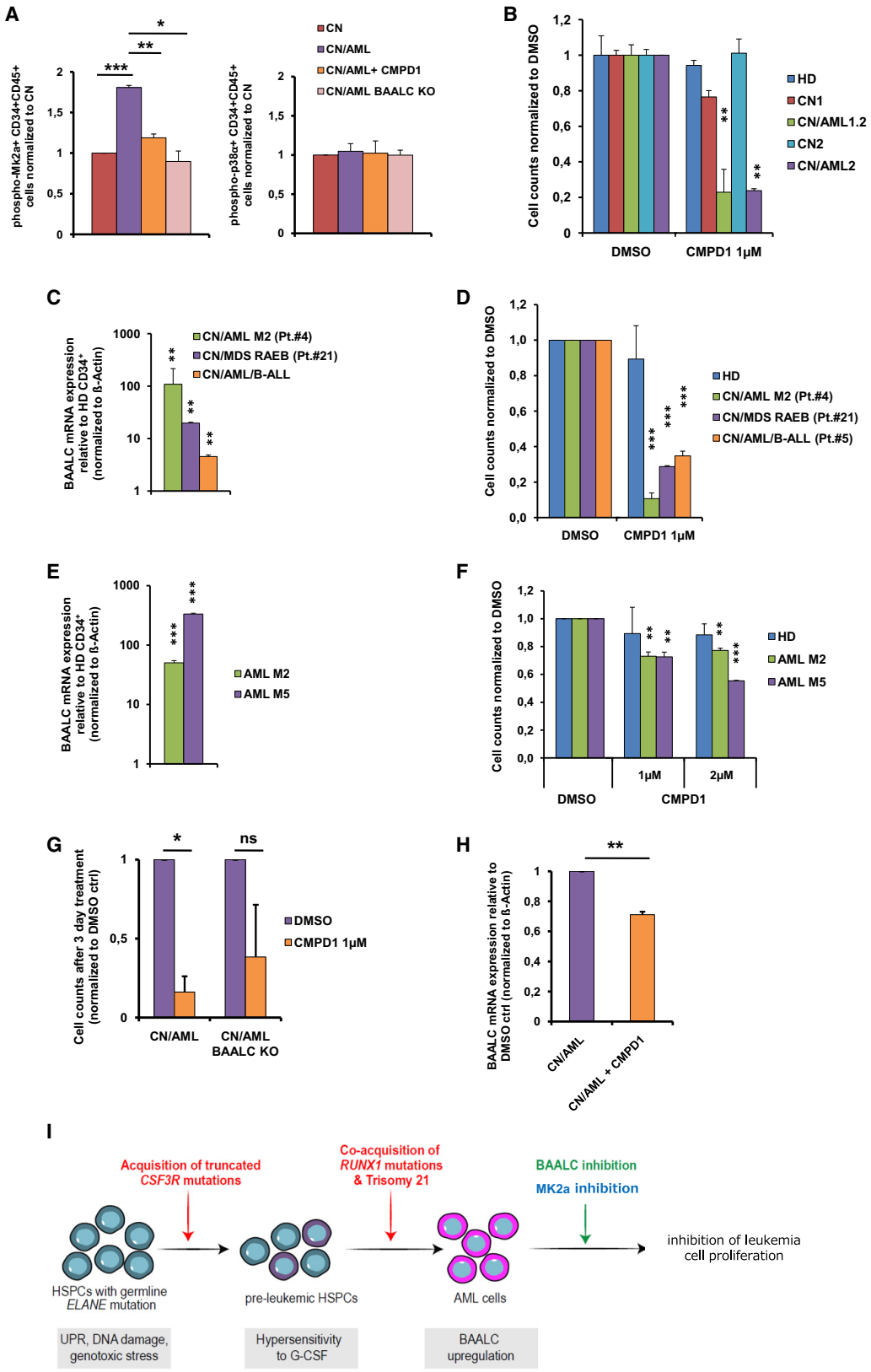

(legend on next page)

Forschungsgemeinschaft (DFG) (J.S. and M. Klimiankou); COST EuNet-INNOCHRON action from the European Union (EU) (J.S., M. Klimiankou, C.Z., and K.W.); and the internal funding program Fortüne of the Medical Faculty of the Tübingen University (M. Klimiankou).

AUTHOR CONTRIBUTIONS

B.D., M. Klimiankou, and J.S. made initial observations, designed the experiments, and analyzed the data. B.D. and M. Klimiankou performed the experiments. B.D. performed iPSC experiments, qRT-PCRs, and western blots (WBs). M. Klimiankou, M.N., A.S., and B.O. performed CRISPR-Cas9 gene editing in iPSCs. A.S. assisted with CFU assays. M.K. and F.S. performed dPCR. J.M. performed drug treatment of Kasumi-1 and AML cells and assisted with BAALC KO. M. Klimiankou and S.K. performed RNA-seq data analysis. A.Z., T. Morishima, N.L., and T. Moritz assisted with the establishment of generation and hematopoietic differentiation of iPSCs. T.R. and D.S. performed array-CGH. C.Z., M.E., and C.M.N. provided patient material. K.W., M.E., C.M.N., P.M., M. Konantz, and C.L. provided insightful comments. J.S. supervised and supported the study and wrote the manuscript (with assistance from B.D., M. Klimiankou, and P.A.-T.).

DECLARATION OF INTERESTS

The authors declare no competing interests.

Received: April 7, 2020
Revised: January 15, 2021
Accepted: March 30, 2021
Published: April 22, 2021

REFERENCES

Alter, B.P. (2017). Inherited bone marrow failure syndromes: considerations pre- and posttransplant. Blood *130*, 2257–2264.

Babicki, S., Arndt, D., Marcu, A., Liang, Y., Grant, J.R., Maciejewski, A., and Wishart, D.S. (2016). Heatmapper: web-enabled heat mapping for all. Nucleic Acids Res. *44* (W1), W147–W153.

Beekman, R., Valkhof, M.G., Sanders, M.A., van Strien, P.M., Haanstra, J.R., Broeders, L., Geertsma-Kleinekoort, W.M., Veerman, A.J., Valk, P.J., Verhaak, R.G., et al. (2012). Sequential gain of mutations in severe congenital neutropenia progressing to acute myeloid leukemia. Blood *119*, 5071–5077.

Chang, C.J., Kotini, A.G., Olszewska, M., Georgomanoli, M., Teruya-Feldstein, J., Sperber, H., Sanchez, R., DeVita, R., Martins, T.J., Abdel-Wahab, O., et al. (2018). Dissecting the contributions of cooperating gene mutations to cancer phenotypes and drug responses with patient-derived iPSCs. Stem Cell Reports *10*, 1610–1624.

Chao, M.P., Gentles, A.J., Chatterjee, S., Lan, F., Reinisch, A., Corces, M.R., Xavy, S., Shen, J., Haag, D., Chanda, S., et al. (2017). Human AML-iPSCs reacquire leukemic properties after differentiation and model clonal variation of disease. Cell Stem Cell *20*, 329–344.e7.

Clarke, D.J.B., Kuleshov, M.V., Schilder, B.M., Torre, D., Duffy, M.E., Keenan, A.B., Lachmann, A., Feldmann, A.S., Gundersen, G.W., Silverstein, M.C., et al. (2018). eXpression2Kinases (X2K) Web: linking expression signatures to upstream cell signaling networks. Nucleic Acids Res. *46* (W1), W171–W179.

Collins, J., and Dokal, I. (2015). Inherited bone marrow failure syndromes. Hematology *20*, 433–434.

Concordet, J.P., and Haeussler, M. (2018). CRISPOR: intuitive guide selection for CRISPR/Cas9 genome editing experiments and screens. Nucleic Acids Res. *46* (W1), W242–W245.

Dale, D.C., Person, R.E., Bolyard, A.A., Aprikyan, A.G., Bos, C., Bonilla, M.A., Boxer, L.A., Kannourakis, G., Zeidler, C., Welte, K., et al. (2000). Mutations in the gene encoding neutrophil elastase in congenital and cyclic neutropenia. Blood *96*, 2317–2322.

Dannenmann, B., Nasri, M., Welte, K., and Skokowa, J. (2020). CRISPR/Cas9 genome editing of human-induced pluripotent stem cells followed by granulocytic differentiation. Methods Mol. Biol. *2115*, 471–483.

Dobin, A., Davis, C.A., Schlesinger, F., Drenkow, J., Zaleski, C., Jha, S., Batut, P., Chaisson, M., and Gingeras, T.R. (2013). STAR: ultrafast universal RNA-seq aligner. Bioinformatics *29*, 15–21.

Dong, F., Brynes, R.K., Tidow, N., Welte, K., Löwenberg, B., and Touw, I.P. (1995). Mutations in the gene for the granulocyte colony-stimulating-factor receptor in patients with acute myeloid leukemia preceded by severe congenital neutropenia. N. Engl. J. Med. *333*, 487–493.

Dong, F., Dale, D.C., Bonilla, M.A., Freedman, M., Fasth, A., Neijens, H.J., Palmblad, J., Briars, G.L., Carlsson, G., Veerman, A.J.P., et al. (1997). Mutations in the granulocyte colony-stimulating factor receptor gene in patients with severe congenital neutropenia. Leukemia *11*, 120–125.

Feurstein, S., Drazer, M.W., and Godley, L.A. (2016). Genetic predisposition to leukemia and other hematologic malignancies. Semin. Oncol. *43*, 598–608.

Figure 7. Inhibition of proliferation of iPSC-derived and primary CN/AML or *de novo* AML blasts by MK2a inhibitor CMPD1

(A) Flow cytometry analysis of intracellular phospho-MK2a and phospho-p38α protein levels in CN, CN/AML, CMPD1-treated CN/AML (1 μM CMPD1; 24 h) and CN/AML *BAALC*-KO iPSC-derived $CD34^+$ cells. Data are represented as mean ± SD from two independent experiments of two CN/AML patients. *$p < 0.05$, **$p < 0.01$, and ***$p < 0.001$ compared with CN/AML.

(B) Proliferation rate of iPSC-derived $CD34^+$ cells from HD, CN, and CN/AML clones treated with either 1 μM CMPD1 or DMSO for 7 days. Data are represented as mean ± SD from two independent experiments. **$p < 0.01$ compared with DMSO control.

(C) mRNA expression of *BAALC* in blasts of CN/AML patients. Gene expression levels were normalized to β-actin and are shown relative to HD. Data are represented as mean ± SD from two independent experiments. **$p < 0.01$ compared with $CD34^+$ cells of three HDs.

(D) Proliferation rate of primary CN/AML blasts treated with 1 μM CMPD1 or DMSO for 7 days. Data are represented as mean ± SD from two independent experiments. ***$p < 0.001$ compared with DMSO control.

(E) mRNA expression of *BAALC* in *de novo* AML blasts. Gene expression levels were normalized to β-actin and are shown relative to HD. Data are represented as mean ± SD; two independent experiments. ***$p < 0.001$ compared with $CD34^+$ cells of 3 HDs.

(F) Proliferation rate of *de novo* AML blasts treated with 1 and 2 μM CMPD1 or DMSO for 7 days. Data are represented as mean ± SD from two independent experiments. **$p < 0.01$ and ***$p < 0.001$ compared with DMSO control.

(G) Proliferation rate of iPSC-derived $CD34^+$ cells from CN/AML and CN/AML *BAALC*-KO clones treated with 1 μM CMPD1 or DMSO for 7 days. Data are represented as mean ± SD from two independent experiments/patient. *$p < 0.05$ compared with DMSO control.

(H) mRNA expression of *BAALC* in CN/AML iPSC-derived $CD34^+$ cells treated with 1 μM CMPD1 for 24 h. Data are represented as mean ± SD from two independent experiments/patient. **$p < 0.05$ normalized to DMSO control.

(I) Schematic diagram of the role of *BAALC* upregulation in CN-related leukemia development. In CN patients with inherited CN-associated mutations (e.g., *ELANE*), genetically "unfit" HSPCs acquire *CSF3R* mutations. The acquisition of *CSF3R* mutations along with prolonged exposures to high doses of G-CSF leads to the clonal selection of pre-leukemia HSPCs, which exhibit elevated proliferation and reduced differentiation upon G-CSF treatment. The co-acquisition of further *RUNX1* haploinsufficiency or missense *RUNX1* mutations along with trisomy 21 leads to elevated *BAALC* expression levels and leukemogenic transformation. Inactivation of *BAALC* in CN/AML cells using CRISPR-Cas9-mediated gene editing restores normal hematopoietic differentiation, while selective inhibition of MK2a phosphorylation with CMPD1 efficiently blocks proliferation of CN/AML cells.

See also Figure S7.

Gaidzik, V.I., Teleanu, V., Papaemmanuil, E., Weber, D., Paschka, P., Hahn, J., Wallrabenstein, T., Kolbinger, B., Köhne, C.H., Horst, H.A., et al. (2016). RUNX1 mutations in acute myeloid leukemia are associated with distinct clinico-pathologic and genetic features. Leukemia *30*, 2160–2168.

Germeshausen, M., Skokowa, J., Ballmaier, M., Zeidler, C., and Welte, K. (2008). G-CSF receptor mutations in patients with congenital neutropenia. Curr. Opin. Hematol. *15*, 332–337.

Göhring, G., Karow, A., Steinemann, D., Wilkens, L., Lichter, P., Zeidler, C., Niemeyer, C., Welte, K., and Schlegelberger, B. (2007). Chromosomal aberrations in congenital bone marrow failure disorders–an early indicator for leukemogenesis? Ann. Hematol. *86*, 733–739.

Gupta, K., Kuznetsova, I., Klimenkova, O., Klimiankou, M., Meyer, J., Moore, M.A.S., Zeidler, C., Welte, K., and Skokowa, J. (2014). Bortezomib inhibits STAT5-dependent degradation of LEF-1, inducing granulocytic differentiation in congenital neutropenia CD34(+) cells. Blood *123*, 2550–2561.

Harada, Y., and Harada, H. (2011). Molecular mechanisms that produce secondary MDS/AML by RUNX1/AML1 point mutations. J. Cell. Biochem. *112*, 425–432.

Hiramoto, T., Ebihara, Y., Mizoguchi, Y., Nakamura, K., Yamaguchi, K., Ueno, K., Nariai, N., Mochizuki, S., Yamamoto, S., Nagasaki, M., et al. (2013). Wnt3a stimulates maturation of impaired neutrophils developed from severe congenital neutropenia patient-derived pluripotent stem cells. Proc. Natl. Acad. Sci. U S A *110*, 3023–3028.

Hsu, J., Reilly, A., Hayes, B.J., Clough, C.A., Konnick, E.Q., Torok-Storb, B., Gulsuner, S., Wu, D., Becker, P.S., Keel, S.B., et al. (2019). Reprogramming identifies functionally distinct stages of clonal evolution in myelodysplastic syndromes. Blood *134*, 186–198.

Imai, Y., Kurokawa, M., Izutsu, K., Hangaishi, A., Takeuchi, K., Maki, K., Ogawa, S., Chiba, S., Mitani, K., and Hirai, H. (2000). Mutations of the AML1 gene in myelodysplastic syndrome and their functional implications in leukemogenesis. Blood *96*, 3154–3160.

Klimiankou, M., Mellor-Heineke, S., Klimenkova, O., Reinel, E., Uenalan, M., Kandabarau, S., Skokowa, J., Welte, K., and Zeidler, C. (2016a). Two cases of cyclic neutropenia with acquired CSF3R mutations, with 1 developing AML. Blood *127*, 2638–2641.

Klimiankou, M., Mellor-Heineke, S., Zeidler, C., Welte, K., and Skokowa, J. (2016b). Role of CSF3R mutations in the pathomechanism of congenital neutropenia and secondary acute myeloid leukemia. Ann. N Y Acad. Sci. *1370*, 119–125.

Komor, A.C., Kim, Y.B., Packer, M.S., Zuris, J.A., and Liu, D.R. (2016). Programmable editing of a target base in genomic DNA without double-stranded DNA cleavage. Nature *533*, 420–424.

Kotini, A.G., Chang, C.J., Chow, A., Yuan, H., Ho, T.C., Wang, T., Vora, S., Solovyov, A., Husser, C., Olszewska, M., et al. (2017). Stage-specific human induced pluripotent stem cells map the progression of myeloid transformation to transplantable leukemia. Cell Stem Cell *20*, 315–328.e7.

Lachmann, N., Ackermann, M., Frenzel, E., Liebhaber, S., Brennig, S., Happle, C., Hoffmann, D., Klimenkova, O., Lüttge, D., Buchegger, T., et al. (2015). Large-scale hematopoietic differentiation of human induced pluripotent stem cells provides granulocytes or macrophages for cell replacement therapies. Stem Cell Reports *4*, 282–296.

Lamb, J., Crawford, E.D., Peck, D., Modell, J.W., Blat, I.C., Wrobel, M.J., Lerner, J., Brunet, J.P., Subramanian, A., Ross, K.N., et al. (2006). The Connectivity Map: using gene-expression signatures to connect small molecules, genes, and disease. Science *313*, 1929–1935.

Lehnertz, B., Zhang, Y.W., Boivin, I., Mayotte, N., Tomellini, E., Chagraoui, J., Lavallée, V.P., Hébert, J., and Sauvageau, G. (2017). *H3* $^{K27M/I}$ mutations promote context-dependent transformation in acute myeloid leukemia with *RUNX1* alterations. Blood *130*, 2204–2214.

Lensch, M.W., Rathbun, R.K., Olson, S.B., Jones, G.R., and Bagby, G.C., Jr. (1999). Selective pressure as an essential force in molecular evolution of myeloid leukemic clones: a view from the window of Fanconi anemia. Leukemia *13*, 1784–1789.

Li, H., Handsaker, B., Wysoker, A., Fennell, T., Ruan, J., Homer, N., Marth, G., Abecasis, G., and Durbin, R.; 1000 Genome Project Data Processing Subgroup (2009). The Sequence Alignment/Map format and SAMtools. Bioinformatics *25*, 2078–2079.

Liang, G., and Zhang, Y. (2013). Genetic and epigenetic variations in iPSCs: potential causes and implications for application. Cell Stem Cell *13*, 149–159.

Love, M.I., Huber, W., and Anders, S. (2014). Moderated estimation of fold change and dispersion for RNA-seq data with DESeq2. Genome Biol. *15*, 550.

Mendler, J.H., Maharry, K., Radmacher, M.D., Mrózek, K., Becker, H., Metzeler, K.H., Schwind, S., Whitman, S.P., Khalife, J., Kohlschmidt, J., et al. (2012). RUNX1 mutations are associated with poor outcome in younger and older patients with cytogenetically normal acute myeloid leukemia and with distinct gene and MicroRNA expression signatures. J. Clin. Oncol. *30*, 3109–3118.

Metzeler, K.H., Maharry, K., Kohlschmidt, J., Volinia, S., Mrózek, K., Becker, H., Nicolet, D., Whitman, S.P., Mendler, J.H., Schwind, S., et al. (2013). A stem cell-like gene expression signature associates with inferior outcomes and a distinct microRNA expression profile in adults with primary cytogenetically normal acute myeloid leukemia. Leukemia *27*, 2023–2031.

Michaud, J., Wu, F., Osato, M., Cottles, G.M., Yanagida, M., Asou, N., Shigesada, K., Ito, Y., Benson, K.F., Raskind, W.H., et al. (2002). In vitro analyses of known and novel RUNX1/AML1 mutations in dominant familial platelet disorder with predisposition to acute myelogenous leukemia: implications for mechanisms of pathogenesis. Blood *99*, 1364–1372.

Mir, P., Ritter, M., Welte, K., Skokowa, J., and Klimiankou, M. (2020). Gene knockout in hematopoietic stem and progenitor cells followed by granulocytic differentiation. Methods Mol. Biol. *2115*, 455–469.

Morishima, T., Watanabe, K., Niwa, A., Hirai, H., Saida, S., Tanaka, T., Kato, I., Umeda, K., Hiramatsu, H., Saito, M.K., et al. (2014). Genetic correction of HAX1 in induced pluripotent stem cells from a patient with severe congenital neutropenia improves defective granulopoiesis. Haematologica *99*, 19–27.

Morita, K., Masamoto, Y., Kataoka, K., Koya, J., Kagoya, Y., Yashiroda, H., Sato, T., Murata, S., and Kurokawa, M. (2015). BAALC potentiates oncogenic ERK pathway through interactions with MEKK1 and KLF4. Leukemia *29*, 2248–2256.

Nanua, S., Murakami, M., Xia, J., Grenda, D.S., Woloszynek, J., Strand, M., and Link, D.C. (2011). Activation of the unfolded protein response is associated with impaired granulopoiesis in transgenic mice expressing mutant Elane. Blood *117*, 3539–3547.

Nayak, R.C., Trump, L.R., Aronow, B.J., Myers, K., Mehta, P., Kalfa, T., Wellendorf, A.M., Valencia, C.A., Paddison, P.J., Horwitz, M.S., et al. (2015). Pathogenesis of ELANE-mutant severe neutropenia revealed by induced pluripotent stem cells. J. Clin. Invest. *125*, 3103–3116.

Papapetrou, E.P. (2019). Modeling leukemia with human induced pluripotent stem cells. Cold Spring Harb. Perspect. Med. *9*, a034868.

Quentin, S., Cuccuini, W., Ceccaldi, R., Nibourel, O., Pondarre, C., Pagès, M.P., Vasquez, N., Dubois d'Enghien, C., Larghero, J., Peffault de Latour, R., et al. (2011). Myelodysplasia and leukemia of Fanconi anemia are associated with a specific pattern of genomic abnormalities that includes cryptic RUNX1/AML1 lesions. Blood *117*, e161–e170.

Ran, F.A., Hsu, P.D., Wright, J., Agarwala, V., Scott, D.A., and Zhang, F. (2013). Genome engineering using the CRISPR-Cas9 system. Nat. Protoc. *8*, 2281–2308.

Rosenberg, P.S., Alter, B.P., Bolyard, A.A., Bonilla, M.A., Boxer, L.A., Cham, B., Fier, C., Freedman, M., Kannourakis, G., Kinsey, S., et al.; Severe Chronic Neutropenia International Registry (2006). The incidence of leukemia and mortality from sepsis in patients with severe congenital neutropenia receiving long-term G-CSF therapy. Blood *107*, 4628–4635.

Rosenberg, P.S., Zeidler, C., Bolyard, A.A., Alter, B.P., Bonilla, M.A., Boxer, L.A., Dror, Y., Kinsey, S., Link, D.C., Newburger, P.E., et al. (2010). Stable long-term risk of leukaemia in patients with severe congenital neutropenia maintained on G-CSF therapy. Br. J. Haematol. *150*, 196–199.

Ruiz-Gutierrez, M., Bölükbaşı, Ö.V., Alexe, G., Kotini, A.G., Ballotti, K., Joyce, C.E., Russell, D.W., Stegmaier, K., Myers, K., Novina, C.D., et al. (2019).

Therapeutic discovery for marrow failure with MDS predisposition using pluripotent stem cells. JCI Insight *5*, e125157.

Savage, S.A., and Dufour, C. (2017). Classical inherited bone marrow failure syndromes with high risk for myelodysplastic syndrome and acute myelogenous leukemia. Semin. Hematol. *54*, 105–114.

Skokowa, J., Germeshausen, M., Zeidler, C., and Welte, K. (2007). Severe congenital neutropenia: inheritance and pathophysiology. Curr. Opin. Hematol. *14*, 22–28.

Skokowa, J., Steinemann, D., Katsman-Kuipers, J.E., Zeidler, C., Klimenkova, O., Klimiankou, M., Unalan, M., Kandabarau, S., Makaryan, V., Beekman, R., et al. (2014). Cooperativity of RUNX1 and CSF3R mutations in severe congenital neutropenia: a unique pathway in myeloid leukemogenesis. Blood *123*, 2229–2237.

Skokowa, J., Dale, D.C., Touw, I.P., Zeidler, C., and Welte, K. (2017). Severe congenital neutropenias. Nat. Rev. Dis. Primers *3*, 17032.

Stengel, A., Kern, W., Meggendorfer, M., Nadarajah, N., Perglerovà, K., Haferlach, T., and Haferlach, C. (2018). Number of RUNX1 mutations, wild-type allele loss and additional mutations impact on prognosis in adult RUNX1-mutated AML. Leukemia *32*, 295–302.

Subramanian, A., Narayan, R., Corsello, S.M., Peck, D.D., Natoli, T.E., Lu, X., Gould, J., Davis, J.F., Tubelli, A.A., Asiedu, J.K., et al. (2017). A next generation Connectivity Map: L1000 platform and the first 1,000,000 profiles. Cell *171*, 1437–1452.e17.

Weber, S., Alpermann, T., Dicker, F., Jeromin, S., Nadarajah, N., Eder, C., Fasan, A., Kohlmann, A., Meggendorfer, M., Haferlach, C., et al. (2014). BAALC expression: a suitable marker for prognostic risk stratification and detection of residual disease in cytogenetically normal acute myeloid leukemia. Blood Cancer J. *4*, e173.

Wegman-Ostrosky, T., and Savage, S.A. (2017). The genomics of inherited bone marrow failure: from mechanism to the clinic. Br. J. Haematol. *177*, 526–542.

Welte, K., and Dale, D. (1996). Pathophysiology and treatment of severe chronic neutropenia. Ann. Hematol. *72*, 158–165.

Welte, K., Zeidler, C., and Dale, D.C. (2006). Severe congenital neutropenia. Semin. Hematol. *43*, 189–195.

Wesely, J., Kotini, A.G., Izzo, F., Luo, H., Yuan, H., Sun, J., Georgomanoli, M., Zviran, A., Deslauriers, A.G., Dusaj, N., et al. (2020). Acute myeloid leukemia iPSCs reveal a role for RUNX1 in the maintenance of human leukemia stem cells. Cell Rep. *31*, 107688.

STAR★METHODS

KEY RESOURCES TABLE

REAGENT or RESOURCE	SOURCE	IDENTIFIER
Antibodies		
CD33 - BV421	Bio Legend	Cat# 303416; RRID:AB_2561690
CD34 - PE-Cy7	BD Biosciences	Cat# 348811; RRID:AB_2868855
CD45 - BV510	Bio Legend	Cat# 304036; RRID:AB_2561940
CD15 - PE	BD Biosciences	Cat# 555402; RRID:AB_395802
CD16 - FITC	BD Biosciences	Cat# 555406; RRID:AB_395806
CD11b - PE-Cy7	Bio Legend	Cat# 301322; RRID:AB_830644
anti-RUNX1/AML1	Cell Signaling	Cat# 4334; RRID:AB_2184099
anti-STAT5a	Cell Signaling	Cat# 4807; RRID:AB_2196903
anti-G-CSFR	Santa Cruz	Cat# sc-74026; RRID:AB_2292136
anti-β-Actin	Cell Signaling	Cat# 4970; RRID:AB_2223172
anti-BAALC	Santa Cruz	Cat# sc-515606
anti-phospho-p38 PE	Santa Cruz	Cat# sc-166182; RRID:AB_2141746
anti-p38 AF 647	Santa Cruz	Cat# sc-81621; RRID:AB_1127392
anti-phospho-MK2a FITC	Santa Cruz	Cat# sc-293139
anti-MK2a AF 647	Santa Cruz	Cat# sc-393609
HRP-linked Ab	Cell Signaling	Cat# 7076; RRID:AB_330924
HRP-linked Ab	Cell Signaling	Cat# 7074; RRID:AB_2099233
Chemicals, peptides, and recombinant proteins		
7AAD	BD Biosciences	Cat# 559925
BMP4	R&D	Cat# 314-BP
bFGF (FGF2)	Peprotech	Cat# 100-18B
VEGF	R&D	Cat# 293-VE
SCF	Peprotech	Cat# 300-07
IL-3	Peprotech	Cat# 200-03
Y-27632 dihydrochloride	Tocris	Cat# 1254
G-CSF (Filgrastim)	Neupogen	Cat# 55513-209-91
CMPD1	Tocris	Cat# 2186
Retronectin	Takara Bio	Cat# T100B
Accutase	Sigma	Cat# A6964
StemFlex Medium	Thermo Fisher	Cat# A3349401
Geltrex	Thermo Fisher	Cat# A1413202
Methocult H4435	Stem Cell Technologies	Cat# 04435
STEMdiff APEL2 Medium	Stem Cell Technologies	Cat# 05270
Pierce ECL solution	Thermo Fisher	Cat# 32106
Amersham Hyperfilm	GE Healthcare	Cat# 28906837
NBT/BCIP staining dye	Sigma	Cat# 11681451001
*Trans*IT®-LT1 Transfection Reagent	Mirus	Cat# MIR2304
Critical commercial assays		
Agilent Human Genome Microarray Kits 2x400K	Agilent Technologies, Santa Clara, CA, USA	Cat# G4448A
TruSeq RNA Sample Prep Kit	Illumina	Cat# RS-122-2001
EpiQuik Total Histone Extraction Kit	Epigentek	Cat# OP-0006
Histone H3 methylated Lys27 ELISA kit	Active Motif	Cat# 53106
RNeasy Micro Kit	QIAGEN	Cat# 74004

(*Continued on next page*)

Continued

REAGENT or RESOURCE	SOURCE	IDENTIFIER
Omniscript RT Kit	QIAGEN	Cat# 205113
SYBR Green qPCR master mix	Roche	Cat# 04887352001
P3 Primary Cell 4D-Nucleofector X Kit L	Lonza	Catalog# V4XP-3024
Deposited data		
RNA-seq – raw data	This paper	ArrayExpress: E-MTAB-10162
Experimental models: Cell lines		
HD iPSC	Thomas Moritz, MHH, Hannover	N/A
CN iPSC	This paper	N/A
CN/AML iPSC	This paper	N/A
SNL-feeder cells	Public Health England	Cat# 07032801
SL/SL feeder cells	Connie Eaves, Terry Fox Laboratory, BC, Canada	N/A
Recombinant DNA		
pRRL.PPT.SF.hOct34.hKlf4.hSox2.i2dTomato.pre.FRT	Axel Schambach, MHH, Hannover	N/A
pRRL.PPT.SFFV.i2RFP	Axel Schambach, MHH, Hannover	N/A
pSpCas9(BB)-2A-GFP (PX458)	Ran F A et al., Nat Protoc. 2013	Addgene Plasmid # 48138
pCMV-BE3	Komor A et al., Nature. 2016	Addgene Plasmid #73021
BAALC_p.19.NLS.BE3.2xNLS.GFP.PX458	This paper	N/A
Software and algorithms		
GraphPad Prism 8	GraphPad Software Inc.	https://www.graphpad.com/
FlowJo V10	BD	https://www.flowjo.com/
QuantStudio 3D Digital PCR Analysis Suite Software	Thermo Fisher	https://www.thermofisher.com/us/en/home/life-science/pcr/digital-pcr/quantstudio-3d-digital-pcr-system/quantstudio-3d-software.html
Connectivity map (CMAP)	CLUE platform	https://clue.io/cmap
Feature Extraction Software	Agilent Technologies	https://www.agilent.com/en/product/mirna-microarray-platform/mirna-microarray-software/feature-extraction-software-228496
Agilent Genomic-Workbench	Agilent Technologies	https://www.agilent.com/en/product/cgh-cgh-snp-microarray-platform/cgh-cgh-snp-microarray-software/agilent-genomic-workbench-228497
CRISPOR	Concordet J et al., Nucleic Acid Research. 2018	http://crispor.tefor.net
STAR v2.4.2a	Dobin A et al., Bioinformatics. 2013	https://github.com/alexdobin/STAR
IGV v2.3.67	Broad Institute	http://software.broadinstitute.org/software/igv/
Samtools v1.1	Li et al., 2009	http://www.htslib.org/
R	The R Project for Statistical Computing	https://www.r-project.org/
RStudio	RStudio	https://www.rstudio.com/
GSEA	Broad Institute	https://www.gsea-msigdb.org/gsea/index.jsp
DESeq2	Love MI et al., Genome Biology. 2014	https://bioconductor.org/packages/release/bioc/html/DESeq2.html
eXpression2Kinases	Clarke D J et al., Nucleic Acids Res. 2018	https://maayanlab.cloud/X2K/

RESOURCE AVAILABILITY

Lead contact

Further information and requests for other reagents may be directed to, and will be fulfilled by, the Lead Contact, Prof. Dr. Julia Skokowa (Julia.Skokowa@med.uni-tuebingen.de).

Materials availability

All unique/stable reagents generated in this study are available from the Lead Contact with a completed Materials Transfer Agreement.

Data and code availability

RNA-seq data have been deposited to the ArrayExpress database at EMBL-EBI (https://www.ebi.ac.uk/arrayexpress/) under accession number E-MTAB-10162.

EXPERIMENTAL MODEL AND SUBJECT DETAILS

iPSC lines

CN and CN/AML patient samples for reprogramming were received from Severe Chronic Neutropenia International Registry (SCNIR), Hannover, Germany. Informed written consent was obtained from all participants of this study. The experiments involving human inducible pluripotent stem cells (iPSCs) were performed with the approval obtained from the Ethical Review Board of the Medical Faculty, University of Tübingen.

Generation of iPSC

Peripheral blood mononuclear cells (PBMNCs) or bone marrow mononuclear cells (BMMNCs) from 2 male CN/AML patients at different stages of leukemic transformation and male healthy donors were reprogrammed using Oct4, Sox2 and KLF4 (OSK) lentivirus (pRRL.PPT.SF.hOct34.hKlf4.hSox2.i2dTomato.pre.FRT, kindly provided by A. Schambach, MHH Germany). Additional mutations in *CSF3R* or *RUNX1* were introduced using CRISPR/Cas9 gene-editing, if not already obtained by reprogramming. iPSCs were cultured on SNL-feeder cells (Public Health England) for general maintenance or feeder-free on Geltrex with StemFlex medium (Thermo Fisher Scientific) for further gene-editing experiments.

METHOD DETAILS

Reprogramming of PBMNCs

$1.5x10^6$ PBMNCs were cultured for 6 days in $CD34^+$ cells expansion medium (Stemline II medium, Sigma-Aldrich) supplemented with 10% FCS, 1% Pen/Strep, 1% glutamine and cytokines: IL-3 (20 ng/ml), Il-6 (20 ng/ml), TPO (20 ng/ml), SCF (50 ng/ml) and FLT3L (50 ng/ml). All cytokines were purchased from R&D Systems. After 1 week, cells were transferred to Retronectin (Clontech)-coated 12-well plates together with OSK lentiviral supernatant at a multiplicity of infection (MOI) of 2. Four days later, cells were seeded on SNL-feeder and cultured in a 1:1 mixture of iPSC-medium and $CD34^+$ cell expansion medium supplemented with 2 mM valproic acid and 50 μg/ml Vitamin C. Medium was gradually changed to iPSCs medium only. First iPSCs colonies appeared approximately three weeks after initiation of reprogramming.

Sequencing of iPSCs

Genomic DNA of iPSCs was isolated using Nucleo-Spin Tissue Kit (Machery-Nagel) and DNA regions for sequencing were amplified using the following primers: *RUNX1*-F 5′-ACATCCCTGATGTCTGCATTTGTCC-3′, *RUNX1*-R 5′-TGTGGGTTTGTTGCCATGAAACGTG-3′, *ELANE*-F 5′-CGCCCTGAGCCTTGGTGACG-3′, *ELANE*-R 5′-AGCCACGGTGCCTGTTGCTG-3′, *CSF3R*-F 5′-ATGGCATGTGTCAGGCATGT-3′, *CSF3R*-R 5′-AGTCACAGCGGAGATAGTGC-3′. Sanger Sequencing was performed by GATC Biotech.

iPSCs culture

iPSCs were maintained on mitomycin-C treated SNL-feeder cells (Public Health England) in iPSC-medium consisting of DMEM F12 (Sigma-Aldrich) supplemented with 20% Knockout Serum Replacement (Invitrogen), 30 ng/ml bFGF (Peprotech), 1% non-essential amino acids solution (Invitrogen), 100 μM 2-mercaptoethanol and 2 mM L-glutamine. iPSC-medium was replaced every day. For CRISPR/Cas9 gene-editing experiments and expansion of single cell derived clones, iPSC lines were cultured on Geltrex with StemFlex medium (Life Technologies).

CRISPR/Cas9 gene-editing of iPSC lines

Corresponding sgRNAs (Table S2) were cloned into all-in one pSpCas9(BB)-2A-GFP (PX458) plasmid, a gift from Feng Zhang (Addgene plasmid # 48138) (Ran et al., 2013). CN- and CN/AML iPSC lines were nucleofected with 1-5 μg PX458-sgRNA construct using P3 Primary Cell 4D-Nucleofector X Kit L (Lonza) and 4D Nucleofector (Lonza) or reverse transfected with *Trans*IT®-LT1 Transfection Reagent (Mirus). *BAALC* KO in HD iPSCs was introduced by transfection with cytosine base editor plasmid BAALC_p.19.NLS.BE3.2xNLS.GFP.PX458 which was generated by sticky end cloning of BE3 into PX458 backbone followed by cloning guide RNA sequence BAALC p.19 (Table S2). BE3 insert was isolated from pCMV-BE3 plasmid which was a gift from the David Liu lab (Addgene plasmid # 73021) (Komor et al., 2016). GFP^+ cells were sorted 48 hours post-transfection and cultured on the Geltrex. Single-cell clones were analyzed by Sanger sequencing at the gene-edited target regions. *BAALC* KO in primary CN/AML cells was achieved by nucleofection of Cas9-sgRNA-BAALC-p.20 ribonucleoprotein (RNP) complex using P3 Primary Cell 4D-Nucleofector X Kit L (Lonza) and 4D Nucleofector (Lonza). The RNP nucleofection protocol has been recently published

by our group (Mir et al., 2020). Off-target sites were predicted using https://crispor.tefor.net (Concordet and Haeussler, 2018). The top 3 sites with the highest off-target scores and/or exon localization were selected for Sanger sequencing (Table S3).

EB-based hematopoietic differentiation of iPSCs

iPSCs were dissociated from SNL-feeders or Geltrex (Thermo Fisher Scientific) coated plates using PBS/EDTA (0.02%) for 5 min. EB generation was done via centrifugation of 20,000 cells per EB in 96-well plates using APEL serum-free differentiation medium (StemCell Technologies, Inc.) supplemented with bFGF (20 ng/μl) and ROCK Inhibitor Y-27632 dihydrochloride (Tocris). Next day, BMP4 (40 ng/ml) (R&D Systems) was added to the culture to induce mesodermal differentiation. On day four, EBs were plated on Matrigel-coated 6-well plates (10 EBs/well) in APEL medium supplemented with VEGF (40 ng/ml) (R&D Systems), SCF (50 ng/ml) (Peprotech) and IL-3 (50 ng/ml) (Peprotech). For neutrophilic differentiation, medium was changed 3 days later to fresh APEL medium supplemented with IL-3 (50 ng/ml) and G-CSF (50 ng/ml) (Amgen). First hematopoietic suspension cells appeared on day 12 - 14. Suspension cells were harvested every 3 - 4 days and analyzed starting from day 14 to day 32 (Dannenmann et al., 2020; Lachmann et al., 2015).

Culture of iPSC-derived CD45$^+$CD34$^+$ cells, *de novo* CN/AML cells and AML cells on SL/SL feeder cells and drug treatment

1-3x10^5 iPSC-derived CD45$^+$CD34$^+$ cells, primary CN/AML blasts, or *de novo* AML blasts were cultured on SL/SL feeder cells producing FLT3L (kindly provided by C. Eaves, Vancouver, Canada) in HLTM/Myelocult H5100 medium (StemCell Technologies, Inc.) supplemented with 10^{-6} M hydrocortisone, IL-3 (20 ng/ml), Il-6 (20 ng/ml), TPO (20 ng/ml), SCF (50 ng/ml) and FLT3L (50 ng/ml) for 7 days with medium change every 3 - 4 days. For drug treatment, 1μM AZD-6244, 1 μM CMPD1 or DMSO was added to culture medium and incubated for 7 days with medium change and addition of fresh drugs every 3 days. After 7 days, cell viability was assessed by Trypan blue staining and counting using Neubauer cell counting chamber.

Transduction of CD34$^+$ cells with RUNX1 constructs

CD34$^+$ cells from healthy donors (2 × 10^5/well) were transduced with lentiviral supernatant at a MOI of 5. Lentiviral particles expressed either control plasmid, WT *RUNX1* or two *RUNX1* mutants (p.R139G and p.R174L) cloned into pRRL.PPT.SFFV.i2RFP vector (kindly provided by A. Schambach, MHH, Hannover, Germany). A second transduction was performed the next day. Seventy-two hours post-transduction, GFP-positive cells were sorted and analyzed for *RUNX1* and *BAALC* mRNA expression by qRT-PCR. Vector and primer information is available upon request.

Quantitative RT-PCR

RNA was isolated using RNeasy Micro Kit (QIAGEN). cDNA was prepared from 0.2-1 μg of total RNA using Omniscript RT Kit (QIAGEN). qPCR was performed using SYBR Green qPCR master mix (Roche) and Light Cycler 480 (Roche). Data were analyzed using ddCT-method. Target genes were normalized to *GAPDH* and/or β-Actin as housekeeper genes. qPCR primer information are available upon request.

Western blotting

1x10^6 cells were lysed in 200 μl of 3x Lämmli buffer. Protein was denatured for 10 min at 95°C. 5 μl of cell lysate in the Lämmli buffer was loaded per lane. Proteins were separated on a 12% polyacrylamide gel and transferred on a nitrocellulose membrane (GE Healthcare) (1 hour, 100V, 4°C). Membrane was blocked for 1 hour in 5% BSA/TBST and incubated with primary antibody overnight (at 4°C). The following primary antibody were used: anti-RUNX1/AML1 (Cell Signaling Technology, #4334, 1:500), anti-STAT5a (Cell Signaling Technology, #4807, 1:500) anti-G-CSFR (Santa Cruz Biotechnology, #sc-74026, 1:500), and β-Actin (Cell Signaling Technology, #4970, 1:1000) and anti-BAALC (Santa Cruz Biotechnology, #sc-515606, 1:500). Next, membranes were washed and incubated with secondary HRP-coupled antibody (Cell Signaling Technology, #7076 or #7074, 1:2000) for 1 hour at room temperature. Pierce ECL solution (Thermo Fisher Scientific) and Amersham Hyperfilm (GE Healthcare) were used to detect chemiluminescence signals of proteins.

Alkaline phosphatase assay

iPSC colonies on SNL-feeders at day 10 of culture were washed with PBS, fixed in 4% PFA /10% sucrose in water and stained with NBT/BCIP staining dye (Sigma-Aldrich) for 20 min at RT.

Array-CGH

Array-CGH was performed using the Agilent Human Genome Microarray Kits 2 × 400K (Agilent Technologies). Labeling and hybridization of genomic DNA was performed according to the protocol provided by Agilent. Microarray slides were scanned using an Agilent microarray scanner G2505B at a resolution of 2 μm. For image analysis, default CGH settings of Feature Extraction Software (Agilent Technologies) were applied. Output files from Feature Extraction were subsequently imported into Agilent's CGH data analysis software, Genomic-Workbench. The Aberration Algorithm ADM2 was applied and Aberration Filters were set to: threshold 7.0, at least 4 probes with mean log2 ratio of ± 0.3 leading to a resolution of approximately 20 kb.

Flow cytometry

30,000 suspension cells collected from EB-based hematopoietic differentiation system were used for flow cytometry. For cell surface staining, cells were prepared in PBS/1% BSA containing 0.05% sodium azide and stained with specific mouse monoclonal anti-human antibodies. For detection of hematopoietic progenitor cells, a multicolor FACS antibody panel for 'early-stage' hematopoietic differentiation using the following antibody was applied: CD33-BV421 (BioLegend, BL), CD34-PeCy7 (BD Biosciences, BD), KDR-AF647 (BL), CD43-PE (BD), CD41a-FITC (BD), CD235a-FITC (BD), CD45-BV510 (BL), 7-AAD (BD). For detection of mature myeloid cells, a multicolor FACS antibody panel for 'late-stage' hematopoietic differentiation using the following antibody was applied: CD15-PE (BD), CD16-FITC (BD), CD14-APC-H7 (BD), CD45-BV510 (BL), CD33, BV-421 (BL), 7-AAD (BD). For iPSCs characterization, the stem cell surface markers TRA1-60-PE (eBioscience) and SSEA4-FITC (BD) were analyzed. TRA1-85-APC (R&D Systems) was used as a human iPSCs marker. Anti-mouse IgGk beads (BD) were used for compensation. Samples were analyzed using FACSCanto II (BD) and FlowJo V10 (BD).

Morphological analysis

Wright-Giemsa stained cytospin slides were prepared using Hema-Tek slide stainer (Ames). Hematopoietic cells were classified into 4 groups according to the differentiation state: myeloblast and promyelocyte (MB/ProM), myelocyte and metamyelocyte (Myelo/Meta), band and segmented neutrophils (Band/Seg) and monocytes/macrophages (Mo/MΦ).

Colony forming unit (CFU) assay

10,000 suspension cells from EB-based iPSC hematopoietic differentiation at day 14 were used for CFU-Assay using Methocult H4435 enriched medium (StemCell Technologies). Colonies were counted after 10-14 days.

Digital PCR (dPCR)

Digital PCR was used for absolute endpoint quantification of gene copy numbers using TaqMan SNP genotyping Assay and QuantStudio 3D Digital PCR System (Thermo Fisher Scientific). dPCR was performed according to QuantStudio 3D Digital PCR protocol using genomic DNA. Data was processed using QuantStudio 3D Digital PCR Analysis Suite Software (Thermo Fisher Scientific).

RNA sequencing (RNA-seq)

mRNA was isolated from iPSC-derived $CD45^+CD34^+$ cells using RNeasy Mini- or Micro Kit (QIAGEN). Isolated RNA was quantified (Qubit RNA assay kit, Thermo Fisher Scientific) and quality was assessed using an Agilent 2100 Bioanalyzer. Samples with high RNA integrity number (RIN > 8) were selected for library preparation. Using the TruSeq RNA Sample Prep Kit (Illumina) and 100-500 ng of total RNA for each sequencing library, poly (A) selected single- and pair-end sequencing libraries were generated according to the manufacturer's instructions. All libraries were sequenced by the c.ATG (University Hospital Tuebingen) on an Illumina NextSeq500 platform at a depth of 20–30 million reads each. Read quality of RNA-seq data in fastq files was assessed using FastQC (v0.11.4). Reads were aligned using STAR (v2.4.2a) (Dobin et al., 2013) allowing gapped alignments to account for splicing against a custom-built genome composed of the Ensembl *Homo sapiens* genome v90. Alignment quality was analyzed using samtools (v1.1) (Li et al., 2009) and visually inspected in the Integrative Genome Viewer (v2.3.67). Read counts per gene were extracted with HTSeq count. Genes covered with less than 50 reads were excluded from the analysis leaving > 12,000 genes for determining differential expression between the experimental groups. Normalized read counts for the genes were obtained in DESeq2 package (Love et al., 2014) (v1.8.2) and used for GSEA to find significant differences between groups. Differential expression analysis was performed using the DESeq2 package. Differentially expressed genes with log2FC > 1 or log2FC < −1, adjusted P value < 0.05 were selected for downstream analysis. Heatmaps were produced in Heatmapper (Babicki et al., 2016). Venn diagrams were created in Venny 2.1 (https://bioinfogp.cnb.csic.es/tools/venny/index.html). eXpression2Kinases algorithm (Clarke et al., 2018) was used to identify upstream transcription factors that regulate differentially expressed genes and to perform kinase enrichment assay.

Connectivity map (CMAP) analysis

CLUE platform (https://clue.io/cmap) was used for CMAP analysis to evaluate the gene expression profiles of CN/AML and CN/AML BAALC KO RNA-seq datasets for connectivity to known perturbagens (Subramanian et al., 2017).

Intracellular flow cytometry for phospho-MK2a, phospho-p38, MK2a and p38 in iPSC-derived $CD34^+$ cells

iPSC-derived $CD45^+CD34^+$ cells were fixed for 15 min with 4% PFA and permeabilized for 30 min with 90% Methanol. Intracellular protein staining was performed with the following antibodies for 45 min at RT: phospho-p38 PE (sc-166182), p38 AF 647 (sc-81621), p-MK2a FITC (sc-293139) and MK2a AF 647 (sc-393609). All antibodies were purchased from Santa Cruz Biotechnology. The following isotype controls were used: IgG2a, k PE (Miltenyi Biotec), IgG1k AF 647 (BD) and IgG1k FITC (BD). Samples were measured on BD FACSCanto II.

Histone H3 trimethyl Lys27 ELISA

Total histone protein extracts were isolated from CN and CN/AML iPSC-derived HSPCs of both CN/AML patients using the EpiQuik Total Histone Extraction Kit (Epigentek, catalog # OP-0006). Yield of the total histone protein extraction was measured by Quant-iT Qubit protein assay kit (Thermo Fisher Scientific, catalog # Q33212). We quantified trimethylated lysine 27 in histone H3 (H3K27me3)

using the Histone H3 methylated Lys27 ELISA kit (Active Motif, catalog #53106) according to the standard protocol. The assay was performed in duplicates using 6 μg of total histone protein extract per well.

QUANTIFICATION AND STATISTICAL ANALYSIS

Data are presented as mean ± standard deviation (SD). Comparison of two groups was performed using unpaired t test. Statistical analyses were performed using GraphPad Prism 8 (GraphPad Software Inc.), Microsoft Excel 2010 (Microsoft Corp.) and DESeq2. A p value < 0.05 was considered significant.

F) Mir, P. et al., 2020, *Methods in Molecular Biology*

Chapter 26

Gene Knockout in Hematopoietic Stem and Progenitor Cells Followed by Granulocytic Differentiation

Perihan Mir, Malte Ritter, Karl Welte, Julia Skokowa, and Maksim Klimiankou

Abstract

In this chapter, we present an optimized CRISPR/Cas9 RNP nucleofection approach for gene knockout (KO) in hematopoietic stem and progenitor cells (HSPCs). With experimentally proved active locus-specific sgRNAs, we routinely reach over 80% gene KO in HSPCs, thus avoiding the need for cell sorting or enrichment of targeted cell population. Additionally, we provide a protocol for in vitro granulocytic differentiation of HSPCs after gene KO and detailed description of granulocyte function tests which can be applied to study the effects of a particular gene KO.

Key words Hematopoietic stem and progenitor cells, Gene knockout, CRISPR/Cas9, Single-guide RNA, Ribonucleoprotein, Nucleofection, Granulocytic differentiation

1 Introduction

CRISPR (clustered regularly interspaced short palindromic repeat) DNA editing technology is becoming a revolutionary tool in biotechnology, medical, and biological research. In less than a decade after publishing the critical discovery that CRISPR/Cas9 can be reprogrammed to target a desired DNA locus in bacteria [1], RNA-programmable gene editing has transformed biological research, thanks to its extreme flexibility, efficiency, and ease of use (*see* Chapters 1 and 19). Currently, the most popular choice for genome editing is CRISPR/Cas9 system from *Streptococcus pyogenes*. Briefly, the complex of Cas9 protein and a guide RNA bind to DNA through base complementarity. This binding induces DNA cleavage [2]. Gene KO can be achieved by error-prone DNA repair mechanism called nonhomologous end joining pathway which induces insertions or deletions (indels) at position of the DNA cut site. Precise nucleotide sequence integration in desired

Mouldy Sioud (ed.), *RNA Interference and CRISPR Technologies: Technical Advances and New Therapeutic Opportunities*, Methods in Molecular Biology, vol. 2115, https://doi.org/10.1007/978-1-0716-0290-4_26,

DNA locus can be achieved by exploiting the homology-directed repair pathway.

CRISPR/Cas9 system is widely used because of the short and simple NGG protospacer-adjacent motif (PAM) sequence, the best characterized on- and off-target profiles, availability of online tools to assist in performing CRISPR/Cas9 experiments, and its existence in different formats (plasmid, RNA, protein) from an expanding number of companies. Over the past few years, many engineered Cas9 variants have been developed. Different Cas9 variants have been generated (e.g., high-fidelity Cas9 variants including eSpCas9 [3], SpCas9-HF1 [4], and HypaCas9 [5], catalytically dead Cas9 (dCas9) [6], Cas9 nickase [7], and Cas9 variant with expanded PAM recognition site [8]). This discovery enables targeted genome modification with unprecedented flexibility and efficiency (*see* Chapter 21).

Another critical part of CRISPR/Cas9 system is a guide RNA. Guide RNA can be used as single-guide RNA (sgRNA) or as a two-component system which includes CRISPR RNA (crRNA) and trans-activating CRISPR RNA (tracrRNA). Additionally, chemical modifications of sgRNA can substantially increase genome editing efficiency in human primary cells ([9], *see* Chapter 2). Availability of highly purified Cas9 protein and chemically modified guide RNA with enhanced stability and low immune-stimulatory properties from commercial vendors makes nucleofection of CRISPR/Cas9 RNP complex the cost-effective and efficient way of generating targeted gene KOs (*see* Chapter 26).

The advantages of CRISPR/Cas9 RNP complex nucleofection over transfection with Cas9 and sgRNA DNA (plasmid) or RNA or virus-assisted delivery are as follows: it is a nontoxic, well-tolerable genome editing approach with short but high activity window, short persistence of RNP complex in the nuclei reduces probability of cuts at off-target DNA loci, CRISPR/Cas9 RNP complex does not require cellular transcription or translation machinery, no/low induction of inflammatory or cell response against foreign DNA and RNA after RNP complex nucleofection, and visualization of RNP by labeling of Cas9 protein [10].

CRISPR/Cas9 gene KO efficiency depends on multiple factors. Among the most important is the on-target score of sgRNA. Although, a broad range of prediction algorithms and methods for on-target sgRNA activity estimation are available online [11–13], the functional sgRNA validation after in silico on-target activity analysis remains the most comprehensive way to identify a highly active locus-specific sgRNA. Usually, 3–5 sgRNAs are tested per gene or gene locus. In our hands, sgRNA efficiencies have varied from 10% to 99% of edited allele. The second most important factor for successful gene KO is the usage of a sufficient number of viable HSPCs (too less or too many cells per nucleofection reaction may lead to suboptimal results). Preliminary tests may help to determine

the optimal amount of CRISPR/Cas9 RNP complex and the number of HSPCs used for nucleofection.

After successful induction of gene KO, HSPCs can be further differentiated in vitro to cells of the myeloid lineage using appropriate culture conditions. If myeloid differentiation is not disturbed by gene KO, then these cells are expected to demonstrate upregulation of myeloid specific surface markers, morphological maturation, and recapitulation of granulocyte functions. Thus, the coupling of targeted gene KO approach via CRISPR/Cas9 RNP nucleofection with a protocol of granulocytic differentiation of HSPCs and granulocyte function tests allows investigation of the role of certain genes in hematopoiesis in a fast and robust way. It should be noted that the entire protocol can be completed in 3 weeks (Fig. 1).

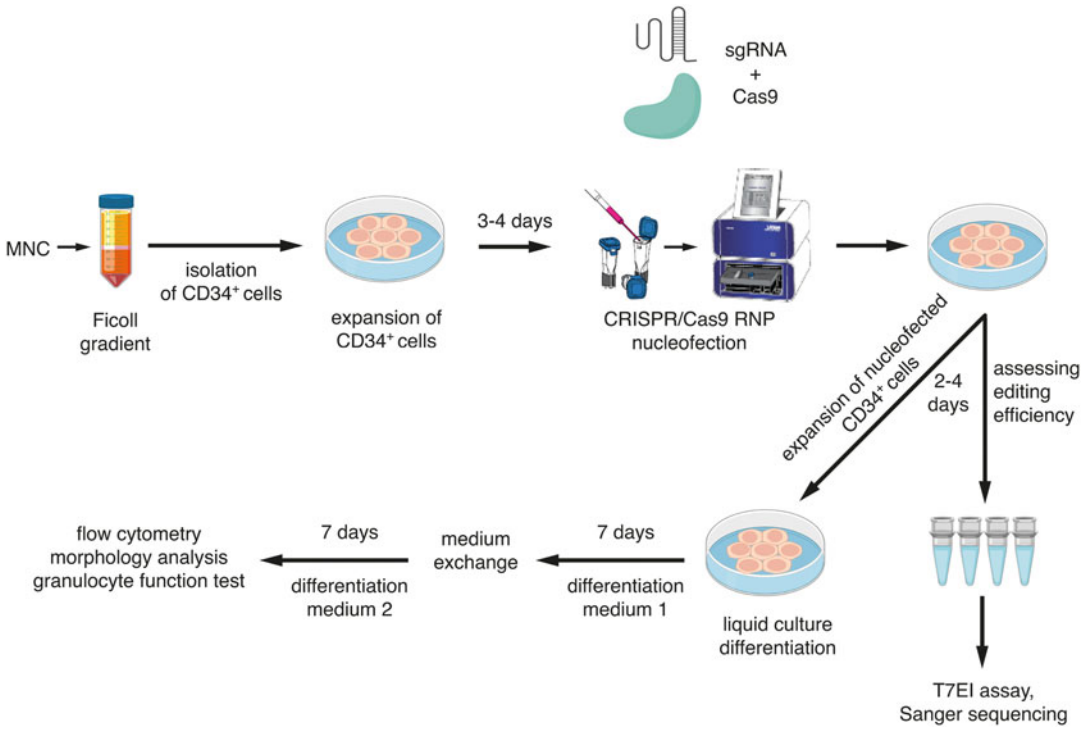

Fig. 1 Scheme of gene KO in HSPCs followed by in vitro granulocytic differentiation. $CD34^+$ cells are isolated from BM or mobilized blood MNCs and expanded in vitro for 3–4 days. After expansion $CD34^+$ cells are nucleofected with CRISPR/Cas9 RNP using the Lonza 4D nucleofection system. Knockout HSPCs are differentiated in vitro toward granulocyte lineage for 14 days and then analyzed by flow cytometry, morphologic analysis, and granulocyte function tests. Gene editing efficiency is assessed 2–4 days after nucleofection by T7EI assay and/or Sanger sequencing. Indel efficiency is determined by TIDE or ICE analysis web tools

2 Materials

All reagents, lab equipment, and web tools described in this section have been successfully tested by us, but other commercially available equivalents can be alternatively used after some optimization steps.

2.1 $CD34^+$ Isolation and Expansion

1. Bone marrow (BM) or mobilized blood from healthy individuals or patients as source for $CD34^+$ cells.
2. Ficoll-Paque density gradient media (density: 1.077 g/mL) for isolation of BM or peripheral blood mononuclear cell (BMMNCs or PBMNCs, respectively).
3. Human CD34 MicroBead Kit for magnetic beads-based isolation of $CD34^+$ cells from BMMNCs or PBMNCs.
4. Cell freezing medium: PSC cryopreservation medium or 90% FCS supplemented with 10% DMSO.
5. $CD34^+$ expansion medium: Stemline II Hematopoietic Stem Cell Expansion medium supplemented with 10% FCS, 1% L-glutamine, 1% penicillin/streptomycin, and a human recombinant cytokine cocktail consisting of 20 ng/mL IL-3, 20 ng/mL IL-6, 20 ng/mL TPO, 50 ng/mL SCF, and 50 ng/mL FLT-3L.
6. 24- or 48-well cell culture plates.

2.2 CRISPR/Cas9 RNP Nucleofection

1. Chemically synthetized CRISPR/Cas9 single-guide RNA with 2′-*O*-methyl 3′phosphorothioate modifications at the 3′ and 5′ termini produced at small scale 15–20 nmol. For selection of the most efficient sgRNA, it is recommended to order and test 3–5 sgRNAs per locus.
2. Alt-R® S.p. Cas9 Nuclease V3 or Alt-R® S.p. HiFi Cas9 Nuclease V3 (IDT).
3. Amaxa 4D-Nucleofector™ System.
4. P3 Primary Cell 4D-Nucleofector Kit.
5. RNase-free aerosol-resistant pipette tips.
6. RNAse-free SafeSeal microcentrifuge tubes.
7. 1x TE Buffer pH 7.5.

2.3 Estimation of Gene-Editing Efficiency

1. DNA extraction kit.
2. Nanodrop or Qubit device and Qubit dsDNA High Sensitivity Assay Kit.
3. PCR: GoTaq Hot Start DNA Polymerase Kit, PCR primers for amplification of genome locus of interest.
4. PCR Nucleotide Mix.

5. T7 Endonuclease I Assay (T7EI) is a quick and cheap method of gene editing efficiency estimation which requires T7 Endonuclease I and NEB buffer 2.
6. PCR product purification kit or enzymatic cleanup using ExoSAP [14].
7. Sanger sequencing by commercial service provider or in-house Sanger sequencing facility.

2.4 Analysis of Granulocytic Differentiation

1. Colony-forming unit (CFU) assay: MethoCult™ Enriched (STEMCELL Technologies), IMDM with 2% FCS (STEMCELL Technologies), Antibiotic-Antimycotic Solution (Sigma Aldrich), 35 mm culture dishes, sterile 16 gauge needles, 1.5 in. long with a metal Luer Lock hub (STEMCELL Technologies).
2. Liquid culture differentiation: Differentiation medium 1 for day 0–7 consists of RPMI 1640 supplemented with 10% FCS, 1% penicillin/streptomycin, and human recombinant cytokines: 5 ng/mL SCF, 5 ng/mL IL-3, 5 ng/mL GM-CSF, and 10 ng/mL G-CSF. Differentiation medium 2 for day 7–14 consists of RPMI 1640 supplemented with 10% FCS, 1% penicillin/streptomycin, and 10 ng/mL G-CSF.
3. Morphology analysis: Shandon Cytospin centrifuge, Cytospin microscope slides, May–Grünwald, and Wright–Giemsa staining solutions.
4. FACS staining: antihuman CD45, antihuman CD34, antihuman CD33, antihuman CD11b, antihuman CD14, antihuman CD15, antihuman CD16 antibodies, PBS supplemented with 2% FCS and 0.02% sodium azide.

2.5 Analysis of Granulocyte Functions

1. Chemotaxis: 24-well Transwell reaction plates, inserts with 5 μm pore size, *N*-formyl-Met-Leu-Phe (fMLP), RPMI 1640 medium, bovine serum albumin (BSA), 5 mL FACS tubes, flow cytometer.
2. Phagocytosis: fluorescein-conjugated *Staphylococcus aureus* BioParticles, RPMI 1640 without Phenol red, 5 mL FACS tubes, flow cytometer capable of measuring FITC signal.
3. Netosis: IncuCyte® Live Cell Imaging system, Phorbol 12-myristate 13-acetate (PMA), RPMI 1640 without Phenol red, BSA, 96-well plate flat bottom, Sytox green dye, 0.001% Poly-L-Lysine Solution.
4. ROS production: ROS-Glo H_2O_2 Assay, bioluminescence reader, and 96-well plates.

3 Methods

3.1 sgRNA Design

1. Usually, the design of sgRNAs is performed with the assistance of online web tools. We routinely use the DESKGEN cloud platform (www.deskgen.com) or Benchling (www.benchling.com). Both online resources require a free registration.
2. For gene KO, make sure to target all possible isoforms of the gene of interest or design multiple sgRNAs (*see* **Note 1**).
3. Select all sgRNA target sites around the ideal position, and evaluate on-target and off-target prediction scores (*see* **Note 2**).
4. Choose from 3 to 5 sgRNAs per locus with the lowest off-target and highest on-target prediction score.
5. Test sgRNAs, as described in the following sections.

3.2 PCR Primers for Assessing CRISPR/Cas9 Gene-Editing Efficiency

1. Primer-BLAST (http://www.ncbi.nlm.nih.gov/tools/primer-blast) is a suitable online tool to design PCR primers [15] for assessing CRISPR/Cas9 gene editing efficiency by sequence trace decomposition.
2. Design PCR primers to ideally have a PCR product length of 700 bp.
3. To allow correct estimation of gene editing efficiency by sequence trace decomposition, the projected Cas9 cut site should be located around 200 bp away from reverse and forward primers used for sequencing.

3.3 $CD34^+$ Isolation and Expansion

1. Pipet 15 mL Ficoll-Paque medium into a 50 mL tube.
2. Dilute BM or mobilized PB sample 1:2 with PBS and carefully layer it onto the Ficoll-Paque medium (*see* **Note 3**).
3. Centrifuge at 500 × *g* for 25 min at room temperature (RT) with the centrifuge brake set off.
4. The mononuclear cell fraction is located in the interphase. Transfer the complete interphase layer to a sterile tube and wash the cells twice with 30 mL ice-cold PBS by centrifuging at 300 × *g* for 8 min at 8 °C.
5. Resuspend cells in ice-cold PBS and the determine cell count of BMMNCs or PBMNCs (*see* **Note 4**).
6. Resuspend cells in 300 μL MACS buffer. Use 200 μL FcR blocking and 100 μL CD34 microbeads for up to 10^8 cells (*see* **Note 5**).
7. Mix gently and incubate for 30 min at 4 °C in the refrigerator.
8. Wash cells with 5–10 mL MACS buffer by centrifugation at 300 × *g* for 10 min. Remove supernatant.

9. Resuspend cells in 500 μL MACS buffer.
10. Place the separation column in the magnetic field.
11. Rinse the column with 3 mL MACS buffer if you use a LS column, and if you use MS column, rinse with 500 mL prior to use (*see* **Note 6**).
12. Apply cell suspension onto the column (*see* **Note 7**). If desired, collect the CD34-negative cells in the flow-through fraction.
13. Wash LS column three times with 3 mL MACS buffer (if you use MS column, wash with 500 μL three times).
14. Remove column from magnetic field and put it onto a 15 mL tube.
15. Pipet 3 mL of MACS buffer on the column (1 mL for MS column) and flush out the cells by pushing the plunger into the column.
16. Determine number of $CD34^+$ HSPCs (*see* **Note 8**).
17. Either use cells freshly for gene editing experiment or freeze them for long-term preservation.
18. Perform cryopreservation in either 0.5 mL PSC cryopreservation medium or in 1 mL 90% FCS supplemented with 10% DMSO.
19. Defreeze $CD34^+$ HSPCs in a pre-warmed standard medium for suspension cells (e.g., RPMI 1640 with 10% FCS and 1% penicillin/streptomycin) (*see* **Note 9**). After centrifugation, resuspend the cells in hematopoietic stem cell expansion medium.
20. Culture $CD34^+$ HSPCs in $CD34^+$ expansion medium at a density of 2×10^5/mL (*see* **Note 10**) at 37 °C and 5% CO_2.
21. Determine cell count at day 3 or day 4 after culturing. If cells proliferate and cell viability is higher than 80% (e.g., by trypan blue), perform CRISPR/Cas9 RNP nucleofection.

3.4 CRISPR/Cas9 RNP Nucleofection

1. Assemble Cas9 protein with sgRNA for 30 min at RT. Use 136 pmol Cas9 protein and 330 pmol sgRNA for 1×10^6 cells.
2. For a single Nucleocuvette™ vessel, mix 18 μL of Supplement 1 and 82 μL P3 Primary Cell Nucleofector™ Solution from P3 Primary Cell Nucleofection Kit (Lonza) (*see* **Note 11**).
3. We recommend to use "mock" nucleofected cells to control the effect of nucleofection itself.
4. Add CRISPR/Cas9 RNP complex to the nucleofection buffer mix (*see* **Note 12**).
5. Wash cells once with PBS. Gently remove as much of the supernatant as possible.

6. Resuspend the cell pellet in the RNP-nucleofection buffer mix and transfer the mixture into the Nucleocuvette™ vessel, avoiding bubbles.
7. Place the Nucleocuvette™ vessel in the retainer of the 4D-Nucleofector X Unit.
8. Select and start the Nucleofector™ program CA-137 (*see* **Note 13**).
9. Carefully transfer the nucleofected cells into $CD34^+$ expansion medium, avoiding repeated aspiration of the sample (*see* **Note 14**). Culture $CD34^+$ cells, as described in Subheading 3.3.
10. After 2–4 days, harvest 1×10^5 cells for DNA isolation to determine the gene editing efficiency.

3.5 Estimation of CRISPR/Cas9 Gene-Editing Efficiency

1. Isolate DNA from harvested cells using the column-based QIAamp DNA Mini Kit according to the manufacturer's protocol and determine the DNA concentration using a Nanodrop or Qubit.
2. Alternatively, for quick estimation of KO efficiency, lyse $0.5–1 \times 10^5$ cells in 25–50 μL of QuickExtract DNA Extraction Solution (Lucigen) and then incubate at 65 °C for 6 min and at 98 °C for 2 min (*see* **Note 15**).
3. Run PCR for target genome locus of interest using the GoTaq Hot Start Polymerase Kit. Per reaction, pipet a master mix consisting of 4 μL of 5x Flexi buffer, 0.5 μL dNTP mix (10 mM each), 1 μL 25 mM $MgCl_2$, 1 μL forward and reverse primer (10 μM each), and 0.125 μL Go-Taq polymerase (5 U/μL). Add 100 ng DNA (or 2–4 μL of QuickExtract DNA Extraction Solution) to the PCR master mix and PCR-grade H_2O to a final volume of 20 μL. The PCR program is as follows: denaturation 1 min at 95 °C, annealing for 1 min at the temperature that is optimal for selected primer pair (usually, it is 5 °C below the Tm of the primers used), and extension 1 min at 72 °C. Repeat PCR cycles for 35 times. A final extension for 5 min at 72 °C is recommended.
4. To quickly estimate gene-editing efficiency, T7EI assay may be performed. T7EI recognizes and cleaves hetero-duplexed DNA (*see* **Note 16**). First, mix 11 μL of PCR product and 2 μL of NEB buffer 2. Anneal PCR sample in thermal cycler using the following hybridization conditions: denaturation at 95 °C for 10 min, annealing at 95–85 °C with ramp rate −2 °C/s followed by second annealing at 85–25 °C with ramp rate −0.3 °C/s. Add 2 μL of T7EI (20 U) to the sample

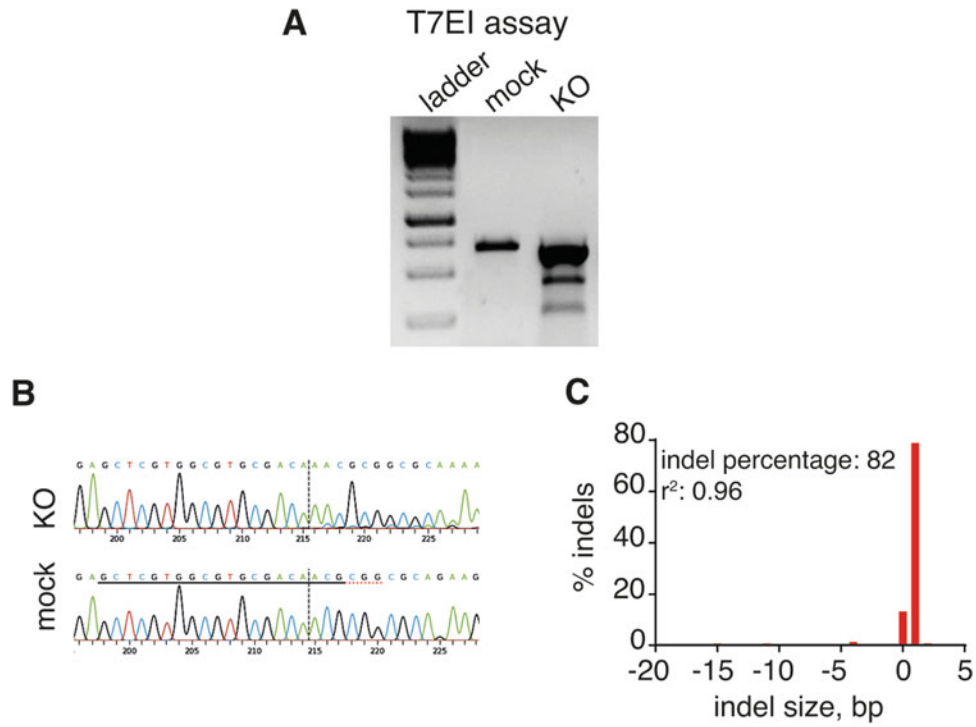

Fig. 2 (**a**) Agarose gel electrophoresis of PCR products after T7EI assay showing two extra bands in KO cells revealed the presence of heteroduplexed DNA resulting from gene editing. (**b**) Representative result of CRISPR/Cas9 RNP-mediated knockout in HSPCs showing Sanger sequencing of total population aligned to sequence track of mock cells. The position of DNA cut is depicted by dashed line. Target DNA sequence for guide RNA is underlined. (**c**) Representative ICE graph reconstructs the spectrum of indels in gene-edited HSPCs. Total editing efficiency is estimated approximately 82% with $r^2 = 0.96$ and one base insertion in the majority of cells. (**b** and **c**) were generated using ICE web tool from Synthego

and incubate at 37 °C for 1 h. Load sample into a 1.5% agarose gel and run it at 85 V for 1 h. Detect PCR products using a gel documentation system. In samples with successful gene editing, two low size extra bands are visible (Fig. 2a). The gene-editing efficiency can be calculated using density profile of the DNA bands by the following formula [16]:

$$\%\ \text{gene modification} = 100 \times (1-(1-\text{fraction cleaved})^{1/2})$$

5. For analysis of gene KO efficiency by sequence trace decomposition, PCR products from mock and CRISPR/Cas9 RNP nucleofected cells should be purified by column-based QIAquick PCR Purification Kit or enzymatic PCR clean-up using ExoSAP. Sanger sequencing traces have to be clean and have sufficient length to allow confident decomposition. Assess the gene modification efficiency using web tools such as TIDE assay [17] (https://tide.deskgen.com) or ICE analysis

(https://ice.synthego.com). For that, upload sgRNA sequence, sequencing traces (.ab1 file) of the mock sample, and the sample after gene editing (Fig. 2b, c).

6. Detailed analysis of mutation composition in the edited cells can be performed by cloning of PCR product into *E. coli* followed by sequencing of single bacteria clones. The most precise method of estimation of mutant allele frequency after gene editing/gene knockout is deep sequencing of PCR product generated from edited DNA locus.
7. Additionally, the analysis of off-target sites may be performed (*see* **Note 17**).

3.6 Characterization of Granulocytic Differentiation of HSPCs

3.6.1 Colony-Forming Unit Assay

1. Resuspend 3–10 × 10^3 cells (*see* **Note 18**) in 300 µL IMDM with 2% FCS, and then add 30 µL Antibiotic–Antimycotic Solution.
2. Add the cell suspension to 3 mL MethoCult™ Enriched medium. Vortex thoroughly, and wait until air bubbles disappear.
3. Seed the cell suspension into two 3.5 cm culture dishes (1.1 mL per dish) using sterile gauge needle.
4. Keep the plates in CO_2 cell culture incubator for 14 days and determine colony numbers and types at day 14 (*see* **Note 19**).

3.6.2 Liquid Culture Granulocytic Differentiation

1. After CRISPR/Cas9 RNP nucleofection, seed the cells at a density of 2 × 10^5/mL. During the first 7 days of differentiation, the cells are kept in differentiation medium 1 with medium exchange every second day (*see* **Note 20**).
2. At day 7, replace medium 1 with differentiation medium 2. The medium has to be changed every second day until day 14.
3. At day 14, perform flow cytometric analysis using antibodies specific for the following hematopoietic/myeloid markers: CD45 (leukocyte marker), CD34 (HSPC marker), CD33 (promyelocyte marker), CD11b (myeloid cell marker), CD14 (monocyte marker), and CD15 and CD16 (neutrophil markers). You may determine neutrophil percentage by gating on neutrophils as follows: $CD45^+CD11b^+CD15^+$, or $CD45^+CD11b^+CD16^+$, or $CD45^+CD15^+CD16^+$ cells.

3.6.3 Evaluation of Cell Morphology

1. Load the Cytoclip™ slide clips by fitting the filter card, the sample chamber, and the glass slide. Place an assemble Cytoclip™ slide clips in the slide clip support plate of the cytospin centrifuge ensuring that the centrifuge is balanced.
2. Pipette 2 × 10^4 cells from liquid culture differentiation (100 µL) into Cytofunnel™.
3. Centrifuge for 3 min at 200 × *g*.

4. Stain cytospin slides for 5 min in May–Grünwald stain, rinse shortly with ddH_2O, and then stain for 10 min in Wright-Giemsa stain. Afterwards rinse shortly with ddH_2O.
5. Determine cell morphology using a microscope.

3.7 Granulocyte Function Tests

3.7.1 Chemotaxis Assay

1. Resuspend the cells at 1×10^6 cells/mL in RPMI with 0.5% BSA and seed 200 μL of the cell suspension on top of the polycarbonate membrane with 5 μm pore size.
2. Fill the bottom well with RMPI 1640 medium supplemented with 0.5% BSA with or without 1 nM fMLP (*see* **Note 21**).
3. Incubate the plate for 2 h at 37 °C, 5% CO_2.
4. Add 70 μL of 50 mM EDTA to the lower chamber and transfer the plate to 4 °C for 30 min.
5. After incubation, remove the inserts, resuspend the cells vigorously, and transfer the cell suspension from the lower chamber into FACS tubes.
6. Count cells on flow cytometer.

3.7.2 Phagocytosis Assay

1. Resuspend 3–10 $\times$ 10^4 cells in 100 μL RPMI 1640 medium supplemented with 2% BSA.
2. Add fluorescent-labeled *Staphylococcus aureus* bioparticles in a ratio of 1:100 per cell and incubate at 37 °C for 2 h. Make sure to have untreated controls to determine background fluorescence.
3. After incubation, wash the cells twice with PBS supplemented with 2% BSA, resuspend cells in PBS with 2% BSA, and then measure the number of FITC-positive cells using f low cytometer.

3.7.3 Netosis Assay

1. Coat the wells of a flat bottom 96-well plate for 30 min at RT with 50 μL/well 0.0001% Poly-L-Lysin solution.
2. Remove the solution after coating and wash twice with PBS.
3. Seed 2×10^4 cells in 100 μL per well, add Sytox Green reagent to a final concentration of 250 nM, and let cells to adhere for 20 min at RT.
4. Carefully add stimulant of choice to induce net release. We used PMA at 100 nM.
5. Place the plates in the IncuCyte® live cell analysis system and perform phase-contrast and GFP imaging every 10 min at 20× magnifications overnight.
6. Analyzed the data on integrated software.

3.7.4 ROS Production

1. Seed the cells at a density of 1×10^5/mL, and then add fMLP at a final concentration of 10 nM to activate ROS production.
2. Incubate for 30 min at 37 °C, 5% CO_2.
3. Measure the level of hydrogen peroxide (H_2O_2) ROS by the ROS-Glo H_2O_2 Assay Kit according to manufacturer's protocol.

4 Notes

1. The preferred localization of guide RNA binding site for introduction of KO by CRISPR/Cas9 system is the first exon, which is present in all coding RNA transcripts. It is important to make sure that the selected DNA sequence is unique, thus reducing the probability of multiple binding of guide RNA to human genome.
2. Benchling and DESKGEN web sites provide on-target and off-target scores for every designed protospacer sequence. For comprehensive analysis of potential off-target sites, a bioinformatics-based tool, COSMID (CRISPR Off-target Sites with Mismatches, Insertions, and Deletions, https://crispr.bme.gatech.edu) [18], may be used. Additionally, calculation of microhomology-associated score can be helpful for the estimation of frequency of undesired in-frame deletion and selection of the gene locus with high out-of-frame score. Microhomology-Predictor tool [19] is available under http://www.rgenome.net/mich-calculator.
3. When layering the PB or BM sample onto Ficoll-Paque medium, pipet it gently to avoid mixing of medium and diluted BM/mobilized blood sample.
4. In case of cells clumps, use a nylon mesh (pre-separation filter with 30 μm, Miltenyi) to remove cell clumps prior to microbead labeling, to avoid a clogged column.
5. You may scale up or down the amount of beads and FcR blocking reagent, according to the cell number.
6. For 1×10^8 PBMNCs or BMMNCs, use either MS or LS columns.
7. For each step, wait until the column reservoir is empty before proceeding to the next step. At the same time, do not let the column to dry out.
8. We recommend to check the isolated $CD34^+$ cell fraction for its purity by staining the cells with an anti-CD34 antibody and flow cytometric analysis before proceeding with gene editing experiments.

9. Hematopoietic stem cell medium and cytokines are expensive cell culture reagents. RPMI 1640 cell medium or other equivalents may be used for the defreezing of $CD34^+$ cells with no adverse effects for the cells.
10. $CD34^+$ HSPCs proliferate better in a dense cell culture with close cell-to-cell contact. Do not seed them with a density lower than 2×10^5/mL.
11. For testing several sgRNAs, you may use the Lonza 16-well Nucleocuvette™ strip to nucleofect 1–10×10^5 cells in a total volume of 20 μL. This way is cost-effective for saving CRISPR/Cas9 RNP and valuable primary cells.
12. The total volume of RNP-nucleofection buffer mix should not exceed 110 μL for nucleofection in the Nucleocuvette™ vessel.
13. Optional: we recommend to let the cells stay for 10 min after nucleofection at RT or in cell culture incubator before transferring them into the cell culture plate.
14. Lonza Nucleocuvette™ vessel may be reused for up to three times. Rinse the cuvettes three times with ddH_2O and once with EtOH. Then expose Nucleocuvette™ vessel with open lid to UV light for at least 30 min.
15. Cell lysis in the QuickExtract DNA Extraction Solution does not allow DNA concentration measurements. Usually, 2–5 μL of the lysate is sufficient for PCR. If PCR yields no product while the positive control shows specific PCR band, then dilute the quicklyzed DNA 1:3–1:5 with the QuickExtract DNA Extraction Solution and repeat PCR.
16. T7EI assay might not give an exact estimation of gene modification efficiency.
17. CRISPR/Cas9 RNP off-targets site analysis may be performed as follows:
    (a) In silico prediction of off-target DNA loci followed by Sanger sequencing of the top predicted off-target sites (low sensitivity, time consuming, low output).
    (b) Custom NGS panel designed for predicted off-target DNA regions (high sensitivity, long turnover time).
    (c) Whole genome or exome DNA sequencing with high depth (can be expensive, especially at the genome level, high quality, and amount of DNA is necessary).
18. $CD34^+$ cells lose stemness during in vitro culture. The number of cells plated for CFU experiment depends on how long cells were kept in culture. If $CD34^+$ cells are cultured more than 1 week, then use 10×10^3 cells per CFU experiment.

19. Place two 3.5 cm CFU dishes and an extra dish with 2 mL of PBS and without a lid in a 10 cm dish to avoid the 3.5 dishes from drying out.
20. It is not recommended to disturb the cells every second day by collecting the whole medium volume. Instead, without disturbing or soaking up the cells, gently remove as much medium as possible and add the same amount of fresh medium to the cells.
21. Each sample needs to be tested with and without chemoattractant (fMLP) to control for spontaneous migration. Additionally, each condition should be conducted at least in technical duplicates.

Acknowledgments

This work was supported by German Cancer Consortium (P.M. and J.S.), DFG (J.S., M.K.), the Fresenius Foundation (M.K.), and the Jose Carreras Leukemia Foundation (M. R.).

References

1. Jinek M, Chylinski K, Fonfara I, Hauer M, Doudna JA, Charpentier E (2012) A programmable dual-RNA-guided DNA endonuclease in adaptive bacterial immunity. Science 337 (6096):816–821
2. Jinek M, East A, Cheng A, Lin S, Ma E, Doudna J (2013) RNA-programmed genome editing in human cells. Elife 2:e00471
3. Slaymaker IM, Gao L, Zetsche B, Scott DA, Yan WX, Zhang F (2016) Rationally engineered Cas9 nucleases with improved specificity. Science 351(6268):84–88
4. Kleinstiver BP, Pattanayak V, Prew MS, Tsai SQ, Nguyen NT, Zheng Z, Joung JK (2016) High-fidelity CRISPR-Cas9 nucleases with no detectable genome-wide off-target effects. Nature 529(7587):490–495
5. Chen JS, Dagdas YS, Kleinstiver BP, Welch MM, Sousa AA, Harrington LB, Sternberg SH, Joung JK, Yildiz A, Doudna JA (2017) Enhanced proofreading governs CRISPR-Cas9 targeting accuracy. Nature 550 (7676):407–410
6. Qi LS, Larson MH, Gilbert LA, Doudna JA, Weissman JS, Arkin AP, Lim WA (2013) Repurposing CRISPR as an RNA-guided platform for sequence-specific control of gene expression. Cell 152(5):1173–1183
7. Mali P, Aach J, Stranges PB, Esvelt KM, Moosburner M, Kosuri S, Yang L, Church GM (2013) CAS9 transcriptional activators for target specificity screening and paired nickases for cooperative genome engineering. Nat Biotechnol 31(9):833–838
8. Hu JH, Miller SM, Geurts MH, Tang W, Chen L, Sun N, Zeina CM, Gao X, Rees HA, Lin Z, Liu DR (2018) Evolved Cas9 variants with broad PAM compatibility and high DNA specificity. Nature 556(7699):57–63
9. Hendel A, Bak RO, Clark JT, Kennedy AB, Ryan DE, Roy S, Steinfeld I, Lunstad BD, Kaiser RJ, Wilkens AB, Bacchetta R, Tsalenko A, Dellinger D, Bruhn L, Porteus MH (2015) Chemically modified guide RNAs enhance CRISPR-Cas genome editing in human primary cells. Nat Biotechnol 33 (9):985–989
10. Nasri M, Mir P, Dannenmann B, Amend D, Skroblyn T, Xu Y, Schulze-Osthoff K, Klimiankou M, Welte K, Skokowa J (2019) Fluorescent labeling of CRISPR/Cas9 RNP for gene knockout in HSPCs and iPSCs reveals an essential role for GADD45b in stress response. Blood Adv 3(1):63–71
11. Doench JG, Fusi N, Sullender M, Hegde M, Vaimberg EW, Donovan KF, Smith I, Tothova Z, Wilen C, Orchard R, Virgin HW, Listgarten J, Root DE (2016) Optimized sgRNA design to maximize activity and

minimize off-target effects of CRISPR-Cas9. Nat Biotechnol 34(2):184–191

12. Chari R, Mali P, Moosburner M, Church GM (2015) Unraveling CRISPR-Cas9 genome engineering parameters via a library-on-library approach. Nat Methods 12(9):823–826
13. Doench JG, Hartenian E, Graham DB, Tothova Z, Hegde M, Smith I, Sullender M, Ebert BL, Xavier RJ, Root DE (2014) Rational design of highly active sgRNAs for CRISPR-Cas9-mediated gene inactivation. Nat Biotechnol 32(12):1262–1267
14. Kim JB, Blackshaw S (2001) One-step enzymatic purification of PCR products for direct sequencing. Curr Protoc Hum Genet. Chapter 11:Unit 11 16. https://doi.org/10.1002/0471142905.hg1106s30
15. Ye J, Coulouris G, Zaretskaya I, Cutcutache I, Rozen S, Madden TL (2012) Primer-BLAST: a tool to design target-specific primers for polymerase chain reaction. BMC Bioinformatics 13:134
16. Guschin DY, Waite AJ, Katibah GE, Miller JC, Holmes MC, Rebar EJ (2010) A rapid and general assay for monitoring endogenous gene modification. Methods Mol Biol 649:247–256
17. Brinkman EK, Chen T, Amendola M, van Steensel B (2014) Easy quantitative assessment of genome editing by sequence trace decomposition. Nucleic Acids Res 42(22):e168
18. Cradick TJ, Qiu P, Lee CM, Fine EJ, Bao G (2014) COSMID: a web-based tool for identifying and validating CRISPR/Cas off-target sites. Mol Ther Nucleic Acids 3:e214
19. Bae S, Kweon J, Kim HS, Kim JS (2014) Microhomology-based choice of Cas9 nuclease target sites. Nat Methods 11(7):705–706

G) Nasri, M. et al., 2020, *Haematologica*

Ferrata Storti Foundation

Haematologica 2020
Volume 105(3):598-609

CRISPR/Cas9-mediated *ELANE* knockout enables neutrophilic maturation of primary hematopoietic stem and progenitor cells and induced pluripotent stem cells of severe congenital neutropenia patients

Masoud Nasri,[1] Malte Ritter,[1*] Perihan Mir,[1*] Benjamin Dannenmann,[1*] Narges Aghaallaei,[1] Diana Amend,[1] Vahagn Makaryan,[2] Yun Xu,[1] Breanna Fletcher,[2] Regine Bernhard,[1] Ingeborg Steiert,[1] Karin Hähnel,[1] Jürgen Berger,[3] Iris Koch,[3] Brigitte Sailer,[3] Katharina Hipp,[3] Cornelia Zeidler,[4] Maksim Klimiankou,[1] Baubak Bajoghli,[1] David C. Dale,[2] Karl Welte[1,5,§] and Julia Skokowa[1,§]

[1]Department of Oncology, Hematology, Immunology, Rheumatology and Clinical Immunology, University Hospital Tübingen, Tübingen, Germany; [2]Department of Medicine, University of Washington, Seattle, WA, USA; [3]Max Planck Institute for Developmental Biology, Tübingen, Germany; [4]Department of Oncology, Hematology, Immunology and Bone Marrow Transplantation, Hannover Medical School, Hannover, Germany and [5]University Children's Hospital Tübingen, Tübingen, Germany

**MR, PM and BD are co-second authors.*

[§]KW and JS are co-senior authors.

ABSTRACT

Autosomal-dominant *ELANE* mutations are the most common cause of severe congenital neutropenia. Although the majority of congenital neutropenia patients respond to daily granulocyte colony stimulating factor, approximately 15 % do not respond to this cytokine at doses up to 50 μg/kg/day and approximately 15 % of patients will develop myelodysplasia or acute myeloid leukemia. "Maturation arrest," the failure of the marrow myeloid progenitors to form mature neutrophils, is a consistent feature of *ELANE* associated congenital neutropenia. As mutant neutrophil elastase is the cause of this abnormality, we hypothesized that *ELANE* associated neutropenia could be treated and "maturation arrest" corrected by a CRISPR/Cas9-sgRNA ribonucleoprotein mediated *ELANE* knockout. To examine this hypothesis, we used induced pluripotent stem cells from two congenital neutropenia patients and primary hematopoietic stem and progenitor cells from four congenital neutropenia patients harboring *ELANE* mutations as well as HL60 cells expressing mutant *ELANE*. We observed that granulocytic differentiation of *ELANE* knockout induced pluripotent stem cells and primary hematopoietic stem and progenitor cells were comparable to healthy individuals. Phagocytic functions, ROS production, and chemotaxis of the *ELANE* KO (knockout) neutrophils were also normal. Knockdown of *ELANE* in the mutant *ELANE* expressing HL60 cells also allowed full maturation and formation of abundant neutrophils. These observations suggest that *ex vivo* CRISPR/Cas9 RNP based *ELANE* knockout of patients' primary hematopoietic stem and progenitor cells followed by autologous transplantation may be an alternative therapy for congenital neutropenia.

Introduction

Autosomal dominant *ELANE* mutations encoding neutrophil elastase (NE) are the most common cause of severe congenital neutropenia (CN), an inherited bone marrow failure syndrome.[1-3] Patients with CN suffer from severe life-threatening bacterial infections starting early after birth due to the absence or very low numbers of neutrophils in the peripheral blood (usually less than 500 cells per μL[3]).

Correspondence:

JULIA SKOKOWA
Julia.Skokowa@med.uni-tuebingen.de

Received: March 14, 2019.

Accepted: June 21, 2019.

Pre-published: June 27, 2019.

doi:10.3324/haematol.2019.221804

Check the online version for the most updated information on this article, online supplements, and information on authorship & disclosures: www.haematologica.org/content/105/3/598

Hematopoietic stem and progenitor cells (HSPC) of CN patients fail to differentiate into mature neutrophils. This differentiation defect can be partially restored with daily or alternate-day subcutaneous injections of recombinant human granulocyte colony stimulating factor (rhG-CSF) in supra-physiological concentrations.[4] Although rhG-CSF therapy improves the life expectancy and quality of life of CN patients, a subgroup does not respond to rhG-CSF. Additionally, about 15 % of CN patients developed myelodysplastic syndrome (MDS) or acute myeloid leukemia (AML) till now.[3] There is a positive correlation between a rhG-CSF dose required to achieve acceptable neutrophil counts and a cumulative incidence to develop MDS or AML in CN patients.[5] Therefore, CN patients, especially patients who either require high rhG-CSF dosages (above 50 μg/kg/day) and those who do not respond at all, need alternative therapeutic options. Hematopoietic stem cell transplantation (HSCT) would be a treatment of choice in CN patients, but it is associated with many adverse events, *e.g.* acute or chronic graft-*versus*-host-disease (GvHD), life-threatening infections, graft failure or graft rejection. Indeed, the overall survival of CN patients after HSCT is approximately 80 % only.

Recently established new technologies of CRISPR/Cas9-mediated gene editing in mammalian cells[6,7] offer novel therapeutic options, especially for inherited monogenic disorders, including *ELANE* mutations associated CN. In this case, CRISPR/Cas9-mediated gene correction or knockout of the mutant gene in patient`s HSPC *ex vivo* followed by autologous transplantation of the corrected HSPC might be a better treatment than high dose rhG-CSF or allogeneic stem cell transplantation.

ELANE mutations induce unfolded protein response (UPR) and endoplasmic reticulum (ER) stress in HSPC of CN patients that leads to increased apoptosis and defective granulocytic differentiation.[8-11] Therefore, inactivation of *ELANE* using CRISPR/Cas9-mediated knockout may abrogate UPR and ER stress caused by mutated *ELANE* with subsequent restoration of granulocytic differentiation. In support of this hypothesis, we recently identified a β-lactam-based inhibitor of human neutrophil elastase (NE), MK0339, which restored defective granulocytic differentiation of induced pluripotent stem cells (iPSC) and HL60 cells expressing mutated NE.[12] In addition, a recent report by Nayak *et al*. demonstrated the restoration of the *in vitro* granulopoiesis of *ELANE*-CN patient-derived iPSC upon treatment with Sivelestat, another NE-specific small-molecule inhibitor.[12,13] Moreover, the fact that individuals showing mosaicism of inherited *ELANE* mutations have a higher proportion of *ELANE* mutated mature neutrophils hematopoietic cells in the bone marrow than in the blood[14,15] supports the hypothesis that inactivation of *ELANE* mutations will improve neutrophil differentiation.

Another possibility to correct the disease phenotype is the direct correction of the specific gene mutation by the activation of homology-directed repair (HDR) of the mutated gene allele after cutting by CRISPR/Cas9 and co-transfection with a repair template. Most CN patients harbor inherited autosomal dominant missense or frameshift *ELANE* mutations that are distributed throughout all five exons and two introns.[16] Therefore, CRISPR/Cas9-mediated correction of *ELANE* mutations would need to be patient/mutation specific. Since mutated *ELANE* may induce UPR and ER stress in edited cells, the introduction of new indels in the *ELANE* gene during the process of CRISPR/Cas9 based editing may be not beneficial for the integrity of the hematopoietic stem cell (HSC) pool.

The first pre-clinical CRISPR/Cas9-based gene therapy study of common inherited blood disorders, sickle cell disease, and β-thalassemia, was reported.[17,18] In these settings, the β-globin gene locus was inactivated by the introduction of deletions in autologous HSPC by CRISPR/Cas9-mediated gene editing. This was done to mimic the hereditary persistence of fetal hemoglobin mutations in HSC.[17,18]

Here, we describe a CRISPR/Cas9 mediated *ELANE* KO by electroporation of HSPC and iPSC with *ELANE* specific CRISPR/Cas9-sgRNA ribonucleoprotein (RNP) complexes. *ELANE* KO induces granulocytic differentiation of HSPC and iPSC of CN patients harboring *ELANE* mutations without affecting their phagocytic functions. These results suggest that it may be possible to use CRISPR/Cas9 based *ELANE* KO in autologous HSCT as a therapy for *ELANE* associated neutropenia.

Methods

Patients

Three healthy donors and five severe congenital neutropenia patients harboring *ELANE* mutations (*ELANE*-CN) were used in the study. Bone marrow and peripheral blood samples from patients were collected in association with an annual follow-up recommended by the Severe Chronic Neutropenia International Registry. Study approval was obtained from the Ethical Review Board of the Medical Faculty, University of Tübingen. Informed written consent was obtained from all participants of this study.

Cell culture

Human CD34$^+$ HSPC were isolated from bone marrow mononuclear cell fraction using Ficoll gradient centrifugation followed by magnetic bead separation using Human CD34 Progenitor Cell Isolation Kit, (Miltenyi Biotech, #130-046-703). CD34$^+$ cells were cultured in a density of 2 x 10^5 cells/mL in Stemline II Hematopoietic Stem Cell Expansion medium (Sigma Aldrich, #50192) supplemented with 10 % FBS, 1 % penicillin/streptomycin, 1 % L-Glutamine and a cytokine cocktail consisting of 20 ng/mL IL-3, 20 ng/mL IL-6, 20 ng/mL TPO, 50 ng/ml SCF and 50 ng/mL FLT-3L (all cytokines were purchased from R&D Systems). Human induced pluripotent stem cells (iPSC) were cultured on Geltrex LDEV-free reduced growth factor basement membrane matrix (Thermo Fisher Scientific, #A1413201) coated plates in a density of 2 x 10^5 cells/mL in StemFlex medium (Thermo Fisher Scientific, #A3349401) supplemented with 1 % penicillin/streptomycin. HL60 cells were maintained in RPMI-1640 supplemented with 10 % fetal bovine serum (FBS) (Gemini Bio Products, West Sacramento, CA, USA), 2 mM L-glutamine, and 1 % penicillin/streptomycin (Thermo Fisher Scientific) at 37°C and 5 % CO2.

Design of the *ELANE*-specific guide RNA (gRNA)

Specific CRISPR-RNA (crRNA) for the knockout of the ELANE gene (cut site: chr19 [CTGCGCGGAGGCCACTTCTG, +852,969 : -852,969], NM_001972.3 Exon 2, 161 bp; NP_001963.1 p.F54) was designed using the CCTop website.[19]

CRISPR/Cas9-gRNA RNP mediated *ELANE* KO in iPSC and HSPC

Electroporation was carried out using the Amaxa nucleofection system (P3 primary kit, #V4XP-3024) according to the manufacturer's instructions. $1x10^6$ human iPSC or $CD34^+$ HSPC were electroporated with assembled gRNA (8 μg) and Cas9 (15 μg) protein (Integrated DNA Technologies).

Isolation of single cell iPSC clones

8×10^3 human iPSC were plated on Geltrex-coated 10-cm dish in StemFlex medium (Thermo Fisher Scientific, #A3349401) and RevitaCell supplement (Thermo Fisher Scientific, #A2644501). The medium was changed every 24 hours without RevitaCell supplement. On day 7, single iPSC colonies were picked and transferred to the Geltrex-coated 96-well plates (one clone/well).

Colony Forming Unit (CFU) assay

$CD34^+$ cells were resuspended in IMDM supplemented with 2 % FBS (Stemcell Technologies, #07700) and enriched Methocult (Stemcell Technologies, #H4435). The cell suspension was plated on 3.5 cm dishes ($3x10^3$ cells/dish) for 14 days.

In vitro phagocytosis assay

Cells were incubated with or without fluorescein-conjugated *Staphylococcus aureus* BioParticles (Invitrogen, #S2851) at a ratio of 100 particles per cell for two hours at 37°C, washed twice with PBS/ 2 % BSA, resuspended in 300 μL FACS buffer and analyzed by flow cytometry.

Statistical analysis

Differences in mean values between groups were analyzed using two-sided, unpaired Student's *t*-tests using GraphPad Prism software.

Additional Material and Methods are available in the *Online Supplementary Material and Methods*.

Results

Inhibition of *ELANE* expression restored defective granulocytic differentiation of HL60 cell lines expressing endogenous *ELANE* mutations

We created CRISPR/Cas9 edited mutant *ELANE* knock-in HL60 human promyelocytic cell lines expressing either p.P139L or p.C151Y *ELANE* mutations. All-trans retinoic acid (ATRA) induced differentiation of wild-type and

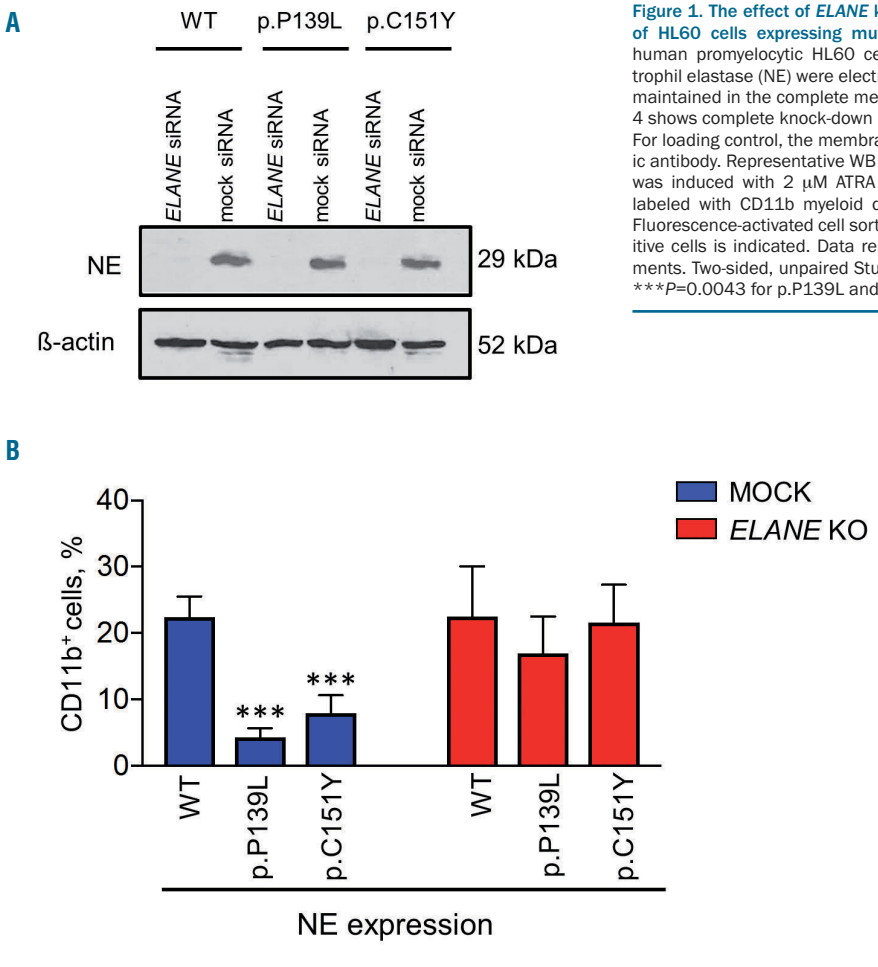

Figure 1. The effect of *ELANE* knock-down on the impaired myeloid differentiation of HL60 cells expressing mutant neutrophil elastase. (A) CRISPR/Cas9 edited human promyelocytic HL60 cells expressing p.P139L and p.C151Y mutant neutrophil elastase (NE) were electroporated with scrambled and anti-*ELANE* siRNA and maintained in the complete medium for five days. Western blot (WB) analysis at day 4 shows complete knock-down of NE detected with an anti-NE monoclonal antibody. For loading control, the membrane was stripped and re-probed with a β-actin-specific antibody. Representative WB membranes are depicted. (B) Myeloid differentiation was induced with 2 μM ATRA (all-trans retinoic acid). After five days, cells were labeled with CD11b myeloid differentiation surface marker and examined using Fluorescence-activated cell sorting (FACS) analysis. The proportion of CD11b-PE positive cells is indicated. Data represent means ± SD from four independent experiments. Two-sided, unpaired Student's *t*-test *P*-values are shown, ***$P<0.0001$ and ***$P=0.0043$ for p.P139L and p.C151Y respectively compared to wild-type (WT).

mutant HL60 clones revealed a typical impairment of granulocytic differentiation capacities in both mutant cell lines, as assessed by the significantly lower proportion of cells expressing CD11b granulocytic differentiation marker in p.P139L and p.C151Y mutant cell lines compared to the wild-type ($P<0.0001$ and $P=0.00043$, respectively) on day 5 of differentiation (Figure 1A-B and *Online Supplementary Figure S1A-C*). These findings are consistent with *ELANE* associated neutropenia patients phenotype.

As a proof-of-principle experiment, we have used RNA interference (RNAi) technology to knock down the expression of the *ELANE* gene in these cell lines. Thereby, we investigated the biological effects of inhibition of mutant NE on the granulocytic differentiation. Indeed, transfection of commercially available siRNA against the exon 4 of *ELANE*, completely knocked down the expression of NE in all cell lines. Production of CD11b positive cells was significantly restored in both mutant cell lines ($P=0.00041$ for p.P139L and $P=0.00048$ for p.C151Y), but not in wild-type cells (Figure 1A-B and *Online Supplementary Figure S1A-C*).

Design and validation of sgRNA targeting *ELANE*

We further generated guide RNA (gRNA) specifically targeting exon 2 of *ELANE* by annealing CRISPR-RNA (crRNA) with trans-activating crRNA (tracrRNA). gRNA was incubated with recombinant Cas9 protein to generate CRISPR/Cas9-gRNA RNP complexes. The gRNA targeting exon 2 of *ELANE* (cut site: chr19[+852.969:-852.969], Figure 2A) was selected to introduce stop-codon mutations and to induce nonsense-mediated mRNA decay (NMD) of *ELANE* mRNA, which is caused by stop-codon or frameshift mutations at the beginning of *ELANE* mRNA. Based on our experimental analysis, the selected gRNA has high on-target activity with low off-target score (*data not shown*). To evaluate inhibition of NE expression by CRISPR/Cas9 RNP mediated targeting of exon 2 of *ELANE*, we generated an *ELANE* KO myeloid cell line

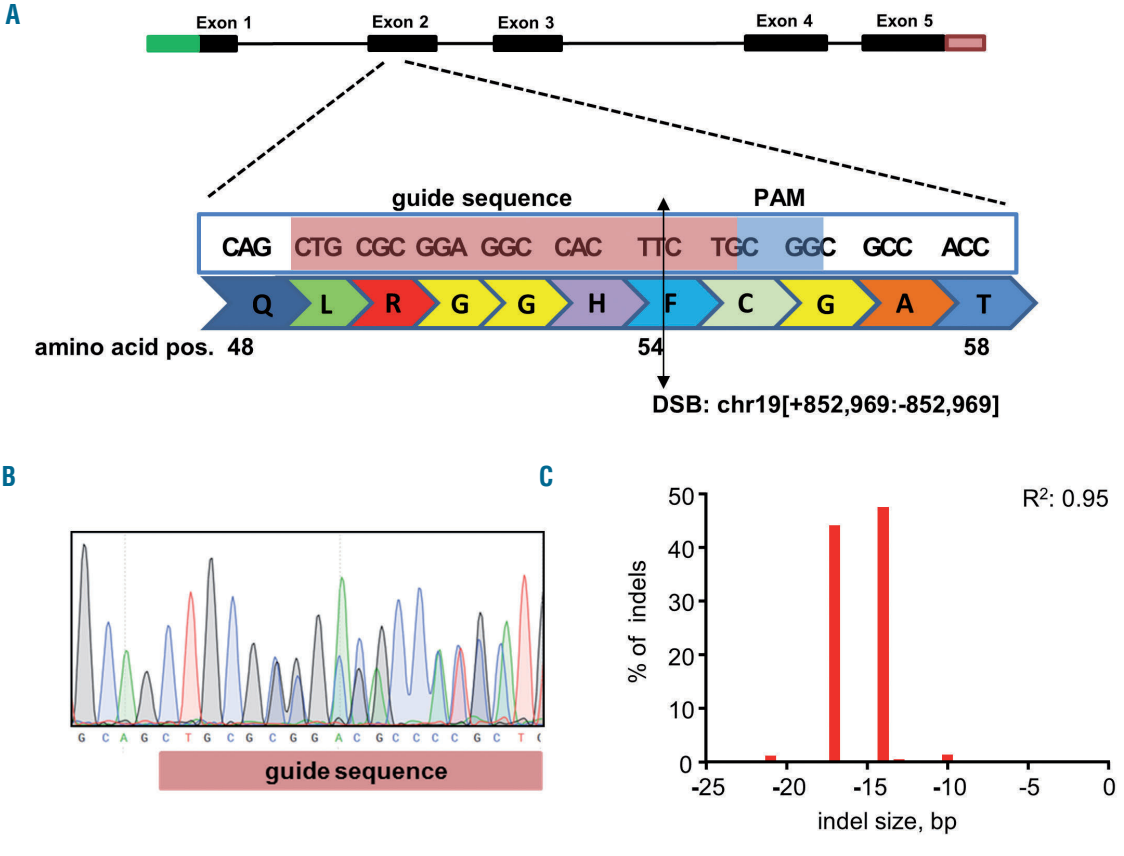

Figure 2. Establishment of CRISPR/Cas9 RNP-mediated *ELANE* knockout in THP-1 cells. (A) *ELANE* was targeted using single guide ribonucleoprotein (RNP)-mediated (highlighted in pink), which creates a double-strand break at NM_001972.2 exon 2, 161 bp after ATG; NP_001963.1, p.F54. Schematic presentation of the cut site by sgRNA. (B-D) Myeloid cell line THP-1 was electroporated with *ELANE*-specific CRISPR/Cas9 RNP. Single cell clones of *ELANE* KO THP-1 cells were generated, as described in the Material and Methods. Representative Sanger sequencing image (B), the bar chart of the TIDE assay (C) and representative Western blotting (WB) images of neutrophil elastase (NE) and α-tubulin protein expression (D) in single cell-derived *ELANE* KO THP-1 cells are depicted.

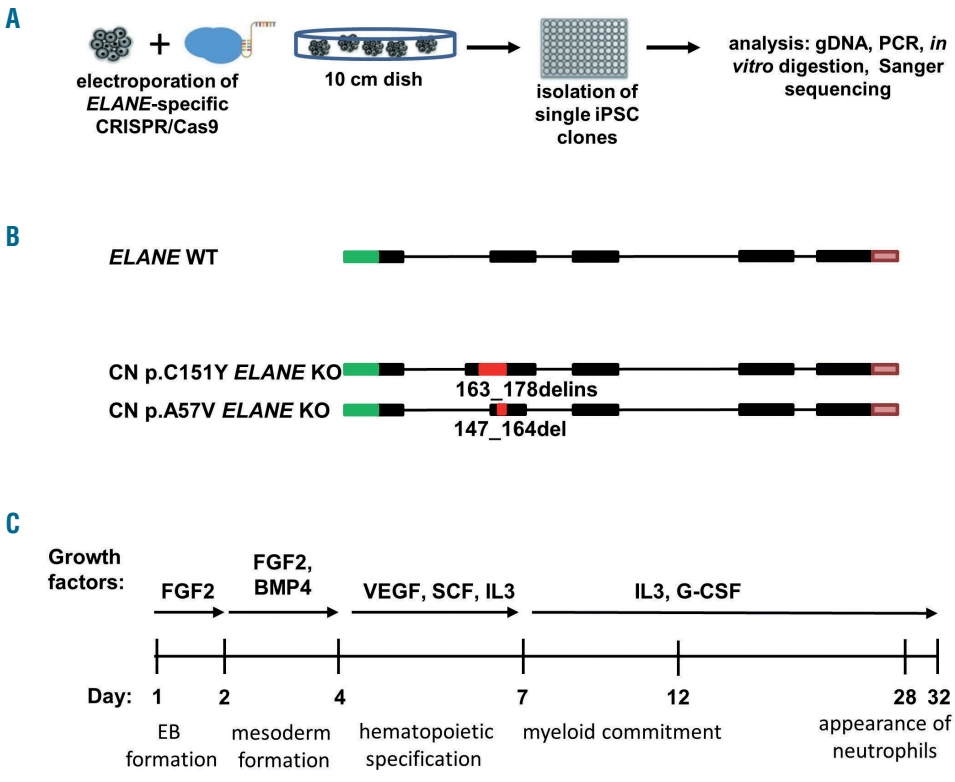

Figure 3. Generation of *ELANE* KO CN iPSC clones. (A) Scheme of the *ELANE*-specific CRISPR/Cas9-gRNA ribonucleoprotein electroporation of induced pluripotent stem cells (iPSC) and generation of *ELANE* KO iPSC clones. Generation of single *ELANE* knockout iPSC clones was made by seeding single iPSC, subsequent picking of each clone and transferring them into 96 well plates. Screening of each iPSC clone was done by Cas9 *in vitro* digestion and Sanger sequencing. (B) Scheme of CRISPR/Cas9 introduced modifications in the *ELANE* gene in iPSC clones of congenital neutropenia (CN) patients. Red inserts show positions of indels in *ELANE* mRNA (NM_001972.2) and numbers refer to bp position after ATG. (C) Scheme of the EB-based hematopoietic/neutrophilic differentiation of iPSC.

THP-1, which has high basal expression levels of *ELANE* and NE. The efficiency of *ELANE* knockout in the total population of edited THP-1 cells was 77 %, as assessed by Sanger sequencing and tracking of indels by decomposition (TIDE) analysis (*data not shown*). The pure *ELANE* KO THP-1 cell clone has compound heterozygosity of 14 and 17 bp deletions on each allele (Figure 2B-C). The NE expression was completely absent in the pure *ELANE* KO THP-1 cell clone, as determined by Western blotting (WB) using anti-NE antibody against the C-terminus of NE protein (Figure 2D, *Online Supplementary Figure S2A-B*). These data suggest that sgRNA targeting *ELANE* that we designed led to a complete loss of NE protein.

Restoration of the *in vitro* granulocytic differentiation in *ELANE*-CN iPSC clones after *ELANE* knockout

We generated iPSC from peripheral blood mononuclear cells (PB MNC) of two *ELANE*-CN patients, harboring *ELANE* mutations p.C151Y or p.A57V (CN p.C151Y iPSC and CN p.A57V iPSC, respectively). Additionally, iPSC of one healthy control (healthy ctrl iPSC) were evaluated. All three iPSC lines expressed elevated mRNA and protein levels of pluripotent stem cell-specific factors, displayed alkaline phosphatase activity and expression of pluripotent embryonic stem cell surface markers (*Online Supplementary Figure 3A-C*).

Next, we used electroporation of iPSC clones with *ELANE*-specific CRISPR/Cas9-sgRNA RNP to generate pure *ELANE* KO CN iPSC clones. For this, electroporated iPSC were seeded on a geltrex coated culture dish and single-cell derived iPSC clones were isolated transferred to geltrex coated 96 well-plates for the subsequent selection of *ELANE* knockout clones (Figure 3A). Confirmed *ELANE* knockout iPSC clones have followed *ELANE* modifications: 274 bp del/ins in CN p.C151Y *ELANE* KO iPSC, and 17 bp del in CN p.A57V *ELANE* KO iPSC (Figure 3B). The editing efficiency of healthy ctrl iPSC was 97 % (*Online Supplementary Figure S4A*), therefore, we used the total population of gene-edited healthy control (ctrl) iPSC for further analysis. We did not detect any off-target activity of the gRNA for the selected cDNA sites in all studied iPSC, as assessed using Sanger sequencing (*Online Supplementary Figure S4B* and *Tables S1, S2*).

Applying a slightly modified *in vitro* embryoid body (EB)-based iPSC differentiation method that allows generation of hematopoietic cells and mature myeloid cells for approximately 30 days,[22,23] we found an increase in the percentage of $CD15^+CD16^+CD45^+$ granulocytes in *ELANE* KO CN-iPSC cell culture, as compared to CN-iPSC. The generation of granulocytes from *ELANE* KO CN-iPSC was comparable to iPSC generated from a healthy donor (Figure 3C, 4A, and *Online Supplementary Figure S5A*). Generation of immature hematopoietic cells ($CD34^+KDR^+$, $CD34^+CD43^+$, $CD45^-CD235^+CD41a^+$ and $CD45^+CD34^+$ cells) and $CD45^+CD33^+$ myeloid progenitor cells in *ELANE* KO CN- and CN-iPSC lines were similar or increased, in comparison to corresponding MOCK treated iPSC lines (*Online Supplementary Figure S6A*).

A CFU assay was performed with $ELANE^{-/-}$ iPSC-derived $CD34^+$ cells from CN patients and showed elevated levels of CFU-G but reduced CFU-M colony numbers, as compared to $CD34^+$ cells derived from MOCK treated CN iPSC clones (Figure 4C). These data suggest that *ELANE* knockout restores granulocytic differentiation in CN.

We did not observe any significant defects in *in vitro* granulocytic differentiation of *ELANE* KO iPSC generated from a healthy donor, as compared to MOCK treated cells (Figure 4A-C, *Online Supplementary Figures S5* and *S6*).

ELANE knockout in HSPC of *ELANE*-CN patients restores diminished granulocytic differentiation

To further evaluate the clinical applicability of *ELANE* KO as a treatment option of *ELANE*-associated CN, we performed CRISPR/Cas9 RNP-mediated gene editing in primary bone marrow CD34$^+$ HSPC of four *ELANE*-CN patients (Table 1) and three healthy donors and differentiated the cells towards neutrophils. *ELANE* knockout in CD34$^+$HSPC was performed by electroporation of human CD34$^+$HSPC with assembled *ELANE* specific sgRNA and Cas9 protein (Figure 5A). The editing efficiency varied between 27 % and 94 % (Figure 5B, *Online Supplementary Figure S7*). As expected, NE levels in neutrophils differentiated from the total population of edited cells were markedly reduced (Figure 5C-D, *Online Supplementary Figure S8A-B*). Moreover, *ELANE* KO leads to elevated granulocytic differentiation, as assessed by the percentage of CD15$^+$CD11b$^+$CD45$^+$ cells (Figure 6A, *Online Supplementary Figure S9A-B*) and morphological examination of cytospin preparations of mature granulocytes generated on day 14 of the *in vitro* granulocytic differentiation using liquid culture (Figure 6B). At the same time, the ratio of *ELANE* KO cells increased from day 7 to day 14 of differentiation (Figure 5B). Simultaneously, the percentage of CD34$^+$CD45$^+$ cells was reduced in *ELANE* KO cells of CN patients, but not in healthy donor cells (*Online Supplementary Figure S10A*). In one patient (CN I120F), no difference in the percentage of CD15$^+$CD11b$^+$CD45$^+$ cells between MOCK and *ELANE* KO samples was observed, but a clear improvement of granulocytic differentiation was detected in cytospin slides. This finding may be explained by relative mild neutropenia (*Online Supplementary Table 3*) and possible expression of CD15 in not fully mature myeloid cells in this patient.

Scanning and transmission electron microscopy revealed that *ELANE* KO cells of both healthy control and one CN patient showed no significant differences in morphology or intracellular structures, compared with MOCK cells of a healthy donor (Figure 6C-D).

Altogether, these data suggest that *ELANE* KO cells have a differentiation advantage over the HSPC carrying mutated *ELANE*.

Neutrophils generated from *ELANE* KO HSPC exhibited unaffected ROS production, phagocytosis and chemotaxis upon activation *in vitro*

We further evaluated *in vitro* activation of neutrophils generated from *ELANE* KO HSPCs in liquid culture for 14 days. We first performed an assessment of H_2O_2 levels (ROS) in fMLP-activated *ELANE* KO neutrophils generated from a healthy donor. We detected no differences between *ELANE* WT and *ELANE* KO neutrophils (Figure 7A).

Phagocytosis was evaluated by incubation of cells with fluorescein-conjugated *Staphylococcus aureus* BioParticles for two hours. Percentage of GFP$^+$ granulocytes that engulfed bacteria were assessed by FACS using gating on granulocyte population in the dot plot of forward-scatter light (FSC) *versus* side-scatter light (SSC) channels. We did not detect any significant differences in phagocytosis of *ELANE* KO neutrophilic granulocytes, as compared to control MOCK cells (Figure 7B). As an independent evaluation of phagocytosis kinetics, we performed live cell imaging of neutrophils incubated with pHrodo Green *E. coli* Bioparticles Conjugate using IncuCyte ZOOM system and observed similar phagocytosis behavior of MOCK and *ELANE* KO neutrophils generated from a healthy donor or one CN patient (Figure 7C).

Chemotactic activity of fMLP-treated neutrophils was also comparable between MOCK and *ELANE* KO groups (Figure 7D).

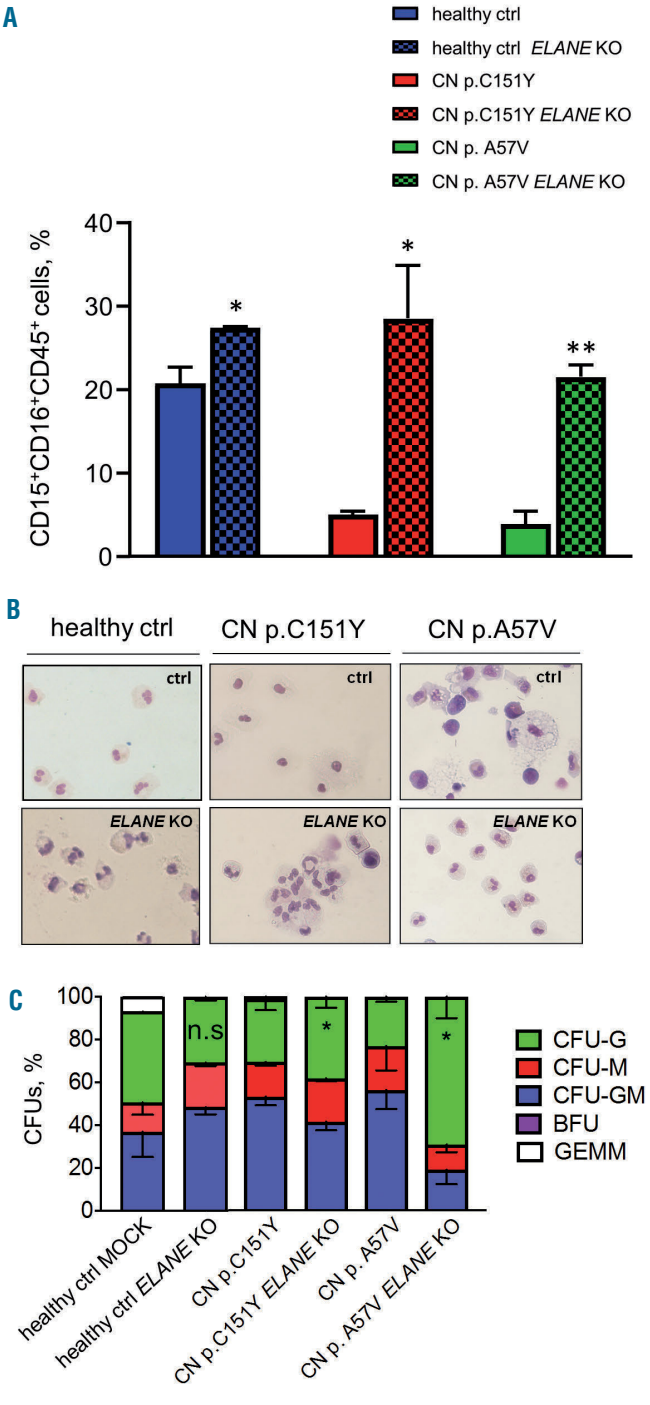

Figure 4. *ELANE* knockout restored granulocytic differentiation of *ELANE*-CN iPSC. (A) Flow cytometry analysis of suspension cells harvested from embryoid body (EB)-based granulocytic cell culture of respective iPSC clones on day 28 or 32 of differentiation. Data represent means ± standard deviation (SD) from two independent experiments. **P*<0.05, ***P*<0.01. (B) Wright-Giemsa staining of cytospin preparations of suspension myeloid cells harvested from iPSC culture at day 28 or 32 of differentiation. Representative images are depicted. (C) Colony-forming unit (CFU) assay of CD34$^+$ cells harvested from EB-based iPSC culture on day 14 of differentiation. Data represent means ± SD from two independent experiments. **P*<0.05.

Unaffected phagocytic activity of *ELANE* KO PMN in zebrafish embryos

To evaluate the phagocytic activity of *ELANE* KO PMN *in vivo*, we transplanted fluorescently labeled polymorphonuclear leukocytes (PMN) generated from *ELANE* KO HD into zebrafish embryos (Figure 8A). PMN were injected into the duct of Cuvier, a wide circulation channel on the yolk sac connecting the heart to the trunk vasculature. Subsequently, Alexa-594-conjugated *Staphylococcus aureus* BioParticles were injected locally in the tail fin close to the caudal vein. Live imaging showed that human neutrophils migrated into the caudal hematopoietic tissue (CHT), which is equivalent to the fetal liver in mammals and provides a human-compatible environment.[24,25] Confocal imaging of this region revealed that most of the *ELANE* KO neutrophils were found inside the perivascular pocket (Figure 8B) and many of them have engulfed bacteria (white arrows in Figure 8B and 8C, *Online Supplementary Movie S1*). Time-lapse *in vivo* imaging of the xenotransplanted embryos also revealed that human *ELANE* KO PMN have the capability to form surface protrusion within the perivascular region (Figure 8D, *Online Supplementary Movie S2*). We could not detect a difference between transplanted human *ELANE* KO and control MOCK PMN in zebrafish embryos (*data not shown*). These observations indicate that human *ELANE* KO PMN are able to migrate and phagocyte *in vivo*.

ELANE KO restores deregulated expression of UPR gene BiP and anti-apoptotic factor Bcl-xl in *ELANE* KO iPSC derived cells of CN patients

We further evaluated the effects of *ELANE* KO on the expression of UPR gene BiP and anti-apoptotic factor Bcl-xl (*Online Supplementary Figure S11*). We analyzed pure *ELANE* KO HSPC (for Bcl-xl) or neutrophils (for BiP) generated from iPSC of two CN patients. We found that *ELANE* KO HSPC express elevated mRNA levels of Bcl-xl and BiP expression was markedly reduced in *ELANE* KO

A

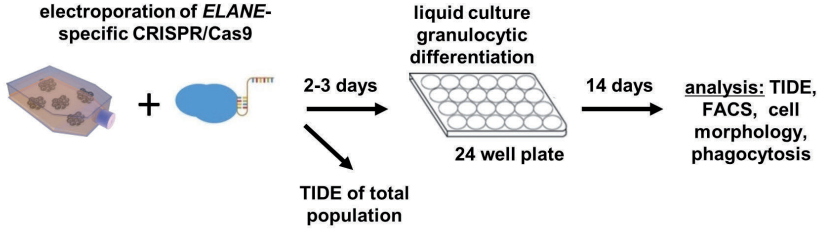

B

Sample, *ELANE* mutation position	Exon	Indel Efficiency, %	
		day 7	day 14
healthy ctrl 1	-	71	69
healthy ctrl 2	-	57	46
healthy ctrl 3	-	86	94
CN p.A57V	Exon 2	52	63
CN p.I120F	Exon 3	81	90
CN p.S126L	Exon 4	45	57
CN p.C223AfsX17	Exon 5	27	37

C

D

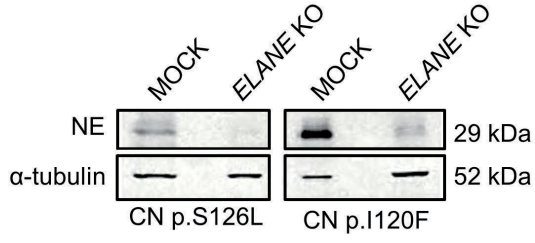

Figure 5. Efficient CRISPR/Cas9 RNP-based *ELANE* knockout in HSPC. (A) Scheme of the generation of *ELANE* KO HSPC using electroporation with *ELANE*-specific CRISPR/Cas9-gRNA ribonucleoprotein (RNP). (B) TIDE results of edited CD34$^+$ HSPC at day 7 and 14 of liquid culture differentiation. (C and D) Hematopoietic stem and progenitor cells (HSPC) of healthy controls (C), or two CN patients (D) were electroporated with *ELANE*-specific CRISPR/Cas9 RNP, on day 14 of culture, cells were lysed in Laemmli buffer and Western blotting (WB) analysis using anti-neutrophil elastase (NE) antibody against C-terminus of NE was performed, staining with α-tubulin antibody was used as loading control. Representative WB images of cells from two independent experiments are depicted.

PMN, compared to cells carrying mutated *ELANE*. As expected, *ELANE* mRNA levels were severely diminished in *ELANE* KO cells (*Online Supplementary Figure S11*).

Discussion

The majority of patients suffering from congenital neutropenia respond well to daily treatment with rhG-CSF leading to a normal quality of life. However, in the last 25 years, we learned that CN is a preleukemic syndrome and that approximately 15 % of patients do not respond to even ultra-high dosages (>50 μg/kg/d) of rhG-CSF. Therefore, we are searching for other treatment modalities for CN patients that may prevent leukemic transformation and may be useful for those who are requiring high dosages of rhG-CSF or not responding at all to rhG-CSF. For these patients, the only available treatment is stem cell transplantation with the risk of transplant-associated adverse events such as acute or chronic GvHD.

In the present study, we described for the first time the establishment of an *in vitro* cellular model of CRISPR/Cas9 mediated gene therapy of CN associated with autosomal dominant *ELANE* mutations, the most frequent cause of

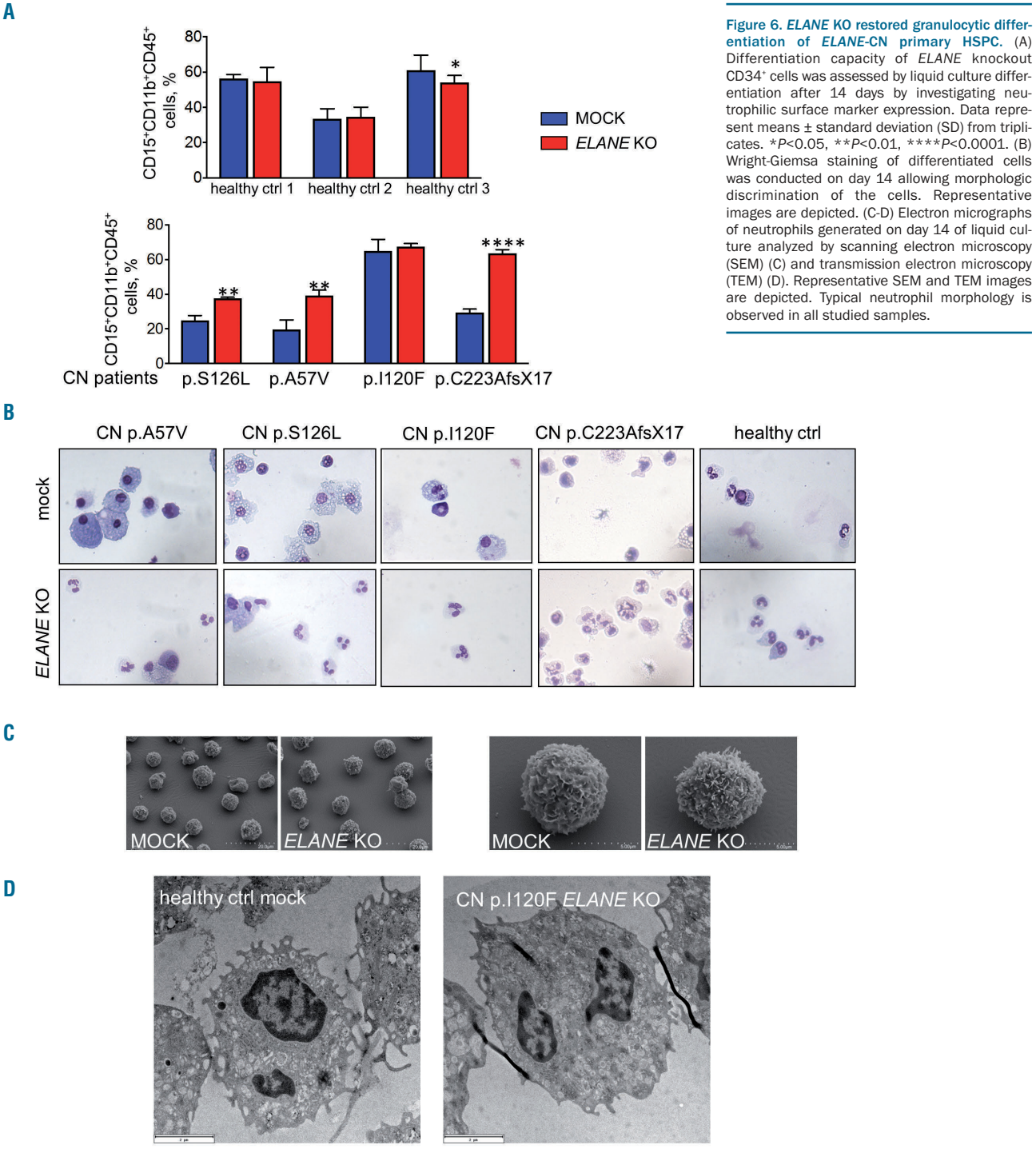

Figure 6. *ELANE* KO restored granulocytic differentiation of *ELANE*-CN primary HSPC. (A) Differentiation capacity of *ELANE* knockout CD34+ cells was assessed by liquid culture differentiation after 14 days by investigating neutrophilic surface marker expression. Data represent means ± standard deviation (SD) from triplicates. **P*<0.05, ***P*<0.01, *****P*<0.0001. (B) Wright-Giemsa staining of differentiated cells was conducted on day 14 allowing morphologic discrimination of the cells. Representative images are depicted. (C-D) Electron micrographs of neutrophils generated on day 14 of liquid culture analyzed by scanning electron microscopy (SEM) (C) and transmission electron microscopy (TEM) (D). Representative SEM and TEM images are depicted. Typical neutrophil morphology is observed in all studied samples.

CN. We tested *ex vivo* CRISPR/Cas9 RNP-based *ELANE* knockout in HSPC of CN patients that may be used for autologous transplantation as a therapeutic approach for *ELANE*-CN patients. Virus- and DNA-free application of CRISPR/Cas9 RNP markedly increases gene editing efficiency and simultaneously decreases the probability and frequency of off-target effects, because CRISPR/Cas9 RNP activity is preserved in cells for only approximately 48 hours. We recently reported the establishment of the fluorescent labeling of CRISPR/Cas9 RNP complexes for gene editing of primary hematopoietic stem cells and subsequent sorting of gene-modified cells for further applications.[26] Implementation of this method will improve the efficiency of gene knockout or gene correction in HSPC, including *ELANE* knockout or correction of *ELANE* mutations.

In case of *ELANE* KO, different combinations of the *ELANE* gene editing are expected: we may generate unedited, monoallelic edited (of mutated or WT allele), or bi-allelic edited HSPC. Since we did not use any selection marker for edited HSPC, we were not able to estimate the proportion of HSPC with inactivation of the mutated *ELANE* allele. The fact that the proportion of *ELANE* KO cells was elevated upon granulocytic differentiation strongly argues for the differentiation advantage of the edited cells lacking *ELANE* (including loss of the mutated allele).

There are several potential unforeseen consequences of the *ELANE* gene knockout strategy. For example, Tidwell *et al.* reported the presence of two in-frame ATG codons in exon 2 and exon 4 of *ELANE*.[27] They showed that the internal translation of NE can be initiated when the canon-

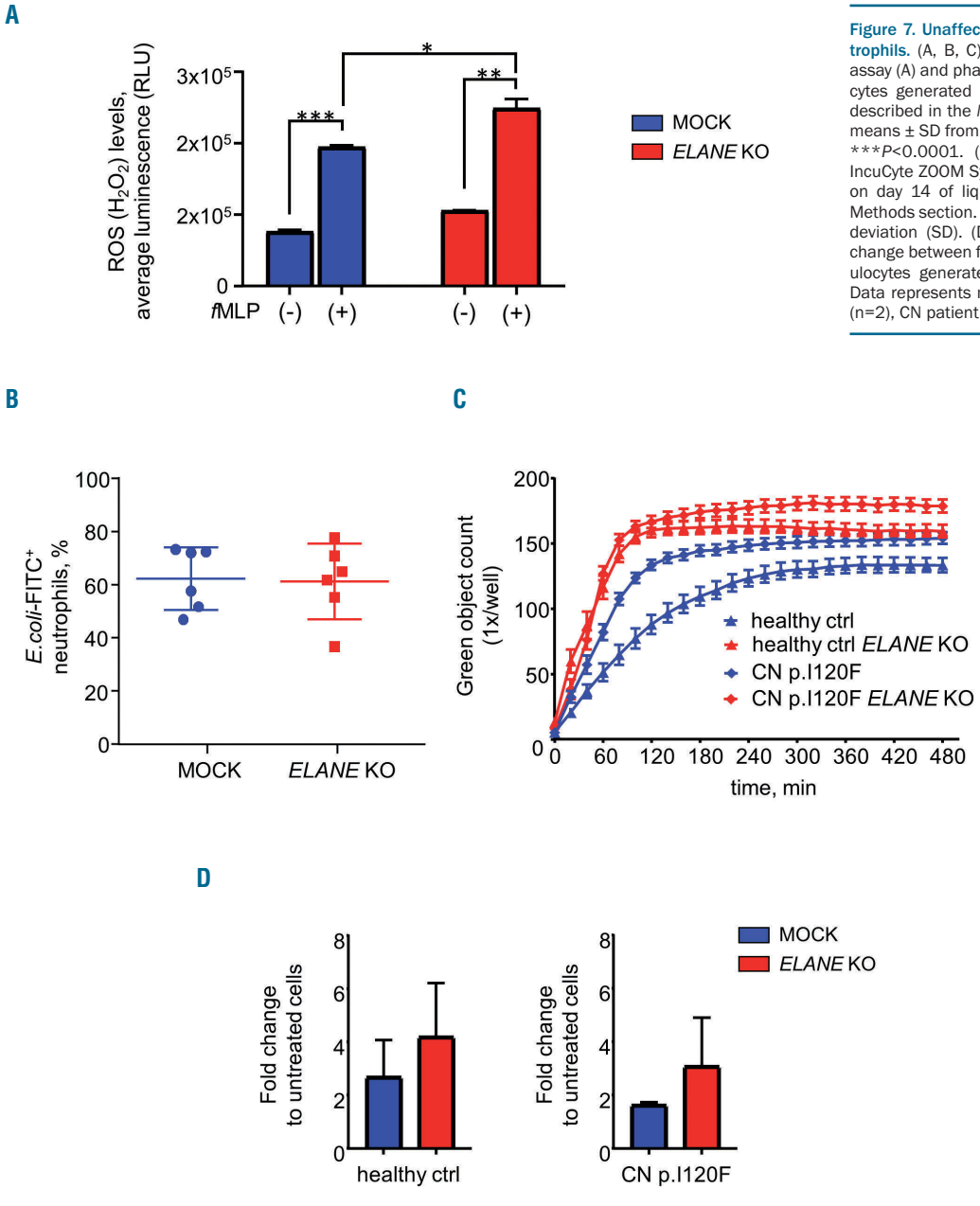

Figure 7. Unaffected functions of *ELANE* KO neutrophils. (A, B, C) Reactive oxygen species (ROS) assay (A) and phagocytosis assay (B, C) of granulocytes generated on day 14 of liquid culture, as described in the *Methods* section. Data represent means ± SD from duplicates. **P*<0.05, ***P*<0.01, ****P*<0.0001. (C) Phagocytosis Kinetic using IncuCyte ZOOM System of granulocytes generated on day 14 of liquid culture as described in the Methods section. Data represent mean ± standard deviation (SD). (D) Chemotaxis depicted as fold change between fMLP-treated and untreated granulocytes generated on day 14 of liquid culture. Data represents mean ± SD, healthy control (ctrl) (n=2), CN patient (n=1).

ical translational start site and/or internal start sites in exon 2 are disrupted and that expression of internally-initiated *ELANE* is pathogenic. We found a marked reduction of *ELANE* mRNA, most probably due to the induction of nonsense-mediated mRNA decay (NMD) of *ELANE* mRNA after exposure of cells to *ELANE*-specific CRISPR/Cas9 sgRNA RNP. We also did not detect any additional NE protein bands on WB analysis of edited cells using antibody recognizing C-terminus of NE. Based on these observations, we concluded that our sgRNA is inducing loss of NE protein without activation of the pathogenic *ELANE* forms from the internal ATG.

We did not detect off-target activity in edited cells, but recent results from Alan Bradley have suggested that the introduction of CRISPR/Cas9 editing can cause multiple genomic changes far beyond the actual target.[28] Therefore, for clinical applications, evaluation of the off-target activity of CRISPR/Cas9 on whole genome level using next-generation sequencing should be performed. In addition, it would be important to evaluate that the editing of *ELANE* occurred in the repopulating hematopoietic stem cell population and that these cells maintained their ability to engraft immunodeficient mice *in vivo*. Since most probably HSC are not expressing NE, we will not expect any damaging effects of the *ELANE* KO on the functions and integrity of HSC.

We demonstrated here, that CRISPR/Cas9 mediated *ELANE* KO in HSPC and iPSC of CN patients induces granulocytic differentiation and *in vitro* generated *ELANE* KO neutrophils have no defects in the phagocytic activity, ROS production, and chemotaxis. NE is a proteolytic enzyme of the neutrophil serine protease (NSP) family,

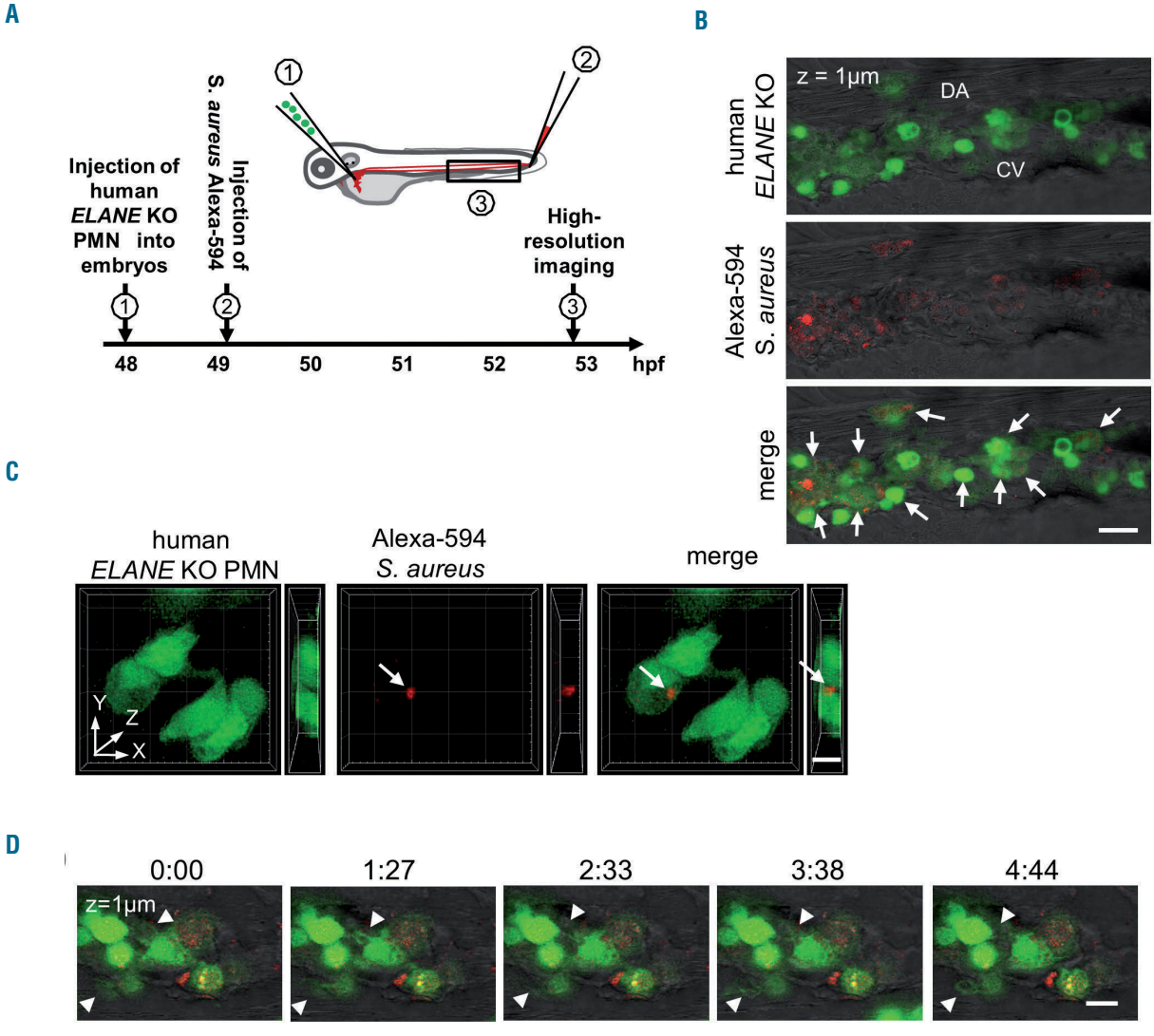

Figure 8. Human *ELANE* KO PMN are capable to migrate and to phagocyte *S. aureus* BioParticles in zebrafish embryos *in vivo*. (A) The scheme of *in vivo* phagocytosis assay in zebrafish embryos xenotransplanted with human fluorescently labeled polymorphonuclear leukocytes (PMN). (B) A representative confocal image highlighting the presence of transplanted human *ELANE* KO PMN in the caudal hematopoietic site of a zebrafish embryo at 53 hpf. White arrows indicate *S. aureus* BioParticles phagocytosed by human *ELANE* KO PMN. CV: caudal vein; DA: dorsal aorta. Scale bar: 20 µm. (C) Three-dimensional rendering of a z-stacks of 12 µm illustrating human *ELANE* KO PMN, one of them has engulfed *S. aureus* BioParticles (white arrow). Scale bar: 10 µm. (D) Still photographs from a time-lapse recording illustrating the phagocytic activity of transplanted human *ELANE* KO PMN in the zebrafish embryo. Arrowheads indicate the formation of neutrophil protrusions. Numbers indicate time in minutes. Scale bar: 10 µm.

including also cathepsin G (CG), proteinase 3 (PR3) and azurocidin (AZU1). NSP are stored in cytoplasmic granules, can be secreted into the extra- and peri-cellular space upon cellular activation and considered to be crucially involved in bacterial defense. NE and PR3 are very similar in their substrate specificity supporting a potentially redundant function for these two enzymes. *Elane*$^{-/-}$ mice have normal neutrophil counts, but there are conflicting results regarding the effect of NE-deficiency on neutrophil extravasation to sites of inflammation, phagocytosis, and neutrophil extracellular traps in mice. NE may or may not be essential for these processes.[29-33] Papillon-Lefevre Syndrome (PLS) is the only human disorder known to cause NE deficiency. This rare autosomal recessive disease is due to loss-of-function mutations in the DPPI gene locus with the loss of the lysosomal cysteine protease cathepsin C/dipeptidyl peptidase I (DPPI). The activation of NSP, including NE, depends on the N-terminal processing activity of DPPI. Therefore, PLS patients exhibit a severe reduction in the activity and stability of all three NSP including NE. Intriguingly, patients with PLS have no defects in their ability to kill bacteria *e.g. Staphylococcus aureus* or *E.coli*, suggesting that redundancies in the neutrophil's bactericidal mechanisms negate the necessity for serine proteases for killing common bacteria.[34] Moreover, since the other serine proteases including CG, PR3 and neutrophil serine protease 4 remain intact, we do not expect for the resultant cells to develop any neutrophil-specific functional anti-bacterial or immunodeficiency phenotype in *ELANE* KO cells. Based on these observations, at this juncture, we believe that CRISPR/Cas9 based knockout of *ELANE* in HSPC of CN patients may restore defective granulopoiesis in CN patients without seriously impairing neutrophil functions. Further studies, including gene expression analysis to understand which pathways are affected by *ELANE* mutations and verifying that these pathways are indeed restored by *ELANE* KO, are essential to justify the therapeutic applications of *ELANE* KO technology in the future. It will also contribute to the understanding of the pathophysiology of the CN caused by *ELANE* mutations. Our first attempts to investigate intracellular signaling pathways affected by mutated *ELANE* revealed the restoration of mRNA expression of anti-apoptotic Bcl-xl factor that is downregulated in CN myeloid progenitor cells.[35] Moreover, we found downregulation of mRNA levels of the key UPR player BiP, normally upregulated in HSPC of CN patients harboring *ELANE* mutations.[8-10]

CRISPR/Cas9 technology also allowed correction of the specific gene mutations. We selected the *ELANE* knockout approach since *ELANE* mutations are heterozygous gain-of-function gene defects that are distributed throughout all five exons and two introns of *ELANE* and specific *ELANE* mutations correction would require specific settings for each patient based on the mutation position. In addition, the requirement of the introduction of the donor repair template DNA in a gene correction approach requires the activation of HDR making it difficult to achieve efficient correction in primary HSPC. We and other investigators have reported that *ELANE* mutations induce UPR and ER stress.[8-11] We also described deregulated signaling pathways in HSPC of CN patients downstream of *ELANE* mutations, such as diminished expression of transcription factors LEF-1, and C/EBPα,[36–39] abrogated expression and phosphorylation of the adaptor protein HCLS1,[40] elevated apoptosis[35] and hyperactivated NAMPT/sirtuins.[41] These intracellular defects may lead to the elevated fragility of HSPC during *ex vivo* gene manipulations and may affect gene correction efficiency. Moreover, gene editing strategy directed to the correction of *ELANE* mutations may lead to the creation of novel missense or frameshift mutations that may result in the novel mutant NE protein with damaging functions and potential generation of the pre-leukemic HSPC clones with proliferative advantage and possible leukemic transformation. Adeno-associated virus (AAV)-based vector may be used for the delivery of the donor repair template and is considered safer than retroviral constructs. Two groups recently published successful gene deletions as a gene therapy approach to cure sickle cell disease, a common inherited blood disorder.[17,18] It should be noted that AAV-based expression constructs may induce anti-viral host immune responses and may non-specifically integrate into the host genome.

In summary, we report here for the first time a method of CRISPR/Cas9 mediated *ELANE* gene deletion in hematopoietic stem cells and iPSC from CN patients harboring *ELANE* mutations. The *ELANE* gene deletion resulted in the increase of granulocytic differentiation to functional normal mature neutrophils in these patients *in vitro*. Therefore, CRISPR/Cas9 based gene knockout of *ELANE* in CN patients harboring *ELANE* mutation might be a useful treatment option especially in patients requiring high G-CSF dosages or do not responding to G-CSF at all. In addition, it remains to be investigated in subsequent clinical studies whether, in CN patients harboring *ELANE* mutations, the *ELANE* gene knockout would also abrogate the leukemogenesis.

Acknowledgments

We would like to thank the FACS core facility of the UKT especially Stella Autenrieth for the assistance in flow cytometry; Michael Schindler and Esther Lehmann for their support in confocal microscopy. This work was supported by the Excellence Initiative of the Faculty of Medicine, University of Tübingen (JS), Jose Carreras Leukemia Foundation (JS, PM, MR), Madeleine Schickedanz Kinderkrebsstiftung (JS, MK, MN), DFG (JS, MK), intramural Fortüne program of the Medical Faculty of the Tübingen University (MK, DA, YX), German-Israeli Foundation for Scientific Research and Development (GIF) (KW, BD), German Cancer Consortium (PM), Else Kröner-Fresenius Stiftung (MK, BD), Fritz Thyssen Foundation (MR and BD), NIH R24 AI 049393 (VM, BF, CZ, DCD).

References

1. Dale DC, Person RE, Bolyard AA, et al. Mutations in the gene encoding neutrophil elastase in congenital and cyclic neutropenia. Blood. 2000; 96(7):2317-2322.
2. Skokowa J, Germeshausen M, Zeidler C, Welte K. Severe congenital neutropenia: inheritance and pathophysiology. Curr Opin Hematol. 2007; 14(1):22-28.
3. Skokowa J, Dale DC, Touw IP, Zeidler C, Welte K. Severe congenital neutropenias. Nat Rev Dis Primers. 2017;3:17032.
4. Welte K, Gabrilove J, Bronchud MH, Platzer E, Morstyn G. Filgrastim (r-metHuG-CSF): the first 10 years. Blood. 1996;88(6):1907-1929.
5. Rosenberg PS, Zeidler C, Bolyard AA, et al.

Stable long-term risk of leukaemia in patients with severe congenital neutropenia maintained on G-CSF therapy. Br J Haematol. 2010;150(2):196-199.
6. Jinek M, Chylinski K, Fonfara I, Hauer M, Doudna JA, Charpentier E. A programmable dual-RNA-guided DNA endonuclease in adaptive bacterial immunity. Science. 2012;337(6096):816-821.
7. Ran FA, Hsu PD, Wright J, Agarwala V, Scott DA, Zhang F. Genome engineering using the CRISPR-Cas9 system. Nat Protoc. 2013;8(11):2281-2308.
8. Grenda DS, Murakami M, Ghatak J, et al. Mutations of the ELA2 gene found in patients with severe congenital neutropenia induce the unfolded protein response and cellular apoptosis. Blood. 2007;110(13): 4179-4187.
9. Nanua S, Murakami M, Xia J, et al. Activation of the unfolded protein response is associated with impaired granulopoiesis in transgenic mice expressing mutant Elane. Blood.2011;117(13):3539-3547.
10. Nustede R, Klimiankou M, Klimenkova O, et al. ELANE mutant-specific activation of different UPR pathways in congenital neutropenia. Br J Haematol. 2016;172(2):219-227.
11. Kollner I, Sodeik B, Schreek S, et al. Mutations in neutrophil elastase causing congenital neutropenia lead to cytoplasmic protein accumulation and induction of the unfolded protein response. Blood. 2006;108(2):493-500.
12. Makaryan V, Kelley ML, Fletcher B, Bolyard AA, Aprikyan AA, Dale DC. Elastase inhibitors as potential therapies for ELANE-associated neutropenia. J Leukoc Biol. 2017;102(4):1143-1151.
13. Nayak RC, Trump LR, Aronow BJ, et al. Pathogenesis of ELANE-mutant severe neutropenia revealed by induced pluripotent stem cells. J Clin Invest. 2015;125(8):3103-3116.
14. Ancliff PJ, Gale RE, Watts MJ, et al. Paternal mosaicism proves the pathogenic nature of mutations in neutrophil elastase in severe congenital neutropenia. Blood. 2002;100(2): 707-709.
15. Benson KF, Horwitz M. Possibility of somatic mosaicism of ELA2 mutation overlooked in an asymptomatic father transmitting severe congenital neutropenia to two offspring. Br J Haematol. 2002;118(3):923; author reply -4.
16. Makaryan V, Zeidler C, Bolyard AA, et al. The diversity of mutations and clinical outcomes for ELANE-associated neutropenia. Curr Opin Hematol. 2015;22(1):3-11.
17. Ye L, Wang J, Tan Y, et al. Genome editing using CRISPR-Cas9 to create the HPFH genotype in HSPCs: An approach for treating sickle cell disease and beta-thalassemia. Proc Natl Acad Sci U S A. 2016;113(38): 10661-10665.
18. Traxler EA, Yao Y, Wang YD, et al. A genome-editing strategy to treat beta-hemoglobinopathies that recapitulates a mutation associated with a benign genetic condition. Nat Med. 2016;22(9):987-990.
19. Stemmer M, Thumberger T, Del Sol Keyer M, Wittbrodt J, Mateo JL. CCTop: an intuitive, flexible and reliable CRISPR/Cas9 target prediction tool. PLoS One. 2015; 10(4):e0124633.
20. Brinkman EK, Chen T, Amendola M, van Steensel B. Easy quantitative assessment of genome editing by sequence trace decomposition. Nucleic Acids Res. 2014;42(22):e168.
21. Bajoghli B, Kuri P, Inoue D, et al. Noninvasive in toto imaging of the thymus reveals heterogeneous migratory behavior of developing T cells. J Immunol. 2015; 195(5):2177-2186.
22. Lachmann N, Ackermann M, Frenzel E, et al. Large-scale hematopoietic differentiation of human induced pluripotent stem cells provides granulocytes or macrophages for cell replacement therapies. Stem Cell Reports. 2015;4(2): 282-296.
23. Dannenmann B, Zahabi A, Mir P, et al. Human iPSC-based model of severe congenital neutropenia reveals elevated UPR and DNA damage in CD34(+) cells preceding leukemic transformation. Exp Hematol. 2019;71-51-60.
24. Hamilton N, Sabroe I, Renshaw SA. A method for transplantation of human HSCs into zebrafish, to replace humanised murine transplantation models. F1000Res. 2018; 7:594.
25. Staal FJ, Spaink HP, Fibbe WE. Visualizing human hematopoietic stem cell trafficking in vivo using a zebrafish xenograft model. Stem Cells Dev. 2016;25(4):360-365.
26. Nasri M, Mir P, Dannenmann B, et al. Fluorescent labeling of CRISPR/Cas9 RNP for gene knockout in HSPCs and iPSCs reveals an essential role for GADD45b in stress response. Blood Adv. 2019;3(1):63-71.
27. Tidwell T, Wechsler J, Nayak RC, et al. Neutropenia-associated ELANE mutations disrupting translation initiation produce novel neutrophil elastase isoforms. Blood. 2014;123(4):562-569.
28. Kosicki M, Tomberg K, Bradley A. Repair of double-strand breaks induced by CRISPR-Cas9 leads to large deletions and complex rearrangements. Nat Biotechnol. 2018;36(8):765-771.
29. Allport JR, Lim YC, Shipley JM, et al. Neutrophils from MMP-9- or neutrophil elastase-deficient mice show no defect in transendothelial migration under flow in vitro. J Leukoc Biol. 2002;71(5):821-828.
30. Martinod K, Witsch T, Farley K, Gallant M, Remold-O'Donnell E, Wagner DD. Neutrophil elastase-deficient mice form neutrophil extracellular traps in an experimental model of deep vein thrombosis. J Thromb Haemost. 2016;14(3):551-558.
31. Hirche TO, Atkinson JJ, Bahr S, Belaaouaj A. Deficiency in neutrophil elastase does not impair neutrophil recruitment to inflamed sites. Am J Resp Cell Mol Biol. 2004;30(4):576-584.
32. Young RE, Thompson RD, Larbi KY, et al. Neutrophil elastase (NE)-deficient mice demonstrate a nonredundant role for NE in neutrophil migration, generation of proinflammatory mediators, and phagocytosis in response to zymosan particles in vivo. J Immunol. 2004;172(7):4493-4502.
33. Belaaouaj A, McCarthy R, Baumann M, et al. Mice lacking neutrophil elastase reveal impaired host defense against gram negative bacterial sepsis. Nat Med. 1998;4(5):615-618.
34. Pham CT, Ivanovich JL, Raptis SZ, Zehnbauer B, Ley TJ. Papillon-Lefevre syndrome: correlating the molecular, cellular, and clinical consequences of cathepsin C/dipeptidyl peptidase I deficiency in humans. J Immunol. 2004;173(12):7277-7281.
35. Cario G, Skokowa J, Wang Z, et al. Heterogeneous expression pattern of pro- and anti-apoptotic factors in myeloid progenitor cells of patients with severe congenital neutropenia treated with granulocyte colony-stimulating factor. Br J Haematol. 2005;129(2):275-278.
36. Skokowa J, Cario G, Uenalan M, et al. LEF-1 is crucial for neutrophil granulocytopoiesis and its expression is severely reduced in congenital neutropenia. Nat Med. 2006;12(10): 1191-1197.
37. Skokowa J, Welte K. LEF-1 is a decisive transcription factor in neutrophil granulopoiesis. Ann N Y Acad Sci. 2007;1106:143-151.
38. Skokowa J, Welte K. Dysregulation of myeloid-specific transcription factors in congenital neutropenia. Ann N Y Acad Sci. 2009;1176:94-100.
39. Skokowa J, Welte K. Defective G-CSFR signaling pathways in congenital neutropenia. Hematol Oncol Clin North Am. 2013;27(1): 75-88, viii.
40. Skokowa J, Klimiankou M, Klimenkova O, et al. Interactions among HCLS1, HAX1 and LEF-1 proteins are essential for G-CSF-triggered granulopoiesis. Nat Med. 2012;18 (10):1550-1559.
41. Skokowa J, Lan D, Thakur BK, et al. NAMPT is essential for the G-CSF-induced myeloid differentiation via a NAD(+)-sirtuin-1-dependent pathway. Nat Med. 2009;15 (2):151-158.

H) Ritter, M. et al., 2020, *Annals of Hematology*

Annals of Hematology (2020) 99:2329–2338
https://doi.org/10.1007/s00277-020-04194-0

ORIGINAL ARTICLE

Cooperating, congenital neutropenia–associated *Csf3r* and *Runx1* mutations activate pro-inflammatory signaling and inhibit myeloid differentiation of mouse HSPCs

Malte Ritter[1] · Maksim Klimiankou[1] · Olga Klimenkova[1] · Axel Schambach[2,3] · Dirk Hoffmann[2] · Amy Schmidt[4] · Lothar Kanz[1] · Daniel C. Link[4] · Karl Welte[5] · Julia Skokowa[1]

Received: 3 March 2020 / Accepted: 20 July 2020 / Published online: 3 August 2020

Abstract

Patients with the pre-leukemia bone marrow failure syndrome called severe congenital neutropenia (CN) have an approximately 15% risk of developing acute myeloid leukemia (AML; called here CN/AML). Most CN/AML patients co-acquire *CSF3R* and *RUNX1* mutations, which play cooperative roles in the development of AML. To establish an in vitro model of leukemogenesis, we utilized bone marrow lin$^-$ cells from transgenic C57BL/6-d715 *Csf3r* mice expressing a CN patient–mimicking truncated *CSF3R* mutation. We transduced these cells with vectors encoding *RUNX1* wild type (WT) or *RUNX1* mutant proteins carrying the R139G or R174L mutations. Cells transduced with these *RUNX1* mutants showed diminished in vitro myeloid differentiation and elevated replating capacity, compared with those expressing WT *RUNX1*. mRNA expression analysis showed that cells transduced with the *RUNX1* mutants exhibited hyperactivation of inflammatory signaling and innate immunity pathways, including IL-6, TLR, NF-kappaB, IFN, and TREM1 signaling. These data suggest that the expression of mutated *RUNX1* in a *CSF3R*-mutated background may activate the pro-inflammatory cell state and inhibit myeloid differentiation.

Keywords Severe congenital neutropenia · Pre-leukemia bone marrow failure syndrome · G-CSFR mutations · RUNX1 mutations

Introduction

Patients with the inborn pre-leukemia bone marrow failure syndrome called severe congenital neutropenia (CN) have a very low level (less than 500 cells/μl blood) or even a complete lack of mature neutrophilic granulocytes in the peripheral blood which is caused by blockade of the terminal differentiation of bone marrow myeloid progenitor cells at the promyelocytes/myelocyte stage [1, 2]. In most CN patients, this granulocyte differentiation defect can be successfully treated by daily subcutaneous administration of recombinant human granulocyte colony–stimulating factor (G-CSF). Approximately 15% of CN patients develop myelodysplastic syndrome or acute myeloid leukemia (MDS or AML). Inherited mutations in the ELANE, HAX1, G6PC3, SRP54, GFI1, and JAGN1 genes cause CN, and leukemic progression has been seen in CN patients of all genetic groups [1].

CSF3R mutations resulting in the production of truncated G-CSFR proteins that lack from one to four phospho-tyrosine residues and exhibit defective receptor

Electronic supplementary material The online version of this article (https://doi.org/10.1007/s00277-020-04194-0) contains supplementary material, which is available to authorized users.

✉ Julia Skokowa
Julia.Skokowa@med.uni-tuebingen.de

[1] Division of Translational Oncology, Department of Hematology, Oncology, Clinical Immunology and Rheumatology, University Hospital Tübingen, Otfried-Müller-Straße 10, 72076 Tübingen, Germany

[2] Institute of Experimental Hematology, Hannover Medical School, Hannover, Germany

[3] Division of Hematology/Oncology, Boston Children's Hospital, Harvard Medical School, Boston, MA, USA

[4] Division of Oncology, Section of Stem Cell Biology, Washington University Medical School, St. Louis, MO, USA

[5] The University Children's Hospital Tübingen, Tübingen, Germany

Published online: 03 August 2020

internalization were reported in a majority of CN patients with overt AML or MDS [3–9]. However, transgenic d715 *Csf3r* mice lacking three tyrosines do not develop AML or MDS [3–9], suggesting that additional genetic alterations in combination with *CSF3R* mutation are needed for the progression of AML. We recently examined a large cohort of CN/AML patients (31 patients) and found cooperative acquired mutations of *CSF3R* and *RUNX1* (runt-related transcription factor 1) in 55% of CN patients with overt AML or MDS [10]. However, the detailed mechanism underlying the leukemogenic transformation downstream of *CSF3R* and *RUNX1* mutations remained unknown.

Acquired mutations in *RUNX1* occur in AML, mostly secondary to MDS, radiation therapy, or chemotherapy [11–16]. Most *RUNX1* mutations are acquired heterozygous point mutations; they are predominantly located in the Runt homology/DNA-binding (RHD) or transactivation (TAD) domains. Interestingly, a majority of patients with familial platelet disorder (FPD) and a predisposition for AML have germline *RUNX1* mutations [17]. Some FPD patients with overt AML gain additional *RUNX1* mutations [17]. Among the described groups of AML patients, the incidence of acquired *RUNX1* mutations is the highest in CN/AML patients. *RUNX1* mutations in CN/AML patients are distributed throughout the RHD (primarily) and TAD of the RUNX1 protein, and some hot spot positions have been noted [10]. For example, amino acid residues 139 and 174 of the RUNX1 protein were found to be mutated in four and three CN/AML patients, respectively [10] (data not shown). The functional outcomes of *RUNX1* mutations at different positions have not yet been clearly defined, but we speculate that they may affect the DNA binding of RUNX1 to target genes or the protein–protein interactions, intracellular localization, protein stability, and/or post-translational modification(s) of RUNX1.

The role of inflammation in cancer was first mentioned in 1863 by Virchow [18]. A growing body of research suggests that pro-inflammatory signaling acts through diverse mechanisms to increase the proliferation rate of hematopoietic stem and progenitor cells (HSPCs), which induces genotoxicity, increases survival, and produces preleukemia stem cells (pre-LSCs) with a high likelihood of leukemic transformation [19].

In the present study, we sought to establish an in vitro experimental model to study the intracellular mechanisms of leukemia development downstream of *CSF3R* and *RUNX1* mutations. Using this model, we identified upregulation of an inflammatory signature signaling in mouse HSPCs expressing mutated *CSF3R* and *RUNX1*. This expression signature may predispose CN patients toward leukemic transformation.

Material and methods

Mice

Male d715 *Csf3r* mice on the C57BL/6J background have been described previously [9]. Mice were housed under pathogen-free conditions in the animal facility of Tübingen University.

Cell purification and separation

Mouse bone marrow cells were isolated by flushing the long bones with ice-cold PBS. Bone marrow mononuclear cells were isolated by Ficoll–Hypaque gradient centrifugation (Amersham Biosciences) and positively selected bone marrow lin^- cells by immunomagnetic labeling with corresponding MACS beads (Miltenyi Biotec). Cells were counted, and viability was assessed by Trypan blue dye exclusion.

Generation of the lentiviral vectors expressing WT or mutant RUNX1 cDNA

To generate RUNX1 mutants, we performed site-directed mutagenesis. As a template, we used Lego-iG/Puro-RUNX1-wt-CTAP plasmid expressing human wild type (WT) RUNX1 generously provided by Dr. Boris Fehse and Dr. Carol Stocking. Specific primers to introduce mutations p.Arg139Gly (R139G) and p.Arg174Leu (R174L) in wild type *RUNX1* nucleotide sequence were designed using the QuickChange Primer Design tool (https://www.agilent.com/store/primerDesignProgram.jsp). Primer sequences are available upon request. Lego-iG/Puro-RUNX1-R139G-CTAP and Lego-iG/Puro-RUNX1-R174L-CTAP plasmids were generated using the QuickChange II Site-Directed Mutagenesis Kit (Agilent Technologies, Inc.) according to the manufacturer's instruction. *RUNX1* cDNAs (WT and two mutants) were subsequently re-cloned into lentiviral pRRL.PPT.CBX3.SFFV.hRUNX1.i2.EBFP.puro.pre vector. Transgene expression was controlled by the spleen focus–forming virus promoter (SFFV) juxtaposed to the minimal ubiquitous chromatin opening element (CBX3). EBFP translation was initiated by an internal ribosomal entry side (i2).

Transduction of cells

Lin^- cells were cultured in a hematopoietic stem cell expansion medium consisting of Stemline II medium supplemented with Pen/Strep, 10% FCS (Sigma-Aldrich), 1 μm dexamethasone, 100 ng/ml of mSCF, 4 ng/ml of mIL-3, 10 ng/ml of hIL-6, 40 ng/ml of murine IGF-1, and 20 ng/ml of human Flt-3L at 2×10^5 cells/ml for 2 days. Cells were transduced at MOIs of 5–10 in the presence of polybrene (5 μg/ml) and re-transduced after 12–24 h. Percentage of $EBFP^+$ cells was assessed by FACS.

Detection of the human RUNX1 protein in transduced bone marrow lin$^-$ cells from d715 *Csf3r* mice using western blotting

A total of 1×10^6 transduced bone marrow lin$^-$ cells from d715 Csf3r mice were lysed in 200 μl 3 × Laemmli buffer, and protein was denatured for 10 min at 95 °C. Five microliter of cell lysate in Laemmli buffer was loaded per lane. Proteins were separated on a 12.5% polyacrylamide gel and transferred on a nitrocellulose membrane (GE Healthcare) (1 h, 100 V, 4 °C). The membrane was blocked for 1 h in 5% milk and incubated with primary rabbit anti-human and anti-mouse RUNX1-specific (Cell Signaling Technology #4334) or GAPDH (Cell Signaling Technology, #2118) antibody overnight (at 4 °C). After that, membranes were washed and incubated with secondary HRP-conjugated antibody (Cell signaling, #7074) for 1 h at room temperature. Pierce ECL solution (Thermo Fisher) and Amersham Hyperfilms were used to detect chemiluminescence signal of proteins.

Liquid culture differentiation of transduced lin$^-$ cells

A total of 2×10^5 of transduced cells/ml were incubated for 7 days in RPMI 1640 GlutaMAX supplemented with 10% FCS, 10 ng/ml hIL-6, 5 ng/ml IL-3, 5 ng/ml GM-CSF, and 10 ng/ml G-CSF. The medium was exchanged every second day. On day 7, the medium was changed to RPMI 1640 GlutaMAX supplemented with 10% FBS, 1% penicillin/streptomycin, and 10 ng/ml G-CSF. The medium was exchanged every second day until day 11. On day 11, cells were analyzed by FACS using the following antibody: rat anti-mouse Gr-1 (BD 553128) and rat anti-mouse CD11b (BD 553312) on FACSCanto II.

Colony-forming unit assay

A total of 1000 transduced EBFP$^+$ cells were plated directly after transduction in 1 ml methylcellulose medium (MethoCult GF M3434; StemCell Technologies) supplemented with 10 ng/ml of G-CSF. After 14 days of culture, the numbers of CFU-G, CFU-GM, and BFU-E colonies were counted. Cells were collected for the colony replating experiments, washed 3 times with PBS, and plated 1000 cells/dish in new methylcellulose for an additional 2 weeks (1st replating). The procedure was repeated one more time (2nd replating).

Microarray-based mRNA expression analysis

After 48 h of lentiviral transduction, lin$^-$ cells were starved for 24 h and subsequently treated with 10 ng/ml of G-CSF for 24 h. After that, transduced cells were sorted, and mRNA was isolated using the RNeasy Mini Kit (Qiagen, #74106) according to the manufacturer's instructions.

RNA from transduced lin$^-$ cells was subjected to microarray analysis using the Affymetrix Microarray Platform. The GeneChip WT cDNA Synthesis and Amplification Kit was used to make double-stranded cDNA from total RNA, which was then labeled with biotin (GeneChip WT Terminal Labeling Kit). After chemical fragmentation of the biotin-labeled cDNA targets, they were hybridized to the GeneChip Mouse Gene 2.0 ST Array using the Fluidics Station 450 and scanned using the Affymetrix GeneChip Scanner 3000 with the GeneChip Operating Software 1.4 (Affymetrix, Santa Clara, CA). Data analysis was performed using Affymetrix Expression Console Version 1.1 for invariant set normalization, and the Ingenuity Pathway Analysis (IPA) software (Qiagen) was used for identification of differentially expressed genes. Motif activity response analysis (MARA) was conducted using the Integrated System for Motif Activity Response Analysis (ISMARA); CEL files were uploaded to the server using the web interface.

Cytospin preparation, staining, and microscopic image acquisition

After sorting, 1×10^4 cells were centrifuge onto microscope slides at 250 rpm for 3 min. The slides were air-dried, and subsequent Wright–Giemsa staining was carried out. Images where acquired on a Nikon Eclipse TS100. Cells were covered with oil, and images were collected at × 630 magnification.

qRT-PCR

RNA isolation was performed using the RNeasy Micro Kit (Qiagen). cDNA was synthesized from 1 μg total RNA with the Omniscript RT Kit (Qiagen). qRT-PCR was conducted with SYBR Green qPCR master mix (Roche) on a Light Cycler 480 (Roche). Target genes were normalized to ACTB. Primers are available upon request.

LSK cell analysis

A total of 2×10^5 cells were incubated with FcR blocking antibody (BioLegend #101320), 7AAD, and lineage cocktail biotin–conjugated antibody (BioLegend #79750, #79748, #79752, #79748, #79749), and stained with APC-Cy7-conjugated streptavidin (BioLegend #405208), anti-mouse Sca-1 BV510–conjugated antibody (BioLegend, #108129), and anti-mouse-c-KIT APC–conjugated antibody (BioLegend, #105812). After staining and washing, cells were analyzed on a CANTO II (BD) flow cytometer.

Statistics

Statistical analysis was performed using a two-sided unpaired Student *t* test for the analysis of differences in mean values between groups.

Results

Diminished formation of myeloid colonies and elevated replating capacity of d715 *Csf3r* lin$^-$ cells transduced with mutated *RUNX1*

We isolated bone marrow lin$^-$ cells from d715 *Csf3r* mice and transduced these cells with lentiviral vectors encoding EBFP and *RUNX1* wild type (*RUNX1*-WT), or mutants, *RUNX1*-R139G, or *RUNX1*-R174L. Amino acids 174 and 139 were found to be "hot spots" for mutation in the RHD domain of the RUNX1 protein, as they were detected in four and three CN-AML patients, respectively (Fig. 1a) [10] (data not shown). At 72 h post-transduction, we performed colony-forming units and replating experiments of sorted EBFP$^+$ cells (Fig. 1b). We observed comparable expression of human WT and mutant RUNX1 proteins in transduced cells (Fig. 1c). Low levels of endogenous murine runx1 protein were detected in BFP$^+$ control transduced cells (Fig. 1c). Interestingly, d715 *Csf3r* lin$^-$ cells transduced with mutated *RUNX1* had markedly diminished capacities to form myeloid colonies, including CFU-G and CFU-GM, as compared with cells transduced with WT *RUNX1* (Fig. 1d). In line with these findings, CFU replating experiments showed that cell transduced with each *RUNX1* mutant had markedly higher replating capacities than *RUNX1* WT–transduced cells (Fig. 1e).

Reduced liquid culture myeloid differentiation of d715 *Csf3r* lin$^-$ cells transduced with mutated *RUNX1*

We next compared the G-CSF-triggered myeloid differentiation of transduced d715 *Csf3r* lin$^-$ cells in vitro. Transduced cells were cultured in liquid culture myeloid differentiation medium for 11 days (Fig. 2a). FACS was used to count the absolute numbers of myeloid CD11b$^+$ and Gr-1$^+$ cells on day 11 of liquid culture, and the results showed that d715 *Csf3r* lin$^-$ cells transduced with each of the *RUNX1* mutants exhibited reduced myeloid differentiation, compared with WT *RUNX1*–overexpressing samples (Fig. 2b). At the same time, no marked difference was observed in the absolute numbers of BFP$^+$ cells between groups transduced with WT *RUNX1* or with each of *RUNX1* mutants on days 3 and day 7 of liquid culture differentiation. On day 11 of culture, numbers of BFP$^+$ cells transduced with *RUNX1*-R139G mutant were significantly ($p < 0.05$) increased, as compared with *RUNX1* WT– or *RUNX1*-R174L–transduced samples (Fig. 2c).

RUNX1 missense mutations induce inflammatory signaling pathways in G-CSF-treated d715 *Csf3r* hematopoietic cells

We further aimed to identify intracellular signaling pathways downstream of *csf3r* and *RUNX1* mutations that may affect the in vitro proliferation and myeloid differentiation of mouse HSPCs. The d715 *Csf3r* lin$^-$ cells were expanded in HSPC expansion medium and transduced with lentiviral vectors carrying *RUNX1* WT, *RUNX1*-R139G, or *RUNX1*-R174L. Transduced cells were starved for 24 h and then treated with G-CSF for 24 h. EBFP$^+$ cells were sorted in RLT buffer, and mRNA expression was evaluated using an Affymetrix MoGene 2.0 Chip (Fig. 3a). Representative images of Wright–Giemsa–stained cytospins prepared from sorted cells show no difference in the cell morphology between studied groups: all samples show immature cell morphology (Fig. 3b). These data suggest that the differences in mRNA expression should not contribute to a strong diversity in the cell composition between studied groups.

After invariant set normalization, the expression levels of the *RUNX1* mutants were normalized to those obtained from WT *RUNX1*–transduced cells. The fold change expression table (Suppl. Table 1) was uploaded to the IPA software, and the cutoff values were set to − 1.7 and + 1.7 for log fold change, with the goal of identifying differentially expressed genes. This analysis showed that 1113 and 1814 genes were differentially expressed in the *RUNX1*-R174L and *RUNX1*-R139G mutant groups compared with the WT *RUNX1* group (Suppl. Table 2). Overlap analysis revealed that 679 genes (37.4% for the *RUNX1*-R139G mutant and 61% for the *RUNX1*-R174L mutant) were co-regulated in both *RUNX1* mutant groups (Fig. 3c). The 15 most highly up- and down-regulated genes were very similar between the *RUNX1* mutant groups. Of the top upregulated genes, 10/15 from the *RUNX1*-R174L group and 14/15 from the *RUNX1*-R139G group were co-activated in both groups. Of the top downregulated genes, 14/15 from the *RUNX1*-R174L group and 11/15 from the *RUNX1*-R139G group were co-downregulated (Fig. 3d). A comparison analysis performed using the IPA software revealed that 46 and 79 canonical pathways were significantly enriched ($\log(p \text{ value}) \geq 1.3$ corresponding to $p \leq 0.05$) in d715 *Csf3r* lin$^-$ cells transduced with *RUNX1*-R174L or *RUNX1*-R139G, respectively. Of these pathways, 11 in the *RUNX1*-R174L group and 18 in the *RUNX1*-R139G group were significantly activated (z-value ≥ 2) or inhibited (z-value ≤ -2). Most of the regulated pathways belonged to members of the activated innate immune pathways category; these included NF-kappaB signaling, toll-like receptor signaling (TLR), acute-phase response signaling, production of nitric oxide and reactive oxygen species, pattern-recognizing receptors, Trem 1 signaling, and IL-1 signaling. Activation was also seen among members of the inflammatory signaling

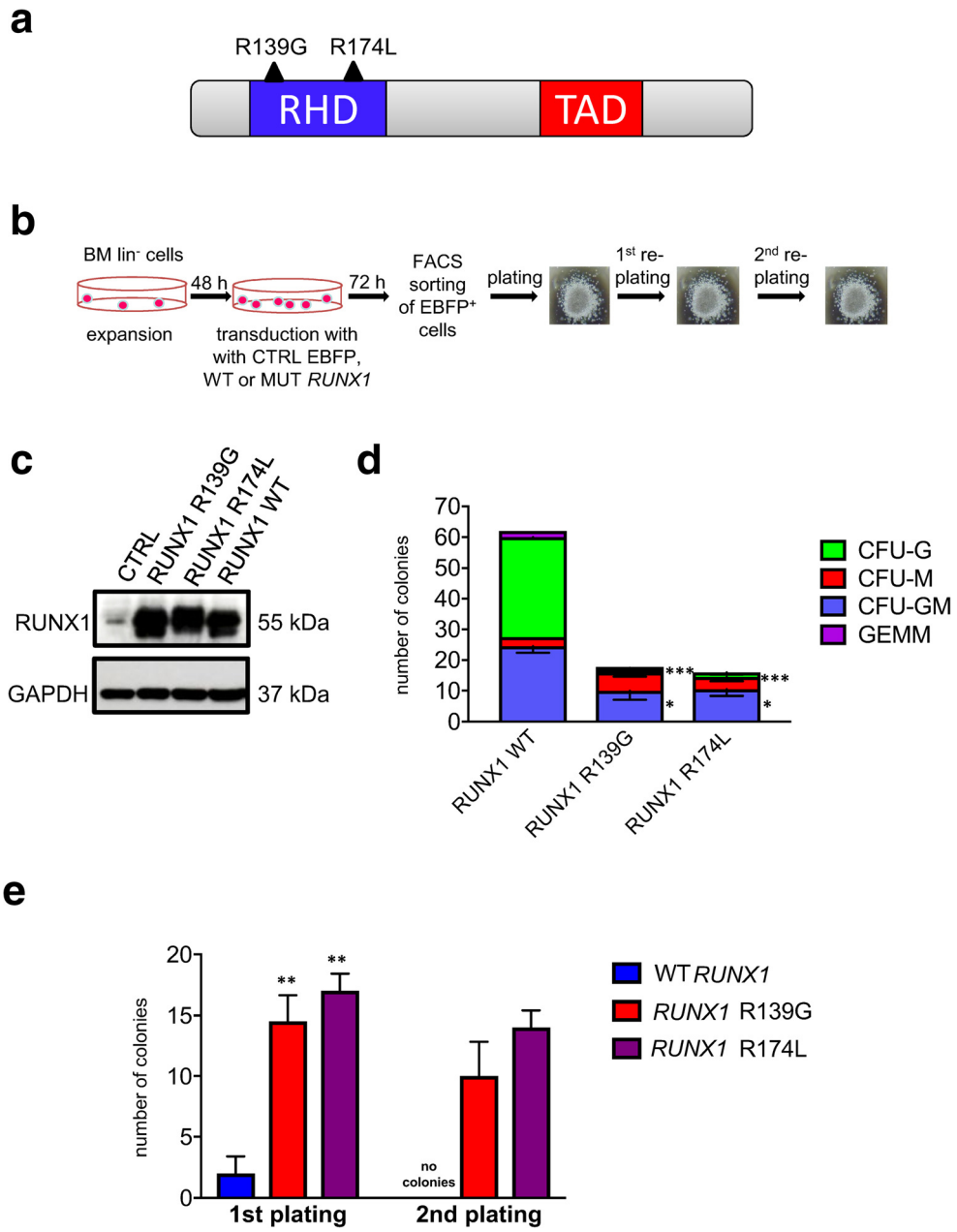

Fig. 1 In HSPCs of d715 *Csf3r* mice, *RUNX1* mutations decrease CFU-G and CFU-GM formation but increase the replating capacity. **a** Schematic of RUNX1 protein showing the location and amino acid changes of the mutations, which are indicated by black triangles. The functionally important Runt homology DNA-binding domain (RHD) is shown in blue, and the transactivation domain (TAD) is shown in red. **b** Schematic of CFU experiments performed using transduced bone marrow lin$^-$ cells of C57BL/6-d715 *Csf3r* mice. **c** Representative WB images of lin$^-$ cells of C57BL/6-d715 *Csf3r* mice transduced with corresponding lentiviral constructs. GAPDH was used as loading control. **d** CFU assay and **e** replating CFU assay of transduced C57BL/6-d715 *Csf3r* lin$^-$ cells. Data represent means ± SD from triplicates of two independent experiments; $^*p < 0.05$, $^{**}p < 0.01$,$^{***}p < 0.001$

pathways, such as IL-6 signaling, interferon signaling, Tec kinase signaling, and leukocyte extravasation signaling (Fig. 3e, Suppl. Table 3).

Representative pathways of the innate immune system activated in d715 *Csf3r* lin$^-$ cells transduced with *RUNX1* mutants

As examples of the activated canonical inflammatory and innate immune signaling pathways, canonical TLR signaling and IL-6 pathways are depicted in Suppl. Figs. 2 and 3. TLR signaling was upregulated in d715 *Csf3r* lin$^-$ cells transduced with the R139G or R174L *RUNX1* mutants; this resulted in activation of transcription factors through Janus kinase 1 (JAK1) and p38 MAPK, promoting the expression of IL-1, TNF-alpha, and IL-12 (Suppl. Fig. 2A, B). Interferon signaling acted through JAK1 and JAK2 to activate the transcription factors, STAT1 and STAT2, thereby upregulating interferon response factors and other pro-inflammatory genes (Suppl. Fig. 2A, B).

The upregulation of IL-6 signaling–dependent genes in d715 *Csf3r* lin$^-$ cells transduced with each *RUNX1* mutant was also mediated through JAK signaling, but relied on the transcription factor, STAT3, to confer translational regulation in the nucleus. Additional IL-6-dependent activation of ERK1 induced the NF-kappaB-NF-IL-6 transcription factor complex (Suppl. Fig. 3A, B).

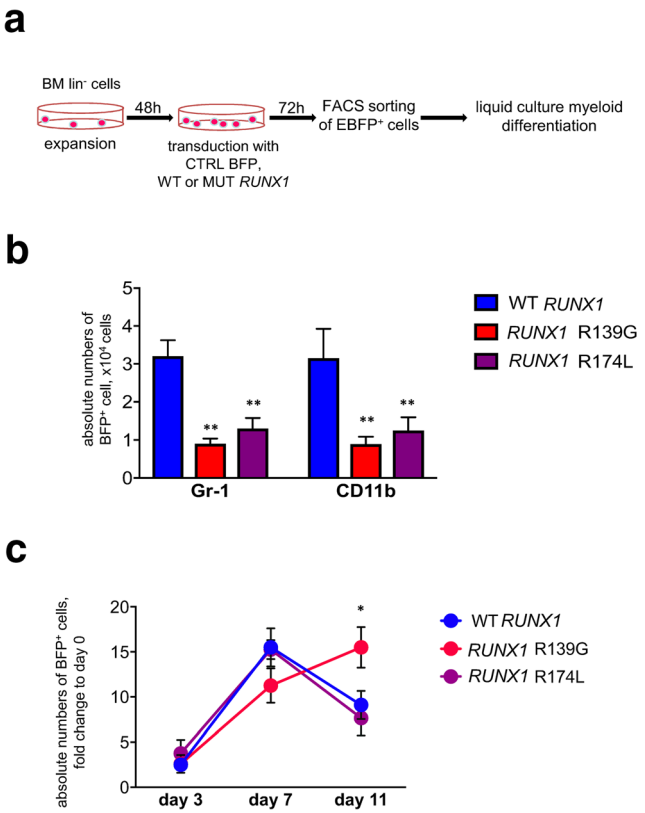

Fig. 2 Liquid culture differentiation of transduced d715 *Csf3r* HSPCs. **a** Schematic of the workflow for liquid culture myeloid differentiation of transduced bone marrow lin$^-$ cells obtained from C57BL/6-d715 *Csf3r* mice. **b** Transduced cells were subjected to liquid culture myeloid differentiation (see "Material and methods" for details). FACS was used to count the myeloid and granulocytic cells on day 11 of culture. Graph bars represent absolute cell counts of Gr-1$^+$ or CD11b$^+$ cells. Data represent means ± SD from triplicates of two independent experiments; $^{**}p < 0.01$

Upstream pathway analysis points toward inflammatory dysregulation

Upstream analysis performed using the IPA software identified potential upstream regulators responsible for the gene expression signatures observed in the studied groups. We detected 768 upstream regulators in the *RUNX1*-R139G mutant group and 875 regulators in the *RUNX1*-R174L mutant group (Suppl. Fig. 4A, Suppl. Table 4). Five hundred upstream regulators were commonly found in both groups: 65.1% in the *RUNX1*-R139G mutant group and 57.1% in the *RUNX1*-R174L mutant group (Suppl. Fig. 4A). Among the 15 top activated upstream regulators, 9/15 for *RUNX1*-R174L and 11/15 for *RUNX1*-R139G were shared between the groups. Among the 15 top downregulated regulators, overlaps were seen in 6/15 for *RUNX1*-R174L and 9/15 for *RUNX1*-R139G (Suppl. Fig. 4B). Selected up- and downregulated candidate genes were validated by qRT-PCR in the independent set of experiments (Suppl. Fig. 4C). Also, staining of transduced G-CSF-treated lin$^-$ cells with Sca-1 and c-kit antibody followed by flow cytometry analysis revealed an increase of lin$^-$Sca-1$^+$c-KIT$^+$ cell population in *RUNX1*-R139G– and *RUNX1*-R174L–transduced groups, compared with cells expressing *RUNX1* WT, or GFP CTRL (Suppl. Fig. 4D).

The top overlapping upstream regulators included a number of inflammatory cytokines, such as IL-15 and IL-18. IL-15 has been described as a responsible driver for chronic inflammation in autoimmune diseases and hematological malignancies [20]. Both IL-15 and IL-18 are confirmed targets for antitumor activity [21, 22]. Another factor that promotes survival of leukemogenic cells, Bcl2a1 [23], was also highly expressed, as were Ly6a and Sca-1, which are known as stemness factors for HSPCs.[24] The top downregulated genes included anti-inflammatory genes, such as Il-10 [25], and the cytokine-processing factor, Dpp4, which can increase proliferation by prolonging cytokine signaling [26]. Interestingly, *Csf3r* was among the highest expressed genes in both groups. This is in accordance with the literature showing that G-CSF sensitivity is increased in AML blasts with missense *RUNX1* mutations.

Motif activity response analysis confirms the central role of inflammatory and innate immunity signaling and the presence of early molecular changes related to MDS/AML downstream of Csf3r and *RUNX1* mutations

We used the ISMARA [27] web tool to analyze the transcription factor binding motifs enriched among the differentially expressed genes. We found that the most highly enriched motif was Irf2_Irf1_Irf8_Irf9_Irf7 (*z*-value 4.564), which corresponds to the interferon regulatory factors. This indicates that an interferon-related change in inflammation signaling is responsible for at least some of the observed gene expression differences. The Stat2 motif was significantly correlated with the expression signature (*z*-value 2.707), and we observed significant activation of the Klf4_Sp3 (*z*-value 2.349) and Mecp-2 (*z*-value 2.627) transcription factor binding motifs known to be associated with AML or MDS, but significant downregulation of the Max–Mycn motif (*z*-value 2.016), upon transduction of d715 *Csf3r* lin$^-$ cells with *RUNX1* mutants (Suppl. Fig. 5A). Finally, our inferred activity analysis of each motif revealed that there was a high degree of similarity in the significantly activated motifs associated with the two different *RUNX1* mutants (Suppl. Fig. 5B).

Discussion

The identification of cooperative *CSF3R* and *RUNX1* mutations in a majority of CN patients with overt MDS or AML brought us one step closer to understanding leukemia development [3]. Truncated *CSF3R* mutations are a very rare event

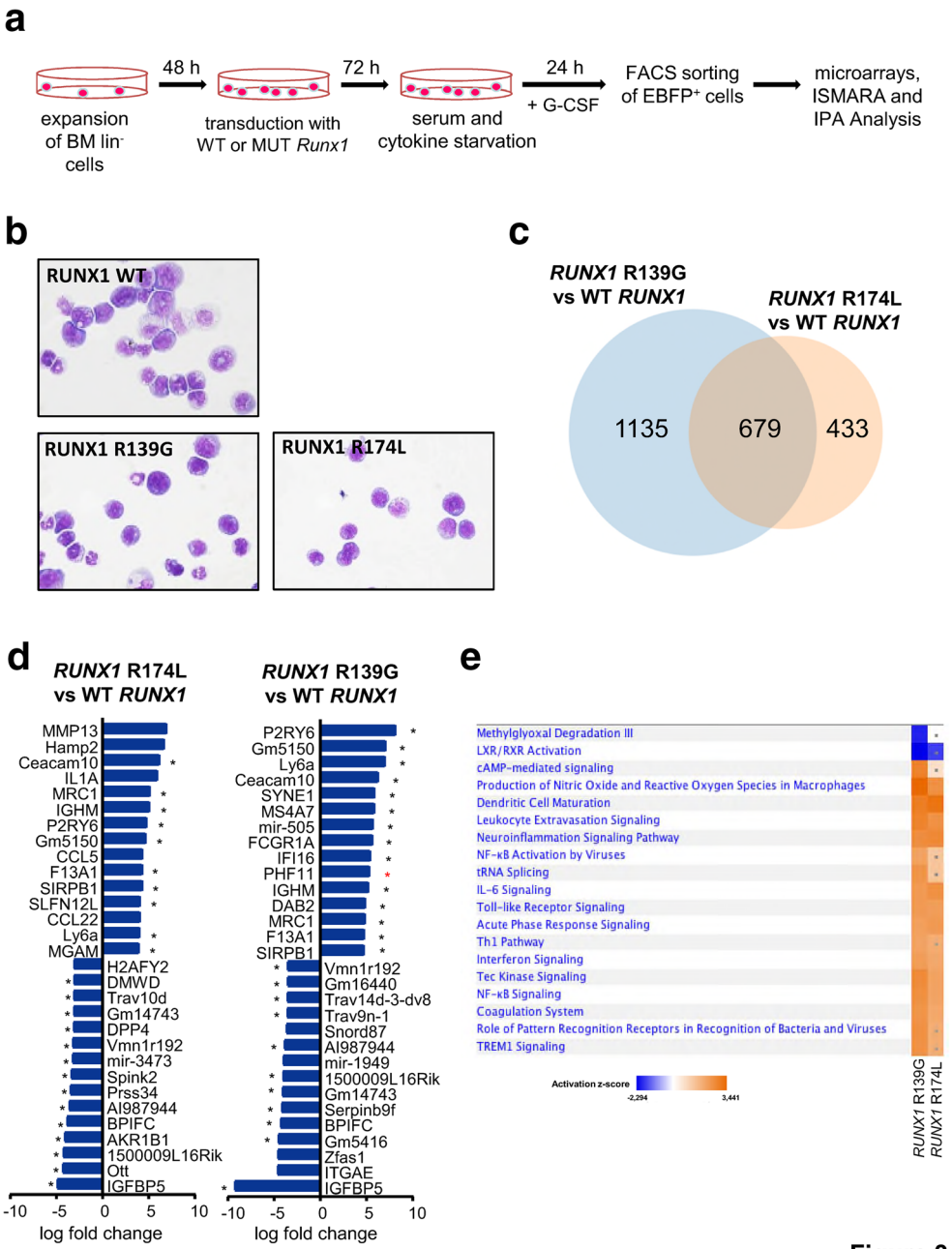

Fig. 3 Canonical pathway analysis of microarray data obtained from transduced d715 *Csf3r* HSPCs. **a** Schematic of the experimental procedure performed for microarray analysis. The experiment was conducted in duplicate. After quality control analysis, one sample from the *RUNX1*-R139G group was excluded from the final analysis. **b** Wright–Giemsa–stained cytospin preparations of *Csf3r* lin$^-$ cells transduced with *RUNX1* WT and mutants and sorted for fluorescent protein expression. Images were acquired at × 630 magnification. **c** Venn diagram depicting the overlay of significantly up- or downregulated transcripts in each *RUNX1* mutant group, as compared with WT *RUNX1*–transduced cells. **d** Canonical pathways that were significantly (−log(*p* value) > 1.3) enriched and significantly predicted (*z*-value > 2 and < − 2) to be up- or downregulated in each *RUNX1* mutant group compared with WT *RUNX1*–transduced cells. Shared pathways are marked with an asterisk (*). **e** IPA analysis of the significantly regulated pathways shared by lin$^-$ cells transduced with each *RUNX1* mutant, as compared with WT *RUNX1*–overexpressing samples. Upregulated pathways are shown in orange, and downregulated pathways are shown in blue

Figure 3

in de novo AML, while *RUNX1* mutations are most frequent among patients with secondary AML (sAML) after chemotherapy or radiation therapy, which represents about 30% of adult AML cases. Acquired cooperative *CSF3R* and *RUNX1* mutations in approximately 55% of CN/AML patients are a unique feature and may reflect the inherited background of patients with CN-associated gene mutations, such as those in *ELANE* or *HAX1*. Mechanistically, *ELANE* mutations induce unfolded protein response (UPR) [28, 29] and endoplasmic reticulum (ER) stress, while mutations in *HAX1* have pro-apoptotic functions [30, 31]. The role of inherited CN-associated mutations in the process of leukemogenesis needs to be investigated. The presence of these mutations may predispose to acquisition of secondary mutations in *CSF3R* and *RUNX1* and the development of leukemia. Similar to secondary leukemias, wherein HSPCs are damaged by chemotherapeutic agents or radiation therapy, inherited CN-specific mutations may induce DNA damage or stress responses in HSPCs. Indeed, using CN patient–derived iPSCs as an experimental model, we recently showed that an elevation of DNA damage in CN HSPCs precedes the leukemic transformation [32]. In the present study, we found that *csf3r* and *RUNX1*

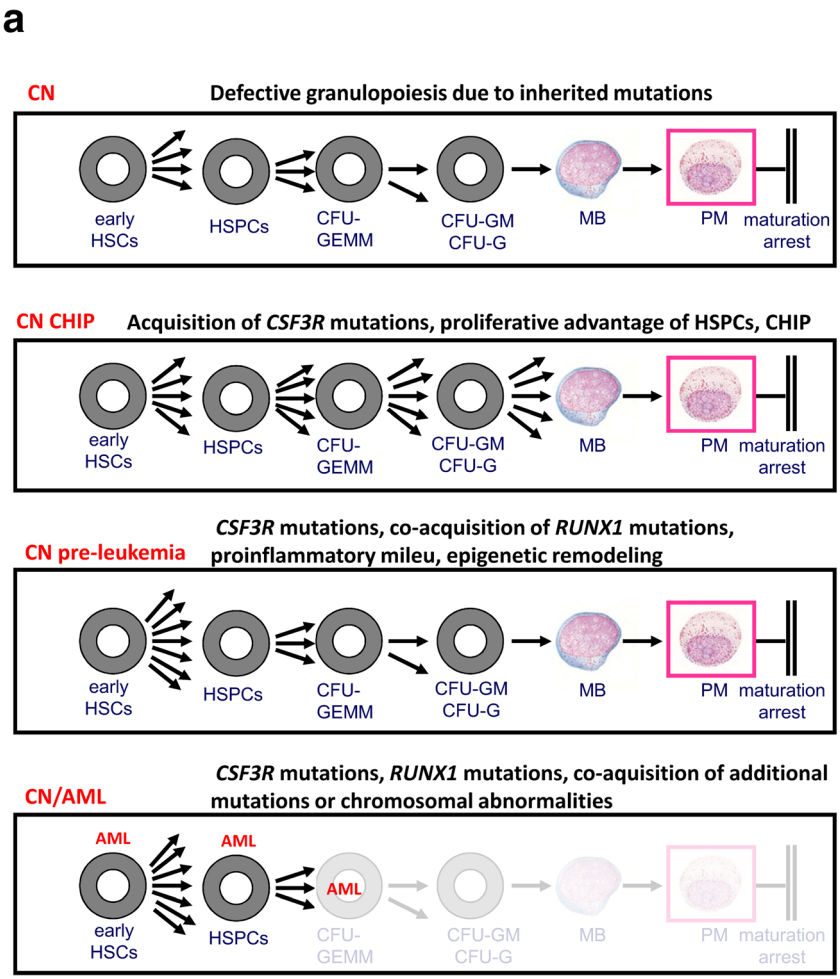

Fig. 4 Proposed model for leukemia development in CN. **a** CN, CN-associated germline mutations cause maturation arrest of granulopoiesis at the stage of promyelocytes/myelocyte. CN CHIP, HSPCs that acquire *CSF3R* mutations gain a proliferative advantage that may mimic the CHIP phenotype. CN pre-leukemia, the co-acquisition of *RUNX1* mutation induces an inflammatory milieu, leading to genotoxicity, additional defects of myeloid differentiation, and elevated proliferation that constitute the pre-leukemia stage. CN/AML, the acquisition of additional leukemia-associated gene mutations or chromosomal abnormalities results in AML or MDS

mutations in HSPCs induce reduced myeloid differentiation and enhanced clonogenic potential. Our findings demonstrated that cells transduced with WT *RUNX1* differentiated and lost the capacity to proliferate, making no colonies in replating experiments. In contrast, cells transduced with *RUNX1* mutants differentiate less, but retain proliferative potential. Leukemogenic activity of *csf3R* and *RUNX1* mutations should be further elaborated in vivo using a mouse model.

Elucidation of the deregulated intracellular signaling pathways downstream of *CSF3R* and *RUNX1* mutations will help to identify druggable targets, with the goal of eliminating leukemia-predisposed HSPCs and/or specifically targeting CN/AML blasts. Interestingly, mRNA expression analysis revealed that HSPCs harboring mutations in *Csf3R* and *RUNX1* exhibit activation of the inflammatory and innate immunity pathways, including interferon signaling; IL-1, IL-6, IL-8, and TLR signaling; and TREM1 signaling. Additionally, we also found marked upregulation of Ly6a (also known as Sca-1), a marker of stemness in HSPCs [24] that is also upregulated upon inflammation [33–35]. IL-6 and IL-8 were previously known to be hyper-activated in MDS and AML [19, 36, 37]. Moreover, the increased genotoxic stress in HSPCs of 40% de novo MDS cases has been associated with elevated TLRs/Myd88-triggered intracellular signaling and IL-8 expression [19]. Most probably, the presence of truncated *CSF3R* and *RUNX1* mutations in HSPCs of CN patients alters the pro-inflammatory cell state, enhances proliferation, and increases the susceptibility of HSPCs to genomic toxicity. Recent reports revealed that pre-leukemic HSPCs carrying an *ETV6-RUNX1* fusion gene or having *Pax5* haploinsufficiency evolved to precursor B cell acute lymphocytic leukemia upon activation of the pro-inflammatory pathways [38, 39]. The role of activated innate immunity and inflammatory pathways in the leukemogenesis of CN HSPCs was not studied yet. It would be interesting to investigate the susceptibility and expression kinetics of TLRs and the receptors for IL-1 and IL-8 on HSPCs from CN/AML patients during the development of leukemia.

We found that the Spi1/PU.1 transcription factor motif is activated in HSPCs downstream of *Csf3r* and *RUNX1* mutations. PU.1 is upregulated in hematopoietic cells of CN patients [40] and is an essential transcription factor for monocytic differentiation [41, 42]. PU.1 also acts as a maintenance factor for pre- and leukemia-initiating cells [43]. The

leukemogenic function of upregulated PU.1 in HSPCs of CN patients has not been studied yet.

Taken together, our results support the following proposed mechanism for leukemia development in CN: *CSF3R* mutations represent a state of clonal hematopoiesis of indeterminate potential (CHIP) in CN patients in that they confer a clonal advantage. Co-acquisition of *RUNX1* mutation further increases proliferation and genotoxicity, including hypersensitivity to pro-inflammatory signaling. This combination may lead to acquisition of additional somatic mutations (e.g., in *SUZ12* or *ASXL1*) or chromosomal abnormalities (e.g., monosomy 7 or trisomy 21), which finally overt to MDS or AML (Fig. 4).

Acknowledgments We would like to thank C. Stocking for providing *RUNX1* expression plasmids.

Authorship contributions JS and MR made initial observations, designed the experiments, analyzed the data, supervised experimentation, and wrote the manuscript; MR performed the main experiments; MK generated *RUNX1* mutants; A Scham. and DH re-cloned *RUNX1* cDNAs into pRRL.PPT.CBX3SF hRUNX1.i2.EBFP.puro.pre backbone; OK assisted with the transduction of mouse lin^- cells and differentiation experiments; A Schm. and DCL provided bone marrow of C57BL/6-d715 *Csf3r* mice; and KW and LK provided insightful comments.

Funding information Open Access funding provided by Projekt DEAL. This study was funded by the Fritz Thyssen Stiftung and DFG. We would like to acknowledge the financial support of the study by the German Jose Carreras Leukemia foundation (M.R. and J.S.).

Compliance with ethical standards

Conflict of interest The authors declare that they have no conflict of interest.

Ethical approval All applicable international, national, and/or institutional guidelines for the care and use of animals were followed. All animal studies included in this manuscript were reviewed and approved by the Regional Board of the City of Tübingen.

Human and animal rights This article does not contain any study with humans participants performed by any of the authors.

References

1. Skokowa J, Dale DC, Touw IP, Zeidler C, Welte K (2017) Severe congenital neutropenias. Nat Rev Dis Prim 3:17032
2. Skokowa J, Germeshausen M, Zeidler C et al (2007) Severe congenital neutropenia: inheritance and pathophysiology. Curr Opin Hematol 14:22–28
3. Hermans MHA, Antonissen C, Ward AC, Mayen AEM, Ploemacher RE, Touw IP (1999) Sustained receptor activation and hyperproliferation in response to granulocyte colony-stimulating factor (G-CSF) in mice with a severe congenital neutropenia/acute myeloid leukemia–derived mutation in the G-CSF receptor gene. J Exp Med 189:683–691
4. Dong F, Brynes RK, Tidow N, Welte K, Löwenberg B, Touw IP (1995) Mutations in the gene for the granulocyte colony-stimulating-factor receptor in patients with acute myeloid leukemia preceded by severe congenital neutropenia. N Engl J Med 333:487–493
5. Dong F, Hoefsloot LH, Schelen AM, Broeders CA, Meijer Y, Veerman AJ, Touw IP, Lowenberg B (1994) Identification of a nonsense mutation in the granulocyte-colony-stimulating factor receptor in severe congenital neutropenia. Proc Natl Acad Sci 91:4480–4484
6. Dong F, van Buitenen C, Pouwels K, Hoefsloot LH, Löwenberg B, Touw IP (1993) Distinct cytoplasmic regions of the human granulocyte colony-stimulating factor receptor involved in induction of proliferation and maturation. Mol Cell Biol 13:7774–7781
7. Ward AC, van Aesch YM, Schelen AM, Touw IP (1999) Defective internalization and sustained activation of truncated granulocyte colony-stimulating factor receptor found in severe congenital neutropenia/acute myeloid leukemia. Blood 93:447–458
8. Liu F, Kunter G, Krem MM, Eades WC, Cain JA, Tomasson MH, Hennighausen L, Link DC (2008) Csf3r mutations in mice confer a strong clonal HSC advantage via activation of Stat5. J Clin Invest 118:946–955
9. McLemore ML, Poursine-Laurent J, Link DC (1998) Increased granulocyte colony-stimulating factor responsiveness but normal resting granulopoiesis in mice carrying a targeted granulocyte colony-stimulating factor receptor mutation derived from a patient with severe congenital neutropenia. J Clin Invest 102:483–492
10. Skokowa J, Steinemann D, Katsman-Kuipers JE, Zeidler C, Klimenkova O, Klimiankou M, Ünalan M, Kandabarau S, Makaryan V, Beekman R, Behrens K, Stocking C, Obenauer J, Schnittger S, Kohlmann A, Valkhof MG, Hoogenboezem R, Göhring G, Reinhardt D, Schlegelberger B, Stanulla M, Vandenberghe P, Donadieu J, Zwaan CM, Touw IP, van den Heuvel-Eibrink MM, Dale DC, Welte K (2014) Cooperativity of RUNX1 and CSF3R mutations in severe congenital neutropenia: a unique pathway in myeloid leukemogenesis. Blood 123:2229–2237
11. Osato M (2004) Point mutations in the RUNX1/AML1 gene: another actor in RUNX leukemia. Oncogene 23:4284–4296
12. Osato M, Asou N, Abdalla E, Hoshino K, Yamasaki H, Okubo T, Suzushima H, Takatsuki K, Kanno T, Shigesada K, Ito Y (1999) Biallelic and heterozygous point mutations in the runt domain of the AML1/PEBP2alphaB gene associated with myeloblastic leukemias. Blood 93:1817–1824
13. Christiansen DH, Andersen MK, Pedersen-Bjergaard J (2004) Mutations of AML1 are common in therapy-related myelodysplasia following therapy with alkylating agents and are significantly associated with deletion or loss of chromosome arm 7q and with subsequent leukemic transformation. Blood 104:1474–1481
14. Harada H, Harada Y, Tanaka H, Kimura A, Inaba T (2003) Implications of somatic mutations in the AML1 gene in radiation-associated and therapy-related myelodysplastic syndrome/acute myeloid leukemia. Blood 101:673–680
15. Schnittger S, Dicker F, Kern W, Wendland N, Sundermann J, Alpermann T, Haferlach C, Haferlach T (2011) RUNX1 mutations are frequent in de novo-AML with noncomplex karyotype and confer an unfavorable prognosis. Blood 117:2348–2357

16. Gaidzik VI, Teleanu V, Papaemmanuil E et al (2016) RUNX1 mutations in acute myeloid leukemia are associated with distinct clinico-pathologic and genetic features. Leukemia 30:2160–2168
17. Preudhomme C, Renneville A, Bourdon V et al (2009) Brief report High frequency of RUNX1 biallelic alteration in acute myeloid leukemia secondary to familial platelet disorder. 113:5583–5588
18. Balkwill F, Mantovani A (2001) Inflammation and cancer: back to Virchow? Lancet 357:539–545
19. Hemmati S, Haque T, Gritsman K (2017) Inflammatory signaling pathways in preleukemic and leukemic stem cells. Front Oncol 7
20. Fehniger TA, Caligiuri MA (2001) Interleukin 15: biology and relevance to human disease. Blood 97:14–32
21. Kim PS, Kwilas AR, Xu W et al (2016) IL-15 superagonist/IL-15RαSushi-Fc fusion complex (IL-15SA/IL-15RαSu-Fc; ALT-803) markedly enhances specific subpopulations of NK and memory CD8+ T cells, and mediates potent anti-tumor activity against murine breast and colon carcinomas. Oncotarget 7
22. Senju H, Kumagai A, Nakamura Y, Yamaguchi H, Nakatomi K, Fukami S, Shiraishi K, Harada Y, Nakamura M, Okamura H, Tanaka Y, Mukae H (2018) Effect of IL-18 on the expansion and phenotype of human natural killer cells: application to cancer immunotherapy. Int J Biol Sci 14:331–340
23. Vogler M (2012) BCL2A1: the underdog in the BCL2 family. Cell Death Differ 19:67–74
24. Holmes C, Stanford WL (2007) Concise review: stem cell antigen-1: expression, function, and enigma. Stem Cells 25:1339–1347
25. Kelly Á, Lynch A, Vereker E, Nolan Y, Queenan P, Whittaker E, O'Neill LAJ, Lynch MA (2001) The anti-inflammatory cytokine, interleukin (IL)-10, blocks the inhibitory effect of IL-1β on long term potentiation. J Biol Chem 276:45564–45572
26. Deng L, Chan R, O'Leary HA et al (2017) DPP4 truncated GM-CSF and IL-3 manifest distinct receptor-binding and regulatory functions compared with their full-length forms. Leukemia 31: 2468–2478
27. Balwierz PJ, Pachkov M, Arnold P, Gruber AJ, Zavolan M, van Nimwegen E (2014) ISMARA: automated modeling of genomic signals as a democracy of regulatory motifs. Genome Res 24:869–884
28. Grenda DS, Murakami M, Ghatak J, Xia J, Boxer LA, Dale D, Dinauer MC, Link DC (2007) Mutations of the ELA2 gene found in patients with severe congenital neutropenia induce the unfolded protein response and cellular apoptosis. Blood 110:4179–4187
29. Nustede R, Klimiankou M, Klimenkova O, Kuznetsova I, Zeidler C, Welte K, Skokowa J (2016) ELANE mutant-specific activation of different UPR pathways in congenital neutropenia. Br J Haematol 172:219–227
30. Boztug K, Appaswamy G, Ashikov A et al (2008) A syndrome with congenital neutropenia and mutations in G6PC3. N Engl J Med 360:32–43
31. Klein C, Grudzien M, Appaswamy G, Germeshausen M, Sandrock I, Schäffer AA, Rathinam C, Boztug K, Schwinzer B, Rezaei N, Bohn G, Melin M, Carlsson G, Fadeel B, Dahl N, Palmblad J, Henter JI, Zeidler C, Grimbacher B, Welte K (2007) HAX1 deficiency causes autosomal recessive severe congenital neutropenia (Kostmann disease). Nat Genet 39:86–92
32. Dannenmann B, Zahabi A, Mir P et al (2018) Human iPSC-based model of severe congenital neutropenia reveals elevated UPR and DNA damage in CD34+ cells preceding leukemic transformation. Exp Hematol
33. Clapes T, Lefkopoulos S, Trompouki E (2016) Stress and non-stress roles of inflammatory signals during HSC emergence and maintenance. Front Immunol 7:1–15
34. Essers MAG, Offner S, Blanco-Bose WE, Waibler Z, Kalinke U, Duchosal MA, Trumpp A (2009) IFNα activates dormant haematopoietic stem cells in vivo. Nature 458:904–908
35. Bujanover N, Goldstein O, Greenshpan Y, Turgeman H, Klainberger A, Scharff Y', Gazit R (2018) Identification of immune-activated hematopoietic stem cells. Leukemia 32:2016–2020
36. Kuett A, Rieger C, Perathoner D et al (2015) IL-8 as mediator in the microenvironment-leukaemia network in acute myeloid leukaemia. Sci Rep 5:1–11
37. Bhattacharyya S, Shastri A, Bartenstein M et al (2015) IL8-CXCR2 pathway inhibition as a therapeutic strategy against MDS and AML stem cells. Blood 125:3144–3152
38. Rodríguez-Hernández G, Hauer J, Martín-Lorenzo A, Schäfer D, Bartenhagen C, García-Ramírez I, Auer F, González-Herrero I, Ruiz-Roca L, Gombert M, Okpanyi V, Fischer U, Chen C, Dugas M, Bhatia S, Linka RM, Garcia-Suquia M, Rascón-Trincado MV, Garcia-Sanchez A, Blanco O, García-Cenador MB, García-Criado FJ, Cobaleda C, Alonso-López D, de Las Rivas J, Müschen M, Vicente-Dueñas C, Sánchez-García I, Borkhardt A (2017) Infection exposure promotes ETV6-RUNX1 precursor B-cell leukemia via impaired H3K4 demethylases. Cancer Res 77:4365–4377
39. Martín-Lorenzo A, Hauer J, Vicente-Dueñas C et al (2015) Infection exposure is a causal factor in B-cell precursor acute lymphoblastic leukemia as a result of Pax5-inherited susceptibility. Cancer Discov 5:1328–1343
40. Skokowa J, Welte K (2009) Dysregulation of myeloid-specific transcription factors in congenital neutropenia: rescue by namptnad+ sirt1. Ann N Y Acad Sci 1176:94–100
41. Friedman AD (2007) Transcriptional control of granulocyte and monocyte development. Oncogene 26:6816–6828
42. Rosenbauer F, Tenen DG (2007) Transcription factors in myeloid development: balancing differentiation with transformation. Nat Rev Immunol 7:105–117
43. Staber PB, Zhang P, Ye M, Welner RS, Levantini E, di Ruscio A, Ebralidze AK, Bach C, Zhang H, Zhang J, Vanura K, Delwel R, Yang H, Huang G, Tenen DG (2014) The Runx-PU.1 pathway preserves normal and AML/ETO9a leukemic stem cells. Blood 124:2391–2399

I) Morishima, T. et al., 2019, *Blood*

blood®
Regular Article

LYMPHOID NEOPLASIA

LMO2 activation by deacetylation is indispensable for hematopoiesis and T-ALL leukemogenesis

Tatsuya Morishima,[1] Ann-Christin Krahl,[1,*] Masoud Nasri,[1,*] Yun Xu,[1] Narges Aghaallaei,[1] Betül Findik,[1] Maksim Klimiankou,[1] Malte Ritter,[1] Marcus D. Hartmann,[2] Christian Johannes Gloeckner,[3,4] Sylwia Stefanczyk,[1] Christian Lindner,[1] Benedikt Oswald,[1] Regine Bernhard,[1] Karin Hähnel,[1] Ursula Hermanutz-Klein,[1] Martin Ebinger,[5] Rupert Handgretinger,[5] Nicolas Casadei,[6] Karl Welte,[5] Maya Andre,[5,7] Patrick Müller,[1,8] Baubak Bajoghli,[1] and Julia Skokowa[1]

[1]Department of Hematology, Oncology, Clinical Immunology and Rheumatology, University Hospital Tübingen, Germany; [2]Department of Protein Evolution, Max Planck Institute for Developmental Biology, Tübingen, Germany; [3]German Center for Neurodegenerative Diseases, Tübingen, Germany; [4]Center for Ophthalmology, Institute for Ophthalmic Research, University Hospital Tübingen, Tübingen, Germany; [5]University Children's Hospital Tübingen, Tübingen, Germany; [6]Institute of Medical Genetics and Applied Genomics, University Hospital Tübingen, Tübingen, Germany; [7]Department of Pediatric Intensive Care, University of Basel Children's Hospital, Basel, Switzerland; and [8]Friedrich Miescher Laboratory of the Max Planck Society, Tübingen, Germany

KEY POINTS

- **LMO2 is deacetylated by the NAMPT/SIRT2 pathway.**
- **LMO2 deacetylation is essential for LIM domain binding 1 binding and TAL1 complex activation during hematopoiesis and T-ALL leukemogenesis.**

Hematopoietic transcription factor LIM domain only 2 (LMO2), a member of the TAL1 transcriptional complex, plays an essential role during early hematopoiesis and is frequently activated in T-cell acute lymphoblastic leukemia (T-ALL) patients. Here, we demonstrate that LMO2 is activated by deacetylation on lysine 74 and 78 via the nicotinamide phosphoribosyltransferase (NAMPT)/sirtuin 2 (SIRT2) pathway. LMO2 deacetylation enables LMO2 to interact with LIM domain binding 1 and activate the TAL1 complex. NAMPT/SIRT2-mediated activation of LMO2 by deacetylation appears to be important for hematopoietic differentiation of induced pluripotent stem cells and blood formation in zebrafish embryos. In T-ALL, deacetylated LMO2 induces expression of TAL1 complex target genes *HHEX* and *NKX3.1* as well as *LMO2* autoregulation. Consistent with this, inhibition of NAMPT or SIRT2 suppressed the in vitro growth and in vivo engraftment of T-ALL cells via diminished LMO2 deacetylation. This new molecular mechanism may provide new therapeutic possibilities in T-ALL and may contribute to the development of new methods for in vitro generation of blood cells. (*Blood*. 2019;134(14):1159-1175)

Introduction

Hematopoietic transcription factors that play crucial roles during different stages of blood development are often deregulated in leukemia,[1-3] strengthening the view that appropriate regulation of transcription factor networks is essential for maintaining proper hematopoietic tissue homeostasis. One example of the importance of dose and cell differentiation stage-dependent expression of transcription factors in blood homeostasis is the LIM domain only 2 (LMO2) protein, an essential transcriptional regulator of early hematopoiesis.[4,5] *LMO2* knockout mice and zebrafish exhibit a complete loss of hematopoietic cells.[6,7] Notably, malignant cells from ~50% of patients with T-cell acute lymphoblast leukemia (T-ALL) express elevated levels of LMO2 or its interaction partner SCL/T-cell acute lymphocytic leukemia 1 (TAL1).[8-10] LMO2 is continuously silenced after commitment to early T-cell progenitors, and its overexpression leads to preleukemic alterations in thymocytes that culminate in T-ALL.[11-15] It has been shown that, in T-ALL, LMO2 reactivates a hematopoietic stem cell (HSC)-specific transcriptional program, leading to enhanced self-renewal and proliferation of early T-cell progenitors with reduced capacity for T-cell differentiation of T-ALL blasts.[16] A recent study by García-Ramírez et al demonstrated that the presence of LMO2 in murine hematopoietic stem/progenitor cells (HSPC) is necessary for the early stages of transformation to T-ALL through in vivo reprogramming.[17]

LMO2, which is highly conserved in organisms ranging from zebrafish to humans,[5] consists of 2 LIM domains (LIM1 and LIM2) connected by a short, flexible hinge region.[18,19] LIM domains are generally composed of 2 consecutive zinc finger motifs that mediate interactions with other proteins. The LMO2 protein forms the core of the transcriptional TAL1 complex, anchoring its interaction partners LIM domain binding 1 (LDB1), TAL1 (also known as SCL), E47 (also known as transcription factor-3), and GATA binding protein 1 (GATA1).[20] Both LMO2 LIM domains serve as scaffolds for assembly of the complex. Whereas the interaction with LDB1 involves all 4 zinc fingers, the interaction with the TAL1:E47 heterodimer is largely localized to the central hinge region, involving the C-terminal zinc finger of LIM1 and the N-terminal zinc finger of LIM2.[19] GATA proteins are thought to interact mostly with the LIM2 domain.[18] Thus, LMO2 functions as an essential adapter protein, allowing the proper assembly of the TAL1 complex.

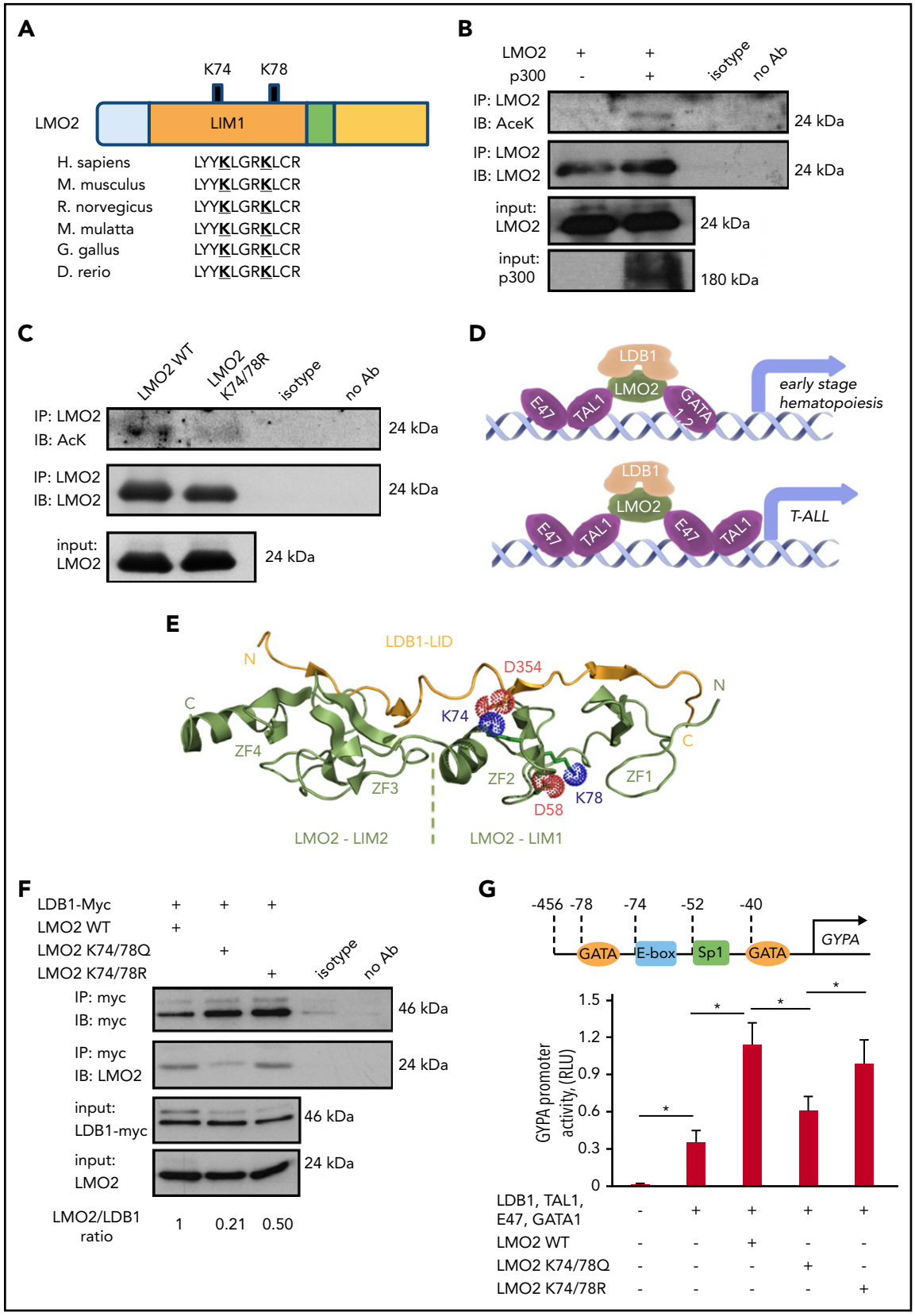

Figure 1. Lysine deacetylation of LMO2 is essential for the LDB1 interaction and transcriptional activity of the TAL1 complex. (A) Schematic of the LMO2 protein showing 2 putative lysines in LMO2 (K74 and K78) within the LIM1 domain that could be deacetylated (bold and underlined) based on in silico analysis. (B-C) Immunoprecipitation (IP) assay of the lysates of HEK293T cells transfected with expression vectors of p300 and WT or K74/78R LMO2 mutant. IP and immunoblot were performed with indicated antibodies. IPs were performed twice; representative western blot images are depicted. (D) Schematic of the activation of target genes during early hematopoiesis (upper) and T-ALL leukemogenesis (lower) by binding of the TAL1 complex (consisting of E47, TAL1, LDB1, LMO2, and GATA1/2 proteins) to the specific putative regions on the gene promoters.

Determining how LMO2 activity may be specifically targeted in T-ALL requires an understanding of the mechanisms of LMO2 activation. There are only a few reports describing the mechanism of LMO2 activation. Two of them demonstrated autoregulatory mechanisms of elevated *LMO2* messenger RNA (mRNA) expression in HSCs and T-ALL cells.[21,22] Posttranslational regulation of protein function through deacetylation mediated by nicotinamide phosphoribosyltransferase (NAMPT) and sirtuin (SIRT) is known to play a pivotal role during myeloid differentiation and leukemogenic transformation of hematopoietic cells. The NAMPT/SIRT pathway serves this function by activating a number of proteins, including the CCAAT/enhancer binding proteins C/EBPα and C/EBPβ, the serine/threonine kinase AKT, the tumor-suppressor p53, and the forkhead box transcription factor FOXO3.[23-27] NAMPT is a NAD^+-generating enzyme, and SIRT family proteins (SIRT1-7) are NAD^+-dependent class III histone deacetylases.[28] Despite their high similarity, SIRT1 and SIRT2 have different functions, targets, and preferential intracellular localizations. In this latter context, SIRT1 is preferentially localized to the nucleus, whereas SIRT2 is a cytoplasmic enzyme that transiently migrates to the nucleus during the G2/M cell-cycle transition.[29,30] It has been demonstrated that a SIRT1 deficiency compromises hematopoietic differentiation of mouse embryonic stem (ES) cells, and embryonic and adult hematopoiesis in the mouse.[31] However, the role of NAMPT and SIRT2 during early stages of blood cell development or T-ALL leukemogenesis is largely unknown. Importantly, specific selective inhibitors of NAMPT, SIRT1, and SIRT2 have been described,[32-34] allowing functional analysis of the specific role of these factors. In the present study, we investigated whether LMO2 is activated by NAMPT/SIRT2-mediated deacetylation in T-ALL and in early blood development in vitro and in vivo.

Methods

Cell culture

HEK 293T and HEK 293FT cells were cultured in Dulbecco's modified Eagle medium supplemented with 10% fetal bovine serum (FBS) and 1% penicillin/streptomycin. MOLT-4 and MOLT-14 cells were cultured in RPMI-1640 medium supplemented with 10% FBS and 1% penicillin/streptomycin. Mononuclear cells isolated from bone marrow or peripheral blood samples of 3 pediatric T-ALL patients were transplanted IV into 8- to 12-week-old female NOD.Cg-Prkdc^{scid}Il2rg^{tm1Wjl}/SzJ (NSG) mice (The Jackson Laboratory, Bar Harbor, ME). T-ALL blasts isolated from spleen of engrafted mice were used for the in vitro experiments and the in vivo zebrafish engraftment. Written informed consent and institutional review board approval of the University Hospital Tübingen in accordance with the Declaration of Helsinki were obtained for the use of T-ALL bone marrow and peripheral blood samples for this study.

Healthy donor-derived human iPS cells (hCD34-iPSC16)[35] were kindly provided by Nico Lachmann and Thomas Moritz (Hannover Medical School, Hannover, Germany). This human iPS cell line was maintained on mitomycin-C-treated (Sigma-Aldrich, St. Louis, MO) SNL feeder cells in Dulbecco's modified Eagle medium/F12 (Sigma-Aldrich) supplemented with 20% Knockout Serum Replacement (Thermo Fisher Scientific, Waltham, MA), 30 ng/mL basic fibroblast growth factor (Peprotec, Rocky Hill, NJ), 1% nonessential amino acids solution (Thermo Fisher Scientific), 100 mM 2-mercaptethanol (Thermo Fisher Scientific), and 2 mM L-glutamine (Thermo Fisher Scientific). The culture medium was replaced daily with fresh medium. Colonies were mechanically passaged onto new SNL feeder cells every 10 days.

Hematopoietic differentiation of iPS cells

Undifferentiated iPS cell colonies were cultured on growth factor-reduced Matrigel (Becton-Dickinson)-coated cell culture dishes in Stemline II HSC expansion medium (Sigma-Aldrich) containing insulin-transferrin-selenium (ITS) supplement (Thermo Fisher Scientific) and cytokines (bone morphogenetic protein 4 [BMP4], 20 ng/mL, R&D Systems, Minneapolis, MN) was added to the culture for the first 4 days and then replaced with vascular endothelial growth factor 165 (VEGF 165) (40 ng/mL, R&D Systems) for 2 days. On day 6, VEGF 165 was replaced with a combination of stem cell factor (50 ng/mL, R&D Systems), interleukin 3 (IL-3; 50 ng/mL, R&D Systems), and thrombopoietin (5 ng/mL, R&D Systems). Thereafter, medium was replaced every 3 or 4 days. FK866 (Sigma-Aldrich), AC93253 (Sigma-Aldrich), EX527 (Sigma-Aldrich), or dimethyl sulfoxide (DMSO; vehicle control, Sigma-Aldrich) were added to the fresh medium. Differentiated iPS cells were dissociated using StemPro Accutase Cell Dissociation Reagent (Thermo Fisher Scientific), harvested through a cell strainer (Miltenyi Biotec, Bergisch Gladbach, Germany), and used for analysis. $CD34^+$ cells were sorted using the CD34 MicroBead Kit, human (Miltenyi Biotec) following the manufacturer's instructions.

Zebrafish experiments

Gene knockdown experiments were performed using wild-type (WT) TE fish and the transgenic line *Tg(-6.35drl:EGFP)*.[36] Antisense morpholino oligonucleotides (MOs) were obtained from GENE TOOLS (Philomath, OR) targeting *nampta* (5′-TGTGTG ACCTGCAATGAAAGAAAGA-3′) or *sirt2*[37] (5′-ACCTCTAAAGGA CACAAAAAAGGCT-3′). MOs and plasmids (pcDNA3.1-pbef [NAMPT], pcDNA3.1-SIRT2-flag, and pSIN4-EF1a-LMO2-IRES-Puro, with WT or K74/78R mutant *LMO2* complementary DNA) were injected into 1-cell stage embryos using a PV830 Pneumatic PicoPump (World Precision Instruments, Sarasota, FL) at nontoxic levels (ie, 3.3 ng *nampta MO*, 2.5 ng *sirt2 MO* and 25 pg plasmids). Primers flanking exon 1 and exon 5 of the *nampta* gene (forward: 5′-AGAGAAGCCGCGGATTTCAA-3′; reverse: 5′-CTCCAGTCC TTCCAGGCTTC-3′) and primers flanking exon 1 and exon 4 of the *sirt2* gene[37] (forward: 5′-GCTGGCTTATAGTTTTAAAGAGGG TA-3′; reverse: 5′-AGTATGTAGCGAGCAACTGAGTC-3′) were used for subsequent reverse transcriptase polymerase chain reaction (RT-PCR) to verify morpholino-induced blocking of splicing. Embryos at 24 hours postfertilization (hpf) were collected and

Figure 1 (continued) (E) Crystal structure of the LMO2:LDB1-LID complex (PDB 2XJY), highlighting electrostatic interactions of the deacetylated lysines 74 and 78 of LMO2 (green). The lysines and neighboring aspartates, D58 from LMO2-LIM1 and D354 from LDB1 (yellow), are shown as sticks; their cationic ammonium and anionic carboxylate groups are outlined with dotted spheres representing their van der Waals radii. If the lysines were acetylated, they would carry 0 net-charge and could not complement the negative charge of the aspartates. N and C termini and the individual zinc fingers (ZF1-ZF4) are labeled. (F) Co-IP of LMO2 and LDB1 proteins in lysates of HEK293T cells transfected with indicated expression vectors. IP and immunoblot were performed with indicated antibodies. Representative western blot images are depicted. (G) Activity of *GYPA* reporter containing the 456-bp upstream region of *GYPA* with putative binding sites for the TAL1 complex (upper). HEK293T cells were transfected with *GYPA* reporter construct and the indicated expression vectors. The activation of *GYPA* reporter was measured as described in "Methods." Data show means ± standard deviation (SD) (n = 8). *$P < .05$.

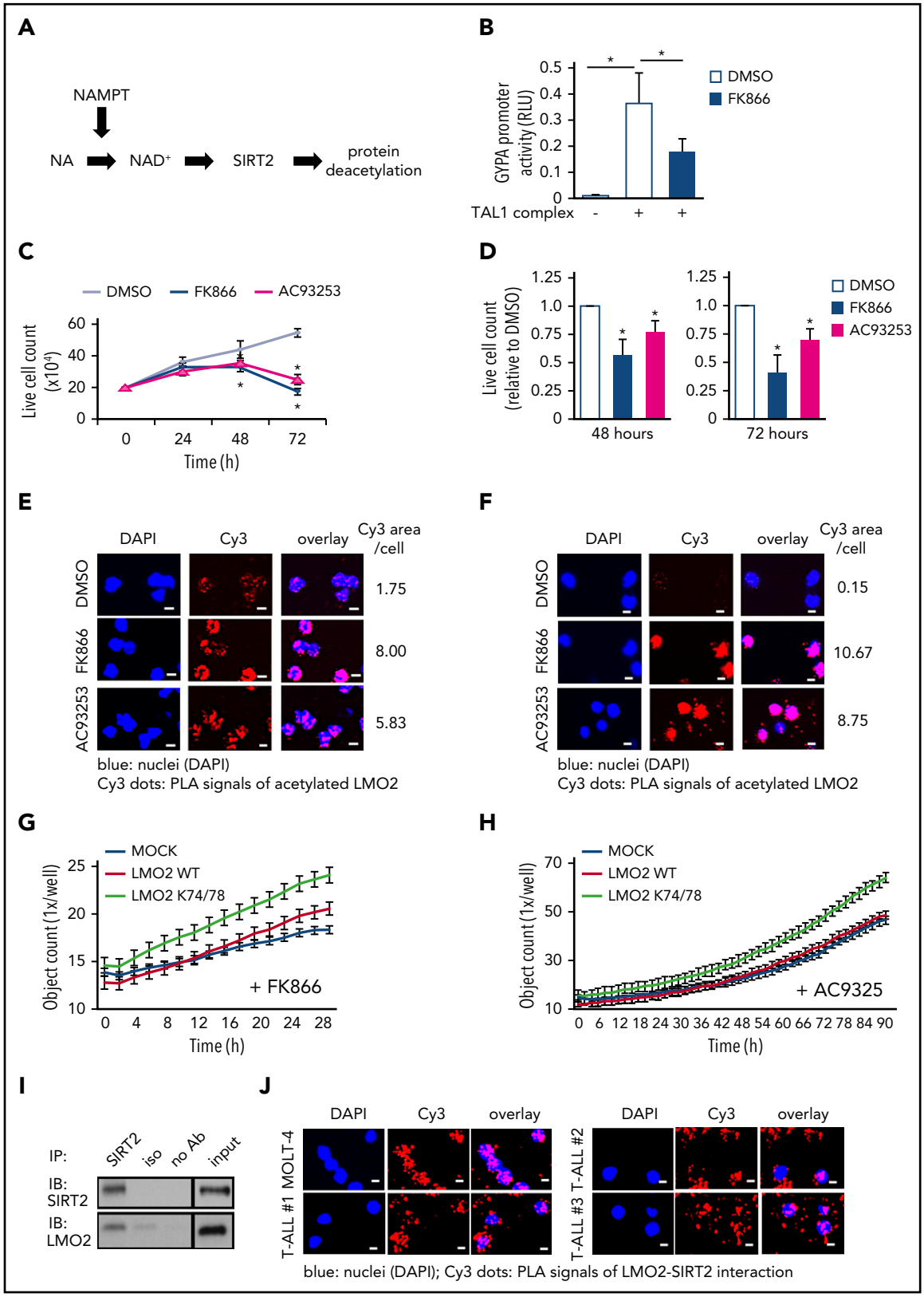

Figure 2. The NAMPT/SIRT2 pathway activates LMO2 by deacetylation in T-ALL cells. (A) Schematic of the NAMPT-NAD^+-SIRTs pathway. (B) Reporter gene assay using *GYPA* reporter construct. HEK293T cells were transfected with a *GYPA* reporter and the indicated expression constructs. Transfected cells were cultured in the presence or absence of FK866 for 24 hours, and the activation of the *GYPA* reporter was measured as described in "Methods." The same concentration of DMSO was added as a vehicle control. Data show means ± SD (n = 8). *$P < .05$. (C) Live-cell counting of MOLT-4 cells treated with 10 nM FK866 or 100 nM AC93253. The same concentration of DMSO was added as a vehicle control. Dead cells were excluded by trypan blue dye staining. Data represent mean ± SD from 3 independent experiments, each in triplicate (*$P < .05$ compared with DMSO-treated cells). (D) Live-cell counting of primary blasts from T-ALL patients (n = 3) treated with 10 nM FK866 or 100 nM AC93253 for 48 or 72 hours. The same

homogenized with a pestle for RNA isolation and NAD^+ measurement. RNA was isolated using the RNeasy Mini Kit (Qiagen) following the manufacturer's instructions. Images were collected using an Axio ZoomV16 microscope (ZEISS).

Xenotransplantation experiments were performed using WT TE or albino fish (alb^{b4}).[38] WT embryos were treated with 0.003% 1-phenyl-2-thiourea to prevent pigment formation. MOLT-4 cells were labeled with Vybrant CFDA SE Cell Tracer Kit (Thermo Fisher Scientific) following the manufacturer's instructions. Labeled cells were suspended in phosphate-buffered saline at a density of 2×10^5 cells/μL, and 1 nL cell suspension (200 cells) was injected into the perivitelline space of embryos at 24 hpf. Injected embryos were incubated at 28°C for 1 hour followed by incubation with DMSO or FK866 for 48 hours at 35°C. Drug-treated embryos were dissociated by passing through a 40-μm cell strainer (Greiner Bio-One) in ice-cold FACS buffer (phosphate-buffered saline, 2% FCS, 0.05% NaN_3) and then analyzed using a BD LSR II Flow Cytometer (Becton-Dickinson) and FlowJo software (FlowJo, LLC).

Xenotransplantation in mice

NSG mice (The Jackson Laboratory) were maintained under specific pathogen-free conditions in the research animal facility of the University of Tübingen, Germany, according to German federal and state regulations (Regierungspräsidium Tübingen, K3/17). Primary T-ALL patient cells or MOLT-4 cells (0.5×10^6 cells each) were injected IV into 8- to 12-week old male NSG mice and randomized to the treatment groups. Seven days after leukemia inoculation, mice were injected intraperitoneally once a day with 20 mg/kg FK866 hydrochloride hydrate (dissolved in 20% [2-Hydroxypropyl]-γ-cyclodextrin [HGC]) or 20% HGC, respectively. Two or 3 weeks after starting the treatment, mice were euthanized, and the bone marrow was analyzed for human $CD45^+$ leukemia cells by flow cytometry. Engrafted T-ALL cells were isolated from bone marrow samples using the human CD45 MicroBeads Kit (Miltenyi Biotec) following the manufacturer's instructions.

Statistical analyses

Statistical analyses were conducted using Student *t* test or BootstRatio.[39] Statistical significance was taken to be $P < .05$.

Results

Lysine deacetylation of LMO2 is essential for the binding to LDB1 protein and activation of the TAL1 complex

Using the in silico prediction algorithms PAIL,[40] LysAcet[41] and LAceP,[42] we identified 2 evolutionarily highly conserved lysine residues, K74 and K78, in the LIM1 domain of LMO2 that may be targets for deacetylation (Figure 1A). Acetylation of LMO2 protein was confirmed in immunoprecipitation assay using HEK293T cells, in which acetylation of LMO2 protein was enhanced by cotransfection with the lysine acetyltransferase p300 (Figure 1B). We confirmed acetylation of the endogenous LMO2 protein in the LMO2-expressing T-ALL cell line MOLT4 in immunoprecipitation assay (supplemental Figure 1A-B, available on the *Blood* Web site).

To evaluate the role of K74 and K78 of LMO2 on its deacetylation, we generated expression constructs containing WT or deacetylation-mimic LMO2 mutant at the predicted lysine residues (K74/78R). Immunoprecipitation assays in HEK293T cells cotransfected with LMO2 constructs and p300 using anti-LMO2 antibody followed by western blot with anti-acetyl-K antibody confirmed acetylation of WT LMO2 and demonstrated that deacetylation-mimic LMO2 mutant at K74/78R could not be acetylated (Figure 1C). LMO2 is a component of the multiprotein transcriptional activation TAL1 complex, consisting of LMO2, LDB1, TAL1, E47, and GATA1/2 proteins that exert transcriptional activity toward target genes activated during early hematopoiesis and in T-ALL blasts (Figure 1D).[43] Therefore, we aimed to investigate whether LMO2 deacetylation on K74 and K78 may affect its interaction with LDB1. Structurally, both K74 and K78 are accommodated in the second zinc finger of LMO2, but only K74 is directly involved in the interaction with LDB1. The association of LMO2 and LDB1 is driven by both polar and hydrophobic contacts. The LDB1-LID domain binds in an elongated conformation along the 2 LMO2 LIM domains by contributing an additional β-strand to each of the 4 zinc finger domains (Figure 1E). Consequently, a large network of backbone hydrogen bonds is formed in these extended β-sheets, which are fortified by several hydrophobic contacts between the LID and both LIM domains. However, there are also several electrostatic interactions, which are exclusively formed via the LIM1 domain.[18] In addition to the described salt bridges between R40, E52, and R70 of LIM1 and E362, R360, and E355 of LDB1-LID, we note that K74 is also in direct van der Waals distance to D354 for an ionic interaction. Together with D352, E353, and E355, D354 forms a strongly anionic DEDE motif, which is counterbalanced by the cationic R70 and K74. Consequently, when K74 is acetylated (and thus neutralized), the interaction with D354 is lost and the electrostatic balance between LMO2 and LDB1 impaired. In contrast, K78 is not directly interacting with LDB1-LID but forms a salt bridge with D58 of the same zinc finger (Figure 1E). It is conceivable that this interaction is stabilizing the geometry of the LIM domain. This notion is supported by the observation that in 1 instance of a LMO2:LDB1-LID crystal structure (PDB 2XJZ, chain C), in which this interaction is broken, the geometry of LIM1 is distorted and the LDB1-LID domain detached from the first zinc finger.[18] It is therefore conceivable that the acetylation of K78 would lead to a similar conformational change and thus abrogate the LMO2:LDB1 interaction.

We compared the interaction between LDB1 and WT K74/78Q (acetylation-mimic) or K74/78R (deacetylation-mimic) LMO2

Figure 2 (continued) concentration of DMSO was added as a vehicle control. Dead cells were excluded by trypan blue dye staining. Live-cell numbers are normalized to those obtained in samples treated with DMSO (defined as 1). Data represent means ± SD of triplicate determinations (*$P < .05$ compared with DMSO-treated cells). Duolink in situ proximity ligation assay (PLA) of MOLT-4 cells (E) or primary blasts (F) from T-ALL patient (patient no. 3) treated with 10 nM FK866 or 100 nM AC93253 for 48 hours using anti-LMO2 and anti-acetylated lysine antibodies. The same concentration of DMSO was added as a vehicle control. Representative images are shown. Scale bars: 10 μm. (G-H) Proliferation of MOCK, WT-LMO2, or K74/78R LMO2-expressing MOLT4 cells (2×10^4 cells/well of a 96-well plate) was evaluated over time with the IncuCyte S3 Live-Cell Analysis System. The experiment was performed twice, each in triplicate. (I) Co-IP assay of SIRT2 and LMO2 protein interaction in lysates of HEK293T cells transfected with SIRT2 and LMO2 expression vectors. IP and immunoblotting were performed using the indicated antibodies. Representative images are shown. (J) Duolink in situ PLAs in MOLT-4 cells and primary blasts of T-ALL patients. Cells were stained with anti-LMO2 and anti-SIRT2 antibodies. Representative images are shown. Scale bars: 10 μm. RLU, relative light unit.

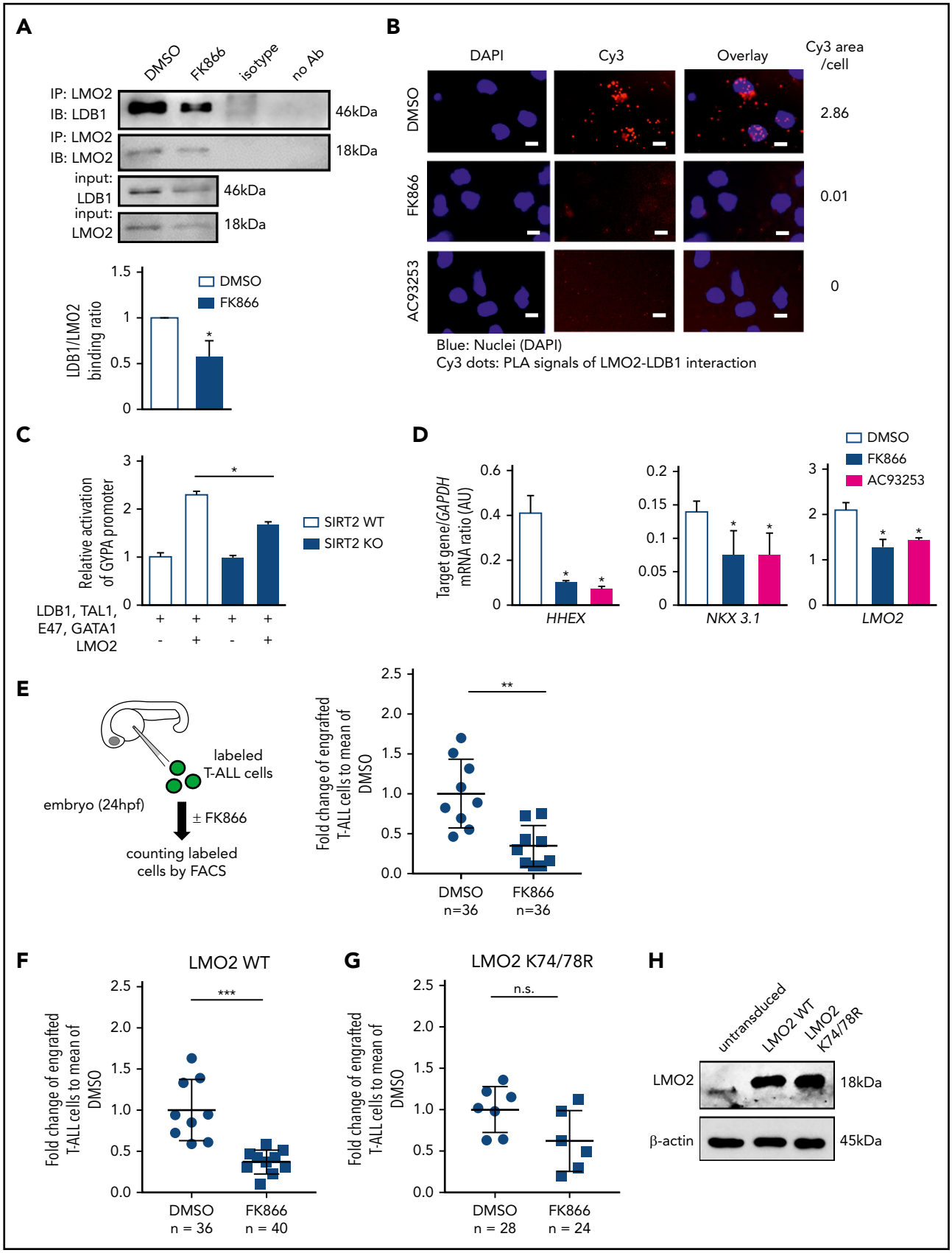

Figure 3. NAMPT/SIRT2-mediated LMO2 deacetylation is essential for LMO2 interaction with LDB1, activation of TAL-1 complex, and proliferation of T-ALL cells. (A) Co-IP of LMO2 and LDB1 from lysates of MOLT-4 cells treated with 10 nM FK866 for 72 hours. IP and immunoblotting were performed using the indicated antibodies. Representative images are shown. Bar graphs of the LDB1/LMO2 binding ratio indicate the LDB1 protein signal divided by the LMO2 protein signal in IP samples. Data show

expression constructs by co-immunoprecipitation and indeed found that the K74/78Q LMO2 mutant showed a weaker interaction with LDB1 in comparison with WT and K74/78R LMO2 (Figure 1F).

Furthermore, we made a reporter gene construct containing a 456-bp upstream regulatory region of the human *GYPA* gene containing GATA binding motifs, an E-box and SP1 binding site specific for TAL1 complex binding[44] and performed reporter gene assay. We found that the acetylation-mimic K74/78Q LMO2 mutant suppressed *GYPA* promotor activity of the TAL1 complex in comparison with WT and the deacetylation-mimic K74/78R LMO2 mutant (Figure 1G). These results demonstrate that deacetylation of LMO2 at lysines 74 and 78 is essential for the transcriptional activity of the TAL1 complex.

Activation of LMO2 by NAMPT-mediated deacetylation

Proteins may be deacetylated by the NAMPT/SIRT pathway.[45] NAMPT is essential for the generation of NAD^+ and activation of NAD^+-dependent protein deacetylases, SIRT (Figure 2A). To evaluate whether transcriptional activity of the TAL1 complex is affected by NAMPT-triggered LMO2 deacetylation, we compared TAL1 complex-dependent activation of the *GYPA* promoter in HEK293T cells in the presence or absence of the specific NAMPT inhibitor FK866. Indeed, we observed markedly diminished activation of TAL1 complex-dependent *GYPA* promoter activity after NAMPT inhibition compared with DMSO-treated control group (Figure 2B).

In vitro inhibition of NAMPT or SIRT2 suppresses proliferation and induces apoptosis of T-ALL cells by inhibiting LMO2 deacetylation

LMO2 and/or other components of the TAL1 complex are hyperactivated in T-ALL.[46,47] Accordingly, we evaluated whether inhibition of NAMPT or SIRTs (SIRT1 and SIRT2) affects the proliferation and/or survival of the LMO2-expressing T-ALL cell lines, MOLT4 and MOLT14 (supplemental Figure 1A). We found that inhibition of NAMPT (FK866) or SIRT2 (AC93253), but not SIRT1 (EX527), led to a marked reduction in cell proliferation, as assessed by cell counts, ^{3}H-thymidine incorporation, and BrdU assays, compared with vehicle (DMSO)-treated samples (Figure 2C; supplemental Figure 1C-H; data not shown). Apoptosis was also elevated in cells treated with FK866 or AC93253 (supplemental Figure 2A) compared with vehicle controls. These phenotypic changes are consistent with the almost completely abolished levels of intracellular NAD^+ (supplemental Figure 2B). Strong dependence of MOLT4 cells on LMO2 was confirmed in CRISPR/Cas9-mediated *LMO2* knockout (KO) studies, where we found dramatically diminished viability, proliferation, and elevated apoptosis of MOLT4 cells upon *LMO2* KO (supplemental Figure 2C-H; supplemental Table 1).

We further evaluated the effects of NAMPT- or SIRT2 inhibition on the survival of primary blasts from T-ALL patients. We selected T-ALL patients expressing LMO2 and *TAL1* levels comparable to that of the LMO2-dependent MOLT4 cell line having high LMO2 levels (supplemental Figure 1A; supplemental Table 2; supplemental Figure 3A). Treatment of LMO2- and TAL1-expressing primary blasts from T-ALL patients with FK866 or AC93253 also led to markedly diminished cell proliferation and reduced NAD^+ levels (in FK866 treated cells) (Figure 2D; supplemental Table 2; supplemental Figure 3A-B). These findings are in line with the diminished deacetylation of LMO2 following treatment of the MOLT4 T-ALL cell line and primary T-ALL blasts with FK866 or AC93253 compared with cells in vehicle control groups (Figure 2E-F; supplemental Figure 3C). The specificity of the Duolink signal of acetylated LMO2 protein was confirmed in *LMO2* KO MOLT4 cells (supplemental Figure 3D). Interestingly, FK866- or AC93253-treated MOLT4 cells stably expressing the K74/78R LMO2 mutant showed better proliferation compared with control transduced cells, as evaluated using an IncuCyte cell proliferation assay (Figure 2G-H).

We further evaluated whether SIRT2 interacts with LMO2 to induce its deacetylation. Indeed, direct interactions between SIRT2 and LMO2 were detected by coimmunoprecipitation and subsequent western blotting of lysates from HEK293T cells cotransfected with SIRT2 and LMO2 (Figure 2I), as well as in Duolink assays of T-ALL cell lines and primary cells from T-ALL patients (Figure 2J; supplemental Figure 4A). Moreover, interactions between endogenous LMO2 and LDB1 in MOLT-4 cells were considerably diminished by inhibition of NAMPT or SIRT2 (Figure 3A-B; supplemental Figure 4B), and TAL1 complex activity toward the *GYPA* reporter was reduced in *SIRT2*-KO HEK293FT cells (Figure 3C; supplemental Figure 3C-D). In addition, mRNA levels of the known LMO2-target genes, *HHEX*[16] and *NKX3.1*,[48] were strongly decreased in cells treated with FK866 or AC93253 (Figure 3D; supplemental Figure 4E). Consistent with the previously reported autoregulation of *LMO2* expression in HSCs and T-ALL cells,[21,22] *LMO2* mRNA levels were reduced after NAMPT or SIRT2 inhibition (Figure 3D; supplemental Figure 4E).

Inhibition of NAMPT results in diminished proliferation of T-ALL cells in vivo due to abrogated deacetylation of LMO2

We further evaluated the effect of NAMPT inhibition on the proliferation and survival of LMO2-expressing T-ALL cells in vivo.

Figure 3 (continued) means ± SD from 3 independent experiments (*$P < .05$). (B) Duolink in situ PLAs of MOLT-4 cells treated with 10 nM FK866 or 100 nM AC93253 for 48 hours. Cells were stained with anti-LMO2 and anti-LDB1 antibodies. Scale bars: 10 μm. (C) WT or *SIRT2*-knockout (*SIRT2*KO) HEK293FT cells were transfected with a *GYPA* reporter and the indicated expression constructs. Transfected cells were cultured for 24 hours; activation of the *GYPA* reporter was measured as described in "Methods." Signals measured in cells cotransfected with LMO2 and *GYPA* constructs were normalized to those in cells without an LMO2 expression plasmid (defined as 1). Data show means ± SD (n = 8; *$P < .05$). (D) mRNA expression levels of the indicated genes in MOLT-4 cells treated with 10 nM FK866, 100 nM AC93253, or DMSO for 72 hours were assessed using quantitative RT-PCR. Target gene/*GAPDH* mRNA expression ratios are shown. Data, expressed as arbitrary units (AUs), are means ± SD from 3 independent experiments, each in triplicate (*$P < .05$ compared with DMSO-treated cells). (E-G) Xenotransplantation of T-ALL cells into zebrafish embryos. Zebrafish embryos were transplanted with labeled primary T-ALL cells (E), MOLT-4 cells transduced with a WT (F), or K74/78R mutant LMO2-expressing lentivirus construct (G). FACS, fluorescence-activated cell sorting. Xenotransplanted embryos were treated with 800 nM FK866 or DMSO for 2 days. Numbers of transplanted cells were assessed as described in "Methods." Data represent percentage of labeled cells normalized to the average percentage of labeled cells in the DMSO-treated group. The black lines represent mean ± SD. Each dot represents 4 embryos pooled as 1 biological sample. The number of analyzed embryos is indicated in the lower panel of each figure (***$P < .0001$; **$P < .001$). (H) Representative western blot images of cell lysates of MOLT-4 cells transduced with the indicated lentivirus constructs using anti-LMO2 and anti-β-actin antibodies. NS, not significant.

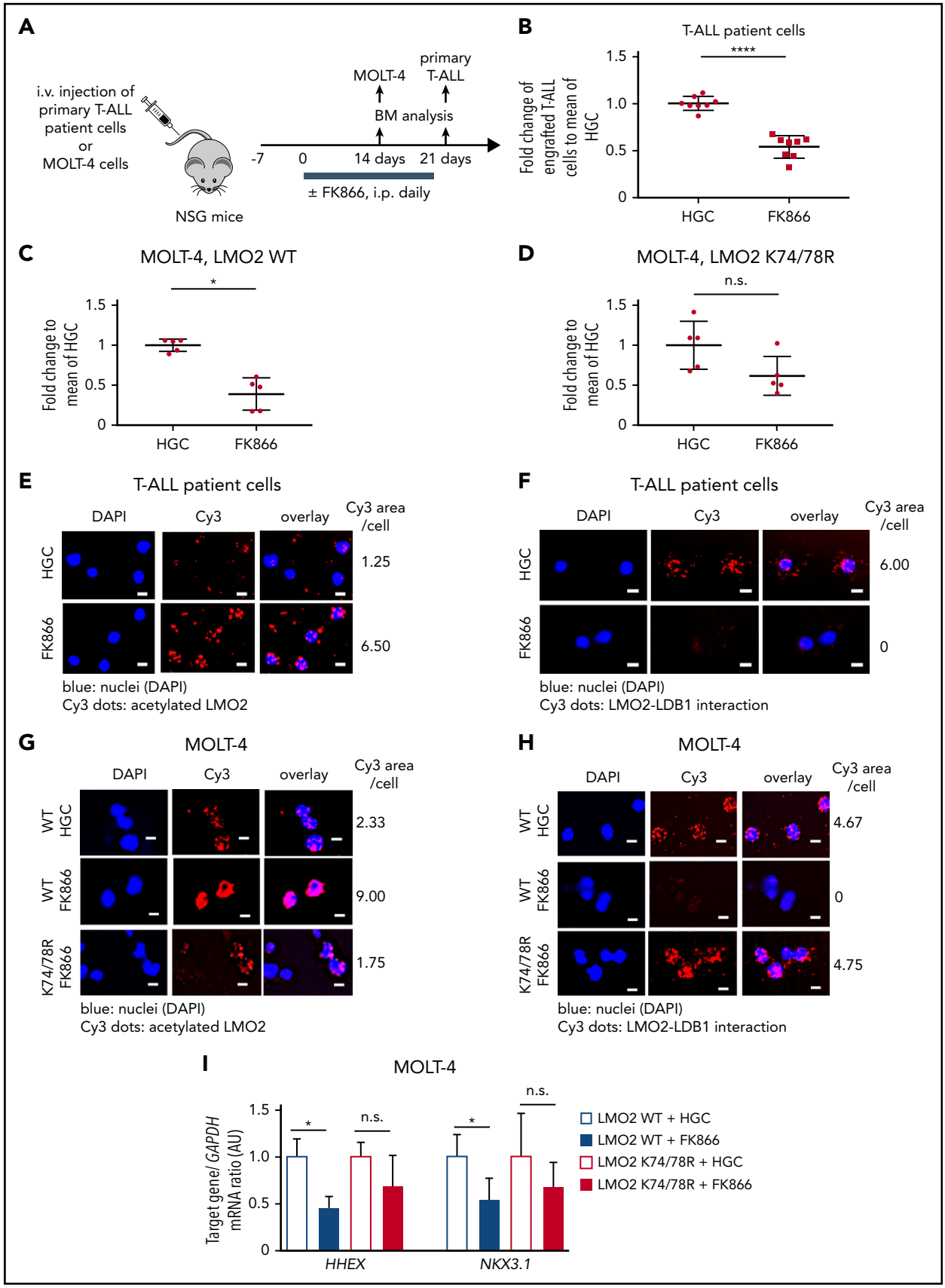

Figure 4. In vivo inhibition of NAMPT results in reduced T-ALL burden in NSG mice owing to abrogated deacetylation of LMO2. (A) Xenotransplantation of NSG mice with either MOLT-4 cells, transduced with WT or K74/78R mutant LMO2-lentivirus, or primary T-ALL patient cells. Transplanted mice were injected intraperitoneally (i.p.) with 20 mg/kg of FK866 once a day for 2 (MOLT4 cells) or 3 (T-ALL patient cells) weeks. The same concentration of HGC was injected as a vehicle control. (B-D) Fold changes of percent

To this end, we injected MOLT-4 T-ALL cells or primary T-ALL patient cells labeled with the dye carboxyfluorescein diacetate succinimidyl ester into zebrafish embryos at 24 hpf and subsequently treated embryos with FK866 or DMSO for 48 hours. In line with our in vitro observations, the number of primary T-ALL patient cells in FK866-treated embryos was markedly reduced compared to control DMSO-treated samples (Figure 3E). In addition, transduction of MOLT-4 cells with a deacetylation-mimicking LMO2 (K74/K78), but not with WT LMO2, protected these cells from FK866-mediated cell death in vivo (Figure 3F-H).

In another series of experiments, we engrafted primary T-ALL patient cells and MOLT-4 cells into immunodeficient nonobese diabetic severe combined immunodeficiency IL2Rγc$^{-/-}$ (NSG) mice. Engrafted mice were treated with 20 mg/kg FK866 or HGC (solvent for FK866) for 14 (MOLT-4 cells) or 21 (primary T-ALL patient cells) days, once a day (Figure 4A-D). Similar to zebrafish xenograft experiments, the percentage of engrafted T-ALL cells was strongly reduced in FK866-treated mice compared with HGC-injected control animals (Figure 4 B-C). LMO2 deacetylation was reduced and interactions between LMO2 and LDB1 were markedly diminished in T-ALL cells isolated from the bone marrow of engrafted FK866-treated mice (Figure 4E-H). mRNA expression levels of *HHEX* and *NKX3.1* were reduced in MOLT4 cells engrafted in FK866-treated mice compared with that observed in HCG-treated mice (Figure 4I). Again, transduction of cells with the deacetylation-mimicking K74/78R LMO2 mutant, but not WT LMO2 (as control) prevented FK866-mediated abrogation of engraftment (Figure 4C-D), and rescued downregulation of LMO2 target genes (Figure 4I). In line with this, LMO2 deacetylation was reduced and interactions between LMO2 and LDB1 were much weaker in LMO2-WT-transduced MOLT4 cells isolated from the bone marrow of engrafted FK866-treated mice, but not in cells transduced with the K74/K78 LMO2 mutant (Figure 4G-H).

Gene expression signature of NAMPT-deacetylated LMO2 in T-ALL

To identify the gene expression program regulated by NAMPT-deacetylated LMO2 in T-ALL, we performed RNA sequencing (RNA-Seq) analysis of WT or K74/78 LMO2-expressing MOLT4 cells treated with FK866 or DMSO for 2 days (Figure 5A). We detected 69 genes to be differentially regulated in WT LMO2-, but not K74/78 LMO2-expressing cells after NAMPT inhibition by FK866 (Figure 5B-C; supplemental Table 3). Among these genes, we found tumor- or leukemia-associated candidates, as *PRDM1*, *HOXD13*, *RASL11B*, *TRAF1*, *IGFBP4*, *SOX7*, *SOX12*, *CYP1B1*, and *CYP2E1* (Figure 5C). Pathway overrepresentation analysis[49] of the candidate genes revealed cytochrome P450, tryptophan degradation, biological oxidation, direct p53 effectors, and tumor necrosis factor α (TNF-α) signaling pathways to be regulated by NAMPT-deacetylated LMO2 (Figure 5D). Using iRegulon analysis of the transcription factor binding sites[50] presented in FK866-treated WT LMO2, but not in K74/78 LMO2 MOLT4 cells, as compared with each DMSO control, we detected PITX-, ZNF695-, MEF2-, and Ep300-binding motifs to be significantly enriched (Figure 5E).

The NAMPT-NAD$^+$-SIRT2 pathway is essential at early-stage hematopoietic differentiation of iPS cells

Previously, we demonstrated that NAMPT activates myeloid differentiation of CD34$^+$ bone marrow-derived HSC.[23] LMO2 plays an important role during early stages of hematopoietic differentiation.[4,5] Knowing that leukemogenic role of LMO2 in T-ALL may be linked to the abnormal reactivation of the HSC-specific transcriptional program in T-lymphocyte progenitors,[16] we aimed to study whether NAMPT-mediated deacetylation of LMO2 is playing a role during early steps of hematopoietic differentiation. We performed a serum- and feeder-free monolayer hematopoietic differentiation of iPS cells[51,52] in the presence of FK866, AC93253, or DMSO (Figure 6A). Interestingly, the percentage of KDR$^+$CD34$^+$ hematopoietic progenitor cells on day 6 of culture was noticeably decreased by inhibition of NAMPT or SIRT2 compared with the control DMSO-treated group (Figure 6B-C), whereas the percentage of KDR$^+$CD34$^-$ was not affected and the percentage of KDR$^-$CD34$^-$ cells was even increased at the highest inhibitor concentration (supplemental Figure 5A-D). Inhibition of SIRT1 had no effect on the formation of hematopoietic cells from iPS cells (supplemental Figure 5E-G). Intracellular NAD$^+$ levels in differentiated iPS cells treated with FK866 were markedly suppressed on day 6 of culture in comparison with the DMSO control group (supplemental Figure 5H). Moreover, the emergence of CD43$^+$ hematopoietic progenitor cells on day 13 of culture as well as colony-forming unit formation was completely suppressed after SIRT2 inhibition (Figure 6D-E). These results indicate that SIRT2 is essential during early hematopoietic differentiation of human iPS cells downstream of the NAMPT-NAD$^+$ signaling pathway.

LMO2 is deacetylated by NAMPT/SIRT2 during the early stages of hematopoietic differentiation of iPS cells

To identify whether LMO2 is a downstream target of the NAMPT-NAD$^+$-SIRT2 mediated deacetylation at the early stage of hematopoietic differentiation, we compared the acetylation state of LMO2 and other hematopoietic transcription factors essential for early-stage hematopoiesis (TAL1 and RUNX1)[5] in iPS-derived hematopoietic cells on day 6 of culture. We used the Duolink-proximity ligation assay (PLA)-FACS,[53] which allows identification of endogenous protein complexes or protein modifications in single cells, and quantified the signal using flow cytometry.[54] Signal from total protein was obtained by staining with a primary antibody specific for the protein of interest; signal from acetylated protein was obtained using a combination of primary antibody and acetyl-lysine antibody. Interestingly, only LMO2 showed increased deacetylation in iPSCs-derived HSCs on day 6 of culture (Figure 6F; supplemental Figure 6A). The Duolink assay revealed an interaction of LMO2 and SIRT2 proteins

Figure 4 (continued) of human CD45$^+$ primary T-ALL patient cells (B) and Molt-4 cells (C-D) in bone marrow of FK866-treated mice to HGC group are shown. Data represent mean ± standard error of the mean (****$P < .0001$), n = 5 to 8 mice per group. (E-H) Duolink in situ PLAs of human CD45$^+$ cells isolated from bone marrow of mice transplanted with primary T-ALL patient cells (E-F) or MOLT-4 cells (G-H). "WT" and "K74/78R" indicate mice transplanted with MOLT-4 cells transduced with WT or K74/48R LMO2 mutant, respectively. Cells were stained with anti-LMO2 and anti-acetylated lysine (E,G) or anti-LMO2 and anti-LDB1 antibodies (F,H). Representative images are shown. Scale bars: 10 μm. (I) mRNA expression levels of the indicated genes in human CD45$^+$ cells isolated from bone marrow of xenotransplanted mice. mRNA expression was assessed using quantitative RT-PCR, and is expressed as arbitrary units (AUs). Target gene/*GAPDH* mRNA expression ratios are shown. Data show means ± SD from 5 independent experiments, each in triplicate (*$P < .05$).

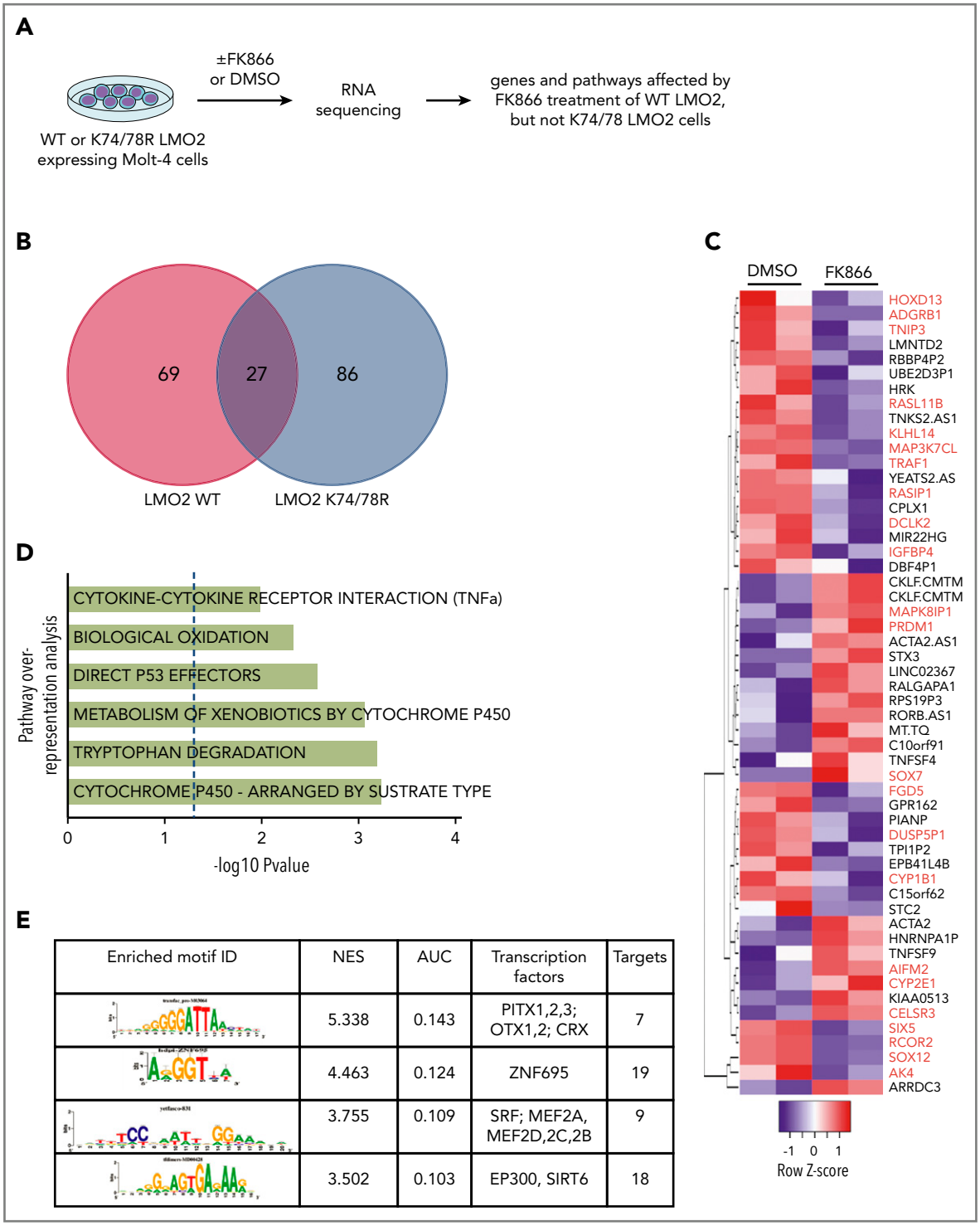

Enriched motif ID	NES	AUC	Transcription factors	Targets
	5.338	0.143	PITX1,2,3; OTX1,2; CRX	7
	4.463	0.124	ZNF695	19
	3.755	0.109	SRF; MEF2A, MEF2D,2C,2B	9
	3.502	0.103	EP300, SIRT6	18

Figure 5. NAMPT-LMO2 dependent gene expression signature in MOLT4 cells. (A) Schematic of the experimental procedure. Venn diagram (B) and heat map (C) of genes that were significantly differentially regulated upon FK866 treatment compared with DMSO-treated groups of WT LMO2 or K74/78 LMO2 expressing MOLT4 cells (adjusted value $P < .05$). Genes known to play a role in tumorigenesis are marked in red. (D) Pathway overrepresentation analysis using a list of significantly regulated genes from panel C revealed top significantly enriched signal transduction pathways that are NAMPT-LMO2 dependent. (E) iRegulon transcription factor motif enrichment analysis using a list of significantly upregulated genes from (C) revealed enrichment of genes (normalized enrichment score >3.0 and area under the curve >0.03) with NAMPT-LMO2–specific transcription factor motifs.

in iPSC-derived HSCs on day 6 of culture (Figure 6G) and inhibition of SIRT2 resulted in elevated acetylation of LMO2 as well as diminished interaction with LDB1 compared with control DMSO treated cells (Figure 6H-I; supplemental Figure 6B-C). Target genes of the TAL1 complex as well as *FOS* and *FRZB* (early hematopoiesis genes) mRNA expression were also suppressed in iPS cell-derived HSCs on day 6 of culture in the presence of NAMPT- or SIRT2-specific inhibitors (Figure 6J; supplemental

Figure 6D). These data suggest an essential role of NAMPT-NAD$^+$-SIRT2-mediated deacetylation of LMO2 for the activation of TAL1 complexes in early hematopoiesis.

Inhibition of the NAMPT-NAD$^+$-SIRT2 pathway with morpholinos abrogates early hematopoiesis in zebrafish embryos

We further evaluated the role of the NAMPT-NAD$^+$-SIRT2 pathway during early hematopoiesis in vivo in zebrafish. In zebrafish embryos, developing blood cells appear in the blood island located just before the yolk extension around 24 hpf.[55] To analyze early hematopoiesis, we used transgenic zebrafish *Tg(-6.35drl:EGFP)* expressing GFP under the control of the *draculin* promoter, which is expressed in hematopoietic progenitor cells within the lateral plate mesoderm.[36] We knocked down zebrafish orthologs for *NAMPT* and *SIRT2*, (*nampta* and *sirt2*) by injecting 1-cell-stage zebrafish embryos with antisense MOs.[37] MO-induced mRNA knockdown was efficient (supplemental Figure 7A). Although *nampta*- or *sirt2*-knockdown embryos showed tail defects, these phenotypes could be rescued by coinjection with expression plasmid encoding human NAMPT or SIRT2, indicating *nampta* and *sirt2* specific knockdown (supplemental Figure 7B). We quantified early hematopoiesis in zebrafish embryos by counting GFP$^+$ cells in the developing blood island at 24 hpf and found that *nampta* and *sirt2* MO-injected embryos had markedly reduced numbers of hematopoietic cells compared with uninjected control embryos (Figure 7A), which could be rescued by coinjection with expression plasmid of human NAMPT or SIRT2 (supplemental Figure 7C-D). In line with impeded hematopoiesis 24 hpf, NAD$^+$ levels as well as mRNA expression levels of downstream target genes of the TAL1 complex were downregulated by knockdown of *nampta* and *sirt2* genes (Figure 7B; supplemental Figure 7E). These data suggest that the NAMPT-NAD$^+$-SIRT2 pathway is indispensable for early hematopoiesis, most likely through the activation of the TAL1 complex in zebrafish embryos.

While the morpholino knockdown data has to be confirmed with genetic mutants, injection of zebrafish embryos with expression plasmid of human deacetylation-mimic LMO2 mutant (K74/78R), but not WT LMO2, rescued *nampta* MO-induced defective hematopoiesis and mRNA expression of TAL1 complex target genes at 24 hpf (Figure 7C-D). Together with our results in human iPS cells, these results indicate that deacetylation of LMO2 at K74/78 by NAMPT and SIRT2 is crucial for early vertebrate hematopoiesis.

Discussion

In the present study, we demonstrated for the first time that NAMPT and SIRT2 are essential for the proliferation and survival of T-ALL blasts in vitro and in vivo. We also found that NAMPT and SIRT2 are important for blood cell formation in an iPS cell model in vitro and in morpholino-mediated knockdown experiments in zebrafish embryos in vivo. Therefore, we have opened a new line of investigation into the role of NAMPT-mediated protein deacetylation in developmental hematopoiesis and T-ALL leukemogenesis. It would be interesting to investigate whether NAMPT/SIRT2-mediated protein deacetylation governs the development of other tissues and organs of, for example, mesoderm origin, and whether SIRT2 or other SIRTs are involved.

The dose- and cell type-dependence of NAMPT in the hematopoietic system is well documented. Thus, hyperactivated NAMPT and SIRT2 have been shown to induce uncontrolled proliferation of hematopoietic progenitors and cause acute myeloid leukemia.[24] We demonstrated that inhibition of NAMPT or SIRT2 suppressed proliferation and induced apoptosis of T-ALL cells in vitro and in vivo. We previously published evidence for an important role of NAMPT in later stages of the myeloid specification of hematopoietic progenitors that depend on granulocyte colony-stimulating factor or granulocyte-macrophage colony-stimulating factor.[23,27] Most likely, NAMPT is also activated by other growth factors essential for the induction of embryonic hematopoiesis, such as BMP4, VEGF, and basic fibroblast growth factor, or the development of T-ALL, such as common γ-chain signaling cytokines (gamma c-cytokines), including IL-2, IL-4, IL-7, and IL-9.[56-58] We recently determined the involvement of the IL-13 pathway in NAMPT-triggered myeloid differentiation.[26] Less is known about the role of NAMPT and SIRTs in T lymphopoiesis. Bruzzone et al showed impaired proliferation and function of activating T lymphocytes upon NAMPT depletion in experimental autoimmune encephalomyelitis.[59] SIRT1 plays a role in Foxp3$^+$ T-regulatory cell function[60] and in human CD8$^+$ memory T cells.[61] Interestingly, we found that SIRT2, but not SIRT1, is important during early stages of blood cell formation and T-ALL development downstream of NAMPT activation. SIRT1 and SIRT2 have a high degree of structural similarity and may have similar functions and targets. However, there are also reports that SIRT1 possesses specific functions that are not shared by SIRT2. The same is true for SIRT2.[27-29] In our system, it is obvious that these 2 SIRTs exhibit different functions and have different downstream effectors. Previous investigations by Han et al and Ou et al demonstrated that a SIRT1 deficiency causes increased apoptosis and diminished hematopoietic differentiation in mouse ES cells.[31,62] In contrast, we found no effect of SIRT1 inhibition on early hematopoietic differentiation, a difference that may be explained by the differences in species and/or cell type used. Whether SIRT2 also plays a role in apoptosis induction and/or hematopoietic differentiation of mouse ES cells remains to be investigated.

Importantly, we indicated for the first time that LMO2 is a downstream target of NAMPT signaling, showing that NAMPT/SIRT2-mediated LMO2 activation by deacetylation on lysines K74 and K78 is essential for LMO2 interaction with LDB1 and formation of a transcriptionally active TAL1 complex (Figure 7E). We found that LMO2 is deacetylated by NAMPT/SIRT2 during early stages of hematopoietic differentiation and T-ALL development (Figure 7E). This is the first report describing activation of LMO2, a developmentally important protein, by deacetylation on K74 and K78 within the LIM1 domain, which is essential for the association of LMO2 with LDB1 protein and TAL1 complex activation. Knowing this, it has become possible to perform structure-based screens of chemical compounds to identify candidates that either prevent LMO2 deacetylation and LDB1 binding in T-ALL, or induce this interaction and enhance blood cell formation. Holen et al[63] and von Heideman et al[64] already described FK866's toxicity and safety analyzing the first clinical studies for FK866 treatment in cancer patients. The dose-limiting toxicity of FK866 is thrombocytopenia and various gastrointestinal symptoms including nausea, vomiting and diarrhea. In our study, daily treatment of NSG mice with FK866 for up to 21 days was well tolerated with no premature deaths, as already described by Nahimana et al[65] and Matheny et al.[66] Only some minor side effects were

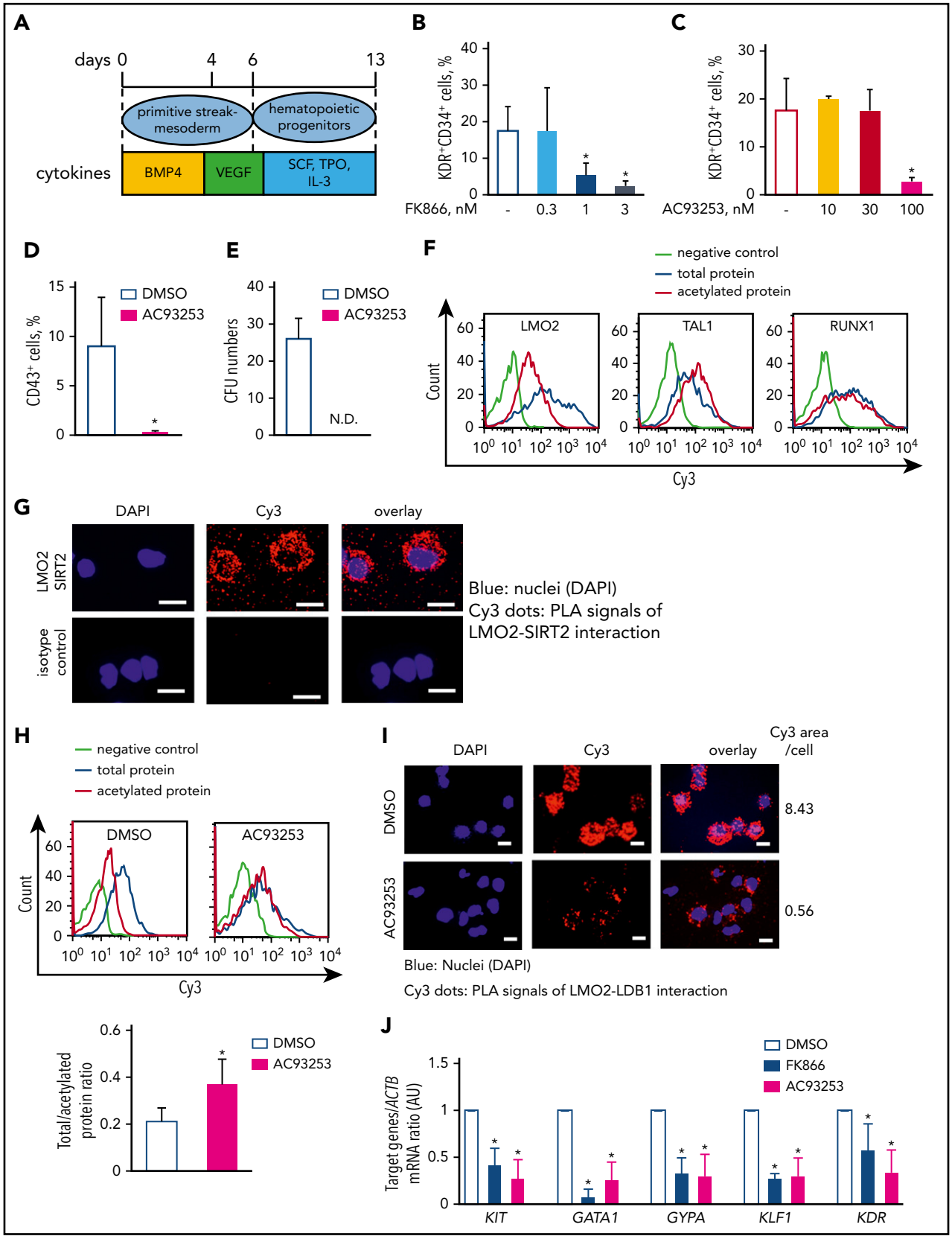

Figure 6. The NAMPT-NAD$^+$-SIRT2 pathway plays an essential role in early-stage hematopoietic differentiation of iPS cells via LMO2 deacetylation. (A) Schematic of the serum- and feeder-free monolayer human iPS cells hematopoietic differentiation system. (B-C) The percentage of KDR$^+$CD34$^+$ cells was evaluated in differentiated iPS cells on day 6 treated with FK866 (B) or AC93253 (C). The same concentration of DMSO was used as a vehicle control. Data show means ± SD and are derived from 3 independent experiments, each in triplicate. *$P < .05$. (D-E) The percentage of CD43$^+$ cells was evaluated by flow cytometry (D), and colony-forming unit assays were performed in differentiated iPS cells on day 13 treated with 100 nM AC93253 during differentiation (E). The same concentration of DMSO was used as a vehicle control. Data are mean ± SD

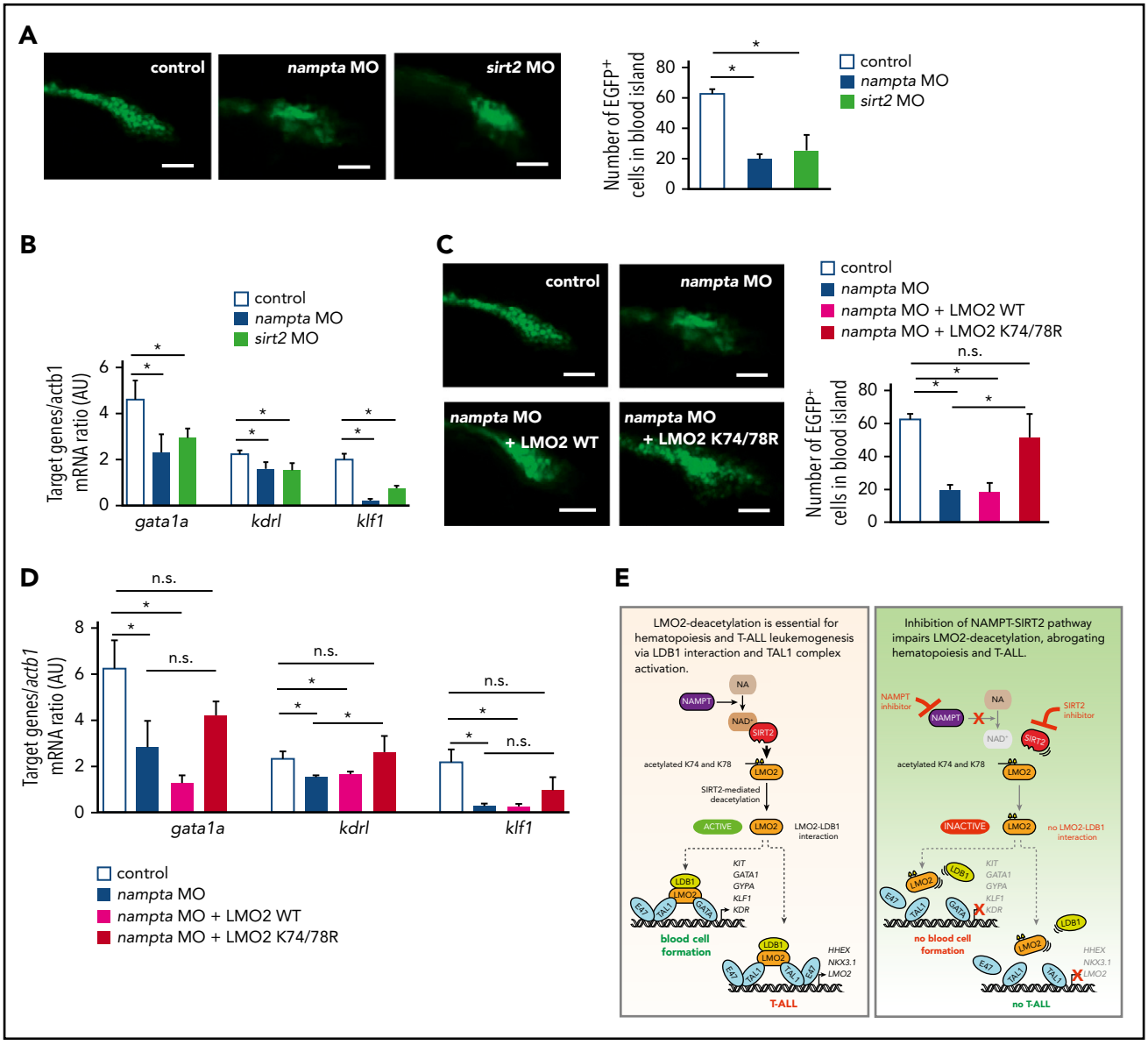

Figure 7. Morpholino-mediated inhibition of the NAMPT-NAD⁺-SIRT2 pathway impedes early hematopoiesis in zebrafish embryos. (A,C) Quantification of EGFP⁺ hematopoietic cells in uninjected control and morpholino (MO)/plasmid injected *Tg(-6.35drl:EGFP)* zebrafish embryos at 24 hpf. Representative images and numbers of EGFP⁺ hematopoietic cells in the blood islands are shown. Data show mean ± SD (n = 5). *$P < .05$. Scale bars: 50 μm. (B,D) mRNA expression levels of the indicated genes in control and MO/plasmid injected zebrafish embryos at 24 hpf were assessed using quantitative RT-PCR. Target gene/*actb1* mRNA expression ratios are shown. Data show mean ± SD from 3 independent experiments, each in triplicate. *$P < .05$. (E) Schematic for the NAMPT/SIRT2-mediated lysine deacetylation of the LMO2 transcription factor that is essential for the interaction of LMO2 with LDB1 and formation of the TAL1 complex. This activates the oncogenic transcriptional program and promotes T-cell leukemia development or induces blood cell formation.

observed, such as mild fatigue and reduced movement compulsion. In zebrafish embryos, FK866 treatment did not show any severe side effects even if used in higher concentrations.

LMO2 is expressed in early T-cell progenitors and is normally switched off during T-lymphocyte differentiation.[11-15] In T-ALL, LMO2 continues to be expressed owing to recurrent chromosomal

Figure 6 (continued) derived from 3 independent experiments, each in triplicate. *$P < .05$. (F) Representative histograms of the Duolink-FACS analysis on the acetylation of the indicated proteins in differentiated iPS cells on day 6. Blue, signal from total protein; red, signal from acetylated protein; lime green, negative control. (G) Duolink in situ PLA assay in the differentiated iPS cells on day 6 of culture. Cells were stained with anti-LMO2 and anti-SIRT2 antibodies. Representative images are depicted. Scale bars: 10 μm. (H) Representative histograms of the Duolink-FACS analysis on the acetylation of LMO2 protein in differentiated iPS cells on day 6 in the absence or presence of 100 nM AC93253. The same concentration of DMSO was added as a vehicle control. Blue, signal from total protein; red, signal from acetylated protein; lime green, negative control. Graph bars of the total to acetylated protein Duolink-FACS signal ratio indicates the mean fluorescence intensity (MFI) of acetylated LMO2 protein signal divided by the MFI of total LMO2 protein signal. Data are mean ± SD from 3 independent experiments. *$P < .05$. (I) Duolink in situ PLA assay in the differentiated iPS cells on day 6 of culture treated with 100 nM AC93253. The same concentration of DMSO was added as a vehicle control. Cells were stained with anti-LDB1 and anti-LMO2 antibodies. Representative images are depicted. Scale bars: 10 μm. (J) mRNA expression levels of the indicated genes in differentiated iPS cells on day 6 of culture in the presence of 3 nM FK866 or 100 nM AC93253 were assessed using quantitative RT-PCR and expressed as AUs. The same concentration of DMSO was added as a vehicle control. Target gene *ACTB* mRNA expression ratio measured in the control DMSO-treated sample was normalized to 1. Data are mean ± SD from 3 independent experiments, each in triplicate. *$P < .05$ compared with DMSO-treated cells. ND, not detected.

translocations, deletions in an upstream negative regulatory region, somatic acquisition of a neomorphic promoter, or gene therapy-related retroviral insertional mutagenesis at the *LMO2* locus.[8,22,67-70] In our T-ALL patient cohort, we did not compare LMO2 expression levels to that of early thymocyte progenitors, but the samples selected for further analysis showed comparable LMO2 expression level to the LMO2 dependent MOLT4 T-ALL cell line. Activated LMO2 reactivates an HSC-specific transcriptional program in T-cell progenitors, leading to enhanced self-renewal and proliferation, with reduced capacity for T-cell differentiation and transformation into T-ALL blasts.[15,16] These data are in agreement with our observation that LMO2 activation by NAMPT/SIRT2-mediated lysine deacetylation is essential for both formation of HSCs and T-ALL leukemogenesis. Most likely, deacetylated LMO2 activates common downstream targets that are important a specific transcriptional program in HSCs and transformation of T-ALL blasts. At the same time, we cannot exclude the involvement of other transcriptional targets in addition to LMO2 that are activated by NAMPT and SIRTs in HSCs and/or T-ALL cells. In addition, NAMPT-independent mechanisms of LMO2 activation in HSCs and T-ALL cells should be considered.

Using RNA-Seq analysis of MOLT4 cells stably expressing WT or deacetylated LMO2 mutant, we were able to identify signaling pathways such as cytochrome P450, tryptophan degradation, biological oxidation, P53- or TNF-α downstream signaling cascades to be regulated by NAMPT-mediated LMO2 deacetylation. Components of the cytochrome pathway, CYPE1 and CYP1B1, that were downregulated upon NAMPT inhibition in a LMO2-dependent manner, are known to play a role in the ALL pathogenesis.[71-73] Additionally, tryptophan degradation may play a role in the tumorigenesis and may be evaluated further for the potential drug targeting.[74,75] Most probably, LMO2 is involved in the metabolic reprogramming of HSCs during T-leukemogenesis.[76-78] *P53* mutations are frequent finding in ALL that correlates with poor chemotherapy response.[79] TNF-α is known to be involved in different steps of leukemogenesis, including cellular transformation, proliferation, survival, and resistance to chemotherapy.[80-83] In iRegulon analysis, we identified target gene enrichment for known T-ALL-associated transcription factors, such as PITX,[84] ZNF695,[85] MEF2 family,[86-91] and EP300.[92] These data further confirmed the important role of the LMO2 activation by NAMPT-mediated deacetylation in the T-ALL development. It would be interesting to investigate functional connection between identified candidate genes and pathways and NAMPT-activated LMO2 in the pathogenesis of T-ALL and early hematopoiesis.

The 2 experimental models for studying early steps in hematopoiesis used here (in vitro iPS cells and in vivo zebrafish) have offered us an excellent opportunity to study the involvement of NAMPT/SIRTs in differentiation processes of diverse layers/organs and at defined developmental stages. Our observations may help establish improved culture conditions for modulating NAMPT/SIRT signaling (eg, for large-scale in vitro generation of hematopoietic cells from iPS cells).

Taken together, our findings demonstrate that a novel posttranslational mechanism, NAMPT/SIRT2-mediated lysine deacetylation, is involved in regulating the developmentally important protein LMO2. This mechanism could prove profoundly important for developmental biologists, tumor biologists, and clinical scientists/oncologists. Our observations have translational significance, suggesting the possibility of clinically targeting T-ALL leukemia cells through specific inhibition of NAMPT-mediated LMO2 deacetylation. They also have implications for the large-scale in vitro production of hematopoietic cells through modulation of the NAMPT/SIRT2/LMO2 axis.

Acknowledgments

The authors thank Nico Lachmann and Thomas Moritz (Institute of Experimental Hematology, Hannover Medical School) for providing the human iPS cell line hCD34-iPSC16, Qiang Tong (Baylor College of Medicine) for providing pcDNA3.1-SIRT2-flag plasmid, Igor Slukvin (University of Wisconsin School of Medicine and Public Health) for providing pSIN4-EF1a-LMO2-IRES-Puro and pSIN4-EF1a-GATA1-IRES-Puro plasmids, and Robert Benezra (Memorial Sloan Kettering Cancer Center) for providing pcDNA3-hE47 plasmid. Cell sorting and flow cytometry sample acquisition was done on shared instruments of the Flow Cytometry Core Facility Tübingen.

This work was supported by the Applied Clinical Research program from the Faculty of Medicine of the Tübingen University (T.M.); the *Fortüne* program from the Faculty of Medicine, the Tübingen University (T.M.); the Research Fellowship of Uehara Memorial Foundation (T.M.); Deutsche Forschungsgemeinschaft (DFG) (J.S., B.B., and N.A.); Sander Stiftung (A.K.); and Schickedanz Kinderkrebsstiftung (J.S.).

Authorship

Contribution: T.M., J.S., and K.W. made initial observations, designed the experiments, analyzed the data, supervised experimentation, and wrote the manuscript; T.M. performed the main experiments, including zebrafish knockdown; A.-C.K., M.R., S.S., and M.A. designed and performed mouse transplantation experiments; T.M. and M.K. performed Duolink experiments; T.M., Y.X., C.L., B.O., and U.H.-K. performed western blots and immunoprecipitation; T.M. and B.F. made reporter gene assays; R.B. cultured human iPS cells; R.B. and K.H. performed quantitative polymerase chain reaction experiments; Y.X. and M.N. performed CRISPR/Cas9-mediated *SIRT2* gene knockout; M.D.H. conducted structural analysis of LMO2; N.C. performed RNA-sequencing; M.N. analyzed RNA-sequencing data; P.M. designed and supervised the zebrafish experiments; B.B. and N.A. performed the zebrafish xenograft experiments and analyzed the data; M.E. and R.H. provided T-ALL patients material; and C.J.G. assisted with the interpretation of data and provided insightful comments.

Conflict-of-interest disclosure: The authors declare no competing financial interests.

The current affiliation for T.M. is International Research Center for Medical Sciences, Kumamoto University, Kumamoto, Japan.

ORCID profiles: T.M., 0000-0003-3876-3217; N.A., 0000-0002-9890-3229; M.D.H., 0000-0001-6937-5677; C.J.G., 0000-0001-6494-6944; S.S., 0000-0002-4134-4171; N.C., 0000-0003-2209-0580; P.M., 0000-0002-0702-6209; B.B., 0000-0002-7368-7523; J.S., 0000-0002-4399-2324.

Correspondence: Julia Skokowa, Department of Hematology, Oncology, Clinical Immunology and Rheumatology, University Hospital Tübingen, Otfried-Mueller Str 10, 72076 Tübingen, Germany; e-mail: julia.skokowa@med.uni-tuebingen.de; and Tatsuya Morishima, International Research Center for Medical Sciences, Kumamoto University, 2-2-1 Honjo, Chuo-ku, Kumamoto City 860-0811, Japan; e-mail: tatsuyam@kumamoto-u.ac.jp.

Footnotes

Submitted 10 February 2019; accepted 1 July 2019. Prepublished online as *Blood* First Edition paper, 31 July 2019; DOI 10.1182/blood.2019000095.

*A.-C.K. and M.N. contributed equally to this work.

The online version of this article contains a data supplement.

The publication costs of this article were defrayed in part by page charge payment. Therefore, and solely to indicate this fact, this article is hereby marked "advertisement" in accordance with 18 USC section 1734.

REFERENCES

1. Skokowa J, Cario G, Uenalan M, et al. LEF-1 is crucial for neutrophil granulocytopoiesis and its expression is severely reduced in congenital neutropenia [published correction appears in *Nat Med*. 2006;12(11):1329]. *Nat Med*. 2006;12(10):1191-1197.
2. Skokowa J, Steinemann D, Katsman-Kuipers JE, et al. Cooperativity of RUNX1 and CSF3R mutations in severe congenital neutropenia: a unique pathway in myeloid leukemogenesis. *Blood*. 2014;123(14):2229-2237.
3. Marcucci G, Haferlach T, Döhner H. Molecular genetics of adult acute myeloid leukemia: prognostic and therapeutic implications. *J Clin Oncol*. 2011;29(5):475-486.
4. Chambers J, Rabbitts TH. LMO2 at 25 years: a paradigm of chromosomal translocation proteins. *Open Biol*. 2015;5(6):150062.
5. Orkin SH, Zon LI. Hematopoiesis: an evolving paradigm for stem cell biology. *Cell*. 2008; 132(4):631-644.
6. Warren AJ, Colledge WH, Carlton MB, Evans MJ, Smith AJ, Rabbitts TH. The oncogenic cysteine-rich LIM domain protein rbtn2 is essential for erythroid development. *Cell*. 1994; 78(1):45-57.
7. Patterson LJ, Gering M, Eckfeldt CE, et al. The transcription factors Scl and Lmo2 act together during development of the hemangioblast in zebrafish. *Blood*. 2007;109(6):2389-2398.
8. Van Vlierberghe P, van Grotel M, Beverloo HB, et al. The cryptic chromosomal deletion del(11)(p12p13) as a new activation mechanism of LMO2 in pediatric T-cell acute lymphoblastic leukemia. *Blood*. 2006;108(10): 3520-3529.
9. Wu L, Xu Y, Wang Q, et al. High frequency of cryptic chromosomal rearrangements involving the LMO2 gene in T-cell acute lymphoblastic leukemia. *Haematologica*. 2015; 100(6):e233-e236.
10. Ferrando AA, Look AT. Gene expression profiling in T-cell acute lymphoblastic leukemia. *Semin Hematol*. 2003;40(4):274-280.
11. Boehm T, Foroni L, Kaneko Y, Perutz MF, Rabbitts TH. The rhombotin family of cysteine-rich LIM-domain oncogenes: distinct members are involved in T-cell translocations to human chromosomes 11p15 and 11p13. *Proc Natl Acad Sci USA*. 1991;88(10): 4367-4371.
12. Fisch P, Boehm T, Lavenir I, et al. T-cell acute lymphoblastic lymphoma induced in transgenic mice by the RBTN1 and RBTN2 LIM-domain genes. *Oncogene*. 1992;7(12): 2389-2397.
13. Dik WA, Pike-Overzet K, Weerkamp F, et al. New insights on human T cell development by quantitative T cell receptor gene rearrangement studies and gene expression profiling. *J Exp Med*. 2005;201(11):1715-1723.
14. Wiekmeijer AS, Pike-Overzet K, Brugman MH, et al. Overexpression of LMO2 causes aberrant human T-Cell development in vivo by three potentially distinct cellular mechanisms. *Exp Hematol*. 2016;44(9):838-849.
15. Herblot S, Steff AM, Hugo P, Aplan PD, Hoang T. SCL and LMO1 alter thymocyte differentiation: inhibition of E2A-HEB function and pre-T alpha chain expression. *Nat Immunol*. 2000; 1(2):138-144.
16. McCormack MP, Young LF, Vasudevan S, et al. The Lmo2 oncogene initiates leukemia in mice by inducing thymocyte self-renewal. *Science*. 2010;327(5967):879-883.
17. García-Ramírez I, Bhatia S, Rodríguez-Hernández G, et al. Lmo2 expression defines tumor cell identity during T-cell leukemogenesis. *EMBO J*. 2018;37(14):e98783.
18. El Omari K, Hoosdally SJ, Tuladhar K, et al. Structure of the leukemia oncogene LMO2: implications for the assembly of a hematopoietic transcription factor complex. *Blood*. 2011;117(7):2146-2156.
19. El Omari K, Hoosdally SJ, Tuladhar K, et al. Structural basis for LMO2-driven recruitment of the SCL:E47bHLH heterodimer to hematopoietic-specific transcriptional targets. *Cell Reports*. 2013;4(1):135-147.
20. Wadman IA, Osada H, Grütz GG, et al. The LIM-only protein Lmo2 is a bridging molecule assembling an erythroid, DNA-binding complex which includes the TAL1, E47, GATA-1 and Ldb1/NLI proteins. *EMBO J*. 1997;16(11): 3145-3157.
21. Landry JR, Bonadies N, Kinston S, et al. Expression of the leukemia oncogene Lmo2 is controlled by an array of tissue-specific elements dispersed over 100 kb and bound by Tal1/Lmo2, Ets, and Gata factors. *Blood*. 2009;113(23):5783-5792.
22. Rahman S, Magnussen M, León TE, et al. Activation of the *LMO2* oncogene through a somatically acquired neomorphic promoter in T-cell acute lymphoblastic leukemia. *Blood*. 2017;129(24):3221-3226.
23. Skokowa J, Lan D, Thakur BK, et al. NAMPT is essential for the G-CSF-induced myeloid differentiation via a NAD(+)-sirtuin-1-dependent pathway. *Nat Med*. 2009;15(2):151-158.
24. Dan L, Klimenkova O, Klimiankou M, et al. The role of sirtuin 2 activation by nicotinamide phosphoribosyltransferase in the aberrant proliferation and survival of myeloid leukemia cells. *Haematologica*. 2012;97(4):551-559.
25. Thakur BK, Lippka Y, Dittrich T, Chandra P, Skokowa J, Welte K. NAMPT pathway is involved in the FOXO3a-mediated regulation of GADD45A expression. *Biochem Biophys Res Commun*. 2012;420(4):714-720.
26. Thakur BK, Dittrich T, Chandra P, et al. Involvement of p53 in the cytotoxic activity of the NAMPT inhibitor FK866 in myeloid leukemic cells. *Int J Cancer*. 2013;132(4): 766-774.
27. Koch C, Samareh B, Morishima T, et al. GM-CSF treatment is not effective in congenital neutropenia patients due to its inability to activate NAMPT signaling. *Ann Hematol*. 2017;96(3):345-353.
28. Nakagawa T, Guarente L. Sirtuins at a glance. *J Cell Sci*. 2011;124(Pt 6):833-838.
29. Feldman JL, Dittenhafer-Reed KE, Denu JM. Sirtuin catalysis and regulation. *J Biol Chem*. 2012;287(51):42419-42427.
30. Vaquero A, Scher MB, Lee DH, et al. SirT2 is a histone deacetylase with preference for histone H4 Lys 16 during mitosis. *Genes Dev*. 2006;20(10):1256-1261.
31. Ou X, Chae HD, Wang RH, et al. SIRT1 deficiency compromises mouse embryonic stem cell hematopoietic differentiation, and embryonic and adult hematopoiesis in the mouse. *Blood*. 2011;117(2):440-450.
32. Hasmann M, Schemainda I. FK866, a highly specific noncompetitive inhibitor of nicotinamide phosphoribosyltransferase, represents a novel mechanism for induction of tumor cell apoptosis. *Cancer Res*. 2003;63(21): 7436-7442.
33. Solomon JM, Pasupuleti R, Xu L, et al. Inhibition of SIRT1 catalytic activity increases p53 acetylation but does not alter cell survival following DNA damage. *Mol Cell Biol*. 2006; 26(1):28-38.
34. Zhang Y, Au Q, Zhang M, Barber JR, Ng SC, Zhang B. Identification of a small molecule SIRT2 inhibitor with selective tumor cytotoxicity. *Biochem Biophys Res Commun*. 2009; 386(4):729-733.
35. Lachmann N, Happle C, Ackermann M, et al. Gene correction of human induced pluripotent stem cells repairs the cellular phenotype in pulmonary alveolar proteinosis. *Am J Respir Crit Care Med*. 2014;189(2):167-182.
36. Mosimann C, Panáková D, Werdich AA, et al. Chamber identity programs drive early functional partitioning of the heart. *Nat Commun*. 2015;6(1):8146.
37. Zhou X, Fan LX, Li K, Ramchandran R, Calvet JP, Li X. SIRT2 regulates ciliogenesis and contributes to abnormal centrosome amplification caused by loss of polycystin-1. *Hum Mol Genet*. 2014;23(6):1644-1655.
38. Dooley CM, Schwarz H, Mueller KP, et al. Slc45a2 and V-ATPase are regulators of melanosomal pH homeostasis in zebrafish, providing a mechanism for human pigment evolution and disease. *Pigment Cell Melanoma Res*. 2013;26(2):205-217.
39. Clèries R, Galvez J, Espino M, Ribes J, Nunes V, de Heredia ML. BootstRatio: a web-based statistical analysis of fold-change in qPCR and RT-qPCR data using resampling methods. *Comput Biol Med*. 2012;42(4):438-445.

40. Li A, Xue Y, Jin C, Wang M, Yao X. Prediction of Nepsilon-acetylation on internal lysines implemented in Bayesian discriminant method. *Biochem Biophys Res Commun*. 2006;350(4):818-824.

41. Li S, Li H, Li M, Shyr Y, Xie L, Li Y. Improved prediction of lysine acetylation by support vector machines. *Protein Pept Lett*. 2009; 16(8):977-983.

42. Hou T, Zheng G, Zhang P, et al. LAceP: lysine acetylation site prediction using logistic regression classifiers. *PLoS One*. 2014;9(2): e89575.

43. Lécuyer E, Hoang T. SCL: from the origin of hematopoiesis to stem cells and leukemia. *Exp Hematol*. 2004;32(1):11-24.

44. Lahlil R, Lécuyer E, Herblot S, Hoang T. SCL assembles a multifactorial complex that determines glycophorin A expression. *Mol Cell Biol*. 2004;24(4):1439-1452.

45. Revollo JR, Grimm AA, Imai S. The NAD biosynthesis pathway mediated by nicotinamide phosphoribosyltransferase regulates Sir2 activity in mammalian cells. *J Biol Chem*. 2004;279(49):50754-50763.

46. Curtis DJ, McCormack MP. The molecular basis of Lmo2-induced T-cell acute lymphoblastic leukemia. *Clin Cancer Res*. 2010; 16(23):5618-5623.

47. Porcher C, Chagraoui H, Kristiansen MS. SCL/TAL1: a multifaceted regulator from blood development to disease. *Blood*. 2017;129(15): 2051-2060.

48. Kusy S, Gerby B, Goardon N, et al. NKX3.1 is a direct TAL1 target gene that mediates proliferation of TAL1-expressing human T cell acute lymphoblastic leukemia. *J Exp Med*. 2010;207(10):2141-2156.

49. Khatri P, Drăghici S. Ontological analysis of gene expression data: current tools, limitations, and open problems. *Bioinformatics*. 2005;21(18):3587-3595.

50. Janky R, Verfaillie A, Imrichová H, et al. iRegulon: from a gene list to a gene regulatory network using large motif and track collections. *PLOS Comput Biol*. 2014;10(7): e1003731.

51. Niwa A, Heike T, Umeda K, et al. A novel serum-free monolayer culture for orderly hematopoietic differentiation of human pluripotent cells via mesodermal progenitors. *PLoS One*. 2011;6(7):e22261.

52. Morishima T, Watanabe K, Niwa A, et al. Genetic correction of HAX1 in induced pluripotent stem cells from a patient with severe congenital neutropenia improves defective granulopoiesis. *Haematologica*. 2014;99(1): 19-27.

53. Söderberg O, Gullberg M, Jarvius M, et al. Direct observation of individual endogenous protein complexes in situ by proximity ligation. *Nat Methods*. 2006;3(12): 995-1000.

54. Leuchowius KJ, Weibrecht I, Landegren U, Gedda L, Söderberg O. Flow cytometric in situ proximity ligation analyses of protein interactions and post-translational modification of the epidermal growth factor receptor family. *Cytometry A*. 2009;75(10):833-839.

55. Kimmel CB, Ballard WW, Kimmel SR, Ullmann B, Schilling TF. Stages of embryonic development of the zebrafish. *Dev Dyn*. 1995; 203(3):253-310.

56. Wang Z, Skokowa J, Pramono A, Ballmaier M, Welte K. Thrombopoietin regulates differentiation of rhesus monkey embryonic stem cells to hematopoietic cells. *Ann N Y Acad Sci*. 2005;1044(1):29-40.

57. Pramono A, Zahabi A, Morishima T, Lan D, Welte K, Skokowa J. Thrombopoietin induces hematopoiesis from mouse ES cells via HIF-1α-dependent activation of a BMP4 autoregulatory loop. *Ann N Y Acad Sci*. 2016; 1375(1):38-51.

58. Oliveira ML, Akkapeddi P, Alcobia I, et al. From the outside, from within: Biological and therapeutic relevance of signal transduction in T-cell acute lymphoblastic leukemia. *Cell Signal*. 2017;38:10-25.

59. Bruzzone S, Fruscione F, Morando S, et al. Catastrophic NAD+ depletion in activated T lymphocytes through Nampt inhibition reduces demyelination and disability in EAE. *PLoS One*. 2009;4(11):e7897.

60. Beier UH, Wang L, Bhatti TR, et al. Sirtuin-1 targeting promotes Foxp3+ T-regulatory cell function and prolongs allograft survival. *Mol Cell Biol*. 2011;31(5):1022-1029.

61. Jeng MY, Hull PA, Fei M, et al. Metabolic reprogramming of human $CD8^+$ memory T cells through loss of SIRT1. *J Exp Med*. 2018; 215(1):51-62.

62. Han MK, Song EK, Guo Y, Ou X, Mantel C, Broxmeyer HE. SIRT1 regulates apoptosis and Nanog expression in mouse embryonic stem cells by controlling p53 subcellular localization. *Cell Stem Cell*. 2008;2(3):241-251.

63. Holen K, Saltz LB, Hollywood E, Burk K, Hanauske AR. The pharmacokinetics, toxicities, and biologic effects of FK866, a nicotinamide adenine dinucleotide biosynthesis inhibitor. *Invest New Drugs*. 2008; 26(1):45-51.

64. von Heideman A, Berglund A, Larsson R, Nygren P. Safety and efficacy of NAD depleting cancer drugs: results of a phase I clinical trial of CHS 828 and overview of published data. *Cancer Chemother Pharmacol*. 2010;65(6):1165-1172.

65. Nahimana A, Attinger A, Aubry D, et al. The NAD biosynthesis inhibitor APO866 has potent antitumor activity against hematologic malignancies. *Blood*. 2009;113(14): 3276-3286.

66. Matheny CJ, Wei MC, Bassik MC, et al. Next-generation NAMPT inhibitors identified by sequential high-throughput phenotypic chemical and functional genomic screens. *Chem Biol*. 2013;20(11): 1352-1363.

67. Hacein-Bey-Abina S, von Kalle C, Schmidt M, et al. A serious adverse event after successful gene therapy for X-linked severe combined immunodeficiency. *N Engl J Med*. 2003; 348(3):255-256.

68. Hacein-Bey-Abina S, Von Kalle C, Schmidt M, et al. LMO2-associated clonal T cell proliferation in two patients after gene therapy for SCID-X1. *Science*. 2003;302(5644):415-419.

69. Howe SJ, Mansour MR, Schwarzwaelder K, et al. Insertional mutagenesis combined with acquired somatic mutations causes leukemogenesis following gene therapy of SCID-X1 patients. *J Clin Invest*. 2008;118(9): 3143-3150.

70. Van Vlierberghe P, Ferrando A. The molecular basis of T cell acute lymphoblastic leukemia. *J Clin Invest*. 2012;122(10):3398-3406.

71. Krajinovic M, Sinnett H, Richer C, Labuda D, Sinnett D. Role of NQO1, MPO and CYP2E1 genetic polymorphisms in the susceptibility to childhood acute lymphoblastic leukemia. *Int J Cancer*. 2002;97(2):230-236.

72. DiNardo CD, Gharibyan V, Yang H, et al. Impact of aberrant DNA methylation patterns including CYP1B1 methylation in adolescents and young adults with acute lymphocytic leukemia. *Am J Hematol*. 2013;88(9): 784-789.

73. Litzenburger UM, Opitz CA, Sahm F, et al. Constitutive IDO expression in human cancer is sustained by an autocrine signaling loop involving IL-6, STAT3 and the AHR. *Oncotarget*. 2014;5(4):1038-1051.

74. Schwarcz R. The kynurenine pathway of tryptophan degradation as a drug target. *Curr Opin Pharmacol*. 2004;4(1):12-17.

75. Sucher R, Kurz K, Weiss G, Margreiter R, Fuchs D, Brandacher G. IDO-mediated tryptophan degradation in the pathogenesis of malignant tumor disease. *Int J Tryptophan Res*. 2010;3: 113-120.

76. Udensi UK, Tchounwou PB. Dual effect of oxidative stress on leukemia cancer induction and treatment. *J Exp Clin Cancer Res*. 2014; 33(1):106.

77. Dyczynski M, Vesterlund M, Björklund AC, et al. Metabolic reprogramming of acute lymphoblastic leukemia cells in response to glucocorticoid treatment. *Cell Death Dis*. 2018;9(9):846.

78. Olivas-Aguirre M, Pottosin I, Dobrovinskaya O. Mitochondria as emerging targets for therapies against T cell acute lymphoblastic leukemia. *J Leukoc Biol*. 2019;105(5): 935-946.

79. Chiaretti S, Brugnoletti F, Tavolaro S, et al. TP53 mutations are frequent in adult acute lymphoblastic leukemia cases negative for recurrent fusion genes and correlate with poor response to induction therapy. *Haematologica*. 2013;98(5):e59-e61.

80. Zhou X, Li Z, Zhou J. Tumor necrosis factor α in the onset and progression of leukemia. *Exp Hematol*. 2017;45:17-26.

81. Munzert G, Kirchner D, Stobbe H, et al. Tumor necrosis factor receptor-associated factor 1 gene overexpression in B-cell chronic lymphocytic leukemia: analysis of NF-kappa B/Rel-regulated inhibitors of apoptosis. *Blood*. 2002;100(10):3749-3756.

82. Edilova MI, Abdul-Sater AA, Watts TH. TRAF1 signaling in human health and disease. *Front Immunol*. 2018;9:2969.

83. Zhang B, Wang Z, Li T, Tsitsikov EN, Ding HF. NF-kappaB2 mutation targets TRAF1 to induce lymphomagenesis. *Blood*. 2007;110(2): 743-751.

84. Nagel S, Venturini L, Przybylski GK, et al. Activation of paired-homeobox gene PITX1 by del(5)(q31) in T-cell acute lymphoblastic leukemia. *Leuk Lymphoma*. 2011;52(7):1348-1359.

85. Li C, Kuang L, Zhu B, Chen J, Wang X, Huang X. Identification of prognostic risk factors of acute lymphoblastic leukemia based on mRNA expression profiling. *Neoplasma*. 2017;64(4):494-501.

86. Nagel S, Venturini L, Meyer C, et al. Transcriptional deregulation of oncogenic myocyte enhancer factor 2C in T-cell acute lymphoblastic leukemia. *Leuk Lymphoma*. 2011;52(2):290-297.

87. Canté-Barrett K, Pieters R, Meijerink JP. Myocyte enhancer factor 2C in hematopoiesis and leukemia. *Oncogene*. 2014;33(4):403-410.

88. Gu Z, Churchman M, Roberts K, et al. Genomic analyses identify recurrent MEF2D fusions in acute lymphoblastic leukaemia. *Nat Commun*. 2016;7:13331.

89. Di Giorgio E, Hancock WW, Brancolini C. MEF2 and the tumorigenic process, hic sunt leones. *Biochim Biophys Acta Rev Cancer*. 2018;1870(2):261-273.

90. Smith S, Tripathi R, Goodings C, et al. LIM domain only-2 (LMO2) induces T-cell leukemia by two distinct pathways. *PLoS One*. 2014;9(1):e85883.

91. Homminga I, Pieters R, Langerak AW, et al. Integrated transcript and genome analyses reveal NKX2-1 and MEF2C as potential oncogenes in T cell acute lymphoblastic leukemia. *Cancer Cell*. 2011;19(4):484-497.

92. Qian M, Zhang H, Kham SK, et al. Whole-transcriptome sequencing identifies a distinct subtype of acute lymphoblastic leukemia with predominant genomic abnormalities of EP300 and CREBBP. *Genome Res*. 2017;27(2):185-195.